

ISSUE NO. 273

OCTOBER 2006

बी ए आर सी
न्यूज़लैटर

BARC
NEWSLETTER

$$(\Delta E_{int})_{AK} = \frac{-(\mu_A - \mu_B)^2}{2} \left(\frac{S_A f_{AK} + S_B f_{BK}}{S_A f_{AK} + S_B f_{BK}} \right)$$

$$\frac{\lambda}{2} \left(\frac{\lambda}{S_A f_{AK} + S_B f_{BK}} \right)$$

Founder's Day

Special Issue

320 nm

Founder's Day

Special Issue



Government of India

BHABHA ATOMIC RESEARCH CENTRE



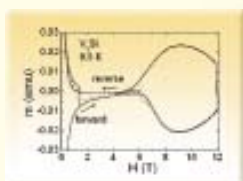
DEDICATED TO THE MEMORY OF

Homi Jehangir Bhabha
(1909 - 1966)

Founder and Architect of
Indian Atomic Energy Programme

CONTENTS

1. **Nature of the order-disorder transition of the vortex matter in weakly pinned superconductors** 1



Ravi Kumar, G.
Recipient of the Homi Bhabha Science and Technology Award for the year 2004.

2. **Development of neutron and x-ray detectors and neutron radiography at BARC** 8



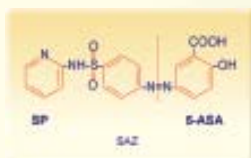
Shaikh, A.M.
Recipient of the Technical Excellence Award for the year 2004.

3. **Role of surface states of semiconductor nanomaterials in interfacial electron transfer dynamics and effect of surface modification** 25



Ghosh, H.N.
Recipient of "The APA-Prize of Young Scientists" awarded by the Asian and Oceanian Photochemistry Association, at Crains, Australia, on 27th July 2005.

4. **Evidence for antioxidant activity and functional moiety of non steroidal anti inflammatory drug sulfasalazine** 36



Joshi, R. and Mukherjee, T.
Recipients of the Young Scientist Award at the 24th Miller Conference on Radiation Chemistry, held at La Londe les Maures, Toulon, France, during 10th to 15th September, 2005.

Newsletter on the web available at URL:<http://www.barc.gov.in>

5. Electronic structure and properties of molecules and clusters : density functional theory based approach 43

Chandrakumar, K.R.S.
Recipient of the Young Scientist Medal at the Indian National Science Academy (INSA), New Delhi, 2005.

6. Density concept in molecules and materials modeling at different length scales 53

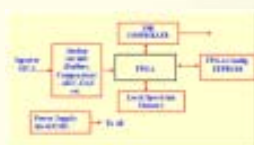
Ghosh, S.K.
Recipient of the Silver Medal of the Chemical Research Society of India (CRSI), Bangalore, February 2005.

7. Differential pulse anodic stripping in aqueous solution of Na₂CO₃ for the determination of trace amounts of cadmium present in UO₂ fuel 64

Kamat, J.V et al
Recipients of the Best Paper Award (First Prize) in the technical session at the twelfth National Convention of Electrochemists (NCE-12), held at Thiagarajar College of Engineering, Madurai, during February 18-19, 2005.

8. Compact 8 K multi-channel analyzer with USB interface and multi-mode operation 67

Kulkarni, C.P. et al
Recipients of the Best Paper Award in the National Symposium on Compact Nuclear Instruments and Radiation Detectors, held at Jodhpur, during March 2-4, 2005.

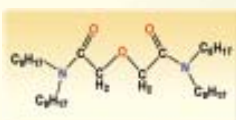


9. Extraction chromatographic studies employing N,N',N'-tetractyl diglycolamide (TODGA) as stationary phase

73

Ansari, S.A. et al

Recipients of the Best Paper (Oral) Award at the DAE-BRNS Symposium in Nuclear & Radiochemistry (NUCAR-2005), held at the Gurunanak Dev University, Amritsar, during March 15-18, 2005.

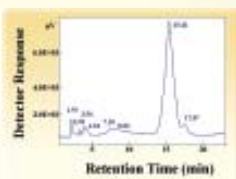


10. Inhibition of chlorophyll degradation in stay-green langra mango (*mangifera indica L.*) fruits

80

Janave, M.T. and Sharma, A.

Recipients of the Best Paper Award (G.S. Sirohi Award 2005) at the National Seminar of the Indian Society for Plant Physiology held at Navasari Agricultural University, Navasari, Gujarat, during November 2005.

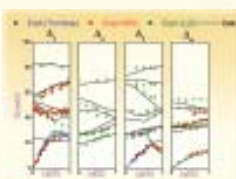


11. Modeling of anomalous thermodynamic properties using lattice dynamics and inelastic neutron scattering

88

Mittal, R.

Recipient of the Golden Jubilee Young Achiever Award at the DAE-Solid State Physics Symposium, held at BARC, Mumbai, during December 5-9, 2005.



12. Role of blend morphology in the radiation processing of SBR-EPDM blends

92

Dubey, K.A. et al

Recipients of the Shri K.M. Philip Award constituted by the Indian Rubber Manufacturers' Research Association during the 19th Rubber Conference, held at Mumbai, during December 19-20, 2005.



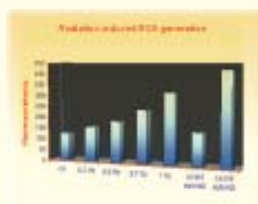
13. **Application of neutron radiography and neutron diffraction techniques in study of zirconium hydride blisters in zirconium based pressure tube materials** 104



Shaikh, A.M. et al

Recipients of the Best ISNT National Award 2004, under the category "Best Paper published in R&D" in the Journal Non Destructive Testing & Evaluation, 2003.

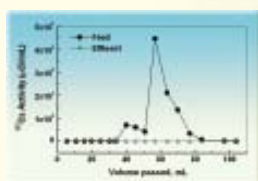
14. **Effect of low dose ionising radiation and ultraviolet radiation on human keratinocyte cell line** 113



Mehrotra, P et al

Recipients of the Best young Scientist Oral Presentation Award at the International Conference on Recent Trends in Radiation Biology, held at BARC, Mumbai, during December 1-3, 2004.

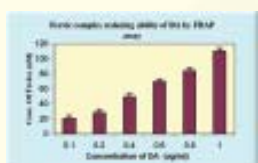
15. **Simultaneous separation and consolidation of ¹³⁷Cs from alkaline intermediate level reprocessing waste using resorcinol formaldehyde polycondensate resin and zeolite sorbent** 119



Banerjee, D. and Samanta, S.K.

Recipients of One of the Best Paper Award at the DAE-BRNS Theme Meeting on "Emerging Trends in Separation Science and Technology" (SESTEC-2004), held at BARC, Mumbai, during July 22-23, 2004.

16. **Antioxidant properties of a novel marine analogue of dendrodoine** 123



Strayo De, et al

Recipients of the Best Poster Paper Award in "The First International Conference on Natural Products for Health and Beauty", at Maha Sarakham, Thailand, during October 17-21, 2005.

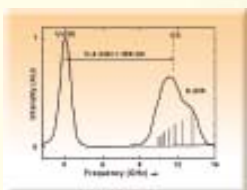
17. **Thermal analysis of solid-cathode holder assembly of indirectly heated cathode EB welding gun** 134



Karmakar, P. et al

Recipients of the Best Poster Paper Award at the DAE-BRNS symposium on "Electron Beam Technology and Application" (SEBTA-2005), held at BARC, Mumbai, during September 28-30, 2005.

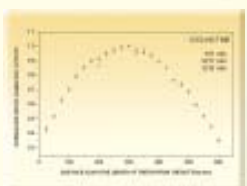
18. **Spectroscopic data for laser isotope by atomic vapour route: a case study in (U-234,U-235) isotopic system** 145



Marathe, A.P. et al

Recipients of the Best Paper Award in the session "Physics Behind Nuclear Technology" at the Indian Nuclear Society's Annual Conference (INSAC-2005), on "Science Behind Nuclear Technology" held at BARC, Mumbai, during November 15-18, 2005.

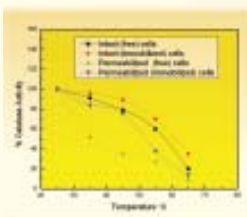
19. **A methodology for gamma ray spectrometric determination of fission rates in fuel specimens** 152



Reddy, A.V.R. et al

Recipients of the Best Paper Award on "Science Behind Nuclear Technology" at the 16th Annual Conference of Indian Nuclear Society, held at BARC, Mumbai, during November 15-18, 2005.

20. **Immobilization of catalase by cross-linking of permeabilized yeast cells in a protein support** 162



Kubal, B.S. and D'Souza, S.F.

Recipients of the Best Poster Presentation Award at the 73rd Annual General Body Meeting of Society of Biological Chemists (India) and International Symposium on "Challenges and Opportunities to Harness Modern Biology for Socio-Economic Development in Genomic Era" held at GB Pantnagar University of Agriculture & Technology, Pantnagar, during November 21-24, 2004.

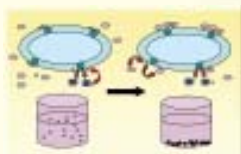
25. Production of biopesticide azadirachtin by hairy root cultures of neem (*azadirachta indica A. juss*) 195



Satdive, R.K. et al

Recipients of the Best Poster Presentation Award at the National Symposium on "Plant Biotechnology: New Frontiers", held at Central Institute of Medicinal and Aromatic Plants, Lucknow, during November 18-20, 2005.

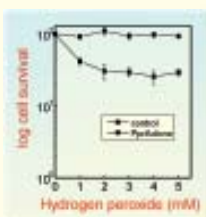
26. Phosphatase mediated bioremediation of cadmium 208



Seetharam Chitra et al

Recipients of the Best Poster Paper Award at the 16th Annual Conference of Indian Nuclear Society (INSAC-2005), held at Mumbai, during November 16-18, 2005.

27. PprA: an important protein of radiation resistance in *Deinococcus stimulates catalase activity in Escherichia coli* 213



Kota Swathi and Misra H.S.

Recipients of the Best Poster Paper Award at the DAE-BRNS symposium on "Molecular Biology of Stress Response and its Applications" held at BARC, Mumbai, during December 19-21, 2005.

28. Screening of Indian corn varieties for aflatoxin resistance 218



Hajare Shruti, S. et al

Recipients of the First Prize Poster Paper Award in the subject area "Infestation Control and Food Protectants" at the 17th Indian Convention of Food Scientists & Technologists (ICFOST 2005), held at NIMHANS, Bangalore, during December 9-10, 2005.

29. Developmental studies of the 20 MeV high intensity linac 231



Singh, P. et al

Recipients of the Best Poster Paper Award at the DAE-BRNS 50th symposium on Nuclear Physics, held at BARC, Mumbai, during December 12-16, 2005.

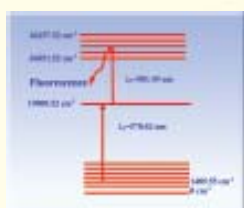
30. Selection for abiotic (salinity and drought) stress tolerance and molecular characterization of tolerant lines in sugarcane 244



Patade, V.Y. et al.

Recipients of the Best Poster Paper Award at the National Conference on "Biotechnological Aspects Towards Cultivation, Utilization and Disease Management of Plants", held at Lal Bahadur Shastri Mahavidyalaya, Dharmabad, Nanded, during December, 24-25, 2005.

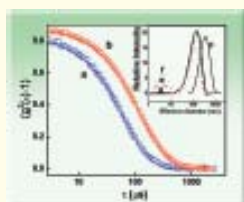
31. Measurement of atomic parameters of Samarium using two-color Laser-Induced Fluorescence (LIF) 258



Shah, M.L. et al

Recipients of One of the Best Poster Paper Awards at the National Symposium on "Recent Trends in Fluorescence Spectroscopy and its applications", held at the Department of Physics, Kumaun University, Nainital, during December 1-3, 2005.

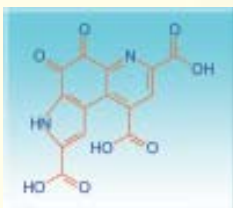
32. Formation of redox active nanoselenium on reactions of oxidizing free radicals with selenourea 262



Mishra Beena et al

Recipients of One of the Best Poster Paper Awards in the National Symposium on Radiation & Photochemistry (MSRP-2005) held at the University of Karnatak, Dharwad, January 2005.

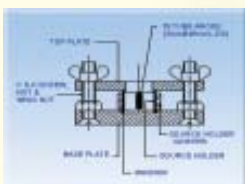
33. **One-electron reduction of pyrroloquinoline quinone (PQQ),
in aqueous solutions : a pulse radiolysis study** 268



Barik Atanu et al

Recipients of One of the Best Poster Paper Awards at the National Symposium on "Radiation & Photochemistry (NSRP-2005), held at the University of Karnatak, Dharwad, during January 17-19, 2005.

34. **Preparation of ⁶³Ni electrodeposited special
custom-made sources** 274



Gandhi S.S. et al.

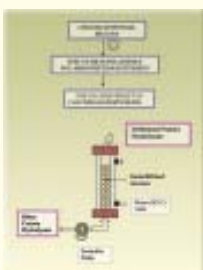
Recipients of Consolation prize in the Poster Presentation Session at the NAARRI Annual Conference (NAC-2005) on "Radioisotopes and Radiation Technology : User's Perception and Experience", held at BARC, Mumbai, during November 10-11, 2005.

35. **Influence of ionizing radiation on protein degradation by
endogenous proteases in poultry viscera** 278

Jamdar, S.N. et al

Third Prize for the Poster Paper at the NAARRI Annual Conference-2005), held at Mumbai, during November 10-11, 2005.

36. **Modification of protein hydrolysates by chicken intestinal
aminopeptidases** 285



Damle, M.V. et al

Third Prize for the Poster Paper in Biochemistry & Nutrition at ICFOST-2005, held at Bangalore, during December, 9-10, 2005.

NATURE OF THE ORDER-DISORDER TRANSITION OF THE VORTEX MATTER IN WEAKLY PINNED SUPERCONDUCTORS

G. Ravikumar
Technical Physics and Prototype Engineering Division
Bhabha Atomic Research Centre

Dr Gurazada Ravi Kumar is the recipient
of the Homi Bhabha Science and Technology Award
for the year 2004.

Abstract

Peak effect in weakly pinned superconductors represents order-disorder transition of the vortex matter. It is accompanied by metastability. Experimental manifestation of the metastability is highlighted and is explained by proposing a phenomenological model, in which each metastable vortex state corresponds to a distinct critical current density J_c . Existence of a unique stable state corresponding to a $J_c = J_c^{st}$ is postulated and established experimentally. It is shown that the stable state can be accessed from any metastable state by subjecting the superconductor to an oscillatory field of a small amplitude. Assuming that the stable state is the thermodynamic equilibrium state, we infer the equilibrium magnetization across the peak effect regime. We present an evidence that the order-disorder transition corresponds to a first order transition.

Superconducting materials lose their resistance below a critical temperature T_c . Besides the zero resistance, they also exhibit Meissner effect (total flux expulsion). Based on their magnetic behavior, superconductors are classified as type I and type II. Application of a magnetic field larger than a critical value H_c restores the normal resistance of Type I superconductors even below T_c . Most type I superconductors are elemental materials having a critical field not more than few hundred Oersteds. On the other hand, type II superconductors exhibit Meissner effect only below a lower critical field H_{c1} .

Between H_{c1} and an upper critical field H_{c2} , magnetic flux penetrates the superconductor in the form of quantized vortices while the resistance remains zero. This state is called the Mixed State or Vortex State. Most of the type II superconductors are alloys and compounds having critical fields in the range of few thousand to several millions of Oersteds. Thus they are extensively used in generating high magnetic fields in particle accelerators, Nuclear Magnetic Resonance Imagers (MRIs), Tokamaks for nuclear fusion experiments and so on. The most popular superconducting materials in use for these applications

are NbTi and Nb₃Sn. High T_c tapes made of YBa₂Cu₃O₇, coated conductors are slowly gaining acceptance, albeit for generating relatively low fields (of the order of 1 – 2 T) but using liquid Nitrogen rather than the expensive and cumbersome liquid helium.

A vortex is an object carrying a quantum of magnetic flux $\phi_0 \approx 2 \times 10^{-15}$ Weber and a persistent circulating supercurrent extending upto the London penetration depth λ . The repulsive interaction due to the circulating supercurrents organizes the vortices into an ordered lattice. However, a transport current through a superconductor exerts a Lorentz force on the vortex lattice. The resulting motion of the vortices causes dissipation. Fortunately, the normal vortex cores of radius equal to the coherence length ξ interact with the underlying material defect structure and various impurities to immobilize or pin the vortices. The interaction of the vortex matter with the defect structure is the basis for all the high field applications of the superconductors. Metallurgists manipulate the material microstructure to enhance the J_c of the superconductors by various metallurgical processing routes.

The pinning interaction is also responsible for destroying the spatial order of the vortex lattice. The competition between the repulsive inter-vortex interaction, which tends to order the vortex lattice and the pinning which tends to destroy that order is interesting from the basic physics point of view. While the success in applications is achieved by metallurgists, the physics of the interaction

between the vortex matter and the pinning is not well understood basically because of the relatively long range interaction between the vortices. The competition between these two interactions determines the critical current density J_c, which is one of the most important properties from the application point of view and also produces various phases of the vortex matter[1]. This study assumed further importance with the advent of high T_c superconductors where thermal energy kT is an additional energy, which makes the vortex phase diagram even more interesting[1]. Mutual competition between the three energy scales, viz., inter-vortex repulsive interaction, pinning interaction and the thermal energy produces mainly three vortex phase transitions (see the vortex phase diagram in Fig. 1) viz., (i) vortex solid to vortex liquid[2], (ii) Vortex solid to vortex Glass or *order-disorder transition*[3] and (iii) Vortex Glass to vortex liquid[4]. The first is established to be a first order transition[2]. My work mainly focuses on the understanding of the thermodynamic nature of the vortex solid to vortex glass transition.

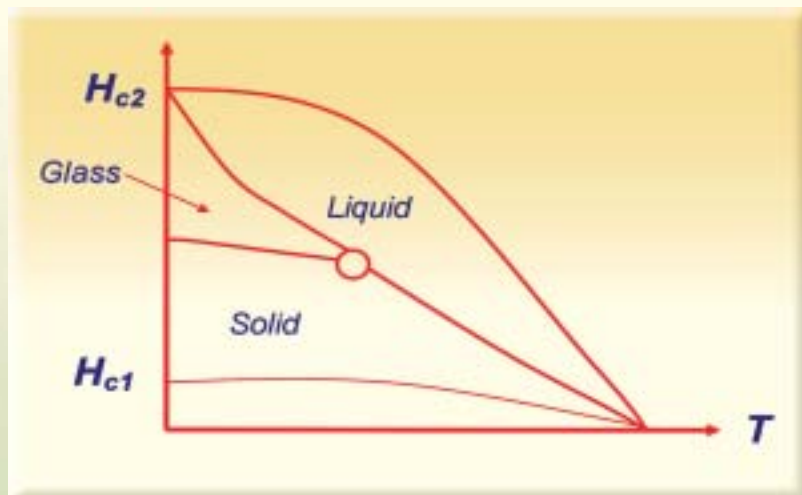


Fig. 1 : Vortex phase diagram of a type II superconductor

Larkin and Ovchinnikov[5] proposed the collective pinning (LO) theory based on the elastic interaction between the vortex lattice with a random distribution of point pins which correlates J_c to the microscopic parameters through the relation

$$J_c = (n \langle F^2 \rangle / V_c)^{1/2} (1/B), \quad (1)$$

where n is the density of microscopic point pins and f is the average force exerted by each of the pins on a vortex. This theory is strictly valid only in the regime of elastic deformations of the vortex lattice and V_c is the volume of the vortex lattice over which the lattice remains correlated. Usually J_c decreases monotonically with increasing magnetic field (B) and/or temperature (T). But many superconductors exhibit a sharp peak in J_c as a function of both field and temperature, the phenomenon known as *peak effect*[6]. Within the LO theory, a sharp increase in J_c signifies a sudden decrease in the long range correlations of the vortex lattice. However, the assumption of elastic deformations may not be strictly valid across the peak effect as indicated by Small Angle Neutron Scattering experiments[7].

Current understanding is that the peak effect is the result of competition between inter-vortex interaction and pinning resulting in a vortex lattice transition from a low field/temperature quasi-ordered Bragg Glass (BG) phase, free of topological defects, into a highly defective disordered Vortex Glass (VG) phase[8]. It occurs just below the normal state boundary in low T_c superconductors but in high T_c superconductors, it occurs well below the normal state boundary. It is established that in high T_c materials the first order vortex melting line and the BG-VG transition line meet at a critical point. Slight variation in the pinning strength simultaneously shifts both the melting and BG-VG transition lines. Based on this fact, it was argued

that the BG-VG transition might represent what is called a “disorder induced melting” transition which may be either weakly first order or second order in nature[3].

The order-disorder transition in the vortex lattice is identified by the sharp change in J_c . Thus, although a non-equilibrium quantity, J_c may be treated as a thermodynamic quantity as it reflects a sharp change in the vortex lattice correlations. But it is necessary to measure the equilibrium magnetization M_{eq} in order to understand the thermodynamic nature of the BG-VG transition. J_c and M_{eq} are usually obtained from magnetization hysteresis measurements using

$$J_c(H) = [M^{rev}(H) - M^{for}(H)] / 2\mu_0gd \quad (2)$$

$$M_{eq}(H) = [M^{for}(H) + M^{rev}(H)] / 2 \quad (3)$$

$M^{for}(H)$ and $M^{rev}(H)$ are the magnetizations in the increasing and decreasing field scans respectively.

g is a factor depending on the sample geometry and d is the sample dimension transverse to the magnetic field. Eqs. (2) and (3) assume that J_c is uniquely determined by the local magnetic field B . However, pronounced thermo-magnetic history dependence in J_c and the vortex state metastability observed near the order-disorder transition[9-12] make Eqs. (2) and (3) inapplicable.

Magnetization hysteresis measurements are carried out using Quantum Design SQUID magnetometer and/or Oxford Vibrating Sample Magnetometer (VSM) on a 2H-NbSe₂ crystal ($T_c = 7.25K$) and a V₃Si crystal ($T_c = 16.5K$). Onset of the sharp increase in the magnetization hysteresis (proportional to J_c) beginning at about 6 T (Fig. 2) signifies the peak effect. The asymmetry in the magnetization curves in the

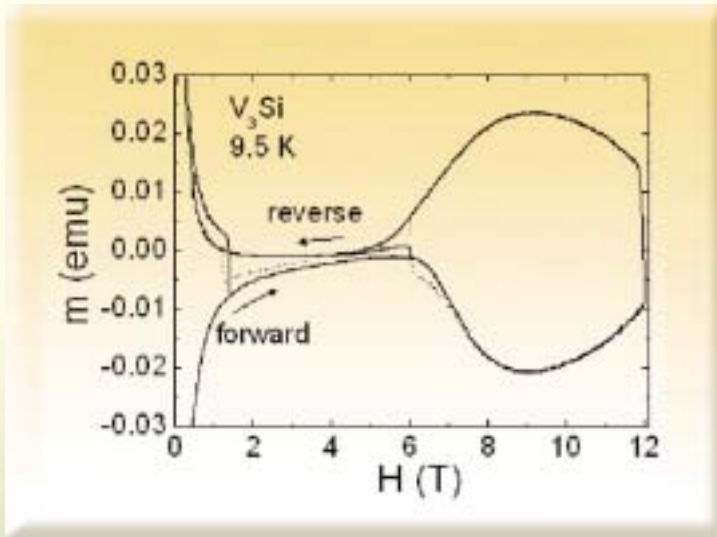


Fig. 2 : M-H loop and minor curves near the peak effect and the low field regime of V_3Si . Full (Dotted) lines are minor curves obtained by decreasing (increasing) the field from a point on the forward (reverse) curve

increasing (forward) and decreasing (reverse) field scans is a primary signature of the history dependence in J_c , which is further investigated by tracing the minor magnetization curves as shown in Fig. 2. The width of the minor curves starting on the forward and reverse curves should be the same if J_c has a unique value at a given field as assumed in the critical state model[13]. However, in the peak regime the minor curves starting on the forward curve are smaller in width compared to those starting on the reverse curve as shown in Fig. 2. This result is summarized by the inequality

$$J_c^{for}(H) < J_c^{rev}(H), \quad (4)$$

where, $J_c^{for}(H)$ and $J_c^{rev}(H)$ are J_c values on the forward and reverse field scans respectively. Minor curves recorded in the low field regime (< 2 T) where J_c falls sharply, exhibit a behavior just opposite to that in the peak regime[14], indicating

$$J_c^{for}(H) > J_c^{rev}(H) \quad (5).$$

This anomalous behaviour cannot be accounted by the critical state model[13], which assumes that J_c is a single valued function of the magnetic field. Qualitative explanation of the history dependence has been provided by invoking supercooling [9,11] and superheating[11] of the VG and BG phases across the BG-VG transition respectively. It is implicit in these arguments that this transition is first order in nature. On the forward curve, the BG (low J_c) phase is superheated to higher fields where VG phase (high J_c) is the stable phase. On the other hand, the disordered VG (high J_c) phase is supercooled to low fields on

the reverse curve where BG phase is the stable phase. This indicates that the vortex state is metastable both on increasing and decreasing field cycles. The main problem in understanding the thermodynamic nature of the transition is that, pronounced metastability in the vortex state obscures the equilibrium state of the vortex lattice. Further, the disorder at the sample edges seems to broaden the transition significantly and contribute to the metastability seen in the bulk magnetization measurements[15]. Therefore, one of the key issues is how to access the equilibrium vortex state.

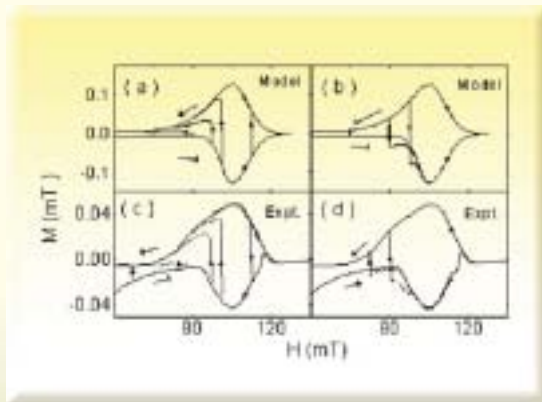
To understand the metastability and quantitatively describe the history effects, we proposed a simple phenomenological model[16], which supposes the existence of multiple metastable configurations of the vortex lattice at a given field and temperature. Each vortex configuration can be accessed by following a certain path in the (B,T) phase diagram. In the model,

J_c is a macroscopic representation of a given metastable configuration. At a given temperature, it is postulated that the transition from one metastable configuration to the other is governed by

$$J_c(B+\Delta B) = J_c(B) + (\pm \Delta B/B_c) [J_c^{st} - J_c(B)] \quad (6)$$

An important assumption is the existence of a unique stable state corresponding to $J_c = J_c^{st}$ at a given field and temperature. B_r is a macroscopic measure of metastability and describes how strongly J_c could be history dependent. In the limit of $B_r \rightarrow 0$, however, the model reduces to the standard critical state model where J_c is unique at a given field and temperature. In the limit of $\Delta B \rightarrow 0$, Eq. 6 reduces to

$$\Delta J_c(B)/\Delta B = \pm(J_c^{st} - J_c)/B_r \quad (7).$$



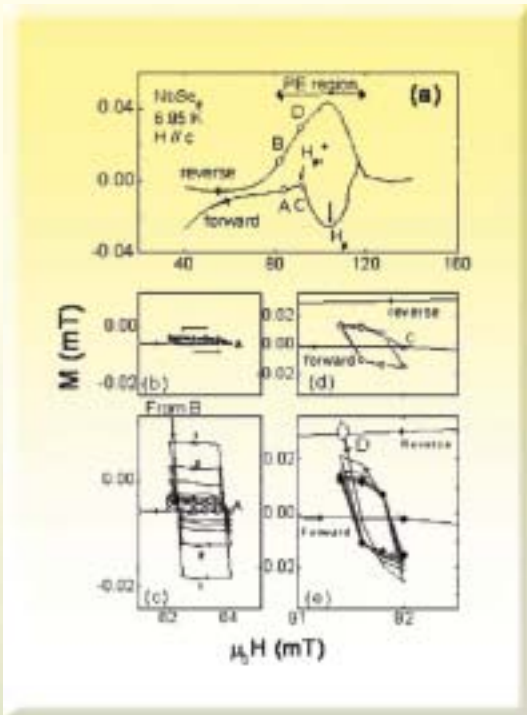
Figs. 3 : (a) and (b) show the two kinds of minor curves calculated using the phenomenological model while (c) and (d) display the corresponding experimentally measured minor curves

Upper (lower) sign is applicable in the case of increasing (decreasing) local field B respectively. Using this simple model, we calculated magnetization hysteresis loops, which turn out to be asymmetric with respect to the direction of field scan as observed in experiments (Fig. 3). Different experimental minor curves are also understood using this simple model.

It can be seen from Eq. 6 and/or Eq. 7 that a metastable vortex state with $J_c \neq J_c^{st}$ can be driven into the stable state by merely oscillating the magnetic field by a small amplitude. An important result of our study is that a unique equilibrium state independent of the past history can be reached by repeated field cycling. In the absence of adequate thermal energy, we argue that the energy imparted in moving the vortices in a metastable configuration allows it to overcome the free energy barrier and enter a lower energy configuration[17].

Fig. 4(a) depicts the hysteresis loop of an NbSe₂ crystal recorded at 6.95 K. A, B, C and D marked in Fig. 4(a) are four representative points at which minor hysteresis loops (MHLs) are initiated. A (C) and B (D) are at a field $H < H_{pl}^+$ ($H > H_{pl}^+$) where H_{pl}^+ is the field at which a sharp change in magnetization occurs on the forward branch. Minor loops were recorded from both forward and reverse branches, spanning the entire peak region by cycling the field by about 10 to 20 Gauss.

Minor loops starting from point A (forward curve, $H < H_{pl}^+$) retrace in different field cycles as shown in Fig. 4(b). It indicates that the vortex state is already in a stable configuration with a J_c proportional to the width of this minor loop (Eq. 2). In Fig. 4(c), minor loops initiated from point B on the reverse curve shrink with each successive field cycle, merging eventually with the loop traced from A (shown in open circles). The vortex state at B is a supercooled metastable state with a J_c higher than the stable value at that field. The final MHL obtained after many field cycles is independent of the history, and therefore corresponds to a stable or equilibrium state with $J_c = J_c^{st}$. Fig. 4(d) shows the MHLs starting at point C (i.e., $H > H_{pl}^+$). The increasing field



Figs. 4 : (a) M-H loop of NbSe2 at 6.95K. (b) MHLs starting from A, (b) MHLs starting from B (full line) shrinks with each successive field cycle. After five cycles it merges with the loop (open circles) shown in (b) which is re-plotted. (d) MHLs starting from C and (e) MHLs starting from D (full line) collapse into the final loop shown in (c) (open circles)

leg of the MHL separates from the forward curve in the first field cycle itself and remains outside the main loop. In other words, the MHL expands on field cycling. This suggests that, for $H > H_{pl}^+$, vortex configuration on the forward curve is also metastable and J_c is initially less than the stable value, which is a signature of the superheated BG phase. The behavior of the minor loop starting from D is again quite similar to that starting from B. Eventually, the MHLs from C and D collapse on to the same loop, again indicating a unique state at this field. We therefore conclude that this new procedure provides an unambiguous way to attain a stable or equilibrium state.

Having succeeded in producing the equilibrium state, we determine the quantities J_c and M_{eq} by applying the relations 2 and 3 to the saturated minor loops obtained after many field cycles. In Fig. 5, we plot the stable state critical current density J_c^{st} and the equilibrium magnetization M_{eq} as a function of applied

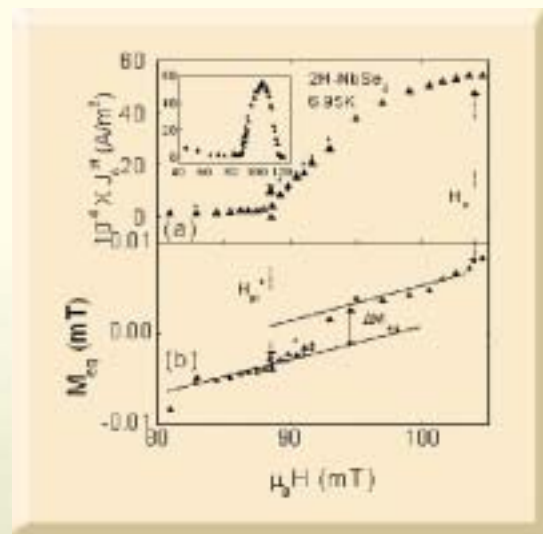


Fig. 5 : J_c^{st} vs H at 6.95K in the field range 80 mT to 120 mT. Filled triangles and open circles are the values obtained from MHLs initiated from forward and reverse curves respectively. Inset shows the J_c^{st} in the entire field range studied. (b) M_{eq} vs H at 6.95K. The increase in M_{eq} coincides with the sharp increase in J_c^{st}

field. M_{eq} exhibits a sharp increase between H_{pl}^+ and H_p signifying an increase in the equilibrium flux density. This is reminiscent of flux lattice melting transition in cuprate superconductors[2]. The observation suggests that the OD transition is a first order transition. The increase in M_{eq} coincides with the sharp increase in J_c at the onset of peak effect. A similar result following our experimental procedure has been reproduced by Nishizaki et al[18] at the onset of the order-disorder transition of twin free YBCO crystals.

In summary, we have presented the generic magnetic behavior near the order-disorder transition of weakly pinned superconductors, which is described by a phenomenological model. An important outcome of the model is that it suggests a definite experimental procedure, viz., the method repeated field cycling with a small amplitude, to access the equilibrium state of the vortex system which is otherwise obscured by the metastability. We have obtained the equilibrium magnetization across the peak regime, which clearly suggests that the order-disorder transition represents a first order transition.

Acknowledgements

This work was done in collaboration with Dr. V. C. Sahni, Late Dr. K. V. Bhagwat, Dr. P. K. Mishra, Dr. T. V. C. Rao, Prof. S. Bhattacharya, Prof. A. K. Grover, Prof. S. Ramakrishnan and Dr. S. S. Banerjee. The NbSe₂ samples studied have been provided by M. J. Higgins. The author is also grateful to Dr. Heinz Kupfer for many discussions.

References

1. G. Blatter et al, Rev. Mod. Phys. **66** (1994) 1125.
2. E. Zeldov et al, Nature (London) **375** (1995) 373; A. Schilling et al, Nature **382** (1996) 791.
3. B. Khaykovich et al, Phys. Rev. B **56** (1997) R517
4. H. Beidenkopf et al, Phys. Rev. Lett. **95** (2005) 257004.
5. A. I. Larkin and Y. N. Ovchinnikov, Sov. Phys. JETP, **38** (1974) 854.
6. M. J. Higgins and S. Bhattacharya, Physica C **257** (1996) 232 and references therein.
7. X. S. Ling et al, Phys. Rev. Lett. **86** (2001) 712
8. T. Giamarchi and P. le Doussal, Phys. Rev. Lett. **72** (1994) 1530; Phys. Rev. **B 52** (1995) 1242
9. S. B. Roy and P. Chaddah, J. Phys: Condens.Matter, **9** (1997) L625.
10. G. Ravikumar et al, Phys. Rev. **B 57** (1998) R11069.
11. G. Ravikumar et al, Phys. Rev. **B 61** (1998) 12490.
12. S. Kokkalis et al, Phys. Rev. Lett. **82** (1999) 5116.
13. C. P. Bean, Phys. Rev. Lett. **8** (1962) 250.
14. G. Ravikumar et al, Phys. Rev. **B 65** (2002) 94507.
15. Y. Paltiel et al, Nature (London) **403** (2000) 398
16. G. Ravikumar et al, Phys. Rev. **B 61** (1998) R6479; G. Ravikumar, Phys. Rev. B
17. G. Ravikumar et al, Phys. Rev. **B 63** (2000) 24505.
18. T. Nishizaki et al, Private communication

ABOUT THE AUTHOR



Dr Ravi Kumar is from the 27th Batch of the training school. For his Ph.D thesis, he worked on the irreversible magnetic response and magnetic relaxation in type II superconductors. Prior to this he worked on developing high homogeneity superconducting magnets. He has been a Indo-European Community Post-Doctoral Fellow in Free University of Amsterdam, in the Netherlands. He has been a Humboldt Fellow since the year 2000 and spent a year in the Forschungszentrum Karlsruhe, Germany. He has also been elected a member of the National Academy of Sciences. Last year he was conferred the Homi Bhabha Science and Technology Award.



DEVELOPMENT OF NEUTRON AND X-RAY DETECTORS AND NEUTRON RADIOGRAPHY AT BARC

A.M. Shaikh
Solid State Physics Division
Bhabha Atomic Research Centre

The author is the recipient of the DAE Technical Excellence
Award for the year 2004.

Abstract

Design and development of neutron and X-ray detectors and R&D work in Neutron Radiography (NR) for non-destructive evaluation are the important parts of the neutron beam and allied research programme of the Solid State Physics Division (SSPD) of BARC. The detectors fabricated in the division not only meet the in-house requirement of neutron spectrometers but also the need of other divisions in BARC, DAE units and some universities and research institutes in India and abroad for a variety of applications. The NR facility set up by SSPD at Apsara reactor has been used for a variety of applications in nuclear, aerospace, defense and metallurgical industries. The work done in development of neutron and X-ray detectors and Neutron Radiography since 1992 is reported in this article.

Neutron and X-ray Detectors

Radiation detectors play an important role in medicine, biology, materials science and high-energy physics for monitoring and imaging applications. Gas filled detector, semiconductor detector and scintillation detector are widely used in flux measurement, area monitoring and scattering experiment applications with each of them having their own advantages and limitations. The detector technology is rapidly evolving by making use of recent developments in material processing, new detector designs, data acquisition and analysis systems [1]. In case of neutron scattering experiments the neutron beam intensities are low due to

collimation, monochromatisation and scattering. Efficient neutron detection or imaging is therefore essential to use the neutron beam time judiciously. Demand for neutron detectors with higher count rates, larger scanning angles and finer position resolutions, is ever increasing.

Among the various types of detectors, gas-filled detectors are widely used especially by the neutron scattering communities around the world. Gas-filled position sensitive detectors [2] are conveniently used in various spectrometers to scan large angles as these detectors can be fabricated with large size and show high detection efficiency. They have the advantages of

low gamma sensitivity, high neutron efficiency, very high noiseless internal amplification, no radiation damage, flexibility of size and fill gas pressure and need simple counting and pulse processing electronics. Large area position sensitive detectors with multiwire geometry developed in 1970s have become widely popular for many applications [3]. At Solid State Physics Division, we are involved in indigenous development of gas filled signal detectors and position sensitive detectors (PSDs) for X-rays and neutrons for various applications at BARC and other laboratories in India. These detectors are widely used as low sensitivity monitor counters to very high sensitivity signal detectors. Continuous efforts are put in towards modification of detection techniques to carry out the experiments efficiently. Various types of detectors

developed are ^3He and BF_3 filled detectors for neutrons, linear 1-D single anode PSD, 1-D and 2-D multiwire PSDs, curvilinear PSD and a microstrip based PSD for both neutrons and X-rays[4-11]. These detectors show excellent operational characteristics and stability over the long periods. Various types of neutron proportional counters fabricated in our laboratory are listed in Table 1 along with their specifications and applications. Fig.1 shows some of these detectors.

Table 2 gives photographs and salient features and applications of various types of position sensitive detectors designed, developed and successfully tested in our laboratory. Many of the 1-D position sensitive neutron detectors are mounted on the neutron spectrometers at

Table 1: Various types of Neutron Proportional Counters developed

Detector Type†	Fill gas	Pressure (bar)	Sensitivity (cps/nv)	Efficiency (%) End-on side-on		Application
4A	BF_3	0.79	0.3	22	3.6	Neutron flux monitor
4C	BF_3	0.79	2.3	22	8.0	Neutron flux monitor
20C	$^3\text{He}+\text{Kr}$	3+1.5	53	99	42	As signal detector for n- γ monitoring of spent fuel bundles and nuclear waste
6D	BF_3	0.79	5.5	45	12	Signal detector on neutron spectrometer and REM monitor
6E	$^3\text{He}+\text{Kr}$ BF_3	3+1.5 0.79	25 11.6	92 45	12 16	
9D	BF_3	0.79	7.0	60	12	As signal detector on neutron spectrometer
18D	BF_3	0.79	23	85	12	Signal detector for characterisation of pulsed neutron sources.
36D	$^3\text{He}+\text{Kr}$ $^3\text{He}+\text{Kr}$	3+1.5 3+1.5	105 108	98 99	55 55	
36E	BF_3	0.79	108	98	16	Nuclear waste monitoring

†Detector type nomenclature: the number before alphabet indicates length of detector in inches and A, B, C, D and E indicate cathode diameter of 0.4", 0.5", 1", 1.5" and 2" respectively. The anode is made of tungsten wire of 25 mm diameter.
Cathode material: brass.



Fig.1: Some of the neutron proportional counters mentioned in Table 1

Dhruva and working over the years satisfactorily.

The gas filled neutron proportional counters are extensively used in BARC over a wide range of application

such as flux and area monitoring, spent fuel activity measurement, study of nuclear reactions, measurement residual activity of nuclear waste, measurement of cosmic neutron radiations and

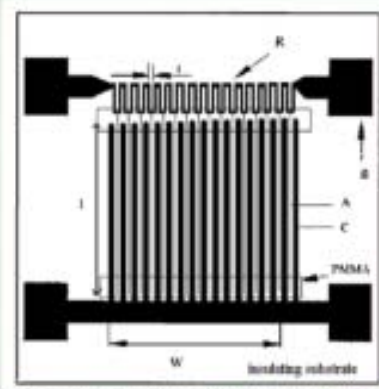
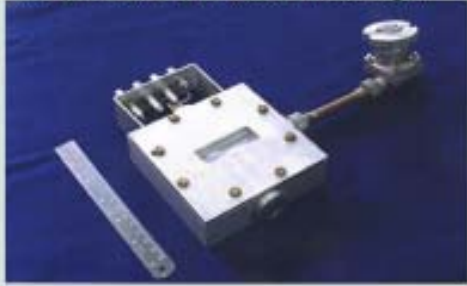
Type of Detectors	Description
<p>³He- filled 1-D Position Sensitive Neutron Detectors</p>	<p>Dimensions: 100 cm (l) x 36 mm (φ) 100 cm x 25 mm 60 cm x 50 mm 20 cm x 50 mm</p> <p>Position Resolution: 4.5 mm - 7 mm Energy Resolution: ~ 6 % Efficiency: 55 % - 80 % at 1 Å</p> <p>Application: Installed on High Q, Profile Analysis, Quasielastic, small angle scattering Neutron spectrometers and Polarised Neutron reflectometer at Dhruva reactor</p>
<p>2-D Multiwire Position Sensitive Neutron Detector</p> <p>Schematic Diagram</p> <p>2-D PSD with gas filling and data acquisition system.</p>	<p>Active area : 345mm x 345mm Active dept : 25mm Window : ~ 18mm thick Dome wall thickness: ~ 9mm Spatial resolution: 69 x 69 pixels Pixel size : 5mm x 5mm Anode grid : 25µm Au-W wire, pitch 5mm X, Y readout grids : 25µm SS wire, pitch 5mm, R=51kΩ</p> <p>Anode-Cathode spacing: 6.4mm Fill gas: ³He + Kr (2:1) in active chamber : ⁴He (3bar) in compensating chamber Efficiency: 70% for 4Å neutrons</p> <p>Application: Small Angle Neutron Scattering, neutron Diffraction</p>

Table 2: Various types of Position Sensitive Detectors for Neutron and X-rays developed

Table 2 contd...

Type of Detectors	Description																
<p data-bbox="411 596 770 621">1-D Position Sensitive X-ray Detector</p> 	<p data-bbox="914 557 1289 610">Cathode: 24 mm (l) x 21 mm (ID) x 3 mm (t)</p> <p data-bbox="914 612 1134 637">Anode : CCQ Fibre</p> <p data-bbox="914 639 1182 664">Sensitive length = 160 mm</p> <p data-bbox="914 666 1230 714">X-ray window : 100µm Al foil, 30% absorption below 6 keV</p> <table border="1" data-bbox="914 737 1289 868"> <thead> <tr> <th>Gas</th> <th>p (atm)</th> <th>ΔE (% 5.9 keV)</th> <th>ΔP (mm)</th> </tr> </thead> <tbody> <tr> <td>Ar+CH₄</td> <td>1.2</td> <td>14.3</td> <td>0.96</td> </tr> <tr> <td>Kr+CH₄</td> <td>1.2</td> <td>10.5</td> <td>0.80</td> </tr> <tr> <td>Xe+CH₄</td> <td>1.2</td> <td>21.6</td> <td>0.64</td> </tr> </tbody> </table> <p data-bbox="914 870 1289 914">Applications: X-ray diffraction and small angle X-ray scattering</p>	Gas	p (atm)	ΔE (% 5.9 keV)	ΔP (mm)	Ar+CH ₄	1.2	14.3	0.96	Kr+CH ₄	1.2	10.5	0.80	Xe+CH ₄	1.2	21.6	0.64
Gas	p (atm)	ΔE (% 5.9 keV)	ΔP (mm)														
Ar+CH ₄	1.2	14.3	0.96														
Kr+CH ₄	1.2	10.5	0.80														
Xe+CH ₄	1.2	21.6	0.64														
<p data-bbox="403 920 778 945">2-D Position Sensitive X-ray Detector</p> 	<p data-bbox="914 920 1270 945">Active Area : 100 mm x 100 mm</p> <p data-bbox="914 948 1150 972">Active Depth : 15 mm</p> <p data-bbox="914 975 1246 1000">Spatial resolution: 64 x 64 pixels</p> <p data-bbox="914 1002 1182 1027">Pixel size : 1.5 mm x 1.5 mm</p> <p data-bbox="914 1029 1182 1054">Inter grid spacing: 2.4 mm</p> <p data-bbox="914 1056 1238 1104">Anode : 10 µm SS grid, 3 mm pitch</p> <p data-bbox="914 1106 1289 1177">X, Y readout grids : 25 µm SS wire 1.5 mm pitch, R = 12.8 kΩ</p> <p data-bbox="914 1179 1289 1204">Fill gas : Ar + CH₄ (9:1)</p> <p data-bbox="914 1206 1182 1231">Detection efficiency: 75%</p> <p data-bbox="914 1233 1270 1258">Case material: SS with Al lining</p> <p data-bbox="914 1261 1182 1285">Window : Be, 4"φ</p> <p data-bbox="914 1288 1289 1313">Overall size: 200 mmOD x 70 mmH</p> <p data-bbox="914 1315 1214 1340">Overall weight: 1.5 Kg</p> <p data-bbox="914 1342 1182 1367">Energy resolution of ~12%</p> <p data-bbox="914 1369 1289 1401">Position Resolution ~ 1.2 mm x 1.4 mm for 3 bar gas pressure</p>																
<p data-bbox="355 1408 826 1433">A Curvilinear multiwire 1-D PSD for Neutrons</p>   <p data-bbox="304 1703 879 1728">Multiwire anode- PCB structure enclosed inside the PSD.</p>	<p data-bbox="914 1408 1289 1433">Detector casing: 8 mm thick 1S-Al</p> <p data-bbox="914 1435 1150 1460">Sensitive length: 70 cm</p> <p data-bbox="914 1462 1150 1487">Overall length: 81 cm</p> <p data-bbox="914 1490 1038 1515">Arc radius: 2 m</p> <p data-bbox="914 1517 1023 1542">Scan angle: 24°</p> <p data-bbox="914 1544 1198 1569">Anode wire: 25 µm SS</p> <p data-bbox="914 1571 1198 1596">Active gas thickness: 35 mm</p> <p data-bbox="914 1598 1198 1623">Scanning height: 35 mm</p> <p data-bbox="914 1626 1150 1651">Fill gas: ³He + Kr</p> <p data-bbox="914 1653 1289 1678">Energy resolution: 15% at 764 keV</p> <p data-bbox="914 1680 1182 1705">Position resolution: 6 mm.</p>																

Table 2 contd...

Type of Detectors	Description
<p data-bbox="391 480 790 503">Microstrip based 1-D PSD for Neutrons & X-rays</p>  <p data-bbox="295 918 885 1043"><i>Schematic of a designed Microstrip pattern on insulating substrate deposited using photolithography. A, anode; C, cathode; B, bonding pad; R, meandering resistive strip; t, meandering strip width; PMMA, poly methyl met acrylate coating for end passivation; w, active area width; l, active area length.</i></p>  <p data-bbox="295 1349 901 1428"><i>Photograph of rectangular chamber containing the Microstrip plate (top plate with X-ray window mounted. similar Al plate without window is used for neutrons)</i></p>	<p data-bbox="917 480 1189 503">Design parameters of microstrip</p> <p data-bbox="917 503 1276 698">Substrate : Borosilicate glass Anode width : 12 μm Cathode width : 300 μm Anode-cathode gap : 150 μm Pitch : 612 μm Active area : 20 mm x 15mm Resistive strip width : 100 μm Resistive strip resistance : 40 kΩ</p> <p data-bbox="917 721 1077 743"><u>As 1-D X-ray PSD:</u></p> <p data-bbox="917 766 1308 839">Energy resolution = 12.3% at 5.9 keV X-rays Position Resolution = 0.49 mm with Xe + CH₄ at 2.1 bar</p> <p data-bbox="917 861 1093 884"><u>As 1-D Neutron PSD</u></p> <p data-bbox="917 907 1284 993">Energy resolution of 16%, 8% and 10.5 % ³He + Ar+CO₂, ³He + Kr and ³He + CF₄ gas mixtures resp.</p> <p data-bbox="917 1016 1300 1065">Position Resolution: 1.8 mm with ³He + Kr in (1:2) ratio at total pressure of 3 bar.</p> <p data-bbox="917 1088 1029 1111"><u>Application:</u></p> <p data-bbox="917 1134 1300 1236">X-ray, neutron scattering measurements with high position resolution and high count rate. Used with synchrotron sources for X-ray scattering studies.</p>

material studies using neutron scattering techniques. The detectors are also supplied to atomic energy establishments of other countries like Bangladesh, Vietnam and Austria (IAEA). Table 3 gives the statistics about different types of detectors designed, fabricated and supplied to various users in BARC and outside institutions. Users other than BARC can procure these detectors through the Technology Transfer & Collaboration

Division of BARC.

Neutron Radiography Facility and Applications

The property of thermal neutrons, which makes them valuable for studying industrial components is their high penetration through widely used industrial materials such

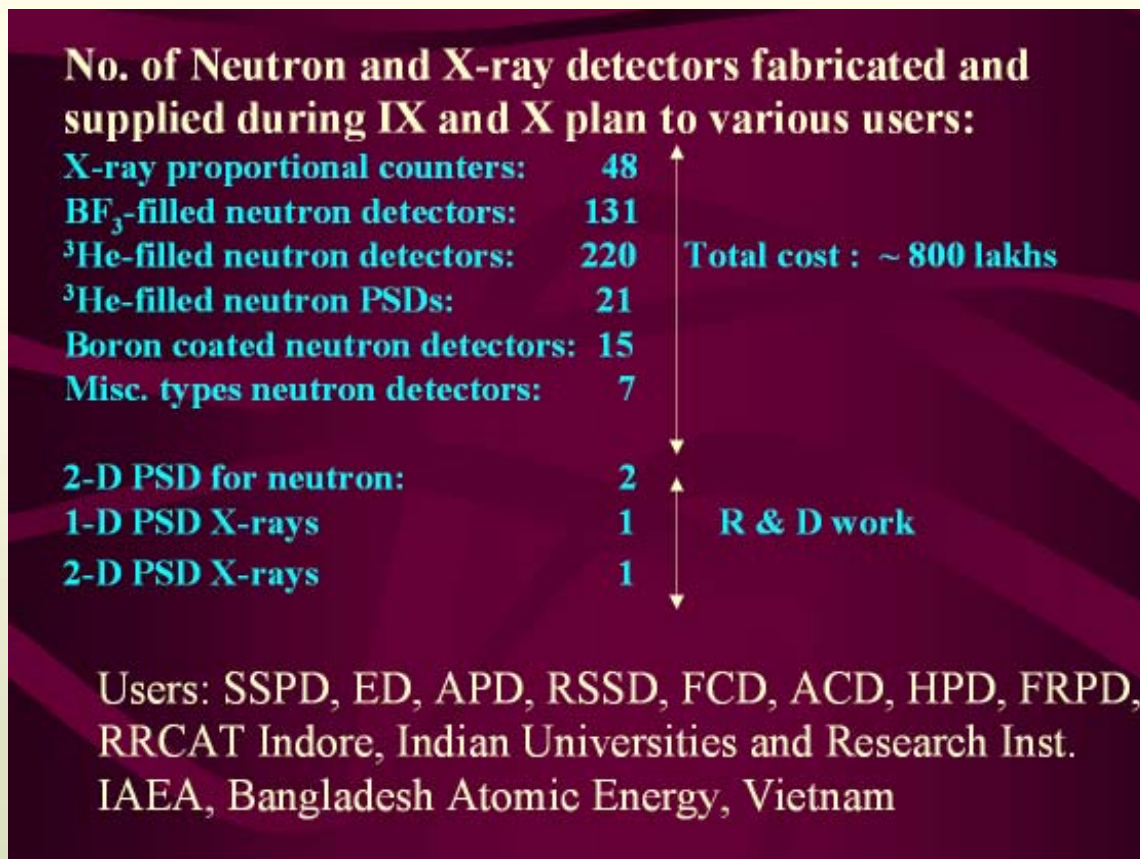


Table 3 : Statistics of Neutron & X-ray Detectors Fabricated and Supplied

as steel, aluminium or zirconium. Neutrons are efficiently attenuated by only a few specific elements such as hydrogen, boron, cadmium, samarium and gadolinium. For example, organic materials or water attenuate neutrons because of their high hydrogen content, while many structural materials such as aluminium or steel are nearly transparent. Neutron Radiography (NR) is a non-destructive imaging technique for material testing. It is similar to X-ray and gamma radiography and has some special advantages in Nuclear, Aerospace, Ordnance and rubber and plastic industries. Information is obtained on the structure and inner processes of the object under investigation by means of transmission. At BARC, neutron

radiography has been actively pursued by the Solid State Physics Division for various applications, using the 400kW swimming pool type reactor, Apsara as the neutron source. In this facility the thermal neutrons from the reactor are collimated by a divergent, cadmium lined aluminum collimator with a length/inner diameter (L/D) ratio of 90. A cadmium shutter facilitates the opening and closing of the beam. The specimen can be mounted about 60 cm from the collimator followed by a cassette containing neutron converter and X-ray film. The whole setup is properly shielded to avoid any radiation exposure to the operator. Table 4 gives the important parameters of the facility, which is schematically shown in Fig. 2.

The NR facility of Apsara has been used for a variety of applications in nuclear, aerospace, defense and metallurgical industries[12]. The facility has been extensively used for recording neutron radiographs of

- experimental fuel elements,
- water contamination in marker shell loaded with phosphorous,
- electric detonators,

Table 4: Apsara Reactor Nr Facility

Useful beam area	: 15 cm dia
Thermal neutron flux	: 1×10^6 n/cm ² /sec
Gamma radiation level	: 4R/h
Cadmium ratio	: 6.3
Neutron/gamma ratio	: 9×10^3 n/cm ² /mR
Neutron converter screens	: Gd 25 μ m, Dy 100 μ m, Kodak CN85-B ⁶ LiF-ZnS(Ag) scintillator and CCD based digital imaging, Fuji neutron image plate

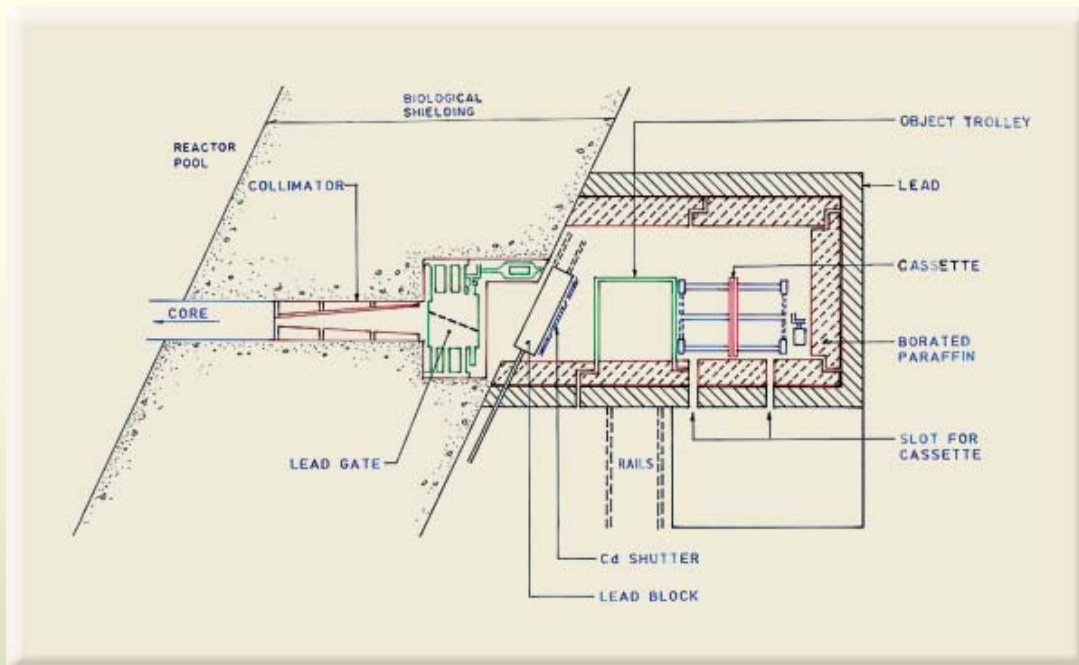


Fig. 2 : Schematic of NR Facility at Apsara Reactor

- satellite cable cutters and pyro valves,
- boron-aluminium composites,
- hydride blisters in irradiated zircaloy pressure tubes,
- variety of hydrogenous and non hydrogenous materials and
- two phase flows in metallic pipes.

While some of the radiographs are shown in Fig.3, the most recent work on NR is described in the following paragraphs.

Assessment of hydriding on Zircaloy-2/Zr-Nb2.5% pressure tube material using Neutron Radiography

One of the most important applications of NR in the nuclear field is the post irradiation examination of pressure tube (PT) to check formation of hydride blisters if any. To ascertain the detection of hydride blisters in zircaloy pressure tubes, detectability limit of hydride was first established[13]. For this purpose hydride blisters were

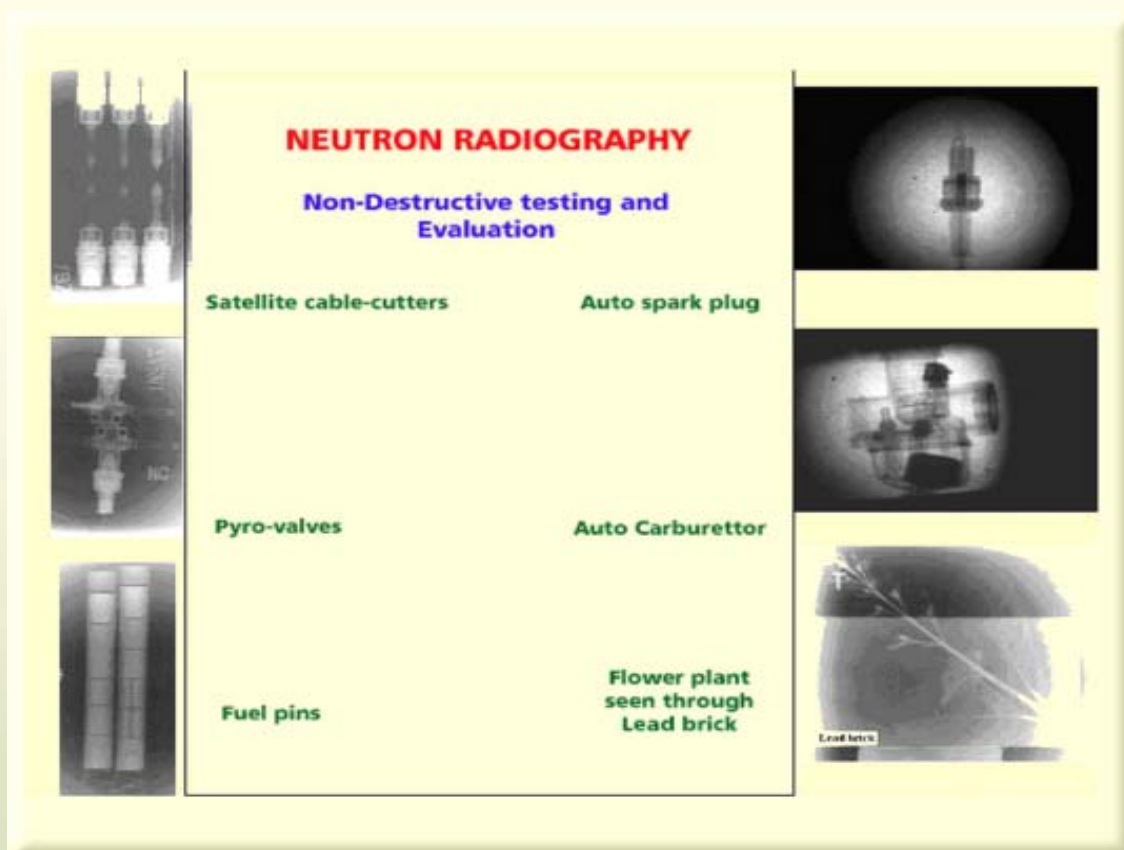


Fig. 3 : Neutron Radiographs of various objects taken with Apsara NR facility.

created in the laboratory on hydrogen charged Zircaloy pressure tubes under thermal gradient are examined using neutron radiography. It was established that a zirconium hydride blister of nearly 0.25% of job thickness could be detected using neutron radiography. The theoretical detectability was also analyzed and found to be in good agreement with the experimental results. This work served as reference to examine an irradiated pressure tube from a power reactor [14, 15, 16]. Neutron radiographs of an irradiated pressure tube [Rajasthan Atomic Power Station (RAPS#2, K-7 position, 8.25 EFPY) sample were recorded using Apsara NR facility after modifying it for handling the radioactive zircaloy-2 pressure tube coupons. The PT sample of size 59mm x 29mm x 4.2mm was radiographed using transfer technique with 100m thick Dysprosium converter screen. A PT strip containing four laboratory generated hydride blisters were also mounted on the same converter screen cassette to act as a reference. Fig.4(a) shows neutron radiographs of laboratory generated hydride blisters in zircaloy-2 and Zr-2.5% Nb

pressure tube coupons where as Fig. 4(b) shows hydride blister streaks in the zircaloy-2 coupon of the pressure tube from power reactor RAPS#2. Enlarged view of one of the blisters is also shown to the right of the figure.

Neutron radiography was also used to study size and shape of the zirconium hydride blister in the zircaloy-2 pressure tube. Figs. 5(a) and (b) show neutron radiographs of a pressure tube with three laboratory generated hydride blisters and with neutron beam incident parallel and normal to the plane of the blisters respectively. Fig.5 (a) shows lenticular shape of the blister with nearly 2/3 of the blister embedded in the wall of the tube. In the present photograph maximum width of the blister corresponds to 1.5 mm in 4 mm thick wall of the pressure tube. However, the smallest blister grown in the laboratory was found to be mainly on the outer surface of the pressure tube with almost no penetration in the wall of pressure tube.

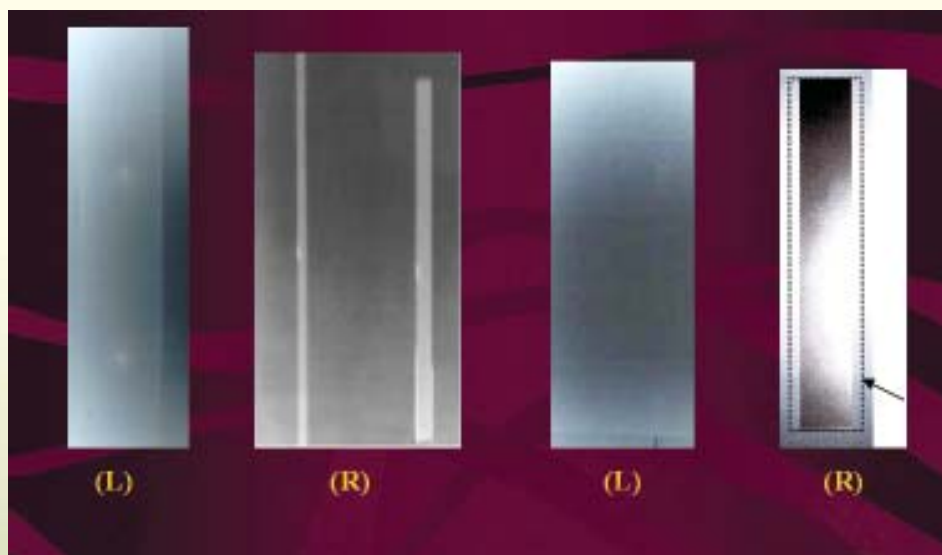


Fig. 4(a) : Hydride blisters in zircaloy-2(L) and Zr-Nb(R) PT coupons (Lab. Generated)

Fig. 4(b) : Hydride blister streak in zircaloy-2 PT coupon (L) from a power reactor. Enlarged view of the blister shown in (R)

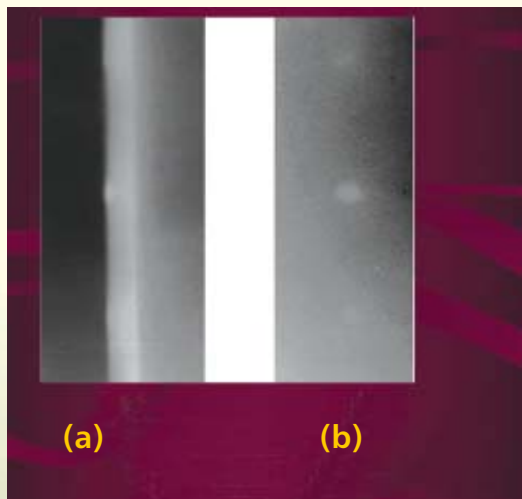


Fig. 5 : NR of zircaloy-2 PT coupons with neutrons incident parallel (a) and perpendicular(b) to the plane of blisters

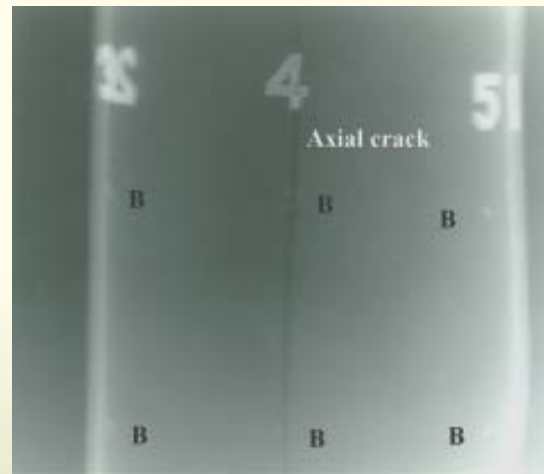


Fig. 6 : Neutron radiograph of Zr-2.5%Nb pressure tube piece containing laboratory generated hydride blisters(B).The axial crack is seen passing through two blisters at position 4 on the tube.

Recently characterization of hydride blisters in burst tested Zr-2.5% Nb pressure tube was done using Apsara NR facility [17]. Hydride blisters were grown in a 16.5 cm long Zr-2.5% Nb pressure tube piece in RED, BARC. The tube was subjected to burst testing. The tube failed axially in brittle manner during testing. The axial crack passed through two hydride blisters which was also seen in the neutron radiograph (Fig. 6).

HYSEN radiography technique with NR facility at Apsara reactor

The technique, referred as Hydrogen Sensitive Epithermal Neutron (HYSEN) radiography technique was first developed for imaging small amounts of hydrogenous materials encapsulated within high thermal neutron absorbers, and found to be useful in study of hydride-induced embrittlement of metals. The HYSEN imaging system consists of a converter screen (In) and a neutron beam filter (In + Cd) with the object placed between

the screen and filter. For neutrons, In has a resonance peak at 1.49 eV. Combination of Cd foil with In foil almost completely cuts off neutrons with energy lower than 1.49 eV. Incident neutrons with energy higher than 1.49 eV, which pass through, are scattered elastically by hydrogen atoms present in the object. The neutrons that are slowed down to the vicinity of 1.49 eV by this scattering are absorbed by the second In foil placed behind the sample. Since the image is induced by the scattered neutrons, the resolution and the sensitivity of the technique are highly dependent on the object dimensions and object to screen distance. Hydrogen concentrations as low as 50 ppm (0.020 mg H/cm²) in 0.62 mm zircaloy coupons have been reported. The detection limit of standard NR techniques is about 0.66 mg H/cm². Thus the sensitivity of this method was found to be about 30 times better than the normal NR techniques.

Setting up of HYSEN radiography technique with existing NR facility at Apsara reactor was undertaken as a part of coordinated research project of IAEA[15,18]. The imaging

system (Fig.7) consisted of a 250 mm indium converter screen and a neutron beam filter comprised of 1 mm cadmium and 1 mm indium foils, with the object being placed between the filter and screen. The system was exposed to neutron beam of the NR facility. Neutron radiograph of 1-, 2-, 3-, 4- layers of cellophane adhesive tape as object was recorded. The gradation of hydrogen concentration in successive layers of adhesive tapes was clearly seen in the radiograph (Fig.8). At present the experimental set up is suitable for recording HYSEN photographs of very thin hydrogenous samples. The results of preliminary measurements are regarded as encouraging, considering the very simple system that was used (Fig. 9). The work on improvement over the



Fig. 8 : Neutron radiograph of 1-, 2-, 3-, 4- layers of cellophane adhesive tape as an object

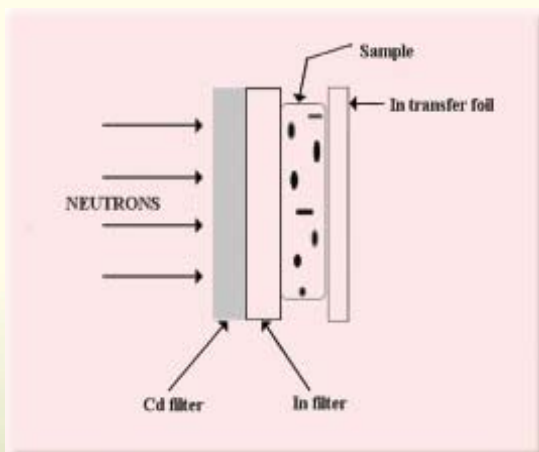


Fig. 7 : Schematic of basic HYSEN Radiography system

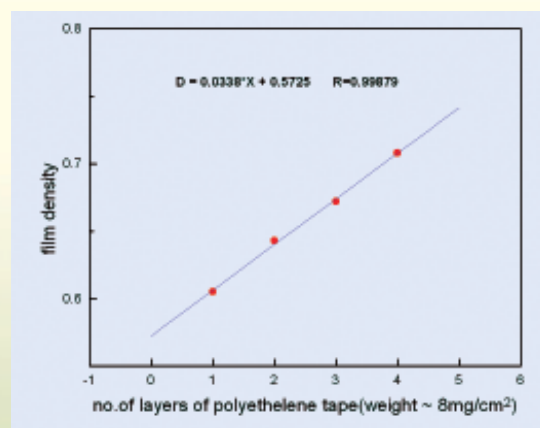


Fig. 9 : Sensitivity of 8 mg/cm² corresponding to 1mg/cm² of hydrogen

existing set up with different neutron detector and filter foils and use of electronic imaging camera for recording the radiograph is in progress.

Digital Neutron Imaging

One of the important radiography methods is Electronic Imaging or Real Time Radiography, which produces

neutron images on a video monitor. This method is especially attractive for the high-throughput inspection of parts requiring instant feedback of information. Unfortunately, it has limitations in its applications. It cannot be used for inspection of the irradiated specimens because of its sensitivity to gamma radiation. Typically, an electronic imaging method utilizes a fluorescent converter screen to produce a light signal that is suitably

amplified and fed into video equipment for viewing. The video output is digitized using frame grabber card and processed using an onboard processor. Image acquisition software performs operations like online thresholding, contrast stretching, integration, averaging etc. Trained human eye can distinguish 50 to 100 gray levels between black and white. Digital imaging accelerates this probing dramatically, up to 4096 gray levels are differentiated. Use of planar detectors like low light cameras (e.g. CCD, C-CCD...) in combination with fluorescent screens is made to record the radiographs.

An electronic imaging system (Figs. 10 and 11) based on commercially available image intensifier tube and low cost CCD camera has been developed and tested [19]. The neutron beam transmitted through the sample is absorbed in a NE-426 scintillator screen. The light produced by the screen is reflected by 90° and focused onto the input fibre optic face of an image intensifier tube. The output image is focused onto a CCD camera using, an F#1.4 lens. The CCD camera used has 756(H) x 581(V) pixel array and image intensifier used has 30 lp/mm resolution with gain of 10^5 Cd/m²/lx. The video output of CCD is digitised using a frame grabber card and processed using onboard processor. Various types of assemblies and components were scanned using the imaging system. Neutron images were instantly seen on the video monitor indicating that flux at Apsara NR facility was adequate

for real time imaging work. Fig.12 shows images of some of the objects scanned using the imaging system.

For Neutron Tomography the sample to be imaged is placed on a platform, which is rotated using a stepper motor. The stepper motor is controlled using a PC based

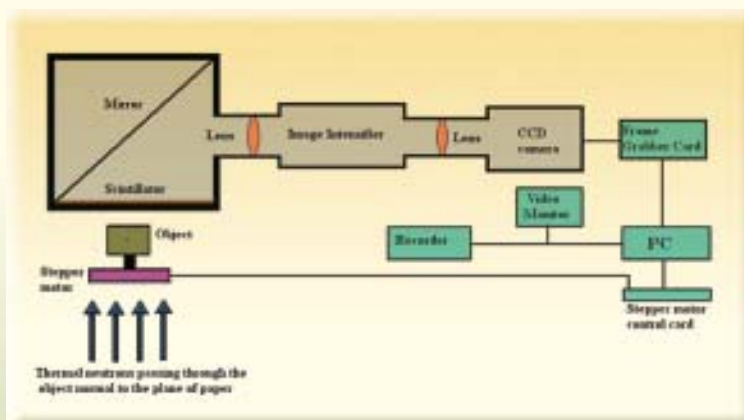


Fig. 10 : Schematic diagram of electronic imaging setup at Apsara



Fig. 11 : Photograph of an electronic imaging system used at Apsara for real time neutron radiography

controller card. The sample rotation, image acquisition and processing have been interfaced together within a single control program. The images were recorded in various angles and used in reconstruction program based on Convolution Back Program method for obtaining CT

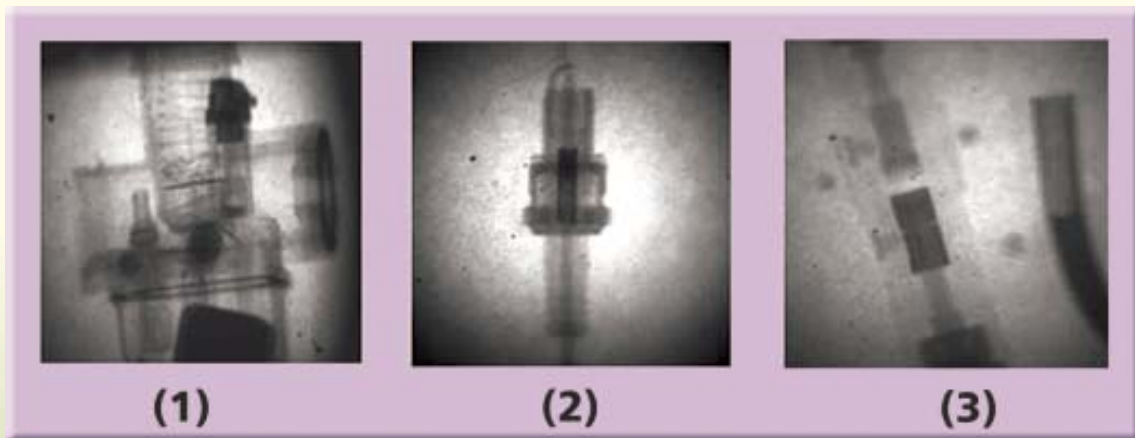


Fig.12 : Neutron images of (1) carburettor, (2) spark plug, (3) INSAT cable cutter & U-tube filled with wax recorded using electronic imaging system at Apsara

scans at various slices. Several sets of samples were fabricated to assess the quality of tomography system [19,20]. One such sample is a cylindrical brass rod of 40 mm diameter with holes ranging from 1 mm to 5 mm, some of them filled with wax, air and Indium wire, is shown in Fig.13. Fig.14 shows the CT scan of this sample. All the holes either wax or air filled, are visible in the image.

Visualisation and analysis of water/air, water/vapour two phase flow inside metallic pipes under high temperature and pressure condition is of considerable importance in thermal hydraulic design of nuclear reactors. It is important to know under what condition bubbly to slug or slug to annular flow transitions occur. Ideally, one would like to have method where one not only determines such transitions quantitatively but also visualize the flow pattern. Neutrons provide this facility. Most of the

cladding metals such as aluminum or steel are transparent to neutrons whereas hydrogenous materials such as water are relatively opaque. This makes neutrons a unique tool for study of flow of water inside metallic pipes. Such two phase flow visualization is done using electronic imaging technique [21]. The prototype electronic imaging system developed by us has been used for

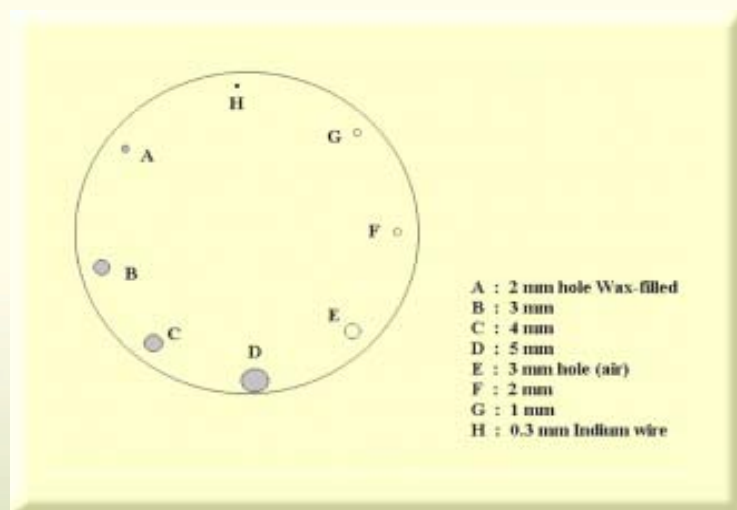


Fig.13 : Schematic diagram of a sample made of solid brass (40 mm ϕ) with holes of 1mm to 5 mm filled with wax, air and indium wire

visualization of two phase flow (water/air) inside metallic pipes. Simulation of bubbly, slug and annular flow was done using various combinations of flow rates of water and air using the experimental arrangement shown in

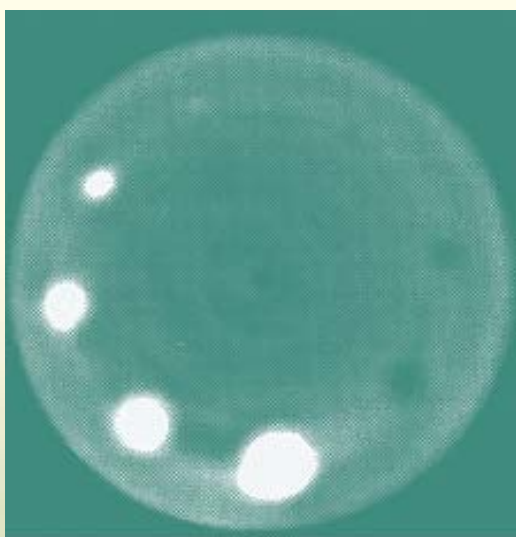


Fig.14 : Neutron computed tomographic image of sample shown above

Fig.15. The transition from one flow regime to other has been visualized (Fig.16). Aluminum pipes of diameter from 12 mm to 25 mm and wall thickness of 1.5 mm to 2 mm, and steel pipe of 12 mm diameter and 1.5 mm wall thickness have been used for visualization purpose.

Acknowledgement

I thank my colleagues Mrs. S. S. Desai, Mr. A.K. Patra, Mr. J.N. Joshi, late Mr. N.D. Kalikar, Mrs. M. Padalakshmi, Mr. A.G. Temkar and Mr. S.M. Patkar for their sincere, valuable assistance and hard work in fabrication and testing of neutron and X-ray detectors. Thanks are also due to Prof. K. Rajanna, Indian Institute of Science, Bangalore for collaboration in microstrip detector work. The work in Neutron Radiography was performed in association with various research groups in BARC. I thank Mr. B.K. Shah and Dr. P.R. Vaidya (AFD), Mr. K.C. Sahoo, Mr.D.N. Sah, Mr. S. Gangotra (PIED) for their interest in investigations of zirconium hydride

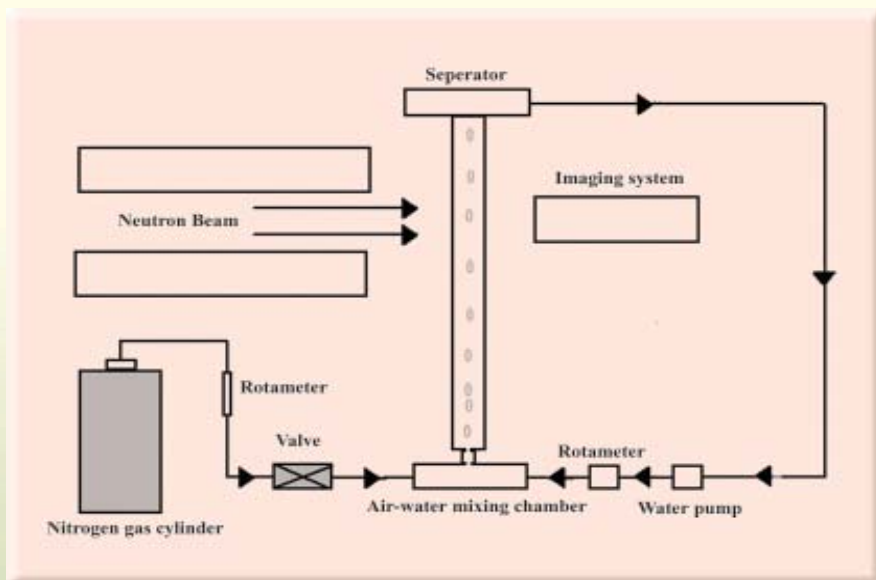


Fig. 15 : Experimental setup for two phase flow study at Apsara reactor NR Facility

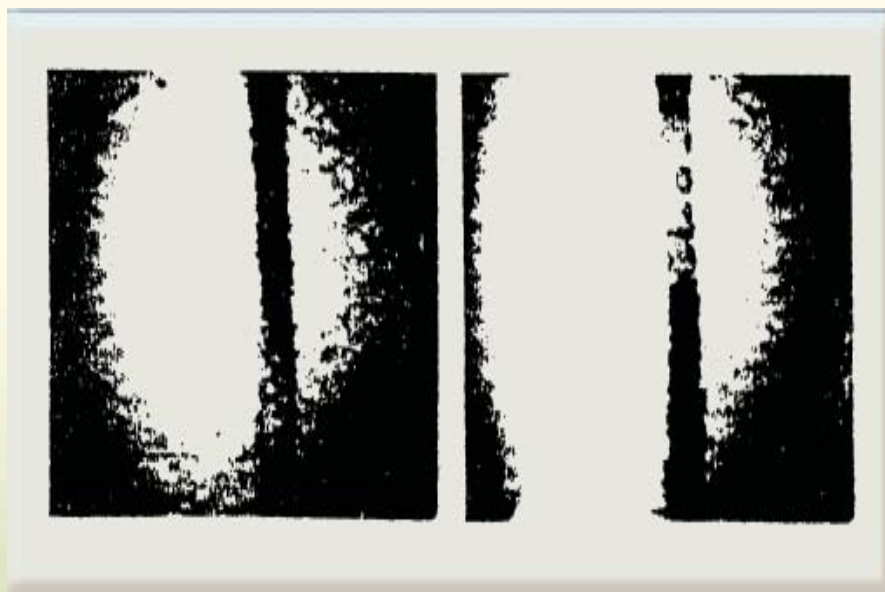


Fig.16 : Single frame image of water/air flow inside aluminium pipe at two different instants

blisters and Dr. Amar Sinha (HPPD) for the work on electronic imaging. My thanks are due to Dr. K.R. Rao (Ex-Director, Solid State and Spectroscopy Group, BARC) for his interest, suggestions and many useful discussions in development of neutron detectors and neutron radiography. I acknowledge support of Dr. A. Sequiera and Dr. M. Ramanadham (Ex- Heads of SSPD) and Dr. S.L. Chaplot, Head, SSPD and for their keen interest in the work. I am indebted to Dr. Anil Kakodkar, Chairman AEC and Dr. Srikumar Banerjee, Director BARC for the recognition of my work with DAE award for Technical Excellence for the year 2004.

References

1. Knoll G. F. Knoll, Radiation Detection and Measurement, 2nd edition John Wiley and Sons, 1989.
2. Position Sensitive Detection for Thermal Neutrons, Edited by P. Convert and J.B., Forsyth Academy press London.
3. G. Charpak, R.Bouclier, T. Bressani, J. Favier and C. Zupanicic, Nucl. Instru. and Meth. 62(1968) 262.
4. Neutron Detection Techniques in Neutron Scattering and Radiography Experiments, A.M. Shaikh, Bulletin of Indian Association of Nuclear Chemists and Allied Scientists Vol.1, No.3 , 66-71, 2002 .
5. Development of Gas Filled Radiation Detectors for X-rays and Neutrons at SSPD, BARC, S.S. Desai and A.M. Shaikh, Proceedings of DAE-BRNS National Symposium on Compact Nuclear Instruments and Radiation Detectors-2005, 495-502, 2005.
6. Two dimensional position sensitive neutron detector, A.M. Shaikh, S.S. Desai, and A.K. Patra, Pramana-J of Physics, 63(2), 465-470 (2004).
7. Development of a microstrip gas chamber to study the effect of drift gap on its performance,

- V. Radhakrishna, K. Rajanna, S.S. Desai and A.M. Shaikh, Rev. Sci. Instr., 72(2), 1361, 2001.
8. Development and Studies on Microstrip detector, V. Radhakrishna, S.S. Desai, A.M. Shaikh and K. Rajanna, Current Science (2003) vol. 84, No.10, 2003, pp 1327.
 9. Study on meandering resistive strip for microstrip position sensitive detector using charge division method, V. Radhakrishna, K. Rajanna, S.S. Desai and A.M. Shaikh, Rev. Sci. Instr., 74(10), 4263-4267(2003).
 10. Development of a microstrip based neutron detector, S.S. Desai, and A.M. Shaikh, V. Radhakrishna and K. Rajanna, Pramana-J of Physics, Vol. 63(2), 465-470 (2004).
 11. A Curvilinear Position Sensitive Neutron Detector, S.S. Desai and A.M. Shaikh, Solid State Physics (India) Vol. 50, 315(2005).
 12. Y.D. Dande et al, Ind. J. Pure and Appl. Phys., 29(1991)721.
 13. Detection of zirconium hydride blister in zircaloy tubes using neutron radiography, A.M. Shaikh, P.R. Vaidya, B.K. Shah and P.G. Kulkarni, International Seminar on Developments on Enhancement of Research Reactor Utilization, IAEA-SR-198/26, 1996.
 14. Neutron Radiography of contact location of irradiated zircaloy-2 pressure tube from RAPS#2, S. Gangotra, P.M. Ouseph, A.M. Shaikh and K.C. Sahoo, in Trends in NDE science and Technology, proceedings of the 14th WCNDT, Vol. 3, 1453-1456, 1996.
 15. Bulk Hydrogen Analysis using Neutrons, A.M. Shaikh et al, IAEA-CRP Report F1-RC-655.3, 2003.
 16. Application of Neutron Radiography and Neutron Diffraction techniques in study of zirconium hydride blisters in zirconium based pressure tube materials", A.M. Shaikh, P.R. Vaidya, B.K. Shah, S. Gangotra and K.C. Sahoo, J. of Non Destructive Testing and Evaluation, Vol.2(3), 9-12, 2003.
 17. Study of hydride blisters grown on Zr-2.5Nb pressure tube spool piece under stimulated condition of in-reactor pressure and temperature, S.K. Sinha, D.N. Shah, Suparna Banerjee, V.K. Suri, K. Gurumurthy, A.M. Shaikh and R.K. Sinha, BARC Report, 2006.
 18. Bulk Hydrogen analysis using Neutrons: Hydrogen Sensitive Epithermal Neutron Radiography Technique (HYSEN), A.M. Shaikh, Proceedings of National Seminar on Non-Destructive Evaluation, 155-157, 2003.
 19. Development of CCD/Image intensifier based 2D/3D tomography system and its application in neutron and gamma tomography, Amar Sinha, A.M. Shaikh, A. Shyam , Nuclear Instruments and Methods in Physics Research B142, 425-431(1998).
 20. Development of CCD/Image intensifier based 2D/3D tomography system and its application in neutron and gamma tomography, Amar Sinha, A.M. Shaikh, A. Shyam and L.V. Kulkarni, Proceedings of Twelfth National Symposium on Radiation Physics, 142-144(1998).
 21. Use of neutrons for visualization of water/air flow inside metallic pipes, Amar Sinha, A.M. Shaikh, A. Shyam and L.V. Kulkarni, Proceedings of Twelfth National Symposium on Radiation Physics, 243-245(1998).

ABOUT THE AUTHOR



Dr. A.M. Shaikh joined BARC in 1992. His areas of specialization are neutron & X-ray detectors, neutron radiography, high temperature X-ray crystallography and instrumentation. A Ph.D. from IISc, Bangalore, he was a postdoctoral fellow at the University of Washington Seattle, USA and has worked as faculty member at IISc, Bangalore and

University of Kuwait. Dr. Shaikh has been associated with IAEA in programmes related to Neutron Radiography and worked as an IAEA expert in this field. He has about 90 research papers in national and international journals and conference proceedings to his credit. Dr. Shaikh is on the Board of Studies and Board of Ph.D. Examiners of many universities and research institutions in India. Dr. Shaikh is the recipient of DAE-Technical Excellence Award-2004 and also the ISNT National Award-2003.

ROLE OF SURFACE STATES OF SEMICONDUCTOR NANOMATERIALS IN INTERFACIAL ELECTRON TRANSFER DYNAMICS AND EFFECT OF SURFACE MODIFICATION

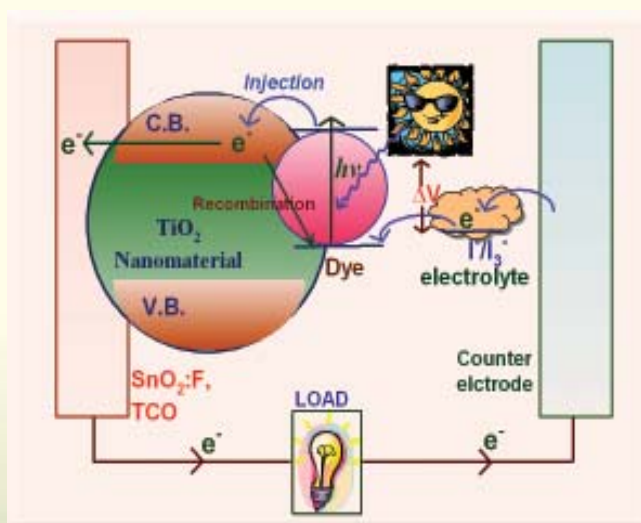
Hirendra N. Ghosh
Radiation & Photochemistry Division
Bhabha Atomic Research Centre

The author is the recipient of "The APA-Prize for Young Scientists" awarded by the Asian and Oceanian Photochemistry Association. This prize was given to top five photo-chemists in Asia and Australia and he was the only Indian to receive the award for the year 2004. The award is based on his original contribution on "Interfacial Electron Transfer Dynamics between Molecular Adsorbates and Semiconductor Nanocrystalline Materials". This award was conferred on the 27th July, 2005, at Crains, Australia.

Introduction

Electron transfer (ET) between molecular adsorbates and semiconductor nanomaterials has been a subject of intense research interest in recent years^{1,2}. This process is intimately related to the application of semiconductor nanomaterials in photography³, solar energy conversion², photocatalytic waste degradation⁴ and quantum dot devices⁵. Solar energy conversion through design and development of dye-sensitized TiO₂ semiconductor solar cell⁶ has been a subject of intense research in recent years.

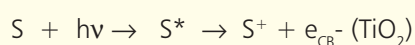
The most efficient cells of this type, based on Ru(dcbpy)₂(NCS)₂ [dcbpy (4,4'-dicarboxy-2,2'-bipyridine)] (or Ru N3) sensitized nanocrystalline TiO₂ thin films, can achieve a solar to electric power conversion efficiency of about 10%. The high conversion efficiency



Scheme 1: Kinetic model for electron transfer from a molecular adsorbate to semiconductor nanomaterials in dye-sensitized solar cell.

can be attributed to efficient solar energy harvesting by the sensitizer and high incident photon to current conversion efficiency (IPCE)². A high IPCE requires a fast electron injection rate from the sensitizer to the semiconductor and a much slower back electron transfer

rate to the sensitizer. A schematic of the interfacial ET processes in dye-sensitized semiconductor nanomaterials in solar cell is shown in Scheme 1. The operation of this solar cell and many devices based on nanocrystalline materials is directly related to the charge transfer and carrier relaxation/recombination dynamics. For this reason, in addition to interfacial ET, carrier relaxation and recombination dynamics in metal and semiconductor nanoparticles have also been actively studied in recent years⁷. The mechanism of solar cell devices is based upon the injection of an electron from a photo-excited state of the sensitized dye into the conduction band of the semiconductor. The efficiency of the dye-sensitized solar cells depends critically on the rates of the forward (dye to semiconductor) and back (semiconductor to dye) electron transfer reactions. For an efficient solar energy conversion it is necessary to establish conditions for both fast electron injection and slow recombination. High yield of long-lived charge separation is expected for useful conversion of sunlight into electric charge. The basic photophysical reactions for the above process can be written as



The dye (S) is excited with visible light ($h\nu$) to the electronically excited state S^* . If this state lies energetically above the conduction band edge of the colloid, electron injection to the semiconductor can occur on a fast or ultrafast time scale⁶⁻¹⁷. The energetic position of the acceptor level plays a key role for the dynamics of the injection mechanism. Most of the reports are available in the literature are the high density (conduction band continuum) of acceptor states was regarded as the main reason for the ultrafast initial charge separation. The lower lying (below conduction band) surface states can also play important role. Surface states in the nanoparticle

are generated due to the intrinsic defect on the surfaces of the nanoparticles. However, one cannot investigate the role of surface states in dye sensitized TiO_2 system in interfacial ET dynamics because the LUMO (lowest unoccupied molecular orbital) of most of the dye molecules are above the conduction band of TiO_2 . As a result the photo-excited dye molecules immediately injected into the conduction band. Higher band gap semiconductor colloids such as ZrO_2 may serve as an ideal system to investigate the role of these surface states, in interfacial ET reaction. Now the question is that is it possible to observe ET reaction in ZrO_2 nanoparticles by any adsorbate. The observation by many others and us reveal that most of the adsorbate do not inject electron in ZrO_2 . So what is the necessary condition for a dye/ ZrO_2 system to realize ET process? To answer this question judiciously we have chosen a series of molecules, which can inject electron in the surface states of ZrO_2 . We have also address the necessary condition in dye/nanoparticle system to observe ET reaction in the surface states.

Presence of surface states in the nano-structured materials actually brings down the efficiency of the devices. It is reported in the literature that involvement of the surface states in the interfacial ET process can actually bring down the efficiency of the solar cell. To gain higher efficiency in the devices it is very important to pacify these surface states. Modification of these states is possible using suitable modifier molecules. By this process it is possible to remove most of the lower lying surface states. Surface modification of semiconductor nanoparticles changes their optical, chemical and photo-catalytic properties significantly¹⁸. It can lead to the following effects: i) it may enhance their excitonic and defect emission by blocking non-radiative electron/hole (e^-/h^+) recombination at the defect sites (traps) on the surface of the semiconductor nanoparticles¹⁹, ii) it

may enhance the photo-stability of semiconductor nanoparticles¹⁹, iii) it may create new traps on the surface of the nanoparticles leading to the appearance of new emission bands²⁰, iv) it may enhance the selectivity and efficiency of light-induced reactions occurring on the surface of semiconductor nanoparticles^{18, 21}. Over all on surface modification density of surface states (lower lying states below the conduction band) can be changed drastically. Now the question is that on surface modification is the surface states which only get affected or the energy level of conduction and valence band also changes. As we are discussing the efficiency of dye-sensitized solar cell where interfacial electron transfer plays an important role. So it is important to see the effect of surface modification on interfacial electron transfer dynamics. In the present article we are going to address the interfacial ET dynamics in the surface states of semiconductor nanoparticles. We are also going to discuss the change of optical and photo-physical of nanoparticles on surface modification by suitable modifier molecule and also the effect of surface modification on ET dynamics. To address above questions we have used Femto-second transient absorption technique to study the ET dynamics in the surface states of ZrO₂ nanoparticles and also the effect of surface modification of TiO₂ nanoparticles on interfacial ET dynamics.

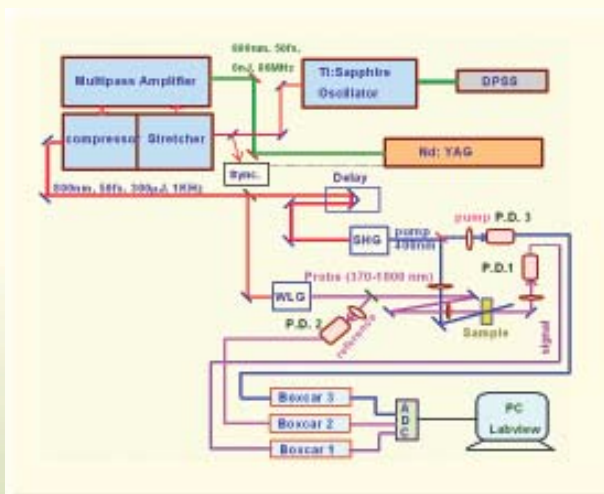
Synthesis of Nanoparticles

Nanometer-size ZrO₂ and TiO₂ particles were prepared by controlled hydrolysis of Zirconium (IV) isopropoxide isopropanol complex and Titanium (IV) isopropoxide and it has been described in detail in our earlier work^{7, 13}. A solution of 5 ml Ti[OCH(CH₃)₂]₄ (Aldrich, 97%) dissolved with 95 ml isopropyl alcohol (Aldich) was added

drop-wise (1 ml/min) to 900 mL of nanopure water (2^oC) at pH 1.5 (adjusted with HNO₃). The solution was continuously stirred for 10-12 hours until a transparent colloid was formed. The colloidal solution was concentrated at 35-40 °C with a rotary evaporator and then dried with nitrogen stream to yield a white powder. ZrO₂ nanoparticle was also prepared by adopting the above procedure.

Femtosecond Spectrometer

The femtosecond tunable absorption spectrometer has been developed in Radiation & Photochemistry Division based on a multi-pass amplified femtosecond Ti:sapphire laser system from CDP-Avesta, Russia (1 kHz repetition rate at 800 nm, 50 fs, 300 μJ/pulse)¹². The 800 nm output pulse from the multipass amplifier is split into two parts to generate pump and probe pulses. One part, with 200 μJ/pulse, is frequency doubled and tripled in BBO crystals to generate pump pulses at 800, 400, or 267 nm. Typical energy of the pump pulse were kept ~6-7 μJ. To generate visible probe pulses, about 3 μJ of the 800 nm beam is focused onto a 1.5 mm thick sapphire window. The intensity of the 800 nm beam has been adjusted by iris size and ND filters to obtain a stable white light continuum in the 470 nm to over 1000 nm region. The probe pulses are split into the signal and reference beams and are detected by two matched photodiodes with variable gain. The noise level of the white light is about ~0.5 % with occasional spikes due to oscillator fluctuation. It has been noticed that most laser noise is low-frequency noise and can be eliminated by comparing the adjacent probe laser pulses (pump blocked vs unblocked using a mechanical chopper). The typical noise in the measured absorbance change is about <0.3 %.



Femtosecond Transient Absorption Spectrometer

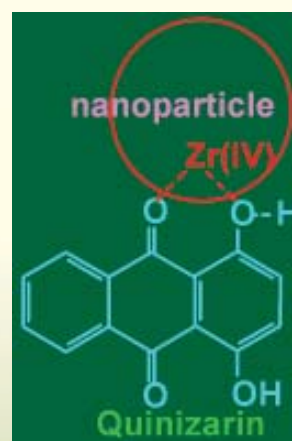
Dye-Nanoparticle Interaction

To understand the mechanism of the dye-sensitized ET reaction in the dye-nanoparticles (NP) system, it is very important to know the type of interaction between the dye molecules and the NPs when they get adsorbed on the nanoparticle surface. In the present article we are going to discuss the involvement of surface states of ZrO_2 NP in ET dynamics. For this purpose a suitable sensitizer (quinizarin) has been identified. Steady state spectroscopic measurements of Qz molecules in TiO_2 and ZrO_2 colloidal solutions suggest that Qz molecule have strong interaction with both the NPs. It is interesting to observe that Qz molecule have stronger interaction with ZrO_2 NP as compared to that TiO_2 NP. It is interesting to observe that on adsorption of the Qz on ZrO_2 nanoparticle surface, a new ligand to metal CT band is formed. The formation of CT complex can be explained by the following equation



The optical absorption spectra of Qz molecule in presence of ZrO_2 nanoparticles are broader and red shifted

as compared to that in presence of TiO_2 nanoparticles. It has already been reported by Rajh et al²² that six-membered ring complexes are more stable on ZrO_2 nanoparticle surface and five-membered ring complexes are more stable on TiO_2 nanoparticle surface for < 20 nm particles. In the present investigation Qz forms chelating type of complex having six-membered ring with ZrO_2 nanoparticles (Scheme 2) forming a stronger complex as compared to that formed on TiO_2



Scheme 2: Molecular structure of quinizarin coupled with ZrO_2

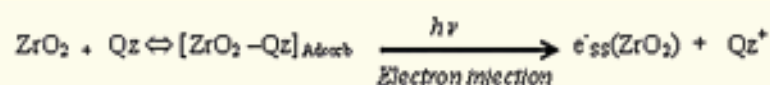
nanoparticle surface. In this scheme, it can be seen that oxygen bonded to the central ring in keto (quinoid) form along with one OH group binds to the Zr (IV) atom, which is sitting on the surface of the nanoparticle. This binding mode results in a six membered ring chelate type of complex with the surface Zr atoms. A six membered ring has larger bond angles that can accommodate the cubic structure of ZrO₂.

Electron Transfer (ET) Dynamics into the Surface States of ZrO₂ Nanoparticles and its Mechanism

The main aim of this article is to study IET dynamics in the surface states of ZrO₂ nanoparticles. It has been observed that all the sensitizers, which inject electron into the conduction band of TiO₂ not necessarily will inject electron in to the surface states of ZrO₂. As the chemical nature of ZrO₂ and TiO₂ nanoparticle surfaces are very similar²³, to understand the photophysics of the dye molecule on a non-injecting nanoparticle surface, we have used ZrO₂ nanoparticles surface, where electron injection was not possible from photoexcited dye. In those systems^{7,8} excited state properties of the dye molecules on ZrO₂ nanoparticles surface were very similar to that in bulk solvents. However, in Qz/ZrO₂ system interesting behavior has been observed in photo-excited condition. Fig.2 shows the time resolved transient absorption spectra of Qz/ZrO₂ system in water. The spectrum at each time delay consists of a bleach in 475-585 nm wavelength region centered around 510 nm, a positive peak at ~660 nm and broad positive feature in the whole spectral region (750 - 1000 nm). From the transient spectrum it is clearly visible that photophysics of Qz molecules on ZrO₂ nanoparticles surface is very different from that in methanol¹³. Temporal characteristics of the transients in the entire wavelength region are also dissimilar to that of free Qz in

solution¹³. The positive peak at 660 nm has been attributed to the combination of cation radical of Qz molecule as well as the injected electron in ZrO₂ nanoparticles and broad absorption band in the region of 750-1000 nm has been attributed to the injected electrons in the nanoparticles. Since the excited singlet state (S1) of Qz molecule is well below the conduction band of ZrO₂ (Scheme II), photo excited Qz molecule will be unable to inject electron in the conduction band of ZrO₂ nanoparticles. Thus, this injection process has been attributed to the injection in the surface states of nanoparticles. The bleach peak appears due to disappearance of ground state of the dye-ZrO₂ complex, on excitation by the laser pulse. The appearance time of the above signal is pulse width limited (<50 fs), it can be attributed to electron injection time into the surface states of ZrO₂ nanoparticles. The electron injection in ZrO₂ nanoparticles can be explained by the equation given below.

The kinetic decay of both electron in the conduction band as well as the parent cation radical and also the recovery kinetics of the bleach can provide the recombination dynamics of the injected electrons and



the parent cation. Fig.1 inset shows the bleach recovery kinetics at 570 nm wavelength. The recovery kinetics has been best fitted with a multi-exponential function with the time constants of 0.6 ps (76.2%), 4.5ps (10.8%) and >200 ps (13%). Recombination dynamics of the above reaction can also be determined by both monitoring the cation radical at 660 nm and also the electron in the nanoparticle at 900 nm.

It has been discussed earlier that Qz forms a strong complex with ZrO₂ nanoparticles than with TiO₂

nanoparticles. Time-resolved absorption studies reveals that electron injection time for both TiO₂ and ZrO₂

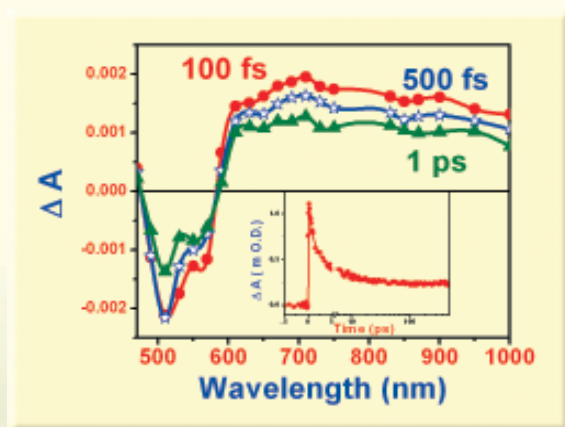


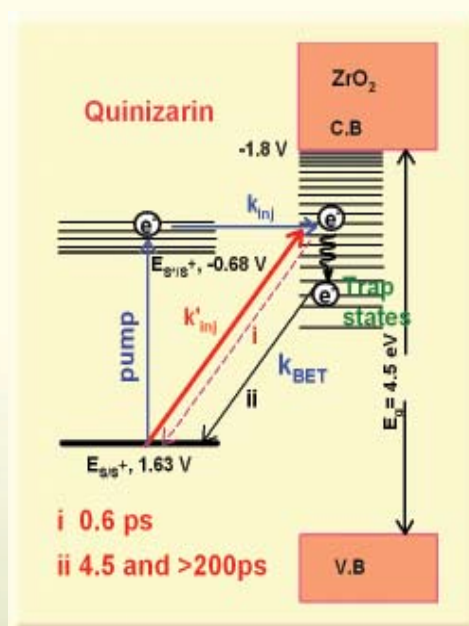
Fig. 1 : Transient absorption spectra of quinizarin sensitized ZrO₂ nanoparticle in water at different time delay after excitation at 400 nm. Inset: Transient decay kinetics at 900 nm.

nanoparticles is pulse width limited (<50 fs) Although, the density of acceptor states in the surface states of ZrO₂ nanoparticles is much smaller compared to that in the conduction band of TiO₂ nanoparticles, still we have observed that electron injection is ultrafast in both the cases. Rego et al²⁴, and Wang et al²⁵ have already explained the direct electron injection into the nanoparticles through charge transfer mechanism. In the present investigation we have observed that Qz forms strong CT complex with ZrO₂ nanoparticles, which can facilitate direct electron injection in to the surface states of the nanoparticles. As the LUMO in the case of a CT complex is located on the metal center (Zr), on excitation with light, the electron gets directly localized on the metal center from where diffusion into either the continuum of conduction band states or surface states of the nanoparticle takes place depending on the semiconductor. However, we have shown in the Scheme 3 that electron injection in Qz/ZrO₂ system can be possible both via photo-excited Qz molecules (k_{inj})

and also direct injection (k'_{inj}) to metal centers (Zr).

Modification of Surface States of Nanoparticles

It is quite clear that surface states play an important role in interfacial ET reaction. Surface states directly involved in the ET process for dye/NP systems where dye molecules couple strongly with the formation CT complex. To make an efficient solar cell devices it is always



Scheme 3 : Mechanistic scheme of electron transfer for the quinizarin/ZrO₂ system Here S*/S⁺ is the excited sensitized dye/cation radical couple, k_{BET} is the back electron transfer rate, k_{inj} is the electron injection through excited state, k'_{inj} is direct electron injection (excitation of CT complex).

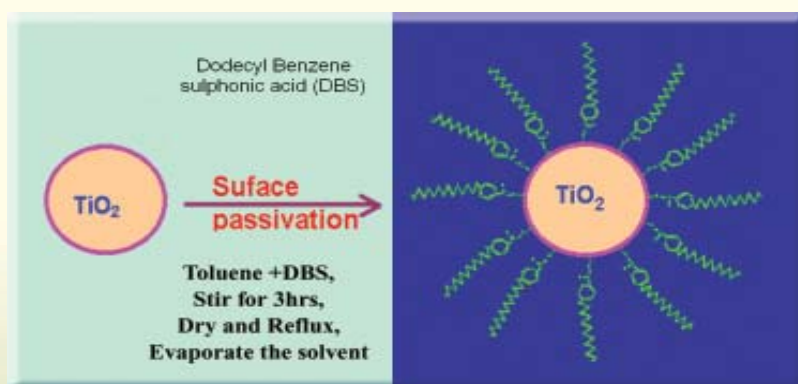
expected that surface states nano-structured materials should not take part. However SS are the unavoidable intrinsic property of nano-structured material. However, these SS of nano-materials can be modified by using suitable capping agent (modifier molecule)²⁶. Where modifier molecules directly interact with the lower lying surface states. As a result density of SS can be changed

drastically in the modified particles as compared to the bare one. DBS ($C_{12}H_{25}C_6H_4SO_3Na$, sodium dodecyl benzene sulphonate) is one of the modifier molecules, which can be dissolved only in water, because it's ionic nature. As TiO_2 nanoparticle is important material for the development of dye-sensitized solar cell, it would be interesting effect of surface modification of it. As the surface of the TiO_2 nanoparticles is positively charged, DBS molecules

can easily bind through sulphonic group (SO_3^-) with the nanoparticles. The newly capped TiO_2 nanoparticles looks like reverse micelle (Scheme 4) and can be dissolved in organic solvent. In this situation TiO_2 nanoparticles migrate from water to organic phase (toluene). Now with the help of a separating funnel the organic phase was separated out. At this stage the organic phase looks little cloudy. The organic phase was dried in $CaCl_2$ and transformed to an optically clear solution. The organic phase was then refluxed for 2 hours and the solvent was taken out with the help of a rotary evaporator in N_2 atmosphere. Dry TiO_2 particles capped by DBS, which were left in the flask, can be dissolved in many non-aqueous solvents to get colloidal solution in that particular solvent. Similarly ZrO_2 nanoparticles can be modified by DBS molecule as the surface nature of ZrO_2 nanoparticles as similar to TiO_2 nanoparticles.

Effect of Surface Modification on Interfacial Electron Transfer Dynamics

The central theme of this article is to demonstrate the effect of surface modification on interfacial electron transfer dynamics in dye-sensitized TiO_2



Scheme 4: Schematic diagram of synthesis of sodium dodecyl benzene sulphonate (DBS) capped TiO_2 nanoparticle

nanoparticles. For that purpose alizarin (Alz) molecule had been chosen for sensitization of semiconductor nanoparticles, which adsorb on the semiconductor surface very strongly with or without the presence of the modifier molecule (DBS)¹². Interestingly Alz does not interact with DBS molecule both in the ground and excited state, this is an ideal system to study the effect of surface modification on dye-sensitized semiconductors¹². It is seen that Alz and TiO_2 nanoparticles interact strongly and similarly both on unmodified and modified surface. It indicates that electronic coupling between Alz and TiO_2 in the ground states is very similar in both cases. Electronic coupling is an important parameter for forward electron transfer (electron injection) process in dye/nanoparticle system. The above observations may lead us to speculate that there will be negligible effect of surface modification on electron injection on Alz/ TiO_2 nanoparticle systems. To verify the above speculation electron injection experiments has been carried out in Alz/ TiO_2 system on both unmodified and modified surface by changing the solvent. Figure 2 shows the comparison of electron injection dynamics in Alz/ TiO_2 system on both unmodified and modified surface in different solvents after monitoring the appearance signal of conduction band electron at 900 nm.

It is very interesting to see that in all the cases electron injection is found to be pulse width limited. This is because of the fact that electronic coupling primarily drives electron injection between initially populated electronic state in the molecular adsorbate and the delocalized electronic states of similar energy in the semiconductor²⁴. Although electron injection dynamics is found to be unaffected by surface modification, however, charge recombination (BET) dynamics found

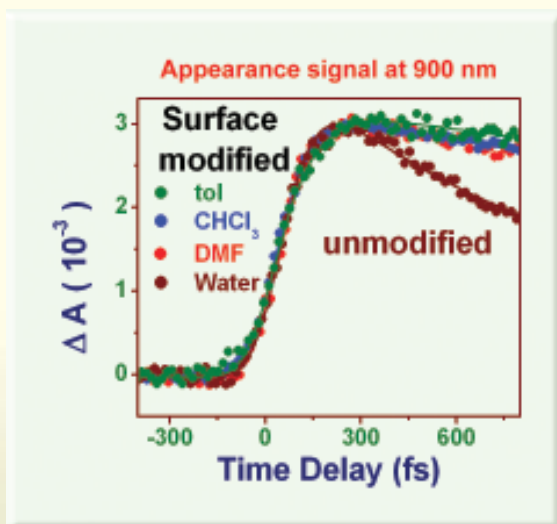


Fig. 2 : Comparison of electron injection dynamics in a) Al₂O₃ sensitized unmodified TiO₂ nanoparticles (O); b) surface modified TiO₂ nanoparticles (•). Probe wavelength is 900 nm.

to be affected substantially on surface modification. Figure 3 shows the transient absorption decay of conduction band electron (eCB-) at 900 nm in Al₂O₃/TiO₂ system on both unmodified and modified surface in different solvents. The decay of the observed signals can be fitted by multi-exponential functions with time constants of 0.6 ps (75%), 7 ps (10%) and > 400 ps (15%) for Al₂O₃/unmodified-TiO₂ system and 1.9 ps (45.3%), 35 ps (12.9%) and > 400 ps (41.8%)

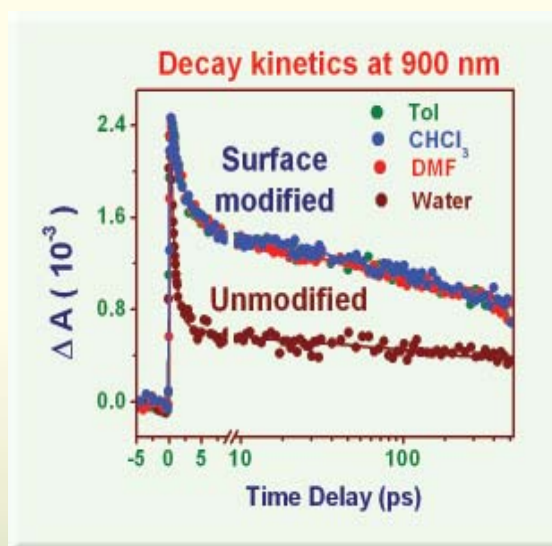


Fig. 3 : Comparison of recombination (BET) dynamics in a) Al₂O₃ sensitized unmodified TiO₂ nanoparticles (O); b) surface modified TiO₂ nanoparticles (•). Probe wavelength is 900 nm.

for Al₂O₃/SM-TiO₂ system. It is striking to see that BET reaction between the injected electron and the parent cation is faster on the unmodified nanoparticle surface compared to that on the modified surface. This interesting behavior of slow BET reaction on modified surface can be explained following Marcus electron transfer theory. As the other factors that can affect the surface modified nanoparticles are not operating for the present system, we are inclined towards applying the semi-classical Marcus ET theory for explaining the results by following expression

$$k_{BET} = \left(\frac{2\pi}{\hbar} \right) |H_{AB}|^2 \frac{1}{\sqrt{4\pi\lambda kT}} \exp \left\{ - \frac{(\Delta G^0 + \lambda)^2}{4\lambda kT} \right\}$$

BET rate constant (kBET) depends on the coupling element (H_{AB}), the overall free energy of reaction (ΔG⁰ = E_C - E_{S⁺}), the potentials of electrons in the conduction band of the semiconductor (E_C = -0.49V)³, and the redox potential of the adsorbed dye (E_{S⁺}) (Scheme 5). It has been observed that on surface

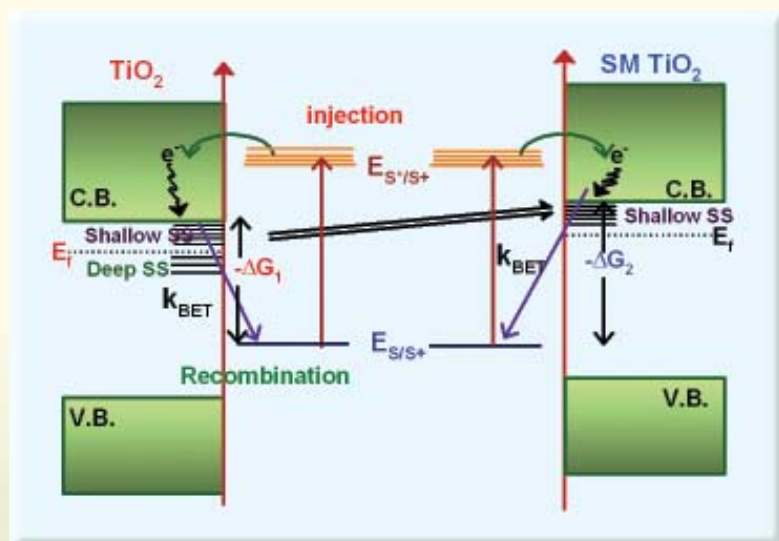
modification both electronic coupling (HAB) and the solvent reorganization parameter (L) of Al₃/TiO₂ nanoparticle system do not alter¹². As a result BET dynamics of Al₃/TiO₂ system may depend mostly on free energy ($-\Delta G^0$) of the reaction for both unmodified and modified surface. Ellis et al²⁷ reported that strong adsorption of negative counter ions on the electrode surface shifts the flat band potential (V_{fb}) and also the valence band (VB) to more negative values. On TiO₂ nanoparticle DBS molecule (modifier) is adsorbed strongly through sulphonic group (SO₃H⁻). So on surface modification the Fermi level of the modified colloids is pushed up in energy, as a result the overall free energy of reaction increases. On modification, both flat band potential and valence band is shifted towards negative values with same extent²⁸ (Scheme 5). As a result the band gap of nanoparticles does not change with

modification but the conduction band edge energy level shifts toward higher energies. According to Marcus ET theory, with increasing thermodynamic driving force ($-\Delta G^0$), the ET rate initially increases to reach a maximum value and then starts decreasing²⁹. This high exoergic region is often termed as "inverted regime". BET processes in dye-sensitized TiO₂ nanoparticles surfaces fall in the Marcus inverted regime for its high free energy of reaction^{30,31}. In this region with increasing driving force ($-\Delta G^0$) of the reaction, the rate of BET decreases. As the free energy for BET for the case of SM-TiO₂ is higher than that of the unmodified TiO₂ nanoparticles, BET rate on the modified surface is slower as compared to that on the unmodified surface.

Conclusions

Electron injection has been demonstrated in the forbidden energy states i.e. surface states of semiconductor

nanoparticles by time-resolved Femto-second transient absorption studies. It is shown that quinizarin (Qz) an adsorbate that can couple very strongly with ZrO₂ nanoparticles can inject electron in the surface states of NP although energy level of photo-excited Qz lies far below the conduction band of ZrO₂ NP. Steady-state absorption studies revealed that quinone moiety of Qzs, form six-membered strong charge transfer (CT) complex with ZrO₂ nanoparticles. It has been observed that CT complex formation facilitates electron injection in the surface states of ZrO₂ nanoparticles. Surface states of NP has been modified by a suitable



Scheme 5: Mechanistic scheme of electron transfer (ET) and effect of surface modification on ET in Al₃-sensitized unmodified (left) and modified (right) TiO₂ nanoparticles. Fermi level pinning is seen due to surface-modification on TiO₂ nanoparticles (right). The energy levels of the modified nanoparticles are pushed up in energy and thereby effective free energy ($-\Delta G$) increases ($-\Delta G_2 > -\Delta G_1$).

modifier molecule namely DBS. Upon surface modification it has been observed that optical and photochemical properties of NP changed. Effect of surface modification on interfacial electron transfer dynamics in surface modified TiO₂ nanoparticles using suitable sensitizer molecule like alizarin (Alz). Electron injection dynamics has been found unaffected by surface modification, however, charge recombination (BET) dynamics is found to be slow on modified surface as compared to that on bare surface. The flat band potential of the modified nanoparticles is pushed up in energy, increasing the overall free energy of reaction ($-\Delta G^0$) for BET; as a result BET rate decreases on modified surface. In conclusion, electron injection into the forbidden states of semiconductor nanoparticles have demonstrated and also it is shown that on surface modification, the rate of BET reaction can be reduced drastically in dye-sensitized nanoparticle system. This observation can, in turn, help the solar energy researchers to build low cost dye-sensitized solar cell with high photo-conversion efficiency.

Acknowledgement

I would like to thank my collaborators Dr. G. Ramakrishna and Dr. D.K. Palit for fruitful discussions. I would also like to thank Dr. S.K. Sarkar, Head, Radiation & Photochemistry Division and Dr. T. Mukherjee, Director Chemistry Group for their encouragements.

References

1. R. D. J. Miller, G. L. McLendon, A. J. Nozik, W. Schmickler, F. Willig, *Surface electron-transfer processes*; VCH publishers, Inc.: New York, (1995).
2. P. V. Kamat, and D. Meisel, *Semiconductor Nanoclusters - Physical Chemical and Catalytic Aspects*; vol 103, Elsevier: Amsterdam, (1997).
3. A. Hagfeldt and M. Gratzel, *Chem., Rev.* 95, 49. (1995).
4. B. Oregan and M. Gratzel, *Nature.*, 353, 737 (1991).& 338, 737 (2001).
5. A. J. Nozik, and R. Memming, *J. Phys. Chem.* 1996, 100, 13061.
6. T. Hannapel, B. Burfeindt, W. Storck and F. Willig, *J. Phys. Chem. B* 101, 6799 (1997).
7. H.N. Ghosh, *J. Phys. Chem. B.*, 103, 10382. (1999).
8. G. Ramakrishna and H.N. Ghosh, *J. Phys. Chem. B.* 105, 7000 (2001).
9. G. Ramakrishna, H. N. Ghosh, A. K. Singh, D. K. Palit and J. P. Mittal, *J. Phys. Chem. B.* 105, 12786 (2001).
10. G. Ramakrishna and H.N. Ghosh, *J. Phys. Chem. B.*, 106, 2545 (2002).
11. G. Ramakrishna, A. Das and H.N. Ghosh, *Langmuir*, 20, 1430 (2004).
12. G. Ramakrishna, A. K. Singh, D. K. Palit and H. N. Ghosh, *J. Phys. Chem. B.* 108, 1701 (2004).
13. G. Ramakrishna, A. K. Singh, D. K. Palit and H. N. Ghosh, *J. Phys. Chem. B.* 108, 4775 (2004).
14. G. Ramakrishna, A. K. Singh, D. K. Palit and H. N. Ghosh, *J. Phys. Chem. B.* 108, 12489. (2004).
15. G. Ramakrishna and H.N. Ghosh, *Langmuir*. 20, 7342 (2004).
16. G. Ramakrishna, D. Amilan Jose, K. Krishna Kumar, A. Das, D. K. Palit and H. N. Ghosh *J. Phys. Chem. B.* 109, 15445. (2004).
17. H. N. Ghosh, J. B. Asbury and T. Lian, *J. Phys. Chem. B* 102, 6482 (1998).
18. J. B. Asbury, E. Hao, Y.Q. Wang, H. N. Ghosh and T. Lian *J. Phys. Chem. B* 104, 4545 (2001).
19. Fox M.A. *Topp. Curr. Chem.* 1987, 72, 142.
20. Spanhel, L.; Haase, M.; Weller, H.; Henglein, A. *J. Am. Chem. Soc.* 1987, 109, 5649.
21. Spanhel, L.; Weller, H.; Fojtik, A.; Henglein. *Ber. Bunsenges. Phys. Chem.* 1987, 91, 88.

22. Fox, M.A.; Dulay, M.T. *Chem. Rev.* **1993**, *93*, 341.
23. Rajh, T.; Chen, L.X.; Lukas, K.; Liu, T.; Thurnauer, M.C.; Teide, D.M. *J.Phys.Chem. B* **2002**, *106*, 10543.
24. A. Kay, R. Humphry-Baker, M. Gratzel, *J. Phys. Chem.* **98**, 952. (1994).
25. G. L. S. Rego, and V. S. Batista, *J. Am. Chem. Soc.* **125**, 7989 (2003).
26. Y. Wang, K. Hang, N. A. Anderson and T. Lian. *J. Phys. Chem. B* . **107**, 9434 (2003).
27. Ramakrishna, G.; Ghosh, H.N. *Langmuir.* **2003**, *19*, 505.
28. Cohen, R.; Kronik, L.; Shanzer, A.; Cahen, D.; Liu, A.; Rosenwaks, Y.; Lorenz, J.K.; Ellis, A.B. *J. Am. Chem. Soc.* **1999**, *121*, 10545.
29. Xagas, A.P.; Bernard, M.C.; Hugot-Le Goff, A.; Spyrellis, N.; Loizos, Z.; Falaras, P. *J. Photochem. Photobiol. A: Chemistry*, **2000**, *132*, 115.
30. R. A. Marcus and N. Sutin, *Biochim. Biophys. Acta* **811**, 265 (1985)
31. Lu, H.; Prieskorn, J.N.; Hupp, J.T.; *J. Am. Chem. Soc.* **1993**, *115*, 4927.
32. Ramakrishna, G.; Ghosh, H.N. *J. Phys. Chem. B.* **2001**, *105*, 7000.

ABOUT THE AUTHOR



After obtaining his M. Sc. In Chemistry from IIT, Kharagpur , in 1989, Dr. Ghosh joined Chemistry Division, BARC, in 1990, through BARC Training School Course (33rd batch, 1989-90). Dr. Ghosh obtained his Ph.D. degree in 1996 from Bombay University for his work on fast photochemical processes in liquid and microheterogeneous

media. He did his Post-doctoral studies for the period of 1997-1998, with Prof. Tim Lian at the Chemistry Department of Emory University, Atlanta, USA, in femtosecond infrared spectroscopy. Dr. Ghosh was awarded the "INSA Young Scientist" Medal for the year of 1998 for his outstanding Ph.D. work. He has also received the prestigious "Anil Kumar Bose Memorial Award" in 2000 for the best output during the year after INSA Young Scientist Award by the Indian National Science Academy, New Delhi. Dr. Ghosh has published more than 50 research papers in highly reputed International Journals, and his research papers have been cited by peers and experts in his field of research for more than 1000 times. He has developed Femtosecond laser spectrometer detecting both invisible and infrared region. His current research interest includes ultrafast interfacial electron transfer and charge carrier relaxation dynamics in semiconductor nanoparticles and quantum dot materials as also development of Femtosecond terahertz spectrometer.

EVIDENCE FOR ANTIOXIDANT ACTIVITY AND FUNCTIONAL MOIETY OF NON STEROIDAL ANTI INFLAMMATORY DRUG SULFASALAZINE

Ravi Joshi and T. Mukherjee
Radiation & Photochemistry Division, Chemistry Group,
Bhabha Atomic Research Centre

This paper received the "Young Scientist Award" at the 24th Miller Conference on Radiation Chemistry held at La Londe les Maures, Toulon, France, from 10th to 15th September 2005 and was also presented at the conference.

Abstract

Kinetics and mechanism of reactions of non-steroidal anti-inflammatory (NSAID) drug sulfasalazine and its metabolites, 5-aminosalicylic acid and sulfapyridine, with various free radicals have been studied. The transients produced in these radical scavenging reactions have been assigned and rate constants have been measured using pulse radiolysis technique. The study shows the mechanistic aspects of drug action against free radicals produced during inflammation. It has been proposed that free radical scavenging activity of 5-aminosalicylic acid may be a major path of pharmacological action of sulfasalazine against inflammatory bowel diseases.

Introduction

Sulfasalazine (SAZ) is a drug, which is used effectively in the treatment of inflammatory bowel diseases (IBD) [2]. The inflammatory diseases are caused by enhanced production of reactive oxygen species (ROS) by phagocytic leukocytes. After ingestion, SAZ is reduced by coliform bacterial enzyme azoreductase into sulfapyridine (SP) and 5-aminosalicylic acid (5-ASA) (scheme 1) in the intestine and colon. SP is absorbed from the gut into blood and is metabolized but 5-ASA is not absorbed and its concentration at the site of inflammation is high. Therefore, the active



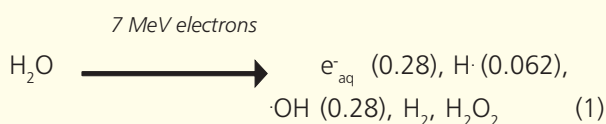
Scheme 1

therapeutic moiety of SAZ in the treatment of IBD is assumed to be 5-ASA. However, antioxidant efficacy

of any compound depends not only on its high local concentration at the target site but also on its reactivity with the free radicals and the fate of drug transients. To study the chemical reactions involved in these processes electron pulse radiolysis technique has been used which is as a clean and direct method.

Experimental

The pulse radiolysis system giving pulses of 7 MeV electrons from a linear electron accelerator for *in-situ* generation and study of free radicals has been used and is described elsewhere [3]. High-energy electrons deposit energy in water to generate its radical and molecular species (equation 1).



The values in the parenthesis in equation 1 are radiation chemical yield in the unit of micromoles per Joule of absorbed energy. Relative absorption of radicals in the UV-visible region has been observed against time and wavelength to get kinetic and absorption characteristics, respectively.

Results and Discussion

The reactions of SAZ, 5-ASA and SP with various oxidizing and reducing radicals have been studied using appropriate chemical systems and following the standard methods for *in situ* generation of the free radicals. Rate constants of the reaction of SAZ, 5-ASA and SP with various radicals and absorption maximum of the transients produced in these reactions are given in Tables 1, 2 and 3 respectively.

Table 1
Rate constants and transient absorption maxima for the reactions of various free radicals with SAZ

Radical	pH	λ_{max} (nm)	k (mol ⁻¹ dm ³ s ⁻¹)
$\cdot\text{OH}$	6.8	450	5.0×10^9
$\text{N}_2\cdot$	6.8	450	9.8×10^8
$\cdot\text{CCl}_3\text{O}_2$	11.3	450	4.5×10^9
e_{aq}^-	6.8	420, 560	1.1×10^{10}
$\cdot\text{CO}_2$	6.8	420, 570	4.0×10^9
$\text{O}_2\cdot^-$	6.8	420, 560	1.2×10^9
$\text{GS}\cdot$	4.6	430, 560	1.5×10^9 (at 560) 6.0×10^7 (at 430)
$\text{LO}_2\cdot$	11	---	4.0×10^9
SAZ + AscH ⁺	6.8	---	3.0×10^9

Table 2
Rate constants and transient absorption maxima for the reactions of various free radicals with 5-ASA

Radical	pH	λ_{max} (nm)	k (mol ⁻¹ dm ³ s ⁻¹)
$\cdot\text{OH}$	6.8	320, 440	6.7×10^9
$\text{N}_2\cdot$	6.8	320, 440	6.0×10^9
$\cdot\text{CCl}_3\text{O}_2$	6.8	320, 440	9.0×10^9
e_{aq}^-	6.8	300	6.0×10^9
$\cdot\text{CO}_2$	6.8	270	5.0×10^9
$\text{GS}\cdot$	4.1	330, 430, ~470	7.0×10^7
Trp	6.8	---	7.3×10^7
L [•]	11	---	2.0×10^9
$\text{LO}_2\cdot$	11	---	8.0×10^9
5-ASA + AscH ⁺	6.8	360, 400, 430, 460	1.5×10^7

Table 3
Rate constants and transient absorption maxima for the reactions of various free radicals with SP

Radical	pH	λ_{max} (nm)	k (mol ⁻¹ dm ³ s ⁻¹)
·OH	6.8	400, 520	1.0 × 10 ¹⁰
N ₃ ⁻	6.8	---	1.0 × 10 ⁹
·CCl ₃ O ₂	6.8	320	6.0 × 10 ⁶
e ⁻ _{aq}	6.8	360	2.1 × 10 ¹⁰
·CO ₂ ⁻	6.8	350	3.8 × 10 ⁹
SP ⁻ + AscH ⁻	6.8	---	2.7 × 10 ⁹

Reaction with the Oxidizing Radicals

Hydroxyl radical (·OH) is the most deleterious oxidizing radical among those physiologically produced and reacts with most of the biomolecules at diffusion-controlled

rates. Since the hydroxyl radical can react by addition, abstraction and one-electron addition reactions, specific one-electron oxidant (azidyl radical, N₃⁻) has been also used to unambiguously resolve the absorption bands of the produced transients.

SAZ, 5-ASA and SP reacted with oxidizing radicals to produce transient absorption spectra with maximum at ~450 nm; 440 & 320 nm; and 390 nm, respectively (Fig. 1). The transient absorption at ~440 nm observed for SAZ and 5-ASA can be ascribed to their phenoxyl radical. The transient absorption observed at 390 nm with SP has been ascribed to the reaction of pyridine ring of SP with ·OH. Reaction of 5-ASA with ·OH and N₃⁻ produced one-electron oxidized transient only. However, in the reaction of SAZ with ·OH, G(SAZ⁻) has been found to be equal to (1/2).G(·OH). Therefore, remaining 50% contributes to other reactions like adduct formation, hydrogen abstraction etc. It should be noted that ·CCl₃O₂ has not been found to oxidize SAZ at pH 6.8. This suggests

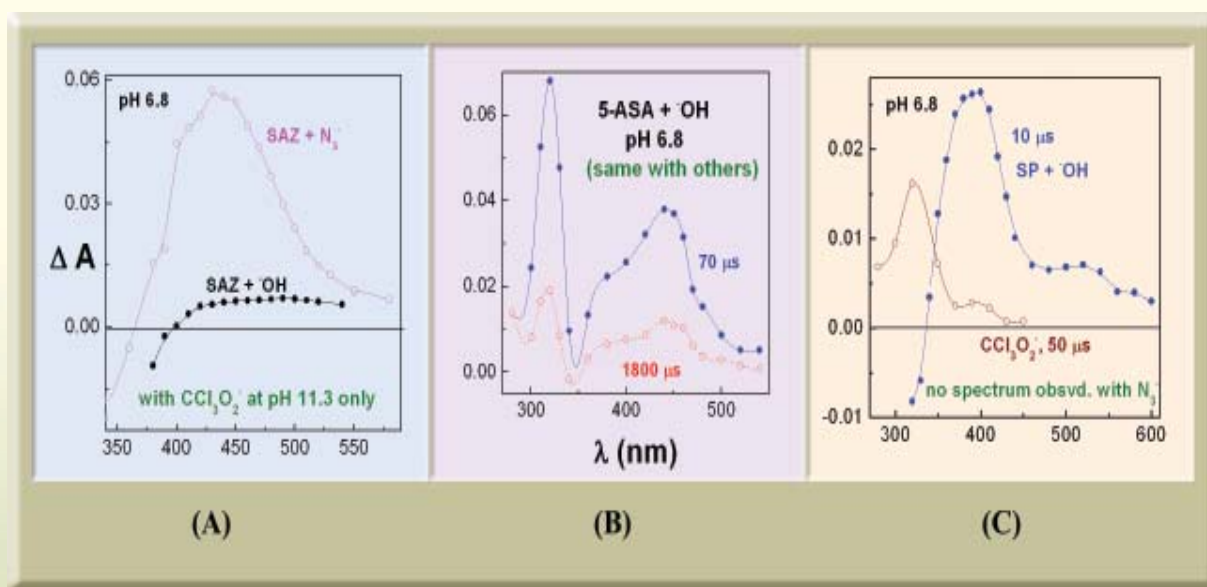


Fig. 1 : Absorption spectrum of the transients obtained in the reaction of (A) SAZ (B) 5-ASA and (C) SP with various oxidizing radicals

that at pH 6.8, 5-ASA can scavenge peroxy radical but SAZ is ineffective. SP reacted with $\cdot\text{CCl}_3\text{O}_2$, at pH 6.8, to produce transient absorption spectrum with a maximum at ~ 320 nm and negligible absorption ~ 350 nm which can be attributed to the adduct of $\cdot\text{CCl}_3\text{O}_2$ with benzene ring of SP.

Reaction with Reducing Radicals

SAZ, 5-ASA and SP reacted with reducing radicals to give transient absorption spectra with maximum at 420 & 560 nm; 270 & 300 nm; and ~ 350 nm, respectively (Fig.2). The absorption maxima produced in the reaction of reducing radicals with SAZ has been ascribed to delocalized molecular radical anion of SAZ, probably at diazo group. 5-ASA reacted with reducing radicals to produce electron/radical adduct with aromatic ring of the molecule. SP reacted with reducing radicals to produce pyridinyl radical.

The reactions of SAZ, 5-ASA and SP with various radicals show that they efficiently scavenge oxidizing and reducing radicals and can be termed as competitive antioxidants. The reactions of 5-ASA with $\cdot\text{OH}$ and $\text{CCl}_3\text{O}_2\cdot$ produce almost 100% one-electron oxidized phenoxyl radical ($\lambda_{\text{max}} = 440, 320$ nm). On the other hand, the reactions of SAZ with $\cdot\text{OH}$ and $\cdot\text{CCl}_3\text{O}_2$ produce $\sim 50\%$ and $\sim 60\%$ one-electron oxidized phenoxyl radical ($\lambda_{\text{max}} = 450$ nm), respectively along with other transients. However, SP molecule having both pyridine and benzene rings reacted with $\cdot\text{OH}$, $\text{N}_3\cdot$ and $\cdot\text{CCl}_3\text{O}_2$ to produce transients corresponding to both the moieties.

The sites of attack of oxidizing and reducing free radicals on SAZ, 5-ASA and SP and the absorption maxima of the produced transients are shown in the scheme 2.

The reactions of SAZ with e_{aq}^- , $\cdot\text{CO}_2^-$ and $\text{O}_2^{\cdot-}$ produced delocalized radical anion ($\lambda_{\text{max}} = 420, 560$ nm). 5-ASA reacted with e_{aq}^- to produce electron-adduct with

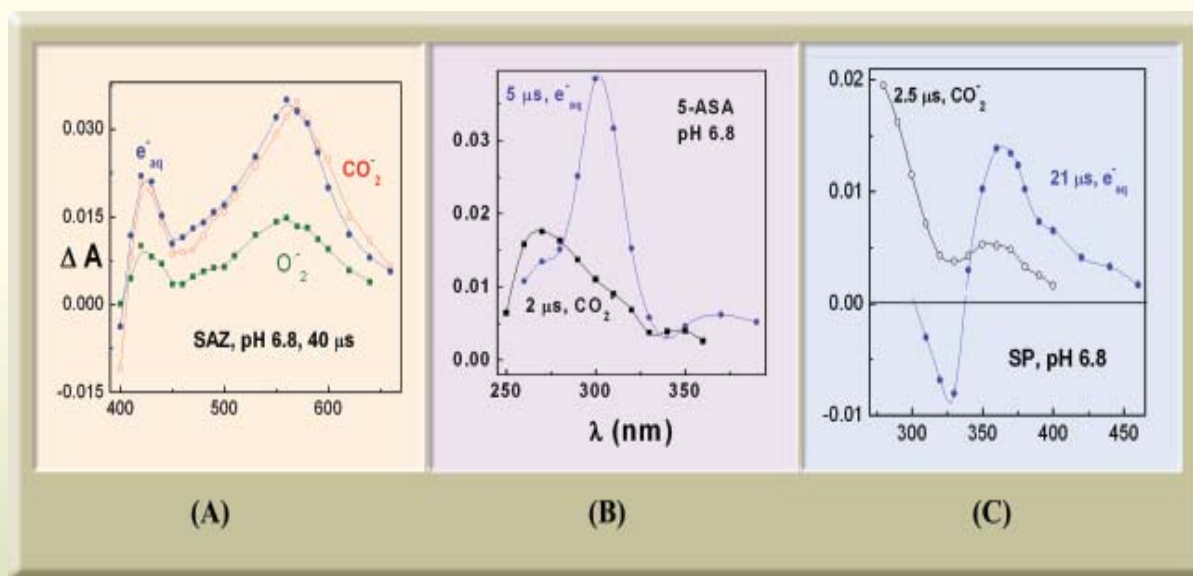
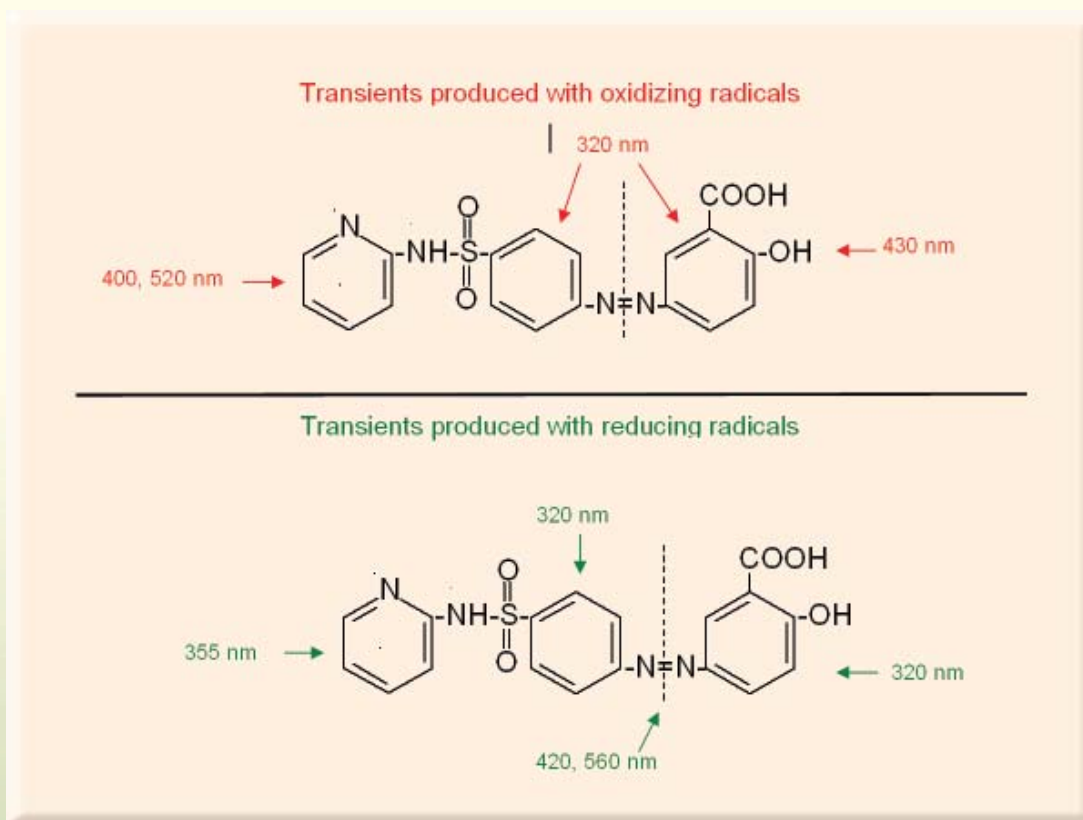


Fig. 2 : Absorption spectrum of the transients obtained in the reaction of (A) SAZ, (B) 5-ASA and (C) SP with various reducing radicals.



Scheme 2

benzene ring ($\lambda_{\max} \sim 310$ nm) but solute-radical adduct ($\lambda_{\max} = 270$ nm) is also produced with $\cdot\text{CO}_2^-$. SP reacted with $\cdot\text{CO}_2^-$ to produce electron-adduct with benzene ring ($\lambda_{\max} \sim 310$ nm) but with e_{aq}^- it produced pyridinyl radical ($\lambda_{\max} \sim 360$ nm) also. The reactions of O_2^- with 5-ASA and SP have not been observed under our experimental conditions. It is clear from the above discussion that more than one transient are produced in the reactions of SAZ, 5-ASA and SP with various oxidizing and reducing radicals.

5-ASA is the component that reaches the site of inflammation in IBD and is anticipated to act as an antioxidant by scavenging free radicals of various biomolecules in addition to primary radicals. Therefore,

an attempt has been made to study these biologically relevant reactions directly using pulse radiolysis technique. Reactions of (1) drug transient with biomolecules and (2) biomolecule transients with drug molecules have been studied and their rate constants are given in Tables 1, 2 and 3.

Reaction with Lipid Radicals

Lipids make the cell membrane and their reaction with $\cdot\text{OH}$ radical (physiologically and pulse radiolytically produced) produce lipid (L \cdot) and lipid peroxy (LOO \cdot) radicals. Both SAZ and 5-ASA have been found to scavenge LOO \cdot radical efficiently. 5-ASA has been found to scavenge L \cdot radical also. This efficient scavenging of

LOO \cdot by SAZ and 5-ASA makes them good antioxidant in the lipid phase also. However, SP has not been found to scavenge either L \cdot or LOO \cdot .

Reaction with Tryptophanyl Radical

Tryptophanyl radical (Trp \cdot) is produced in the reactions of proteins with oxidants in the first step before producing tyrosine radical followed by protein damage and cross-linking. Electron transfer to Trp \cdot by antioxidant can prevent the damage to the protein molecule. 5-ASA has been found to efficiently scavenge Trp \cdot at pH 7. However, SAZ and SP have not been found to scavenge Trp \cdot radical. This suggests that 5-ASA can reduce the damage to proteins by acting as radical scavenger as well as repair agent.

Reaction with Glutathyl Radical

Thiyl radicals (RS \cdot) generated in the cellular redox processes and antioxidant action are reactive oxidants. Hence repair of thiyl radical is necessary for the storage of thiols (RSH) for their antioxidant activity as well as to protect lipids from thiyl radical attack.

Transient absorption spectrum for the reaction of glutathyl radical with 5-ASA showed absorption maxima at 330, 430 and \sim 470 nm (Fig.3A). The transient absorption at 470 nm has been assigned to solute-radical adduct (5-ASA \cdot GS \cdot) produced in addition to phenoxyl radical ($\lambda_{\text{max}} = 430, 330$ nm) of 5-ASA. SAZ reacted with GS \cdot to produce transient absorptions at 560 and 430 nm. The absorption at 560 nm is attributed to solute-radical adduct (SAZ \cdot GS \cdot) and that at 430 nm to the phenoxyl radical on 5-ASA group. Transformation of

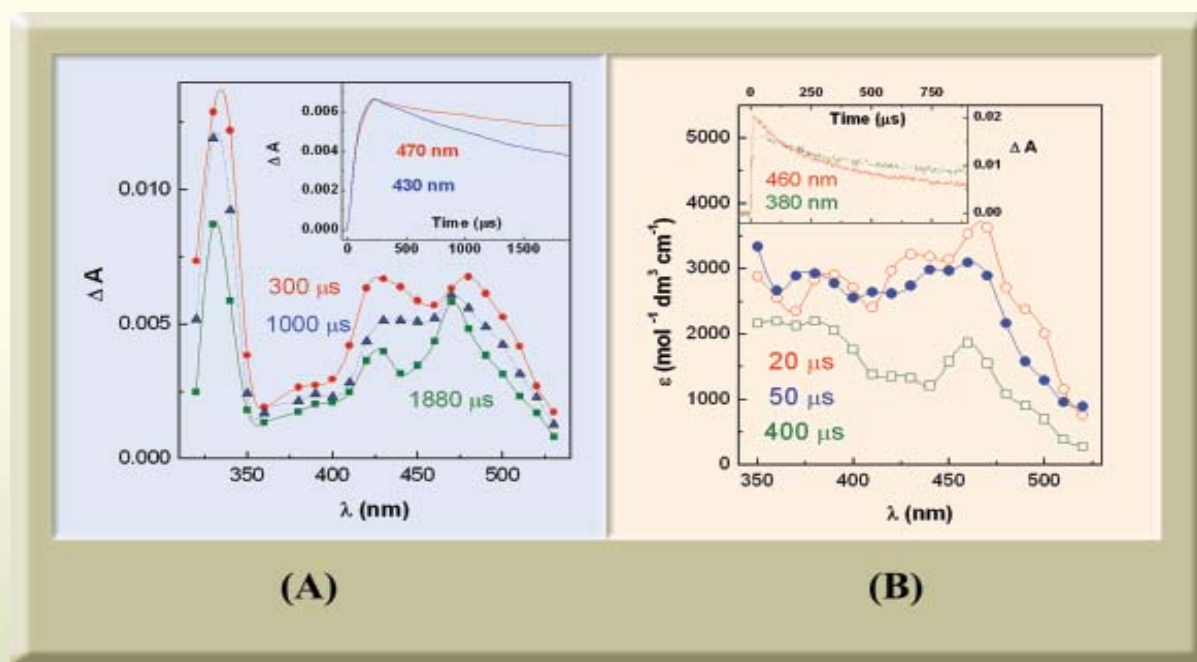


Fig. 3(A) : Reaction of glutathyl radical with 5-ASA at pH 4.1
Inset : kinetic traces under identical conditions

Fig. 3(B) : Reaction of 5-ASA with ascorbic acid at pH 6.8
Inset : kinetic traces under identical conditions

solute-radical adduct into solute radical has not been observed in these cases. SP, however, has not been found to scavenge GS[•] radical.

These studies clearly show that physiologically relevant oxidizing radicals (LO₂[•], Trp[•], GS[•]) are scavenged by the phenoxyl group of 5-ASA whereas the superoxide radical anion is efficiently scavenged by SAZ only.

Reaction of One-electron Oxidized Solutes with Vitamin C

Vitamin C is a well-known water-soluble physiological antioxidant. Transient absorption spectrum for the reaction of one-electron oxidized radical of 5-ASA with AscH[•] has been shown in the Fig.3B. Simultaneous decay of absorption band of 5-ASA[•] (~430 nm) with formation of Asc[•] (~370 nm), and solute-radical complex, (5-ASA[•]...AscH)[•] at ~460 nm is evident from the spectrum. This suggests that 5-ASA[•] is scavenged by vitamin C. Similarly, SP[•] and SAZ[•] have been found to be repaired by vitamin C (AscH[•]).

Conclusion

SAZ, 5-ASA and SP efficiently scavenged various reducing and oxidizing radicals. 5-ASA scavenged glutathyl, tryptophanyl and lipid peroxy radicals also. SAZ scavenged lipid peroxy and superoxide radical. However, 5-ASA and SP have not been found to scavenge superoxide radical. In the antioxidant activity of SAZ, phenoxyl group of 5-ASA has been found to act as an electron (or H-atom) donor. One-electron oxidized SAZ, SP and 5-ASA are scavenged by ascorbate. This study suggests that free radical scavenging activity of 5-ASA may be the major mode of action of SAZ in IBD.

References

1. Ravi Joshi, M. Sudheer Kumar, M. K. Unnikrisnan and T. Mukherjee, *Free Rad. Res.* (2005) **39**, 1163 and references cited therein.
2. (a) A. H. Azad-Khan, J. Piris and S. C. Truelove, *Lancet* **2** (1977) 892. (b) S. Ardizzone and G. B. Porro, *Drugs* **55**, (1998) 519.
3. (a) T. Mukherjee in Ahmad S. A. (1997) *Atomic, Molecular and Cluster Physics*. Narosa, New Delhi. (b) S. N. Guha, P. N. Moorthy, K. Kishore, D. B. Naik and K. N. Rao, *Proc. Ind. Acad. Sci. (Chem. Sci.)* **99**, (1987) 261.

ABOUT THE AUTHOR



Dr. Ravi Joshi (M. Sc.- Chem, MLS Univ. Udaipur) graduated from 38th batch of Training school and joined Chemistry Division, BARC in 1995. He obtained

Ph. D. degree from Mumbai Univ. in 2002. His research interests include free radical reactions of biomolecules, natural products, drugs and solvent effects on chemical reactions.

ELECTRONIC STRUCTURE AND PROPERTIES OF MOLECULES AND CLUSTERS: DENSITY FUNCTIONAL THEORY BASED APPROACH

K.R.S. Chandrakumar
Theoretical Chemistry Section,
Chemistry Group,
Bhabha Atomic Research Centre

The author is the recipient of the Young Scientist Medal of the Indian National Science Academy (INSA), New Delhi for the year 2005.

Abstract

A theoretical basis for the concepts of chemical reactivity, selectivity and stability of molecular complexes has been discussed within the framework of density functional theory. In particular, special attention has been focused on the development of a theoretical formulation to establish a relation between the total energy changes with respect to the changes in the chemical potential and hardness parameters. A model based on local hard-soft-acid-base principle has been proposed to evaluate the intermolecular interaction energy of the molecular complexes in terms of the reactivity descriptors. In addition, we have also presented the quantum size effects on the electronic response properties of alkali metal clusters and some issues on the effects of electron correlation in the evaluation of the polarizability of these clusters. Further, we have briefly outlined the concept of magic clusters and their potential use as building blocks of cluster-assembled materials.

Introduction

Theoretical modelling and simulation methods based on the quantum chemical and statistical theories play a crucial role in understanding the fundamental aspects of a vast range of problems of chemical interest [1,2]. The major goal of theoretical chemistry is the prediction of structure and properties of simple molecules as well as complex materials. In particular, the study of intermolecular interactions is very important for applications in many different fields [3]. The work

presented here focuses on some aspects of the electronic structure and reactivity of molecules and clusters within the framework of density functional theory (DFT) and the work is broadly categorized into two parts. In the first part, the concepts of reactivity descriptors and their application for different class of molecular systems are presented. In addition, a method is provided for the evaluation of the intermolecular interaction energy of the molecular complexes in terms of these reactivity descriptors. In the second part, we discuss the quantum size effects.

Development of Semi-Quantitative Theoretical Models based on the Concepts of Reactivity Descriptors

One of the important questions concerning the molecular interactions is the prediction and interpretation of the preferred direction of a reaction and product formation under different conditions. The study of molecular interactions has been a great challenge from the experimental and theoretical points of view [3]. Although, the quantum chemical methods provide a basic framework to study the molecular interaction rather accurately, the applicability of these methods has been limited to small molecular systems with the precision to the experimental findings. For large molecular systems, these methods become prohibitively expensive from the computational point of view. The molecular orbital wave function obtained from the Hartree-Fock method or highly correlated methods, embodies all the information about the structure, stability and reactivity of the system. However, the wave function containing this information is in such a complex form that is difficult to translate into heuristic concepts and ad-hoc models that are familiar to the chemists [4]. In general, what we need in chemistry, in addition to specific details about individual molecules, is an understanding of how the reactivity of molecular systems is classified within the broad range of molecular systems. Hence, it is necessary to develop very systematic and effective models, which should at least provide the correct qualitative order and a good prediction of the phenomenon involved. Such approximate models or indices have been used in the literature to explain the reactivity of molecular systems, e.g. valency, charge density, delocalization, electrical moments, molecular electrostatic potential and several other molecular orbital indices [1-4].

In recent years, DFT has been shown to provide a framework for the simple physical interpretations of complex reactive phenomena and build a bridge to the chemist's intuitive concepts in an elegant way [5]. The quantification of some of the most widely utilized concepts in chemistry, such as, electronegativity, hardness, softness [6] and the Fukui function or frontier orbitals [3], as realized in terms of the basic parameters in the DFT, presents an important development in quantum chemistry. Using these density-based parameters, two important chemical principles, viz., Hard-Soft Acid-base (HSAB) principle and the principle of maximum hardness, have been proved under some constraints [6]. The development made in this area has illustrated the usefulness of these parameters in a great detail to understand the structure, stability and the chemical reactivity of molecules.

Our work also deals with some aspects of the reactivity of molecular systems using the recently developed density-based descriptors. In particular, an attempt has been made to correlate the reactivity pattern of molecular systems using these descriptors in a semi-quantitative way. Essentially, a method is provided to evaluate the intermolecular interaction energy of the molecular complexes in terms of these descriptors. The basis of these models emerges from the second order energy-density perturbation method using the external potential and the number of electrons as the basic perturbation variables. This model can describe the interaction between the molecular systems occurring only through single sites. The formulation of a theoretical model to describe the intermolecular interactions that are occurring through the multiple reaction sites has also been done. These models have been tested through some of the systems that are well studied experimentally as well as theoretically. The validity

of the approximation that is used in the proposed model is also discussed.

Reactivity Descriptors and their Applications

Some of the chemical phenomena can be understood and predicted by some theoretical quantities that have a direct relationship with the characteristic sets of important chemical properties. These quantities are, in general, called descriptors. The reactivity descriptors are very much pertinent to the reactivity of the molecular systems and are intended to provide a qualitative and semi-quantitative measure of the extent to which a particular site will be affected in a given condition. In the last two centuries, there have been several attempts to explain the nature of bonding and reactivity of molecular systems based on some intuitive ideas, models and empirical rules in terms of the reactivity descriptors [1-6]. These are essentially derived from several experimental observations and many of the chemical facts. These ideas are more *connected* with respect to the small domain of experimental facts rather than to *be systematic* in a general sense and hence, it was only partially successful in explaining the chemical and physical aspects of the systems. It has also been realized that the formulation of a systematic generalization is not so simple from these qualitative ideas and models. This fact is due to the existence of the limitless number of different classes of molecules and consequently, the fascination as well as frustration started emerging out from chemists' community.

Quantum mechanics in terms of molecular orbital theory tried to advance the degree of integration of all the conceptual models and principles, and formed mathematical foundations to it. The development of

quantum chemical methods led to the rigorous definition of many of the empirical chemical concepts and has provided a method for the calculation of the properties of chemical systems and the bonding that is involved in the molecular systems. Among all the important developments in the field of descriptors, some have been remarkably successful in explaining the reactivity of the molecular systems. In particular, the concept of the highest occupied molecular orbital and lowest unoccupied molecular orbital (HOMO-LUMO) developed by Fukui (frontier molecular orbital theory) [3], Woodward-Hoffmann's molecular orbital symmetry [7] and Pearson's hardness and softness concept (HSAB principle) [6]. These descriptors or principles have made a profound impact on our understanding of the experimental observations at the microscopic level in an elegant way. Along with these descriptors, other descriptors have also been proposed, such as charge density and its derivatives, molecular electrostatic potential, electric field, etc. Thus, there have been many such descriptors and all of them have their own merits and demerits in describing various aspects of chemical phenomena.

Among all, the work contributed by Pearson is considered to be one of the most important works and it has been found to be very useful for correlating and better understanding of a very large amount of chemical information in terms of the hard and soft parameters [6]. More over, these concepts have got further momentum after the proposition of HSAB principle by Pearson in 1963 and it became one of the most useful concepts among the chemist's community. The HSAB principle says that there is an extra stabilization if hard acids bind to coordinate with hard bases and soft acids bind to coordinate with soft bases. It is a condensed statement of very large amount of chemical information from experimental observations.

This concept, which found its first applications in rationalizing inorganic stability constants, was shown to be useful even in organic chemistry.

In the present work, we have focused on the developments of the density-based descriptors, such as chemical potential, hardness, softness, Fukui function and their derivatives for the investigation of reactivity of molecular systems in a semi-quantitative way.

The Global and Local Reactivity Descriptors from Density Functional Theory Viewpoint

In DFT, the ground state energy of an atom or a molecule in terms of its electron density $\rho(r)$ is written as [5],

$$E[\rho] = F[\rho] + \int v(r)\rho(r)$$

where $v(r)$ is the external potential that includes the nuclear potential also, and $F[\rho]$ is the universal Hohenberg-Kohn functional composed of the electronic kinetic energy and the electron-electron repulsion energy. The first and second partial derivatives of $E[\rho]$ with respect to the number of electrons, N , for a fixed external potential $v(r)$ are defined as the chemical potential (μ) and the global hardness (η) of the system respectively.

$$\mu = \left(\frac{\partial E}{\partial N} \right)_{v(r)} \quad \eta = \left(\frac{\partial^2 E}{\partial N^2} \right)_{v(r)}$$

The inverse of the hardness is expressed as the global softness, $S = 1/2\eta$. The physical meaning of chemical potential in DFT is the measure of the escaping tendency of an electron cloud from one system to

another. It is constant in three-dimensional space for the ground state of an atom, molecule or solid and equals the slope of E versus N curve at constant external potential. It has also been noted that this parameter is exactly identical with the definition of one of the important concepts, electronegativity. The global descriptor of hardness has been an indicator of overall stability of the system. The parameter hardness is also interpreted as the resistance of the chemical potential to change in the number of electrons or resistance to deformation or change. The minimum value of hardness is zero and it corresponds to the maximum softness. Since these parameters (chemical potential, hardness and softness) are obtained by averaging over atomic or molecular space, these are called as global reactivity descriptors. The site-selectivity of a chemical system, can not be studied using the global descriptors of reactivity. For this, appropriate local descriptors have been derived, particularly, for the cases of local softness $s(r)$ and Fukui function $f(r)$ parameters. The local softness parameter is given by, $s(r) = f(r)S$, where the function $f(r)$ is known as Fukui function,

$$f(r) = \left(\frac{\partial \rho(r)}{\partial N} \right)_{v(r)}$$

These descriptors have been very useful in analyzing many important aspects of the chemical reactions. It has been shown that when any two different sites with similar dispositions interact with another given reagent, the reagent prefers the one which, on the reagent's approach, is associated with the maximum response of the system's chemical potential. In addition, the preferred attack of any molecular system by another is shown to be the one with the largest value of Fukui function at the reaction site. Thus, these theoretical formulations of the chemical potential, hardness and softness parameters have paved a way for the understanding of HSAB principle and many

other chemical principles related to the reactivity of the chemical systems [8].

A Semi-Quantitative Approach for Chemical Reactivity Using Energy Density Perturbation Methods

The global and local reactivity descriptors, as defined above, have been successful in describing about the nature of the reactivity and stability of the molecular systems. They have also substantially helped in laying the foundations of chemical reactivity theory within the framework of DFT. Despite the partial success in describing the reactivity of the chemical systems, such studies have remained primarily qualitative. Although the concepts of hardness and softness parameters permits the organization of a very large number of reactions based on the knowledge of molecular structure and properties of the constituent atoms, it does not provide the reaction energies. It merely predicts interactions between the molecular systems qualitatively. It should also be noted that the transformation of this qualitative principle into a quantitative form has been considered to be one of the challenging and difficult problems. Since the reaction enthalpy is an experimental quantity, the reproduction of this quantity would be a greater challenge than the qualitative reactivity order. The present work focuses on the formulation of such relations and discusses various aspects of chemical binding in terms of these descriptors.

In general, the interaction between the chemical systems can be qualitatively perceived from the evaluation of the responses of a system to any perturbation due to other chemical systems or external fields. In other words, the chemical effects may be described by some suitable response functions of the unperturbed isolated systems.

Such descriptions have been known for many decades ago [3-5]. Examples of such approximate methods are the computation of intermolecular interaction energies in terms of the experimental multipole moments of empirical atomic contributions [9].

In density functional description, chemical binding has been viewed as a result of the reorganization and redistribution of electron density among the atoms in a molecule. Ghanty and Ghosh have proposed such model for studying the process of chemical binding and numerically demonstrated for different chemical reactions using DFT as a starting point [10]. Our quantitative approach is essentially based on the energy density perturbations up to the second order, as a functional of the number of electrons and the external potential. It comprises the energy and density response functions (global and local function) of the reagents, i.e. the response of the electrons to a local or global change of the electron number of the system. The total interaction energy can be partitioned into several terms involving different density response quantities by truncating the perturbation series. This can facilitate the understanding of the role of the individual descriptors in stabilizing the molecular complexes. In our approach, the interaction between the systems A and B is assumed to take place in two steps. In the first step, the interaction takes place at constant external potential through the equalization of chemical potential (ΔE_V). In the second step, the systems A and B evolve toward the equilibrium state through changes in the electron density of the global system, by making changes in the external potential at constant chemical potential (ΔE_μ). The second step is actually a manifestation of principle of maximum hardness. Without going into much details of the derivation, we will now provide the interaction energy expression [11,12],

$$(\Delta E_{\text{int}})_{AB} = \frac{-(\mu_A - \mu_B)^2}{2} \left(\frac{S_A S_B}{S_A + S_B} \right)_v + \frac{-1}{2} \left(\frac{\lambda}{S_A + S_B} \right)_\mu$$

From the local point of view, if the interaction between the systems occurs through the k-th atom of A with the molecular system B, one can express the total interaction energy as,

$$(\Delta E_{\text{int}})_{AK} = \frac{-(\mu_A - \mu_B)^2}{2} \left(\frac{S_A f_{Ak} S_B}{S_A f_{Ak} + S_B} \right)_v + \frac{-1}{2} \left(\frac{\lambda}{S_A f_{Ak} + S_B} \right)_\mu$$

The parameter λ has been defined as,

$$\lambda_A = \sum_i^M N_{A,i}^{eq} - \sum_i^M N_{A,i}^0$$

where the terms $N_{A,i}^{eq}$ and $N_{A,i}^0$ are the number of electrons present in A in the system AB and isolated system A, respectively. This single reactive site model, as initially formulated by Gazquez and coworkers, forms the basis for the local HSAB principle [11]. It states that *the interaction between two molecular systems is favored, when it occurs through those atoms whose local softnesses are approximately equal*. Further, we have extended the above principle for general cases involving many reaction centers present in the systems [13]. In such cases, the interaction can take place by the cooperative or non-cooperative effects, for instance, inter and intra molecular interactions (via multiple hydrogen bonds) present in nucleic acids (DNA and RNA). Accordingly, two models have been

developed, namely Localized Reactive Model and Smeared Reactive Model. The details of these can be referred elsewhere [14].

The developments discussed above have substantially helped in laying the foundations of chemical reactivity theory within the framework of DFT, by relating the structure-reactivity relationships in terms of the reactivity descriptors in a quantitative way. Using these models, we have made an attempt to answer the following questions.

1. How each reactant molecule influences or dominates the other molecule?
2. How important are chemical potential equalization and maximum hardness principle in a reaction?
3. What parameters act as driving forces for the interaction between them so as to have a maximum hardness (stability)?
4. How these individual molecular descriptors determine or distinguish the nature of various types of interactions - covalent, ionic, van der Waals, hydrogen bonding, other short and long range interactions?

In order to validate the reliability of the proposed models, we have considered a wide range of systems that encompasses a variety of chemical reactions, for instance, Lewis acid-base interaction, charge transfer interaction, hydrogen bonding and van der Waals complexes. It has also been demonstrated that the present models can be considered as a tool to monitor the influence of these descriptors in determining the reactivity of several types of complexes in a quantitative way. These developments has actually strengthened the applicability of these reactivity descriptors and broadened its usage in rationalizing different types of the molecular interactions.

Size dependent response properties of Alkali Metal Clusters

Atomic clusters are small particles that bridge the gap between atoms/molecules and condensed matter and exhibit a range of unusual structural, electronic and other properties [15,16]. In recent years, the study of small metal clusters has been a subject of intense interest from experimental as well as theoretical points of view, mainly because of the strong dependence of their electronic structure and properties on their size and geometry. Their physical and chemical properties can even be tuned in desired manner by simply changing the cluster size and the charge in the system. Most of the properties of the materials at the nano scale are often very discrete and oscillating in nature due to the quantum size effects and hence, these small clusters can exhibit properties quite different from the bulk. As the size of the clusters becomes large, the properties of the clusters smoothly saturate to yield the bulk properties [15,16].

Static dipole polarizability is one of the important fundamental properties of any atomic or molecular system and has been well studied by both theoretical and experimental methods [17]. The polarizability indirectly provides a measure of the extent of electron density redistribution under the action of an external electric field. It is quite sensitive to the nature of the bonding and geometrical structure of the clusters. In particular, the study of polarizability of metal and molecular clusters has been considered to be one of the challenging and interesting fields and has emerged as an active research topic in recent years [16]. A fundamental understanding of the size sensitive properties is very essential in view of their potential applications. Such size evolution of properties, such

as, ionization potential, electron affinity, polarizability, binding energy, etc. has been best studied for sodium metal clusters [15,16]. Although the general qualitative trend is found to be similar in all the experimental and theoretical results, the reproducibility of the values is rather poor in both the results. Thus, a reliable and systematic all electron calculation of the polarizability by accurate theoretical methods is essential to resolve the ambiguity present in the experimental as well as theoretical results. Accordingly, some of the pertinent questions have been addressed, especially on the study of the static dipole polarizability of sodium and lithium clusters using the post Hartree-Fock as well as density functional methods with different exchange-correlation functionals, thus making a critical appraisal on the polarizability values obtained by various theoretical as well as experimental methods.

Another important issue is concerned with the study of the relationship between the important molecular properties, viz., the polarizability and the ionization potential of the systems. The concept of relating these two quantities is still one of the long-standing problems in the area of chemical physics [17]. In addition, the reactivity of these metal clusters can also be studied from DFT based descriptors, namely, the chemical potential, global hardness and softness parameters. Since the polarizability of the systems can be directly related to the global softness of the systems, an attempt has also been made to relate the softness and polarizability of the metal clusters. Moreover, a correlation between the binding energy and polarizability of alkali metal clusters has also been studied by invoking the minimum polarizability principle [18].

Our results on the polarizability of sodium clusters reveal that all the pure DFT functionals (except the now

Hartree-Fock exchange along with one-parameter functional) have been found to considerably underestimate the calculated polarizability values as compared to the MP2 results [19]. One of the most important conclusions of this study is that the effect of electron correlation plays a significant role in determining the polarizability of the clusters and MP2 method can be considered to be one of the most reliable methods for their prediction. The polarizability and the binding energy of the clusters are found to be inversely related to each other and their correlation is rationalized by invoking the minimum polarizability principle. A good linear correlation between the polarizability, ionization potential, softness and volume of the clusters has been shown to exist [18].

Similarly, the effect of electron correlation on the estimation of polarizability of lithium clusters has been carried out by *ab initio* and DFT methods [21]. Comparing the polarizability of the lithium with sodium clusters, we find some unusual features on the size evolution of the polarizability of lithium clusters. Some of the important remarks are as follows. (1) the electron correlation has insignificant role on the evaluation of polarizability of the lithium clusters (2) since the polarizability values are much sensitive to the temperature, it is normally expected that the zero temperature polarizability values would be less than the experimental results which are carried out at high temperature. In the present case, however, we observe that the polarizability trend is reversed.

The Concept of Magic Clusters and Cluster Aggregation

The main motivation in pursuing the subject of cluster science is to design novel (cluster-assembled) materials with unique and size-specific properties [21]. We will

briefly discuss the problems associated with the assembly of clusters. Since the clusters are generally metastable, they have a tendency to coalesce when they are brought or assembled together. This poses an interesting and challenging problem in the area of cluster-assembled materials. Different ways have been followed to stabilize such metastable clusters, for instance, by trapping these clusters in different matrices or by coating those clusters by other suitable ligands. An alternative route is to find the clusters, which are so stable that the intracluster interaction is stronger than the intercluster interactions. Such types clusters will tend to regain their individual identity even in the assembled materials. In this context, the nature of the interaction between two metal clusters becomes very important. It has been recognized that the structural identity of the individual clusters in the assembly can be best retained if they belong to the class of magic clusters, which arise due to shell closings of the associated valence electrons. As is well known, the magic clusters are in general associated with exceptional stability as reflected through peaks in the mass spectra, high ionization potential, low electron affinity, high symmetry and reduced reactivity [16].

In this connection, we have investigated the properties of the two clusters TiAu_4 and ZrAu_4 to evaluate the extent to which they belong to the class of magic clusters in the context of cluster-assembled materials and studied the process of their dimer formation [22]. The objective has been to probe if these two clusters satisfy all the criteria mentioned above for being magic clusters and hence forming the building blocks for cluster-assembled materials. Our results reveal that the Ti and Zr doped gold clusters have tetrahedral structures and are found to be associated with large values of the ionization potential, HOMO-LUMO gap as well as the binding energies, which are characteristic of the magic clusters. However, the cluster-cluster interaction energy

corresponding to a dimer formation is found to be unusually high (5 – 7 eV) in contradiction to the usual properties of a magic cluster and is attributed to a 3-center–2-electron M–Au–M type bridge bonding as well as aurophilic attraction. Based on these observations, it has been concluded that the requirement of a weak inter-cluster interaction may be relaxed if the condition of retention of identity in the assembled materials is satisfied. In addition, we have also remarked that the conventional ideas of magic clusters may have to be reframed to judge their suitability as building blocks for cluster assembled materials. These results will have some important implications in the design of novel cluster-based nanomaterials for various nanoscale applications.

Concluding Remarks

Theoretical developments made towards the broad subject of chemical reactivity using the quantum chemical methods are briefly discussed. We have also described how the empirical conceptual ideas (electronegativity, chemical potential, hardness, softness, etc.) have been theoretically quantified within the framework of DFT. Their successes as well as failures in predicting the reactivity of molecular systems have also been discussed. We have outlined the energy-density perturbation methods within the domain of DFT and the different semi-quantitative models, including local HSAB principle, in finding a direct correlation between the density based descriptors and the molecular stabilization or interaction energy.

Further, the size dependent response properties of sodium and lithium metal clusters are presented. We have found that the electron correlation is found to play a major role in evaluating the polarizability of sodium metal clusters while for the lithium clusters, the electron correlation effects are found to be

insignificant. The relationship between polarizability with softness, ionisation potential and binding energy of the neutral clusters has also been discussed. In addition, we have explained the concept of magic clusters and the necessary conditions as well as the various factors that govern the assembly of clusters.

Acknowledgements

It is a pleasure to thank Dr. Sourav Pal and Dr. Swapan K Ghosh for their kind interest and encouragement. I also wish to acknowledge Dr. T. K. Ghanty and others who have contributed to the present work. I am also thankful to Dr T. Mukherjee for his encouragement.

References

1. Pauling, L. *The Nature of Chemical Bond and Structure of Molecule and Crystals* (1967) Oxford University Press.
2. Mc Weeny, R. *Coulson's Valence*, (1979) Oxford University Press, Oxford.
3. Fukui, K. *Theory of Orientation and Stereo Selection* (1975), Springer-Verlag, Berlin.
4. Klopman, G. *Chemical Reactivity and Reaction Path*, (1974), Wiley, New York.
5. Parr R G and Yang W, *Density Functional Theory of Atoms and Molecules* (1989) (Oxford Univ. Press, New York).
6. Pearson, R. G. *Chemical Hardness: Applications from Molecules to Solids* (1997) Wiley-VCH Verlag GMBH: Weinheim.
7. Woodward, R. B.; Hoffmann, R. *The Conservation of Orbital Symmetry* (1989) New York, Academic Press.
8. Geerlings, P.; De Proft, F. and Langenaeker, W. *Chem. Rev.* **103** (2003), 1793.
9. Stone, A. J. *The Theory of Intermolecular Forces*.

- (1996) Oxford University Press, New York.
10. (a) Ghanty, T. K.; Ghosh, S. K.; *J. Phys. Chem.* **95** (1991) 6512. (b) *ibid. Chem. Comm.* (1992) 1502.
 11. (a) Mendez, F; Gazquez, J. L. *J. Am. Chem. Soc.* **116** (1994) 9298; (b) Gazquez, J. L. *J. Phys. Chem. A* **101** (1997) 9464; (c) Gazquez, J. L. *J. Phys. Chem. A* **101** (1997) 8967.
 12. Pal, S; Chandrakumar, K. R. S. *J. Am. Chem. Soc.*, **122** (2000) 4145.
 13. (a) Chandrakumar, K. R. S.; Pal. S. *J. Phys. Chem. B* **105** (2001) 4541; (b) *ibid. J. Phys. Chem. A* **106** (2002) 5737.
 14. Chandrakumar, K. R. S. *Theoretical Studies on Some Aspects of Chemical Reactivity Using Density based Descriptors*, Ph. D. Thesis submitted to Pune University, India (2002).
 15. Moskovits, M. *Annu. Rev. Phys. Chem.* **42** (1991) 465.
 16. (a) De Heer, W. A. *Rev. Mod. Phys.* **65** (1993) 611; (b) Brack, M. *Rev. Mod. Phys.* **65** (1993) 677.
 17. Hohm, U. *Vacuum* **58** (2000) 117.
 18. Chandrakumar, K. R. S.; Ghanty, T. K. Ghosh, S. K. *J. Phys. Chem. A* **108** (2004) 6661.
 19. Chandrakumar, K. R. S.; Ghanty, T. K. Ghosh, S. K. *J. Chem. Phys.* **120** (2004) 6487.
 20. Chandrakumar, K. R. S.; Ghanty, T. K. Ghosh, S. K. *Int. J. Quan. Chem.* **105** (2005) 166.
 21. Alivistaos, A. P. *J. Phys. Chem.* **100** (1996) 13226.
 22. Ghanty, T. K.; Chandrakumar, K.R.S. and Ghosh, S. K. *J. Chem. Phys.* **120** (2004) 11363.

ABOUT THE AUTHOR



Dr K.R.S. Chandrakumar is currently working in the Theoretical Chemistry Section, Chemistry Group. He joined BARC as a K.S. Krishnan Research Associate (6th batch) in 2003 after completing his Ph. D. from Pune University, working at the National Chemical Laboratory, Pune. He is also the recipient of young scientist award from Indian Science Congress Association for the year 2002. His research interests are in general theoretical chemistry, hydrogen generation and storage, cluster-assembled materials, electronic structure and properties metal and carbon nano tubes, etc.

DENSITY CONCEPT IN MOLECULES AND MATERIALS MODELING AT DIFFERENT LENGTH SCALES

Swapan K. Ghosh
Theoretical Chemistry Section,
Chemistry Group,
Bhabha Atomic Research Centre

The author is the recipient of the Silver Medal of the Chemical Research Society of India (CRSI), Bangalore for the year 2005.

Abstract

The basic ideas underlying the versatile uses of the concept of density in the modeling of molecules and materials, as visualized in various length scales, are outlined. In the microscopic length scale, it is the electron density that has played a major role in providing a deeper understanding of chemical binding in atoms, molecules and solids. In the intermediate mesoscopic length scale, an appropriate picture of the equilibrium and dynamical processes has been obtained through the single particle number density of the constituent atoms or molecules. A wide class of problems involving nanomaterials, interfacial science and soft condensed matter has been addressed using the density based theoretical formalism as well as atomistic simulation in this regime. In the macroscopic length scale, however, matter is usually treated as a continuous medium and a description using local mass density, energy density and other related density functions has been found to be quite appropriate. The unique single unified theoretical framework that emerges through the density concept at these diverse length scales and is applicable to both quantum and classical systems is the so called density functional theory (DFT) which essentially projects the many-particle picture to a single particle one. Selected illustrative applications through examples of the electron density based microscopic modeling of chemical binding as well as intermolecular interaction and classical density based mesoscopic physics of soft condensed matter systems with particular reference to confined fluids are presented.

Introduction

Advances in modern science and technology can be intimately linked with the dream of discovering molecules and materials with properties and functions

tailored to intended applications. Modeling and simulation thus play a major role in molecule and materials design which has been one of the important and broad areas of research in recent times. A major challenge that one faces, however, arises due to the wide

range of length and time scales involved in the act of modeling. Although at the fundamental level, the properties of materials are dictated by the basic laws of quantum mechanics, their prediction through a direct ab-initio electronic structure calculation is often too ambitious even with the state of the art computational techniques and resources. One can, however, view the materials through the windows of different length scales and develop modeling in three broad domains, viz. microscopic, mesoscopic and macroscopic regimes covering the length scales of 0.1-1 nm, 1-100 nm and larger than 100 nm respectively.

In the macroscopic length scales, matter is considered as a continuous medium and the theoretical tools used are the conventional approaches of continuum mechanics and hydrodynamics of classical physics. The property parameters needed in this approach as input can be obtained from a consideration of the so called mesoscopic length scale with an atomistic description using classical and statistical mechanics of interacting particles (atoms and molecules), their movements and distributions. The major input parameters in this intermediate length scale are the interparticle interactions which can be generated through a quantum mechanical investigation within the microscopic length scale. In this shorter length scale, one can deal with the interacting electrons and the nuclei, employing a complete ab-initio electronic structure description within the framework of available approximate theories.

Although the electronic, atomistic and continuum descriptions for materials modeling at the three respective length scales appear to be quite diverse, there lies a unified theoretical framework which can encompass all of them and the present work aims at presenting a glimpse of this area of research. The concept

that plays the role of a common underlying thread in this endeavour is the concept of density and the associated theoretical approach is the density functional theory (DFT) [1-5].

In the microscopic length scale, the DFT based description of a many-electron system employs the single-particle electron density [6] as the basic variable bypassing the many-electron wavefunction, providing thereby tremendous simplification, computational economy and foundation of widely used chemical concepts. DFT has also been formulated [7] for the mesoscopic length scale, with the density distribution of the atomistic particles as the basic variable, leading to wide applications in the field of soft condensed matter [8] physics. The recent upsurge in nanomaterials research has also led to greater opportunities for materials modeling in this mesoscopic size regime. The effective interparticle interaction potentials needed for the mesoscopic DFT can be obtained through the microscopic or quantum DFT either through a detailed electron density calculation or a modeling of chemical binding using DFT based atomic parameters. One can also couple the interatomic potential calculation based on quantum DFT for electrons with the classical mesoscopic DFT for the atomistic particles in the spirit of the well known Car and Parrinello [9] approach for DFT based ab-initio simulation. For simplicity, one can also employ empirical pair potentials in the mesoscopic DFT as is often done in usual classical simulation. In the domain of macroscopic length scale, a density based continuous medium description is possible using the mass, current, energy and other property densities as the basic variables, reminiscent of the classical hydrodynamics.

Thus, in DFT as applied to materials modeling [10] in

the short, intermediate and large length scales, the respective basic variables are the electron density, the single particle number density and the property density, corresponding to the electron, atom and the volume element as the respective building blocks. A central common feature in DFT is the collection of building blocks with an inhomogeneous density distribution arising due to the field of an external potential. However, there are many phenomena such as freezing, nucleation, crystallization, formation of liquid crystals, micelles etc. where the density inhomogeneity is created through stabilisation of thermal density fluctuations even in absence of external potentials.

Besides the DFT corresponding to different individual length scales, many of the areas of materials science and engineering dealing with the material properties needs a bridging of the microscopic, mesoscopic and macroscopic length scales. Building such bridges can enhance the possibility of opening new windows to view the details of the microstructure which determines the properties of different forms of matter that matters in many applications of interest.

We present here a unified view of the density concept as applied to diverse situations and length scales as mentioned above with the aim of solving the many-particle problem through a single-particle picture. An important and unique feature of the description is that it provides a common unified framework for quantum as well as classical systems encompassing the diverse length scales involved in materials modeling highlighting the interconnections among the various approaches. Thus, we first discuss the basic theoretical formalism of quantum and classical DFT as used in different regimes of length scales and then consider in the next section, a specific application of quantum DFT for the modeling of chemical binding to obtain the

interatomic potential that can be used in the mesoscopic DFT. This is followed by discussion of DFT based modeling in soft matter. Besides the equilibrium aspects, the density viewpoint also covers the study of response properties as to how a material evolves and can cope with an applied stress. Thus, extension beyond the equilibrium situations covering some of the dynamical aspects is also discussed.

A Unified Density Functional Theory of Quantum and Classical Systems

The single-particle density $\rho(r)$ which is the basic variable in DFT, is defined, for an N-particle quantum or classical system, by integrating the full distribution function $P(r_1, r_2, \dots, r_N)$ over N-1 variables, as

$$\rho(r_1) = N \int dr_2 \int dr_3 \dots \int dr_N P(r_1, r_2, \dots, r_N)$$

For a quantum system, the distribution function $P(r_1, r_2, \dots, r_N)$ is given by $|\Psi(r_1, r_2, \dots, r_N)|^2$ where $\Psi(r_1, r_2, \dots, r_N)$ is the many-electron wave function. The density variable which is a function in three-dimensional space and represents locally the number density clearly satisfies the normalisation $\int dr \rho(r) = N$. For interacting particles, the possibility of describing a quantum or classical many-particle system completely in terms of the single-particle density is not obvious and has been established rigorously through the theorems proved by Hohenberg and Kohn [1] and Mermin [3]. Although the birth of a formal DFT is rather recent, approximate versions of DFT have existed for a very long time in the forms of the Thomas-Fermi and Debye-Huckel theories for quantum and classical systems respectively dealing with the distribution of electrons around the nuclei in atoms and that of ions in electrolyte solutions. In spite of a wide difference in the nature of these systems, the two approximate theoretical descriptions have close similarities.

For a many-particle system characterized by an external potential $v(r)$ (arising due to the nuclei in the case of electrons and due to the walls or pores in the case of confined classical fluid particles), the proofs of Hohenberg-Kohn-Mermin [1,3] follow by establishing a one to one mapping between the density and the potential. In the resulting formal DFT, the ground state energy $E_v[\rho]$ (for a many-electron quantum system) or, the grand potential $\Omega_v[\rho]$ (for a many-particle classical system) is treated as the unique functionals of density, given respectively by

$$E_v[\rho] = F[\rho] + \int dr \rho(r)v(r),$$

and

$$\Omega_v[\rho] = F[\rho] + \int dr \rho(r)[v(r) - \mu],$$

with μ denoting the chemical potential [11]. The true equilibrium densities in both cases are determined by the Euler-Lagrange equations corresponding to the minima of the respective energy density functionals, as given by

$$\mu = v(r) + \delta F[\rho] / \delta \rho(r)$$

For many-electron systems, the functional $F[\rho(r)]$ is universal and can be expressed as

$$F[\rho] = T_s[\rho] + E_{\text{coul}}[\rho] + E_{\text{xc}}[\rho],$$

where $T_s[\rho]$, $E_{\text{coul}}[\rho]$ and $E_{\text{xc}}[\rho]$ represent respectively the non-interacting kinetic energy, classical Coulomb energy and the exchange-correlation (XC) energy density functionals.

For a classical fluid with inhomogeneous density distribution [7], the functional $F[\rho(r)]$ representing the

intrinsic Helmholtz free energy is universal only for a specified inter-particle interaction and can be expressed as

$$F[\rho] = F_{\text{ideal}}[\rho] + F_{\text{excess}}[\rho]$$

where $F_{\text{ideal}}[r(r)]$ represents the ideal-gas free-energy functional corresponding to absence of internal interactions and is the analogue of the non-interacting kinetic energy functional $T_s[\rho]$ for quantum systems, while $F_{\text{excess}}[\rho(r)]$ representing the excess free energy for the classical system is analogous to the interaction energy functional ($E_{\text{coul}}[\rho] + E_{\text{xc}}[\rho]$) of a quantum system.

For quantum systems, a minimisation of the energy functional $E_v[\rho]$ with the known exact expression of $E_{\text{coul}}[\rho]$, neglect of $E_{\text{xc}}[\rho]$ and the so called local density approximation for the kinetic energy functional leads to the well known Thomas-Fermi theory. On the other hand, using the known exact expression for $T_s[\rho]$, in the energy functional, one obtains, on minimization, the effective one-particle Kohn-Sham equation [2], viz.

where the orbitals $\{\psi_k\}$ define the density $\rho(r)$ as the sum $\rho(r) = |\psi_k|^2$ and the effective potential is given by the density functional

$$v_{\text{eff}}(r; [\rho]) = v(r) + [\delta E_{\text{coul}} / \delta \rho(r)] + [\delta E_{\text{xc}} / \delta \rho(r)]$$

Analogously, for a classical system, on using the known exact expression for the ideal-gas free energy functional $F_{\text{ideal}}[r(r)]$, the Euler-Lagrange equation leads to the density equation

$$\rho(r) = \Lambda^{-3} \exp[\beta_0 \mu] \exp[\beta_0 v_{\text{eff}}(r; [\rho])]$$

where Λ is the thermal de-Broglie wavelength and β_0 ($=1/k_B T$) is the inverse temperature. This equation represents essentially a Boltzmann-like distribution of an ideal gas in the field of an effective potential v_{eff} given by

$$v_{\text{eff}}(r) = v(r) + [\delta F_{\text{ex}}[\rho] / \delta \rho(r)],$$

with the last term representing the first order direct correlation function (DCF) provides the extra contribution to the effective potential, arising from interparticle interactions and correlations in analogy to the exchange-correlation contribution to the Kohn-Sham potential for quantum systems. The Debye-Huckel theory can be obtained from an extension of this exact classical DFT to a two-component ionic system with an approximation of the excess free energy functional as the pure Coulomb contribution.

It is thus clear that DFT provides a formally exact single-particle framework for many-particle systems, providing the density distribution through that of a system of non-interacting particles, viz. the one-particle Schrodinger equation for a quantum system and Boltzmann-like distribution for classical particles. This has emerged through an exact mapping of the actual system of N interacting particles in the field of an external potential $v(r)$ to another model system of N non-interacting particles of the same density $\rho(r)$ but moving in an effective potential $v_{\text{eff}}(r; [\rho])$, itself depending on the density, thus requiring a self-consistent iterative procedure for solving the resulting equations.

Although the DFT framework is exact, the crux of the problem lies in the fact that the exact form of the density

functionals is not known for an inhomogeneous density distribution and hence approximations are needed for the XC energy functional $E_{\text{xc}}[\rho]$ for quantum systems, and the excess free energy functional $F_{\text{ex}}[\rho]$ or its derivatives for classical systems. The approximate procedures usually are based on the knowledge of the functionals for the corresponding systems with homogeneous density. The simplest approximation scheme is the so called local density approximation (LDA) where the expression for the energy functional of the homogeneous system is directly evaluated using the inhomogeneous density. While this approximation is reasonable for many-electron systems, for the excess free energy of the classical systems where the particle sizes are finite, the so called weighted density approximation (WDA) where an effective density, obtained by coarse graining of the actual density distribution $\rho(r)$ with a suitable weight function has been found to be a successful approach [12]. Other procedures include improvements of LDA by including the gradient corrections for quantum systems and functional perturbation techniques in the theory of fluids [13]. Although the discussion so far has been restricted to a single density quantity, it may be noted that the spin-polarized quantum systems and the classical two-component fluid mixtures can also be treated through analogous unified DFT descriptions by considering the two spin components of the density and the individual component densities as the respective basic variables. In the following Sections, we consider specific illustrative applications of these generalized DFT for two-component systems for quantum as well as classical systems.

Microscopic Density Modeling of Interatomic Interaction Potential: A Light Approach to a Sound Interpretation

The electron density based quantum DFT has been highly successful in the electronic structure calculation of atoms, molecules, clusters and solids. The interatomic or intermolecular interaction potential obtained through such an ab-initio calculation using suitable XC energy functionals can be used in the study of mesoscopic DFT or computer simulation in the atomistic length scale. In this work, however, we discuss a simpler and appealing alternative model which is based on the conceptual aspects of quantum DFT, the basic foundation of which lies in the chemical potential equalisation within a many-electron system which can be generalised to the spin-polarised situation [14,15] as

$$\begin{aligned}\mu_{\alpha} &= v(r) + \delta F[\rho_{\alpha}, \rho_{\beta}] / \delta \rho_{\alpha}(r); \\ \mu_{\beta} &= v(r) + \delta F[\rho_{\alpha}, \rho_{\beta}] / \delta \rho_{\beta}(r).\end{aligned}$$

Here, μ_{α} and μ_{β} are the up- and down-spin chemical potentials which correspond to the spin-polarised version of the energy functional, expressed as functionals of the two spin-component densities $\rho_{\alpha}(r)$ and $\rho_{\beta}(r)$, as

$$E[\rho_{\alpha}, \rho_{\beta}] = F[\rho_{\alpha}, \rho_{\beta}] + \int dr \rho(r) v(r)$$

We propose to obtain the energy change in a many-electron system arising from a reorganization of its electron density through a functional Taylor expansion [16] (up to second order) in terms of the density changes $\delta \rho_{\nu}(r)$ (for $\nu = \alpha, \beta$) as

$$\begin{aligned}\Delta E &= \sum_{\nu} \mu_{\nu} \delta \rho_{\nu}(r) \\ &+ \frac{1}{2} \sum_{\nu} \sum_{\nu'} \int dr \int dr' \eta_{\nu, \nu'}(r, r') \delta \rho_{\nu}(r) \delta \rho_{\nu'}(r')\end{aligned}$$

where the hardness kernel [17,18] $\eta_{\nu, \nu'}(r, r')$ represents the energy functional derivative $[\delta^2 F[\rho_{\alpha}, \rho_{\beta}] / \delta \rho_{\nu}(r) \delta \rho_{\nu'}(r')]$. It also determines the corresponding changes in the two chemical potentials μ_{α} and μ_{β} .

The objective now is to develop a lattice model of a set of interacting atoms (say, M in number) located at the fixed positions (lattice sites) $\{R_i\}$ corresponding to a particular (say, equilibrium) configuration and express the density change due to the interaction between the atoms by partitioning it as a sum of the atomic contributions as $\delta \rho_{\nu}(r) = \sum_i \delta \rho_{\nu, i}(r_i)$, with $\{r_i\}$ denoting the atomic region around the i-th atomic site location $\{R_i\}$. Without loss of generality, for simplicity, we assume the density components $\delta \rho_{\nu, i}(r)$ to vanish outside this region r_i belonging to the i-th site. After Taylor series expansion of the hardness kernel around the atomic sites retaining the first order term and proper regrouping of the terms, the final expressions for the interaction energy and chemical potentials of the individual atoms can be written in terms of the charges and dipole moments at the atomic sites [16]. For simplicity, we write here only the atomic charge contributions given by

and

$$\begin{aligned}\Delta E &= \sum_{\nu} \sum_i \mu_{\nu}^0(i) q_{\nu}(i) \\ &+ \frac{1}{4} \sum_{\nu} \sum_{\nu'} \sum_i \sum_j \eta_{\nu, \nu'}(i, j) q_{\nu}(i) q_{\nu'}(j)\end{aligned}$$

where $q_{\nu}(j) = \int dr_j \delta \rho_{\nu}(r_j)$ denotes the charge at the j-th atomic site. The lattice model of the set of interacting atoms thus correspond to a set of point charges (zeroth moment of the density) located at the M lattice sites. An equalization of the effective chemical potentials corresponding to each spin as given

by the above equations for all the M atomic sites leads to M-1 linear equations in the charge variables for each spin which along with the charge conservation condition yield the individual site charges. It may be noted that while the conventional chemical potential equalization schemes which usually consider only the net charges on atomic sites predict only zero charge and interaction among identical atoms, the present scheme which consider spin-dependent charge can predict the interaction energy even for similar atoms if the atoms concerned are open shell ones. This scheme has been further generalized by considering the bond sites between the bonded atoms in addition to the atomic sites. While the form of the final equations remains the same, the number of sites and linear equations for obtaining the site and bond charges for each spin become larger in number.

The final energy expression given above is reminiscent [14] of the binding energy of molecules as obtained by semiempirical quantum chemistry and calculations based on this procedure lead to binding energies and partial atomic charges of homonuclear as well as heteronuclear simple molecular systems [15,19] in good agreement with more detailed ab-initio calculations. The present formalism has also resemblance to the Miedema model for predicting the heat of formation of simple alloy systems. It is also expected to play an important role in the investigation of cluster-assembled materials [20].

The input parameters in the present approach [16] are the chemical potentials of the constituent atoms and also the diagonal and off-diagonal elements of the hardness matrix $\eta_{\nu,\nu'}(i,j)$ corresponding to different spins and sites. The atomic chemical potentials and the corresponding diagonal hardness parameters of each atom can be obtained from spin-

polarised DFT calculations. If bond sites are used, the corresponding chemical potential and hardness parameters can be approximated by suitable averaging of the corresponding values for the bonded atoms. The off-diagonal (i'j) elements of the hardness kernel can be modeled by using the atom-in-molecule hardness matrix concept generalised to spin-polarised situation following an electrostatic analogy. The Coulomb potential approximation is quite suitable for a nonbonded pair of sites, while for bonded sites, a better modeling along the lines of semiempirical quantum chemistry is found to be more appropriate. The simplified DFT framework presented here provides a simple scheme for predicting the interatomic interaction potential and hence the forces which can be used in computer simulation as well as in mesoscopic DFT to be discussed in the next Section.

Mesoscopic DFT: Application to Soft Condensed Matter

The DFT in the mesoscopic regime involves atomistic length scale and uses the single-particle number density as the basic variable. An important application that is considered here is in the area of soft condensed matter systems where the collective interaction and correlation effects are known to play important role and thus the DFT formalism is a highly effective tool [21] for the study of these many-body systems. The building blocks in this intermediate mesoscopic length scale are the atomistic particles and thus a typical system that is considered here is a two-component fluid mixture, with specified interparticle interaction $\phi_{\mu\nu}(r_{12})$ with μ and ν denoting the two components, which can be obtained either through a microscopic DFT calculation or by using simple models such as hard sphere or Lennard-Jones (for neutral species), charged hard sphere (for ionic fluids), DLVO screened Coulomb (for colloids) etc. In particular, our interest is

in the equilibrium arrangement of the fluid particles at interfaces due to confinement of the fluid mixture, for example, in a planar slit, spherical cavity or cylindrical pore. The fluid components are subjected to the external potentials $v_\alpha(r)$ and $v_\beta(r)$ which lead to the inhomogeneous density distributions $\rho_\alpha(r)$ and $\rho_\beta(r)$ and are considered to be in equilibrium with the corresponding bulk phase of component densities and chemical potentials as ρ_α^0 , ρ_β^0 and μ_α , μ_β respectively.

Minimization of the two-component generalized grand potential and subsequent equalization of the chemical potentials of the two components with those of corresponding bulk phases, lead to the Euler-Lagrange equations given by

$$\rho_\nu(r) = \rho_\nu^0 \exp[-\beta_0 v_{\nu,eff}(r; [\rho_\alpha, \rho_\beta])]$$

which is of Maxwellian form corresponding to an ideal gas subjected to the effective potential given by

$$v_{\nu,eff}(r; [\rho_\alpha, \rho_\beta]) = v_\nu(r) + c_\nu^{(1)}(r; [\rho_\alpha, \rho_\beta]) - c_\nu^{(1)}([\rho_\alpha^0, \rho_\beta^0])$$

where the first order direct correlation function $c_\nu^{(1)}(r; [\rho_\alpha, \rho_\beta]) = [\delta F_{excess}[\rho_\alpha, \rho_\beta] / \delta \rho_\nu(r)]$ and the excess free energy are contributed by inter-particle interaction and correlation.

In absence of knowledge of the exact functionals for an inhomogeneous density distribution, one can consider its functional Taylor expansion in powers of the density inhomogeneity. The second order DCF which is often known for some model pair potentials can be used for this purpose and the third order DCF if needed can also be approximated in terms of the second order DCF. The parameters introduced in the approximation are often evaluated by demanding the

approximate density functional to yield the correct bulk partial pressures in the homogeneous limit. We have also proposed alternative routes for evaluating the correlation function using the bridge function concept of integral equation theory of homogeneous fluid mixtures.

Besides these fully or partially perturbative approaches, one can also employ nonperturbative WDA based methods, where the basic approach is to approximate terms of all orders by evaluating the excess free energy or the first order DCF at suitable effective weighted densities. In the partially nonperturbative approaches, WDA is used to evaluate the short range contribution to the first-order DCF and for the long range contribution, one employs a functional perturbative expansion. A typical application that has been considered involves the structure of electrode-electrolyte interface, with the ionic components modeled as charged hard spheres, and the solvent as a dielectric continuum. For this restricted primitive model, the long range contribution leads to an electrostatic potential analogous to that in the many-electron systems and the short range correlation is evaluated through WDA or functional perturbative method. For walls or cavities of planar, spherical or cylindrical shapes, the density variation is along only one coordinate and hence the numerical calculation becomes much simpler.

An important consequence of the inhomogeneous density distribution at the interfaces is the solvation or structural force which can be directly measured experimentally. The interaction between colloidal particles in a suspension is also essentially an interaction between the overlapping electric double layers. DFT has been used successfully to predict the solvation force for simple liquids and the results are in

good agreement with simulation results. We have also calculated the interaction energies between the walls for a neutral liquid and have been able to reproduce the experimental results for a real liquid quite well by choosing a suitable value for the hard sphere diameter. The DFT approach has also been used to calculate the interaction between colloidal particles. There is also interest in the study of the effect of surface induced inhomogeneity in density and the surface forces on the dynamics in condensed phase.

Besides these cases involving density inhomogeneity as a consequence of external potential due to confinement, there are situations where one has spontaneous appearance of density inhomogeneity, for example, in phase transitions. Here thermal density fluctuations leading to density inhomogeneity get stabilised at suitable values of the external parameters such as temperature, density etc. DFT has been quite successful in its prediction of the phase transition from liquid phase to an ordered phase due to the pioneering works of Ramakrishnan and Yussouff [22] who laid the foundation of the DFT of freezing. The theory employs the free energy or the grand potential functionals to locate the physical parameters at which the ordered phase with an inhomogeneous periodic density distribution is energetically more stabilised as compared to the uniform density fluid phase. The original theory has been extended and applied extensively to a large class of soft matter systems including colloidal suspensions, liquid crystals and other forms of complex fluids. With a simple modeling of the interfacial density as a decaying oscillatory function in the perpendicular direction and periodic in the parallel plane, DFT has been able to predict the surface energy as a function of the number of interfacial layers in good agreement with simulation results. Application to various other phase transitions,

nucleation and many other phenomena has also been found to be quite successful.

Density Functional Theory of Dynamical Phenomena

The applicability of DFT is not restricted to equilibrium situations alone, but is extended to time-dependent (TD) situations [23-25] for both quantum and classical systems. The basic variables involve the TD density $\rho(r,t)$ and TD current density $j(r,t)$. The TD DFT for quantum systems involves the TD one-particle Kohn-Sham like equations of the form

$$[-(\hbar^2 / 2m)\nabla^2 + v_{\text{eff}}(r,t;[\rho, j])]\psi_k(r,t) = i\hbar[\partial\psi_k(r,t) / \partial t]$$

where the orbitals $\{\psi_k(r,t)\}$ define the density $\rho(r,t)$ and the current density $j(r,t)$ as the sum

$$\rho(r,t) = \sum_k |\psi_k(r,t)|^2 \quad \text{and} \quad j(r,t) = (i\hbar / 2m) \sum_k [\psi_k(r,t)\nabla\psi_k^*(r,t) - \psi_k^*(r,t)\nabla\psi_k(r,t)]$$

while the effective potential is given by a density functional derivative analogous to that for the time-independent situations, but is determined by density as well as the current density.

There is also an equivalent quantum hydrodynamic formulation [6] consisting of the continuity equation corresponding to the time evolution of the density given by

$$(\partial\rho(r,t) / \partial t) + \nabla \cdot j(r,t) = 0$$

and an Euler type equation for the time-evolution of the current density as

$$(\partial j(r,t) / \partial t) = -\rho(r,t)\nabla[v(r,t) + (\delta F / \delta\rho)] - \nabla \cdot (jj / \rho)$$

which are reminiscent of the conventional hydrodynamic

equations and differ only in the additional force of quantum origin which augments the classical force. A local thermodynamic picture [26] of the electron cloud has also emerged and has led to simpler approaches [27] to the calculation of various properties.

The classical TD DFT consists of the same continuity equation and a modified equation for the current density, involving the dissipation kernel. The quantum and classical TD DFT thus involve closely analogous frameworks, suitable for bridging the microscopic and mesoscopic length scales. The TD DFT equations have also been extended to spin-polarized situations, and multi-component fluid mixtures leading to many applications to dynamical phenomena.

The interconnections of TD DFT formalism with mode coupling theories of diffusion in fluid mixtures have also been demonstrated recently and simple scaling laws [28,29] for the diffusivities of fluid mixtures in terms of the entropy defined through the pair distribution functions have been derived. One such scaling law is given by

$$D_{\mu}^* = A \exp[S_{\mu}^*];$$

$$S_{\mu}^* = -(1/2) \sum_{\nu} \rho_{\nu} \int dr [g_{\mu\nu}(r) \ln g_{\mu\nu}(r) - (g_{\mu\nu}(r) - 1)].$$

The theoretical investigation [30] of the probability density distribution of the end-to-end distance of a flexible polymer chain molecule using a generalized diffusion equation has led to insight into the diffusion-influenced end-to-end conformational relaxation which can be probed using fluorescence resonance energy transfer experiments.

Concluding Remarks

This work presents a brief review of the role of density concept in building bridges among the microscopic, mesoscopic and macroscopic length scales and providing

the underlying threads which are woven into the colourful fabric of multiscale modeling of molecules and materials. The emphasis has been on the unified nature of the theoretical framework, with close analogies and interconnections among the density based descriptions encompassing quantum as well as classical systems. Its promise for future applications in diverse interdisciplinary areas of research has been highlighted, although the discussion has been only illustrative, guided more by the author's limited knowledge and perception. With the advancement of theoretical and computational techniques, it is expected that more and more challenging developments with density as central unifying theme will emerge, and the materials and molecular modeling research will be more and more exciting.

Acknowledgements

It is a pleasure to thank my colleagues Drs Alok Samanta, Tapan K. Ghanty, Chandra N. Patra, Niharendu Choudhury, Asish K. Dhara, Musharaf Ali, Tusar Bandyopadhyay and K.R.S. Chandrakumar for collaboration and many helpful discussions. I am deeply indebted to Dr R. Chidambaram, Dr R.M. Iyer, Dr C. Manohar, Dr J.P. Mittal, and Dr H.K. Sadhukhan for their immense help and support during the early years of my life in BARC. I am also thankful to Dr T. Mukherjee for his encouragement.

References

1. Hohenberg P. and Kohn W., Phys. Rev. **136** (1964) B864.
2. Kohn W and Sham L J Phys. Rev. **140** (1965) A1133.
3. Mermin N D, Phys. Rev. **137** (1965) A1441.
4. Kohn W. (Nobel Lecture), Rev. Mod. Phys. **71** (1999) 1253.
5. Parr R G and Yang W, *Density Functional*

- Theory of Atoms and Molecules* (1989).
(Oxford Univ. Press, New York).
6. Ghosh S K and Deb B M, Phys.Rep. 92 (1982)1.
 7. Henderson D, Editor, *Fundamentals of Inhomogeneous Fluids*, (1992) (Marcel Dekker, New York).
 8. de Gennes P G, (Nobel Lecture) Rev. Mod. Phys. 64 (1992) 645.
 9. Car R and Parrinello M, Phys. Rev. Lett. 55 (1985) 2471.
 10. Ghosh, S.K., Bull. Mater. Sci. 26 (2003) 3
 11. Parr R G, Donnelly R A, Levy M and Palke W E J. Chem. Phys. 68 (1978) 3801.
 12. Patra C.N. and Ghosh S.K., Phys. Rev. E50 (1994) 5123; E47 (1993) 4088.
 13. Choudhury N. and Ghosh S.K., J. Chem. Phys. 110 (1999) 8628; 118 (2003) 1327.
 14. Ghosh S.K. Int. J. Quant. Chem. 49 (1994) 239.
 15. Ghanty T K and Ghosh S K J. Am. Chem. Soc. 116 (1994) 8801.
 16. Wadehra A and Ghosh S K, J. Chem. Sci. 117 (2005) 401.
 17. Berkowitz M, Ghosh S K and Parr R G, J. Am. Chem. Soc. 107 (1985) 6811.
 18. Ghosh S. K., Chem. Phys. Lett. 172 (1990) 77.
 19. Ghanty T K and Ghosh S K J. Phys. Chem. 100 (1996) 17429
 20. Ghanty T K, Chandrakumar K.R.S. and Ghosh S. K., J. Chem. Phys. 120 (2004) 11363.
 21. Choudhury N., Patra C.N. and Ghosh S.K., J. Phys.: Cond. Matter, 14 (2002) 11955.
 22. Ramakrishnan T V and Yussouff M, Phys. Rev. B 19 (1979) 2775.
 23. Deb B M and Ghosh S.K., J. Chem. Phys. 77 (1982) 342.
 24. Runge E and Gross E.K.U. Phys. Rev. Lett. 52 (1984) 997.
 25. Ghosh S.K. and Dhara A.K. Phys. Rev. A 38 (1988) 1149.
 26. Ghosh S.K., Berkowitz M. and Parr R.G., Proc. Natl. Acad. Sci USA 81 (1984) 8028
 27. Parr R.G., Rupnik K. and Ghosh S.K., Phys. Rev. Lett. 56 (1986) 1555.
 28. Samanta A., Ali M. and Ghosh S.K. Phys. Rev. Lett. 87 (2001) 245901
 29. Samanta A., Ali M. and Ghosh S.K, Phys. Rev. Lett. 92 (2004) 145901.
 30. Bandyopadhyay T. and Ghosh S.K. J. Chem. Phys. 119 (2003) 572.

ABOUT THE AUTHOR



Dr Swapan K. Ghosh is currently Head of the Theoretical Chemistry Section, BARC and also Dean-Academic (BARC) for Chemical Sciences, HBNI. He joined Heavy Water Division, BARC through the Training School (19th Course, Chemistry) in 1976 and moved

to the Chemistry Group in 1998. He received his Ph.D. in Chemistry from Indian Institute of Technology, Bombay in 1982. His early work encompassed deuterium isotope effects and development of formulation and code for the accurate prediction of thermodynamic and transport properties of water and heavy water at any desired temperature and pressure. His current research interests include topics in theoretical chemistry, computational materials science and soft condensed matter physics. He is a Fellow of the Indian Academy of Sciences, Bangalore, Indian National Science Academy, New Delhi and National Academy of Sciences, Allahabad, India.

DIFFERENTIAL PULSE ANODIC STRIPPING VOLTAMMETRY STUDIES IN AQUEOUS SOLUTION OF Na_2CO_3 FOR THE DETERMINATION OF TRACE AMOUNTS OF CADMIUM PRESENT IN UO_2 FUEL

J.V. Kamat, N. Gopinath and S.K. Aggarwal
Fuel Chemistry Division
Bhabha Atomic Research Centre

This paper received the Best Paper Award (First Prize) in the Technical Session at the Twelfth National Convention of Electrochemists (NCE-12) held at Thiagarajar College of Engineering, Madurai during February 18-19, 2005.

Cadmium possesses a high neutron absorption cross-section for thermal neutrons and therefore its presence in amounts greater than 1 ppm is not tolerated in UO_2 fuel. The technique to be used for its determination in the fuel as part of quality control should be selective and sensitive. The Differential Pulse Anodic Stripping Voltammetry (DPASV) technique coupled with Hanging Mercury Drop Electrode (HMDE) is ideally suited for determination of trace amount of cadmium in UO_2 fuel due to the fact that there is a large enhancement in the limit of elemental detection in stripping technique using mercury electrode.

The solid UO_2 sample is dissolved in HNO_3 acid for performing various quality control tests. This solution

medium is unsuitable for the determination of cadmium in presence of UO_2^{2+} by Voltammetry technique because not only Cd^{2+} but also UO_2^{2+} will simultaneously take part in the electrode reaction since the value of redox potential of Cd^{2+} , - 0.434V, is less positive to that value of UO_2^{2+} , + 0.327V. As a result, the current efficiency of reduction of Cd^{2+} will be too small to be able to determine Cd in presence of very large excess of UO_2^{2+} .

It has been observed recently in our laboratory that the value of the reduction potential of Cd^{2+} is more positive than that of UO_2^{2+} in saturated aqueous solution of Na_2CO_3 .

This paper will discuss the results of experiments

performed in Na_2CO_3 aqueous solution to develop a method and optimize the parameters associated with the Differential Pulse Anodic Stripping Voltammetry (DPASV) technique for the determination of trace amounts of cadmium present in UO_2 fuel.

The experimental procedure has been designed as follows. The size of the sample, UO_2 , to be taken for determination of cadmium has been fixed at about one gram and should be dissolved quantitatively in minimum volume of dilute (1:1) HNO_3 . Later, the solution has to be evaporated to near dryness and then the residue to be dissolved in 25 mL of Na_2CO_3 aqueous solution. Two aliquots, each of 10 mL (the minimum volume of solution required for all the three electrodes are in good contact with the solution) are to be taken for the purpose of determination of Cd.

It has been observed that the evaporated acid dissolved one gram UO_2 is completely soluble with the production of a clear solution in 25mL of aqueous solution Na_2CO_3 of concentration 0.4M and more. The concentration of UO_2^{2+} in this solution is about 0.15M.

Stock solutions of 0.15M UO_2^{2+} , 0.35mM Cd^{2+} (1ppm) and a mixture of 0.15M UO_2^{2+} and 0.35mM Cd^{2+} (1ppm) in 0.5M Na_2CO_3 were prepared for use as test solutions in the appropriate experiments.

The values of peak reduction potential, E_{pr} , for Cd^{2+} and UO_2^{2+} in 0.5M Na_2CO_3 aqueous solutions were determined by Linear Scan Voltammetry. It was found that the value for Cd^{2+} , -0.776V, was more positive by an amount of 0.25V than that of UO_2^{2+} , -1.025V.

The optimum DPASV experimental parameters for the determination of Cd^{2+} in 10mL volume of synthetic mixture solution containing both Cd^{2+} and UO_2^{2+} prepared in 0.5M Na_2CO_3 aqueous solution were

found to be dissolution of cadmium in HMDE at an accumulation voltage, E_{acc} , of -0.75V(Ag/AgCl, 3M KCl) for a duration of 600s and followed by stripping it by changing the voltage of HMDE from -0.75V to -0.60 V at a scan rate of 10mVs^{-1} superimposing a pulse voltage of 50mV for 5s.

The DPASV current peak heights were determined for different concentrations of Cd^{2+} ($1 \times 10^{-7}\text{M}$ to $3.9 \times 10^{-7}\text{M}$) in presence of 0.15M UO_2^{2+} using the optimized experimental conditions. A linear relation between the values of DPASV current peak heights and their corresponding concentration of Cd^{2+} was observed. The value of correlation coefficient (R^2) obtained was 0.94.

The developed methodology is suitable for the determination of trace amounts of cadmium in UO_2 .

ABOUT THE AUTHORS



Ms. J.V. Kamat has obtained her M.Sc degree from Mumbai University. She joined Mass Spectrometry Section, Fuel Chemistry Division. After joining, she obtained her Ph.D from Mumbai University. She is involved in the application of electroanalytical techniques for developing methods for the analysis of elements of interest in nuclear fuels. She is the Treasurer of Indian Society for Electro Analytical Chemistry (ISEAC).



Mr N.Gopinath has obtained M.Sc. Degree in Physical Chemistry from Sri Venkateswara University, Tirupati. He joined the Chemical Methods Group, Radiochemistry Division, BARC. Since then he is actively involved in developing and employing various Electroanalytical techniques for different applications in the nuclear fuel cycle. He is a coauthor of a good number of scientific publications. He is the Secretary of the Indian Society for ElectroAnalytical Chemistry (ISEAC)



Dr. S.K. Aggarwal is presently Head, Fuel Chemistry Division, BARC. He received his B.Sc.(Hons) from Guru Nanak Dev University, Amritsar, in 1972 with two Gold Medals. He joined the 16th Batch of BARC Training School in 1972 and received Homi Bhabha Award. He did his Ph.D from Mumbai University in 1980. He is a coauthor of about 300 scientific publications, which include 100 articles published in reputed journals. Dr. Aggarwal has participated in several international and national conferences and in different international intercomparison experiments. He is a specialist in the field of atomic mass spectrometry and alpha spectrometry and is interested in various mass spectrometry techniques. His other areas of interest include electrochemistry and solvent extraction. He represents India in the Executive Committee of International Mass Spectrometric Conferences. He has visited several countries in Europe, America and Australia as an expert as well as for delivering lectures. He is a recognized Ph.D. Guide of the Mumbai University.

COMPACT 8 K MULTI-CHANNEL ANALYZER WITH USB INTERFACE AND MULTI-MODE OPERATION

C. P. Kulkarni, M. Vinod, M. Paulson, P. P.Vaidya,
M.D. Ghodgaonkar and S. K. Kataria
Electronics Division
Bhabha Atomic Research Centre

This paper received the Best Paper Award in the National Symposium on Compact Nuclear Instruments and Radiation Detectors, organised at DLJ Jodhpur, during March 2-4, 2005.

Abstract

A Multi-Channel Analyzer (MCA) is the heart of a nuclear spectroscopy system. The paper describes a new, high-performance MCA with many advanced features. Some of them are in-built hardware for List and MCS modes in addition to the standard PHA mode of operation, local spectrum memory and USB bus interface. The mode of operation is selectable through GUI. The MCA uses an FPGA to integrate all the digital circuits in one chip and it has state-of-the-art analog chips in analog side for superior performance. The resolution is selectable from 256 channels to 8 K channels suitable for all needs. It supports good input pulse rate (typically more than 100 KHz) without significant dead time penalty. The USB bus interface offers a truly universal and simple connectivity with almost any modern PC or Simputer for MCA data manipulation, control and display. The applications of the MCA include energy spectroscopy, half-life analysis and analysis of individual events and it is a good fit for embedded and battery-operated instruments as well as for standard desktop instruments.

Introduction

An MCA is a major part of nuclear spectroscopy systems. Depending on the application, it is used in either PHA or MCS or List mode of operation. The MCA presented here, supports all of them in one system and it is satisfactorily working as per the specifications in the real world. The digital circuitry which includes control registers, timers, sequencer, memory controller, 8 bit

generic bus interface and ADC linearization circuits, etc. is designed using VHDL with 200 K gates FPGA. The analog part of the circuit uses state-of-the-art analog chips like low power, high speed and high precision comparators, op-amps, ADC and DAC. It utilizes the isolated power supplies using DC-DC converters and regulators, which run only on +5V input supply. Use of isolated power supplies and ground also scales down the effect of noise associated with feeding power supply,

resulting into superior performance. The PHA (Pulse Height Analysis) mode is the most common mode of operation. Here the incident pulses are counted in individual memory channels depending on their energy and the plot of *count vs. energy* is available after the experiment. This PHA mode is useful for isotope identification, calibration and nuclear spectroscopy experiments. The MCA supports 256 to 8 K channels resolution with a DNL of better than + 1 % at 8 K, and has a fixed conversion time of 7 ms.

The MCS (Multi-Channel Scaling) mode records the counting rate of events as a function of time. The count is recorded for each *dwell time* slice and is stored in memory at incremental channel locations. It is useful for isotope half-life analysis. The MCA supports 32K channels length of MCS with dwell time of 4 ms to 4000 s. It has an internal dwell timer as well as provision of external channel incrementing pulse. In the List mode, the energy (amplitude) information of individual event is recorded at incremental memory locations. It is useful for analysis of individual events with respective to time or any other variable. The MCA supports a list of 32 bit into 32 K

optional support for individual data tagging to create 2D spectrums.

Design methodology

The following are the few aspects of the MCA design presented here:

- Low power precision analog design
- Low power, fully synchronous digital design
- Generic and portable VHDL code, independent of FPGA platform
- Hierarchical
- Power-down mode for SRAM memory

Functional Brief

The block schematic of MCA card is shown in Fig.1. The analog circuit consists of LLD and ULD comparators, peak stretcher and peak detect comparator, 16-bit successive approximation ADC and DAC for sliding scale correction. When the input pulse height exceeds the lower level discriminator (LLD) threshold, the peak stretcher is enabled. It stores the peak amplitude of



Fig. 1 : Block diagram of the MCA

the input pulse. If the input pulse amplitude falls within the LLD and ULD thresholds, the control and logic circuit is enabled and the ADC conversion process starts. The required mode of the MCA operation (*PHA*, *MCS*, or *List*) is selected through the GUI and accordingly the internal sequencers and other digital circuitry processes the ADC data.

PHA operation

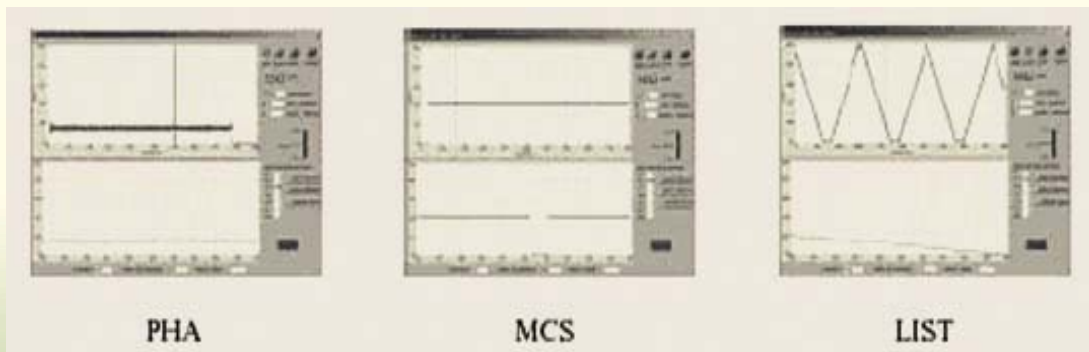
The ADC code corresponding to the specific input pulse amplitude is used as a memory address pointer and the 31-bit count value stored at the memory location is incremented by 1. This is done on "byte by byte" basis to speed-up the process of spectrum building and to maintain 8-bit bus interface. The process typically takes a minimum of 400 ns to a maximum of 1.6 μ s, depending on the number of byte access (1, 2, 3 or 4). This process is parallel with the ADC conversion time (5 μ s max), using a 1 stage buffer and thus the dead time is minimized.

incremented. The counter then starts fresh counting for next channel. The process continues for the 32 K channels or the acquisition time set. The process can be interrupted by external TTL input of MCS reset, which resets the channel pointer to 0 and restarts from channel 0.

List operation

The ADC data is written in the first channel in the memory and the channel pointer is incremented to next. The next data from the ADC is written there. This process repeats for 32 K channel length, which can store the energy information for 32 K events.

The screen-shots below show the data acquired in various modes with input from a sliding pulse generator:



MCS operation

An internal 32-bit counter counts the input pulses validated by LLD and ULD (SCA) for the duration of the *dwell time*, and then the count is written in the first channel in the memory and the channel pointer is

Bus arbitration logic

The MCA has a memory management with bus arbitration logic for single port SRAM chip. It resolves the Read / Write requests from ADC side and PC side, giving higher priority to the ADC side, so that the histogram doesn't

miss any input event. The PC side read request is processed intermittently and is notified by raising a flag bit embedded as a MSB bit of the 32-bit channel count. The maximum resolution supported by the digital hardware is 32 K channels of 31 bits each for future expansion, but presently, the maximum resolution available is 8 K channels. The on-board histogram memory makes the hardware to operate independently, once initialized and thus doesn't require frequent PC access. The SRAM reset function is user driven through GUI, so that the spectrum is protected from automatic erasing.

USB bus interface

The MCA has an on-board USB controller chip. It supports a data transfer rate of 12 MBPS and provides an excellent connectivity with most of the new PCs and palm-top type computers like *Simputer*, which helps make a compact and portable spectroscopy system.

Specifications

Following are the specifications for the MCA:

1. PHA mode:

- MCA resolution : 256, 512, 1K, 2K, 4K and 8K channels
- Spectrum memory : 128 K Bytes single port SRAM
- Max counts / channel : 31 bit (2 Giga counts)
- Pulse processing time : $7 \mu s$
- Pile up rejection : Active high TTL input
- DNL : + 1 % at 8K resolution
- INL : + 0.05 % F.S.

2. LIST mode:

- List size : 32 K x 32 bit
- Pulse processing time : $7 \mu s$
- Supports all PHA controls : Yes

3. MCS mode:

- Input (through SCA) : 100 KHz max, single channel
- Memory length (channels) : 32 K
- Max counts / channel : 31 bits (2Giga counts)
- Channel increment : External TTL pulse or internal dwell timer
- Dwell timer setting : $4 \mu s$ to 4000 seconds, set through software

4. Common specifications:

- MCA Input : Single channel, 0 to +10 volts
- Timer : 32 bit, integrated in FPGA
- Preset Time : LIVE or CLOCK, 2^{32} seconds (136 yrs) max.
- ADC conversion time : $5 \mu s$
- LLD, ULD, Baseline : Set through on-board DACs using application GUI
- Power requirement : 5V, ~ 500 mA

Future Plans

The digital part of the MCA may be transformed into indigenous digital ASIC to replace the FPGA and to make the system lower power and more compact as well as self-reliant. The analog circuits may be replaced with indigenous analog hybrid circuits to make it more compact.

References

1. EG&G-ORTEC catalog 1995.
2. Radiation Detection and Measurement by G. F. Knoll.
3. Xilinx Data Book CDROM 2003.
4. Technical Manual of MCA-2000, Electronics Division, BARC.

ABOUT THE AUTHORS



Mr C.P. Kulkarni did his BE (Electronics) from Shivaji University in 1995. He joined 39th batch of training school. After training, he was posted in Electronics division in 1996. He has developed a variety of MCAs and spectroscopy systems for different applications. His major areas of work include FPGA based system design and development of nuclear instruments for embedded and portable systems. Currently, he is working on the development of ASICs for MCAs.



Mr M.Vinod did his B.Tech. (Electronics) from Calicut University in 2000, and joined 44th batch of training school. After training, he joined the Electronics division in 2001. He has specialised in analog and digital circuit designs for MCAs. His major area of work includes micro controller based system design. Currently, he is working on development of portable spectroscopy systems.



Ms Molly Paulson joined BARC in 1979. Since then she has been actively involved in development of various nuclear medical instruments like Gamma Camera, Isotope calibrator etc. She is also involved in development of various Spectroscopy Systems and data acquisition modules for nuclear instrumentation



Dr. P. P. Vaidya obtained his B.E. degree from Regional Engineering College, Nagpur and joined Electronics Division after completion of 15th batch of BARC Training School. He has been working on developments of various nuclear instruments for more than 25 years. He obtained PhD in Electrical Engg. from IIT Mumbai for his work on Nuclear Analog to Digital converters. He has researched several new methods for high resolution nuclear ADCs, which have been published in journals of international repute. Dr.Vaidya is presently leading Nuclear System Section of Electronics Division, BARC. His main fields of interest include high-speed low power electronics, design of portable spectroscopy systems and other compact portable nuclear and test equipment.



Mr M.D. Ghodgaonkar obtained his M. Sc. (Physics) from the University of Indore and joined Electronics Division in 1969 after the completion of 12th batch

of BARC Training School. His contributions to Nuclear Instrumentation program over the last 37 years include Neutronic instrumentation (Purnima, FBTR and Cirus and Apsara upgradation), Transputer based Parallel Processing for nuclear applications, CAMAC Instrumentation for Accelerator control systems (FOTIA and LINAC) and high performance Multi-parameter systems for Nuclear Research. He has been instrumental in establishing the indigenous development of CAMAC instrumentation. During IX plan, he initiated the development of ASICs and Hybrids, which is being rigorously pursued. He has several publications in the filed of nuclear instrumentation. At present he heads Electronics Division of BARC and his current electronics interests are indigenous development of ASICs, radiation detectors, embedded instrumentation for radiation monitors and front end electronics for physics experiments, High speed high throughput Data Acquisition Systems and Radiation Security Instrumentation relevant to DAE programs.



Dr S. K. Kataria obtained his B.Sc. Degree from Rajsthan University in 1965 (Gold Medalist in Physics) and completed the BARC Training School Course in 1966 as Homi Bhabha

Awardee. He did his postgraduate degree and doctoral work in the area of experimental nuclear physics. For three decades, he worked in the area of nuclear experimental studies and nuclear instrumentation for accelerators and nuclear reactors while in NPD, BARC. Since the last decade, he has been working with a mission of modernisation of Electronics and Radiation Detectors and related Instrumentation. During this period he has led the development of new radiation detectors, HMCs, and ASICs for nuclear electronics, bio-medical and reactor instrumentation. He has published over 120 research papers in journals of international repute and over 200 in national and international symposia. He retired as an Associate Director, E&I Group of BARC and is at present Raja Ramanna Fellow at the Electrical Engineering Department, IIT Mumbai with the aim to promote collaborative development programs in these areas amongst DAE Institutes and IIT Bombay.

EXTRACTION CHROMATOGRAPHIC STUDIES EMPLOYING N,N,N',N'-TETRAOCTYL DIGLYCOLAMIDE (TODGA) AS STATIONARY PHASE

S.A. Ansari, P.N. Pathak and V.K. Manchanda
Radiochemistry Division
Bhabha Atomic Research Centre

and

M. Hussain, A.K. Prasad and V.S. Parmar
Department of Chemistry, University of Delhi, Delhi

This paper received the Best Paper (oral) Award at the DAE-BRNS Symposium in Nuclear & Radiochemistry (NUCAR-2005) held at Gurunanak Dev University, Amritsar, during March 15-18, 2005.

Abstract

N,N,N',N'-tetraoctyl diglycolamide (TODGA) sorbed on chromosorb-W has been used as the stationary phase in the extraction chromatographic separation of actinide ions from nitric acid solution. Uptake behaviour of metal ions such as Am(III), Eu(III), Pu(IV), U(VI), Fe(III), Sr(II) and Cs(I) was investigated from pure nitric acid as well as from simulated high level waste (SHLW) solution by batch studies employing the chromatographic resin material. Effect of macro concentration of Nd, Fe and U suggested that the uptake of Am(III) is mainly influenced by the presence of trivalent lanthanide ions.

Introduction

High level waste (HLW) solution generated as a consequence of the reprocessing of the spent nuclear fuel by PUREX process contains long lived minor actinides such as ^{241}Am , ^{243}Am , ^{245}Cm and ^{237}Np apart from the small amounts of unrecovered plutonium and uranium. At present, the most accepted concept for the management of HLW is to vitrify it in the glass matrix followed by disposal in deep geological repositories. Since

the half lives of the minor actinides concerned range between a few hundred to millions of years, the surveillance of this high active waste for such a long period of time is needed, which is a rather difficult proposal. An alternative concept is the partitioning and transmutation (P&T) option, which envisages the complete removal of minor actinides from HLW solution and their consequent burning in reactors as mixed oxide fuels [1,2]. This process will lead to generation of extra energy and at the same time would alleviate the waste

disposal problems. In the last two decades, all over the world, efforts have been made in several international laboratories to use the already known reagents and also to synthesize several new class of reagents for the efficient partitioning of minor actinides from high level waste solutions.

Organophosphorus extractants such as CMP, CMPO and TRPO (Cyanex-923) have been found useful for the partitioning of minor actinides from HLW solutions of PUREX origin. However, in recent years, penta alkyl malonamides have been evaluated extensively as alternative extractants to organophosphorus compounds for the partitioning of actinides. In addition to their improved extraction behavior towards actinide ions and fission products, these extractants offer distinct

identified as one of the most promising extractant being considered for the partitioning of trivalent actinides and lanthanides from HLW solutions [3]. This tridentate neutral ligand represents higher affinity for trivalent actinides and lanthanides than the DIAMEX solvent i.e. dimethyl dibutyl tetradecyl malonamide (DMDBTDMMA). In the present paper, extraction chromatographic material prepared by impregnating TODGA on chromosorb-W has been evaluated with respect to the uptake of Am(III) for the first time. Comparison of this material was also made with extraction chromatographic materials prepared using Cyanex-923, CMPO and DMDBDTDMMA for Am(III) uptake studies. Batch studies have been carried out for the uptake of Am(III), Eu(III), Pu(IV), U(VI), Fe(III), Sr(II) and Cs(I) ions from pure nitric acid as well as from Simulated High Level Waste (SHLW) solution.

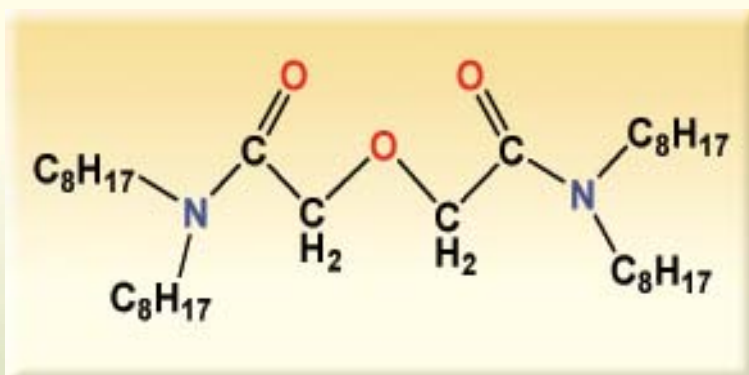


Fig.1 : TODGA

advantages, especially with respect to their complete incinerability and the innocuous nature of their radiolytic degradation products (mainly carboxylic acids and amines) that can be easily washed out. To further increase the efficiency of diamides towards the extraction of Am(III) and Cm(III), several modifications have been suggested. A recently developed, tridentate ligand, N,N,N',N'-tetraoctyl diglycolamide (TODGA) (Fig.1) has been

procedure as reported earlier [4]. The weight percentage of the extractant loaded on the resins was calculated from the difference in the weight of the resin before and after loading and was found to be about 50% w/w, which was subsequently confirmed by elemental analysis. The weight distribution coefficient of the metal ions was investigated by equilibrating 1 mL of aqueous solution containing radionuclides with ~ 25mg resin in a

Experimental

TODGA was synthesized at the Chemistry Department, University of Delhi, Delhi under DAE-BRNS Project. The purity of the product was checked by TLC, FT-IR, NMR and CHN elemental analysis. Chromosorb-W (60-80 mesh) obtained from Johns Manville, USA was washed with water and acetone followed by air drying before use. The chromatographic resin material was prepared by the

thermostated water bath at $25 \pm 0.1^\circ\text{C}$. Suitable aliquots of aqueous phase were taken before and after equilibration for assaying radiometrically. The distribution coefficient (K_d) was calculated by employing the formula,

$$K_d = [(C_0 - C) / C] \times V / W \quad (1)$$

Where C_0 and C are the concentrations of metal ions (in counts per unit time per unit volume) before and after equilibration, V is the volume of aqueous phase used (mL) and W is the weight of the resin material employed (g).

Results and Discussion

The solid phase extraction profile of Am(III) as a function of nitric acid concentration with different extractants viz. TODGA, CMPO, Cyanex-923 and DMBTDMA sorbed on Chromosorb-W is represented in Fig. 2. In case of TODGA and CMPO, there was a sharp increase in the K_d values of Am(III) upto 1M HNO_3 beyond which saturation was observed. However, in case of DMBTDMA, Am(III) uptake increased gradually with nitric acid concentration and reached only to moderate values above 3M HNO_3 . On the other hand, Cyanex-923 shows moderate K_d value only at low acidity ($K_d = 140$ at 0.5M HNO_3). The K_d values of Am(III) at 3M HNO_3 followed the order: 7200 (TODGA) > 2000 (CMPO) > 35.3 (DMBTDMA) > 3.2 (TRPO), suggesting TODGA as the most promising extractant for trivalent actinide. It is worth noting that

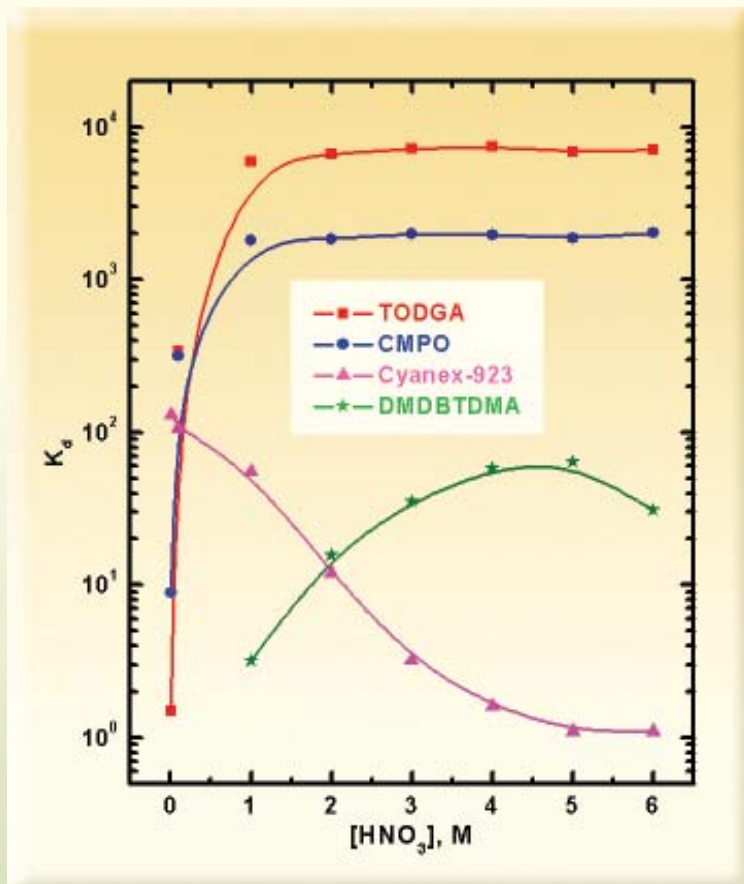


Fig.2 : Variation of K_d of Am by different extractant impregnated on Chromosorb-W

the commonly used neutral diamides act as bidentate ligand whereas the presence of additional etheric oxygen (in addition to two carbonyl oxygen, Fig.1) in TODGA makes the molecule tridentate thereby increasing the complexation with the metal ion. This clearly demonstrates that tridentate diglycolamide represents excellent extraction properties for actinide(III) over bidentate diamides. On the other hand, though TODGA and CMPO display comparable extraction properties for Am(III), there is distinct advantage of employing TODGA over phosphorous-based extractant in the secondary waste management due to its complete incinerability.

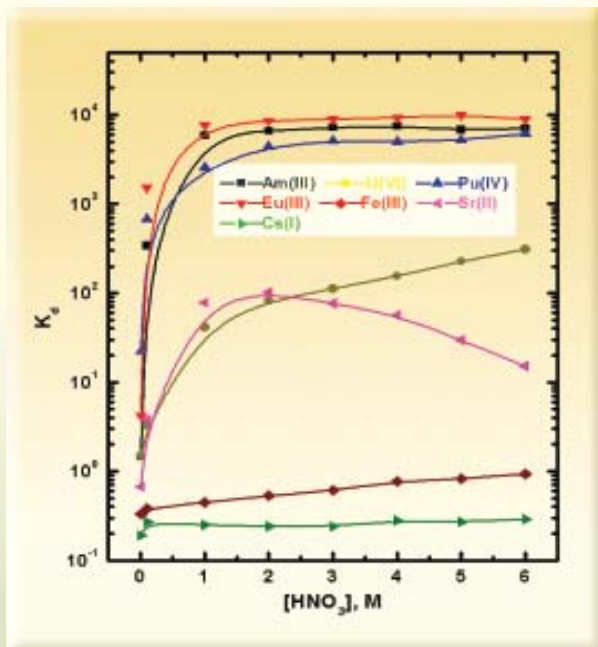


Fig. 3 : K_d of metal ions from pure nitric acid
Extractant : TODGA sorbed on Chromosorb-W

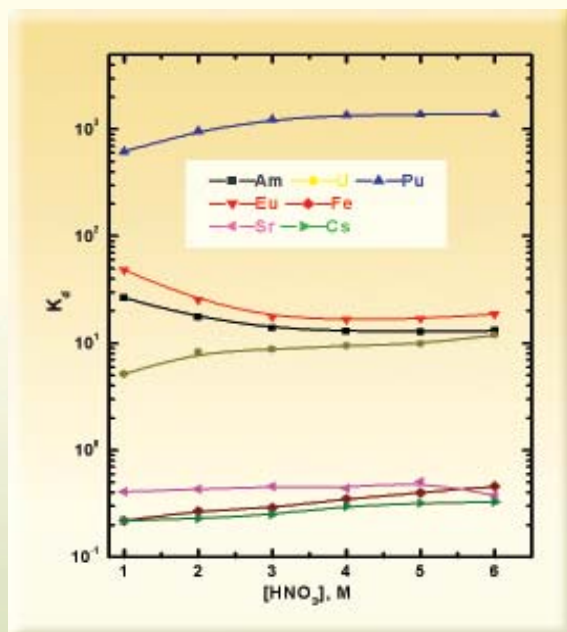


Fig. 4 : K_d of metal ions from SHLW
Extractant : TODGA sorbed on Chromosorb-W

The uptake profiles of metal ions such as Am(III), Eu(III), Pu(IV), U(VI), Fe(III), Sr(II) and Cs(I) were obtained from pure nitric acid as well as from SHLW employing TODGA / Chromosorb-W resin. The composition of the SHLW used in the present studies is reported elsewhere [4]. Fig.3 shows the variation of K_d values of metal ions as a function of HNO_3 concentration. It can be seen that the uptake of Am(III), Eu(III) and Pu(IV) increases sharply with the acidity upto 2M HNO_3 beyond which saturation was observed. The order of K_d values observed for lanthanides and actinides were similar to those obtained in solvent extraction studies i.e. $\text{Eu(III)} > \text{Am(III)} > \text{Pu(IV)} > \text{U(VI)}$, demonstrating that TODGA molecule in the adsorbent plays an analogous role to the liquid-liquid extraction systems [5]. In case of Sr(II), the K_d value increased with the aqueous phase acidity up to 3M HNO_3 and decreased thereafter. For Cs(I) and Fe(III), the K_d values were less than 0.5 in the entire range of acidity investigated, suggesting insignificant uptake of these metal ions. Fig.4 shows the variation of the K_d values of metal ions as a function of HNO_3 concentration from SHLW. Interestingly, the K_d values are distinctly higher for Pu(IV) as compared to those of Am(III) and Eu(III). Also, at any acidity, the K_d value of a given metal ion is less in the SHLW as compared to that in

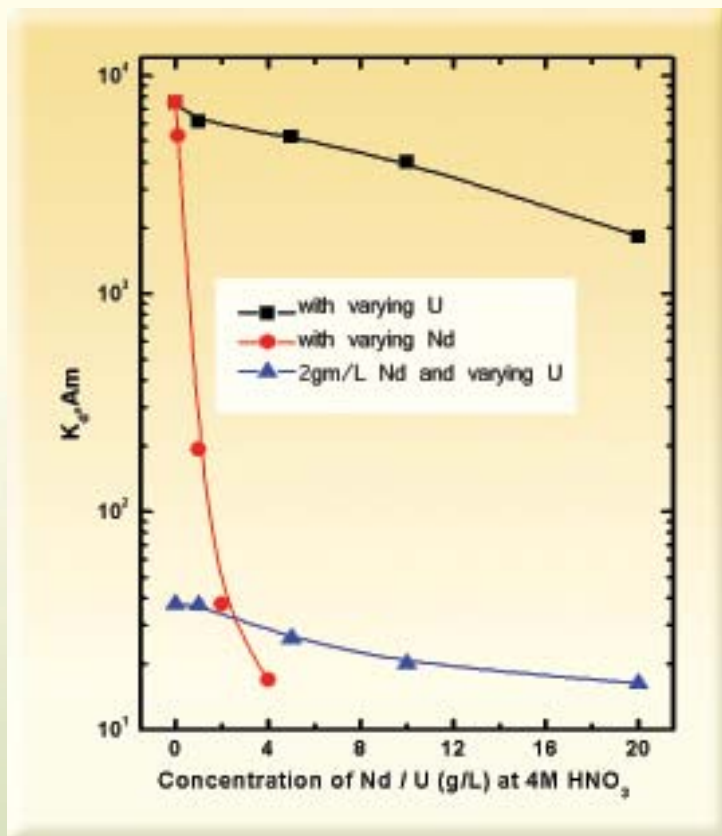


Fig. 5 : Effect of macro concentration of U and Nd on the uptake of Am(III) by TODGA/chromosorb-w resin

the presence of 2g/L of Nd and varying concentration of U. This result clearly demonstrated that the lanthanides are the major cations responsible for the decrease in the Am(III) uptake by the resin from SHLW.

Conclusions

The chromatographic resin material prepared by impregnating TODGA on chromosorb-W was found to be promising for the partitioning of trivalent actinides as compared to other extractants employed in actinide partitioning. Whereas the macro concentration of U(VI) did not influence the uptake of Am(III), trivalent lanthanides influence the uptake significantly.

pure HNO_3 (Fig.3), apparently due to the co-extraction of other metal ions present in SHLW. Also, no significant extraction of Sr(II) was observed from SHLW as maximum K_d , Sr(II) was ~ 0.5 in the entire range of acidity investigated. Fig.5 shows the uptake of Am(III) in the presence of varying concentration of U(VI) and Nd(III). The results reflected that even the presence of 20g/L of uranium does not affect the uptake behaviour of Am(III). This is attributed to the higher uptake of trivalent actinide as compared to hexavalent uranium as reflected in the batch studies. However, in case of Nd(III) (taken as a representative element of lanthanide), the K_d value of Am(III) decreased sharply with increase in the lanthanide concentration. Similar effect could also be observed in

References

1. Status and Trends of Spent Fuel reprocessing, IAEA TECDOC-1103, 1999.
2. L.H. Baestle; Burning of Actinides: A complementary waste management option? IAEA Bulletin, 34, 1992, 32.
3. Y. Sasaki, Y. Sugo, S. Suzuki and S. Tachimori; Solv. Extr. Ion Exch., 19, 2001, 91.
4. S.A. Ansari, M.S. Murali, P.N. Pathak and V.K. Manchanda; Solv. Extr. Ion Exch., 22, 2004, 1013.
5. S.A. Ansari, P.N. Pathak, M. Hussain, A.K. Prasad, V.S. Parmar and V.K. Manchanda; Solv. Extr. Ion Exch., 23, 2005, 463.

ABOUT THE AUTHORS



Mr S.A. Ansari obtained his M.Sc. degree in Analytical Chemistry from University of Mumbai in 2002. He is working as Senior Research Fellow in Radiochemistry Division, Bhabha

Atomic Research Centre, Mumbai since January 2003 under the collaboration scheme between University of Mumbai and Department of Atomic Energy. His area of specialization is separation of actinides and fission products using novel extractants. He has seven journal and fifteen conference / symposium papers to his credit.



Dr P.N. Pathak joined Radiochemistry Division in 1995 after completing 38th batch of Chemistry Training course. He has contributed towards the basic studies dealing with reprocessing of thorium-based fuels using branched dialkyl

amides and the use of macrocyclic ligands for ⁹⁰Sr / ⁹⁰Y separation. Currently, he is working as a post-doctoral research fellow in Prof. G.R. Choppin's laboratory at the Florida State University, Tallahassee, Florida, USA. Dr. Pathak's work has been published in leading international journals (40) and in national / international conferences (75).



Dr V.K. Manchanda joined the Radiochemistry Division, B.A.R.C. in 1969 after graduating from Delhi University and from B.A.R.C. Training School (one year orientation Course in Nuclear Sciences). He was

awarded Ph.D. by Bombay University in 1975 and carried out Post-Doctoral work at UTEP, Texas, U.S.A. as a Fulbright Scholar (1985-87). His research interests include; Thermodynamics and kinetics of complexes of macrocyclic ligands with lanthanides and actinides,

physico-chemical studies on lanthanide/actinide chelates, design and synthesis of novel extractants of actinides relevant into the back end of the fuel cycle, chemical quality control of Pu based fuels and speciation of actinides in aquatic environment. A recognised teacher of University of Mumbai, he has guided 15 Ph.D scholars. He has about 150 publications in international journals and about 400 conference/symposium papers. He is the founder convener of the Indian Association of Separation Scientists and Technologists (INASAT). He is a member of the Advisory Board of the well known international journal "Radiochimica Acta". He currently heads the Radiochemistry Division of BARC.



Mr Mofazzal Husain obtained his M.Sc. degree in Organic Chemistry from Dr. Ram Manohar Lohiya Avadh University, Faizabad in 2000. He is pursuing his Ph.D. work with

joint supervision of Professor VS Parmar (Department of Chemistry, University of Delhi) and Dr RK Gupta at the GGSIP University, Delhi. He worked as a visiting research scholar for a period of three months at KU Leuven, Belgium. He has ten scientific publications and seven conference papers to his credit. His major research interests are focused on the development of new methodologies for the synthesis of amides, biotransformation reactions and synthesis of biologically active heterocycles.



Dr A.K. Prasad received his PhD in Chemistry from University of Delhi in 1990. After postdoctoral research at the University of Southern Denmark, Denmark, Max-Plank Institute for Molecular Physiology, Germany, he

joined the Department of Chemistry at University of Delhi as a Reader in 2001. His research interests include Biotransformations, Nucleic Acid Chemistry, Natural Products Chemistry and Synthesis of Bioactive Compounds. He has worked as visiting scientist at the University of Copenhagen, Denmark and at University of Massachusetts, Lowell, USA. Dr Prasad has authored nearly a hundred scientific publications in international journals.



Dr V.S. Parmar received his Ph.D degree in Chemistry from the University of Delhi in 1978. After two years of postdoctoral studies at Cornell University (USA) and the University of Basle (Switzerland), Dr Parmar joined the

Department of Chemistry, University of Delhi as a Reader in 1984, where he has been full Professor since 1994. His research interests are biocatalytic reactions, nanotechnology, synthetic organic

chemistry, polymer chemistry, green chemistry and natural products chemistry. He has been a visiting scientist/visiting Professor at different institutions, i.e. Massachusetts Institute of Technology (MIT), Harvard University, Polytechnic University (New York) and the University of Massachusetts Lowell (USA), Imperial College of Science, Technology and Medicine and the University of Warwick (UK), the University of Basle (Switzerland) and the University of Southern Denmark. He has authored more than 275 scientific publications and has supervised the research work of a large number of PhD (38) and M.Phil (14) students.

INHIBITION OF CHLOROPHYLL DEGRADATION IN STAY-GREEN LANGRA MANGO (*MANGIFERA INDICA L.*) FRUITS

Machhindra T. Janave and Arun Sharma
Food Technology Division
Bhabha Atomic Research Centre

This paper was adjudged for the Best Paper Award (G.S. Sirohi Award-2005) at the National Seminar of the Indian Society for Plant Physiology, organised at Navasari Agricultural university, Navasari, Gujarat, during November 2005.

Abstract

Langra mangoes (Mangifera Indica L) ripened at tropical temperature (25-30 °C) appear green due to incomplete degradation of chlorophyll even though the fruits are table ripe. About 30% of total chlorophyll was retained and two fold increase in total carotenoids was observed during ripening. Ripening at lower temperature resulted in more loss of chlorophyll and reduced levels of carotenoids. RP-HPLC of the pigments extracted from various stages of ripening indicated accumulation of an unknown Chl derivative (retention time 7.32 min) and pheophytin a (retention time 20.4 min). Soluble protein fraction from peel catalyzed faster degradation of Chl a as compared to Chl b. Screening of the intermediates of enzymatic Chl a degradation by RP-HPLC indicated operation of chlorophyllase pathway. Accumulation of the unknown intermediate was observed when Chl b was used as a substrate with respect to incubation time up to 60 min. However, other polar intermediates were formed and disappeared after 30 min. The results indicated that upon ripening possibly a derivative of Chl b and pheophytin a accumulate giving the fruit a 'stay-green' character.

Introduction

Disappearance of green colour is the first visible result of degradation of chlorophyll as a consequence of maturation and ripening of fruits. Chlorophyll breakdown is a regulated process and various enzymes catalyzing the different reactions have been identified. Brown *et al* (1991) has classified these reactions into two groups,

type I and type II. Type I comprise the reactions catalyzed by the enzymes chlorophyllase, Mg-dechelataase, pheophorbide a oxygenase to opening of tetrapyrrole ring V. Type II reactions lead to cleavage and opening of the porphyrin macrocycle. The biochemistry underlying the Chl decomposition during leaf senescence has been elucidated (Hörtensteiner 1999, Takamiya *et al* 2000). Some of the enzymes have been cloned and studied in

more detail (Jacob-Wilk *et al* 1999, Wüthrich, *et al* 2000). Apart from this, Chl is also degraded by chlorophyll oxidase and peroxidase (Schoch *et al* 1984, Yamauchi & Watada 1994).

During ripening of fruits disappearance of Chl is normally associated with unmasking of carotenoids and the fruit acquiring bright yellow-red colour. Langra mango and Cavendish banana are commercially important fruits of India. Despite their pleasant pulp colour, flavor and general acceptance, these fruits fail to develop yellow colour due to incomplete degradation of Chl when ripened at temperatures above 25-30 °C (Thomas and Janave 1992). These 'green-ripe' fruits affect consumer preference and consequently fetch a lower price. In 'stay-green' Cavendish bananas evidence has been provided for operation of two distinct degradative pathways, Chlorophyllase pathway and Chl oxidase pathway (Janave 1997). Although degradation of Chl by Chl oxidase was reported earlier (Schoch *et al* 1984), no information is available on how the product, 13²-OH-Chl is further metabolized. Also, there are very few reports on how Chl *b* is metabolized during senescence. In the present paper attempt has been made to understand the mechanism of inhibition of Chl *a* and Chl *b* degradation in Langra mango which show similar ripening character as Cavendish banana.

Materials and Methods

Mature unripe fruits of mango (cv. Langra) were procured from a local market and stored in perforated polyethylene bags in cardboard boxes in dark for ripening at 25-30 °C and 20 °C. The peel was used for acetone powder preparation and pigment extraction. Acetone powder was prepared at different ripening stages as detailed in the previous paper (Janave 1997). The weighed amounts of

the acetone powder were sealed in polyethylene bags and stored at -30 °C until further use. Authentic pigments Chl *a*, Chlorophyllide (Chlide) *a*, Chl *b* and pheophytin (Pheo) *a* and *b* were prepared from spinach leaves as detailed earlier (Janave 1997).

Pigments from the peel (20 g) in triplicate after removing adhering pulp were extracted four times with 60 ml of acetone: hexane mixture (60:75). A pinch of NaHCO₃ was added to prevent Chl from pheophytinization. The filtrate was diluted with distilled water and separated in a separating funnel. The hexane epiphase containing all the pigments was washed with distilled water, dried over anhydrous Na₂SO₄, volume was made up and an aliquot was used for pigment analysis. An aliquot (1 ml), was evaporated by a stream of N₂, dissolved in 1 ml of spectroscopy grade diethyl ether and total chlorophylls, Chl *a*, Chl *b* and total carotenoids content was determined spectrophotometrically by using the equations of Lichtenthaler (1987). Another aliquot from hexane layer was evaporated by stream of N₂, dissolved in HPLC grade methanol. The pigments after passing through 0.22 µ GVWP filters were analyzed by JASCO HPLC system. The sample was loaded into a 100 Å Enertsil ODS RP C-18 column (4.6 ID X 250 mm) with an autoinjector and eluted with HPLC grade methanol isocratically. The operation conditions set were, flow rate 1 ml min⁻¹, detection at 425 nm and results were analyzed by using Borwin chromatography software.

The soluble enzyme from acetone powder was extracted as detailed earlier (Janave 1997). To 40 ml 0.02 M HEPES buffer (pH 7.2) containing 0.1 M NaCl, 10% glycerol and insoluble 2% PVPP, 2g acetone powder was added and stirred on magnetic stirrer at 4 °C in dark for 2h. The slurry after passing through muslin cloth was centrifuged at 27,000 X g for 10 min. The supernatant was used as soluble enzyme.

Protein content was determined by the Bradford dye binding (Bradford 1976) using bovine serum albumin as a standard.

The disappearance of Chl *a* and Chl *b* was measured as enzyme activity as detailed in the previous paper (Janave 1997). Reaction mixture (1.5 ml) in 30% acetone contained 70 mM phosphate buffer (pH 7), 10 μ M substrate (Chl *a* or Chl *b*) in acetone and 0.5 ml enzyme and incubated at 25 °C for specified time intervals. The reaction was stopped by 0.1 ml of 1 N NaOH followed by addition of 3 ml of acetone/hexane mixture (2/4, v/v). The contents were vigorously vortexed until emulsion formation, allowed to stand for 10 min and centrifuged at 3000 X g for 5 min. The reaction mixture after separating in acetone/hexane mixture (2/3, v/v), absorbance of hexane layer at 663 nm and 642 nm for Chl *a* and *b*, respectively was recorded. Concentrations of Chl *a* and Chl *b* were determined by employing extinction coefficients 94.5 (Chiba *et al.* 1967) and 56.2 (Schoch and Ihl 1998) respectively. The aqueous acetone layer was used for HPLC analysis after extraction with diethyl ether. Ether layer was evaporated with a stream

of N₂, dissolved in HPLC grade methanol and analyzed by HPLC as detailed under pigment preparation section. For control experiment, authentic chlorophylls were treated with reaction mixture components without enzyme under identical conditions.

Results and Discussion

Langra mangoes remain green at table-ripe stage showing about 32% and 22% retention of total chlorophylls when ripened at 25-30 °C and 20 °C respectively (Table 1). At 'Green-Unripe' stage, the concentrations of Chl *a* and Chl *b* were 11.37 mg and 5.1 mg 100g⁻¹, respectively, and upon ripening about 67-80% loss was observed at both the temperatures. However, at 20 °C, the Chl content at ripe stage was much lower than that in fruits ripened at room temperature indicating that Chl degradation is inhibited at higher temperature. Total carotenoids increased by about two folds in 'RT-Ripe' and 1.6 folds in '20 °C-ripe' mangoes. Ripening at lower temperatures is known to affect carotenoid synthesis in Alphonso mango (Thomas and Janave 1975).

Table 1: Changes in pigment content during ripening of Langra mangoes at room temperature (28-32 °C) and 20 °C.

Ripening Stage	Total Chl* (mg 100g ⁻¹)	Chl a* (mg 100g ⁻¹)	Chl b* (mg 100g ⁻¹)	Total Carotenoids* (mg 100 g ⁻¹)	*Unknown Pigment (Rt 7.32 min) (Area μ V)	*Pheophytin a (Rt 20.4 min) (mg 100g ⁻¹)
Green-Unripe	16.48(100)	11.37(100)	5.1 (100)	3.63 (100)	6589737(100)	2.67 \pm 0.57(100)
RT-Semiripe	10.19(38.2)	7.23(36.5)	2.96(41.9)	4.70(129.7)	4872839(26 \pm 1.4)	3.58 \pm 0.25(134.6)
RT-Ripe	5.29(67.9)	3.81(66.5)	1.49(70.9)	6.93(191.3)	4291820(35 \pm 0.3)	0.97 \pm 0.11(63.5)
20 °C-Semiripe	9.06(45.0)	5.91(48.0)	3.15(38.2)	4.27(117.9)	6401414(2.9 \pm 0.1)	2.53 \pm 0.3 (5.0)
20 °C-Ripe	3.59(78.2)	2.33(80.0)	1.27(75.2)	5.67(156.3)	2940524(55 \pm 1.2)	0.71 \pm 0.1 (73.8)

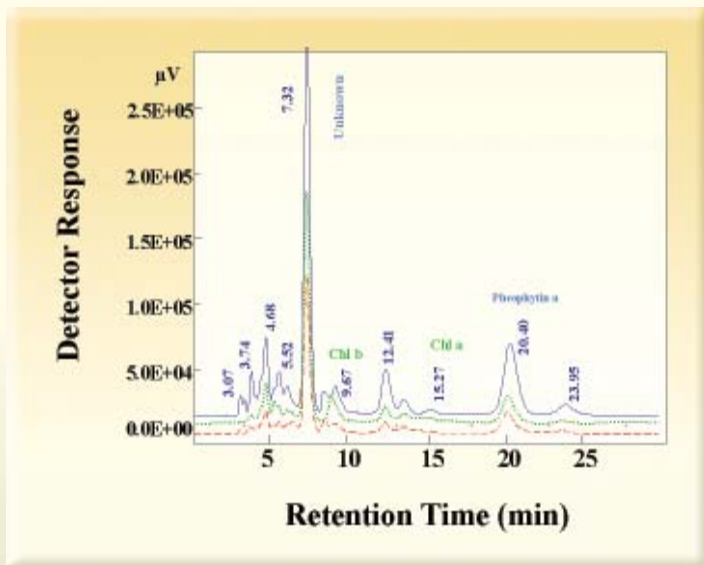


Fig. 1. RP-HPLC separation profile of pigments of Langra mangoes at (-) Green-Unripe, (· · ·) Green-Ripe and (- - -) Yellow-Ripe stages. The pigments after phase separation were subjected to RP-HPLC using JASCO HPLC system as detailed under Materials and Methods. The figures on the heads of peaks indicate retention time.

RP-HPLC of pigments extracted from mango peel is shown in Fig. 1. It was observed that an unknown pigment (Rt 7.32 min) and pheophytin a (Rt 20.4 min) were accumulated and very slowly degraded during ripening. Comparison of the area of the peak of unknown pigment revealed that it was degraded only 35% and 55% in 'RT-Ripe' and '20 °C-Ripe' mangoes respectively (Table 1). Pheophytin loss was about 63-74% in the two stages of ripening studied. These mangoes in unripe stage are very sour due to high

acidity thereby resulting in conversion of Chl to pheophytins. As pheophytins are not on direct route of enzymic Chl degradation (Janave 1997; Vicentini *et al.* 1995), its accumulation may be resulting in 'stay-green' character. Very small amounts of Chl a (Rt 15.27 min) and Chl b (Rt 9.67 min) were detected (Fig.1). This is in contrast to the spectrophotometric data of Chl a and Chl b levels reported in Table 1. This may be due to the degradation products of Chl exhibit almost similar spectral characteristics as that of parent chlorophyll a or b. Degradation of Chl a and Chl b by soluble enzyme revealed that Chl a degradation was faster than that of Chl b (Table 2). Chlorophyll b degradation was about half of that when Chl a was used as substrate. Activity of Chl a breakdown was much higher in 'RT-ripe' mangoes than that in '20 °C-ripe'

mangoes. The total protein content of green-ripe mango increased by 1.5 fold, whereas, in fruits ripened at 20 °C, about 2 fold increase was observed.

Table 2. Degradation of Chl a and Chl b by soluble enzyme fraction from acetone powder of Langra mangoes at three stages of ripening.

Ripening Stage	Volume (ml)	Protein ($\mu\text{g g}^{-1}\text{fw}$)	Chl a* hydrolyzed (nmol)	Chl b* hydrolyzed (nmol)
Green-Unripe	60	1335	222.0	123.2
RT-Semiripe	60	1170	301.2	289.2
RT-Ripe	60	2038	328.0	106.4
20°C-Semiripe	60	1512	324.0	278.4
20 °C-Ripe	60	2539	177.0	100.9

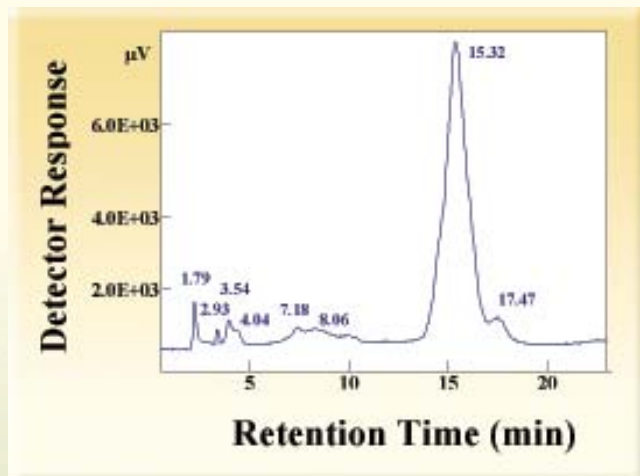


Fig. 2 : RP-HPLC separation of Chl *a* degradation products catalyzed by soluble enzyme from Green-Ripe Langra mangoes after 15 min of incubation. The assay of Chl *a* degradation was carried out as described in Materials and Methods. The pigments in acetone phase were subjected to HPLC. Peak eluting at Rt of 15.32 min is unutilized Chl *a*, the substrate.

Fig. 2 shows the RP-HPLC profile of degradation products of Chl *a* catalyzed by soluble enzyme fraction. Almost similar trend was observed when the reaction was carried out for 5-60 min, hence, data for 15 min incubation is shown. Most of the polar intermediates eluting between the Rt of 1.79 min to 4.04 min indicate operation of chlorophyllase pathway. As was the case in Cavendish banana (Janave, 1997), not a single intermediate of oxidase pathway was detected. However, the intermediates (Rt 7.18 and 8.06 min) possibly may be formed by the oxidative enzymes as revealed by their longer retention time.

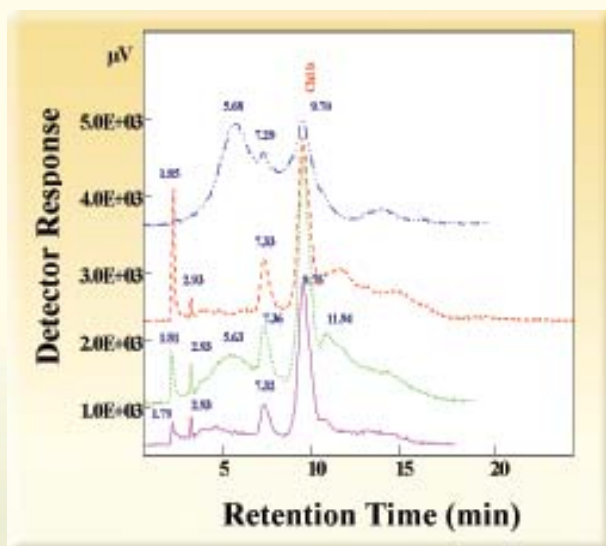


Fig. 3 : RP-HPLC separation of Chl *b* degradation products catalyzed by soluble enzyme from Green-Ripe Langra mangoes with respect to time of incubation. The assay of Chl *b* degradation and separation of products by phase separation was carried out as described in Materials and Methods. The pigments in acetone phase were subjected to HPLC. Peak eluting at Rt of 9.7-9.75 min is unutilized Chl *b*, the substrate.

Fig. 3 shows the profile of HPLC separation of enzymatic degradation products of Chl *b* with respect to time of incubation. Apart from the dephytylated polar intermediates eluting between Rt 1.79 - 4.64 min, an unknown intermediate (Rt 7.33 - 7.36 min) was constantly formed up to 60 min of incubation. This product showed identical retention time to that of unknown pigment accumulated during ripening (Fig. 1). Since the nature of the intermediate is not known at present, no attempts were made to quantitate its concentration. Another intermediate eluting at Rt 5.63-5.68 min was observed at 15 min and 60 min of incubation, the nature of which is not known at present. This intermediate might be a later step after the chlorophyllide *b* or pheophorbide *b* formation as it is detected after longer

time of incubation. The results indicate Chl *b* is also decomposed by the chlorophyllase pathway. Further studies are essential to explore whether the product (Rt 7.36 min) is formed by the chlorophyllase pathway or the oxidase pathway.

The inhibition of Chl degreening responsible for 'stay-green' character of Cavendish bananas and Langra mangoes is an intriguing problem. Yah *et al* (1998) also observed that Kent variety of mango remained green upon ripening and treatment with ethephon resulted in development of yellow-red colour. These fruits ripen giving soft and edible pulp at tropical temperature with green peel. In Cavendish bananas, Blackbourn *et al* (1990) have suggested the inhibition may be due to the retention of thylakoid membranes and loss of electron transport capacity due to non-functional Chl. In non-yellowing senescent leaves of *Festuca pratensis* Huds Bf 993, Vicentini *et al.* (1995) have reported that the thylakoid were deficient in pheophorbide *a* oxygenase thereby resulting in senescence-induced-deficiency. Apart from this no reports are available to understand the mechanism of inhibition of Chl degreening on enzymatic basis. In the present paper, attempts have been made to study the enzymes at different stages of ripening in Langra mango.

RP-HPLC analysis of pigments (Fig. 1) at different stages of ripening indicated accumulation of unknown intermediate (Rt 7.32 min) and pheophytin *a* (Rt 20.4 min) RP-HPLC pattern of enzymatic Chl *b* degradation (Fig. 3) showed constant formation of an hitherto unknown intermediate (Rt 7.33-7.36 min) which is identical with the Rt of accumulated unknown pigment during ripening (Fig. 1). These results suggest this intermediate could be a derivative of Chl *b*. The accumulation of pheophytin *a* and the unknown derivative of Chl *b* during ripening of Langra mango

could be responsible for the stay-green character of this fruit.

References

1. Blackbourn, H..D., Jeger, M..J., John, P. and Thompson, A. .K. (1990). Inhibition of degreening in the peel of bananas ripened at tropical temperatures. III. Changes in plastid ultrastructure and chlorophyll-protein complexes accompanying ripening in bananas and plantains. *Annals of Applied Biology*. 117: 147-161.
2. Bradford, M..M. (1976). A rapid and sensitive method for the quantitation of microgram quantities of protein utilizing the principle of protein-dye binding. *Analytical Biochemistry*. 72: 248-254.
3. Brown, S. B., Houghton, J. D., and Hendry, G. .A.. F. (1991). Chlorophyll breakdown. In *Chlorophylls*, (Scheer H., ed.), CRC Press, Boca Raton, Fl., 465-489.
4. Chiba, Y., Aiga, I., Idemori, M., Satoh, Y., Matsushita, K. and Sasa, T. (1967). Studies on chlorophyllase of *Chlorella protothecoides*. I. Enzymatic phytylation of methyl chlorophyllide. *Plant & Cell Physiol*. 8: 623-635.
5. Hörtensteiner, S. (1999) Chlorophyll breakdown in higher plants *CMLS, Cell. Mol. Life Sci*. 56: 330-347.
6. Jacob-Wilk, D., Holland, D., Goldschmidt, E. E., Riov, J. and Eyal, Y. (1999). Chlorophyll breakdown by chlorophyllase: isolation and functional expression of the *Chlase1* gene from

- ethylene-treated *Citrus* fruit and its regulation during development. *The Plant Journal* 20(6): 653-661.
7. Janave, M. T. (1997). Enzymic degradation of chlorophyll in cavendish bananas: *In vitro* evidence for two independent degradative pathways. *Plant Physiol. & Biochem.* 35(11): 837-846.
 8. Janave, M. T. and Sharma, A. (2004). Partial purification of chlorophyll degrading enzymes from Cavendish banana (*Musa cavendishi*). *Indian J. Biochem. Biophys.* 41: 154-161.
 9. Lichtenthaler, H. K. (1987). Chlorophylls and carotenoids: Pigments of photosynthetic biomembranes. *Methods in Enzymol.* 148: 350-382.
 10. Schoch, H., Rudiger, W., Luthy, B. and Matile, P. (1984). 13²-Hydroxy chlorophyll *a*, the first product of the reaction of chlorophyll oxidase. *J. Plant Physiol.* 115: 85-89.
 11. Schoch, H., and Ihl, M. (1998). Substrate specificity of chlorophyllase from different plants. *Z. Naturforsch.* 53(c): 21-26.
 12. Takamiya K., Tsuciya T. and Ohta H. (2000) *Trends Plant Sci.* 5: 426-431.
 13. Thomas P. and Janave M. T. (1975). Effects of gamma irradiation and storage temperature on carotenoids and ascorbic acid content of mangoes on ripening. *J. Sci. Fd. Agric.* 26: 1503-1512.
 14. Thomas P. and Janave M. T. (1992). Effect of temperature on chlorophyllase activity, chlorophyll degradation and carotenoids of Cavendish bananas during ripening. *International Journal of Food Science & Technol.* 27: 57-63.
 15. Vicentini F., Hörtensteiner S., Schellenberg M., Thomas H. and Matile P. (1995). Chlorophyll breakdown in senescent leaves: identification of the biochemical lesion in a *stay-green* genotype of *Festuca pratensis* Huds. *New Phytologist* 129: 247-252.
 16. Wüthrich K. L., Lucien Bovet., Hunziker P. E., Donnison I. S. and Hörtensteiner S. (2000) Molecular cloning, functional expression and characterisation of RCC reductase involved in chlorophyll catabolism. *The Plant Journal* 21(2): 189-198.
 17. Yah-A-R-Centurion, Gonzalez-Novelo S. A., Tamayo-Cortes J. A., Argumedo J. J., and Duch-E-Sauri. (1998). The effect of Ethephon on the colour, composition and quality of mango (*Mangifera indica*, cv. Kent). *Food Science & Technology-International* 4(3): 199-205.
 18. Yamauchi, N. and Watada, A. E. (1994) Effectiveness of various phenolic compounds in degradation of chlorophyll by *in vitro* peroxidase-hydrogen peroxide system. *J. Japan. Soc. Hort. Sci.* 63(2): 439-444.

ABOUT THE AUTHORS



Dr M.T. Janave joined B.A.R.C. in 1971 after completing B. Sc. in Chemistry from Shivaji University, Kolhapur. He obtained his Masters degree in Biochemistry in 1983 and Ph. D. degree in Biochemistry in 1992 from

Bombay University. He was a Post-Doctoral Research Associate at the Horticultural Sciences Dept., Univ. of Florida, Gainesville, USA, during 2000-2001, where he worked with Prof. Andrew Hanson on plant 5-formyl tetrahydrofolate cycloligase and dimethylsulfoniopropionate (DMSP)-amine oxidase from cord grass *Spartina alterniflora*. After returning to India, Dr. Janave continued further work on chlorophyll degradation in stay-green fruits namely, Cavendish banana and Langra mango. His research activities are mainly focused on understanding the ripening associated

biochemical mechanisms in various tropical fruits and shelf-life extension by gamma irradiation.

Currently Dr. Janave is actively involved on the studies on possible causative factors of spongy tissue development in Alphonso mango. He has isolated *Staphylococcus* bacteria from spongy pulp, characterized this organism and showed that the spongy tissue development in Alphonso mangoes is due to this bacterial infection. This also is the first report for involvement of microbial infection as a causative agent for spongy tissue development. He has extended these studies to explore the source of infection of this organism on the Alphonso trees in Trombay area of BARC campus to show that the insects around the inflorescence harbor these bacteria to the fruits. His further research work is to develop control measures to minimize this bacterial infection, which will be beneficial in quality improvement and more export trade of this economically important fruit crop of India.



Dr Arun Sharma joined Training School of Bhabha Atomic Research Centre, Mumbai, in 1975, after finishing Masters degree in Microbiology from National Dairy Research Institute, Karnal. He obtained his Ph. D.

degree in Biochemistry from University of Bombay in 1984. He was a Post-Doctoral Associate at the Department of Plant Pathology, University of California, Riverside, USA, during 1990-1991, where he worked with Prof. Noel T. Keen on the avirulence gene D of *Pseudomonas syringae* pv. tomato. After returning to India, Dr. Sharma initiated work on *Xanthomonas campestris* pv. glycines, the etiological agent of bacterial pustule disease of soybean. Since then he has

been actively involved in studying the molecular biology of *Xanthomonas* with special reference to the mechanism of host-pathogen interaction. His other interests include biogenesis and control of aflatoxin in food and feed. Simultaneously, he has also been engaged in research related to radiation processing of food. He has more than 150 publications in national and international journals, including chapters in books and encyclopedias. He has participated as a delegate and expert in the co-ordinated research programs of the International Atomic Energy Agency. He has been the secretary of the Environmental Mutagen Society of India and Vice-President of Indian Society for Environmental Science & Technology. Dr. Sharma is currently Head, Food Technology Division, Bhabha Atomic Research Centre, Mumbai, India.

MODELING OF ANOMALOUS THERMODYNAMIC PROPERTIES USING LATTICE DYNAMICS AND INELASTIC NEUTRON SCATTERING

R. Mittal
Solid State Physics Division
Bhabha Atomic Research Centre

The author has received the "Golden Jubilee Young Achiever Award" during the DAE-Solid State Physics Symposium held at BARC, Mumbai, India, during December 5-9, 2005.

Abstract

This paper summarizes the recent developments of the modeling of anomalous thermodynamic properties. It has been shown that lattice dynamics calculations along with inelastic neutron scattering measurements can be employed to reveal phonon properties and to predict thermodynamic properties of various compounds including materials with negative thermal expansion. There is a large variation in the thermal expansion, specific heat and equation of state pertaining to the compounds described in this paper. The interatomic potentials as determined for various compounds have been able to successfully model the thermodynamic behaviour. The variations in phonon spectra manifest in the thermodynamic properties of various compounds at high pressure and temperature.

Introduction

The study of lattice vibrations is of considerable interest because several physical properties of crystals like specific heat, thermal expansion, thermal conductivity and phase transitions are related to the vibrations of atoms in solids [1-4]. We have developed models of interatomic potentials for several compounds of interest, which allow to calculate the structural and dynamical properties as a function of pressure and temperature. The data obtained from neutron scattering and optical experiments are used to test and validate models of interatomic potentials

[1,2]. The models are then used for calculating various thermodynamic properties at high pressures and temperatures. We are able to provide the predictions of equation of state, specific heat and thermal expansion. A brief description of the scientific interest and results obtained for various compounds are given below.

Results and discussion

The compounds ZrW_2O_8 , HfW_2O_8 and $ZrMo_2O_8$ are of considerable interest [5] due to their large

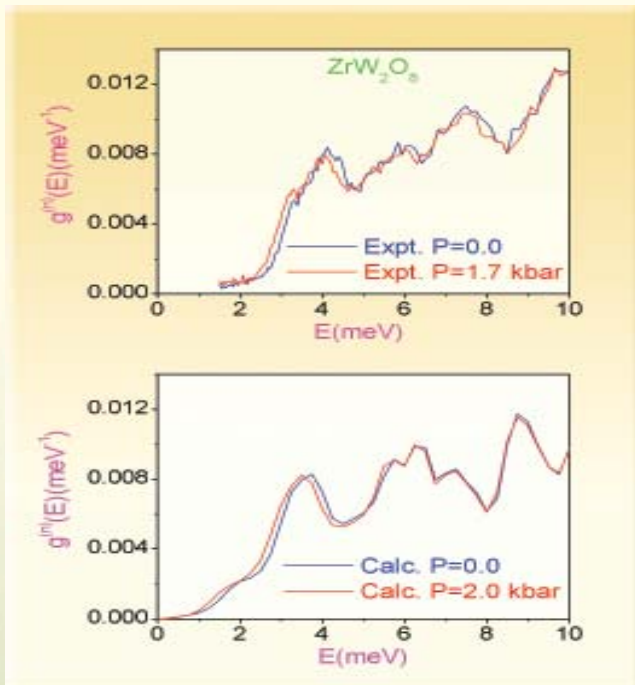


Fig. 1 : The comparison between the calculated and experimental inelastic neutron scattering spectra for cubic ZrW_2O_8 . The experimental data for cubic ZrW_2O_8 is at 160 K and at pressures of 0.0 and 1.7 kbar. The experimental spectra at P=0.3 kbar and 1.0 kbar fall in between those of P=0 and 1.7 kbar, and have not been shown here for the clarity (after ref. [11]).

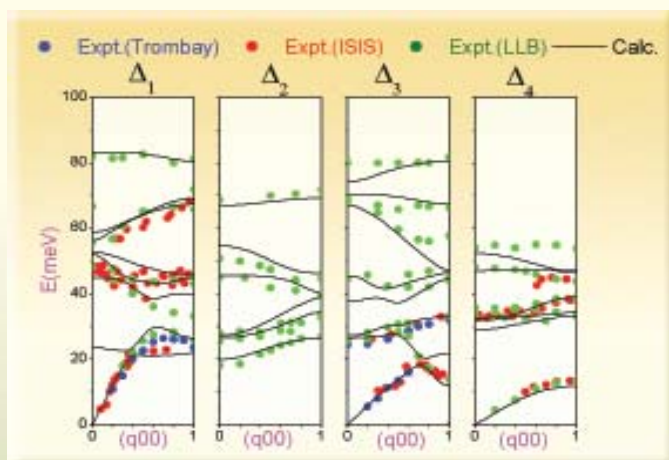


Fig. 2 : The experimental phonon data (symbols) along [100] with the lattice dynamical calculations (lines) for zircon (after refs. [13-15]).

isotropic negative thermal expansion (NTE) in their cubic phase over a wide range of temperatures up to 1443 K, 1050 K and 600 K, respectively. Our lattice dynamical calculations for ZrW_2O_8 and HfW_2O_8 [5-10] reproduced the observed anomalous thermal expansion in these compounds. The unusually dominant contributions of the transverse acoustic, librational and translational optic modes below 8 meV lead to a large NTE. High pressure inelastic neutron scattering experiments conducted [9-12] by us on polycrystalline samples of cubic ZrW_2O_8 and $ZrMo_2O_8$ confirm phonon softening (Fig. 1). The thermal expansion as derived from the phonon measurements is in good agreement with that obtained from diffraction data. This indicates that unusual phonon softening of low energy modes is able to account for the NTE in these compounds.

Zircon, $ZrSiO_4$ is an important host silicate mineral for radioactive elements uranium and thorium in the earth's crust. Initially, phonon dispersion relation in this compound were measured [13] at Dhruva reactor at low energies upto 32 meV. For the reasons of high intensity and good resolution further measurements [14,15] upto 80 meV were extended at ISIS (UK) and LLB (France) (Fig.2). These extensive measurements upto 80 meV provide a rare example of such studies carried out on any material. The lattice dynamical model produces a very good description of the available data. The model is further used to calculate [15,16] the free energies as a function of pressure and

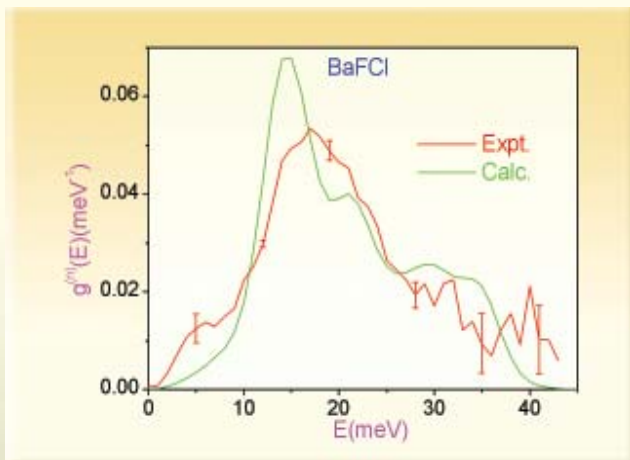


Fig. 3 : The experimental and calculated neutron-weighted phonon density of states for BaFCl. The multi-phonon contribution has been subtracted from the experimental data to obtain the experimental one-phonon spectrum (after ref. [20]).

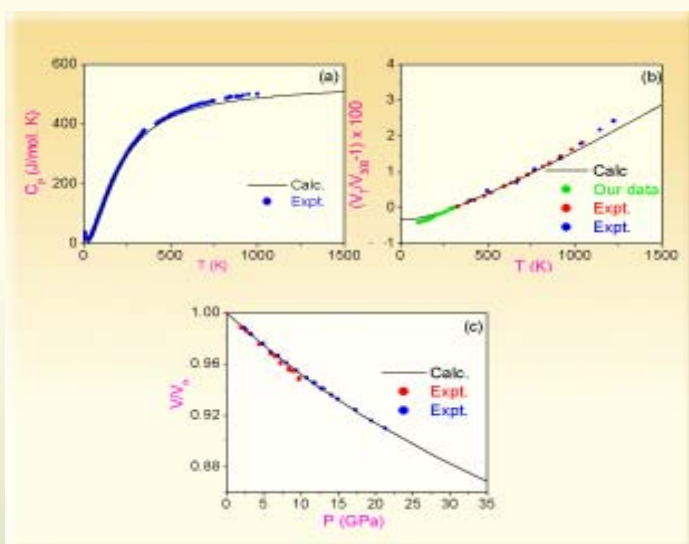


Fig. 4 : Comparison of the calculated (a) specific heat, (b) thermal expansion and (c) equation of state of the garnet mineral almandine $Fe_3Al_2Si_3O_{12}$ with available experimental data (symbols). The references for the experimental data are available in ref. [18] (after ref. [18]).

temperature in the zircon as well as the high-pressure scheelite phase, which reproduce the relative stability of the two phases across their observed phase transition

pressure of about 10 GPa.

Neutron inelastic scattering experiments (Fig. 3) to determine the phonon density of states and lattice dynamical calculations of thermodynamic properties (Fig. 4) were successfully carried out [16-26] for compounds MPO_4 ($M=Al, Ga, Fe$), garnet minerals $M_3Al_2Si_3O_{12}$ ($M=Fe, Mg, Ca$ and Mn), X-ray image storage materials MFX ($M=Ba, Sr, Pb; X=Cl, Br, I$), $LiYF_4$, $LiYbF_4$ and $ZnCl_2$. These studies have enabled a microscopic understanding of the variations in the phonon spectra in these compounds and their manifestations in various thermodynamic properties like the specific heat, thermal expansion and equation of state.

Conclusion

A combination of lattice dynamics calculations and inelastic neutron scattering measurements have been successfully used to study the phonon properties and their manifestations in thermodynamic quantities. These studies have also been exploited to study the anomalous properties like large negative thermal expansion in various compounds.

References

1. S. L. Chaplot, N. Choudhury, S. Ghose, M. N. Rao, R. Mittal, P. Goel, European Journal of Mineralogy 14, 291 (2002).
2. R. Mittal, S. L. Chaplot and N. Choudhury, Progress in Materials Science (Invited review article) 51, 211 (2006).

3. G. Venkataraman, L. Feldkamp and V.C. Sahni, *Dynamics of perfect crystals*, MIT Press, Cambridge (1975).
4. P. Bruesch, *Phonons: Theory and experiments II*, Springer-Verlag, Berlin, Heidelberg, New York, (1986).
5. R. Mittal and S. L. Chaplot, Phys. Rev. B **60**, 7234 (1999).
6. S. L. Chaplot and R. Mittal, Phys. Rev. Lett. **86**, 4976 (2001).
7. R. Mittal and S. L. Chaplot, Solid State Communication **115**, 319 (2000).
8. R. Mittal, S. L. Chaplot, A. I. Kolesnikov, C. -K. Loong and T. A. Mary, Phys. Rev. B **68**, 54302 (2003).
9. R. Mittal, S. L. Chaplot, H. Schober, A. I. Kolesnikov, C. -K. Loong, C. Lind and A. P. Wilkinson, Phys. Rev. B **70**, 214303 (2004).
10. R. Mittal, S. L. Chaplot, H. Schober, T. A. Mary and A. P. Wilkinson, Acta Cryst. A **58**, C334 (2002).
11. R. Mittal, S. L. Chaplot, H. Schober and T. A. Mary, Phys. Rev. Lett. **86**, 4692 (2001).
12. R. Mittal, S. L. Chaplot, H. Schober and T. A. Mary, Neutron News **13**, 36 (2002).
13. R. Mittal, S. L. Chaplot, Mala N. Rao, N. Choudhury and R. Parthasarathy Physica B **241**, 403 (1998).
14. R. Mittal, S. L. Chaplot, R. Parthasarathy, M. J. Bull and M. J. Harris, Phys. Rev. B **62**, 12089 (2000).
15. S. L. Chaplot, L. Pintschovius, N. Choudhury and R. Mittal, Phys. Rev. B **73**, 94308 (2006).
16. S. L. Chaplot, R. Mittal, E. Busetto and A. Lausi, Phys. Rev. B **66**, 64302 (2002).
17. R. Mittal, S. L. Chaplot, N. Choudhury and C.-K. Loong, Phys. Rev. B **61**, 3983 (2000).
18. R. Mittal, S. L. Chaplot and N. Choudhury, Phys. Rev. B **64**, 94302 (2001).
19. R. Mittal, S. L. Chaplot, A. I. Kolesnikov, C. -K. Loong, O. D. Jayakumar and S. K. Kulshreshtha, Phys. Rev. B **66**, 174304 (2002).
20. R. Mittal, S. L. Chaplot, A. Sen, S. N. Achary and A. K. Tyagi, Phys. Rev. B **67**, 134303 (2003).
21. R. Mittal, S. L. Chaplot, A. Sen, S. N. Achary and A. K. Tyagi, Appl. Phys. A **74**[S], S1109 (2002).
22. R. Mittal and S. L. Chaplot, Physics Teacher **45**, 48 (2003).
23. R. Mittal, S. L. Chaplot, A. I. Kolesnikov, C. -K. Loong, O. D. Jayakumar and S. K. Kulshreshtha, Pramana: Journal of Phys. **63**, 405 (2004).
24. A. Sen, S. L. Chaplot and R. Mittal, Phys. Rev. B **64**, 24304 (2001).
25. A. Sen, S. L. Chaplot and R. Mittal, Phys. Rev. B **68**, 134105 (2003).
26. A. Sen, Mala N. Rao, R. Mittal and S. L. Chaplot, J. Phys.: Condens. Matter J. Phys.: Condens. Matter **18**, 6431 (2006).

ABOUT THE AUTHOR



Dr R. Mittal joined the 34th batch of BARC Training School after completing M.Sc (Physics) from H. N. B. Garhwal University. Subsequently

he joined the Solid State Physics Division, BARC in 1991. Since then, he is involved in inelastic neutron scattering experiments and lattice dynamics computations.

ROLE OF BLEND MORPHOLOGY IN THE RADIATION PROCESSING OF SBR-EPDM BLENDS

K. A. Dubey, Y. K. Bhardwaj, C. V. Chaudhari and S. Sabharwal
Radiation Technology Development Section
Bhabha Atomic Research Centre

This paper was adjudged for the Shri K.M. Philip Award, constituted by the Indian Rubber Manufacturers' Research Association, during the 19th Rubber Conference, held at Mumbai during December 19-20, 2005.

Abstract

The effect of gamma radiation on the morphological and physical properties of Styrene-butadiene rubber (SBR) and Ethylene-propylene diene monomer (EPDM) blends has been investigated. The enhancement in the miscibility of blend components in solution phase was observed after irradiation. The probability of spur overlap has been found to increase with the increase in EPDM content in the blends in solid phase, which in turn results in significant improvement in the mechanical properties of the irradiated SBR-EPDM blends with higher EPDM fraction. The efficiency of four multifunctional acrylates as crosslinking aid for the radiation induced vulcanization of SBR-EPDM blend was also studied. The results established lower efficiency of methacrylates over acrylates in the process and indicated that among the crosslinking agents studied trimethylolpropane triacrylate (TMPTA) is the most efficient.

Introduction

Blending of polymers is a well-known, economically viable and versatile way to prepare new engineering material. It allows to overcome certain deficiencies of the parent material by incorporating other suitable component and also to develop new structural systems by mixing different polymers¹⁻². Elastomers/elastomers or elastomers/plastic blends are usually vulcanized by using conventional chemical methods) to improve their mechanical and physical characteristics. However,

high-energy ionizing radiation has recently received a great deal of attention, primarily because of its ability to produce crosslinked networks with a wide range of polymers. The low operation cost, additive free technique and room temperature operations are among the added advantages of radiation vulcanization over the existing vulcanizing techniques³⁻⁷.

The blends of SBR (unsaturated) with EPDM (saturated) are of the special interest because incorporation of suitable amount of EPDM in SBR is expected to impart

significant heat and ozone resistance to SBR matrix⁸. On the other hand, EPDM has weak adhesion property and the products based on sulfur vulcanized EPDM have poor tear strength⁹. Hence, radiation induced vulcanization of SBR/EPDM blends would combine their desired properties including good weatherability and high mechanical strength. However, requirement of high radiation dose for desired extent of crosslinking enhances the cost of radiation vulcanization process as well as it may adversely affect the mechanical properties. To overcome these two disadvantages of radiation processing, the use of multifunctional acrylates (MFAs) and allylic reactive molecules in the process has been proposed¹⁰⁻¹³.

The objective of the present work is to study the interaction between the EPDM and SBR segments and to seek a correlation of blend morphology with the radiation sensitivity of the matrix. In addition to it, an attempt has also been made to look for a suitable multifunctional acrylate for efficient radiation crosslinking of these blends.

Experimental

Materials

Styrene-butadiene rubber (SBR) (Synaprene-1502, Styrene content 25 %) and Ethylene-propylene diene monomer (EPDM) (Kelton -512, Ethylene content 55%) was supplied by local supplier in block form. The multifunctional acrylates employed in the present study were procured from Aldrich chemicals, USA and used as such without further purification.

Sample preparation

Blends of SBR and EPDM of different composition were prepared by initially mixing both rubbers on a 2-roll laboratory mill (Table 1). The blends were then molded

into sheets of dimension 15x15x0.2 (lxbxh) cm using a compression-molding machine at 150 kg/m² pressure at 130°C.

Table 1: Compositional characteristics and designation of the blends

Sample designation	SBR (%)	EPDM (%)
S ₁₀₀ E ₀₀	100	00
S ₇₅ E ₂₅	75	25
S ₅₀ E ₅₀	50	50
S ₂₅ E ₇₅	25	75
S ₀₀ E ₁₀₀	00	100

Irradiation

Irradiation was carried out under aerated condition using a gamma chamber 5000 (GC-5000) having Co-60 gamma source supplied by M/s BRIT India. The dose rate of gamma chamber was ascertained to be 5 kGy/hr by using Fricke dosimetry prior to irradiation of samples.

Gel Content

The Gel content was determined by refluxing the samples with xylene for 24 Hrs. The remaining insoluble portion was rinsed with methanol and dried in vacuum oven at 60°C to a constant weight. Gel content was evaluated using following relationship.

$$\text{Gel content} = \left(\frac{W_g}{W_i} \right) \quad (1)$$

Where W_g and W_i are the weight of insoluble fraction and initial weight respectively.

Differential scanning calorimetry

Differential scanning calorimetry (TA 2000) was used to observe glass transition behavior. The instrument was calibrated for temperature and heat flow using high purity standard. The mid point of the slope change of heat capacity plot of second scan was taken as the glass transition temperature. Heating rate of $20^{\circ}\text{Cmin}^{-1}$ was adopted and an inert atmosphere was maintained throughout the DSC run.

Morphological Studies

Cryogenically fractured surfaces were examined by a scanning electron microscope (SEM). Acceleration voltages of 30 kV and magnification range from 200 x to 10000 x have been used. The fractured surfaces were coated with a thin layer of gold prior to SEM examination.

Mechanical properties

For tensile strength measurements at least five dumbbell shaped specimens were cut from blend sheets using a steel die of standard width. The thickness of the samples were determined to the nearest of 1 mm. The tensile strength and elongation at break were measured by INSTRON universal testing machine using crosshead speed of 300 mm/min at room temperature.

Result and discussion

Compatibility analysis of SBR EPDM blends in solution

Fig. 1 represents the variation of hydrodynamic interaction parameter $[\eta]_{\text{mix}}^{\text{exp}}$ with change in composition of blends for un-irradiated blends; the straight line represents the additive value of intrinsic viscosity of mixture ($[\eta]_{\text{mix}}^{\text{id}}$)¹⁴⁻¹⁶. It can be seen that in the composition range studied the experimental value of intrinsic viscosity is higher than the theoretical value

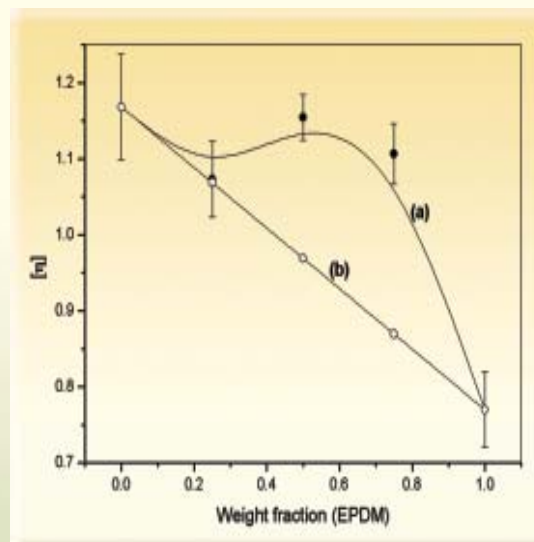


Fig. 1 : Intrinsic viscosity variation for un-irradiated SBR-EPDM blends in toluene (a) experimental profile (b) theoretical profile

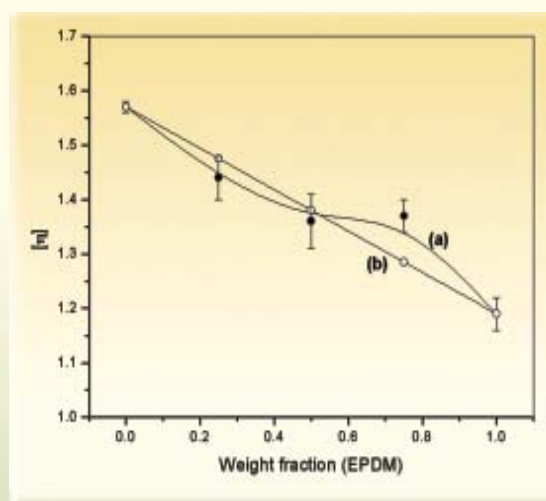


Fig. 2 : Intrinsic viscosity variation for SBR-SPDM blends irradiated to a dose of 10 kGy (a) experimental profile (b) theoretical profile

calculated on the basis of ideal behavior assumption. According to the assumption, positive deviation from ideal solution behavior means repulsive interaction between the two polymers, indicating that

un-irradiated SBR/EPDM blends are incompatible over the whole composition range. Based on the sign convention, it is clear that miscibility criteria are not satisfied for the SBR/ EPDM blends in the composition range of present study. Fig 2 shows profiles for the blends irradiated to a dose of 10 kGy. The experimental value of intrinsic viscosity was found to be lower than theoretical value for blends up to 60 % EPDM content and it was $>[\eta]_{\text{mix}}^{\text{id}}$ values for blends of higher EPDM content. As all of the miscibility criteria is satisfied in the composition range 0-60 % of EPDM, it was concluded that the SBR-EPDM blends are compatible in the above-mentioned range, when it is pre irradiated to an absorbed dose of 10 kGy.

Glass transition variation with blend composition

In general the miscibility of two blends is inferred from the presence of single glass transition temperature, however, in the present SBR/EPDM system the glass transition values are very closely spaced ($<5\text{K}$) hence, a conclusive remark on the immiscible or miscible nature of these two components can not be made on the basis of T_g evaluation. Nevertheless, we tried to quantitatively evaluate the T_g -composition relationship to get information about the scale of blend homogeneity. Accordingly, fitting of the T_g data with following models available for the estimation of interaction strength between the blend components were examined¹⁷⁻¹⁹. The value of K (Gordon-Taylor parameter) was found to be 1.38 ± 0.15 with the intercept value 216.66K from the least square method. K value clearly indicates about the poor interfacial interaction between the blend components. T_g 's predicted by additive rule and Fox equation found to be less than the experimental values, whereas a good correlation was observed with the T_g evaluated from Gordon-Taylor (Fig. 3).

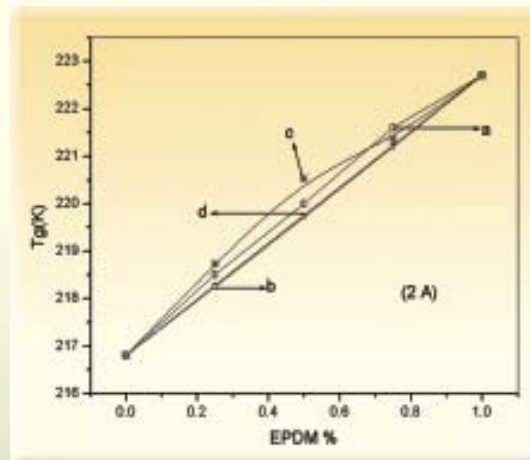


Fig. 3 : Comparison of DSC determined T_g 's and T_g 's predicted by different equations for un-irradiated SBR-EPDM blends (a) experimental profile (b) additive rule (c) Gordon-Taylor equation (d) Fox equation

The extent of homogeneity of SBR/EPDM blends has also been evaluated from the heat of mixing of SBR/EPDM blend system, calculated according to the following equation.²⁰

$$\Delta H_m = (1-w_b)M_a\rho_a(\delta_a - \delta_b)^2 x \left[\frac{w_b}{(1-w_b)M_b\rho_b + w_bM_a\rho_a} \right] \quad (2)$$

Where M , w , δ and ρ are the molecular weight of monomer unit, weight fraction, solubility parameter and the polymer density respectively and subscript a and b refers to SBR and EPDM respectively. The behavior of heat of mixing over the whole composition range is shown in Fig. 4, it was found to lie between 0.05 - 0.13J . It is clear that ΔH_m increases with increase in weight fraction of EPDM in the blend, attains maximum value at $\sim 70\%$ and decreases afterwards. Scheneir²² has calculated the ΔH_m value for many polymer pairs and showed for compatible polymer pairs, the value lies in the range 4×10^{-3} to $4 \times 10^{-2}\text{J}$. Therefore, thermodynamics of the system predicts immiscibility of SBR-EPDM blends over the entire composition range in the present scenario.

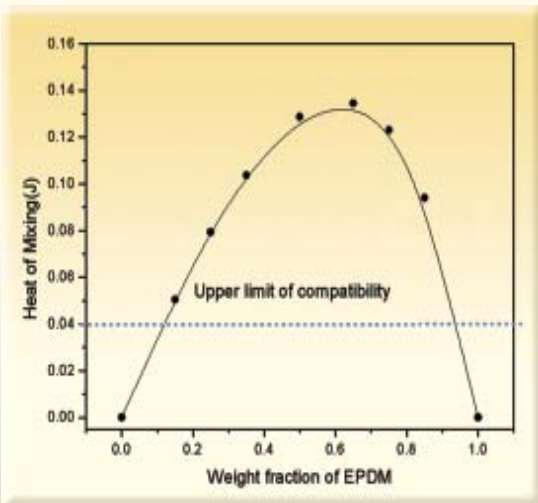


Fig. 4 : Variation of heat of mixing for SBR/ EPDM blends of different composition

clearly figured whereas for the $S_{75}E_{25}$ it is not that conspicuous. At higher EPDM fractions, the SBR matrix was found to be embedded (disperse phase) in the continuous EPDM phase, whereas, at lower EPDM weight fractions co-continuous morphology of SBR and EPDM were observed. These results resembles to our observations in an earlier investigation on the segmental interactions of EPDM and SBR in the presence of solvent, where, by using solvent permeation techniques, the co-continuous phase of EPDM was established in all the composition range²³. SEM of the blends also indicated the higher rigidity of EPDM phase in comparison to SBR phase.

Effect of gamma radiation on SBR/ EPDM blends

Scanning electron microscopy

The scanning electron micrographs of fractured and OsO_4 treated surfaces have been shown in Fig. 5. For the compositions $S_{25}E_{75}$ and $S_{50}E_{50}$ phase separation can be

Gel content of blends

Fig. 6 shows the change in the gel content of SBR-EPDM blends on irradiation. Un-irradiated samples were found to be easily soluble in hot xylene, however

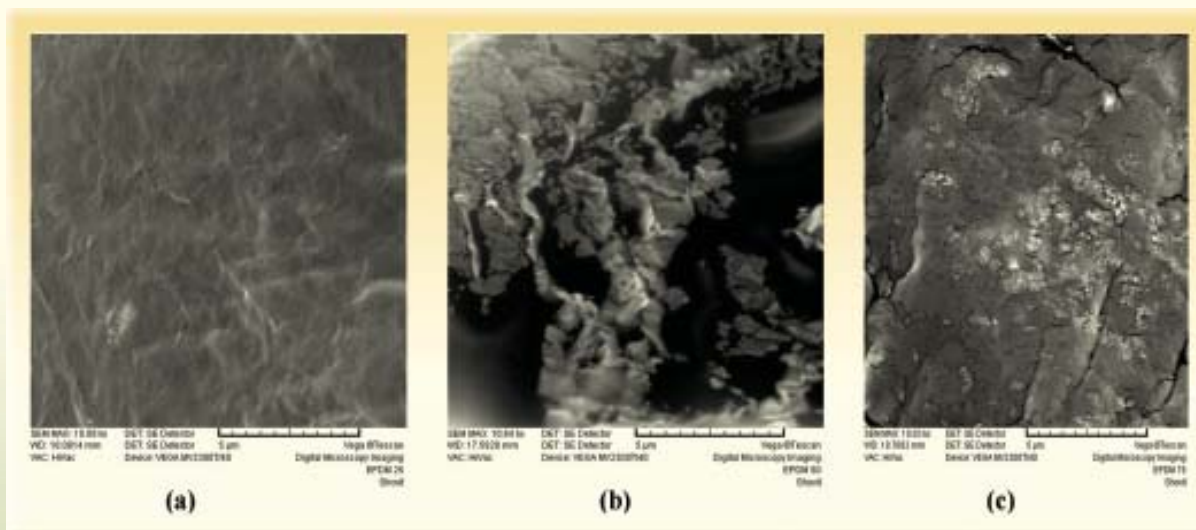


Fig. 5 : Scanning electron micrographs of SBR/EPDM blends (a) EPDM 25 %(b) EPDM 50 %(c) EPDM 75 %

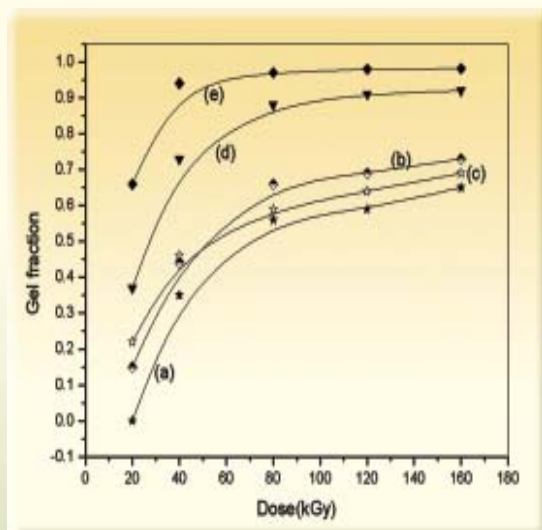


Fig. 6 : Change in Gel fractions of blends on irradiation at a dose rate of 5 kGyh⁻¹ for different compositions of SBR/EPDM blends (a) EPDM 0 % (b) EPDM 25 % (c) EPDM 50 % (d) EPDM 75 % (e) EPDM 100 %

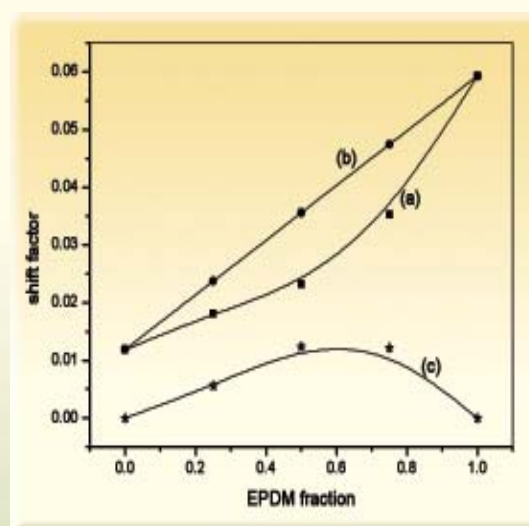


Fig. 7 : Shift parameter variation for SBR-EPDM blends (a) Experimental profile (b) Theoretical profile (c) Difference between theoretical and experimental values

blends irradiated to a dose >20 kGy were insoluble due to the formation of a three-dimensional network²³⁻²⁵. Sol-gel studies revealed higher sensitivity of EPDM to irradiation, as for a dose of 40 kGy gel fractions of 94% and 30% were found for pure EPDM and SBR respectively. It was expected that for a particular radiation dose, the gel-content of the blends would lie in between the pure SBR and pure EPDM depending on their composition however, it was interesting to note that the gel content value of S₂₅E₇₅ was very close to pure EPDM whereas S₇₅E₂₅ and S₅₀E₅₀ showed value of gel contents closer to pure SBR in the dose range studied.

Fig. 7 represents the variation in chemical shift parameter with EPDM weight fraction, it can be clearly seen that the difference in the chemical shift factor from the experimental and calculated values is maximum at 1:1 blend composition indicating the highest lifetime of the spurs formed at this composition. This high deviation in the b value can be attributed to morphological

variations, as it can be clearly seen from the SEM profiles that loosening of the structure is the highest at 1:1 composition. In addition to this an increase in interatomic distance is also expected due to poor polymer-polymer interaction parameter at 1: 1 composition. It is well documented that for any polymer during irradiation crosslinking and degradation proceed simultaneously and the net effect seen is due to the predominant process between the two²⁶ and the crosslinking efficiency or the gel content is decided by the efficient recombination of macro-radicals generated in the irradiated matrix²⁷⁻²⁸. Hence, based on these observations it can be safely concluded that in the blends of immiscible SBR/EPDM system, presence of SBR decreases the interaction probability between close lying macromolecule radicals and this effect is highest at 1:1 composition.

Tensile strength of blends

One of the most obvious effects brought about by

irradiation on the blends due to their crosslinking/ degradation is in their tensile strength. Fig. 8 illustrates the tensile strength of the blends as a function of radiation dose. Tensile strength of pure EPDM, pure SBR and their blends was found to increase continuously in the dose range of study.

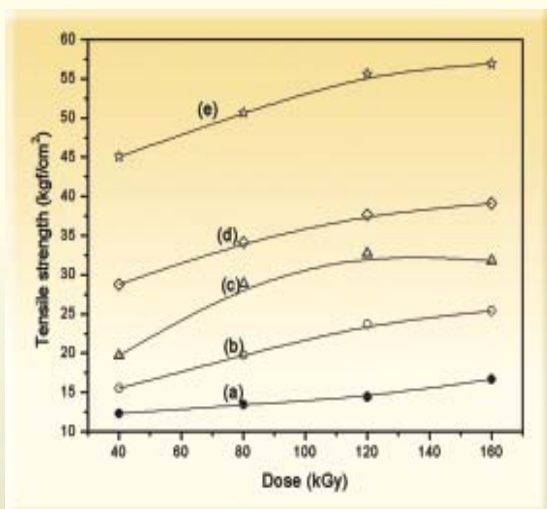


Fig. 8 : Change in tensile strength of blends on irradiation at a dose rate of 5 kGyh⁻¹ for different compositions of SBR/EPDM blends (a) EPDM 0 % (b) EPDM 25 % (c) EPDM 50% (d) EPDM 75 % (e) EPDM 100 %

Further, the observed trend for the intermediate blend compositions is on the expected lines i.e. the tensile strength of the blends increases with increase in EPDM content and absorbed dose. Fig. 9 shows the relationship between elongation at break and irradiation dose of the samples. The elongation at break decreased with dose for all blends due to more crosslinked structures produced in the sample matrix, which prevents the structural organization during drawing and brings about a decrease in internal chain mobility and elongation.

Simple kinetic adjustments were also carried out by means

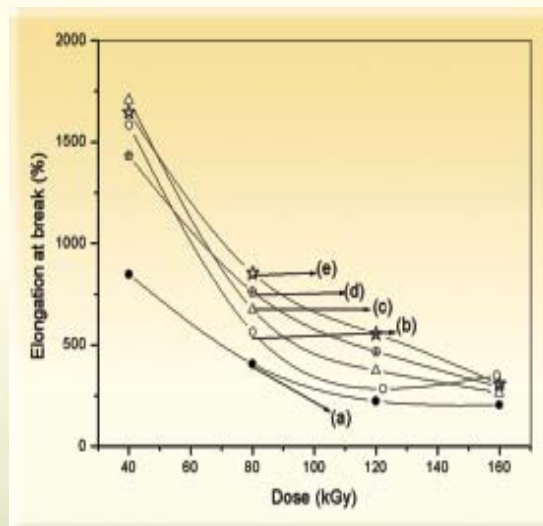


Fig 9 : Change in elongation at break of blends on irradiation at a dose rate of 5 kGyh⁻¹ for different compositions of SBR/EPDM blends (a) EPDM 0 % (b) EPDM 25 % (c) EPDM 50 % (d) EPDM 75 % (e) EPDM 100 %

of mathematical equations to the mechanical properties analyzed namely tensile strength and elongation at break in order to theoretically predict the radiation dose up-to which improvement in these properties will be observed as reported by other workers for other blends²⁹⁻³⁰. The observed behavior of the variation of tensile strength and elongation at break for different compositions of SBR/EPDM blends were fitted in a third order polynomial behavior, which is indicative of complex cross linking and chain scission mechanism, that predominantly depend upon the radiation dose. General third order equation correlating tensile strength (σ) and elongation at break (ϵ) to radiation dose (D) can be written as follows

$$\sigma = \alpha + \beta D + \gamma D^2 + \delta D^3 \quad (3)$$

$$\epsilon = a + bD + cD^2 + dD^3 \quad (4)$$

The mathematical expressions corresponding to the kinetic behavior of the blends showed a correlation

Table 2: Kinetic parameters for the radiation vulcanized SBR: EPDM blends

→ Composition	EP 00	EP25	EP50	EP75	EP100
Parameters					
α	9.56612	12.94847	5.03796	21.79106	42.07648
β	09953	0.02722	0.43831	0.19378	0.01673
γ	-0.00094	0.00112	-0.00183	-0.00045	0.00179
δ	3.729E-6	5.0182E-6	8.3235E-7	-5.3646E-7	-8.1889E-6
a	1638.32	3739.19258	3368.06072	2725.12923	4020.57541
b	-24.92	-71.39741	-58.36117	-42.211	-78.26856
c	0.1384	0.4785	0.42775	0.27316	0.5685
d	-0.00024	-0.00103	-0.00114	-0.00065	-0.00141

index (r^2) between 0.9 and 1. The values of fitting parameters α , β , γ , δ , a, b, c and d for different blend compositions are listed in Table 2.

It is clear from the values of parameters presented in Table 2 that kinetic parameters acquire significantly different values depending on composition of blends, where positive value of parameters are indicative of cross-linking and negative numbers of chain scission. These values reflect that there is difference in the radiation sensitivity of the blends and the effect of irradiation is not exactly in the weighted average of individual components in the blend. This observation further supports our explanation provided for the gel-fraction behavior with radiation dose and composition discussed in the previous sections. However, it may be noticed that the tensile strength variation with dose and composition does not similitude with the gel fraction mainly because (1) the tensile strength results does contains some contribution from sol part present in the

specimens (2) the contribution from the other radiolytic reactions like double bond formation, disproportionation, and hydrogen abstraction during irradiation. It has been stated that these parameters can also be extrapolated to the other physical properties P, and then the modification law of the property can be represented as

$$P = \lambda P_0 * g(D) \quad (5)$$

where P_0 is the property prior to irradiation, λ is an adjustment factor, and g is function of integral dose²⁹.

Effect of addition of MFAs on the addition sensitivity of 50:50 SBR/EPDM blend

Various properties of irradiated SBR/EPDM blends reported in earlier sections, indicate poor radiation sensitivity of 50:50 SBR/EPDM blend composition, hence this composition has been chosen to investigate the efficiencies of MFAs listed in Table 3.

Table 3: Properties of multifunctional acrylates employed in the study

Multi functional acrylate(MFA)	Structure	Functionality	M.W.	Designation
Blank	-----	Nil	---	(S _{0.5} E _{0.5}) _B
Ethylene glycol dimethacrylate (EGDMA)	[H ₂ C=C(CH ₃)CO ₂ CH ₂] ₂	2	198.22	(S _{0.5} E _{0.5}) _E
Tri(propylene glycol) diacrylate (TRPGDA)	H ₂ C=CHCO(OC ₃ H ₆) ₃ O ₂ CCH=CH ₂	2	300.25	(S _{0.5} E _{0.5}) _T
Trimethylolpropane triacrylate (TMPTA)	(H ₂ C=CHCO ₂ CH ₂) ₃ CC ₂ H ₅	3	296.32	(S _{0.5} E _{0.5}) _{TM}
Trimethylolpropane trimethacrylate (TMPTMA)	[H ₂ C=C(CH ₃)CO ₂ CH ₂] ₃ CC ₂ H ₅	3	338.40	(S _{0.5} E _{0.5}) _{TMM}

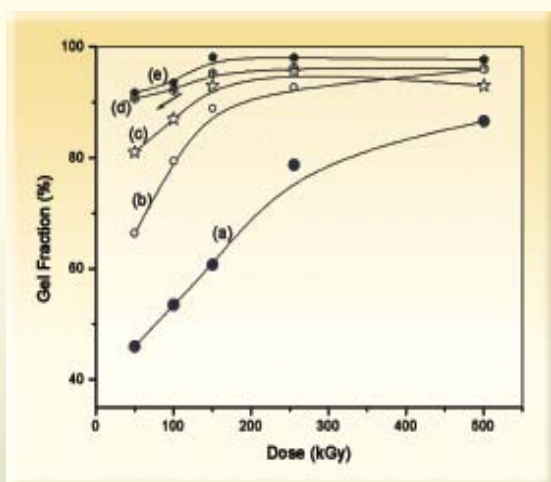


Fig. 10 : Change in Gel fraction of 50:50 SBR/EPDM blends on irradiation at a dose rate of 5 kGyh⁻¹ (a) Blank (b) EGDMA (c) TRPGDA (d) TMPTMA (e) TMPTA

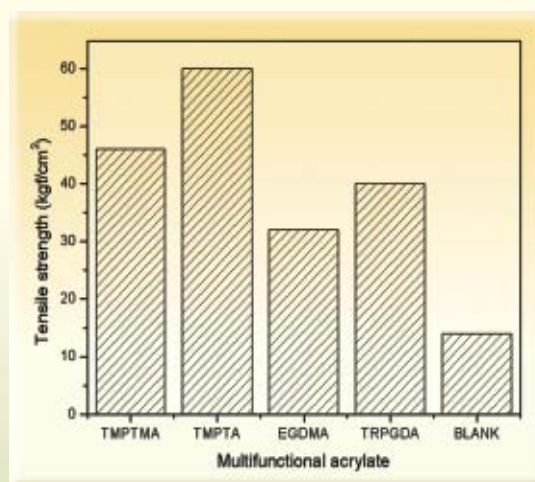
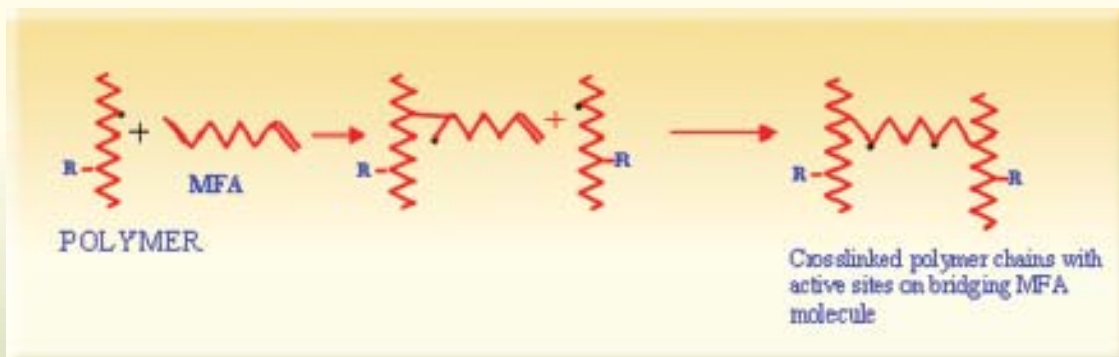


Fig. 11 : Effect of multifunctional acrylates on tensile strength of SBR:EPDM (50:50) blend irradiated to a dose of 25 kGy at a dose rate of 5 kGyh⁻¹ (a) Blank (b) EGDMA (c) TRPGDA (d) TMPTMA (e) TMPTA

The variation in gel content when different MFAs were added to the blend matrix (1%w/w) is shown in Fig. 10. As expected there is an increase in gel content on introduction of MFAs in the pure blends because the multifunctional acrylates employed in this study are well known reactive additives that form bridges by radiation-induced free radical mechanism and produces

a network structure at lower doses (Scheme 1)¹⁰⁻¹³. The effect of addition of MFAs on the tensile strength of SBR/EPDM (50:50) blend irradiated to 25 kGy is shown in Fig. 11. As shown in the Fig. 9, the variation in T_s follows the order (S_{0.5}E_{0.5})_{TM} > (S_{0.5}E_{0.5})_{TMM} > (S_{0.5}E_{0.5})_T > (S_{0.5}E_{0.5})_E > (S_{0.5}E_{0.5})_B, which is in close agreement with the gel content studies in presence of these MFAs.



Scheme 1

Conclusion

In summary, our studies show that gamma irradiation of SBR-EPDM blends to a threshold dose induces good compatibility between the two components SBR and EPDM which otherwise show poor compatibility. The study confirmed that the gamma irradiation of SBR-EPDM blend causes improvement in certain properties of interest and significant reduction in the dose demand can be achieved with the incorporation of multifunctional acrylates. The SBR/EPDM system was found to be immiscible in nature; this conclusion has been verified in the light of various parameters like Gordon-Taylor parameter and shift parameter. Gel fraction of the blends increased with EPDM content in the blend but not as expected on the weighted average value of SBR and EPDM incorporated in the blend. Tensile strength, hardness studies showed a good agreement with gel content studies. Reduction in elongation at break of the blends with increase in radiation dose has been attributed to prevention of the structural organization during drawing due to the formation of crosslinked network. Physical and mechanical properties of the blends were found to be significantly enhanced by using MFAs as radiation vulcanizing aid and TMPTA was found to be most effective crosslinking agent for the system.

References

1. Raghavan, D.; Gu, X.; Nguyen, T.; VanLandingham, M.; Karim, A. *Macromolecules* 2000; 33: 2573-2538.
2. Koing, C.; Duin V.M.; Pagnouille, C.; Jerome, R. *Prog. Polym. Sci.* 1998; 23: 707-757.
3. Aoshuang, Y.; Zhengtao, G.; Li, L.; Ying, Z.; Peng, Z. *Radiat. Phys. Chem.* 2002; 63: 497-500.
4. Sharif, J.; Aziz, S.H.S.A.; Hasim, K. *Radiat. Phys. Chem.* 2000; 58: 191-195.
5. Ahmed, S.; Basfar, A.A.; Aziz, M.M.A. *Polym. Degrad. & Stab.* 2000; 67: 319-323.
6. Basfar, A.A.; Silverman, J.; *Radiat. Phys. Chem.* 1995; 46(4-6): 941-944.
7. Banik, I.; Bhowmick, A.K. *Radiat. Phys. Chem.* 2000; 58: 293-298.
8. El-Sabbagh, S.H. *Polymer Testing* 2003; 22: 93-100.

9. Zaharescu, T.; Meltzer, V.; Vilcu, R. Polym. Degrad. & Stab. 2000; 70: 341-345.
10. Vijayabaskar, V.; Bhatatacharya, S.; Tikku, V.K., Bhoiw Mick A.K. Radiat. Phys. Chem. 2003; 9-19.
11. Yasin, T.; Ahamed, S.; Yoshii, F.; Makuuchi, K. React. & Funct. Polym. 2002;53: 173-181.
12. Banik, I.; Dutta, S.K.; Chaki, T.K.; Bhowmick, A.K. Polymer 1999; 40: 447-458.
13. Jayasuriya, M. M.; Makuuchi, K.; Yoshii F. Eur. Polym. J. 2001; 37: 93-98.
14. Kulshrestha, A. K.; Singh, B. P.; Sharma, Y. N. Eur. Polym. J. 1988; 24: 29-32.
15. Kulshrestha, A. K.; Singh, B. P.; Sharma, Y. N. Eur. Polym. J. 1988; 24: 33-37.
16. Chee, K. K. Eur. Polym. J. 1990; 26: 423-428.
17. Minto, F.; Gleria, M.; Pegoretti, A.; Fanbri L. Macromolecules 2000; 1173-1180.
18. Kuo W.S.; Chang, C.F. Macromolecules 2001; 34: 4089-4097.
19. Chiuf, C.; Huang, K.H.; Yang, C. J. Polym. Sci. Part B: 2000; 412: 2264-2274.
20. Zhong-Yu, W., J. Poly. Sci. Part B Polym Phy. 2003; 41: 2296-2301.
21. Gardon, J.L. Cohesive energy density In Encyclopedia of polymer science and Technology, Mark, H.F.; Gaylord, N. G.; Bikales N. M. (Eds.) Interscience, New York NY, 1965; 3: pp 833-863.
22. Schneier, B. J. Appl. Polym Sci 1973; 17: 3175-3185.
23. Dubey, K. A.; Bhardwaj, Y. K.; Chaudhari, C. V.; Sabharwal, S. J. Appl. Polym. Sci., 2005 (In press)
24. Hopfenberg, H.B.; Paul, D.R., S., Mewman(Eds.), polymer blends, Academic Press, New York, 1978; 1: P445.
25. Chapiro, A.; Radiation chemistry of polymeric systems 1962. John Wiley & Sons, New York pp 339-383 .
26. Woods, R. J. ; Pikaev, A. K. Polymer Modification 1993. In: Applied radiation chemistry: Radiation Processing, John Wiley & Sons. Inc. pp. 339-391.
27. Zagorski, Z.P. Radiat. Phys. Chem. 2002; 63: 9-19.
28. Sonntag, C.V.; Bothe, E.; Ulanski, P.; Adhikary, A. Radiat. Phys. Chem. 1999; 55: 559-603.
29. Albano, C., Reyes, J., Ichazo, M. N., Gonzalez, J., Rodriguez, M. Nucl. Instr. and Meth. B 2003; 208: 485-488.
30. Chipara, M. I. Nucl. Instr. and Meth. B 1997;131: 180.

ABOUT THE AUTHORS



Mr K. A. Dubey did his M. Sc. From IIT Roorkee in the year 2000. After graduating from 42nd batch of training school he joined RTDS. His research interests include radiation induced

compatibility behaviour of elastomers in solutions and solid blends. radiation modification of elastomers to synthesize TPE and suitable compatibilizers for elastomer blends of diverse properties and radiation cured elastomer based nano-composites for novel applications.



Mr C.V. Chaudhari graduated from the University of Poona in 1986. He joined Radiation Technology Development Section in 1988 and has since been involved in radiation processing of polymers particularly

elastomers. He did his M. Sc. from University of Mumbai. His present interests include modification of elastomers to TPE by radiation induced grafting, synthesis of suitable compatibiliser for elastomer blends, radiation vulcanization of synthetic and natural rubber latex.



Dr Y. K Bhardwaj joined Radiation Technology Development Section in 1989 and later did his Ph. D from the University of Mumbai. His research interests include development of grafted polymer matrices, elastomer blends, high performance coatings utilizing electron beam and gamma radiation for industrial applications. He has been actively involved in the studies on radiation polymerization/crosslinking of monomers/polymers, development of radiation processed hydrogels for medical and pharmaceutical applications, synthesis of fast stimuli-responsive hydrogels and radiation crosslinking behaviour of water soluble polymers.

APPLICATION OF NEUTRON RADIOGRAPHY AND NEUTRON DIFFRACTION TECHNIQUES IN STUDY OF ZIRCONIUM HYDRIDE BLISTERS IN ZIRCONIUM BASED PRESSURE TUBE MATERIALS

A.M. Shaikh

Solid State Physics Division
Bhabha Atomic Research Centre

P.R. Vaidya and B.K. Shah

Atomic Fuels Division
Bhabha Atomic Research Centre

and

S. Gangotra and K.C. Sahoo

Radiometallurgy Division
Bhabha Atomic Research Centre

This paper was awarded the ISNT National award 2004, under the category
"Best Paper published in R&D" in the Journal *Non Destructive
Testing & Evaluation*, 2003.

Abstract

A programme of examining hydride blisters created in the laboratory on zircaloy pressure tubes and that in the irradiated pressure tube from one of the PHWR, which was suspected to have developed hydride blisters, was undertaken using neutron radiography. It was observed that a zirconium hydride blister of nearly 0.35% of job thickness could be detected using neutron radiography. This work served as a reference in examining irradiated zircaloy pressure tubes from a power reactor with residence time of ~ 8.25 effective full power years. Neutron radiography was also used to study size and shape of the zirconium hydride blisters embedded in the zircaloy-2 pressure tube. The zircaloy and Zr-2.5%Nb pressure tube coupons in which hydride blisters were created in the laboratory were also studied using neutron diffraction to identify the zirconium hydride phase and to find the extent to which the sample has hydrided. In order to determine the amount of hydride phase, a Rietveld refinement of the neutron diffraction pattern was carried out.

Introduction

R & D related to hydrogen in materials has been in vogue for a long time now because importance of such hydrogen containing materials for various industrial and technological applications. Some of these applications include: metal hydrogen systems for energy storage, metal hydrides as moderators in nuclear reactors, hydrogen storage alloys for automobiles. Measurement of concentration of hydrogen in such materials is obvious importance. There are other situations wherein presence of hydrogen in materials is not desirable as it leads to deleterious effects. For example presence of hydrogen in cladding materials of nuclear fuel, pressure tubes systems of nuclear plants and aircraft components can lead to hydride-induced embrittlement. Hydrogen embrittlement has to be taken into account in choice of materials for containers and heat exchangers in system containing hydrogen.

In most of the cases hydrogen is required to be measured in a bulk medium, rather than merely at a surface. For this reason neutrons are used because of their high penetrating power in the dense material. In addition the very low mass of hydrogen and its unique moderating properties, relatively large neutron energy loss per scatter together with high elastic scattering cross section (particularly incoherent scattering) compared to accompanying elements, can be exploited to study variety of details of hydrogen in metals, alloys and other materials. Various techniques using neutrons are available for hydrogen analysis. Some of them are neutron radiography, neutron diffraction, inelastic and quasielastic neutron scattering. As a part of the IAEA Co-ordinated Research Project, "Bulk Hydrogen analysis, using Neutrons" we have attempted to demonstrate application of neutrons for study of hydride blisters in zirconium based nuclear reactor

pressure tube materials, using neutron radiographic and scattering techniques.

Application of Thermal Neutron Radiography in study of zirconium Hydride blisters in zircaloy pressure tube

Pressure tubes are the most vulnerable zircaloy components in the Pressurised Heavy Water Reactor (PHWR) core. The pressure tubes operate in severe environment of high temperature($\sim 300^{\circ}\text{C}$), high pressure(11Mpa) and high neutron flux (3×10^{13} n/cm²/sec). The pressure tubes are surrounded the calandria tubes operating at 70°C . Pressure tube and calandria tube are separated by a pair of loose fit garter springs. The garter springs get displaced from their design location due to channel vibrations creating large unsupported span of pressure tube which can sag due to irradiation creep and may come in contact with the cold calandria tube. This contact can lead to a cold spot on outside surface of pressure tube. Hydrogen absorbed in the tube can migrate to the cold spot under the action of thermal gradient and form a hydride blister. These blisters hard and brittle could eventually grow and crack. Formation of series of cracked blisters could lead to rupture of the pressure tube by the delayed hydrogen cracking mechanism.

Neutron radiography is known to be capable of detecting inclusions containing low atomic number elements in a matrix of relatively higher atomic number materials. Presence of zirconium hydride blisters/ platelets in zircaloy matrix can therefore be detected by neutron radiography. In order to ascertain detection of hydride blisters in zircaloy pressure tubes, it was first necessary to establish detectability limits of hydride. To do this hydride blisters were created in the laboratory

on hydrogen charged zircaloy pressure tubes under the thermal gradients and examined using neutron radiography.

Neutron radiography was done at Apsara, a 400kw swimming pool type reactor using thermal neutrons collimated by a divergent collimator with L/D ratio of 90. Radiographs were taken by direct technique using 25mm Gd screen and D-7 type industrial x-ray film. A zircaloy plate (thickness 4mm) containing four hydride blisters of size 80 μ m, 50 μ m, 30 μ m and 10 μ m was

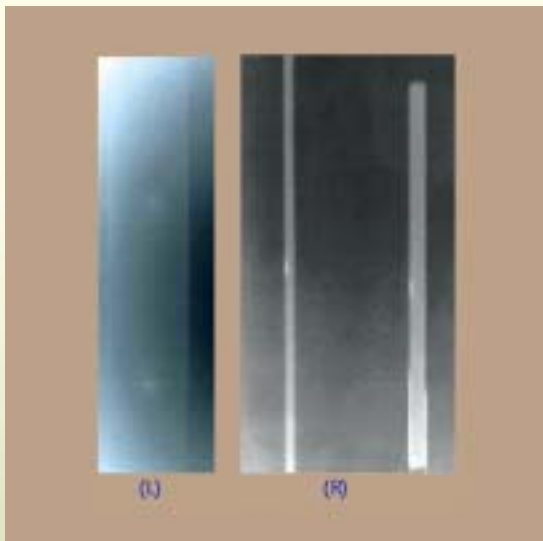


Fig. 1: Hydride blisters in zircaloy-2 (L) and Zr-Nb(R) PT coupons (Lab. Generated)

radiographed. It was observed that a zirconium hydride blister of nearly 0.35% of job thickness could be detected using neutron radiography. This work served as a reference in examining irradiated zircaloy pressure tubes from a power reactor with residence time of \sim 8.25 effective full power years. Figs.1 and 2 show neutron radiographs of the various hydride blisters examined.

Neutron radiography was also used to study size and shape of the zirconium hydride blister in the zircaloy-2 pressure tube. Figs. 3(a) and 3(b) show neutron radiographs of a pressure tube with three laboratory generated hydride blisters and with neutron beam incident parallel and normal to the plane of the blisters. Fig.3 (a) shows lenticular shape of the blister with nearly 2/3 of the blister embedded in the wall of the tube. In the present photograph maximum width of the blister corresponds

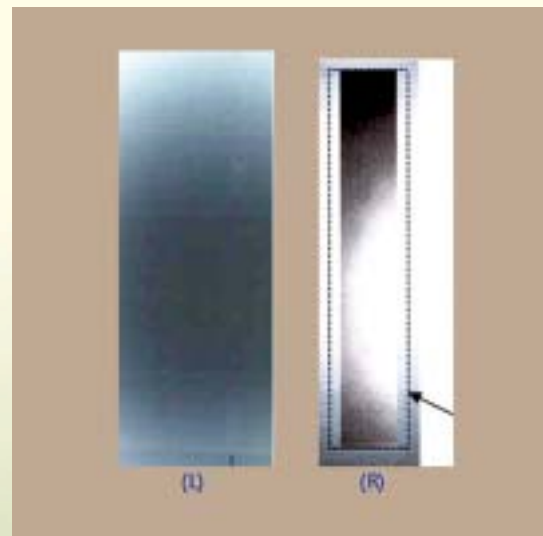


Fig. 2: Hydride blister streak in zircaloy-2 PT coupon (L) from a power reactor. Enlarged view of the blister shown in (R)

to 1.5 mm in 4 mm thick wall of the pressure tube. However the smallest blister grown in the laboratory was found to be mainly on the outer surface of the pressure tube with almost no penetration in the wall of pressure tube.

Application of Neutron Diffraction

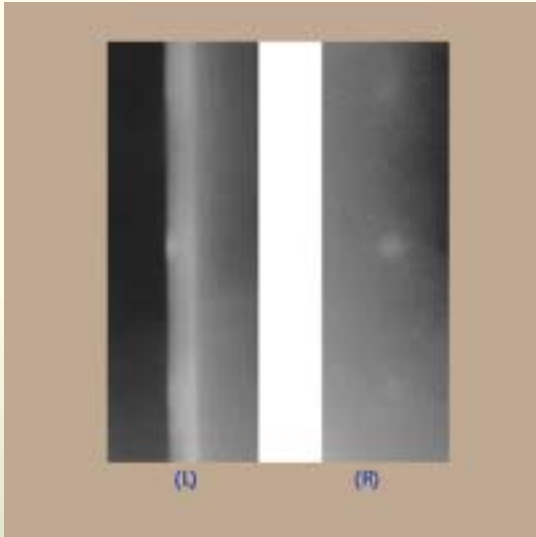


Fig. 3 : NR of zircaloy-2 PT coupons with neutrons incident parallel (L) and perpendicular(R) to the plane of blisters

The zircaloy pressure tube coupons in which hydride blisters were created in the laboratory were studied using neutron diffraction to identify the zirconium hydride phase and to find the extent to which the sample has hydrided. Neutron diffraction measurements were made with the neutron spectrometer at Dhruva reactor using $\lambda = 1.216 \text{ \AA}$. Fig. 4 shows neutron diffraction pattern of a nearly 100% hydrided sample of a zircaloy pressure tube. High background in the spectrum indicates the large proportion of hydrogen present in the system. Fig.5 is the diffraction pattern of a 1.75 mm thick zircaloy containing hydride blister of 8mm diameter and 1.75mm thickness. The pattern predominantly consists of zirconium hydride peaks. Fig.6 shows diffraction pattern of the same zircaloy plate exposed to neutrons at a position away from the

blisters. The spectrum consists mainly zircaloy peaks. All the diffraction patterns confirm formation of $\delta\text{-ZrH}_{1.66}$ phase in the zircaloy sample on hydriding. Neutron diffraction patterns were also recorded on the samples of zircaloy pressure tube with zero, 400 ppm and unknown amount of hydrogen loading respectively. All the three patterns were similar, showing absence of hydride formation. Formation of hydride blister takes place only when hydrogen concentration exceeds 13000 ppm.

In order to determine the amount of hydride phase present in the hydrided zircaloy sample, a Rietveld refinement of the neutron diffraction pattern was carried out. As described earlier, neutron diffraction pattern on various zircaloy plates with laboratory generated hydride blisters were recorded using a neutron spectrometer at Dhruva reactor with neutrons of wavelength 1.216 \AA and 2θ from 20° to 73° in steps of 0.1° . Initial survey of the data showed broadening and overlapping of the diffraction lines. This may be due to various metallurgical

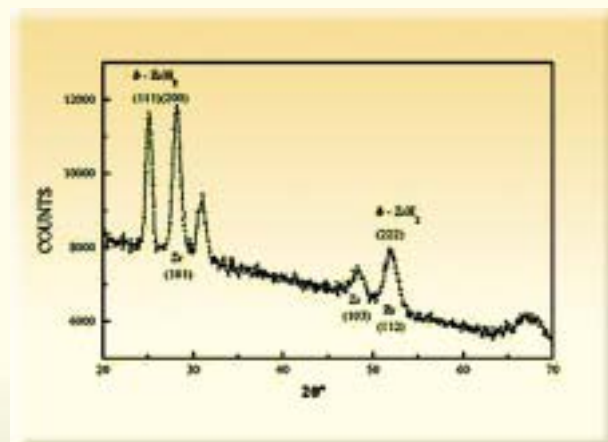


Fig. 4 : Neutron diffraction pattern of almost 100% hydrided zircaloy-2 plate ($\lambda = 1.216 \text{ \AA}$).

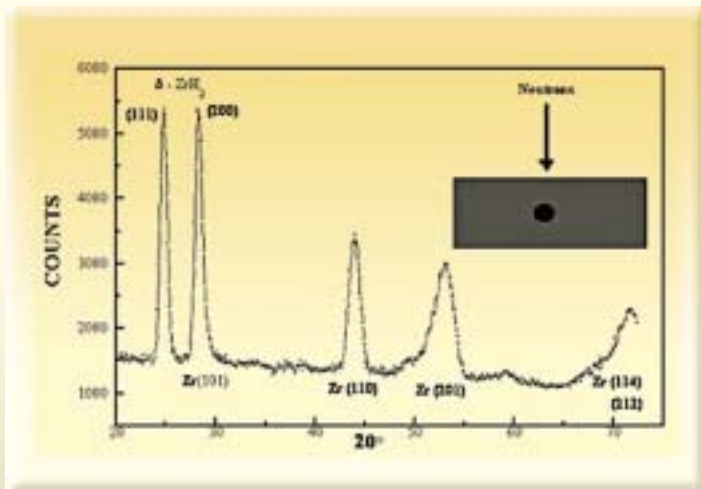


Fig. 5 : Neutron diffraction pattern of zircaloy-2 plate with 1.75 mm thick hydride blister with neutrons ($\lambda = 1.216 \text{ \AA}$) incident on the blister

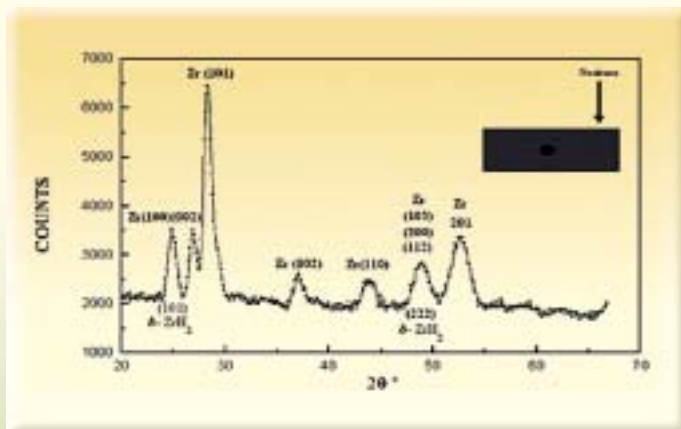


Fig. 6 : Neutron diffraction pattern of the plate of Fig. 5 with neutrons incident on the plate away from the blister

processes the zirconium sample undergone in making the zircaloy pressure tubes. The Rietveld refinement program modified version of DBLS-9411 (Young R.A., Sakthivel A., Moss T.S. and Paiva-Santos C.O., J. Appl. Cryst. 28,366, 1995) was used in resolving the peaks and refining the structure with two phases namely zirconium (hexagonal with space group P63/mmc) and $\delta\text{-ZrH}_{1.66}$ (cubic with Fm3m space group). The lattice

parameters of these compounds were taken from JCPDS files. The data was found to have high-preferred orientation, along [111] in case of zirconium and [010] for hydride phase. In the final cycles of refinement with both the phases $R(\text{profile}) = 4.60\%$ and $R(\text{Bragg}) = 6.05\%$ was achieved. The lattice parameters of both the changes showed drastic changes. The lattice parameters of zirconium were found to change from $a = 3.232 \text{ \AA}$ $c = 5.147 \text{ \AA}$ (input) to $a = 3.179 \text{ \AA}$ $c = 4.994 \text{ \AA}$ (final) and in case of hydride the a parameter changed from 4.781 \AA (input) to 4.8218 \AA (final). Results of structural refinement showing the observed and calculated profiles are shown in Fig. 7(L). The analysis gave 12 peaks for zirconium and 7 peaks for hydride phase. Except the peak at 29.02° all other peaks from hydride phase are weak. The refinement gave 98.75 % molar of zirconium phase and 1.25% molar of hydride phase. Neutron diffraction data was also collected on another pressure tube material, Zr-2.5% Nb alloy, which is superior in its properties compared to zircaloy. Fig. 7(R) shows the neutron

diffraction pattern of one such samples recorded with neutrons of wavelength 1.0940 \AA and 2θ from 11.14° to 101.38° in steps of 0.030° on a position sensitive detector based neutron powder diffractometer at Dhruva reactor, BARC. Results of the refinement showing the observed and calculated profiles are also given in Fig. 7(R). At this stage of refinement $R(\text{profile}) = 17.77\%$ and $R(\text{Bragg}) = 23.59\%$ was reached. The structures need

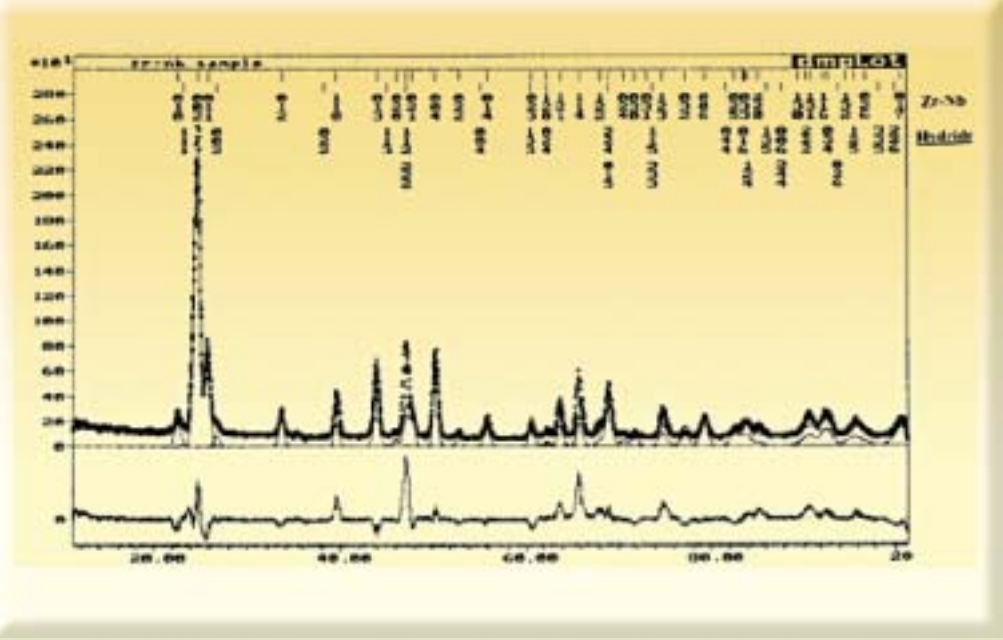
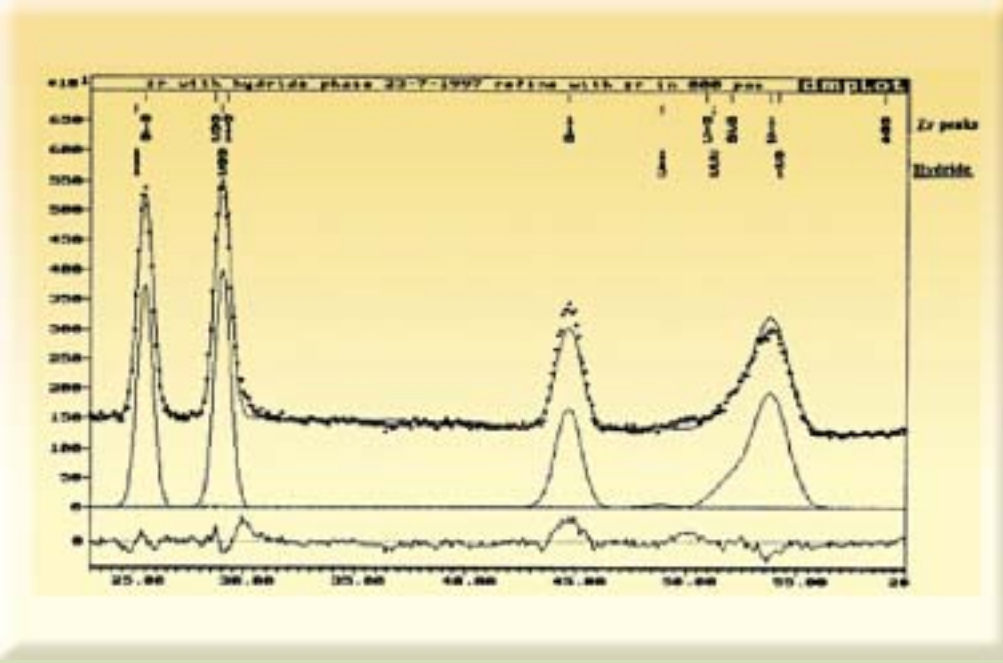


Fig. 7 : Results of structural refinement from neutron diffraction data of (A) zircaloy-2 and (B) Zr-2.5%Nb PT coupons with hydride blister, showing the observed and calculated profiles of Zr and Zr-hydride phases.

further refinement taking preferred orientations, texture and other parameters into consideration. The refinement gave 39 peaks for zirconium and 18 peaks for hydride phase. The analysis showed $\sim 99.53\%$ molar of zirconium phase and $\sim 0.47\%$ molar of hydride phase.

Application of Quasi-elastic Neutron Scattering

In order to understand the diffusion mechanism of hydrogen into zircaloy, quasi-elastic neutron scattering (QENS) measurements on the hydrided zircaloy pressure tube coupons was also undertaken. In QENS experiment the process of diffusion of hydrogen can be monitored by measuring the line broadening of a monoenergetic neutron beam. Various zircaloy coupons pure, loaded with hydrogen and containing hydride blisters were examined by QENS, using a MARX (Multi Angle Reflection Xtal) spectrometer at Dhruva reactor using $\lambda = 4 \text{ \AA}$. QENS spectra were recorded for five samples along with the instrument resolution data for comparison. The resolution data was separately recorded with standard Zr-hydride sample and superimposed on the sample data. All the QENS spectra showed no quasi-elastic peak, indicating absence of free hydrogen in the interstitial sites of Zr lattice. The appearance of only elastic peak confirmed presence of hydrogen in hydride phase as indicated by the neutron diffraction study. All the QENS spectra were recorded under the same conditions, the intensity scale in each spectrum indicates proportionately the amount of hydrogen present in each sample. QENS experiment with in situ movement of hydrogen in zircaloy is essential to study the diffusion of hydrogen.

Acknowledgements

One of the investigators(AMS) thank International Atomic Energy Agency, Vienna for sanction of the CRP project and the financial support. Thanks are also due to Dr. M. Ramanadham, Head Solid State Physics Division for the interest and support in this work. Thanks are also due to Drs. Amitabh Das and S. Mitra for the help rendered in collecting data on neutron spectrometers.

ABOUT THE AUTHORS



Dr A.M. Shaikh joined BARC in 1992. His areas of specialization are neutron & X-ray detectors, neutron radiography, high temperature X-ray crystallography and instrumentation. A Ph.D. from IISc, Bangalore, he was a post doctoral fellow at the University of Washington Seattle, USA and has worked as faculty member at IISc, Bangalore and University of Kuwait. Dr. Shaikh has been associated with IAEA in programmes related to Neutron Radiography and worked as IAEA expert in this field. He has about 90 research papers in national and international journals and conference proceedings to his credit. Dr. Shaikh is on the Board of Studies and Board of Ph.D. Examiners of many universities and research institutions in India. He is the recipient of the ISNT National Award 2003 and DAE Technical Excellence Award 2004.



Dr P.R. Vaidya a graduate of Gujarat University obtained his M.Sc and Ph.D degrees from the University of Bombay. Passing from the 13th Batch of Training School in Physics discipline, he joined Atomic Fuels Division, BARC in 1970. He has been involved in the quality control of nuclear fuels of various designs. He has carried out NDT of different reactor systems and sub assemblies apart from fuel elements. In radiography, his specialization is microfocal radiography and real time radiography. Dr Vaidya was on the Standing committee constituted by Director BARC, for Radiography Cameras and Sources from 1990 to 1997. He has been in AERB teams for regulatory inspection of operating nuclear plants and projects. He is a member of the RT Sub-committee of Bureau of Indian Standards for the last two decades. He was given the 'Ron Halmshaw Award' of the British Institute of NDT for the best paper in their journal INSIGHT. He received the 'Achievement Award (R&D)' of ISNT Mumbai Chapter, 'NDT Man of the Year' from ISNT and the 'Best paper award' for a paper published in the Journal of NDE. He has over 50 research publications in journals and symposia. He is a popular science writer and has been on the 'Consultative Panel of All India Radio, Bombay on Science & Technology Broadcast' for four years.



Mr. B.K. Shah did his B.Sc.Engg.(Metallurgy) from Regional Institute of Technology (RIT), Jamshedpur and M.Tech.(Corrosion Science and Engg.) from Indian Institute of Technology (IIT), Bombay. He joined the 17th batch of BARC Training in 1970. Presently, he is Head, NDT & Quality Evaluation Section, Atomic Fuels Division, BARC. His field of work includes: Quality assurance in the manufacture of nuclear fuel and reactor core components, Material

characterization by NDT, Metallurgical failure analysis, In-service inspection and Corrosion studies on reactor materials. He has published more than 160 papers in various national and international journals and conference proceedings. He is the recipient of the NDT National Award 1998 and ISNT Mumbai Chapter NDT Achievement Award 2001. He is Life Fellow of ISNT and Regional Controller of Examination(Western Region), National Certification Board on NDT. Presently he is the Head of the Quality Assurance Division, BARC.



Mr Suresh Gangotra is a gold medalist in Metallurgical Engineering from M.S. University for the year 1983. After completing training from the 27th Batch of Training School, he joined Radiometallurgy Division. His areas of work are Non Destructive Testing of Irradiated Nuclear Fuels and Reactor Components, Laser applications for hot and development of equipment for Pool Side Inspection of irradiated nuclear fuels.



Mr. K.C. Sahoo is a graduate in metallurgy from Sambalpur University. He joined the 14th batch of BARC Training in 1970. He worked at the hot cells Facility of Riso National Laboratory of Denmark under IAEA fellowship programme during 1976-1977. He is a specialist in the field of irradiation behaviour of nuclear fuels and reactor core components. His field of interest is non-destructive testing and metallurgy of nuclear materials. He was Head of Post Irradiation Examination Division of BARC and retired on 28th February 2006. Presently he is Raja Ramanna fellow in Health, Safety & Environment Group, BARC.

EFFECT OF LOW DOSE IONISING RADIATION AND ULTRAVIOLET RADIATION ON HUMAN KERATINOCYTE CELL LINE

P. Mehrotra, V.P. Sinkar and G. Banerjee
Environmental Safety Laboratory,
Hindustan Lever Research Centre, Mumbai

and

K.P. Mishra
Radiation Biology and Health Sciences Division
Bhabha Atomic Research Centre

This paper won the award for the Best Young Scientist Oral Presentation at the International Conference on Recent Trends in Radiation Biology, held at BARC, Mumbai, during December 1-3, 2004.

Ultraviolet (UV) and Ionising radiation (IR) are the most important external stimulus that affect skin by inducing immuno-suppression, cancer, aging, inflammation and cell death. In all these cases skin require continuous exposure of moderate to higher doses of radiation. Studies have been carried out for years to estimate the human health hazards associated with radiation but the effects of low dose of radiation are still a mystery. It has been proven that the linear threshold theory (LNT) is not applicable for low dose of radiation. There are controversial opinions exist about the effect of low doses of radiation on human health. The first hypothesis indicates the absence of a complete safe dose of radiation and any kind of exposure to radiation is always associated with risk versus benefit. The second hypothesis suggests that the health risks of IR doses below a threshold limit (less than 10 cGy) are not measurable and hence the effects are negligible and not harmful.

Radiation effects are generally categorized as somatic and genetic. Somatic effects appear within a time frame of a few hours to years. Depending on the dose received and the duration, the consequence is greater for higher doses incurred in short time periods. On the other hand, genetic effects are main cause for concern at the lower doses. The radiation doses may be small and appear to cause no observable damage, but the probability of chromosomal damage, with the consequence of mutations giving rise to genetic defect. The radiation dose received by an individual is generally low and few exposed cells damaged due to the failure of protective intracellular repair mechanism. The effects of low level ionizing radiation may accumulate over the period of time and could represent a potential health hazard.

Free radicals like reactive oxygen species (ROS) and nitric oxide (NO) are generated during stress response including radiation that activate a number of

cellular signalling cascades involved in both cell death (apoptosis, necrosis) or survival (cancer, aging) . These free radicals are known to link with Protein Kinase C (PKC) and/or Mitogen Activated Protein Kinase (MAPK). We have recently reported that UVB may induce apoptosis or transformation to human keratinocytes in a dose dependent manner. IR is also known to induce similar effects at higher dose.

In this report, we are demonstrating the cellular signaling mechanism activated by low dose of both UV and IR on human keratinocytes cell line in vitro. This may help us to understand the effects of low doses of radiation and help us to modulate the adverse responses.

Results

Induction of Free radicals (ROS, NO) by UV/IR radiation

UV radiation induced ROS generation was investigated as a function of time and dosage. An increase in the ROS level was detected immediately after the exposure to radiation, which increased linearly with time (15 and 30 min). A saturation of intensity was detected post 45 min post exposure. The results are shown in Fig. 1a.

IR induced ROS showed a linear relationship with dose. Even a low dose like 0.2 Gy showed an increase in ROS level that increased with increasing dose. On the other hand, a low dose of UV (10mJ/cm²) failed to induce ROS generation but as the dose of UV was increased to 30mJ/cm² a drastic

increase in ROS level was detected. The results are shown in Fig. 1b.

We have also investigated the role of UV/IR on NO release by A431. No statistically significant change was detected in the NO level post exposure (data not shown).

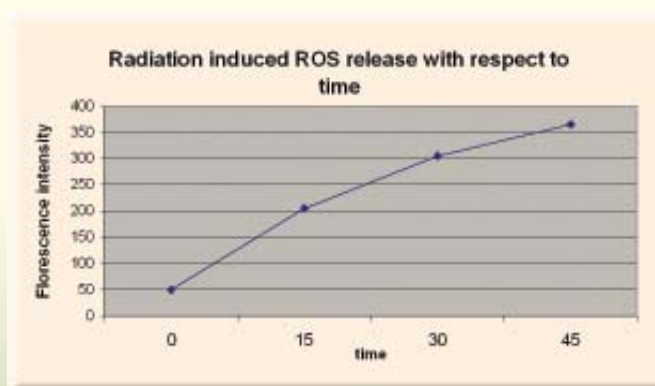


Fig.1a : Release of radiation induced ROS as a function of time using DCFDA as the dye

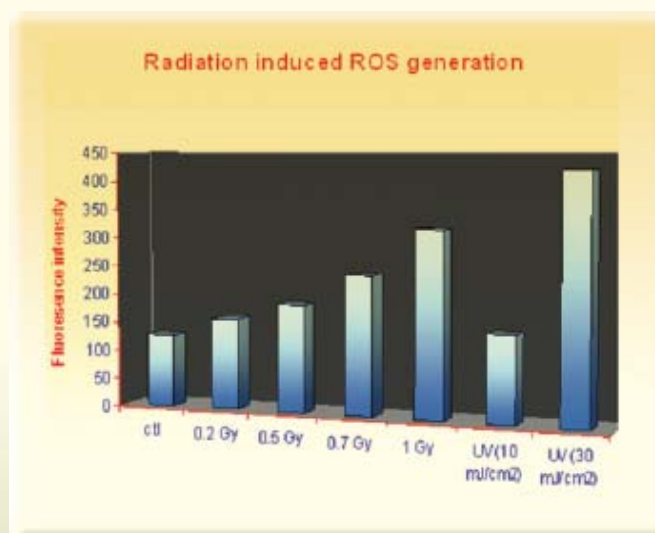


Fig. 1b : Radiation (UV and IR) induced ROS release as a function of dose after post 30 min exposure in A431 cell line. The results are a mean of three different experiments (n=3)

Alteration of mitochondrial membrane potential by UV/IR

A linear increase of the intensity of the dye was observed as a function of dose of IR upto 0.7 Gy. At a dose of 1 Gy of IR, a drastic increase of ROS was observed. Even though the generation of ROS by UV was higher than that of by IR, the alteration of mitochondrial potential was similar. Low dose of UV (10mJ/cm²) did not induce a change in mitochondrial potential. The result is shown in Fig 2.

Radiation induced change in cell membrane fluidity

Radiation induced change in cell membrane fluidity was

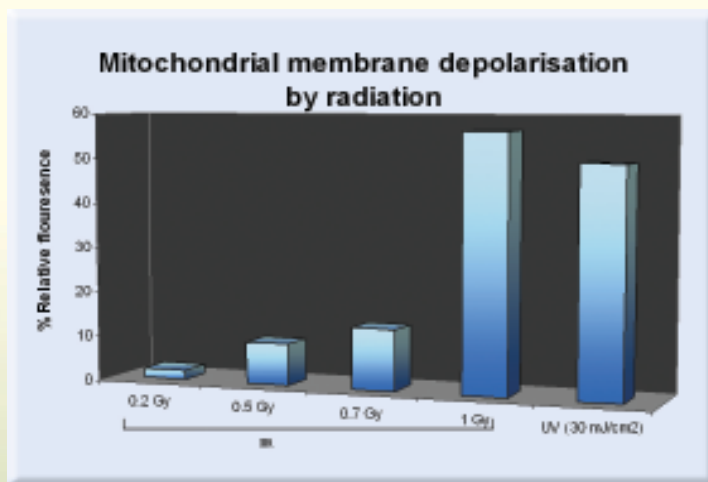


Fig. 2 : Alteration in the mitochondrial membrane by UV and IR post 1 Hr exposure in A431 cell line using Rhodamine as the dye. The results are a mean of three different experiments (n=3)

studied for over a time period of 4 hrs with 1 hr interval. By 5 hrs membrane fluidity was the same as untreated control. Membrane fluidity of keratinocytes was increased

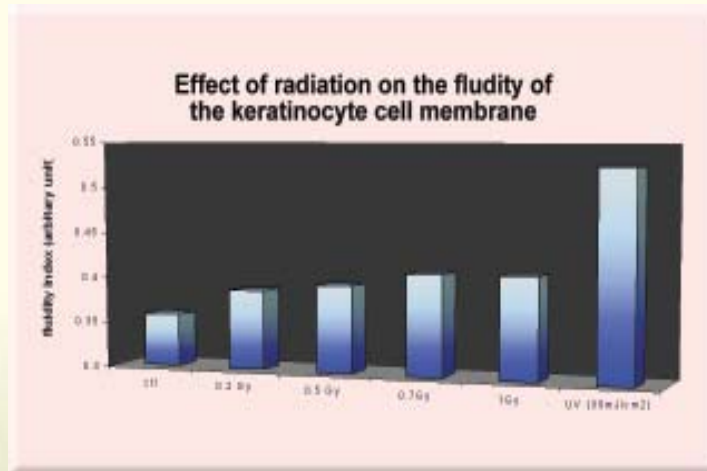


Fig. 3: UV/IR induced changes in the microviscosity of cell membrane in A431 cell post 1 Hr exposure. The results are a mean of three different experiments (n=3)

post IR as well as UV exposure. IR induced change in membrane dynamics was independent of the dose used while significant alteration of the membrane fluidity was observed when cells were exposed to UV. The result is shown in Fig. 3.

Effect of UV/IR on PKC/MAPK isoforms

Regulations of the expression of various known PKC isoforms by UV and IR in A431 cell line were investigated as a function of time and dose of radiation.

(a) Atypical PKC : Ionizing radiation had no effect on transcription level of PKC delta at 1 and 6 hrs. Complete down regulation in response to UV was seen at 1 hr but became same as that of untreated control at 6hrs.

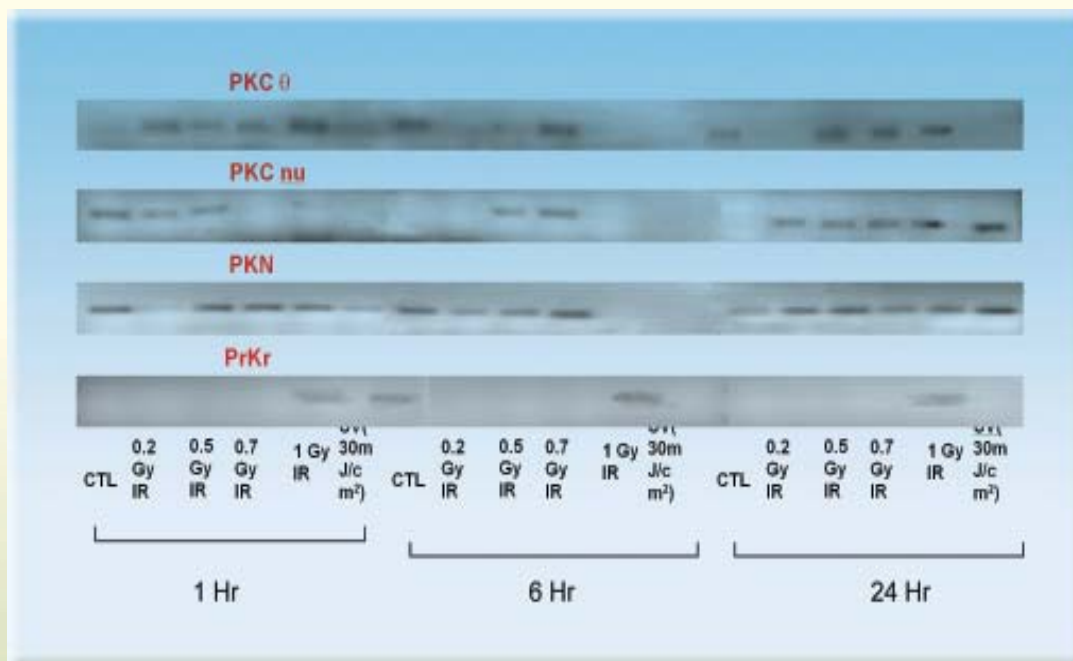


Fig. 4 : Effect of radiation (UV/IR) on PKC isoforms in A431 cell line. The results are a mean of three different experiments (n=3)

Induction of PKC θ in the untreated control was detected only at 6 hrs. Upregulation of PKC θ was observed at all doses of IR at 1 hr. At 6 hrs down regulation was observed. Complete down regulation of PKC θ was observed in UV exposed cells at all time points. The results are depicted in Fig. 4a.

Other atypical PKC isoforms were not detected in treated/untreated A431 cells at the transcriptional level.

(b) *Novel PKC*: Very low doses of ionizing radiation (0.2 and 0.5 Gy) down regulated of PKC λ at early time point (1 and 6 hrs). At higher doses (0.7 and 1 Gy) the intensity was increased and became similar to that of untreated control. On the other hand, UV down regulated PKC λ at both 1 and 6 hrs. The results are shown in Fig. 4b.

PKC ξ was not detected at the transcriptional level.

(c) *PKC related enzymes*: PKC nu was down regulated by IR radiation at 1.0 Gy post 6 hrs of exposure. No detectable change was observed at lower dose at any time point. In case of UV, the level was lower at 1 hr and completely down regulated at 6 hrs.

Upregulation of PrKr in response to IR was observed at all time points investigated. In contrary, UV induced PrKr was observed only at 6 hrs. The results are shown in Fig. 4c.

No change in PKN level was detected post exposure (data not shown).

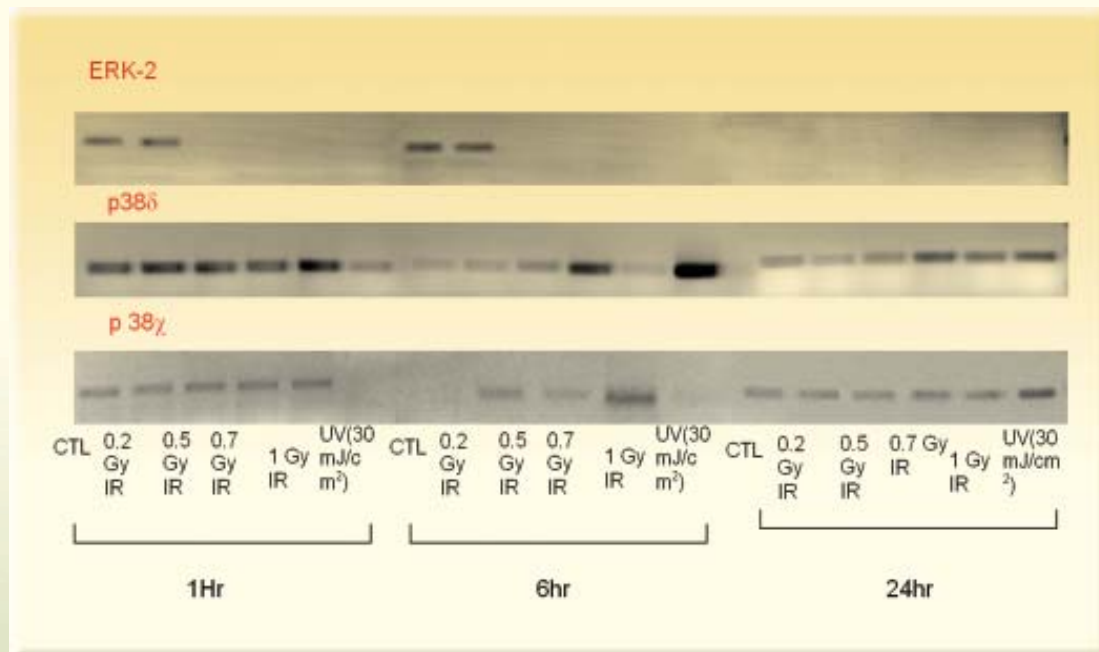


Fig. 5 : Effect of radiation (UV/IR) on MAPK isoforms in A431 cell line. The results are a mean of three different experiments (n=3)

Effect of UV/IR on MAPK isoforms

At 1 hr IR had no effect on ERK-2 except at 0.2 Gy where a complete down regulation was observed. At 6 hrs post exposure, Erk-2 was up regulated at all doses except 0.2Gy of IR. UV induced ERK-2 was observed only at 6 hrs.

No change was seen for p38MAPK δ by IR radiation (at all dose) post 1/ 6hrs. In case of UV, down regulation was seen at 1 hr but significant upregulation was seen at 6-hrs post exposure. The results are shown in Fig. 5.

p38 gamma was not affected by either IR or UV radiation (data not shown).

ABOUT THE AUTHORS



Ms Purvi Mehrotra obtained her M.Sc. degree in Biophysics from Mumbai University. She carried out her Ph.D. work in Life Science from Mumbai University under Dr. K.P. Mishra, Head, Radiation Biology and Health Sciences Division, Bhabha Atomic Research Centre, Mumbai. She was the recipient of "The Young Scientist Award" in the International Conference in Recent Trends in Radiation Biology held at BARC, December 1-3, 2004. Currently, she is pursuing her Post Doctoral Fellowship at the Tata Institute of Fundamental Research, Mumbai.



Dr Gautam Banerjee obtained his B.Sc and M.Sc degrees (Chemistry) from Jadavpur University, Calcutta. He is working as Principal Scientist at Department of Toxicology, Hindustan

Lever Research Center, Mumbai and Bangalore since 1999. His main area of interest is skin allergy and irritation. He has done his Post-Doctoral work from Yale University, USA in Immunology/ Molecular Biology (1997-99). He pursued his Ph.D. at Indian Institute of Chemical Biology, Calcutta and specialized in cell biology/ toxicology/drug delivery system (1989-95).



Dr. V.P. Sinker is currently working as the Head, Environmental Safety Laboratory in Hindustan Lever Research Center. He has done his graduation as well as post graduation

from University of Mumbai in Microbiology. He got his doctorate degree from University of Worcester in Biological Sciences. His postdoctoral experience is in Plant Molecular Biology from the University of Washington.



Dr Kaushala Prasad Mishra, Ph.D. joined BARC through 12th Batch of Orientation Course in Nuclear Research and Technology after completing postgraduation in

Chemistry from Allahabad University in 1968. He has about 38 years of experience in his field of research and his work has been well recognized internationally. His field of research spans radiation biology, free radical biology and biophysical studies on biological systems. He has published more than 125 research papers in national and international journals and chapters in books. Dr Mishra has delivered almost equal number of invited talks, including keynote lectures and inaugural addresses in national and international conferences. He has edited a book titled Radiobiology and Biomedical Research. He has received professional recognition for his significant research contributions in the area of radiation biology and life science. He was visiting scientist to

Japan, Germany, France, USA and other countries. He is a recipient of Distinguished Science Service Award of Asia Pacific EPR Society in 2004. Dr Mishra is an Adjunct Visiting Professor at Institute of Technology, Manipal Academy of Higher Education, Manipal. He is a Fellow of National Academy of Sciences, India, Fellow of Maharashtra Academy of Science, Fellow and Senior Vice President of Microscope Academy of India, and past President of Section of New Biology, 88th Indian Science Congress. Dr Mishra is the President of the Indian Society for Radiation Biology for 2004-2006, Vice President of Asia Pacific ESR/EPR Society for 2004-06, President of Indian Biophysical Society for 2005-2007 and Vice President of Asian Association of Radiation Research, 2005-2009. He was the Vice President of Society of Free Radical Research, 2003-2005. Dr Mishra is on the Editorial Board of International Journal of Low Radiation, Iranian Journal of Radiation Research and Editor-in-Chief of Indian Journal of Radiation Research. Dr Mishra is a Member of Life Research Board of DRDO, Ministry of Defence.

SIMULTANEOUS SEPARATION AND CONSOLIDATION OF ^{137}Cs FROM ALKALINE INTERMEDIATE LEVEL REPROCESSING WASTE USING RESORCINOL FORMALDEHYDE POLYCONDENSATE RESIN AND ZEOLITE SORBENT

D. Banerjee and S.K. Samanta
Back End Technology Development Division
Bhabha Atomic Research Centre

This paper was adjudged as one of the Best Papers at the DAE-BRNS theme meeting on "Emerging Trends in Separation Science and Technology" (SESTEC-2004), at BARC, Mumbai, during July 22-23, 2004.

An innovative process has been adopted in India for highly efficient separation of ^{137}Cs from alkaline reprocessing waste using cesium-selective Resorcinol Formaldehyde Polycondensate Resin (RFPR) in repeated loading-elution cycles [1-3]. Elution of ^{137}Cs leads to its concentration in a small volume of dilute nitric acid. Further consolidation of ^{137}Cs has been found possible by passing the accumulated eluate through a small column containing synthetic zeolite of mordenite type [4]. The zeolite can be encapsulated for use as a radiation source or stored for future processing and recovery of ^{137}Cs . In this connection, it is of interest to see if ^{137}Cs can be loaded as effectively on the zeolite column by directly connecting it downstream to the RFPR column during elution. The composition of the feed to the zeolite column is not constant in this case but varies continuously with progress of elution. In fact, the peak ^{137}Cs concentration could be several times higher than its average concentration in the accumulated eluate.

Satisfactory performance of the zeolite column during such on-line loading could lead to a simplification of process flowsheet by eliminating the eluate accumulation step. This report summarizes the results of experiments using actual waste solution to test the simultaneous separation and consolidation of ^{137}Cs as noted above.

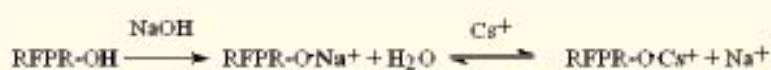
The waste is generated as an acidic concentrate from the waste evaporation cycle of a reprocessing plant. It is made alkaline and stored in carbon steel tanks as intermediate level waste. The sample used in this work had a pH of 12 and contained 90 g/L of dissolved solids, mainly due to the presence NaNO_3 , Na_2CO_3 and NaNO_2 . The major radionuclide present in the waste was ^{137}Cs (4.57 $\mu\text{Ci/mL}$). Traces of ^{106}Ru , ^{125}Sb and ^{90}Sr were also found.

The schematic of the experimental set-up used in this work is shown in Fig.1. The separation of ^{137}Cs from

the waste was carried out during the loading cycle. The waste solution, pre-treated with NaOH to contain 0.1 M free alkali, was passed through the RFPR (5 mL) column at a flow rate of 5 bed volumes per hour using a peristaltic pump. Effluent samples were collected periodically. The loading run was continued without break for 60 hours, during the course of which 300 bed volumes of waste solution was passed. Rinsing of the column with 5 bed volumes of water followed loading. In the next stage, elution of ¹³⁷Cs-loaded RFPR column was carried out in two steps, using 8 bed volumes of 0.1 M HNO₃ followed by 12 bed volumes of 0.5 N HNO₃ in up-flow direction at a flow rate of 3 bed volumes per hour (15 mL/h). The eluate was directly passed through a small column containing 1.5 mL of mordenite type synthetic zeolite. The flow rate through the zeolite column was thus 10 bed volumes per hour. Samples of RFPR column eluate were collected on-line using a hypodermic syringe through a self-sealing rubber septum connected to the tube joining the two columns. Samples of zeolite column effluent were also collected. The ¹³⁷Cs activities in all samples collected were analyzed using HPGe detector coupled with 8 KMCA. The results obtained in the experiments are discussed below.

The performance of RFPR column in the loading cycle is shown in Table 1. It is seen that the activity of ¹³⁷Cs is reduced from 4.57 mCi/mL to 5.4x10⁻⁴ mCi/mL in 300 bed volumes of waste. The separation efficiency is > 99.9% and the column is

expected to treat further quantities of waste with high efficiency. From an analysis of the accumulated effluent, it was estimated that 6.8 mCi of ¹³⁷Cs was loaded on the column. As noted above, the waste was pre-treated with alkali. This was done in view of the negligible amount of free alkali in the waste. Adequate alkalinity is essential for generation of cesium-selective phenolate ion sites, which are responsible for uptake of ¹³⁷Cs as per the following scheme:



The results obtained in the elution cycle are presented in Fig. 2. The activity of ¹³⁷Cs eluting from RFPR and entering the zeolite column is shown with progress of elution along with the activity of ¹³⁷Cs in zeolite column effluent.

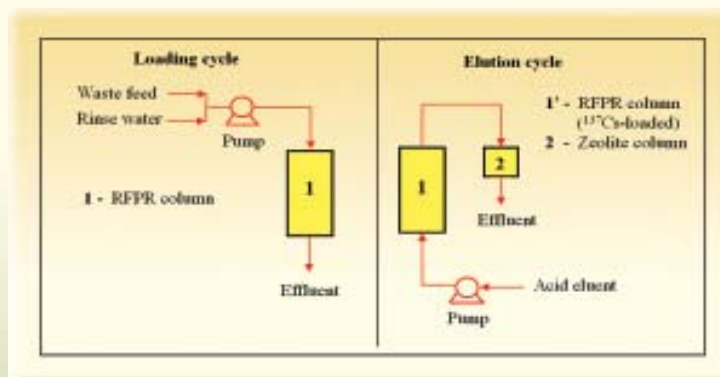


Fig. 1 : Schematic of experimental set-up for loading and elution cycles

Table 1. Performance of RFPR in separation of ¹³⁷Cs
¹³⁷Cs activity in waste: 4.57 μCi/mL, RFPR bed volume: 5 mL, Flow rate: 25 mL/h

Bed volumes of waste passed	100	150	200	250	300	Accumulated effluent
¹³⁷ Cs activity in effluent (μCi/mL)	5.3 x 10 ⁻⁴	6.3 x 10 ⁻⁴	7.9 x 10 ⁻⁴	6.7 x 10 ⁻⁴	4.7 x 10 ⁻⁴	5.4 x 10 ⁻⁴

Though the activity of ^{137}Cs in the feed to the zeolite column varied from 0.1 to as high as $446 \mu\text{Ci/mL}$, only a small amount of activity, $7 \times 10^{-3} \mu\text{Ci/mL}$, was present in the accumulated effluent. The ^{137}Cs activity present in 1500 mL of waste was thus consolidated in 1.5 mL of zeolite, leading to a high volume reduction factor (VRF)

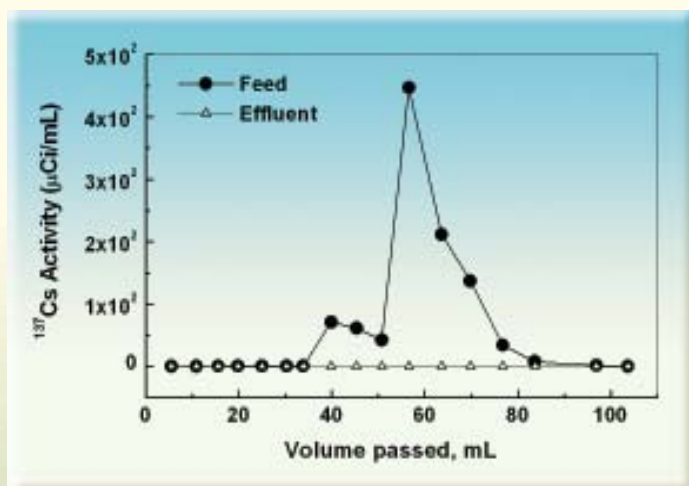


Fig. 2 : Behavior of zeolite column during on-line loading of RFPR column eluate

of 1000 for this process. Still higher VRF can be achieved by repeated use of the same zeolite column for multiple RFPR loading-elution cycles. The results also demonstrate the usefulness of the two-step elution scheme which leads to much lower concentration of competing Na^+ ions in the second step [5] and thereby facilitates the efficient sorption of ^{137}Cs by the zeolite even when its activity is very high.

In conclusion, the results of this experimental work show that direct loading of ^{137}Cs from RFPR column eluate on zeolite is feasible and can be utilized for high volume reduction as well as preparation of radiation sources for various applications.

References

1. S.K. Samanta, M. Ramaswamy; Sep. Sci. Technol., 27(2), 255 (1992).
2. P.D. Ozarde, S.K. Samanta, K. Raj; "Management of intermediate level wastes from past reprocessing using cesium-specific resorcinol formaldehyde resin", International Conference on Issues and Trends in Radioactive Waste Management, December 9-13, International Atomic Energy Agency, Vienna, Austria (2002).
3. D. Banerjee, S.K. Samanta; "Process Chemistry and Resin Performance in the Treatment of Alkaline Intermediate Level Waste by Selective Ion Exchange", 14th Annual Conference of Indian Nuclear Society, IGCAR, Kalpakkam, Dec 17-19, 2003.
4. D. Banerjee, M.A. Rao, M.N. Unni, S.K. Samanta; "Loading of ^{137}Cs from Acidic Eluate of Ion Exchange Column on Synthetic Zeolite", Nuclear and Radiochemistry Symposium, Mumbai, Feb 10-13, 2003.
5. M.A. Rao, S.K. Samanta; "Sequential Elution of Sodium and Cesium from Resorcinol Formaldehyde Polycondensate Resin", Nuclear and Radiochemistry Symposium, Mumbai, Feb 10-13, 2003.

ABOUT THE AUTHORS



Mr D. Banerjee obtained his M.Sc. degree in Chemistry from Burdwan University. He joined Back End Technology Development Division, BARC, in 1999 after graduating from 42nd batch of BARC Training School. He is presently involved in the development of processes for decontamination of radioactive wastes and recovery of ^{137}Cs for use as a radiation source.



Dr. S.K. Samanta joined the 19th batch of BARC Training School in 1975 after graduating from the University of Calcutta and is presently in the Back End Technology Development Division, BARC. He obtained his Ph.D. degree from the University of Bombay in 1992. He has made substantial contribution to the development of a number of processes based on radionuclide separation using functional polymers, chelating resins, inorganic sorbents and zeolites for the treatment of radioactive waste streams. Some of these processes have been successfully translated into plant applications. Dr. Samanta has profound interest in the large scale recovery and utilization of ^{137}Cs as a radiation source for industrial and medical applications and has developed processes for this purpose. He has over 50 publications in International Journals and various Symposia/Conferences.

ANTIOXIDANT PROPERTIES OF A NOVEL MARINE ANALOGUE OF DENDRODOINE

Strayo De and T. P. A. Devasagayam
Radiation Biology and Health Sciences Division
Bhabha Atomic Research Centre

S . Adhikari
Radiation and Photochemistry Division
Bhabha Atomic Research Centre

and

V. P. Menon
Department of Biochemistry,
Annamalai University, Annamalai Nagar-608 002

This paper received the best poster award in "The first International Conference on Natural Products for Health and Beauty", 17-21 October, 2005, Maha Sarakham, Thailand.

Abstract

Marine algae are among the richest natural sources of known and novel bioactive compounds. Several of these unique compounds have shown pharmacological activities for many of the deadly diseases.

Dendrodoin (5-[(3-N-dimethylamino)-1,2,4-thiadiazolyl]-3-indanyl methanone) is an alkaloid extracted from the marine alga *Dendrodoa grossularia*. It possesses a 1,2,4- thiadiazole unit, a rarity among natural products.

Aminothiazoles have a wide range of biological activities such as anti-tumor and antioxidant properties.

The aim of our study was to examine the antioxidant ability of a novel compound, an aminothiazole derivative,

dendrodoin analogue; DA (4-Amino-5-benzoyl-2-(4-methoxy phenylamino) thiazole which has been chemically synthesized and is similar to dendrodoin. In all the biochemical assays corresponding to different levels of protection, DA showed concentration dependent antioxidant ability. DA (1 mg/ml) showed an ability to inhibit ABTS radical formation to the extent of 0.18 times of Trolox. The ferric complex reducing ability of 1 mg/ml DA was equivalent to 110 mM Trolox. 1 mg/ml DA gave 84% protection against deoxyribose degradation.

DA also has an ability to scavenge ·NO radical, 1 mg/ml DA effecting 20% scavenging. Concentration dependent inhibition of lipid peroxidation and protein oxidation was observed with low concentrations of DA (0.5-1 mg/ml). Pulse radiolysis studies revealed that DA scavenges peroxy radicals with a bimolecular rate constant of $3 \times 10^8 \text{ M}^{-1}\text{s}^{-1}$. Moreover, the initially formed nitrogen centered radical gets transformed into sulfur-centered radical before furnishing any final product. Our results indicated that DA can be a valuable antioxidant with potential application as a therapeutic agent.

Introduction

Nature has been a source of medicinal treatment for thousands of years. Much of the world's biological diversity remains unexplored as a source of novel biological compounds and the search for new bio-active agents from natural sources, including extreme environmental niches is expanding. Several of these unique compounds have shown pharmacological activities for many of the deadly diseases like cancer, AIDS, diabetes, arthritis, etc.

Marine algae, popularly known as seaweeds, are of immense industrial, human and agricultural value since time immemorial, especially in the Orient. Marine algae consisting of red, brown, green and microalgae have several potential applications. They are being used as a source of food and materials for industrial uses. Some species are being cultivated, mainly in the Asian countries like Japan, China and Korea. Recent studies show that many marine algae have significant antioxidant abilities. Marine antioxidant research is not yet fully explored. There are very few reports on the antioxidant capacity of algae. Algae (marine and fresh water) that have been used as sources of antioxidants include *Dunaliella salina*, *Haematococcus pluvialis*, *Spirulina* and *Chlorella*. Several Indian species of marine algae have potential applications and technologies to utilize them commercially will yield rich dividends. Several species of microalgae, especially green algae, accumulate high concentrations of carotenoids such as β -carotene, astaxanthin and canthaxanthin. These carotenoids have wide application as natural colourants and antioxidants. *Euglena gracilis* produces significant amount of α -tocopherol.

A marine edible green alga, *Ulva reticulata*, is a known source of proteins, vitamins and sulfated

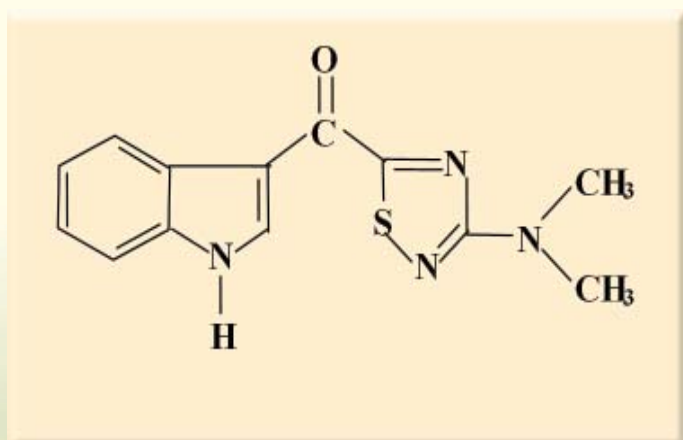
polysaccharides. Recently Rao et al (2004) have shown antihepatotoxic and antioxidant effects of the water extract of this alga in rats. Oral pretreatment with the hot water extract of this alga reduced the hepatotoxicity induced by acetaminophen considerably by improving the antioxidant status and by reducing lipid peroxidation. Murthy et al (2005) have evaluated the ability of *D. salina* algal powder extract to protect against oxidative stress in animal models. Treatment of rats with this extract showed significant protection against toxicity induced by CCl_4 . The algal powder treatment restored the levels of catalase, superoxide dismutase (SOD) and peroxidase decreased by CCl_4 treatment. The rats pretreated with seaweed extract reversed the depleted levels of antioxidant enzymes and reduced the elevated levels of lipid peroxidation. Their results indicated that the seaweed extract contains some anti-ulcer agents, which may maintain the volume/acidity of gastric juice and improve the gastric mucosa antioxidant defense system against HCl-ethanol induced gastric injury in rats. The antioxidant activities of fucosterol, isolated from the marine alga *Pelvetia siliquosa* were investigated by Lee et al (2003). Fucosterol exhibited a significant decrease in serum transaminase activities elevated by hepatic damage induced by CCl_4 . It also showed increase in the antioxidant enzymes SOD, catalase and glutathione peroxidase. Their results suggest that fucosterol not only possesses antioxidant, but also the hepatoprotective activities in rats.

Dendrodione (5-[(3-N-dimethylamino)-1,2,4-thiadiazolyl]-3-indanyl methanone) is an alkaloid extracted from the marine alga *Dendrodoa grossularia*. It possesses a 1,2,4-thiadiazole unit, a rarity among natural products. Aminothiazoles have a wide range of biological activities including antioxidant properties. Secondary metabolites with five membered thiazole

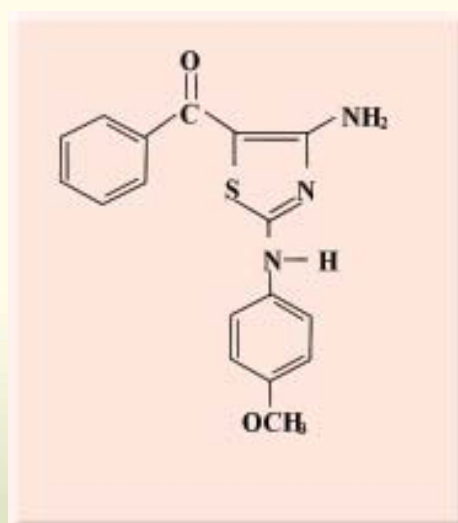
rings are known. They also generate new surface for interactions with proteins, RNA and DNA in sequence discriminating modes. Some of the tandem heterocycles (oligothiazoles/thiazolines) could function as minor groove binders of DNA similar to the oligopyrrole and oligoimidazole reading of bases in the DNA minor groove by antibiotics such as netropsin and distamycin. Indeed, thiazole-containing analogues of these molecules bind in the minor groove of DNA with significant sequence bias. Among the enzymatic post-translational modifications of peptide-based natural products are heterocyclizations of serine, threonine and cysteine side chains. These create five ring heterocycles in the oxazole and thiazole series. Initial products of cyclodehydration are the dihydroheteroaromatic oxazolines and thiazolines, which can undergo redox changes. A two-electron oxidation generates the heteroaromatic oxazole and thiazole systems, while two electron reductions of the carbon nitrogen double bonds would create the thiazolidine and oxazolidine rings. All three oxidation

states are seen in natural products. The heterocyclization not only alter peptide backbone connectivity and electronic distribution, but also afford new recognition elements for interaction with such targets as DNA and RNA and with proteins that effect the specific biological readouts of the natural products.

The synthesis of complex natural products has been challenging and has led to the discovery of many novel reactions. The synthesis of several compounds has permitted the preparation of large number of designed analogues. These studies have analyzed desirable modifications, which inevitably lead to the development of more suitable bio-active compounds. Marine algae are the richest natural sources of known and novel bio-active compounds, many of which belong to totally novel chemical classes not found in terrestrial sources. In this article we report a on the antioxidant ability of a novel compound, an aminothiazole derivative, dendrodoine analogue; DA (4-Amino-5-benzoyl-2-(4-methoxy phenylamino) thiazole which has been chemically synthesized and is similar to dendrodoine.



Dendrodoine



Dendrodoine analogue

Materials and methods

Ascorbic acid, 2,2'-azobis-3-ethylbenzthiazoline-6-sulfonic acid (ABTS) diammonium salt, butylated hydroxy toluene (BHT), chloroform, dinitrophenyl hydrazine (DNPH), 1,1'-diphenyl-2-picrylhydrazyl (DPPH), deoxyribose, ethylene diamine tetra acetic acid (EDTA), ferric chloride, ferrous ammonium sulphate, ferrous sulphate, Folin-Ciocalteu reagent, guanidine hydrochloride, hydrogen peroxide, myoglobin, potassium ferricyanide, potassium hydroxide, potassium phosphate, potassium dihydrogen phosphate, sodium acetate, sucrose, 1,1,3,3-tetraethoxypropane, 2-thiobarbituric acid (TBA), trichloroacetic acid, triphenylphosphine, 2,4,6-tripyridyl-s-triazine (TPTZ), xylol orange were purchased from Sigma Chemical Co., U.S.A., 2,2'-Azobis (2-amidinopropane) dihydrochloride (AAPH) (=2,2'-azobis(2-methylpropionamide) dihydrochloride) and 6-hydroxy-2,5,7,8-tetramethylchroman-2-carboxylic acid (Trolox) were from Aldrich Chemical Co., U.S.A. Other chemicals used in our studies were of the highest quality commercially available from reputed suppliers. The solvents used for pulse radiolysis experiment were freshly prepared in de-ionized 'nanopure' water (conductivity < 0.06 mS cm⁻¹) from a Barnstead nano-pure system. Antioxidant activity was evaluated by the standard biochemical techniques and the mechanism was studied using pulse radiolysis technique.

Results

Antioxidant Properties of Dendrodoine analogue

The antioxidant effect of DA was studied using standard biochemical assays corresponding to different levels of antioxidant protection. These include inhibition of radical formation by ferrylmyoglobin/ABTS assay, radical scavenging assays such as DPPH besides its ability to inhibit deoxyribose degradation and to reduce ferric by FRAP assay. In all these assays DA showed concentration dependent antioxidant ability. The results of FRAP assay is shown in Fig1. The ferric complex reducing ability of 1 mg/ml of DA showed a TEAC of 110.25. DA also showed an ability to inhibit ABTS formation to the extent of 0.17 times of Trolox. The data on Ferrylmyoglobin/ABTS assay is shown in Table 1. Our results showed that DA is not an efficient DPPH radical scavenger even at higher concentrations (Table 2.) The inhibition of deoxyribose degradation capacity of various concentrations of DA is expressed in Table 3. 1 mg/ml of DA gave 84% protection (Table 3).

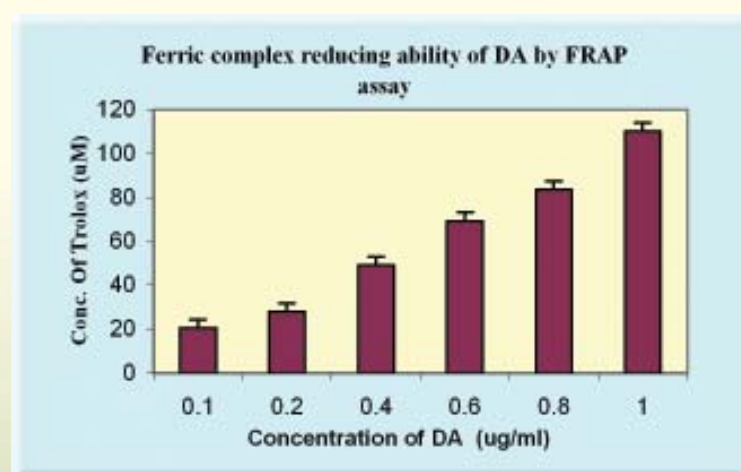


Fig. 1 : Antioxidant activity of DA (Dendrodoine Analogue) as measured by FRAP assay. Data represented as mean \pm S.E. from four individual experiments.

Table 1 Antioxidant activity of DA as measured by Ferrylmoglobin/ABTS assay

Concentration of DA ($\mu\text{g/ml}$)	TEAC (mM)	AEAC (mM)
0.1	0.12 \pm 0.3	0.14 \pm 0.3
0.5	0.15 \pm 0	0.17 \pm 0
1.0	0.17 \pm 0.3	0.19 \pm 0.3

Data represented as mean \pm S.E. from four individual experiments. DA: Dendrodoine Analogue; TEAC: Trolox equivalent antioxidant capacity; AEAC: Ascorbic acid equivalent antioxidant capacity

Table 2 Radical scavenging activity of DA as measured by DPPH assay

Concentration of DA ($\mu\text{g/ml}$)	TEAC (mM)
0.1	0.00 \pm 0.04
0.5	0.00 \pm 0.17
1.0	0.02 \pm 0.05
2.0	0.04 \pm 0.37
3.0	0.05 \pm 0.34
4.0	0.06 \pm 0.60

Data represented as mean \pm S.E. from four individual experiments. DA: Dendrodoine Analogue; TEAC: Trolox equivalent antioxidant capacity; AEAC: Ascorbic acid equivalent antioxidant capacity

Table 3 Deoxyribose degradation assay of different concentrations of DA

Concentration of DA ($\mu\text{g/ml}$)	% Protection
0.1	29.35 \pm 0.008
0.5	75.42 \pm 0.011
1.0	84.01 \pm 0.009

Data represented as mean % protection \pm S.E. from four individual experiments. DA: Dendrodoine Analogue

We have also studied the capacity of DA to prevent mitochondrial damage in terms of lipid peroxidation induced by AAPH and ascorbate- Fe^{2+} . Lipid peroxidation was assessed as formation of lipid hydroperoxides (LOOH) and thiobarbituric acid reactive substances (TBARS). 0.1, 0.5, 1 mg/ml of DA was tested and the concentration dependent inhibition of lipid peroxidation by DA is shown in Table 4 and Fig.2-4. Inhibition of protein carbonyls by DA (table 5) and its NO^{\bullet} scavenging (Fig.5) activities was also studied. Table 5 presents data on the protection by DA against AAPH-induced protein damage in rat liver mitochondria. 0.1 mg/ml, 0.5 mg/ml gave 84% and 96% protection respectively whereas 1 mg/ml of DA gave complete (100%) protection. Our results showed that DA showed concentration dependent antioxidant effects. With concentrations of 0.5-1 mg/ml, it gave significant protection.

In pulse radiolysis study, $\text{CCl}_3\text{OO}^{\bullet}$ radical has been used

Table 4 Protection against AAPH- induced lipid peroxidation in rat liver mitochondria by different concentrations of DA

Concentration of DA ($\mu\text{g/ml}$)	nmoles TBARS/mg protein *
Control	8.59 \pm 0.18
Damage	38.60 \pm 0.15 (0)
0.1	35.22 \pm 0.01 (9.01)
0.5	30.53 \pm 0.003 (38.48)
1	18.27 \pm 0.008 (65.13)

Data represented as mean \pm S.E. from four individual experiments. DA: Dendrodoine Analogue. *Rat liver mitochondria (2 mg protein/ml in 5 mM phosphate buffer, pH 7.4) TBARS: Thiobarbituric acid reactive substances. % protection values are given in brackets.

Table 5 Protection against AAPH-induced damage to proteins in rat liver mitochondria by different concentrations of DA

Concentration of DA ($\mu\text{g/ml}$)	nmoles of protein carbonyls/mg protein*
Control	2.08 \pm 0.13
Damage	3.951 \pm 0.059
0.1	2.38 \pm 0.61 (83.96%)
0.5	2.142 \pm 0.33 (96.68%)
1	1.856 \pm 0.36 (>100%)

Data presented as mean \pm S.E. from two individual experiments. DA: Dendrodoine Analogue. *Rat liver mitochondria (2 mg protein/ml in 5 mM phosphate buffer, pH 7.4) % protection values are given in brackets.

as a representative lipid peroxy radical to understand free radical induced damage to membranes. DA scavenges peroxy radicals with a bimolecular rate constant of $3 \times 10^8 \text{ M}^{-1}\text{s}^{-1}$. It has been observed that an initially formed nitrogen centered radical gets

transformed into sulfur-centered radical before furnishing any final product (Fig. 6).

Discussion and Conclusion

In a normal, healthy individual there exists a well-maintained balance between free radical production and antioxidant defense mechanisms. However, in diseased states, this balance shifts towards the over-production of free radicals or deficit in antioxidant defense and leads to oxidative stress. Oxidative damage to cellular components can further increase the damage (Packer and Ong, 1998). Endogenous antioxidants such as ascorbic acid, vitamin E, uric acid, thiols and bilirubin present in extracellular fluids act as primary defense system that protects against oxidative damage. Ample experimental and epidemiological studies support the involvement of oxidative stress in the pathogenesis and progression of several chronic diseases. (Tewari et al 2000). However, in pathophysiological conditions, there is an extra requirement for exogenous antioxidants from food and medicinal plants (Sies, 1996; Tilak and Devasagayam, 2001). There is an increasing interest in natural antioxidants (Amarowicz, R, et al 2000) and recent studies reveal that marine algae form a novel and important sources of antioxidants.

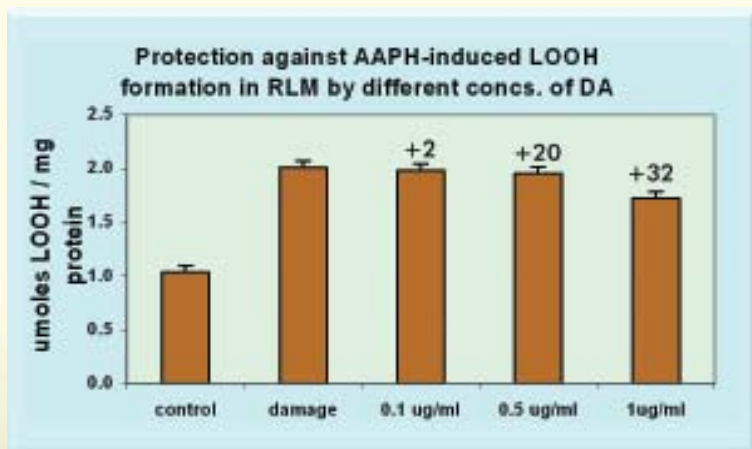


Fig 2 : Protection against AAPH- induced lipid peroxidation in rat liver mitochondria by different concentrations of DA in terms of LOOH. LOOH:Lipid hydroperoxide. DA: Dendrodoine Analogue. Data represented as mean \pm S.E. from four individual experiments. RLM: Rat liver mitochondria (2 mg protein/ml in 5 mM phosphate buffer, pH 7.4) * % protection values.

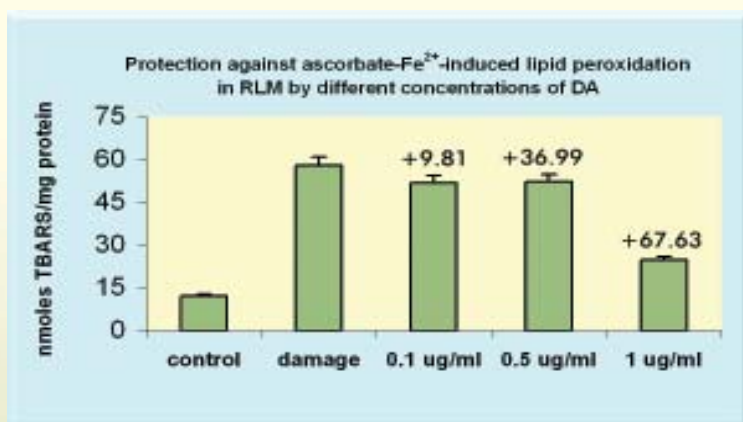


Fig. 3 : Protection against ascorbate-Fe²⁺- induced lipid peroxidation in rat liver mitochondria by different concentrations of DA in terms of TBARS. TBARS: Thiobarbituric acid reactive substances. DA: Dendrodoine Analogue. Data represented as mean \pm S.E. from four individual experiments. RLM: Rat liver mitochondria (2 mg protein/ml in 5 mM phosphate buffer pH 7.4) * % protection values

Antioxidants are substances, which prevent/delay oxidation of substrates when present in low concentrations compared to the substrate, which otherwise gets oxidized by the pro-oxidants. Non-enzymatic antioxidants react with pro-oxidants and inactivate them. In a redox reaction, antioxidants act as 'reductants'. In this context, the antioxidant power can be referred to as 'reducing ability'. In FRAP assay, an easily reducible oxidant, Fe III is used in excess. Thus on reduction of Fe III-TPTZ complex by antioxidant, blue colored Fe II-TPTZ is formed, which can be measured spectrophotometrically at 595 nm (Pulido et al 2000). The first line of defense is the preventive antioxidants, which suppress the formation of free radicals. In Ferrylmyoglobin/ABTS assay, on addition of an antioxidant, the formation of ABTS⁺ radical by reaction of ferrylmyoglobin and ABTS, is delayed and inhibition of formation of the radical is measured as the lag time in seconds (Alzoreky and Nakahara, 2001). Free radicals are formed *in vivo* or taken into body exogenously. The second line of defense is the antioxidants that scavenge free radicals to suppress chain initiation and/or break the chain propagation reactions. Scavenging of DPPH radical is routinely used as preliminary test for estimating the antioxidant activity of natural compounds (Aquino et al., 2001).

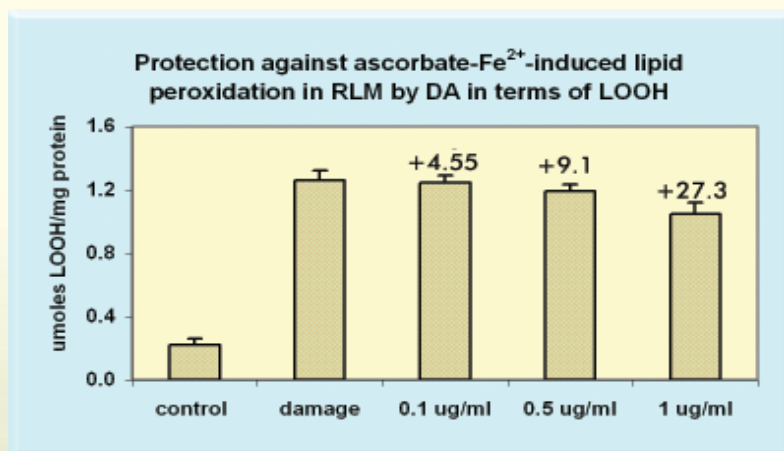


Fig. 4 : Protection against ascorbate-Fe²⁺-induced lipid peroxidation in rat liver mitochondria by different concentrations of DA in terms of LOOH. LOOH:Lipid hydroperoxide. DA: Dendrodoine Analogue. Data represented as mean \pm S.E. from four individual experiments. RLM: Rat liver mitochondria (2 mg protein/ml in 5 mM phosphate buffer pH 7.4) * % protection values

antioxidant properties. The aim of our study was to examine the antioxidant ability of DA, which is an aminothiazole derivative of dendrodoine. In all the biochemical assays corresponding to different levels of protection, DA showed concentration dependent antioxidant ability. Our studies have shown that DA has significant antioxidant capacity in terms of scavenging ABTS radical, degradation of deoxyribose and ferric reducing ability. DA, however, is not an efficient DPPH radical scavenger even at high concentrations.

Aminothiazoles have a wide range of biological activities such as anti-tumor, anti-anoxic and

The antioxidant action also can be assessed by inhibiting the damage caused by free radicals. The

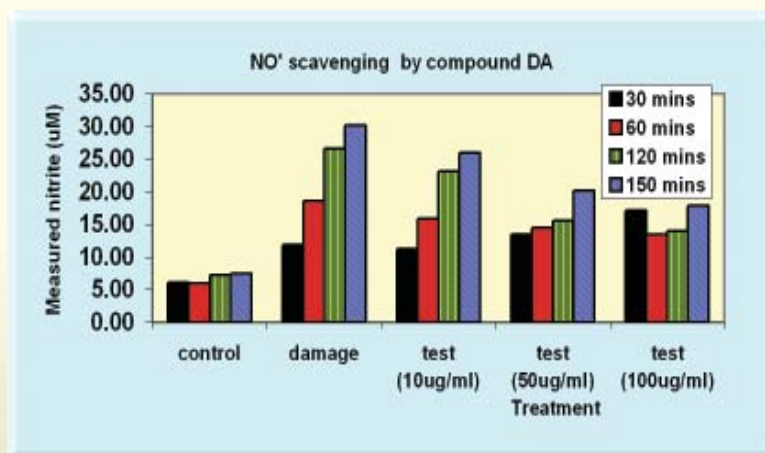


Fig. 5 : NO' scavenging effects of different concentrations of DA at different incubation times. Time range of 30-150 minutes was used. Data represented as mean of two individual experiments. DA: Dendrodoine Analogue.

mechanisms involved in many human diseases such as hepatotoxicities, hepatocarcinogenesis, diabetes, malaria, acute myocardial infarction, skin cancer include lipid peroxidation as a main source of membrane damage (Yoshikawa et al, 2000). To examine the possible mechanisms of action we have studied the ability of DA to prevent oxidative damage in mitochondria isolated from rat liver. The two endogenous systems for inducing damage were AAPH that releases peroxy radical (ROO) and ascorbate- Fe²⁺ that generates OH-radical like species on incubation at the physiological temperature of

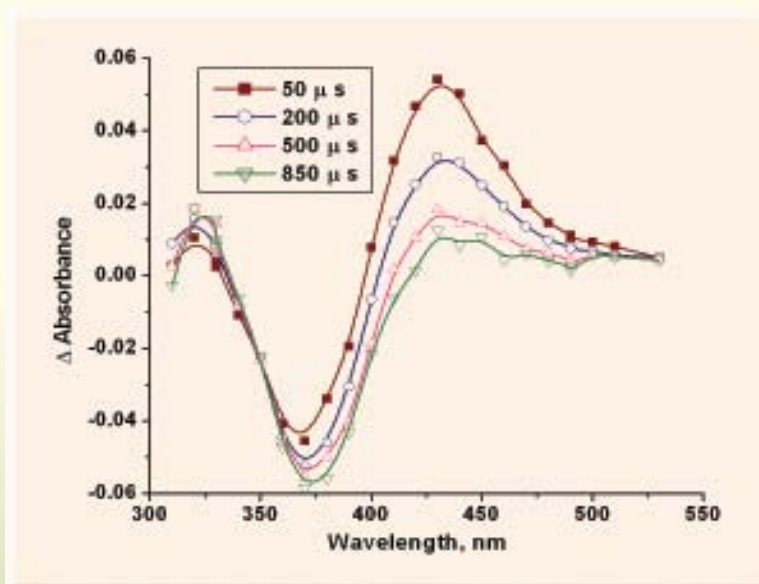


Fig. 6: Transient absorption spectrum obtained from a reaction between DA and $\text{CCl}_3\text{OO}\cdot$

the membrane. DA gave protection against oxidative damage in all our experiments. The inhibition is observed with lipid peroxidation as well as against protein damage in rat liver mitochondria.

The ability to scavenge secondary radicals can also be determined using pulse radiolysis. The possible reason for the observed antioxidant effect of DA can be due to radical scavenging as observed by pulse radiolysis. $\text{CCl}_3\text{OO}\cdot$ radical is a representative peroxy radical that has been used to study

free radical interaction. Pulse radiolysis studies revealed that DA scavenges peroxy radicals with a bimolecular rate constant of $3 \times 10^8 \text{ M}^{-1}\text{s}^{-1}$. Moreover, the initially formed nitrogen centered radical gets transformed into sulfur centered radical before furnishing any final product.

37 °C. The above two systems also differ in their mechanisms in inducing lipid peroxidation.

Lipid peroxidation in tissues is controlled by the interaction of several factors. These include: a) availability of substrates for peroxidation in the form of unsaturated fatty acids mainly present in phospholipids; b) inducers of peroxidation such as ascorbate, Fe^{2+} , compounds which can convert Fe^{3+} to Fe^{2+} , oxygen, initiators of free radical reactions and functioning of the electron transport chain which serve as source of reactive species; c) antioxidant defense in the form of glutathione, α -tocopherol, SOD, carotenoids, substances chelating Fe^{2+} , substances reducing lipid hydroperoxide, glutathione peroxidase system etc.; and d) the physical properties of the membrane lipid such as fluidity and surface charge and the location of the polyunsaturated fatty acid in

Ascorbic acid and trolox are water-soluble and ethanol-soluble antioxidants respectively. As compared to these well-known antioxidants, DA showed significant antioxidant potentials. Our results indicated that an aminothiazole derivative, DA, an analogue of a compound from a marine alga can be a valuable antioxidant with potential applications in health. Further studies are underway in our laboratory to determine its antioxidant properties *in vivo*.

References

1. Alzoreky N, Nakahara K. Antioxidant activity of some edible Yemeni plants evaluated by Ferrylmyoglobin/ABTS^{•+} assay. *Food Sci. Technol. Res.* 2001; 7: 141-144.
2. Amarowicz R, Naczek M, Shahidi F. Antioxidant activity of various fractions of non-tannin phenolics of Canola hulls. *J. Agric. Food Chem.* 2000; 48: 2755-2759.
3. Aquino R, Morelli S, Lauro MR, Abdo S, Saija A, Tomaino A. Phenolic constituents and antioxidant activity of an extract of *Anthurium versicolor* leaves. *J. Natl. Prod.* 2001; 64: 1019-1023.
4. Halliwell B, Gutteridge JMC, *Free Radicals in Biology and Medicine*, Oxford University Press, Oxford, 1997.
5. Lee S, Lee YS, Jung SH, Kang SS, Shin KH. Antioxidant activities of fucosterol from the marine algae *Pelvetia siliquosa*. *Arch Pharm Res.* 2003; 26: 719-722.
6. Murthy CKN, Vanitha A, Rajesha J, Mahadeva Swamy M, Sowmya PR, Ravishankar GA. *In vivo* antioxidant activity of carotenoids from *Dunaliella salina*- a green microalga. *Life Sci.* 2005;76:1381-1390.
7. Packer L, Ong ASH. *Biological oxidants and antioxidants: Molecular mechanisms and health effects*. AOCS Press, Champaign, IL. 1998.
8. Pulido R, Bravo L, Saura-Calixto F. Antioxidant activity of dietary polyphenols as determined by a modified Ferric Reducing/Antioxidant Power assay. *J. Agric. Food Chem.* 2000; 48: 3396-3402.
9. Rao BRH, Sathivel A, Devaki T. Antihepatotoxic nature of *Ulva reticulata* (Chlorophyceae) on acetaminophen-induced hepatotoxicity in experimental rats. *J Med Food.* 2004;7: 495-497
10. Sies H. *Antioxidants in disease, Mechanisms and Therapy*, Academic Press, New York, 1996.
11. Tewari S, Gupta V, Bhattacharya S. Comparative study of antioxidant potential of tea with and without additives. *Ind. J. Physiol. Pharmacol.* 2000; 44: 215-219
12. Tilak JC, Devasagayam TPA. Free radicals in human disease. *ISRAPS Bull* 2001;12:30-37.
13. Yoshikawa T, Toyokuni S, Yamamoto Y, Naito Y, eds. *Free Radicals in Chemistry, Biology and Medicine*, OICA international, London, 2000.

ABOUT THE AUTHORS



Ms. Strayo D. De has received her B.Sc. degree in Microbiology (Applied component: Biotechnology) in 2002 and M.Sc. degree in Biophysics in 2004 from Mumbai

University. During her Post Graduation, she was a topper in her subject and overall fifth in the University. At present, she is a DAE fellow attached to Radiation Biology and Health Sciences Division, BARC, pursuing her Ph.D. on a subject entitled "Studies pertaining to potential applications of some novel materials in human health and radioprotection"



Dr. T.P.A. Devasagayam joined the Bhabha Atomic Research Centre in 1975, after completing the BARC Training School in Biology

and Radiobiology. At present he is working as Scientific Officer (H) in the Radiation Biology and Health Sciences Division of BARC. His major area of research relates to role of free radicals in human health and radiation biology with emphasis on the mechanistic aspects, potential applications, role of ROS in cellular damage and natural antioxidants from dietary sources and medicinal plants. He has done his post-doctoral research in Germany with Prof. Helmut Sies and at the School of Medicine, Wayne State University, Detroit, USA. He holds the post of Honorary of SFRR-India and SFRR-Asia's President-Elect (for 2006-2007)

been appointed as the Assitant Editor for the Indian Journal of Radiation Research in 2005. His recent research focus is the mechanistic aspect of free radical interaction of bio and bio-active molecules including natural and synthetic antioxidants.



Venugopal P. Menon completed his B.Sc. (Chemistry) in 1969 and M.Sc. (Biochemistry) in 1971 from Bombay University and Ph.D from University of Kerala in 1976. He

did his Post Doctoral studies in the Institute of Human Nutrition, Czechoslovakia in 1984. He worked as a visiting scientist at Johns Hopkins University, USA and US Department of Agriculture, Beltsville. He worked as a Lecturer and Reader in the Department of Biochemistry, University of Kerala till 1992. In 1992 he moved to Annamalai University as a Professor and started the Biochemistry Department in 1994. He established a Center for Micronutrient Research at Annamalai University and now he is the Dean, Faculty of Science from 2006. He has successful collaborations with Johns Hopkins University, USA, National University of Singapore and University of Connecticut, USA. Many students have completed their Ph.D and M.Phil degrees under him. His current field of research includes dietary factors in health and diseases, role of different spices and medicinal plants in disease prevention, micronutrient interventions in humans and connective tissue metabolism in health and diseases. He is a member of a number of scientific societies and academic bodies.



Dr Soumyakanti Adhikari joined Chemistry Group in 1991 from the 34th batch of BARC Training School. He is the recipient of the

prestigious IUPAC (International Union for Pure and Applied Chemistry) Prize for Young Chemists in 2001. He had also been conferred the Distinguished Service Award in 2004 from the Asia Pacific Society for EPR/ESR Spectroscopy. Currently, he is holding the honorary post of Secretary General of the Society for Free Radical Research-India. He has

THERMAL ANALYSIS OF SOLID-CATHODE HOLDER ASSEMBLY OF INDIRECTLY HEATED CATHODE EB WELDING GUN

P. Karmakar, N. Maiti, A. V. Bapat, A. K. Sinha and A. K. Ray
Laser and Plasma Technology Division
Bhabha Atomic Research Centre

This paper was selected as the Best Paper (poster) at the DAE-BRNS Symposium on Electron Beam Technology and Application (SEBTA 2005) held at BARC Training School Hostel, Anushaktinagar, Mumbai, during September 28-30, 2005.

Abstract

Directly heated filament may change its shape and move with respect to the grid cup due to thermal expansion under high temperature. Directly heated filament generates strong magnetic field due to the heating current flowing through it. The effects of cathode distortion and self-induced magnetic fields may result in inconsistency of the energy density distribution, focus position and angle of convergence of the EB. These effects may be avoided by the use of the indirectly heated cathode source. It is observed that solid-cathode gives better operation life than directly heated filament.

Alignment of the solid-cathode button (electron source) with respect to the components of the EB gun is very important for optimum performance (in terms of beam shape, focus, energy distribution etc.) of the gun. The cylindrical solid-cathode button (made of Tungsten) is expected to reach 2800 K temperature during operation. Solid-cathode will be heated due to electron bombardment and radiation heat from the directly heated filament.

Solid-cathode interacts thermally with the holder assembly by conduction and to surrounding sub-assemblies by radiation. The solid-cathode holder assembly should maintain its structural integrity during this high temperature operation and also minimize conduction heat loss from the solid-cathode. The solid-cathode holder assembly is designed to maintain the relative positional uniformity between the solid-cathode and the grid cup within the acceptable limit.

This paper focuses upon the thermal design and analysis of solid-cathode holder assembly for 24 kW, 90 kV EB welding gun. The 3-D FEM model has been analyzed for the temperature distribution, thermal stress distribution and deformation for optimized heat flux on the solid-cathode to reach steady emission temperature of 2800K. The two types of holder assemblies, i.e. cup type and pin type, have been compared in view of the structural integrity (deformation) and thermal efficiency (heat loss).

Introduction

Design and development of indirectly heated cathode EB gun has gained importance in view of its better beam quality (beam shape, focus, energy distribution etc.) than the conventional directly heated cathode type gun. Performance of indirectly heated cathode gun is mainly dependent upon the structural integrity and alignment of the solid-cathode under high temperature operation. The solid-cathode should retain its alignment with respect to other gun components (filament, grid cup, anode and gun housing) within permissible limits to maintain the beam quality. Precision tolerance should be maintained on mating part dimensions for thermal stress relieving and also keeping deflection/distortion within acceptable limit. These requirements are contradictory; hence rigorous design and analysis (thermal & structural) of the solid-cathode and its holder assembly is required for selection of optimized dimensions. Transient thermal analysis is carried out to find the temperature ramp, temperature distribution, time required to achieve operating condition, and required input heat flux on solid-cathode. Based on the temperature distribution structural analysis is carried out to find the thermal stress distribution taking care of the contact conditions and displacement restraints. Two types of cathode holder arrangements, namely cup type and pin type, have been modeled, analyzed (by FEM) and compared.

System Description

The assembly of the 24 kW, 90 kV indirectly heated cathode EB gun consists of cylindrical solid-cathode, cathode holder assembly, grid cup and cylindrical housing. Guns considering two types of cathode holders have been designed.

1. Cup type cathode holder: The solid-cathode (Tungsten) is welded (by EB welding) with the tapered holder cup (17.5 mm (OD) 5 mm (ID) 39° 0.25 mm thick material: Tantalum) at four equiangular positions around its periphery.
2. Pin type holder: The solid-cathode is held by three pins (10mm(ϕ) x25mm(L), Material: Molybdenum) at equiangular positions (120° apart). The solid-cathode is supported by sliding type fit with the pins.

2D section view (engg. drawing) of the gun assembly considering both the holding methods are shown under Fig. 1. 3D model of the individual assemblies has been shown under Fig. 2.

Mesh Generation

The activity of discretization of the model with finite number of small pieces of simple shapes (elements) connected at common points (nodes) is called mesh generation. 3D tetrahedral solid element has been used. Fine mesh control has been used for discretization of solid-cathode and its holder assembly and contact surfaces. Discretized model of the solid-cathode and its holder assembly has been shown under Fig. 3.

Analysis

Thermal Analysis

Power Balance for Solid-Cathode: Heat transfer details between the subsystems has been shown under Fig. 4. The Tungsten filament gains power by resistance heating from DC source. It emits electrons on reaching the thermionic emission temperature. The emitted electrons are attracted towards the solid-cathode due

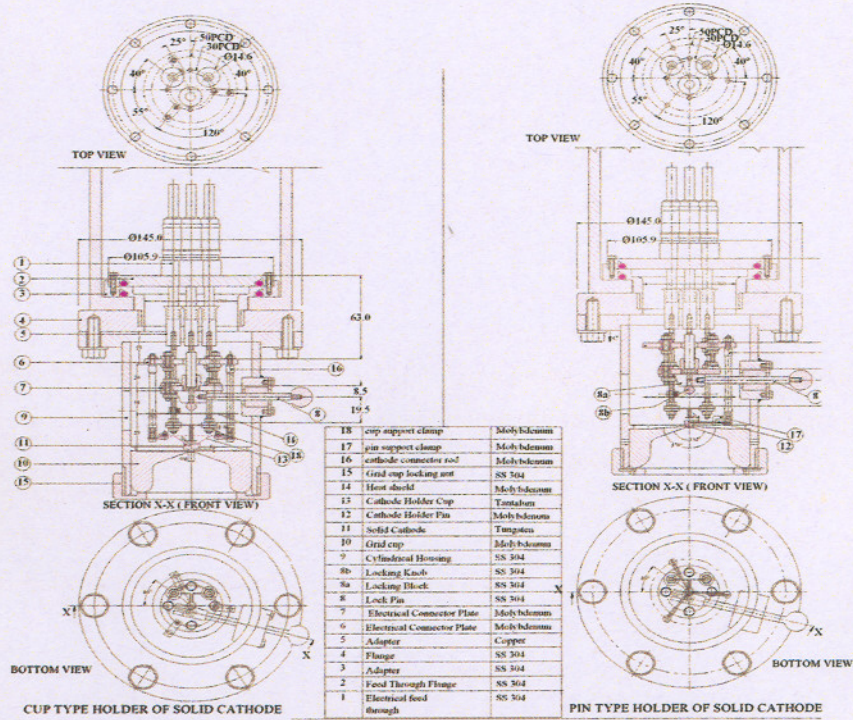


Fig.1 : 2D section view (Engg. Drawing) of the gun assembly

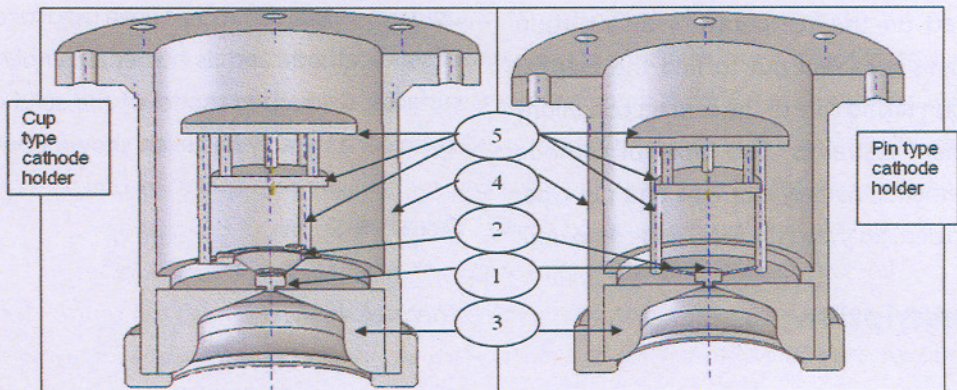


Fig. 2 : 3-D model (showing half section) of the gun assembly consisting of
1) Solid cathode (ϕ 10 X 4) with emitting projection (ϕ 3 X 2); 2) Cathode holder (either cup type or rod type); 3) Grid cup (ID 4 X OD 78 X 32); 4) Gun housing ; 5) Electrical feed through connector rods, plates and radiation shield

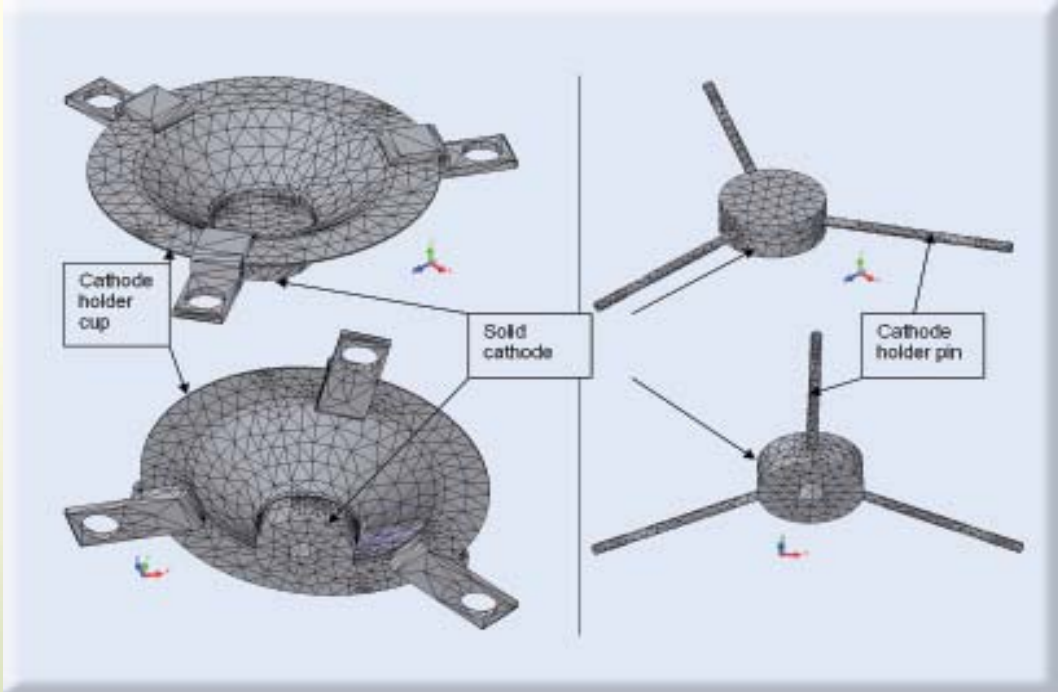


Fig. 3 : Solid mesh using 3-D Tetrahedral solid element (view shown excluding gun housing, grid cup, holder rod and electrical feed)

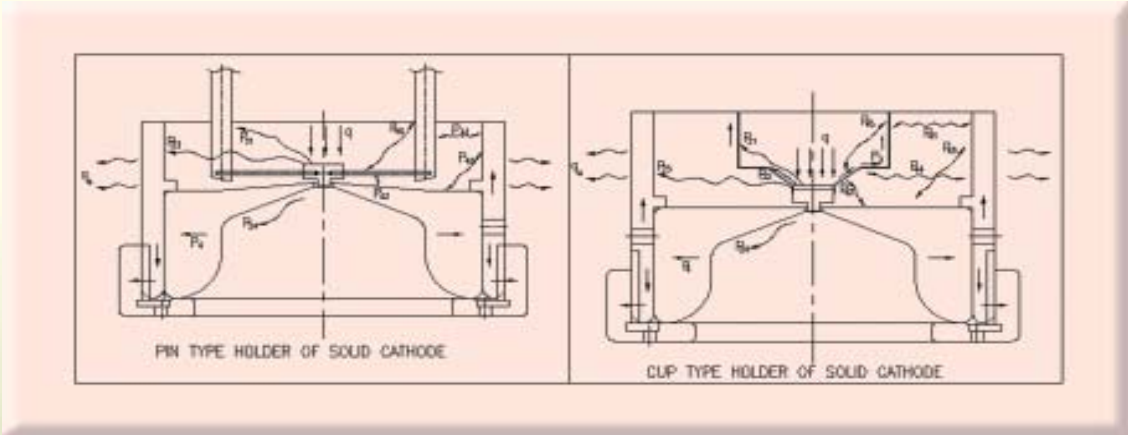


Fig. 4 : Schematic of heat transfer from solid cathode to other parts due to radiation (shown by curved line) and conduction (shown by straight line)

to relative positive potential of solid-cathode with respect to the filament. Solid-cathode gains power by electron bombardment and radiation heat from the filament. It loses power simultaneously by radiating heat to its surrounding sub-assemblies (grid cup, cathode holder, gun housing, electrical feed throughs and connector plates). Solid-cathode will also lose heat by conduction to its holder assembly. The power balance equation for the solid-cathode is as follows:

$$C_c \cdot \frac{dT_c(t)}{dt} = q + P_1 - P_2 - P_3 \quad \dots\dots\dots(1)$$

$$q = I_b \cdot V_b \quad \dots\dots\dots (2)$$

Where,

- C_c = specific heat of cathode,
- T_c = cathode temperature,
- q = power exchange from the filament to the solid-cathode by electron bombardment
- V_b = bombardment voltage,
- I_b = electron current density from Richardson-Dushman equation = $C \cdot T_f^2 \cdot \exp[-q \cdot \phi / k \cdot T_f]$
- P_1 = heat input on the solid-cathode due to radiation heat exchange with surrounding interacting surfaces having temperature higher than the solid-cathode = radiation heat input from the filament to the solid-cathode

$$P_1 = A \cdot \epsilon \cdot \sigma \cdot \left((T_f(t))^4 - (T_c(t))^4 \right) (\text{view factor}) \dots\dots (3)$$

- $T_f(t)$ = filament temperature
- A = heat transfer area
- P_1 is negligible with respect to the $I_b \cdot V_b$. Hence P_1 has been ignored in the analysis and model of filament has not been incorporated in the assembly.

P_2 = heat output from the solid-cathode due to radiation heat exchange with surrounding interacting surfaces with temperature lower than the solid-cathode,

$$P_2 = P_{21} + P_{22} + P_{23} + P_{24} = \sum_i P_{2i} = \sum_i \left[\epsilon \cdot \sigma \cdot \left(T_c(t)^4 - (T_i(t))^4 \right) \right] A_i \cdot (\text{view factor})_{2i} \dots\dots (4)$$

where,

- P_{21} = radiation heat transfer from the solid-cathode to cathode-holder rods
- P_{22} = radiation heat transfer from the solid-cathode to cathode-holder cup
- P_{23} = radiation heat transfer from the solid-cathode to gun housing
- P_{24} = radiation heat transfer from the solid-cathode to grid cup
- ϵ = emissivity = 0.3
- σ = Stefan Boltzman Constant = $5.67 \times 10^{-8} \text{ W/m}^2\text{K}^4$
- $T_c(t)$ = solid-cathode temperature
- $T_i(t)$ = temperature of interacting surface
- A_i = heat transfer area of interacting surface
- $(\text{view factor})_{2i}$ = View factor between the interacting surfaces of the solid cathode and the 'i'-th surface.

t = time

P_3 = conduction heat loss from the solid-cathode to the subsystems in contact,

P_3 is governed by the conduction equation:

$$\frac{1}{\alpha} \frac{\partial T}{\partial t} = \frac{\partial^2 T}{\partial x^2} + \frac{\partial^2 T}{\partial y^2} + \frac{\partial^2 T}{\partial z^2} \quad \dots\dots\dots (5)$$

where α = thermal diffusivity = $\frac{k}{\rho C_p}$

Radiation heat transfer between interacting surfaces has been incorporated in the analysis. This constitutes the following:

- P_{41} = radiation heat transfer in between the cathode holder rods and the gun housing
- P_{42} = radiation heat transfer in between the cathode holder pins/cup and the grid cup
- P_{43} = radiation heat transfer in between grid cup and gun housing
- P_{44} = radiation heat transfer in between the cathode holder cup and the gun housing
- P_{45} = radiation heat transfer in between the cathode holder pins and rods.

System Boundary Condition : The system gains energy from the kinetic energy of electrons hitting the solid-cathode. The kinetic energy of electrons is transferred into heat energy. Uniform heat flux has been assumed on the solid-cathode, which is equal to $I_B V_B$.

The system loses energy by radiating heat to the ambient. The heat out flux is from the gun housing to the ambient. It is formulated as

$$q_a = \sum_i \left[\epsilon_i \sigma \left(T_i(t)^4 - T_a(t)^4 \right) \right] A_i (\text{view factor}) \dots\dots\dots(6)$$

where $T_i(t)$ = temperature of interacting surface, T_a = ambient temperature = 350 K, view factor is considered equal to 1.

Contact Condition: Contact condition plays major part in the conduction heat transfer between the mating parts. Grid cup is push fitted in the slot of gun housing. A locking ring maintains its position. Grid cup is made of Mo, whereas gun housing is made of SS. Thermal expansion co-efficient of Mo ($5 \times 10^{-6}/K$) is lesser than that of SS ($1.8 \times 10^{-5}/K$). Hence finite gap is generated in

between the grid cup and gun housing during temperature increment. Hence free contact surface condition is defined in between the grid cup and gun housing. Free contact surface assumes adiabatic boundary.

Node to surface contact condition is defined in between the gun housing and locking ring. Node to surface contact condition generates gap element, which can define thermal contact resistance. Distributed contact resistance of $0.003 \text{ K.m}^2/\text{W}$ has been used in the analysis.

Analysis: Transient analysis has been carried out to optimize the heat influx ($I_B V_B$) on the solid-cathode in view of achieving solid-cathode emission temperature of 2800 K immediately after energizing the filament and maintenance of the steady emission temperature for minimum 15 minutes operating period.

Static Analysis

Temperature distribution of the thermal analysis (for a particular time step) is fed as boundary condition in the static analysis model. Based on the temperature input, static analysis has been carried out considering contact restraints (free, node to node and node to surface) between the touching parts. Distribution of stress & displacement has been calculated.

Results and Observations

Thermal Analysis

Temperature distribution of the complete assembly for both the cathode holding options after 15 min of operation has been shown under Fig.5. It has been observed that the heating power (i.e. ion

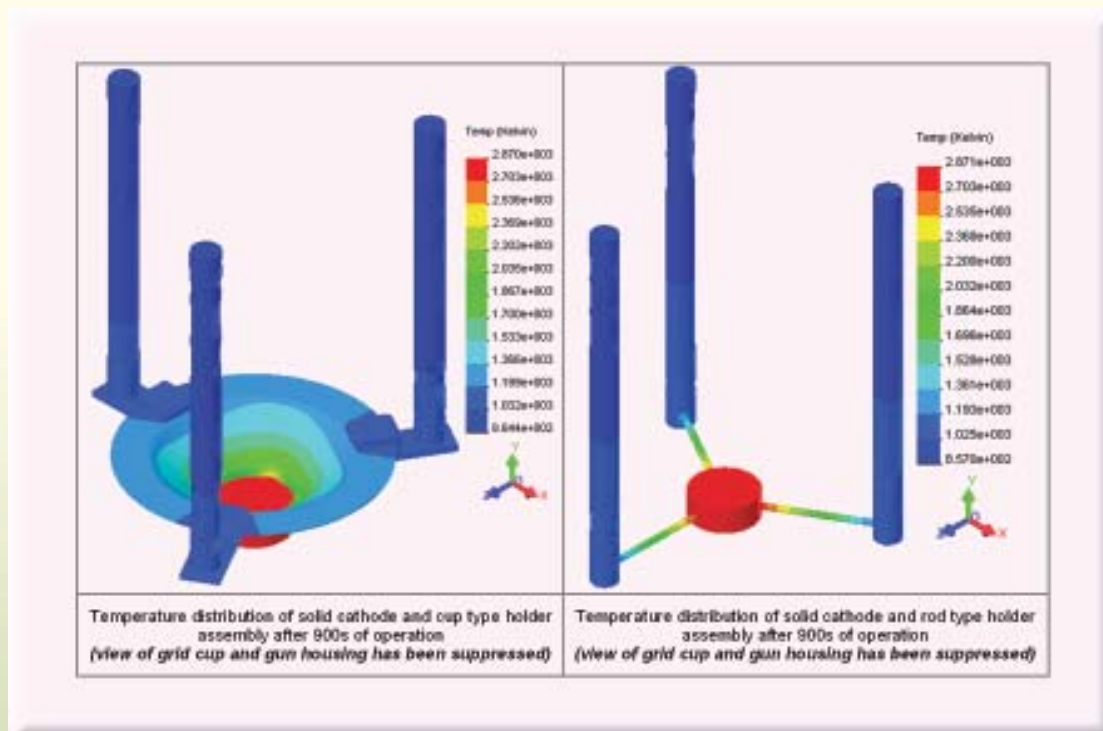


Fig. 5 : Temperature distribution

bombardment power) required for solid-cathode with pin type holder to reach 2800K emission temperature of solid-cathode (235.6 W), is lesser than that with cup type holder (251.3 W). Heat input on solid-cathode with cup type holder is more, as dissipation of heat through holder cup is more. It is lesser for solid-cathode with rod type holder because of lesser contact area between the solid-cathode and holder rod.

Temperature distribution of the solid-cathode in three views (top, front and bottom) has been shown under Fig. 6. The comparative view of the two type holder assemblies shows that the heat dissipation is more for cup type holder than the rod type holder. It happens due to larger contact surface area between the cathode and holder cup than the cathode and holder rod.

Static Analysis

Stress distribution after 900s of operation has been shown under Fig. 7. It has been observed that the maximum stress on solid-cathode holder cup ($1.459 \times 10^9 \text{ N/m}^2$) is higher than the allowable secondary stress for Tantalum ($9.2 \times 10^7 \text{ N/m}^2$). Region of this peak stress is very localized and concentrated on the cathode holder cup at the welding joint between the cup and the cathode (Fig. 7). This is because of the higher thermal expansion co-efficient of Tantalum ($6.3 \times 10^{-6}/\text{K}$) than Tungsten ($4.5 \times 10^{-6}/\text{K}$). The rigid type of joint (welding) prevents the differential expansion between the holder cup and the cathode. Hence plastic failure of the joint will take place during the operation.

However in the case of pin type support, the stress is

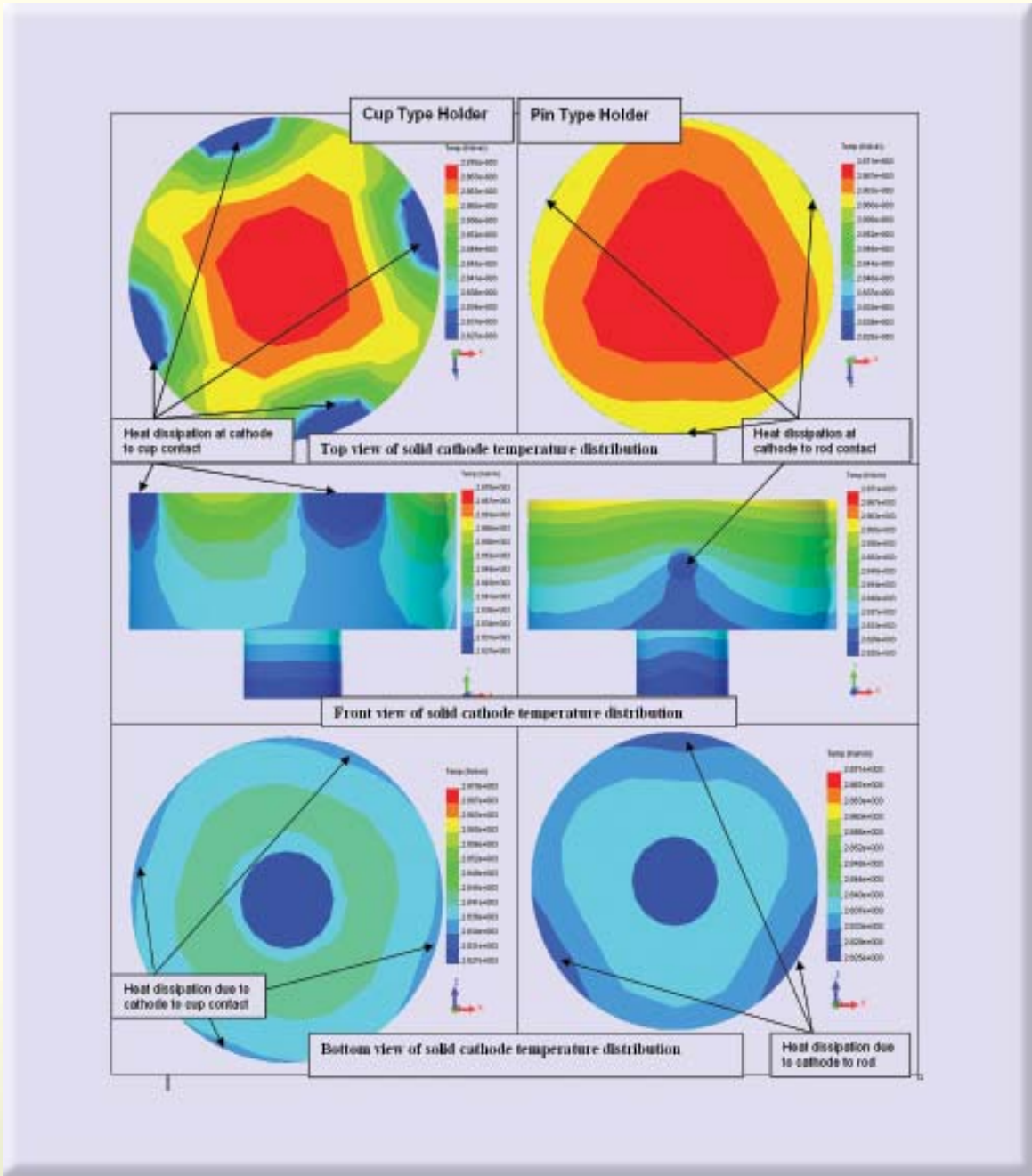


Fig. 6 : Temperature distribution of solid cathode after 900s of operation

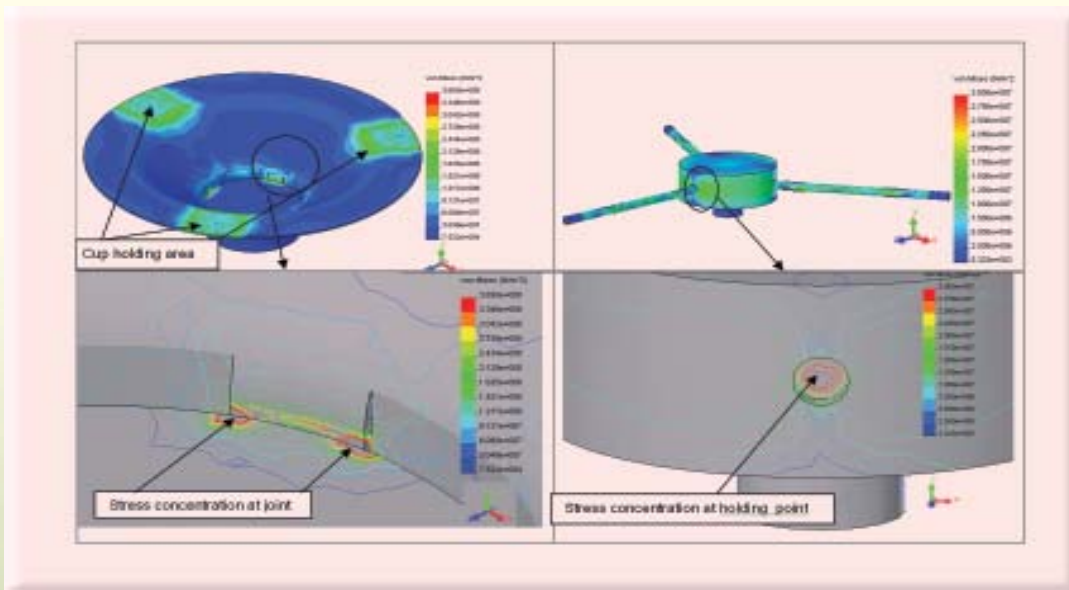


Fig.7 : Stress distribution of solid cathode and holder assembly after 900s of operation

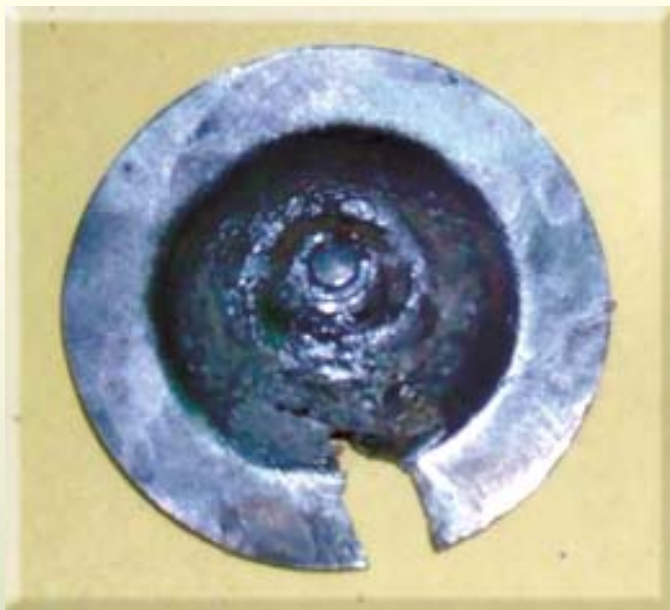


Fig. 8 : View of the cracked cathode holder cup. Crack has been generated at the weld joint between the cathode and cup and it has been propagated into the cup body

always within the acceptable limit (maximum stress = $5.955 \times 10^7 \text{ N/m}^2$). The stress due to differential expansion has been relieved due to clearance fit (in the order of $1 \times 10^{-5} \text{ m}$) provided in between the solid-cathode and holder rod.

Experimental Study

EB welding gun with cup type holder was tested with similar power condition. Crack generation was observed at the cathode to cup weld joint. The crack has been propagated towards the cup periphery. Recorded temperature of solid-cathode is 2400K. The photograph of the cracked cup has been shown under Fig. 8. The experimental result is as per the stress distribution prediction.

Conclusion

Solid-cathode with pin type cathode holder assembly provides better power efficiency than cup type holder assembly, as conduction heat loss is lesser. Thermal stress distribution is under safe region for this type of assembly. However for cup type assembly there is rigid

type of joint (welding) at localized regions in between the cathode and the cathode holder cup, which resist thermal expansion. This gives way for high localized stress at the joint positions, which in long term may cause plastic failure and subsequent crack. Considering these factors, pin type holder assembly becomes a better option for holding of solid-cathode.

ABOUT THE AUTHORS



Mr Pallab Karmakar completed his graduation in Mechanical Engineering from North Bengal University in

the year 1998. He joined BARC in 1999 through 43rd batch Training School. He has been working in L&PTD, BARC. He is involved in the design, analysis, fabrication, installation and commissioning of power beam equipment, such as electron beam welding, melting, evaporation and coating systems. His activities include code design of pressure vessels, thermal-structural analysis of high heat flux equipments and design of vacuum systems. He has contribution in different major projects of L&PTD, i.e. AVLIS at Engg. Hall-6, 300 kW EB Furnace, Coating Unit and Graphite Degassing Furnace.



Ms Namita Maiti received B.E. (Electrical Engineering) from Calcutta University in 1986, M.Tech.

(Control Instrumentation) from Indian Institute of Technology, Bombay in 1995. She joined BARC in 1986 through 30th batch of training school. She has been involved in design, development, installation, commissioning and testing of several electron beam welding machines inside and outside BARC. She has developed transverse electron gun for electron beam coating system. Currently, she is involved in the design of indirectly heated cathode based electron beam welding and melting machines and box coater system for multilayer coating. Her research interest includes high power gun design, high voltage DC power source and digital signal processing.



Dr. A. V. Bapat joined the Plasma Physics Division of BARC in 1976. He initially worked on design and development of MHD Power Generators for the Indian MHD Program. Since 1990 he has been working on the design and development of power beam (electron and plasma) equipments for welding, melting and evaporation. Presently he is head of Electron Beam Technology Section of LPTD, BARC.



Dr. A. K. Ray joined Technical Physics Division of BARC in 1968 through 11th batch of training school. Development of electron beam guns for metallurgical applications has been his main area of work. He has also developed magnetron sputtering unit for coating. He has been guiding development of high power electron beam gun systems for the last 10 years. Presently he is Director, BTDG, BARC.

A. K. Sinha joined Technical Physics Division of BARC in 1968 through 11th batch of training school. Development of high voltage DC power supply for electron beam gun has been his main area of work. He has been guiding work on high voltage insulation and discharge problems.

SPECTROSCOPIC DATA FOR LASER ISOTOPE SEPARATION BY ATOMIC VAPOUR ROUTE: A CASE STUDY IN (U-234, U-235) ISOTOPIC SYSTEM

A.P. Marathe, K.G. Manohar and B.N. Jagatap
Laser & Plasma Technology Division

and

A. Venugopalan
Spectroscopy Division
Bhabha Atomic Research Centre

This paper won the Best Paper Award in the session "Physics Behind Nuclear Technology" at the Indian Nuclear Society's Annual Conference (INSAC-2005), on "Science Behind Nuclear Technology" held at BARC, Mumbai, during November 15-18, 2005.

A b s t r a c t

Involvement of atomic physics in the development of Laser Isotope Separation (LIS) technology with atomic vapour route is discussed with a case study in (U-234, U-235) isotopic system. Importance of atomic data, i.e. isotope shift, hyperfine structure and transition strength in configuration of an isotope selective three-step photoionisation sequence is discussed. Spectroscopic techniques for generating this data are presented along with results on one specific uranium transition. The study is a prototype of spectroscopic investigations for separation of isotopes with one neutron difference in elements with complex energy level structures.

Introduction

Importance of LIS process in the nuclear fuel cycle has been recognized world over for quite some time now. While the technology can be gainfully employed for separation of isotopes involved in the front- and back-end of the nuclear fuel cycle, specific applications that merit mention are enrichment of uranium, denaturing of Zr and Gd and removal of U-232 from U-233, the later being very crucial for the third phase of the Indian

nuclear fuel cycle [1-4]. From the physics perspectives, LIS is a resonant multi-step laser photoionisation process in an atomic vapour, which is made isotope selective by selecting proper atomic energy levels and use of narrow band lasers. Atomic data and intricacies of laser-atom interactions, therefore, form the basis of configuration of a LIS process [4-6].

In this paper we discuss the essential features of generating atomic data for a LIS process and for this

purpose we select separation of U-234 from the isotopic system (U-234, U-235) as a case study. This system has all the trappings of a difficult isotope separation process, namely, one neutron difference in atomic masses ($\Delta M = 1$), blend of an odd and even isotope and need of high temperature for vaporization and, in that sense, is representative of a separation task in high Z elements. Additionally, since the concentration of U-234 in natural uranium is ~ 60 ppm, the spectroscopy of (U-234, U-235) system can provide valuable clues for removal of a trace isotope from an isotopic mixture.

Spectroscopic Data and Level Scheme

Spectroscopic selectivity in LIS arises primarily from the isotope shift (IS) between a pair of isotopes and the hyperfine structure (HFS) exhibited by the odd isotope. As a general rule the levels chosen for LIS must have large IS and narrower HFS widths. Typically, in the heavy elements, e.g. uranium, the IS is of the order of ~ 0 -3 GHz/ ΔM , whereas the HFS widths may vary in the range 1-15 GHz depending on nuclear multi-polar coupling constants. Consequently for $\Delta M = 1$, the selection of atomic levels becomes a very critical issue. Without loss of generality, we consider here a Three-Step Photo Ionisation (TSPI) process involving a common level excitation (CLE) scheme as described in Fig.1. Importance of CLE in uranium LIS lies in improving the atom utilization efficiency, since for evaporation at high temperatures (~ 3000 K), the lowest metastable level of energy 620 cm^{-1} is appreciably populated. TSPI sequence is conveniently driven using Copper Vapour Laser pumped Dye Lasers (CVLDL) and as a consequence the wavelength range is restricted to 540-700 nm.

Isotope Shifts and Transition

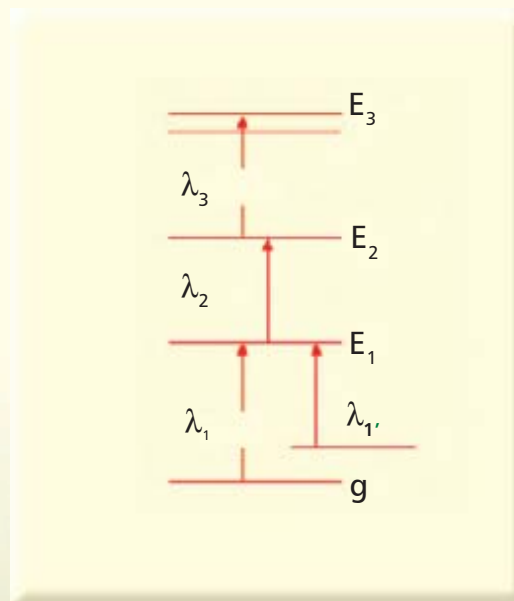


Fig. 1 : Schematic representation of a TSPI sequence with CLE where g = ground level, m = metastable level, E₁= first excited level, which is the common level for photoexcitation from g and m, E₂= second excited level and E₃ = autoionising level. Ionization limit is $\lambda \sim 50,000 \text{ cm}^{-1}$ for uranium. λ_1 and λ_1' are wavelengths for first step transitions $g \rightarrow E_1$ and $m \rightarrow E_1$. Wavelengths for second and third step transitions, $E_1 \rightarrow E_2$ and $E_2 \rightarrow E_3$, are denoted by λ_2 and λ_3 respectively.

Strengths

IS for low-lying atomic levels of uranium have been measured and compiled in several works [7-9]. This information is useful to identify at least the first excited level E₁, which can serve as a possible common level. In Table-1 we present five such possibilities arranged in descending order of IS (234, 235). Note in Table 1 that IS is same for transitions $g \rightarrow E_1$ and $m \rightarrow E_1$.

A transition constituting a TSPI scheme is required to have a good photoabsorption cross-section. It is convenient to provide the strength of the transition in terms of weighted oscillator strength (gf) for it helps to

Table -1 Isotope shifts and Oscillator Strengths for a few common level of U

E_1 in cm^{-1} (J)	λ_1, λ_2 in nm	IS(235,238) in mK [7,9]	IS(234,238) in mK [7,9]	IS(234,235) in mK	gf
14643 (6)	682.7, 712.9	-380	-459.6	-79.6	0.15
14839 (5)	673.7, 703.1	-380	-443.5	-63.5	0.007
15720 (5)	635.9, 662.1	-210	-266.5	-56.5	0.022
18406 (5)	543.1, 562.1	-220	-272.8	-52.8	0.006
17389 (5)	575.8, 596.9	280	330	50	0.001

Note: 1 mK = 30 MHz for errors in IS refer to Ref.[7-9], $IS(234,235) = IS(234,238) - IS(235,238)$

obtain cross-sections for any arbitrary atomic line shape. The gf values given in Table 1 are derived from the emission intensity data and a limited validation of this procedure has been done in the past [10].

For the purpose of this paper we consider the common level 14643 cm^{-1} , which has the largest IS (234, 235) and gf among the transitions in the CVLDL wavelength region. In addition to IS and gf, we need data on HFS to assess feasibility of this level for LIS process. This information is, however, not available in the literature and needed to be generated experimentally.

Hyperfine Structure Measurement

Nuclear spin (I) of U-235 is 7/2, which combines with the angular momentum (J) of the atomic electron to split a level into hyperfine levels ($F = I + J$). The splitting is characterized by the hyperfine constants A and B, which originate respectively from the nuclear magnetic dipole and electric quadrupole interactions. The spectrum of 0 cm^{-1} ($J=6$) \rightarrow 14643 cm^{-1} ($J=6$) transition belonging to

U-235 is expected to exhibit HFS with 8, 7, and 7 components belonging to $\Delta F=0, \pm 1$ with $\Delta F=0$ components being the strongest.

For the purpose of measurement of HFS of $0 \text{ cm}^{-1} \rightarrow 14643 \text{ cm}^{-1}$ transition at 682.7 nm, we take recourse to high-resolution emission spectroscopy in the first phase [5,6,11]. This is done conveniently using an indigenously developed REcording Fabry Perot Optical Spectrometer (REFPOS) and a specially designed Hollow Cathode Discharge Lamp (HCDL) as a source of atomic lines. The instrument has a resolving power of 10^6 and has been extensively used for measurement of IS in heavy elements. The special HCDL used here is liquid nitrogen cooled and requires sample sizes of 1 mg or less [5,11].

In Fig.2, we show the high-resolution emission spectrum of 682.7 nm line recorded on REFPOS. This spectrum can be used to verify the IS (235, 238) which is defined as the frequency separation between the Center of Gravities (CG) of spectral features of U-238 and U-235. The HFS of U-235, however, is not resolved in the spectrum largely due to the instrumental

bandwidth and Doppler width associated with source. This, however, is not a major concern for many transitions since the hyperfine constants can be extracted by subjecting the spectrum to a detailed theoretical analysis. For this purpose we have developed sophisticated HFS ANALysis software, HFSANAL, which takes into account various details such as intensities, center of gravity, spectral line shapes and base line corrections to yield HFS constants A and B from an unresolved spectrum. We analyze the spectrum of Fig. 2 to yield the values of A and B coefficients for 14643 cm^{-1} levels and use these to reconstruct the complete HFS spectrum consisting of 22 components. For convenience we have displayed 8 strong components belonging to $DF=0$ in respect of their frequency positions under the envelope of the unresolved U-235 spectrum in Figure 2.

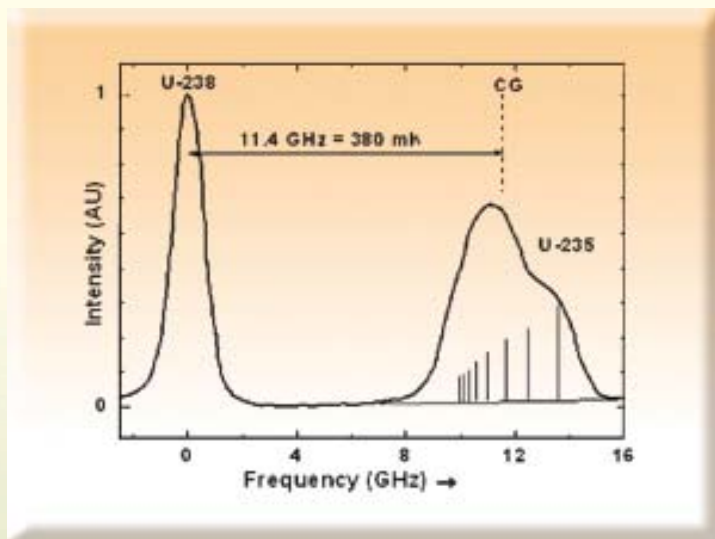


Fig. 2: High resolution emission spectrum of 682.7 nm line of U-235 and U-238. CG of unresolved U-235 spectrum and $IS(235, 238) = 11.4 \text{ GHz}$ are marked. Analysis of U-235 spectrum gives all HFS components of which 8 with $DF=0$ are shown with vertical lines with appropriate frequency separations and intensities. These components ($F \otimes F' = F$) correspond to $F = 5/2, 7/2, 9/2, 11/2, 13/2, 15/2, 17/2$ and $19/2$ in the increasing order of intensity and frequency. See text for details.

The validity of the HFS constants obtained through the theoretical analysis of unresolved emission spectrum can be tested by use of laser spectroscopic techniques or by obtaining HFS pattern of another odd isotope of the same element (e.g. U-233) having larger nuclear magnetic moment. In the present case, we combine both these aspects and obtain a high-resolution spectrum of the 682.7 nm line for U-233 isotope using single mode (mode width $\sim 1 \text{ MHz}$) laser-based Opto Galvanic (OG) spectroscopy [12]. The spectrum of U-233 reported in Ref. [12] is analyzed using HFSANAL program to yield hyperfine constants A and B for U-233. The consistency of the hyperfine constants is checked by the relations and $B^{(233)} / B^{(235)} = Q^{(233)} / Q^{(235)}$ where $\mu^{(M)}, I^{(M)}$ and $Q^{(M)}$ are the nuclear magnetic moment, spin and quadrupole moment of isotope of mass M , respectively.

Spectrum of (U-234, U-235) system

Once the spectral information relating to the IS (cf. Table 1) and hyperfine coupling constants (cf. Sec.4) is available, it is straightforward to construct the spectrum of (U-234, U-235) isotopic system for the transitions $g \rightarrow E_1$ and $m \rightarrow E_1$ where $E_1 = 14643 \text{ cm}^{-1}$. We show in Fig. 3 these spectra generated for atomic vapour with an axial temperature of 300 K. Spectra such as these can be used to address a number of questions relating to the selectivity and accessibility to arrive at LIS process parameters such as bandwidths of the lasers and collimation of an atomic beam.

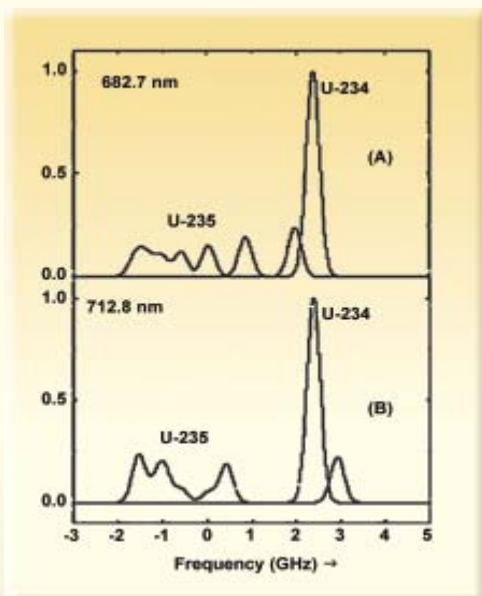


Fig. 3 : Spectra of $g \rightarrow 14643 \text{ cm}^{-1}$ (A) and $m \rightarrow 14643 \text{ cm}^{-1}$ (B) transitions as will be experienced in a uranium atomic beam of axial temperature of 300 K.

The spectra are constructed using experimental data of IS and HFS discussed in Sec. 3-4. The frequency scale is relative with center of gravity of U-235 taken as zero. Ordinate is intensity in arbitrary units.

For convenience of presentation U-234 and U-235 are taken in the same concentration ratio. U-234 spectra may be scaled appropriately to realized the situation for natural uranium. While IS (234, 235) is $\sim 2.4 \text{ GHz}$, there is a considerable overlap of spectral features of U-234 and U-235 owing to comparatively large HFS.

The value of axial temperature used for Fig. 3 is sufficiently low; typical range being 600-800 K. Despite this the spectrum of U-234 shows a partial overlap with that of U-235 for $g \rightarrow E_1$ transition while in case of $m \rightarrow E_1$ transition the spectrum of U-234 lies inside the broad HFS of U-235 although 14643 cm^{-1} level has largest IS (234,235) in the CVLDL wavelength range. Consequently the isotope selectivity in the photoionization process with this transition as the first step is expected to be poor. This conclusion, however, applies for a TSPI process driven

in a standard fashion and with only first step being isotope selective [13].

Second Step Transitions

The next step in constructing a TSPI sequence is to identify second excited step $E_1 \rightarrow E_2$. Usually while moving towards the continuum the absorption cross-section continues to decrease. The level chosen as E_2 must have large absorption cross-section for the step $E_1 \rightarrow E_2$ and further there must exist an autoionizing level E_3 with large enough cross-section for the final step $E_2 \rightarrow E_3$. In a TSPI process, a straightforward way of improving isotope selectivity is to make the second excited step $E_1 \rightarrow E_2$ isotope selective simultaneously. In that case IS and HFS of transition $E_1 \rightarrow E_2$ is an added constraint in the choice of suitable E_2 .

In our experiments we identify these levels using multi-colour photoionisation spectroscopy [6] with an indigenously developed Time Of Flight Mass spectrometer (TOFMS). Multi-colour and multi-step photoionisation in TOFMS is affected using Nd:Yag laser pumped dye lasers. A rich two-colour ($\lambda_1 + \lambda_2$) photoionization spectrum of uranium, obtained by fixing λ_1 and scanning λ_2 , helps to figure out suitable odd parity levels E_2 in the energy range $32500 - 33000 \text{ cm}^{-1}$. The experimental set-up, configured for three colour ($\lambda_1 + \lambda_2 + \lambda_3$) photoionization spectroscopy, further helps to identify suitable autoionising levels E_3 to complete a typical TSPI sequence.

Conclusions

In this paper we have discussed a case study in the spectroscopy of (U-234, U-235) isotopic system to illustrate the importance of atomic physics as the base discipline for LIS. While the paper primarily deals with

investigations of field-free properties of atomic systems, atomic physics plays even a greater role in understanding and quantification of several radiative and non-radiative processes intrinsic to an LIS process. These include, for example, laser-atom interaction processes both in the coherent and non-coherent regime, electric and magnetic field interactions and a variety of atomic collisions involving energy, momentum and charge transfer. We have discussed here the role of atomic data in configuration of an isotope selective and energy efficient TSPI sequence and provided a brief account of experimental techniques and data analysis. The conclusions drawn in this paper are valid for a TSPI process where the origin of isotope selectivity is entirely from the spectral separation that is governed by IS and HFS. It may be possible to invoke innovative ideas in laser-atom interactions to build selectivity in case of isotopes with partially overlapping spectra [13].

Authors thank Dr. L.M. Gantayet, Head, Laser & Plasma Technology Division and Dr. A.K. Ray, Director, Beam Technology Development Group for their support and interest in this work.

References

1. A. Kakodkar, 'Advanced Heavy Water Reactor', Indian Nuclear Society Annual Conference, INSAC-94, Mumbai, February 28-March 2, 1994.
2. A. Kakodkar, BARC News Letter, 182, 1 (1999).
3. L. M. Gantayet, B. N. Jagatap, K. G. Manohar and K. C. Sahoo, in Proceedings of 11th Annual Conference of Nuclear Society (INSAC-2000) on "Power from Thorium: Status, Strategies and Directions", June 1-2, 2000, Mumbai, Part I, p.123.
4. B. N. Jagatap, BARC News Letter, 201, 1 (2000).
5. B. N. Jagatap, L. M. Gantayet, S. A. Ahmad, A. Venugopalan, A. Ramanujam, A. P. Marathe and B. K. Ankush, Proceedings of 11th Annual Conference of Nuclear Society (INSAC-2000) on "Power from Thorium: Status, Strategies and Directions", June 1-2, 2000, Mumbai, Part II, p.235.
6. A. P. Marathe, S. Pradhan, A. Venugopalan, K. G. Manohar and B. N. Jagatap, *ibid*, p.238.
7. J. Blaize and L. J. Radziemski, *J. Opt. Soc. Am.* 66, 644 (1976).
8. R. Engleman and B. A. Palmer, *J. Opt. Soc. Am.* 70, 308 (1980).
9. S. A. Ahmad, P. M. Rao and B. N. Jagatap, BARC-1413 (1988).
10. B. N. Jagatap (unpublished work).
11. A.P. Marathe, A.Venugopalan and B.N. Jagatap, BARC News Letter, 237, 218 (2003).
12. K. G. Manohar, A. P. Marathe, S. Pradhan and B. N. Jagatap, Technical Paper-F8, in the proceedings of 14th Annual conference of Nuclear Society (INSAC-2003) on 'Nuclear Fuel Cycle Technologies: Closing the Fuel Cycle', Dec. 17-19, 2003 at IGCAR. Figure-1 in this paper gives the high resolution spectrum of 682.7 nm line of U-233 obtained using diode laser based opto-galvanic spectroscopy.
13. A. P. Marathe, K. G. Manohar, A. Venugopalan and B. N. Jagatap (Unpublished work).

ABOUT THE AUTHORS



Ms. Asawari Marathe graduated from the 40th batch of training school, after completion of her post graduation in Physics from the Indian Institute of Technology, Mumbai.

She is currently working in the field of laser spectroscopy and laser-atom interactions.



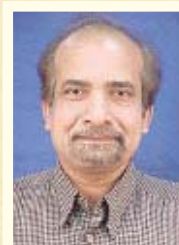
Dr. K.G. Manohar graduated from the 24th batch of BARC training school and obtained his Ph.D. (physics) from University of Mumbai in 1992. He has been

associated with the University of Kaiserslautern, Germany as a Post Doctoral Fellow (1993-94). His research interests include laser physics and spectroscopy.



Dr. A. Venugopalan joined BARC in 1970 after graduating from Kerala University. He obtained his Ph. D (Physics) from University of Mumbai in 1982. He has worked as a visiting scientist at

the ISOLDE facility of CERN, Geneva in 1985 and at the Institute of Physics, University of Mainz, Germany in 1989-90. His field of specialization is high-resolution spectroscopy.



Dr. B.N. Jagatap is a recipient of the Homi Bhabha Award for Science & Technology in 1999. He is a senior visiting fellow at the Centre for Chemical Physics, University of Western Ontario,

Canada. His research interests are atomic physics and quantum optics.



A METHODOLOGY FOR GAMMA RAY SPECTROMETRIC DETERMINATION OF FISSION RATES IN FUEL SPECIMENS

A.V.R. Reddy, T. Newton Nathaniel, G.K. Gubbi, T.P. Chaturvedi and N.S. Tawde
Radiochemistry Division
Bhabha Atomic Research Centre

S. Muralidhar
Metallic Fuels Division
Bhabha Atomic Research Centre

and

K. N. Vyas
Light Water Reactor Division
Bhabha Atomic Research Centre

This paper won the Best Paper Award at the 16th Annual Conference of Indian Nuclear Society, "Science Behind Nuclear Technology", INSAC-2005, held at BARC, Mumbai, during November 15-18, 2005.

Abstract

A methodology was developed to determine the fission rates of compact fuel specimens using high-resolution gamma ray spectrometry, which has been extended to fuel specimens of various dimensions. The absolute efficiency data were generated from the activities of the fission products and the gamma ray activity of ^{238}U at 1001 keV. Axial profiles of the gross gamma ray activity of the fission products were generated using NaI(Tl) detector using discrete scanning and automated fuel pin scanner. Axial profiles of the neutron flux along the 600 mm length of the irradiation position, were also measured using Cu as a flux monitor. The measured fission rates were compared with the values obtained from the neutron flux measurements. Applicability of this methodology for cooling periods as long as 210 d, was also demonstrated by obtaining the fission rates from the measured activities of long-lived fission products like ^{103}Ru (39.25 d), ^{95}Zr (64.03 d) and ^{144}Ce (284.6 d).

Introduction

Non-destructive assay (NDA) methods are used in the quality control of the finished fuel products like pellets, pins and assemblies. These NDA methods are based on the measurement of gamma radiations emanating from or neutrons produced in the samples. Radiations are produced either spontaneously in the

sample or subsequent to active interrogation. A method has been developed to measure fission rates in different fuel specimens and the methodology has been applied to specimens of extended dimensions. This method consists of the following steps (i) High resolution γ -ray spectrometric measurements of some selected fission products produced in the fuel specimens and accounting for attenuation,

(ii) correlating fission product activity to fission rates, (iii) choosing proper energy window for gross gamma ray activity measurement, (iv) Accounting for the decay during the cooling period for different fuel specimens, (v) Extending the methodology to specimens of different dimensions and (vi) validation of the methodology to determine fission rates under simulated conditions.

Absolute fission rates were determined in fuel specimens by high-resolution gamma ray spectrometry[1]. For this purpose a novel method for in-situ determination of detection efficiency was developed which accounts for self-attenuation in thick samples. An energy window of 400 keV – 1500 keV was chosen for measuring fission products activity. A variety of fuel specimens were subjected to active neutron interrogation at a constant low power for short duration in the research reactor Apsara and gross gamma ray activities were measured. After correcting for the decay and attenuation in the sample, fission rates were calculated for samples containing different amounts of uranium. The measured fission rates were found to be consistent with the uranium content and total neutron flux seen by it in the reactor. Reliable data could be obtained based on the measurements carried out during various spans of cooling periods like 2 to 7 days, 15 to 60 days and further even upto 220 days, demonstrating the applicability of the developed methodology. This was extended to a few long fuel specimens with the objectives of (i) determining total fission rates from the measured gross activity, (ii) comparing these fission rates with those obtained using high resolution gamma ray spectrometric measurements and (iii) measurement of fission rates as a function of length of the specimen using a fuel pin scanner. All the three sets of data obtained were found to be consistent. Fission rates of fuel specimen of 600 mm lengths obtained using the

fuel pin scanner were compared with those computed using the simultaneously measured neutron flux using a flux monitor and the observed consistency demonstrated the validity of the methodology [2]. In this paper details of measurements of fission rates in various fuel specimens using γ -ray spectrometry are described.

Experimental

The experiments done were in three categories: (i) compact specimens of less than 10 mm in size, containing about 1 g of natural uranium, irradiated at low power levels, (40 W, 100 W, 400 W) and measurements done in short cooling periods (72 h), (ii) extended specimens like test fuel pins upto 600 mm length, irradiated at 40 W and 100 W and measured at short cooling periods (72 h) and (iii) compact specimens irradiated at high power levels (10 kW and 50 kW), and measurements done at long cooling periods (29 d to 220 d). The irradiations were carried out in Apsara reactor. The axial profile of the neutron flux was determined in the 600 mm length of the irradiation position by irradiating copper wire of 1mm diameter and measuring the gamma ray activity. After a cooling period of 4 h, the irradiated assembly consisting of the extended specimen, the laterally fastened Cu wire along with the aluminum housing, was retrieved from the reactor pool. After adequate cooling period, about 10 mm sections of the Cu wire corresponding to 26 positions with 25 mm spacing were made. The activity of the radionuclide ^{64}Cu (511 keV), was measured for all the samples using an efficiency calibrated HPGe detector to determine neutron flux.

Gamma ray spectra of the fuel specimens/pins were acquired using a High Purity Germanium Detector and a PC-based multi channel analyzer. The detector is shielded with lead bricks, allowing the detector to face

the pin, which is 17 cm away. The width of the collimator was suitably optimized, depending on the level of activity. The pin was supported before the collimator, and the spectra were acquired at each of the 24 positions with spacing of 25 mm from one end to the other to generate the axial profiles of the fission product activity of the pin. The cooling times were varied from a few hours to 72 h for the pin. The compact samples were placed before the detector face while the detector and the sample were inside the shielding. The gamma ray spectra were analysed using the software PHAST. Some of the prominent gamma ray energies corresponding to the fission products are ^{131}I (364.5 keV, $T_{1/2} = 8.02$ d), $^{140}\text{Ba-La}$ (328.8, 487, 815.8 and 1596.5 keV, $T_{1/2} = 12.75$ d), ^{103}Ru (497.1 keV, $T_{1/2} = 39.25$ d) and ^{95}Zr (724.2 and 756.7 keV, $T_{1/2} = 64.03$ d).

Determination of Fission Rates

The activity of a radionuclide produced in nuclear fission, after a cooling period T_c , is given by the equation,

$$A = N \cdot \sigma \cdot \phi \cdot Y (1 - e^{-\lambda \cdot T_i}) \cdot e^{-\lambda \cdot T_c}, \quad (1)$$

where, N = number of ^{235}U atoms in the sample, σ = thermal neutron fission cross section of the target nucleus ^{235}U , ϕ = the average neutron flux at the irradiation position, Y is the cumulative fission yield of the fission product for the thermal neutron fission of ^{235}U , λ = the decay constant of the radionuclide, T_i = the time of irradiation in the reactor, activity is related to the measured peak area (P_A) under a characteristic gamma ray by equation (2).

$$A \cdot \epsilon_\gamma \cdot a_\gamma = \text{CPS} = \frac{P_A \cdot (RT/LT) \cdot \lambda}{(1 - e^{-\lambda \cdot RT})} \quad (2)$$

where, ϵ_γ = detection efficiency at the gamma ray energy chosen, a_γ = abundance of the gamma ray from the radionuclide, P_A = peak area of the gamma ray, LT = live time of the detector during the counting period of RT ,

From the above two equations, the product of the average fission rate in the irradiated specimen ($N\sigma\phi$) and the efficiency of the detector, is given by

$$N \cdot \sigma \cdot \phi \cdot \epsilon_\gamma = \frac{P_A \cdot \lambda \cdot e^{-\lambda \cdot T_c}}{(1 - e^{-\lambda \cdot RT}) \cdot a_\gamma \cdot Y} \quad (3)$$

The peak areas under various gamma ray energies corresponding to the fission products ^{91}Sr ($T_{1/2} = 9.52$ h), ^{133}I ($T_{1/2} = 20.8$ h), $^{132}\text{Te-I}$ ($T_{1/2} = 3.26$ d), $^{140}\text{La-Ba}$ ($T_{1/2} = 12.75$ d), ^{103}Ru ($T_{1/2} = 39.25$ d), ^{95}Zr ($T_{1/2} = 64.03$ d) and ^{144}Ce ($T_{1/2} = 284.9$ d) were used to generate the values of the term ($N\sigma\phi \cdot \epsilon$) from equation (3). These values were used to generate the relative efficiency values of the detector at the respective energies, w.r.t. 1596.5 keV. The relative efficiency data were plotted against the gamma ray energy in the log-log form and is fitted to a 3rd order polynomial, to generate relative efficiency of the detector at any desired energy. The absolute efficiency of the detector for the chosen geometry at 1001 keV (^{238}U), was determined from the peak area at this energy and the amount of U in the sample. This was used to convert the relative efficiency curve to that of the absolute efficiency (Fig. 1). The gamma ray abundance for 1001 keV was taken as 0.837% (3). The data for the half-lives, gamma ray energies and their intensities (4) and the cumulative fission yields (5) for ^{235}U are presented in Table 1.

Fission Rates in Compact Fuel Specimens

Few sets of experiments were carried out with compact fuel specimens. After appropriate cooling, fission

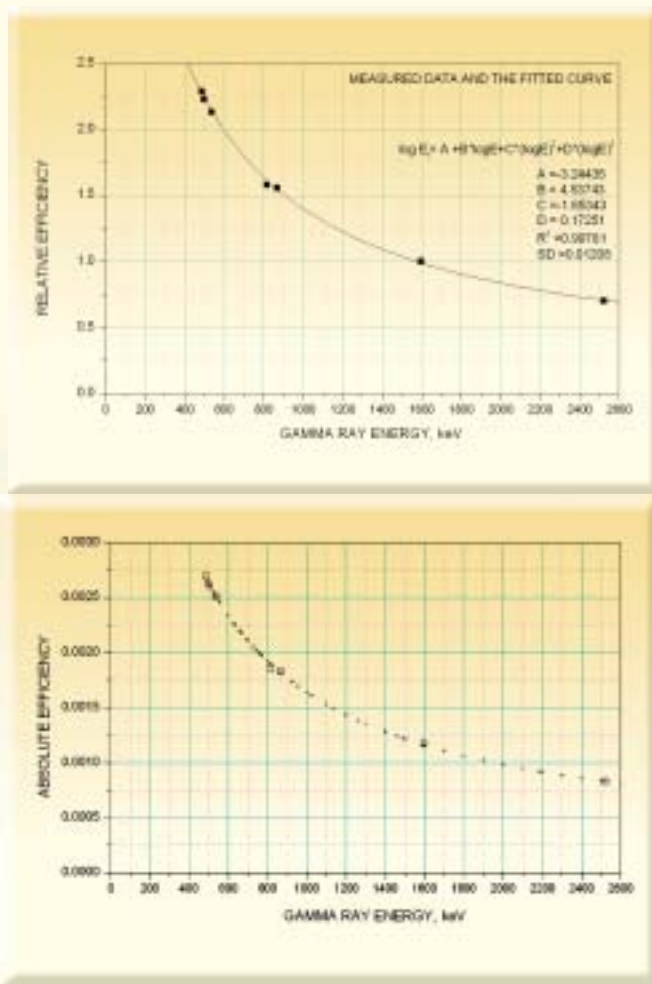


Fig. 1 : Relative efficiency and absolute efficiency curves of sample irradiated at 10 kW, 30 min, cooling time = 67 d

product activities were obtained using high-resolution gamma spectrometric measurements. Activities corresponding to various fission products were obtained by using the absolute detection efficiency, which are used to obtain fission ratios (Fig. 1 and Table 2). A good agreement was observed between the measured values and the computed rates using the amount of uranium, flux and irradiation time. The results of the measurements on the same sample, done at various cooling periods, using different sets of gamma rays also show good consistency.

Gross Gamma Ray Activity : Fission Rates

From the high-resolution gamma ray spectrometric measurements, the energy window of 400 – 1500 keV was chosen for gross gamma counting. In this energy region, many fission products have characteristic gamma rays and for a quick measurement of fission rates a methodology was developed that incorporates correction for radioactive decay. By this methodology it is possible to correlate the measurements carried out at various cooling times. The gross activity (in this energy window) from a typical specimen was measured using a NaI(Tl) detection system in multichannel scaling mode. The obtained composite decay profile is shown in Fig. 2.

Fission Rates in a Long Specimen

After establishing the methodology for compact specimens, fission rates produced in specimens of 600 mm length were measured. As described in earlier section a long specimen was irradiated in Apsara reactor at 100 W for 30 minutes along with a copper wire. The measured neutron flux in the axial direction is shown in Fig. 3. High-resolution gamma ray spectrometric measurements were carried out at 24 discrete points on the long specimen. Fission rates were computed by the methodology described in section 3.1 and the normalized fission rate profile data is shown in Table 3 along with one set of the spectral data.

Table 1 : Nuclear Data for Some Important Fission Products

S. No	Isotope	Half life	γ -ray energy, keV	Abundance %	Fission yield, (%)
1	⁹⁹ Mo	2.75 d	140.5	90.7	6.135614
2	¹⁴¹ Ce	32.5 d	145.4	48.4	5.867379
3	¹³² Te	3.26 d	228.2	88.1	4.115895
4	¹⁴⁰ Ce	33.0 h	293.3	42.8	5.887210
5	¹³¹ I	8.02 d	364.5	81.2	2.774209
6	¹⁴⁰ Ba-La	12.75 d	487.0	52.9	6.300256
7	¹⁴¹ Ra	39.25 d	497.1	89.5	3.105414
8	¹³¹ I	20.8 h	529.9	87.0	6.762420
9	¹⁴⁰ Ba	12.75 d	537.3	24.4	6.300256
10	⁹¹ Sr	9.52 h	555.6	61.3	5.722228
12	⁹¹ Zr	17.0 h	657.9	106.0	5.933895
13	¹³⁰ Te-I	3.26 d	667.7	102.0	4.115895
12	⁹⁹ Mo	2.75 d	739.4	12.1	6.135614
14	⁹¹ Zr	17.0 h	743.4	92.6	5.933895
15	⁹¹ Zr	64.09 d	756.7	55.4	6.502666
16	¹³⁰ Te-I	3.26 d	772.6	78.7	4.115895
17	¹⁴⁰ Ba-La	12.75 d	815.8	27.2	6.300256
18	⁹¹ Sr	9.52 h	1024.3	33.4	5.722228
19	¹³¹ I	6.61 h	1260.4	28.6	6.386041
20	¹⁴⁰ Ba-La	12.75 d	1596.5	109.9	6.300256
21	¹⁴⁶ Ce	284.9 d	2185.7	0.70	5.455421
22	¹⁴⁰ Ba-La	12.75 d	2521.7	3.95	6.300256

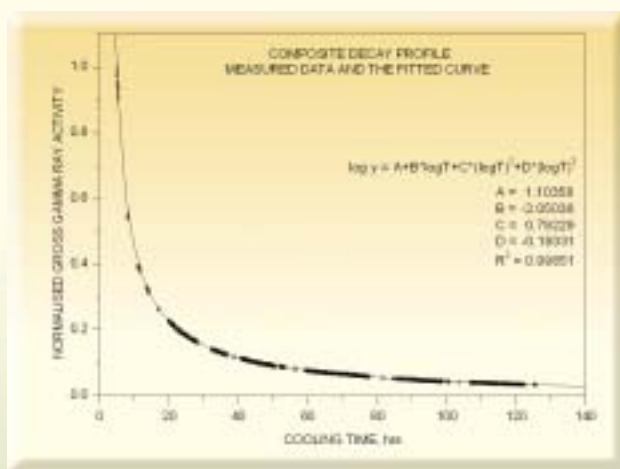


Fig. 2 : Composite decay profile of an extended specimen used to correct the gross gamma ray activities measured at various cooling times to the reference cooling time : gross gamma ray activity (400 - 1500 keV), measured at various cooling times and normalised w.r.t 5 h of cooling time

The measurement done for 1 cm segment of the specimen was assigned to 25 mm length so that the sum of the 24 normalised values is proportional to the total fission rate in the specimen for 600 mm length of fuel. Thus the total fission rate of the 600 mm length of the specimen pin was arrived at as $3.04224E8 \text{ sec}^{-1}$ and $3.06037E8 \text{ sec}^{-1}$ from the activities at 555.6 and 1024.3 keV, respectively, while the value at the centre of the specimen is $6.7223E6 \text{ sec}^{-1}.\text{cm}^{-1}$. Also the gross gamma ray activities measured at 24 discrete points on the

Table 2: Fission Rates of Compact Fuel Specimens of Uranium, Determined at Various Cooling Periods and The Gamma Ray Energies Used

Gamma Ray Energy keV	Fission Rate, $\times 10^8 \text{ sec}^{-1}$	Fission Rate $\times 10^8 \text{ sec}^{-1}$	Fission Rate $\times 10^8 \text{ sec}^{-1}$	Fission Rate $\times 10^8 \text{ sec}^{-1}$
	Samp. wt: 2.582 g Irr. Power: 400 W Irr. Period: 15 m Cool. Period: 50 h	Samp. wt: 0.5681 g Irr. Power: 10 kW Irr. Period: 30 m Cool. Period: 67 d	Samp. wt: 0.5414 g Irr. Power: 50 kW Irr. Period: 30 m Cool. Period: 46 d	Samp. wt: 0.5414 g Irr. Power: 50 kW Irr. Period: 30 m Cool. Period: 210 d
487.0		2.134	1.075	
497.1	3.461	2.105		1.098
529.9	3.466			
537.3	3.359	2.116	1.079	
555.6	3.503			
657.9	3.380			
667.7	3.547			
696.5				1.042
739.4	3.462			
724.2			1.118	
743.4	3.347			
756.7			1.075	1.109
772.6	3.502			
815.8		2.074	1.066	
867.8		2.134		
1024.5	3.446			
1489.2			1.151	1.112
1596.5		2.146	1.092	
2185.7				1.062
2521.7		2.111	1.120	
	3.447 ($\pm 1.92\%$)	2.117 ($\pm 1.14\%$)	1.097 ($\pm 2.71\%$)	1.095 ($\pm 4.93\%$)

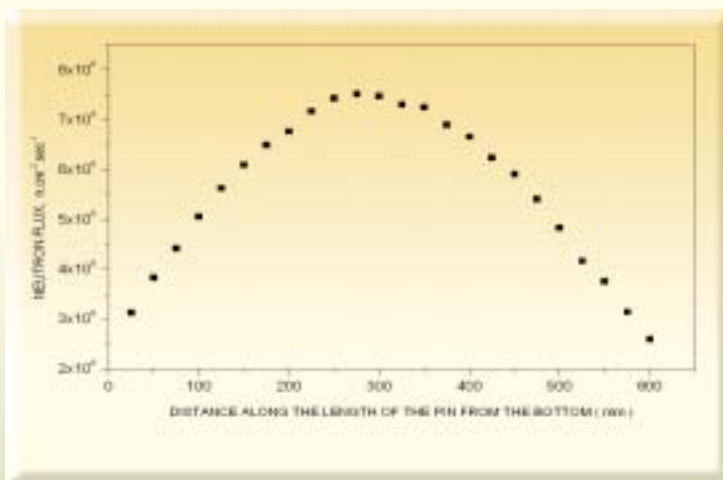


Fig. 3 : Axial profile of neutron flux in the irradiation position of Apsara (F7, 100 W) determined by Cu wire method

at 24 discrete points on the specimen at various cooling times was corrected to a reference cooling time using the correction factors from the composite decay profile (Fig. 2) to give the normalized fission rate profiles (Fig.4), which was used to determine the fission rate of the entire specimen, as $3.12630E8 \text{ sec}^{-1}$ (Table 3).

Fission rates in long Specimens Using NaI(Tl) Detector Based Fuel Pin Scanner.

The gross gamma ray activity

Table 3 - Axial Profile of The Fission Rate of The Extended Fuel Specimen of Uranium Irradiated at 100W for 30 min in Apsara, from Discrete Scanning Measurements Using HPGe and NaI(Tl) Detectors

S.No.	Distance From Bottom End mm	Normalized Gamma Ray Activity of ¹³⁷ Sr 555.6 keV	Fission Rate From Activity of ¹³⁷ Sr 555.6 keV sec ⁻¹ .cm ⁻¹	Fission Rate From Activity of ¹³⁷ Sr 555.6 keV sec ⁻¹ (per 25 mm)	Fission Rate From Activity of ¹³⁷ Sr 1024.3 keV sec ⁻¹ (per 25 mm)	Fission Rate From Gross γ -ray Activity Using NaI(Tl) Detector sec ⁻¹ (per 25 mm)
1	25	0.44065	2.96221E6	7.40551E5	7.01155E5	7.87176E5
2	50	0.48630	3.26909E6	8.17271E5	8.38457E5	8.94048E5
3	75	0.62182	4.18004E6	1.04501E7	9.97727E5	1.09527E7
4	100	0.63864	4.29510E6	1.07327E7	1.22107E7	1.21645E7
5	125	0.85776	5.76612E6	1.44153E7	1.41879E7	1.36283E7
6	150	0.88631	5.95671E6	1.48918E7	1.27410E7	1.46165E7
7	175	0.82701	5.55938E6	1.38985E7	1.40780E7	1.51862E7
8	200	0.86545	5.81781E6	1.45445E7	1.38766E7	1.53332E7
9	225	0.95675	6.43157E6	1.60789E7	1.50848E7	1.60491E7
10	250	0.94185	6.33143E6	1.58286E7	1.68058E7	1.62647E7
11	275	0.94866	6.36373E6	1.59093E7	1.62016E7	1.65879E7
12	300	1.00000	6.72230E6	1.68058E7	1.64762E7	1.68058E7
13	325	0.93417	6.25975E6	1.56994E7	1.61467E7	1.61199E7
14	350	0.95867	6.44440E6	1.61112E7	1.66776E7	1.60954E7
15	375	0.86833	5.83710E6	1.45930E7	1.61833E7	1.56614E7
16	400	0.85103	5.72090E6	1.43023E7	1.55095E7	1.51215E7
17	425	0.91699	6.16022E6	1.54006E7	1.45540E7	1.43353E7
18	450	0.78376	5.20860E6	1.31710E7	1.41512E7	1.31850E7
19	475	0.73522	4.94239E6	1.23590E7	1.24487E7	1.23865E7
20	500	0.73667	4.95208E6	1.23802E7	1.09668E7	1.16754E7
21	525	0.61989	4.16712E6	1.04178E7	1.05265E7	1.04107E7
22	550	0.46949	3.15602E6	7.85006E5	8.18315E5	8.87696E5
23	575	0.43585	2.92990E6	7.32476E5	8.09166E5	7.8724E5
24	600	0.32388	2.17724E6	5.44309E5	5.51038E5	6.30803E5
			Total	3.04224E8 (for 600mm)	3.06370E8 (for 600mm)	3.12630E8 (for 600mm)

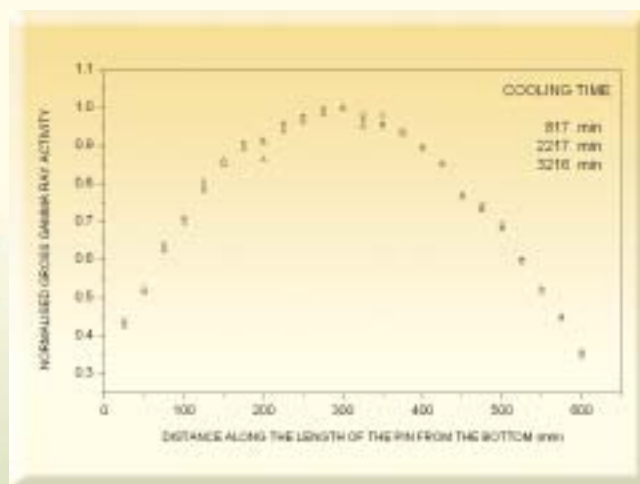


Fig. 4 : Axial power profiles of an extended fuel specimen measured by discrete scanning using NaI(Tl) detector, after various cooling periods, irradiated at 100 W, 30 min. in F7, Apsara

(400–1500 keV) of the long specimen was measured by an automatic fuel pin scanner. The scanner consists of a shielded NaI(Tl) detector and a PC based multi channel analyzer. The extended specimen was loaded on to the cassette, which moves with the help of a stepper motor, so that the specimen moves horizontally before the slit of the collimator (55 mm wide x 15 mm height). Thus 55 mm section of

the specimen was always facing the detector. The scanning speed and the dwell time were optimized as 2 mm.sec⁻¹ and 1 sec, respectively. The axial profiles were obtained from 12 h to 150 h of cooling periods.

The area under the axial profile after correcting for the passive background activity, is plotted as a function of the cooling time to obtain the composite decay profile. The curves when normalized w.r.t. the value at 12 h of cooling period remains identical for the sample-detector geometry chosen, irrespective of the power levels of irradiation (100 W, 100 W and 40 W). The sum of the normalized axial profile data obtained at any cooling time, multiplied by the fission rate determined at the centre of the specimen using HPGe measurements, also gives the total fission rate of the entire specimen. This confirms that the methods developed can be extended to measurements on long specimens at different cooling periods to arrive at total fission rates during the irradiation.

Summary

A methodology for the determination of fission rates was developed for compact fuel specimens using high-resolution gamma ray spectrometry and the applicability of the same for extended fuel specimens and also for cooling periods as long as 220 d was demonstrated. High-resolution gamma ray spectrometry and discrete scanning method was used to measure the activity due to different long-lived fission products. Using the intensities of the characteristic gamma ray(s) of different products, ¹⁴⁰Ba-La, ¹⁰³Ru and ⁹⁵Zr, their cumulative yields for the fission of ²³⁵U with thermal neutrons and the detector efficiency, fission rates were calculated, incorporating irradiation and cooling time corrections. The normalized axial profiles of the fission product activities determined using discrete scanning, as well as the axial profiles of the

gross gamma ray activity of the fission products, were used to determine the total fission rate in the extended specimens.

Acknowledgements

The authors are grateful to Dr. V.K.Manchanda, Head, Radiochemistry Division, Dr. V.Venugopal, Director, Radiochemistry and Isotope Group, Shri H.S. Kamath, Director, Nuclear Fuels Group and Shri V.K. Mehra, Director, Reactor Projects Group for their keen interest in the programme and their constant encouragement.

References

1. A.V.R.Reddy, G.K.Gubbi, T.Newton Nathaniel, R.N.Acharya, T.P.Chaturvedi, and S.B. Manohar, Nuclear and Radiochemistry Symposium, February 7-9, 2001, NUCAR2001, University of Pune, Pune.
2. T.Newton Nathaniel, G.K.Gubbi, A.V.R.Reddy, S. Muralidhar, T.P.Chaturvedi, N.S.Tawde and S.B. Manohar, Nuclear and Radiochemistry Symposium, February 10-13, 2003, NUCAR2003, BARC, Mumbai.
3. Richard B. Firestone and Virginia S. Shirley, Table of Isotopes, 8th Edition, John Wiley Interscience, 1999.
4. U. Reus and W. Westmeier, Catalogue of Gamma Rays From Radioactive Decay, Atomic Data and Nuclear Data Tables, 29, 193-406, 1983.
5. M.E. Meek, and B.F. Rider, Compilation of Fission Product Yields, General Electric, Vallecitos Nuclear Centre, Pleasanton, California-94566., NEDO-12154-1, 74NED6, Class 1, January 26, 1974 & B.F. Rider, NEDO 12154 3c ENDF-327(1981).

ABOUT THE AUTHORS



Dr. A.V.R. Reddy obtained his M.Sc. in Chemistry, in 1974, from Sri Venkateswara University, Tirupati. He joined Radiochemistry Division, BARC, in 1977 after completion of

the one year Orientation Course in Chemistry of the BARC Training School. His areas of research are nuclear fission, nuclear reactions, nuclear spectroscopy, radiochemical separations, heavy element chemistry and activation analysis. He has worked on the chemistry of the elements 104 to 106 at the Institute of Nuclear Chemistry, Mainz, Germany, during 1992-93. He has also worked for IAEA, Vienna, during 1999-2000. He has about 70 publications in journals and more than 100 papers presented in national and international conferences. In addition to this he is a co-author of three books on radiochemistry and the editor of few more books. He is a fellow of the International Union of Pure and Applied Chemistry (IUPAC).



Dr. G.K. Gubbi is from the 11th Batch of BARC Training School. He obtained his M.Sc. in Nuclear Physics from Karnatak University, Dharwad, in 1967. Initially he worked on the

experimental determination of reactor physics parameters for heavy water moderated multi-rod UO_2 clusters using ZERLINA reactor. He was deputed to the Australian Atomic Energy Commission for a year under the Indo-Australian Exchange Programme. He was actively associated with the development of gamma scanners for the quality control of FBTR as well as plutonium-based fuel elements for Tarapur reactors. His recent interests include heavy ion induced nuclear fission and the development of non-destructive assay techniques at various stages of nuclear fuel cycle. He obtained his Ph. D. from University of Mumbai in heavy ion induced nuclear reactions. He has more than 60 publications.



Mr T. Newton Nathaniel is from the 19th Batch of BARC Training School. He completed his M.Sc. in Chemistry at Andhra University, Visakhapatnam, in 1974. He joined BARC in 1976 and worked for the development of high

temperature materials technology for

Magnetohydrodynamic (MHD) Electrical Power Generation Project, jointly executed by BARC and BHEL, in collaboration with the Institute of High Temperatures, Moscow. He was deputed to MHD installations at Moscow and Kiev and participated in the installation and commissioning of the Indian MHD experimental facility (5 MW_{Th}) at Tiruchirappalli. His experience includes work on electrode and insulator materials for MHD generators and air preheaters, component development, performance testing of test

generators, high- T_c ceramic superconductors, zinc oxide varistors, ceramic magnetic cores for transmission line transformers and arc sprayed coatings. His current interest is in reactor irradiation experiments, fission rate determination methods, non-destructive assay techniques by radiation metrology using gamma ray spectroscopy, fuel pin scanners, gamma-well counters based on gas-filled detectors, prompt gamma ray neutron activation techniques and online monitoring of reactor coolant for early detection of failed fuel. He has about 40 publications.



Mr N.S.Tawade joined Radiochemistry Division, BARC in 1998, after graduating in Physics from Mumbai University. His experience is in the field of radiation detectors and the associated instrumentation. He obtained his M.Sc. in Physics by research, from Mumbai University in 2004.



Mr T.P. Chaturvedi, an electronic engineer, joined the Radiochemistry Division, BARC, in 1981. He has extensive experience in radiation detection systems and nuclear instrumentation. He has developed computerized data acquisition systems for the fuel pin scanners and LVDT microscanner for post irradiation examination of reactor components. He has interfaced and automated the cryogenic temperature controllers for positron annihilation spectrometry and data acquisition systems for photo acoustic spectrometer. His current interests include development of magnetic Barkhausen noise acquisition system for the study of stresses in reactor components, digital signal processing for zero dead time spectrometers and assessment of high field radiation in power reactor systems. He is a member of The Institute of Engineers (I).



Mr S. Muralidhar is from 21st batch of BARC Training School. He has done his M.Sc. in Physics at University of Pune in 1976. He joined Radiometallurgy Division, BARC in 1978. Since then, he has been working in the field of non-destructive testing with specialization in ultrasonic testing and radiometry. He has developed NDA methods for the quality control of fuel pins for FBTR using gamma scanners and neutron well coincidence counting techniques. He has about 20 publications.



Mr K.N.Vyas is a Mechanical Engineer from 22nd Batch of BARC Training School. He obtained B.E. from M.S. University, Baroda in 1978. He joined the Reactor Engineering Division, BARC in 1979. His experience in reactor engineering, encompasses design and development of nuclear fuels.

IMMOBILIZATION OF CATALASE BY CROSS-LINKING OF PERMEABILIZED YEAST CELLS IN A PROTEIN SUPPORT

B.S. Kubal and S.F. D'Souza
Nuclear Agriculture and Biotechnology Division
Bhabha Atomic Research Centre

This paper won the Best Poster Presentation Award at the 73rd Annual General Body meeting of the Society of Biological Chemists (India) and at the International symposium on "Challenges and opportunities to harness modern biology for socio-economic development in Genomic era" held at GB Pantnagar University of Agriculture & Technology, Pantnagar, during November 21-24, 2004.

Abstract

Catalase was induced in yeast cells through aeration. The cells were permeabilised for expression of intracellular catalase activity by treatment with toluene. Permeabilised cells were then immobilized in hen egg white using glutaraldehyde as the cross-linking agent. Immobilized cells could be reused for the removal of H₂O₂ from milk.

Introduction

Immobilized catalase (EC 1.11.1.6) can find applications in the food industry in the removal of excess H₂O₂ after cold pasteurization of milk and in combination with a variety of oxidase including glucose oxidase in the production of gluconic acid, removal of oxygen and / or glucose and in the treatment of waste water containing H₂O₂ [1-4]. All these studies have been carried out by immobilization of cell free enzyme of animal and microbial origin [1,2,4]. Major limitation has been the cost and the inactivation of such systems during continuous use. Unlike cell free enzyme preparation, the enzymes have been often found to be more stable inside the whole cells [5]. Even though a number of aerobically grown *Culture Conditions and Induction of*

microbial cells exhibit high catalase activity, not many reports are available on their use in an immobilized form. The present paper describes a simple method for the preparation of immobilized permeabilized yeast cell based catalase by cross-linking in hen egg white, its characterization and its use for the removal of H₂O₂ from milk.

Materials and methods

Materials

Leghorn varieties of hen eggs were purchased from local market. The media constituents including yeast extract, bactopectone and agar were procured from Difco Laboratories. Other chemicals were obtained from standard sources.

Culture conditions and induction of Catalase

Saccharomyces cerevisiae (ATCC 3177) was maintained on agar slants. Catalase was induced in yeast by the method described by D'Souza [6]. The cells were grown anaerobically in a medium containing 2% glucose; 1% bactopectone and 0.3% yeast extract and transferred after 24h to "non-growth" medium (pH 6.8) containing 1% glucose, 1% KH_2PO_4 , 0.01% CaCl_2 and 0.01% $\text{MgSO}_4 \cdot 7\text{H}_2\text{O}$. Catalase was induced in these cells by subjecting them to aeration for 6h at 27° C. The cells were then washed with cold saline and suspended in a 0.05 M phosphate buffer pH 7.0.

Cell permeabilization

Yeast cells (1g) in 5ml 0.05M phosphate buffer (pH7.0) were stirred in cold (0-4° C) for 15 min with 5ml of toluene. This treatment was repeated, after which the cells were washed with phosphate buffer. Permeabilization of yeast cells with toluene increased the catalase activity from 300 to 1880U/g of cells.

Method of enzyme immobilization

The yeast cells were immobilized in hen egg white as follows. The egg white (10ml) obtained from fresh eggs was mixed thoroughly with permeabilized yeast cells (2g) and then treated with glutaraldehyde to a final concentration of 2%. The mixture was stirred well and allowed to stand for 2h at 4°C. The hard gel obtained was shattered by passing through a syringe, and washed with water to remove excess of glutaraldehyde and stored in phosphate buffer at 4°C.

Assay of Catalase Activity

Yeast cells (40mg, entrapped or otherwise) were stirred with 20 ml of 0.08 M H_2O_2 in 0.05M phosphate buffer pH 7.0, and the rate of disappearance of the substrate was measured according to the method described by

Sinha [7]. One unit of enzyme activity is defined as the enzyme responsible to degrade one micromole of substrate (H_2O_2) in one minute.

Results and Discussion

Optimum condition for the immobilization

Gel preparations with optimal retention of enzyme activity and mechanical stability were obtained when cross-linking was carried out for 2 h at 4°C using 2 % glutaraldehyde (Fig 1). Higher temperature (27°C) even though gave mechanically stable gels resulted in considerable inactivation of the enzyme activity.

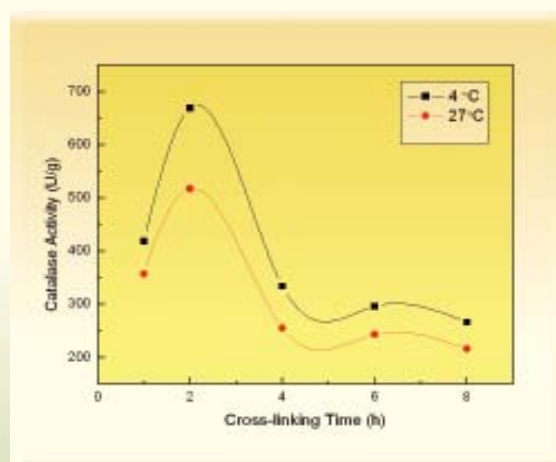


Fig. 1: Optimum condition for immobilization

Properties of immobilized catalase

All the cell preparations (intact and permeabilized) in free and immobilized form exhibited pH optima at 7.0. (Fig.2). Optimal activity was obtained with a buffer concentration of 50 mM. (Fig.3). The thermo stability characteristics of catalase in yeast cells was studied by subjecting the cell suspension to the desired temperature for 10 min followed by rapid cooling in ice. The residual enzyme activity was determined at room temperature. Immobilization was found to

enhance the thermostability (Fig.4). Thus at 45°C the free cells retained only 35% of the original activity as compared to 75% retention of activity seen with the immobilized cells. Immobilized cell preparation can be stored at 4° C for about 40 days retaining over 90% of the original activity.

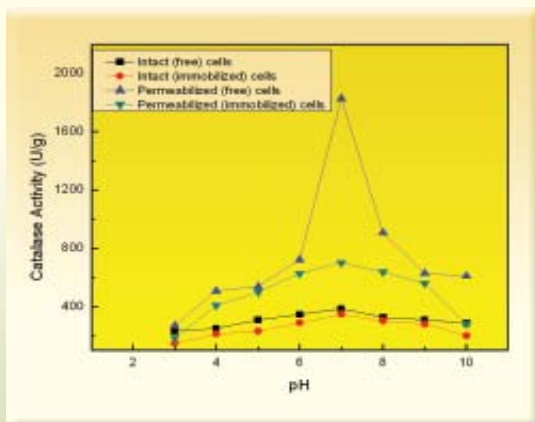


Fig. 2 : pH Effect

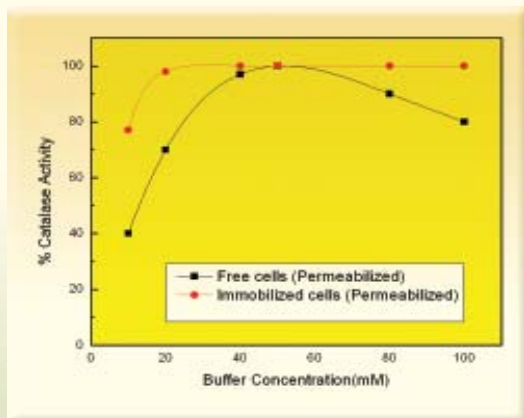


Fig. 3 : Effect of buffer concentration in Catalase

Operational stability of the immobilized catalase

Reuse of immobilized permeabilized yeast cell catalase for the removal of H_2O_2 was studied in a batch reactor

system. The gel particles containing 7g of permeabilized cells was mixed in 400ml of 0.05mM, phosphate buffer pH 7.0 containing 500ppm of H_2O_2 at room temperature for 1 h under stirring. The enzyme gel particles were recovered by filtration using a sieve, washed with buffer and resuspended in a fresh batch of buffer containing 500ppm of H_2O_2 . The process was repeated 10 times. It was observed that the immobilized enzyme was stable for repeated use.

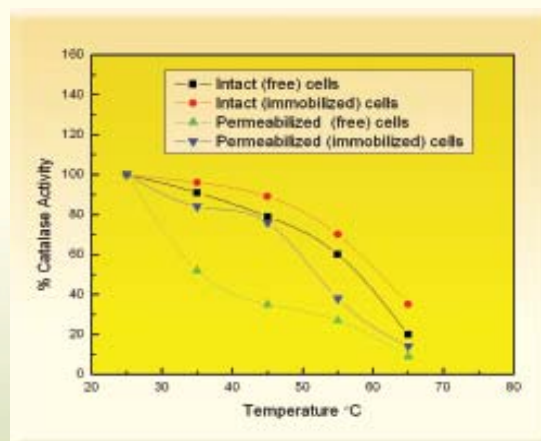


Fig. 4 : Thermostability of Catalase

Application of immobilized enzyme

One of the major applications of catalase is in the removal of H_2O_2 from milk after cold pasteurization. Milk (350 ml) was mixed with 500ppm of H_2O_2 and then treated with 7.0g of entrapped permeabilized yeast cells. The time required for complete degradation of H_2O_2 from the milk was found to be 1h. The immobilized enzyme was reused in 12 batches over a period of 5days without loss in efficiency. The decomposition of H_2O_2 in milk due to immobilized catalase in a batch process was measured by first precipitating the milk proteins with equal volume of 6% trichloroacetic acid. Residual H_2O_2 concentration was measured at 415 nm after addition of 2ml $TiCl_4$ solution (4mg/ml, 5.5N HCl) into 5ml of

sample that had been membrane filtered (0.2µm) after protein precipitation [8].

Conclusions

Permeabilization of yeast cells was found to be essential for maximum expression of intracellular catalase activity. Permeabilization of yeast cells with toluene increased the catalase activity from 300 to 1880U/g of cells. Permeabilized cells in turn can act as an economical source of catalase as compared to commercially available purified enzyme preparations. Further the permeabilized cells can be immobilized in hen egg white by cross-linking with glutaraldehyde for its economical reuse. This technique could find potential in the future for immobilization of microbial catalases. The major advantage as compared to the earlier described technique of entrapment in synthetic polymers like polyacrylamide [6] is the non-toxicity of the hen egg white support thus paving its use in food industry as in the treatment of milk. One of the major problems in the treatment of food material such as milk is the possible microbial contamination of the support. Our earlier studies have shown that hen egg white can serve as a self sterilizing support in view of the large quantities of lysozyme naturally present in the egg white which also gets co-cross-linked (9). Glutaraldehyde used for cross-linking has also been classified under Generally Regarded as Safe (GRAS) category.

References

1. Tarahan L., Use of immobilized catalase to remove H₂O₂ used in the sterilization of milk. *Process Biochem* 1995; 30:623-8.
2. Sankaran K. Godbole S.S., D'Souza SF. Preparation of spray-dried, sugar free egg powder using glucose oxidase and catalase coimmobilized on cotton cloth. *Enzyme Microb Technol* 1989; 11:617-9.
3. Fiedurek J., Production of gluconic acid by immobilized mycelium of *Aspergillus niger* in pumic stones using unconventional oxygenation of culture. *Biochem Lett* 2001; 23:1789-92.
4. Siligia A.C., Tzanko T, Filipa C, George MG, Arhour CP. Recycling of textile bleaching effluents for dyeing using immobilized catalase. *Biochem Lett* 2002;24:173-6
5. D'Souza S.F., Immobilized enzymes in bioprocess. *Curr Sci* 1999; 77:69—79.
6. D'Souza S.F., Nadkarni GB. Immobilized catalase containing yeast cells: Preparation and enzymatic properties. *Biochem Lett* 1980; 22:2191-205.
7. Sinha A.K., Colorimetric assay of catalase. *Anal Biochem* 1972; 47:389-94.
8. Ferrier L.K., Olson NF, Richardson T. Analysis of hydrogen peroxide in milk using titanium tetrachloride. *J. Dairy Sci* 1972; 53; 598-9.
9. Marolia K.Z., D'Souza SF. Enhancement of the lysozyme activity of the hen egg white foam matrix by cross-linking in the presence of N-acetyl glucosamine. *J. Biochem Biophys Method* 1999; 39:115-7.

ABOUT THE AUTHORS



Mr. Bansidhar S. Kubal is currently working in the Nuclear Agriculture and Biotechnology Division. His major research contributions have been in the field of immobilized enzyme technology with special reference to invertase, catalase and amylase. He has to his credit 14 research papers in the national, international journals and symposia.



Dr. S. F. D'Souza is currently the Associate Director-A, Biomedical Group and Head of the Nuclear Agriculture and Biotechnology Division of BARC. His major research interests are in the field of Enzyme and Microbial Biotechnology with special reference to immobilized enzymes and cells for use in bioprocessing, biosensors and bioremediation.

ENHANCEMENT OF CYTOTOXIC EFFECTS OF RADIATION AND DRUG BY ELECTROPORATION IN CANCER CELLS: *IN VITRO* AND *IN VIVO* STUDIES

Pratip Shil and P. B. Vidyasagar
Biophysics Laboratory, Department of Physics,
University of Pune, Pune

and

S. H. Sanghvi and K.P. Mishra
Radiation Biology and Health Sciences Division
Bhabha Atomic Research Centre

This oral presentation was adjudged the Best Oral Presentation and won the prestigious Indian Biophysical Society Young Scientist Award 2005, at the National Symposium on "Recent Trends in Molecular and Medical Biophysics" – IBS 2005, held at the University of Pune, Pune, during January 22-25, 2005.

Introduction

Radiation therapy and chemotherapy are important modalities of cancer treatment. However, each field has its inherent limitations. The major challenges faced by the clinicians and researchers are the development of radio-resistance and chemoresistance in cancer cells. This requires the development of new protocols for improvement of cancer therapy. Electroporation is a biophysical technique which involves transient increase in the cell membrane permeability by application of electric pulses of high voltage and short duration.

The dramatic temporary increase in permeability is generally ascribed to formation of micro-pores in the membrane that allows incorporation of otherwise impermeant biomolecules / drugs.

Theory of electroporation

The cell (in suspension), exposed to electric field, behaves as a non-conducting spherical shell (Fig. 1).

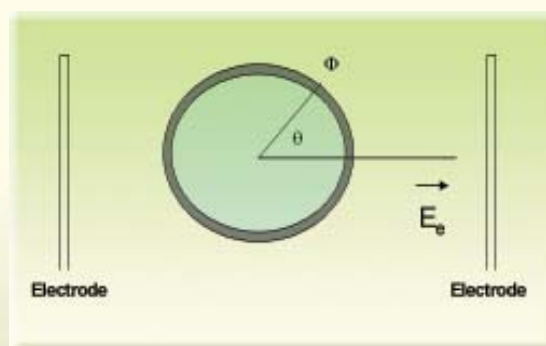


Fig. 1 : Cell (in suspension) exposed to electric field. F – induced transmembrane potential due to applied field E_0

The transmembrane potential of the spherical cell with an non-conducting membrane and placed in an external electric field E_e is given by

$$\Phi = 1.5 r_{cell} E_e \cos\theta \quad (1)$$

where Φ is the transmembrane voltage, r_{cell} is the radius of cell, θ is the angle between the site on the cell membrane where Φ is measured and the direction of E_e .

At $\theta = 0$, $\Phi = 1.5 r_{cell} E_e$; at $\theta = \pi$, $\Phi = -1.5 r_{cell} E_e$. The difference in potential at two diametrically opposite regions of the cell destabilizes the organization of the membrane resulting in formation of micropores [1,2].

Recent research considers cellular plasma membrane as the common target for both radiation and electroporation. The present study is an attempt to explore the modification the effects of radiation and drug by electroporation [3,4].

Materials and Methods

For *in vitro* studies Ehrlich Ascites Carcinoma (EAC) cells were isolated from intra-peritoneal fluid of tumor bearing Swiss mice. For *in vivo* studies, Swiss mice (7 weeks old; weighing ~20g) transplanted with solid tumor fibrosarcoma in right hind legs were used. All experiments were performed according to rules of BARC Institutional Animal Ethics Committee, which are at par with the national laws on animal ethics and experimentation, Republic of India.

Electroporation treatments were performed by using Monophonic square wave pulses (pulse duration: 200 μ s, No. of pulses per train: 8; No of trains: 10) from the medical Electropulsator (BARC/RB&HSD/01-04) designed

and developed in RB&HSD, BARC. For cell electroporation specially designed cuvettes were used, whereas the tumors in animals were electroporated percutaneously with specially designed parallel plate electrodes. To reduce the skin resistance, standard *Electrode gel*[™] (Technomed, INDIA) were applied on the tumor legs prior to the electroporation.

Exposure of cells and mice to Co^{60} γ rays (0.36 Gy/ min) were carried out using the Junior Theratron Teletherapy (MDS, Canada) facility. The cellular effects of treatments were evaluated in terms of generation of Reactive Oxygen Species (ROS) and changes in membrane fluidity using fluorescence spectroscopy with fluorescence probes Dihydrodichloro-fluorescein diacetate (H_2DCFDA) and 1,6-Diphenyl-1,3,5-hexatriene (DPH) respectively. Cellular viability was determined by Trypan Blue dye exclusion assay.

For *in vivo* studies, the tumor growth kinetics was monitored. Tumor size measurements were made using digital Vernier calipers (Mutitoyo, Japan). Two orthogonal diameters a and b were registered. The volume of the tumor was considered to be ellipsoid and calculated by using the formula: V (mm³) = $(\pi / 6) a . b^2$, where a is the largest diameter and b is the diameter perpendicular to a [5].

Results and Discussions

The combination of radiation followed by electroporation treatment (2 kV/cm, 200 μ s, No. of pulses/ train: 8, No. of trains: 10) induced more cytotoxicity in EAC cells as compared to other treatment protocols. The cellular viability dropped significantly in case of the combined treatment. It was observed that the combined treatment with Radiation and Electroporation generated enhanced ROS (Fig. 2) and subsequently greater membrane damage

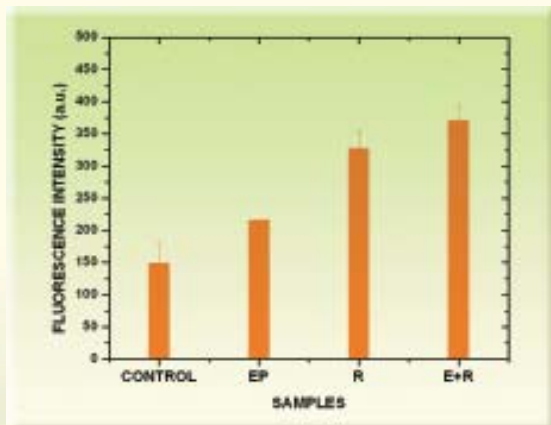


Fig. 2: ROS level in EAC cells determined by H₂DCFDA fluorescence. Abbreviations: EP= electroporation, R= radiation, E+R= combined

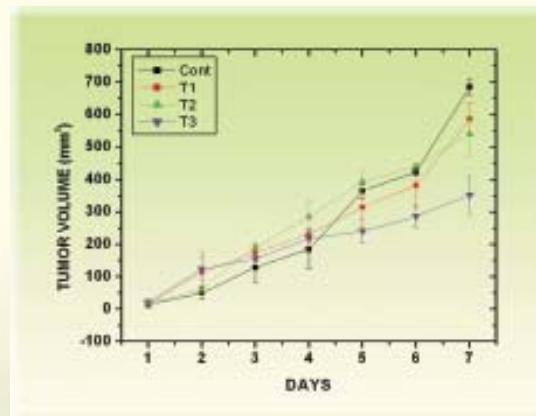


Fig. 4 : Tumor growth kinetics in Murine fibrosarcoma following treatment with Electroporation (T1), Co⁶⁰ γ-radiation 2 Gy (T2) and combination of Electroporation and Radiation (T3).

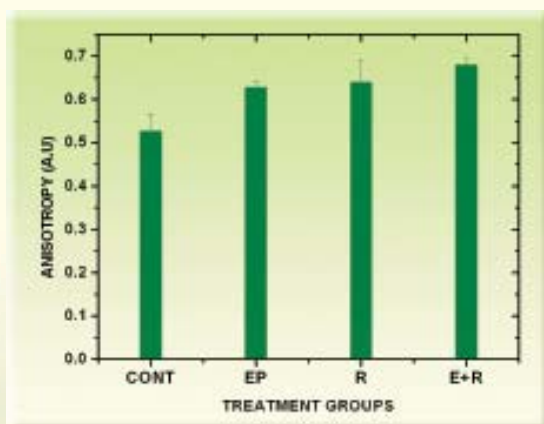


Fig. 3: Changes in membrane fluidity evaluated in terms of DPH-anisotropy. Abbreviations: EP= electroporation, R= radiation, E+R= combined

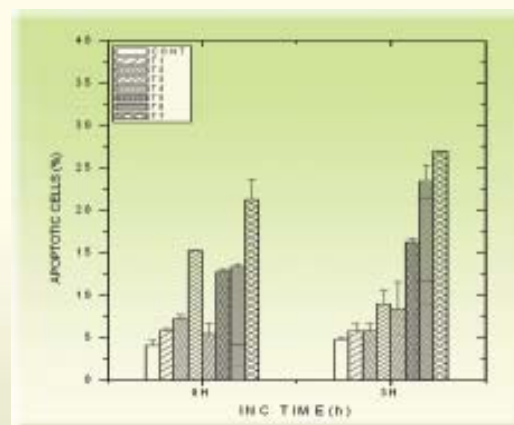


Fig.5 : Apoptosis in EAC cells following ECT. Treatment groups : Control (Cont), Dox 1 μg/ml (T1), Dox 5 μg/ml (T2), Dox 10 μg/ml (T3), Electroporation (T4), Dox 1 μg/ml + EP(T5), Dox 5 μg/ml + EP(T6), Dox 10 μg/ml + EP(T7)

(Fig. 3) in EAC cells indicating that the greater toxicity in cells being mediated by oxidative stress. Significantly enhanced apoptosis (> 25%) was observed in EAC cells subjected to electro-chemotherapy (ECT) with anticancer drug (Dox: 1-10 μg/ml) and electroporation(2 kV/cm,

200 μs, No. of pulses/ train: 8, No. of trains: 10) as compared to the individual treatment modalities (Fig. 5).

The combined treatment of the fibrosarcoma tumor involving electroporation and radiation has produced

greater toxic effects as evident from the significant growth delay (Fig. 4). On 7th day after treatments, the average tumor volumes of treatment groups Electroporation (T1), Radiation (T2) and both (T3) were 85%, 80% and 51 % of that of control respectively.

Conclusions

From the present study we can conclude that the monophasic rectangular electric pulses significantly enhanced the radiation and drug induced cytotoxicity in cancer cells both *in vitro* and *in vivo*(6). This suggests prospects for possible clinical applications in future.

References

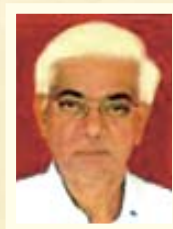
1. Kinoshita K. et al Nature ,268 (1977),438-441.
2. Mishra et al, Bibl. Heamt.,51 (1985), 115.
3. Sersa G. et al, Int.J Radiat. Oncol. Biol. Phys, 46(4) (2000), 1037.
4. Puc M. et al, Bioelectrochem, 64(2004), 13.
5. Kenji M. et al, Intl. J. Clin. Oncol., 5 (2000), 303-307.
6. Pratip Shil et al, J.Env. Pathol. Toxicol. Oncol. (In Press) 2005.

ABOUT THE AUTHORS



Mr Pratip Shil has worked for his Ph.D. under the BARC-Pune University Collaborative Research Program and has submitted his thesis to Pune University in 2005.

He obtained his B.Sc. (Hons.) degree in Physics from the University of Calcutta and M.Sc. (Physics) Degree from University of Pune. He is a recipient of the prestigious R.K Bhalla Award 2004 conferred by the Indian Physics Association to the best Research Scholar in Physics, registered at the University of Pune.



Dr. S.H. Sanghvi, is currently working as a Professor and Head, Department of Bio-Medical Engineering, MGM College of Engineering and Technology, Kamothe,

Navi Mumbai. His main area of interest is biomedical instrumentation. He has obtained his B.Sc and M.Sc. degrees in Physics from Mumbai University. He completed his Ph.D. in Biophysics, in 2004, under the guidance of Dr K.P. Mishra. Dr Sanghvi retired on superannuation from Electronics Division, BARC in Aug. 1999, after rendering a dedicated service of 39 years.



Dr. P. B. Vidyasagar is presently Professor (Biophysics), Department of Physics, University of Pune, Pune. He is also Director, School of Basic Medical Sciences and Director,

School of Energy Studies, at the University of Pune, Pune. He is associated with interdisciplinary research in the University of Pune for two decades and has been a pioneer in the field of research in Medical Physics, Biophysics of Photosynthesis and Thermoluminescence in Biological systems. His contributions have been included in the History of Thermoluminescence in the world and History of Photosynthesis research in India. He is presently Senior Associate, Abdus Salam - International Centre for Theoretical Physics, Trieste, Italy. He is member of the UNESCO Medical Physics Syllabus Committee since 2005. He is the winner of the prestigious Vidya Vyas Award (2003) as an eminent educationist and for his contribution to the popularization of science. He is also the winner of G. R. Paranjpe Award (2005) from the Maharashtra Sahitya Academy, for his contribution to popularization of science, through Marathi medium and science fiction novels in Marathi.



Dr Kaushala Prasad Mishra, Ph.D. joined BARC through 12th Batch of Orientation Course in Nuclear Research and Technology after completing his

postgraduation in Chemistry, from Allahabad University in 1968. He has about 38 years of experience in his field of research and his work has been well recognized internationally. His field of research spans radiation biology, free radical biology and biophysical studies on biological systems. He has published more than 125 research papers in national and international journals and chapters in books. Dr Mishra has delivered almost equal number of invited talks, including keynote lectures and inaugural addresses in national and international conferences. He has edited a book titled Radiobiology and Biomedical Research. He has received several professional recognitions for his significant research contributions in the area of radiation biology and life science. He was visiting scientist to Japan, Germany, France, USA and other countries. He is a recipient of Distinguished Science Service Award of Asia Pacific EPR Society in 2004. Dr Mishra is an Adjunct Visiting Professor at Institute of Technology, Manipal Academy of Higher Education, Manipal. He is a Fellow of National Academy of Sciences, India, Fellow of Maharashtra Academy of Science, Fellow and Senior Vice President of Microscope Academy of India and past President of Section of New Biology, 88th Indian Science Congress. Dr Mishra is the President of Indian Society for Radiation Biology for 2004-2006, Vice President of Asia Pacific ESR/EPR Society for 2004-06, President of Indian Biophysical Society for 2005-2007 and Vice President of Asian Association of Radiation Research, 2005-2009. He has been the Vice President of Society of Free Radical Research, 2003-2005. Dr Mishra is on the Editorial Board of International Journal of Low Radiation, Iranian Journal of Radiation Research and Editor-in-Chief of Indian Journal of Radiation Research. Dr Mishra is a Member of Life Research Board of DRDO, Ministry of Defence.

COMPACT HIGH TEMPERATURE REACTOR (CHTR)

I.V. Dulera, A. Basak, P.P. Kelkar and R.K. Sinha
Reactor Engineering Division,
Bhabha Atomic Research Centre

This paper was judged as the Best Poster Paper under the theme “Emerging Nuclear Energy Systems and Concepts” at the Sixteenth Annual Conference of Indian Nuclear Society (INSAC 2005) held at Mumbai, during November 15-18, 2005.

Abstract

CHTR is mainly a ^{233}U -Thorium fuelled, lead-bismuth cooled and beryllium oxide moderated reactor. This reactor, initially developed to generate about 100 kW_{Th} power, will have a core life of 15 years and will have several advanced passive safety features, to enable its operation as compact power pack in remote areas not connected to the electrical grid. The reactor is being designed to operate at 1000°C, to also facilitate demonstration of technologies for high temperature process heat applications such as hydrogen production from water. Larger power reactors would be designed subsequently.

Introduction

In the long term, nuclear energy would emerge as the primary source of energy replacing fossil fuels. Thus, in addition to producing electricity, it would provide necessary energy for producing alternate fuel or energy carrier for transport applications. Considering very small petroleum reserves and increasing oil prices worldwide, it is prudent that India find an alternative to oil for its transport applications. High temperature reactor assisted fluid fuel production is a long-term sustainable alternative. CHTR, being developed in BARC, is a prototype technology demonstrator reactor in the direction of fulfilling these objectives.

Description

The reactor core [1] consists of nineteen prismatic beryllium oxide (BeO) moderator blocks. These 19 blocks contain centrally located graphite fuel tubes. Each fuel tube carries fuel inside 12 equi-spaced longitudinal bores made in its wall. The fuel tube also serves as coolant channel. The fuel is based on TRISO coated particle fuel, which can withstand very high temperature (1600°C). These particles are mixed with graphite powder as a matrix and made into cylindrical fuel compacts. The fuel compacts are packed in fuel bores in the walls of each of the nineteen fuel tubes. Eighteen blocks of beryllium oxide reflector surround the moderator blocks. These eighteen blocks have central holes to accommodate

passive power regulation system. This system works on temperature feedback and in case of rise of coolant outlet temperature beyond design value, inserts negative reactivity inside the core. Graphite reflector blocks surround these beryllium oxide reflector blocks. This part of the reactor is contained in a shell of a material resistant to corrosion against Pb-Bi eutectic alloy coolant and suitable for high temperature applications. Top and bottom closure plates of similar material close this reactor shell. The fuel, moderator and reflector blocks are contained in a reactor shell made of high temperature and liquid metal corrosion resistant material. Top and bottom closure plates of the same material close the reactor shell. Above the top cover plate and below the bottom cover plate, plenums are provided for core-outlet and core-inlet coolant respectively. These plenums have graphite flow guiding blocks, having passages for coolant flow, to increase the velocity of the coolant between the fuel tube and down comer tube. The reactor shell is surrounded by two gas gaps that act as insulators during normal reactor operation and reduce heat loss in the radial direction. There is an outer steel shell, surrounded by heat sink. This outer shell has fins to improve heat dissipation. Schematic of a single fuel bed and cross-sectional layout of the reactor core are shown in Fig.1 and Fig. 2 respectively.

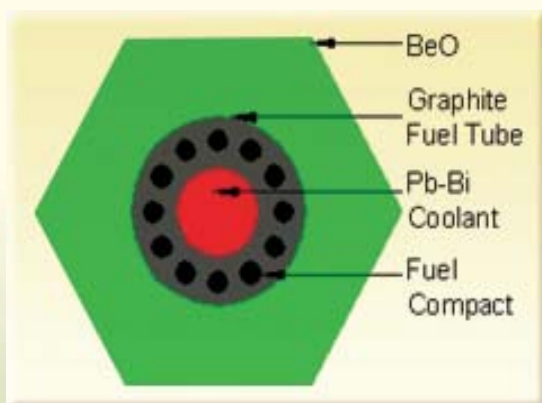


Fig.1 : Single CHTR fuel bed

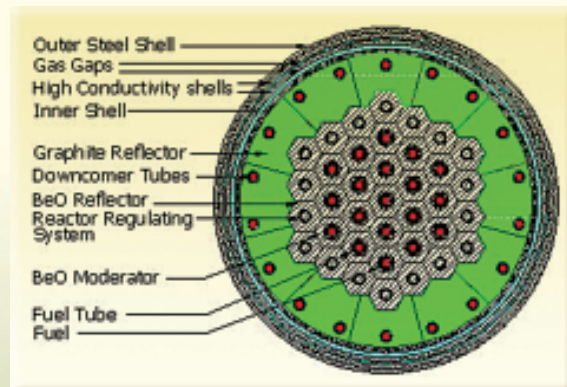


Fig. 2 : CHTR core cross-sectional layout

A passive system has been provided to fill the gas gaps with molten metal in case of abnormal rise in coolant outlet temperature so as to facilitate a conduction path for the reactor heat to outside heat sink. Nuclear heat from the reactor core is removed passively by a lead-bismuth eutectic alloy coolant, which flows due to natural circulation between the bottom and top plenums, upward through the fuel tubes and returning through the downcomer tubes. On top of the upper plenum, the reactor has multi-layer heat utilisation vessels to provide an interface to systems for high temperature heat applications. A set of sodium heat pipes is in the upper plenum of the reactor to passively transfer heat from the upper plenum to the heat utilisation vessels with a minimum drop of temperature. Another set of heat pipes transfers heat from the upper plenum to the atmospheric air in case of a postulated accident. To shut down the reactor, a set of seven shut-off rods has been provided, which fall by gravity in the central seven coolant channels. Instrumentation like neutron detectors; sensors and auxiliary systems such as a cover gas system, purification systems etc. would be incorporated in the design. CHTR component layout is shown in Fig.3. Major design and operating characteristics of CHTR are shown in Table 1.

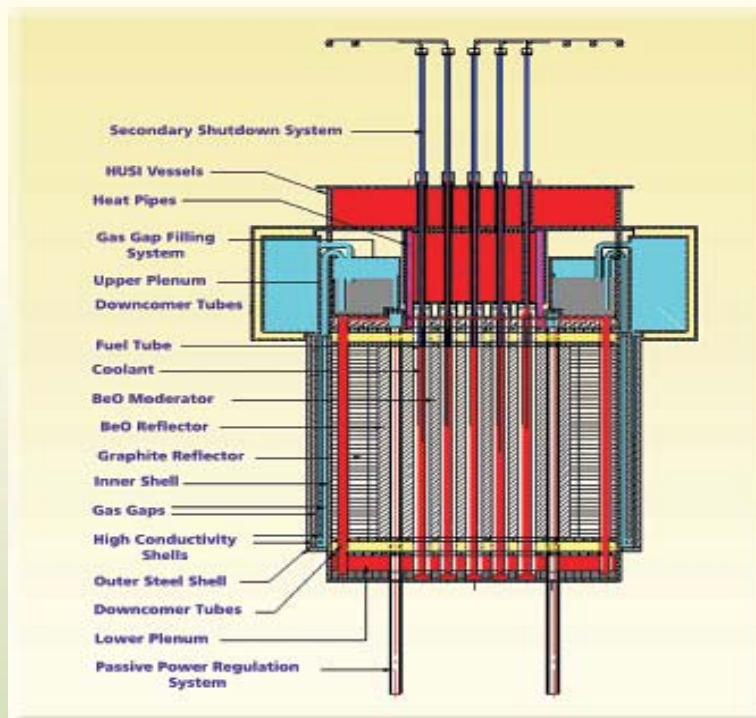


Fig. 3 : CHTR components layout

Table -1: Major design and operating characteristics of CHTR

Attributes	Design Parameters
Reactor power	100 kW(th)
Core configuration	Vertical, prismatic block type
Fuel	$^{233}\text{UC}_2 + \text{ThC}_2$ based TRISO coated fuel particles shaped into fuel compacts with graphite matrix
Fuel enrichment by ^{233}U	33.75 weight %
Refuelling interval	15 effective full power years
Fuel Burnup	≈ 68000 MWd/t of heavy metal
Moderator	BeO
Reflector	Partly BeO and graphite
Coolant	Molten Pb-Bi eutectic alloy (44.5% Pb and 55.5% Bi)
Mode of core heat removal	Natural circulation of coolant
Coolant flow rate through core	6.7 kg/s
Coolant inlet temperature	900 °C
Coolant outlet temperature	1000 °C
Loop height	1.4 m (actual length of the fuel tube)
Core diameter	1.27 m (including radial reflectors)
Core height	1.0 m (Height of the fuelled part and axial reflectors)
Primary shutdown system	18 floating annular B_4C elements of passive power regulation system
Secondary shutdown system	7 mechanical shut-off rods

Fuel Elements

Cylindrical fuel compacts are packed in fuel bores located in the walls of each fuel tube. These fuel compacts comprise TRISO coated fuel particles embedded in graphite matrix. Fig. 4 shows schematic of TRISO coated particle fuel and fuel compact.

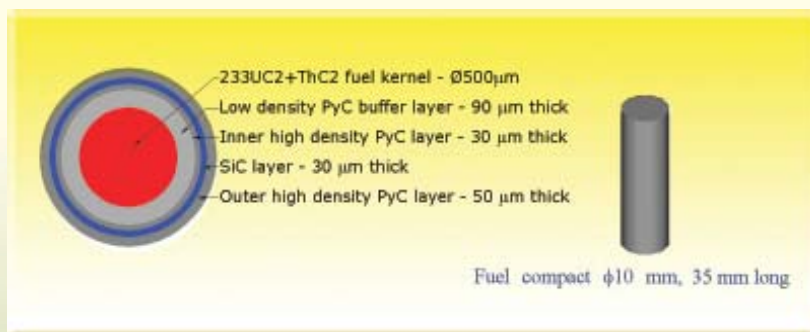


Fig. 4: Schematic of a TRISO coated particle fuel and fuel compact

Passive Core Heat Removal Under Normal Operation

During normal operation of the reactor, the core heat is removed by natural circulation of lead-bismuth eutectic alloy coolant. The coolant at 900° C enters the fuel tube in lower plenum, takes the reactor heat and at 1000° C

it is delivered to the upper plenum. Heat is transferred from the upper plenum to a system of heat utilising vessels by heat pipes [3]. Thermal hydraulic analyses were carried out to study natural circulation of the primary loop. A computer model based on the law of conservation of momentum was developed for this analysis. The mass flow rate of coolant and velocity in the fuel tube was found to be 6.7 kg/sec and 0.04 m/sec respectively.

Passive Power Regulation System (PPRS) and Shutdown System [2]

CHTR incorporates a Passive Power Regulation System (PPRS). This system works on the principle of increase of gas pressure with temperature thereby pressurising and forcing a column of molten metal with floating absorbing material into the core. This introduces negative reactivity in the core. Depending on the temperature rise sensed, the system would stabilize at a particular value of reactivity insertion. The PPRS operation was analyzed using an in-house developed computer code. CHTR has been provided with a passive secondary shutdown system. Under normal operation this system has a set of seven shut-off rods held on top of the reactor core by individual electro-magnets, which are passively released under abnormal conditions when the temperature of the core goes up.

Passive Heat Removal Under Accident Conditions [3]

CHTR has three independent and redundant passive heat removal systems to cater to different postulated accident conditions. These heat removal systems, which are individually capable of removing neutronically limited power of 200 kW_{Th}, may operate together or independently to prevent the temperature of the core and coolant from increasing beyond a set point. For the loss of load condition, when coolant circuit is intact, a system of six variable conductance heat pipes delivers heat to atmosphere. A system of twelve carbon-carbon composite variable conductance heat pipes provided in reactor core caters to the need when coolant is lost. Another passive heat removal system involves filling of the gas gaps by siphon with

a molten metal to provide a conduction heat path from reactor core to heat sink provided outside the outer steel shell.

Inherent safety features and passive safety systems

CHTR is being designed to have many features, which make it inherently safe. In addition, many passive systems for reactor control, reactor shutdown and reactor heat removal under normal and postulated accident conditions, have been incorporated. These are listed below:

CHTR has following inherent safety features

- i. A strong negative Doppler coefficient of the fuel for any operating condition;
- ii. High thermal inertia of the all-ceramic core and low core power density;
- iii. A large margin between the normal operating temperature of the fuel (around 1100 °C) and the leak tightness limit of the TRISO coated particle fuel (1600 °C) to retain fission products and gases;
- iv. A negative moderator temperature coefficient;
- v. Due to the use of the Pb-Bi coolant, which operates at low pressure, there is no over pressurisation and no chance of reactor thermal explosion due to coolant overheating;
- vi. Due to a very high boiling point (1670 °C), there is a very large thermal margin to Pb-Bi boiling. This also eliminates the possibility of heat exchange crisis and increases the reliability of heat removal from the core;
- vii. There is a negligible thermal energy stored in the coolant and available for release in the event of a leak or accident;
- viii. The high temperature Pb-Bi coolant is chemically inert. Even in the eventuality of contact with air or

water, it does not react violently with explosions or fires;

- ix. No pressure in the coolant allows the use of a graphite coolant channel, improving neutronics of the reactor;
- x. A low induced long-lived gamma activity of the coolant; in case of a leakage, the coolant retains iodine and other radionuclides;
- xi. For Pb-Bi coolant, the reactivity effects (void, power, temperature, etc.) are negative.

CHTR employs following passive systems

- i. Natural circulation of coolant to remove reactor heat during normal operation;
- ii. Passive regulation of reactor power under normal operation;
- iii. Passive shutdown for postulated accidental conditions;
- iv. Passive means of conduction of core heat by filling up the gas gaps with molten metals;
- v. Passive transfer of reactor heat by heat pipes under normal and postulated accident conditions;
- vi. Passive removal of heat from the reactor core by carbon-carbon composite heat pipes.

Thermal analysis

A three-dimensional finite element method (FEM) was used for thermal analysis of the CHTR. Fig. 5 shows a steady state distribution of the reactor middle plane temperature. The temperature is seen to be almost constant within the reactor core and the reflector region. The drops in temperature, as expected, occur in two gas gaps provided to prevent loss of heat in the radial direction. Under postulated accident conditions, neutronic limited power becomes 200% of normal power. Temperature distribution under this condition when molten liquid is filled in the gas gaps

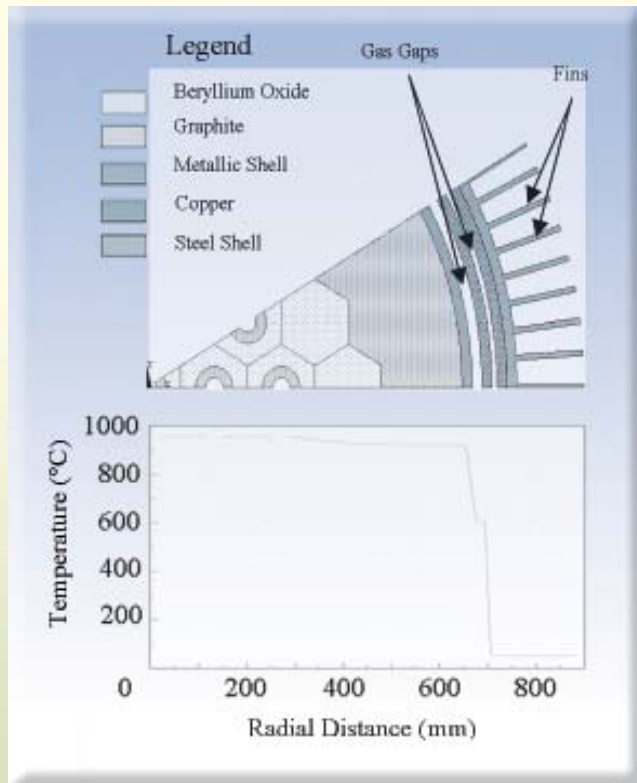


Fig. 5 : Steady state radial temperature distribution within and outside the core

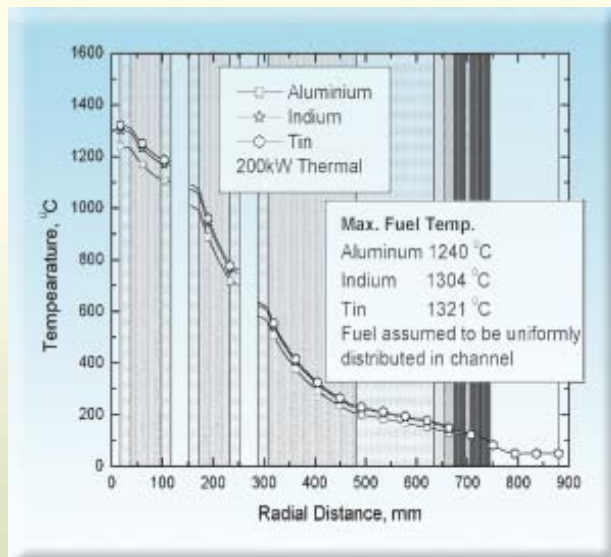


Fig. 6 : Temperature distribution under postulated accident condition

is shown in Fig. 6. Transient analysis under postulated accident condition and in perfect adiabatic conditions showed that the temperature of the fuel would not reach its design limit for 50 minutes, thereby providing sufficient time for operator action.

Major Research and Development Issues and Critical Technologies for CHTR

This reactor calls for research and development activities in many areas of nuclear engineering. There are requirements of high chemical purity special materials like beryllium oxide, graphite and refractory metals with oxidation and corrosion resistant coatings. The fuel needed is high performance high temperature capable special type of TRISO coated particle fuel. In addition to this, the reactor design incorporates many passive systems for reactors control and heat removal. Table 2 lists some of the prominent development areas and their current status.

Current status and schedule

At present, a feasible design of the CHTR has been established after completing the conceptual design of the reactor and associated systems. Experimental facilities are under various stages of development to carry out various studies related to liquid metals, passive safety and heat

Table-2: Important research & development areas for CHTR

Objective	Enabling Technologies	Status of Development
Development of TRISO coated particle fuel	Production of fuel kernels by sol-gel technique	The technique exists
	Technology for development of multi-layer coatings	Coating trials initiated on surrogate material
Development of BeO based moderator and reflector	Manufacture of high density BeO blocks	Sample pieces manufactured
Development of liquid metal coolant technology	Natural circulation of Pb-Bi coolant in the primary circuit	Experimental loop fabricated
	Validated codes for simulation of thermal-hydraulic behaviour of Pb-Bi coolant in primary circuit, under natural circulation	
	Compatibility of materials with Pb-Bi coolant	Under development
Development of passive power regulation system	Validated computer codes to simulate operation of passive power regulation system	Experimental set up under procurement
Development of passive heat removal systems	Manufacture of heat pipes	Experimental set-ups under design
	Testing of heat pipes	
	Gas gap filling system	
Development of graphite and carbon materials	High density isotropic graphite	Under development
Development of high temperature structural materials	Refractory metals	Under development
Development of oxidation- and corrosion-resistant coatings	PyC, SiC, Silicide etc. based coatings development	Under development
Development of codes for design of brittle materials	Validated codes and databases for design of brittle materials	Under development

removal systems. The manufacturing capabilities for BeO, carbon components and fuel micro-spheres have been demonstrated. Trials for TRISO coatings have already started. Subsequent to the manufacture of fuel, materials and other systems, an experimental facility for CHTR would be set up around 2011-12.

References

1. R.K. Sinha and S. Banerjee, Nuclear Energy to Hydrogen, International conference on roadmap to hydrogen energy organized by INAE, Hyderabad, March 4-5, 2005.
2. P.P. Kelkar, A. Basak, S.S. Jana and R.K. Sinha, Passive Power Regulation and Shut down System in Compact High Temperature Reactor, INSAC-2005.
3. A. Basak, I.V. Dulera and R.K. Sinha, Passive Accident Condition Heat Removal Systems for CHTR, INSAC-2005.

ABOUT THE AUTHORS



Mr I. V. Dulera joined Reactor Engineering Division in 1987 after graduating from 30th batch of BARC training school. His field of interest is design and development work related to advanced nuclear systems and components and energy related studies especially, non-electricity applications of nuclear power. Currently he is involved in carrying out design and development work related to Compact High Temperature Reactor, Nuclear Power Pack and Indian High Temperature Reactor for hydrogen production by splitting water.



Mr Abhishek Basak joined Reactor Engineering Division after graduating from the 45th batch of BARC Training School in 2002. He was awarded Homi Bhabha Award in Mechanical Engineering discipline. He is involved in design and development work related to Compact High Temperature Reactor (CHTR), Nuclear Power Pack and 600 MWth High Temperature Reactor. His interest areas are in the fields of thermal and stress analysis using FEM, design, development and testing of high temperature heat pipes, design of brittle components and discrete element based simulations of pebble movement.



Mr Prashant P. Kelkar joined Reactor Engineering Division in 1999 after completing the one-year orientation course conducted by the training school, BARC. He is a B. E. (Mech) by background. He completed his M. E. (Mech.) in 2005 from Indian Institute of Science, Bangalore. Shri Kelkar has been working on various aspects of HTR technology, in particular related to CHTR. He is currently part of the team responsible for the design of Compact High Temperature Reactor (CHTR), Nuclear Power Pack and 600 MWth High Temperature Reactor. His interest areas are in the fields of reactor engineering, structural design, coupled thermal-hydraulic-neutronic phenomenon, application of finite element method.



Mr R.K. Sinha after completing the one year Course of BARC Training School joined Reactor Engineering Division in the year 1973. At present he is serving as Director, Reactor Design & Development Group and Director, Design, Manufacturing and Automation Group, BARC and has been designated a Distinguished Scientist. Shri Sinha has handled several major assignments relating to the Indian research and power reactors. In particular he has specialised in design, development and safety related activities relating to Coolant Channels of Heavy Water Reactors. He is currently guiding the design and development of the innovative Advanced Heavy Water Reactor, Compact High Temperature Reactor, Nuclear Power Pack and Indian High Temperature Reactor being developed for hydrogen production. He is a nationally and internationally recognised expert in the area of nuclear reactor technology. Shri Sinha has received several awards and honours.

STUDIES ON THE ADSORPTION OF ^{125}I ON METALLIC PELLETS FOR THEIR POTENTIAL APPLICATION IN BONE DENSITOMETRY FOR THE DIAGNOSIS OF OSTEOPOROSIS

S.K. Saxena, Ramu Ram, A. Dash and Meera Venkatesh
Radiopharmaceuticals Division, Bhabha Atomic Research Centre
Nilima S. Rajurkar
Department of Chemistry, University of Pune, Pune
S.K. Srivastava
Atomic Fuels Division, Bhabha Atomic Research Centre
and
K.T. Pillai
Fuel Chemistry Division, Bhabha Atomic Research Centre

This Paper won the award for Best Poster Presentation at the Sixteenth Annual Conference of Indian Nuclear Society (INSAC-2005) on 'Science behind Nuclear Technology' held at Multipurpose Hall, Training School Hostel, Anushaktinagar, Mumbai, during November 15-18, 2005.

Abstract

^{125}I - bone densitometry sources find extensive application in the diagnosis of osteoporosis by using single photon absorption (SPA) technique. Silver pellets of size $\sim 2.5 \text{ mm (f)} \times 0.6 \text{ mm (l)}$ were developed as base matrix for adsorption of ^{125}I . Determination of specific surface area and pore size analysis of plain silver and palladium coated silver pellets was carried out. Experimental conditions for quantitative adsorption of ^{125}I were optimized and the sources containing upto $\sim 1.48 \text{ GBq}$ of ^{125}I were prepared. The leachability of sources was found to be $< 0.01\%$. Such ^{125}I - bone densitometry sources developed at our end have potential of application in the diagnosis of osteoporosis after encapsulation of sources within titanium capsules.

Introduction

Osteoporosis is a condition in which the bones become porous and fragile due to the loss of bone matrix (Ca^{+2} etc.), leading to the decrease in the density of bones. It is often seen in persons with impaired bone metabolism, particularly in women during post menopause stage. Osteoporosis is common in absence of medical

intervention^[1]. Measurement of bone density is a useful diagnostic parameter for treatment planning. Some of the established procedures for bone density measurement are Single Photon Absorptiometry (SPA), Dual Photon Absorptionometry (DPA), Quantitative Computerized Tomography (QCT), Dual Energy X-ray Absorptiometry (DEXA) and Ultrasonography. Among these, SPA is a precise and accurate quantitative method available for

the determination of bone density. This is based on the attenuation of a photon that is passed through the bone, where the degree of attenuation is proportional to the bone density. SPA technique uses photons from a single energy radioactive source. In most cases radioisotopes such as ^{125}I or ^{241}Am are used. The use of ^{125}I is preferred over ^{241}Am , on account of its relatively easy availability and low radiotoxicity. In a typical SPA analysis, the extremity is scanned in a rectilinear fashion, and the intensity of the photon beam after passage of the body is registered by a scintillation detector. SPA is mainly used for bone mineral measurements of the forearm or in the lower extremities from the distal femur and below [2-3]. Depending upon various conditions, the choice of technique to be used in bone densitometry is left with the clinicians. However, despite several developments, SPA technique is still used widely as it is very reliable, relatively inexpensive and precise. It also involves very low radiation exposure and many SPA units can be used even in private offices. Preparation of a very small source of ^{125}I [pellet of size ~ 2.5 mm (ϕ) x 0.6 mm (l)] with uniform dose distribution is an intricate job. Techniques such as impregnation of ^{125}I on charcoal beads, electrodeposition of ^{125}I on metallic substrates, etc. have been employed by some manufacturers for the preparation of ^{125}I - bone densitometry sources. In all these substrates, ^{125}I is confined to a minimal area of the base matrix and point sources incorporated with ^{125}I are encapsulated in titanium capsules of dimension ~ 3 mm (OD) x 10mm (l).

In the studies carried out at our end, metallic silver pellets of ~ 2.5 mm (ϕ) x 0.6 mm (l) were developed as a base matrix and conditions for the adsorption of ^{125}I on plain silver pellets as well as on palladium coated silver pellets were optimized. The sources were coated with

thin film of polystyrene as a protective barrier to reduce the spread of contamination during handling and encapsulation of sources.

Materials

Reducing agent free ^{125}I was procured from M/s Institute of Izotop, Hungary. High purity silver powder having particle size of ~ 20 -25 micron (ϕ) was procured locally. Silver pellets of required size were fabricated with the help of a hydraulic press located at AFD, BARC. Specific surface area and pore size determination was done with the help of 'SORPTOMATIC-1990 Analyzer', procured from M/s C.E. Instruments, Italy. The well type NaI (TI) scintillation counter and well type re-entrant ion chamber were used for source activity measurements. Polystyrene beads of ~ 6 mm (ϕ) manufactured by M/s Fluka Chemicals were used for polymer coating of ^{125}I - adsorbed pellets. All other chemicals used were of GR/AR grade procured from reputed manufacturers.

Experimental

Fabrication of Metallic Pellets

The fabrication of silver pellets of ~ 2.5 mm (ϕ) x 0.6 mm (l) was carried out through powder metallurgy route by 'Cold Die Compaction Technique'. Silver powder of ~ 20 -25 micron (ϕ) grain size was compressed at a moderate pressure of ~ 0.5 kg/cm² with the help of hydraulic press. A stroke controlled multiple hole cold die made from stainless steel was developed and employed to shape the silver powder in required pellet form and the stroke length was suitably adjusted to obtain silver pellets of ~ 0.6 mm (l).

Specific Surface Area and Porosity Determination

The specific surface area and pore size analysis of plain silver / palladium coated silver pellets was carried out by using 'SORPTOMATIC 1990' analyzer by studying adsorption- desorption isotherms. The lower part of the adsorption or desorption isotherm (i.e. $0.05 \leq P/P_0 \leq 0.35$) was used for the measurement of specific surface area by multipoint B.E.T. Method [4]. The entire adsorption / desorption isotherm was used for pore size analysis. The pore volume and pore radius were calculated by considering the adsorbed film at the pore walls as cylindrical pores model [5].

Adsorption of ^{125}I on Metallic Pellets

The cleaned silver pellets were treated with 0.5% (w/v) PdCl_2 solution at $\sim 100^\circ\text{C}$ for ~ 15 min to coat them with palladium. Experimental conditions such as reaction volume, reaction temperature etc. were optimized for the quantitative adsorption of ^{125}I on both plain silver pellets as well as on palladium coated silver pellets. Initial tracer experiments were performed by adsorbing ~ 370 KBq (10 mCi) of ^{125}I in the presence of ~ 30 mg of carrier iodide (equivalent to ~ 18.9 GBq) and later, the higher activity pellets were prepared under optimized conditions by using concentrated ^{125}I solution of radioactive concentration $\sim 3.33 - 3.7$ GBq/mL. The activity associated with the pellets in tracer experiments was measured with the help of NaI (TI) scintillation counter and that of having higher activity was measured by using a pre-calibrated re-entrant ionization chamber.

Leachability

The radioactive pellets were subjected to leachability test in accordance with a procedure prescribed by AERB [6]. Individual ^{125}I - adsorbed pellets containing upto

1.48 GBq of ^{125}I were kept in 100 mL of still double distilled water at room temperature for 48 h. At the end of the test, the leached out activity was estimated by assaying the samples of leachant with the help of a NaI (TI) scintillation counter of known efficiency.

Polymer Coating on Pellets Adsorbed with ^{125}I

^{125}I - adsorbed palladium coated silver pellets were coated with polystyrene by treating them for ~ 10 seconds with polystyrene solution at a concentration of ~ 175 mg/mL. Coated pellets were washed with luke warm water at $\sim 30-35^\circ\text{C}$ after drying.

Results and Discussion

Silver pellets of required size could be fabricated with the help of a multiple hole cold compaction die set [Fig.1]. The specific surface area of plain silver pellets and palladium coated silver pellets as determined by B.E.T. Method was found to be $6.7 \text{ m}^2/\text{g}$ and $6.8 \text{ m}^2/\text{g}$ respectively. The pore volume for both the types of pellets was found to be $\sim 0.003 \text{ cc/g}$. Both these parameters (i.e. high surface area and low porosity) are highly favorable for optimum adsorption of ^{125}I on metallic substrates. The pore size distribution of both the types of pellets is shown in [Fig.2]. The shrinkage of pore size in case of palladium coated silver pellets may be attributed to the coating of palladium within the pores. The reaction temperature of $\sim 60-70^\circ\text{C}$ and reaction time of ~ 6 h were found to be optimum for the adsorption of ^{125}I in the presence of ~ 30 mg of carrier iodide. Adsorption of ^{125}I was found to depend upon the reaction volume as shown in [Table 1]. It was observed that as the effective iodide concentration increases (reaction volume decreases), the percentage adsorption also increases. However, below a certain reaction volume, it was impractical to work with low volumes. More

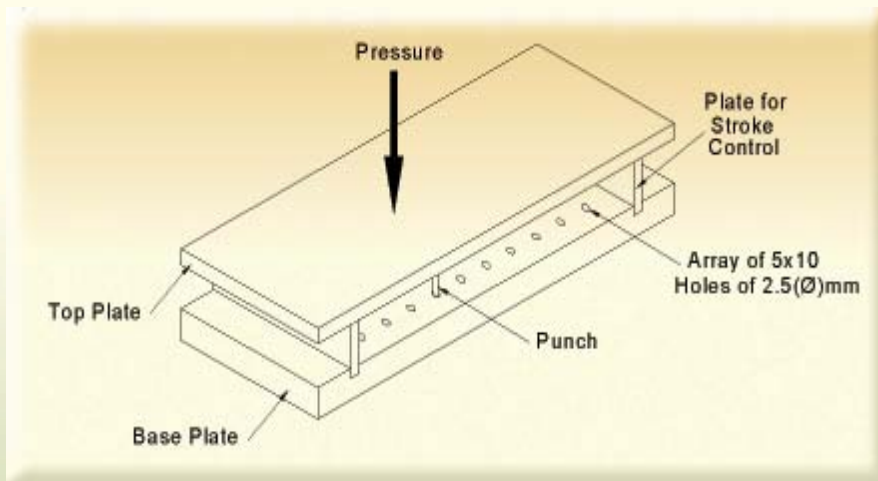


Fig. 1 : Die for Making Silver Pellets

with thin layer of polystyrene without appreciable radiation cut-off. The results of leachability test are depicted in [Table 2]. On account of lower leachability, palladium coated silver pellets were preferred over plain silver pellets as a base matrix for the adsorption of ^{125}I . ^{125}I - sources upto $\sim 1.48 \text{ GBq}$ (40 mCi)

than 75 % adsorption of ^{125}I was obtained on both silver /palladium coated silver pellets, when the reaction volume was kept as $\sim 250 \mu\text{L}$. The sources could be coated

of ^{125}I and containing $\sim 30 \text{ mg}$ of carrier iodide (equivalent to $\sim 18.5 \text{ GBq}$ of ^{125}I) could be prepared by repeating two adsorption cycles.

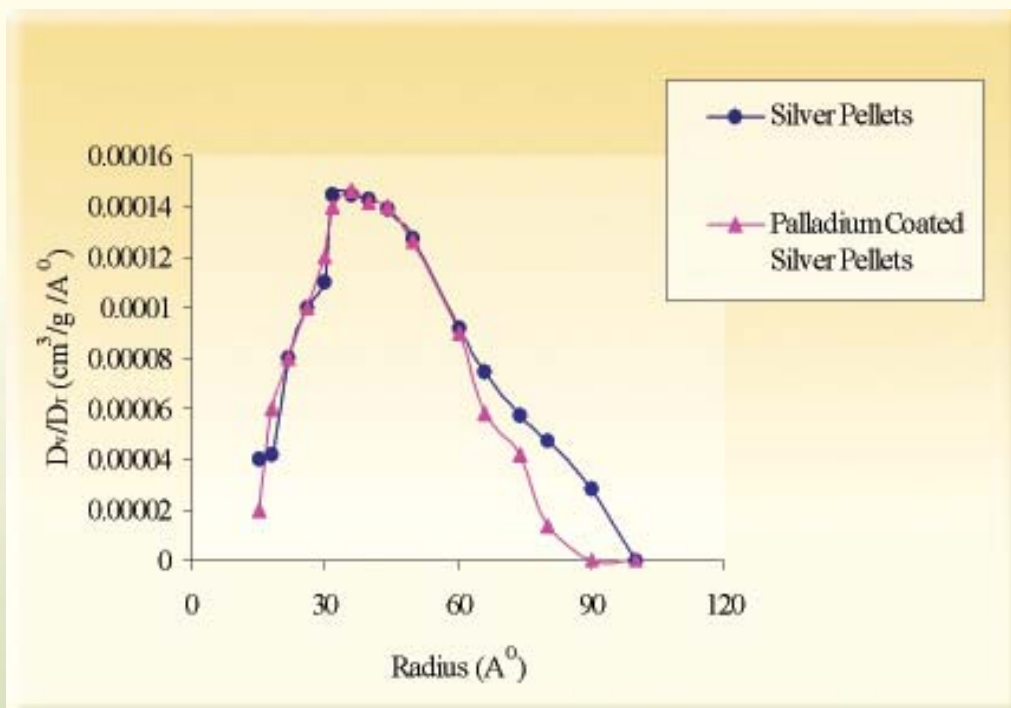


Fig. 2 : Pore Size Distribution of Metallic Pellets

Table-1: Effect of Reaction Volume on (%) Adsorption of ¹²⁵I

S.No.	Reaction Volume (μL)	Effective Iodide Concentration (μg/mL)	Percentage Adsorption (Mean ± SD)	
			Plain Silver Pellet	Palladium Coated Silver Pellet
1.	800	37.5	42.5 ± 8.7	45.7 ± 4.9
2.	600	50.0	47.7 ± 9.3	49.5 ± 3.7
3.	450	66.7	63.56 ± 5.1	65.6 ± 7.2
4.	250	120.0	75.3 ± 6.9	78.6 ± 4.8

n = 5, amount of carrier - 30 μg, reaction time - 6 h, reaction temperature - 60-70 °C.

Table-2: Leachability of ¹²⁵I - Bone Densitometry Sources

S.No.	Source Matrix	Average Source Activity MBq (mCi)	(% Leachability)	
			Mean ± SD	
			Uncoated Source	Polystyrene Coated Source
1.	Silver Pellet	372.5 (10.06)	7.9 ± 3.4	1.76 ± 0.23
2.	Palladium Coated Silver Pellet	365.9 (9.89)	0.007 ± 0.002	0.002 ± 0.001

n=3, test duration- 48 h, temperature - 22° C ambient, leachant- 100 mL d.d. water

Conclusion

A method for the adsorption of ¹²⁵I on metallic pellets could be developed for the fabrication of ¹²⁵I-bone densitometry sources for the diagnosis of osteoporosis. Silver pellets of required size could be fabricated and surface area and pore size determination was carried out. Conditions for adsorption of ¹²⁵I on plain silver pellets as well as on palladium coated silver pellets could be optimized. Palladium coated silver pellets exhibited lower leachability (< 0.01%) and were used for preparation of sources upto the radioactive strength of ~1.48 GBq each.

The sources developed at our end have potential application in the diagnosis of osteoporosis. The encapsulation of sources within the titanium capsules of ~ 50 micron thin window is warranted for their deployment in the diagnosis of osteoporosis.

Acknowledgements

The authors wish to thank Dr. V. Venugopal, Director, RC & IG for his keen interest, encouragement and support. Our thanks are due to Dr. N. Ramamoorthy, former Associate Director, RC & IG and Dr. M.R.A. Pillai, former Head, RPhD for their encouragement.

References

1. Diagnostic methods in Osteoporosis - N. Thomacos and T. Liakatos - Arch Hellen Med, 17(2), March-April 2000, 146-151.
2. Radiographic Absorptiometry- A simple method of determination of bone mass - Cosman F., Herrington B., Himmelstein S., Lindsay R. - Osteoporosis Int. 1991,;2: PP-34 - 38.
3. Bone mineral measurements at the knee using Dual Photon and Dual Energy X-ray Absorptiometry - Michael Mark Petersen - Acta Orthopedica Scandinavica Supplementum No.- 293, Vol.- 71, 2000.
4. Adsorption of gases on multi molecular layers -S. Brunauer, P.H. Emmekte and E. Teller - J. Am. Chem. Soc., 60, (1938), PP-309.
5. The determination of pore volume and area distributions in porous substances -I - Computations from nitrogen isotherms- E.P. Barratte, C.G. Joyner and P.P. Halende - J. Am. Chem. Soc., 73, (1951), PP-373.
6. Testing and Classification of Sealed Radioactive Sources. - AERB SS-3 (Rev-1), 2001.

ABOUT THE AUTHORS



Mr S. K. Saxena after graduation from Allahabad University joined BARC in 1987. He also obtained his M.Sc. degree in Chemistry from University of Pune. In the initial years, he

was engaged in short lived fission products separation programme. He has significantly contributed to indigenous development of ^{137}Cs and ^{125}I - brachytherapy sources for their application in the treatment of gynaecological and eye cancers respectively. He has also been involved in the development of $^{186/188}\text{Re}$, ^{166}Ho etc., based beta emitting liquid radioactive formulations for their potential application in endovascular brachytherapy. He has over 25 research papers to his credit including 12 national/international journal publications. Presently, in addition to the fabrication and supply of brachytherapy sources, he is also involved in the development of emerging brachytherapy and diagnostic radiation sources. He is a life member of IANCAS, INS, NAARRI. Kendriya

Sachivalaya Hindi Parishad and Hindi Vigyan Sahitya Parishad.



Mr Ramu Ram joined BARC in 1998 after completing his graduation from Maharshi Dayanand Saraswati University. He obtained his M.Sc. degree in Chemistry from Mumbai University in 2004.

He has contributed to the production and supply of therapeutic radiation sources. He is presently involved in the regular fabrication of ^{137}Cs brachytherapy and industrial sources. He is also involved in the regular production of different therapeutic isotopes such as $^{186/188}\text{Re}$, ^{166}Ho and ^{90}Y . He is associated with the isolation of isotopes of therapeutic interests such as ^{90}Y etc. He is a life member of IANCAS, INS, NAARRI and Hindi Vigyan Sahitya Parishad. He has more than 10 publications in various symposia, conferences etc.



Dr Ashutosh Dash joined BARC in 1983 after successful completion of the 26th batch of training school. He obtained his PhD degree in Chemistry from Mumbai University in 1994. His areas of

expertise are fission products separation, large scale handling and vitrification of ¹³⁷Cs, separation of radioisotopes by ion exchange methods etc. He had been on deputation to Korean Atomic Energy Research Institute (KAERI) as a Visiting scientist from November 2002 to April 2003. He was a member of IAEA sponsored CRP projects related to development of therapeutic radiation sources and development of generator technologies for therapeutic radionuclides. He is presently heading the T&RS Section of RPhD and looking after the program of production and supply of brachytherapy, industrial and reference sources. He has been involved in various capital plan projects of the Radiopharmaceuticals Division. He is a member of various departmental committees. He has more than 50 research publications including 10 publications in international journals. He is a life member of NAARRI, IANCAS and INS.



Dr (Ms.) Meera Venkatesh joined the Training School of BARC in the year 1976 after completing Bachelor's Degree in Chemistry from Bombay University. She joined the Radiopharmaceuticals

Division in 1977 and has been engaged in the research and development of Radiopharmaceuticals and radiometric assays since then. Dr. Meera obtained her doctorate degree from the Bombay University in 1986 for her work in the field of Radioimmunoassays. She did her post-doctoral fellowship at the University of Missouri, during 1992-94 in the field of therapeutic radiopharmaceuticals and later in 1999 served as a visiting professor at the same university. Currently, Dr. Meera is heading the Radiopharmaceuticals Division, BARC and concurrently serves in the capacity of General Manager of Quality Control at the Board of Radiation and Isotope Technology. She has published over 150 papers in international journals, international and national symposia / conferences and has authored a few invited articles. She has served as an expert in the field of Radiopharmaceuticals and Radiometric assays for the International Atomic Energy Agency.



Dr (Ms) Nilima S. Rajurkar is professor in Physical Chemistry at University of Pune and is working in the field of Nuclear and Radiochemistry. She has guided 20 research students for M.Sc., Ph.D. and M.Phil. Degrees and has to her credit more than 100 research publications. She has written a book entitled "Nuclear Chemistry through Problems" and has contributed to the UGC sponsored Countrywide Classroom Programme on "Radioactivity". She has been the vice president of "Indian Association of Nuclear Chemists and Allied Scientists" and is presently holding the post of convener of "Indian Women Scientists Association", Pune Chapter. She has attended several international and national conferences and has also delivered several lectures abroad.



Mr S.K. Srivastava joined the Atomic Fuels Division, BARC in 1982. Later, he completed Metallurgical Engineering from 'The Institution of Engineers (India)', Calcutta. He has been involved in

powder metallurgy development work and fabrication of control blades for BWR's. He is also associated with development and fabrication of dispersion type fuel elements, regulating pins, control rods and burnable poison rods for PWRs. He is a life member of Powder Metallurgy Association of India, Indian Vacuum Society, Indian Nuclear Society, Indian Association of Nuclear Chemists and Allied Scientists, Indian Society for Non Destructive Testing and has several national and international technical papers and reports to his credit.



Dr K.T. Pillai joined the Fuel Chemistry Division of BARC in 1977. Since then he has been working on the development of Sol-Gel Process for nuclear materials and advanced ceramics. In 2002, he obtained his PhD Degree from

Mumbai University for his work carried out on Sol-Gel Process for alumina and alumina based ceramics. He has published several research papers for his work related to the process development for the preparation of alumina spheres, YAG, YBCO etc.

RADIATION PROCESSED CHITOSAN A POTENT ANTIOXIDANT

M. Shobita Rao, Ramesh Chander and Arun Sharma
Food Technology Division
Bhabha Atomic Research Centre

This paper won the Best Poster Award at the NAARI Annual Conference on Radioisotopes and Radiation Technology : Users' Perception and Experience (NAC 2005) at BARC Guest House and Training School Hostel, Anushaktinagar, Mumbai during November 10-11, 2005.

Abstract

Chitooligosaccharides prepared from chitosan have wide applications in various fields. We have investigated the efficacy of gamma radiation in the preparation of chitooligosaccharides from chitosan. Viscosity and molecular weight of chitosan solution decreased with dose. Radiation dose-dependent increase in free radical scavenging activity and reducing power was observed up to 30 kGy. Irradiated chitosan could scavenge superoxide and hydroxyl radicals in test systems. The efficacy of irradiated chitosan coating in reducing the lipid peroxidation in radiation processed shelf stable intermediate moisture meat products like mutton sheekh kababs and bacon was evaluated. The Thiobarbituric acid reactive substances (TBARS) values in uncoated-irradiated product were higher than the coated-irradiated meat samples after the processing. The chitosan coated, irradiated samples had lower TBARS values up to a storage period of 4 weeks at ambient temperature than uncoated samples. The results suggest the potential use of irradiated chitosan as an antioxidant in maintaining the nutritional quality of radiation processed meat products.

Introduction

Chitosan is derived from chitin which is the second most abundant natural polymer on earth and a waste product of seafood industry. Chitosan, a biodegradable, polycationic polysaccharide has wide range of applications in agriculture, food industry and in medical field ⁽¹⁾. High molecular weight and viscosity limits its use in various applications. Gamma radiation is known to cause main chain scissions in polysaccharides and

decrease the viscosity average molecular weight of the polymers. We have earlier reported increase in antioxidant activity of chitosan solution as a result of irradiation ^(2,3). Radiation technology has been established as an alternative technology for improvement of shelf life, safety and quality of food products. Radiation processing leads to oxidative changes in foods, which may affect the sensory acceptability of foods. We have explored the use of radiation-produced chitooligosaccharides as antioxidants in radiation processed meat products.

Materials and methods

Chitosan solution (1%) was prepared in 1% acetic acid and irradiated at various doses of gamma radiation (0-50 kGy) in Gamma Cell 5000 at a dose rate of 8.7 kGy/h. The viscosity of 1% chitosan solutions (untreated and irradiated) was measured with spindle no. 5 at 50 rpm using Brook field DV-II viscometer at 25°C. Further the molecular weight was calculated using Mark-Houwink equation ⁽³⁾.

Antioxidant assays

Antioxidant activity was measured by 1,1-Diphenyl-2-picrylhydrazyl (DPPH) radical scavenging assay and reducing power assay. The ability to scavenge DPPH radical by chitosan was estimated by method of Yamaguchi and others ⁽⁴⁾. The reducing power was quantified by the method described by Oyaizu ⁽⁵⁾. The mechanism of antioxidant activity of chitosan was elucidated by superoxide radical assay⁽⁶⁾ and hydroxyl radical scavenging ability ⁽⁷⁾.

Antioxidant activity in meat products

Intermediate moisture sheekh kababs and bacon were prepared by reducing the water activity and were coated with chitoooligosaccharide solution. The products were then irradiated with a dose of 4 kGy and stored at ambient temperature. To determine the efficiency of irradiated chitosan as an antioxidant lipid peroxidation was assessed in terms of TBARS ⁽⁸⁾ in products over a storage period of 4 weeks at ambient temperature.

Results and discussion

Irradiation of chitosan solution led to formation of low molecular weight chitoooligosaccharides with reduced viscosity. Viscosity average molecular weight was reduced from a range of 10⁵ to 10³ Da with increasing dose of radiation. Chitoooligosaccharides scavenged the DPPH free radical and dose dependent increase was observed in free radical scavenging activity (Fig.1). A maximum of 80% scavenging was observed for 30-kGy samples. There was no significant increase ($p < 0.05$) in radical scavenging activity with increase in dose above 30 kGy. The scavenging activity of chitosan may be due to reaction between the free radicals and the residual free amino to form stable macromolecule radicals ⁽⁹⁾. Irradiation treatment has been reported to depolymerise chitosan ⁽³⁾, thereby exposing free amino groups and subsequent increase in DPPH free radical scavenging activity.

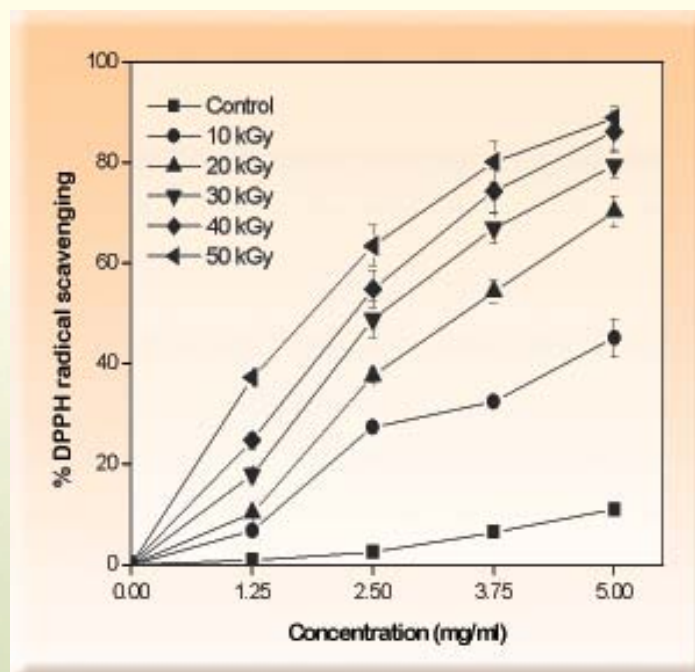


Fig. 1 : Effect of radiation on DPPH radical scavenging activity of chitosan

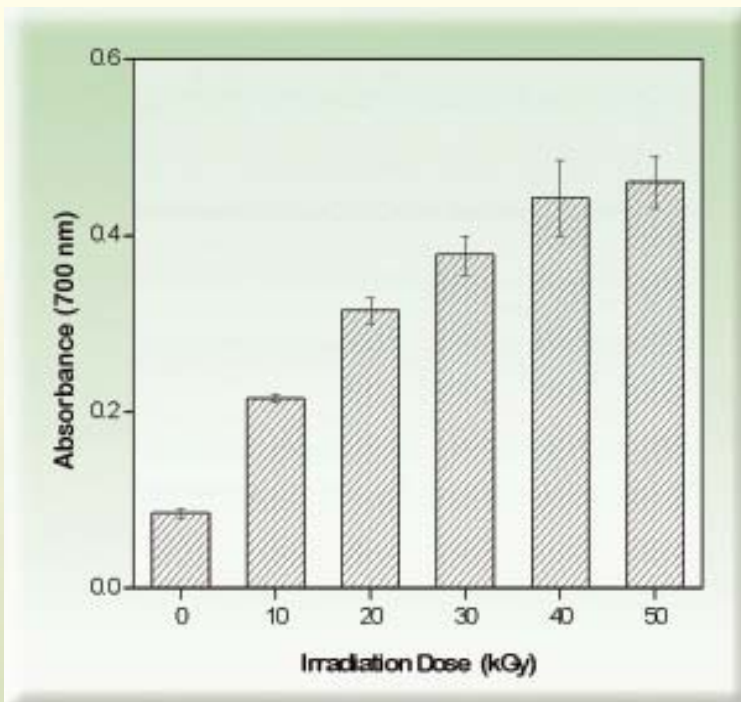


Fig. 2 : Reducing power of chitosan irradiated at various doses

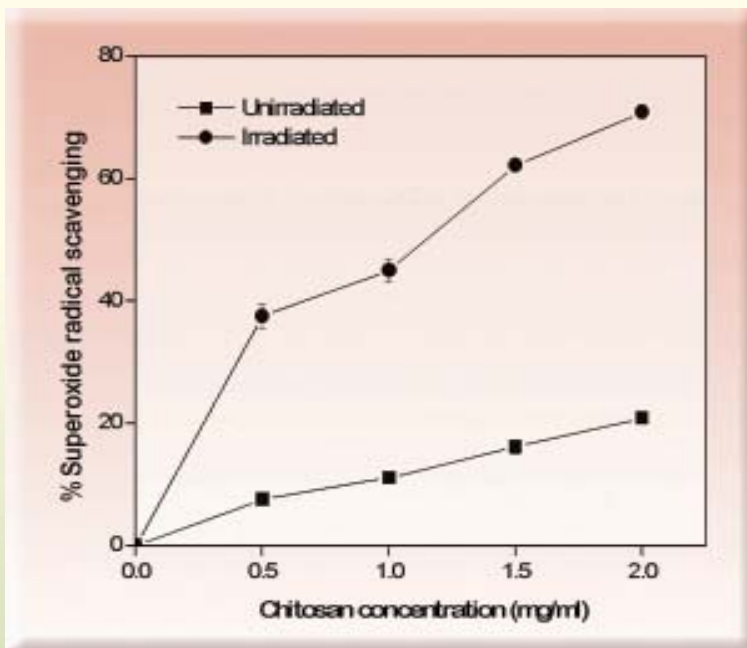


Fig. 3 : Effect of radiation on superoxide radical scavenging activity of chitosan

Reducing power also increased significantly up to 30-kGy doses (Fig. 2) and a linear positive correlation ($r^2=0.953, p < 0.01$) was observed between reducing power and DPPH radical scavenging activity. Increase in reducing power upon irradiation indicates the enhanced antioxidant activity that can be exploited for radiation-processed food and preventing flavor changes caused by lipid peroxidation.

The ability of chitooligosaccharides to act as antioxidant was related mainly to superoxide radical scavenging. The IC_{50} for superoxide radical was found to be 1.15 mg/ml for irradiated chitosan whereas only 20% scavenging activity was observed for unirradiated sample at a concentration of 2 mg/ml (Fig. 3). Superoxide is a relatively weak oxidant but it decomposes to form stronger reactive oxidative species, such as singlet oxygen and hydroxyl radicals, which initiate peroxidation of lipids. Superoxide radical is a zwitterionic radical and it could react with free hydroxyl and amino groups in chitosan thereby leading to scavenging effect. Chitosan has compact structure owing to the intramolecular hydrogen bonding so the scavenging effect is relatively less in untreated chitosan, as the reactive groups are not exposed. The pronounced superoxide scavenging

activity of irradiated chitosan could be related to the fact that irradiation treatment depolymerises the chitosan and the availability of reactive hydroxyl and amino groups increases.

The hydroxyl radical scavenging activity of irradiated chitosan was less as compared to superoxide radical but more than double fold increase in activity was observed as compared to unirradiated solution (Fig. 4). The chitooligosaccharides showed up to 50% hydroxyl radical scavenging activity whereas the activity of untreated was low. The free radical scavenging activities are closely related to bond dissociation energy of O-H or N-H and the stability of the formed radicals. The OH and NH₂ groups in chitosan are difficult to dissociate and react with hydroxyl radical. So chitosan has very low intrinsic scavenging activity⁽⁹⁾. Irradiation is known to cause the breakage of different kinds of bonds. Irradiation treatment led to breaking up of hydrogen bonds and increased availability of OH and NH₂ in the solution for hydroxyl radical scavenging.

The prime objective of this study was to depict the effect of irradiated chitosan on lipid peroxidation in IM shelf stable kababs and bacon respectively. Irradiation led to significant increase ($p < 0.05$) in lipid peroxidation in both the products

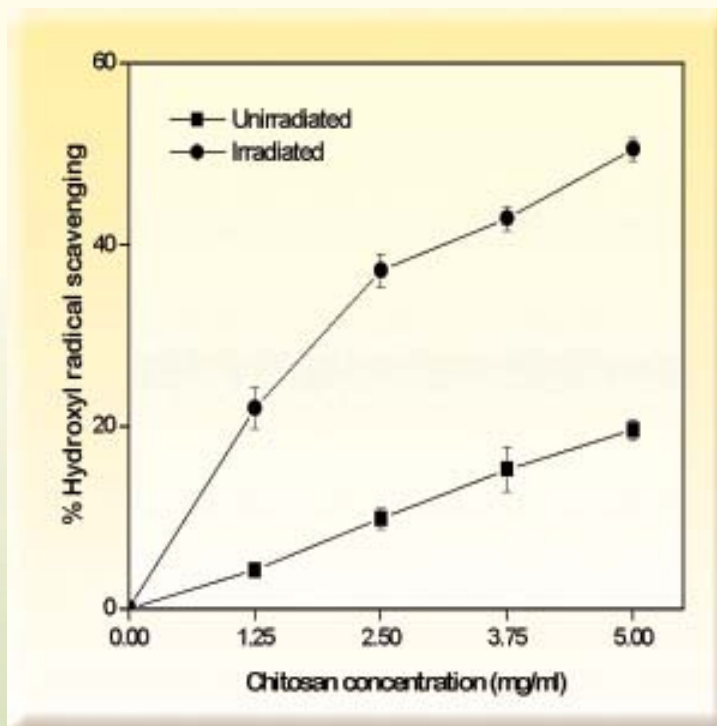


Fig. 4: Effect of radiation on hydroxyl radical scavenging activity of chitosan

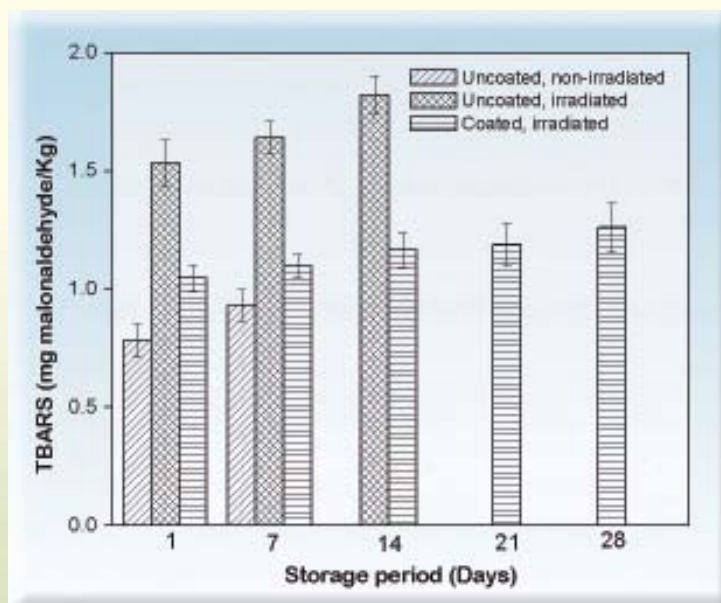


Fig. 5 : Lipid peroxidation in IM mutton sheekh kababs during storage

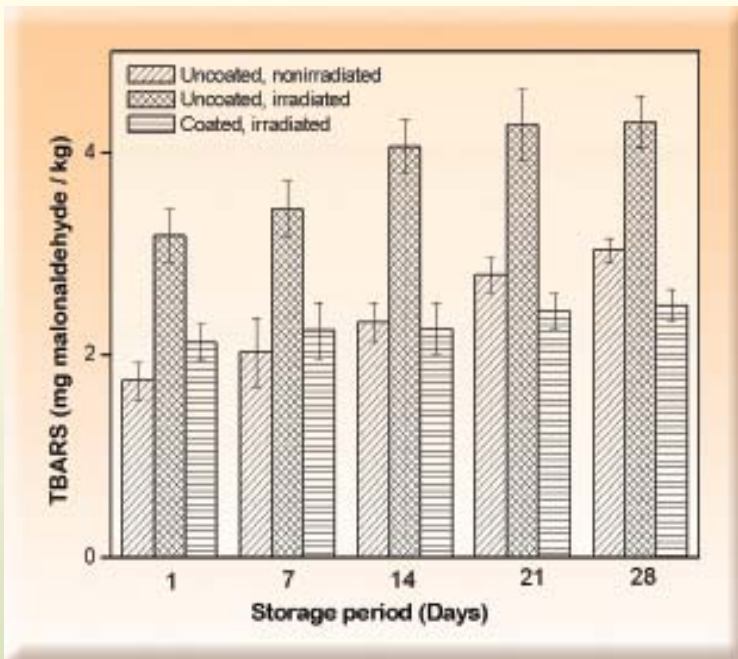


Fig. 6 : Lipid peroxidation in IM bacon during storage

and the values increased upon storage (Figs. 5, 6). Cooked meat is highly susceptible to lipid peroxidation because the cooking processes denature the antioxidant components, damages the cell structure and exposes the membrane lipids to the environment. Like other food processing procedures, irradiation also induces the autoxidative process. Irradiation-induced oxidative changes are dose dependent and the presence of oxygen has significant effect on the rate of oxidation. Irradiated chitosan coating led to 28% and 55% lower TBARS values in irradiated samples than



Fig. 7 : Shelf stable mutton kababs and bacon after storage period of four weeks

uncoated kababs and bacon samples respectively. In this study we found coating was effective in inhibiting the lipid oxidation during irradiation and also during post irradiation storage for four weeks at ambient temperature (Fig. 7).

Conclusion

This is the first published report wherein chitooligosaccharides produced by radiation treatment have been used as antioxidant to retard the lipid peroxidation in shelf stable meat products. Radiation technology can be used to produce chitooligosaccharides with high antioxidant potential, which can be effectively used for maintaining the chemical and sensory quality of radiation processed food products.

References

1. Shahidi F., Synowiecki J. (1991). Isolation and characterization of nutrients and value-added products from snow crab (*Chinocetes opilio*) and shrimp (*Pandalus boreliasis*) processing discards. J. Agric. Food Chem. 39, 1527-1532.
2. Rao M. S., Chander R, Sharma A. (2005). Development of shelf stable intermediate moisture meat products using active edible chitosan coating and irradiation. J. Food Sci. 70 (7), 325-331.
3. Kanatt S. R., Chander R, Sharma A. (2004). Effect of irradiated chitosan on the rancidity of radiation-processed lamb meat. Int. J. Food Sci. Technol. 39, 997-1003.
4. Yamaguchi T., Takamura H., Matoba T., Terao J. (1998). HPLC method for the evaluation of the free radical-scavenging activity of foods by using 1,1-Diphenyl-2-picrylhydrazyl. Biosci. Biotechnol. Biochem. 62 (6), 1201-1204.
5. Oyaizu M. (1986). Studies on products of browning reactions: Antioxidative activities of products of browning reaction prepared from glucosamine. Jap. J. Nutr. 44, 307-315.
6. Liu F., Ooi V. E. C., Chang S. T. (1997). Free radical scavenging activity of mushroom polysaccharide extracts. Life Sci. 60, 763-771.
7. Halliwell B., Gutteridge J. M. C., Aruoma O. I. (1987). The deoxyribose method: a simple test tube assay for determination of rate constants for reaction of hydroxyl radicals. Anal. Biochem. 165, 215-219.
8. Alasnier C., Meynier M. V., Gandmer G. (2000). Hydrolytic and oxidative changes in the lipids of chicken breast and thigh muscles during refrigerated storage. J. Food Sci. 65(1), 9-14.
9. Xie W., Xu P., Liu Q. (2001). Antioxidant activity of water-soluble chitosan derivatives. Bioorg. Med. Chem. Letters. 11, 1699-1701.

ABOUT THE AUTHORS



Ms M. Shobita Rao joined the Food Technology Division, BARC in the year 2003 after one year orientation course from 46th batch of training school. She has done her M.Sc. in Biotechnology from Guru Jambheshwar University, Hisar. She received gold medal in M.Sc. in academics. She has been working on biodegradable packaging material for irradiated foods. Her work also involves development of edible, active packaging for safe, shelf stable meat products using novel antioxidants and antimicrobials. Her other interests include studies on organic solvent tolerant bacteria and its applications.



Dr Ramesh Chander joined Food Technology Division in 1975 after graduating from BARC Training School. He received his M. Sc. from H.A.U. both in microbiology and his Ph. D. from University of Bombay and . He was

a post doctoral fellow at University of Florida, USA from 1988-1990. He is a Fellow of the "Maharashtra Acedemic of Sciences". He is a recipient of outstanding paper award in the pharmaceutical field conferred by Controlled Release Society at Orlando, Florida (USA) on July 28, 1992. He is the author of 40 publications and he also coauthored a book. His work pertains to development of safe, shelf-stable meat products using hurdle technology. He has invented Vibro-thermal disinfestor for disinfestation of food grains. He is also investigating several natural antioxidants for minimising lipid peroxidation in processed food. His major contribution is development of "Artificial Viral Envelopes" for targeted intracellular delivery of peptides, enzymes, toxins and gene constructs for which he holds a US and a European patent. At present he is the Head of the Meat and Meat products Section, Food Technology Division, BARC.



Dr Arun Sharma joined the Training School of Bhabha Atomic Research Centre, Mumbai, in 1975, after finishing Masters degree in Microbiology from National Dairy Research Institute, Karnal. He

obtained his Ph. D. degree in Biochemistry from University of Bombay in 1984. He was a Post-Doctoral Associate at the Department of Plant Pathology, University of California, Riverside, USA, during 1990-1991, where he worked with Prof. Noel T. Keen on the avirulence gene D of *Pseudomonas syringae* pv. tomato. After returning to India, Dr. Sharma initiated work on *Xanthomonas campestris* pv. glycines, the etiological agent of bacterial pustule disease of soybean. Since then he has been actively involved in studying the molecular biology of *Xanthomonas* with special reference to the mechanism of host-pathogen interaction. His other interests include biogenesis and control of aflatoxin in food and feed. Simultaneously, he has also been engaged in research related to radiation processing of food. He has more than 150 publications in national and international journals, including chapters in books and encyclopedias. He has participated as a delegate and expert in the co-ordinated research programs of the International Atomic Energy Agency. He has been the secretary of the Environmental Mutagen Society of India and Vice-President of Indian Society for Environmental Science & Technology. Dr. Sharma is currently Head, Food Technology Division, Bhabha Atomic Research Centre, Mumbai, India.

PRODUCTION OF BIOPESTICIDE AZADIRACTIN BY HAIRY ROOT CULTURES OF NEEM (*AZADIRACHTA INDICA* A. JUSS)

Ramesh K. Satdive, Devanand P. Fulzele and Susan Eapen
Plant Biotechnology and Secondary Products Section,
Nuclear Agriculture and Biotechnology Division,
Bhabha Atomic Research Centre

This paper won the Best Poster Presentation award at the "National Symposium on Plant Biotechnology : New Frontiers" held at Central Institute of Medicinal and Aromatic Plants, Lucknow, during November 18-20, 2005.

A b s t r a c t

Azadirachtin is one of the most potent biopesticides so far developed from a plant source Azadirachta indica. Plant hairy root cultures obtained by genetic transformation with Agrobacterium rhizogenes have been recognized as an alternative source for production of important phytochemicals and in the present study, hairy root cultures induced in A. indica were used for determining the various factors, which influence the production of azadirachtin.

Different ionic strength culture media and elicitation on growth and production of azadirachtin by hairy root cultures were studied. Hairy roots were cultured on the three different media, namely Ohyama and Nitsch's (ionic strength 132.5 mM), Murashige and Skoog's (ionic strength 93.3 mM) and Gamborg's (ionic strength 60 mM) without growth regulators. HPLC chromatogram revealed that hairy roots cultured on Ohyama and Nitsch's medium produced maximum yield of azadirachtin (0.016% DW) and secreted 0.00705 g l⁻¹ azadirachtin into the culture medium. Addition of fungal cell wall fragments of Claviceps purpurea as a biotic elicitor enhanced the production of azadirachtin by ~5 fold (0.074% DW). Similarly, hairy root cultures treated with signal compounds such as jasmonic acid and salicylic acid showed a ~6 (0.095% DW) and ~9 fold (0.14% DW) enhancement respectively in production of azadirachtin.

Introduction

Azadirachta indica A. Juss (Neem) is a fast growing evergreen tree belonging to mahogany family (Meliaceae) and it can grow up to 200 years and is generally propagated by seeds (Fig. 1). Seeds lose their viability within few weeks after ripening and hence storage of

seeds is a major problem for propagation. Therefore, plant cell and tissue culture provides an alternative source for multiplication of the tree and also gives the opportunity to understand biosynthesis of important metabolites.

The biological activities of *A. indica* extracts have been investigated intensively. In general, extracts of *A. indica*



Fig. 1: A mature tree of *Azadirachta indica*

fruits, seeds, seed kernels, twigs, stem bark, and root bark have been shown to possess anti - tumour anti - inflammatory, immunostimulating, insect antifeedant, insecticidal, fungicidal, nematocidal and bactericidal activities (Satdive et al., 2001). Azadirachtin is one of the most potent biopesticides currently in use (Fig. 2), and is isolated from seeds of *A. indica* (neem). Azadirachtin is the most important constituent of neem based biopesticides and is chemically a limonoid tetranortriterpenoid effective against a wide spectrum of insect pests (Satdive et al., 2001). With increase in global demand for this important biopesticide, plant cell and organ cultures

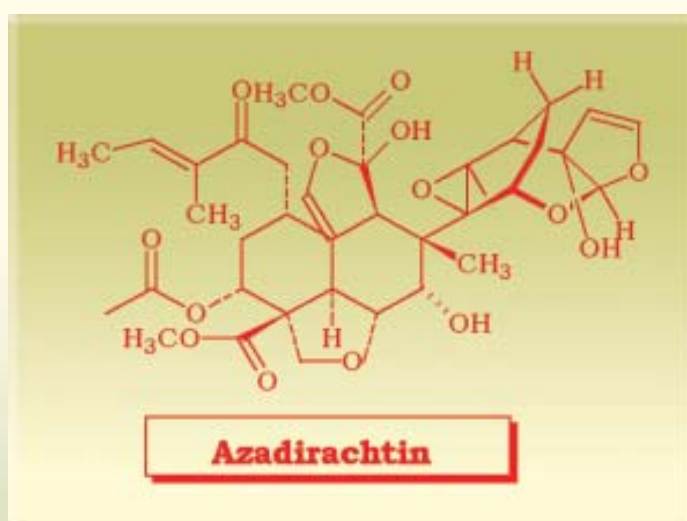


Fig. 2 : Azadirachtin an important biopesticide compound of *Azadirachta indica*

have been recognised as an alternative and continuous source for year round production of azadirachtin (Van der Esch et al, 1993).

Hairy root cultures obtained by genetic transformation with *Agrobacterium rhizogenes* have been recognised as a suitable source for production of bioactive molecules (Doran, 1997; Wysokinska and Chmiel, 1999; Eapen and Mitra 2001; Sevon and Oksman-Caldentey 2002). In addition, they have also been shown to produce novel compounds, which are not found in the parental plant and could be used as a source for biologically active compounds. Allan et al, (2002) have reported production of azadirachtin and related compounds from hairy root cultures of *A. indica*, but the concentration of azadirachtin was very low (0.007% DW).

Elicitation of cell cultures with biotic elicitor and signal compounds has been recognised as an important strategy for enhancement of secondary metabolites (Eilert et al, 1986; Savitha et al, 2006). Use of bacterial and fungal cell wall fragments are also known to enhance the production of secondary metabolites by plant cells (Komaraiah et al, 2003; Namdeo et al, 2002). Methyl jasmonate and jasmonic acid, due to their role in signal transduction pathway are used as wide spectrum elicitors (Grundlach et al, 1992; Zid and Orihara, 2005). Salicylic acid and acetylsalicylic acid are also known to enhance the production of secondary metabolites by plant cells (Jeong et al, 2005). Another strategy to stimulate secondary metabolite production by cultured plant tissues is by altering the macro and micronutrient composition of the media (Pan et al, 2004; Sivakumar et al, 2005). In this study, the effect of different ionic strength media, biotic elicitor and signal compounds on growth and production of azadirachtin by hairy root cultures of *A. indica* is presented.

Materials & Methods

Plant materials and tissue culture

Fresh seeds of *A. indica* (A. Juss) were obtained from a mature tree grown at Bhabha Atomic Research Centre, Mumbai, India. Seeds were washed in running tap water for 30 min and subsequently treated with Dettol for 5 min. The seeds were surface sterilised with 70% ethanol (1 min) followed by 0.1% HgCl₂ (3 min). Thereafter, seeds were washed 4-5 times with sterile distilled water. Finally, disinfected seeds were cultured on 50 ml test tubes containing 20 ml of Murashige and Skoog's (MS) (Murashige and Skoog 1962) medium supplemented with 30 g l⁻¹ sucrose for germination. The medium was adjusted to pH 5.8 prior to the addition of 0.25% gelling agent Phytigel (Sigma, USA) and autoclaved at 121°C at 15 lbs for 20 min. Cultures were incubated at 26 ± 1°C and maintained under 16 hr light (40 mmol m⁻²S⁻¹, Philips white fluorescent light) and 8 hr dark period.

Agrobacterium rhizogenes and hairy root cultures

A. rhizogenes strain LBA 9402 (obtained from INRA, France) was grown on solid YMB medium (Hooykass et al, 1977) with 50 mg l⁻¹ rifampicin at 28°C and 48 hr old cultures were used for infection. Three-week-old germinated seedlings were infected with *A. rhizogenes* by making a wound with a sterile needle and smearing the bacteria on the wounded areas. Co-cultivation was carried out for two days. They were then cultured on MS medium devoid of growth regulators and supplemented with 3% sucrose, cefotaxime (500 mg l⁻¹) and solidified with 0.8% agar (w/v). Hairy roots which developed at the end of three weeks from the infected areas were excised singly and transferred to MS medium containing 500 mg l⁻¹ of

cefotaxime. Hairy roots were subcultured every three weeks for 3-4 passages on MS medium supplemented with 250 mg^l⁻¹ cefotaxime and in subsequent passages the antibiotic was eliminated. Hairy roots obtained from a single clone were transferred to 70 ml MS liquid medium in 250 ml flasks, kept at 40-50 rpm and used for experiments. This clone was selected on the basis of fast growth. The cultures were subcultured every three weeks and used for the experiments.

Confirmation of transformation and isolation of genomic DNA

Genomic DNA from hairy roots and normal roots (control) of *A. indica* was isolated according to the protocol of Dellaporta with a few minor modifications (Dellaporta et al., 1983). The DNA samples thus obtained were subjected to PCR amplification with specific primers.

Isolation of plasmid DNA

Plasmid DNA from *A. rhizogenes* strain LBA 9402 was extracted as described by Sambrook et al, (1989) by alkaline lysis method.

PCR analysis

PCR amplification of the isolated DNA samples was carried out using specific primers for ORF-13 coding sequence of T_L DNA and *mas1*' sequence of T_R DNA of pRiLBA9402. The primers used for amplification of ORF-13 coding sequence of T_L DNA of pRiLBA9402 defined a 498 bp domain of ORF-13 coding sequence (Slightom et al, 1986). For amplification of *mas1*' sequence of T_R DNA of pRiLBA9402, the primers used defined a 970 bp domain of the *mas1*' coding sequence of T_R DNA (Bouchez and Tourneur 1991). DNA amplification was performed on a Hybaid thermal cycler. 25µl of reaction mixture used consisted of 25 ng of template DNA, 2.5µl

of 10x Taq DNA polymerase buffer, 100µM of dNTPs, 0.2µM of primer and 0.5 U Taq DNA polymerase (Bangalore Genei Pvt. Ltd. India) and the mixture was overlaid with paraffin oil.

The primers used for ORF-13 sequence were (+)5' CAG CTT CTA AAT GTG GTG GAG GCC 3' and (-)5' CCT TGC CGA TTG CCA GTA TGG C 3'. These primers defined a 498 bp domain of ORF-13 coding sequence of T_L DNA (Slightom et al., 1986). For amplification of *mas1*' sequence of TR DNA, the primers used were (+)5' CGG TCT AAA TGA AAC CGG ACG 3' and (-)5' GGC AGA TGT CTA TCG CTC GCA CTC C 3'. These primers defined a 970 bp domain of the *mas1*' coding sequence of TR DNA (Bouchez and Tourneur 1991). PCR amplification was programmed at an initial denaturation step at 94°C for 4 min, followed by 45 cycles of denaturation at 94°C for 1 min, annealing at 36°C for 1 min and extension at 72°C for 2 min.

Gel electrophoresis of amplified DNA

Amplified products were separated by electrophoresis on 1.5% agarose gel in 1X Tris-borate buffer (TBE), detected by staining with ethidium bromide and visualized under UV light using a Transilluminator.

Growth and production of azadirachtin on different ionic strength media

To study the effect of different media on growth and production of azadirachtin in hairy root cultures of *A. indica*, three different media namely MS, B5 (Gamborg et al, 1968) and ON (Ohyama and Nitsch 1972) were used.

Preparation of biotic elicitor and signal compounds

The fungus *Claviceps purpurea* (MTCC 1479) obtained

from Institute of Microbial Technology, Chandigarh, India was cultured on potato dextrose agar and incubated for seven days at 30°C. From seven-day-old cultures, 1 cm² mycelium was transferred to 500 ml Erlenmeyer flasks containing 150 ml potato dextrose medium and kept on gyratory shaker for a week at 120 rpm. After seven days of incubation, cells were harvested, filtered and dried at 60°C for 24 hr and ground with a mortar and a pestle. Dry cell powder was dissolved in water (10 g l⁻¹) and autoclaved for 20 min at 121°C. The autoclaved fungal suspension was used as the elicitor to induce azadirachtin production. Jasmonic acid (Sigma, USA) and salicylic acid (Hi Media, India), at 100 and 200 mM concentrations were used as signal compounds and added to 10 day old hairy root cultures and both hairy roots and medium were analysed for azadirachtin.

Growth parameters

Methods for determination of fresh weight (FW) and dry weight (DW) have been described elsewhere (Fulzele et al, 1995). All the experiments were repeated three times.

Extraction of azadirachtin

Dried powdered material (20 mg) was homogenized with 1 ml of methanol by sonication (33 KH₂) for 20 min at room temperature. After sonication, the samples were transferred to polypropylene micro-centrifuge (Eppendorf) tubes and centrifuged at 12000xg for 5 min. The supernatant was transferred to clean glass vials and applied directly onto a HPLC column.

The spent medium was filtered and extracted with chloroform three times. The chloroform fraction was dried (Na₂SO₄), filtered (Whatman No. 1) and subsequently evaporated on a BÜCHI rotavapor at 45°C

to obtain a concentrate and stored at 4°C prior to bioassay and HPLC. For determination of azadirachtin, the concentrates were analysed on HPLC.

Quantification of azadirachtin by HPLC

An Isocratic analytical HPLC was performed on a JASCO Liquid Chromatography equipped with an autosampler injector with a 20 µl sample loop and a variable wavelength detector. The HPLC column was a HI-Q sil C-18 (particle size 5µm, 100 Å, 4x150 mm ID) packed column. The mobile phase for alkaloid elution was acetonitrile : water (60:40) at a flow rate of 1 ml^{-min} and UV detection at 227 nm. Data collection and integration were accomplished using BORWIN software (Japan). This method is sensitive and accurate with good reproducibility. Validation of quantitative method was performed with samples five times. The results of the five injections from the same samples at the five concentrations (0.1 mg–0.5 mg) showed similar retention time. A retention time of azadirachtin was 5.39 min. Peak identification was carried out on the basis of an authentic sample of azadirachtin (SIGMA, USA). Detection of azadirachtin from tissue cultures was also performed with standard sample of azadirachtin by chromatography co-injection. Each experiment was carried out with a minimum of three replicates and repeated twice.

Results

Establishment of A. indica hairy root cultures

After infection of *A. indica* seedlings with *A. rhizogenes*, 55-60% of seedlings showed initiation of hairy roots from the wounded surface. Hairy roots were isolated singly and grown on MS medium without growth regulators, but fortified with cefotaxime (500 mg l⁻¹). The induced roots were successfully cleared off bacteria by several passages through medium containing decreased

concentrations of cefotaxime. After 3-4 subcultures, the roots were able to grow in culture in the absence of cefotaxime and were negatively geotropic. After 4th subculture, hairy roots maintained on MS liquid medium devoid of growth regulators and containing 3% sucrose were used as inoculum for further experiments (Fig. 3).



Fig. 3 : Hairy root cultures of *A. indica* initiated using *A. rhizogenes* strain

Molecular analysis

Transformation was confirmed by polymerase chain reaction using specific primers. PCR amplification with specific primers was used to show the presence of T-DNA of the Ri plasmid in the genomic DNA of hairy roots of *A. indica*. DNA, isolated from hairy roots induced by LBA 9402 when amplified with primers specific for ORF 13 and *mas 1* sequence showed the expected fragments at 498 bp and 970 bp respectively, thus confirming transformation (Fig. 4). Amplification was obtained using positive control (plasmid DNA), while DNA from non-transformed roots (used as control) did not show any amplification at expected sites.

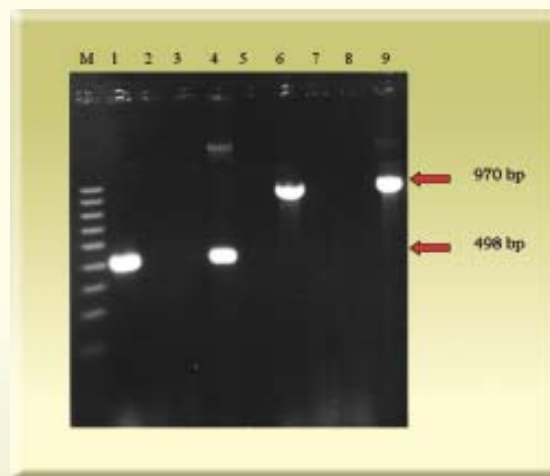


Fig. 4 : PCR amplification of DNA from hairy roots of *A. indica* showing amplification of ORF 13 and *mas 1* genes at 498 bp and 970 bp respectively

M : Molecular marker (100 bp ladder)
Lane 1 and 6 : Plasmid DNA pRi9402
Lane 2,3,5,7 & 8 : Non transformed roots
Lane 4 and 9 : Transformed roots

Influence of different ionic strength media on growth and production of azadirachtin

Hairy roots were cultured in 70 ml of different ionic strength media (ON, MS and B5) in 250 ml Erlenmeyer flasks containing 3% sucrose were tested and kept in gyratory shaker at 60 rpm. HPLC chromatogram showed that both the hairy roots and the medium showed the presence of azadirachtin in all the tested media combinations. Azadirachtin started leaching out into the medium only after 10 days in all the tested media. The present results revealed that hairy roots cultured in ON medium produced highest levels of azadirachtin followed by B5 and MS respectively (Fig. 5). The roots grown in ON medium produced 0.016% DW of azadirachtin on the 30th day. Maximum concentrations 0.00705 g l⁻¹ of azadirachtin was

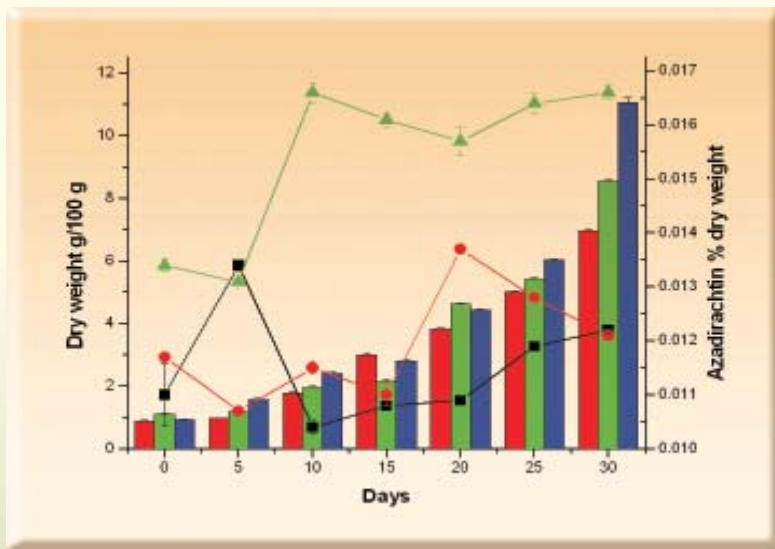


Fig. 5: Growth and production kinetics of transformed root cultures of *A. indica*

Dry Weight : ON : (■) ; B5 : (■) ; MS : (■)
Azadirachtin : ON : (▲) ; MS : (●) ; B5 : (■)

secreted into the culture medium on day 25 (Fig. 6). The pH of the ON medium slightly increased for the first 5 days and after that it remained stable up to the 25th day. The pH of the medium increased to 5.8 at the end of 30 days. The pH of the B5 medium increased from acidic condition to neutral as the days progressed. MS liquid medium did not show much fluctuation in pH like the other two media tested.

Influence of biotic elicitor and signal compounds on production of azadirachtin

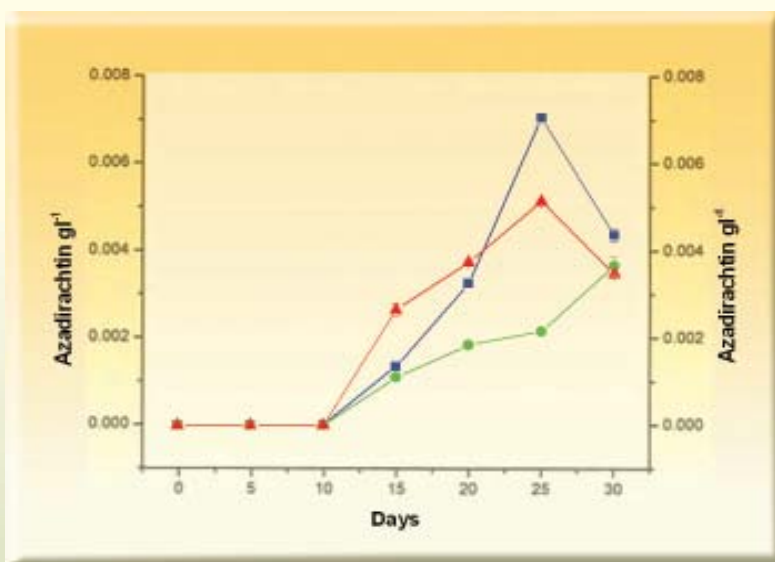


Fig. 6: Azadirachtin secreted into different ionic strength medium

ON : (■) ; MS : (▲) ; B5 : (■)

Fungal cell wall fragments of *C. purpurea* at a concentration of 7 gl⁻¹ were added as a biotic elicitor into the 10-day-old hairy root cultures grown in ON medium. Hairy roots cultivated with biotic elicitor showed similar growth profile compared to hairy roots grown without biotic elicitor. Hairy roots grown with biotic elicitor produced 0.074% DW of azadirachtin on day 25 (Fig. 7), which is ~5 fold more than hairy root grown without biotic elicitor. The present results showed that addition of biotic elicitor increased the yield of azadirachtin in hairy root cultures of *A. indica*. The HPLC profile showed that azadirachtin

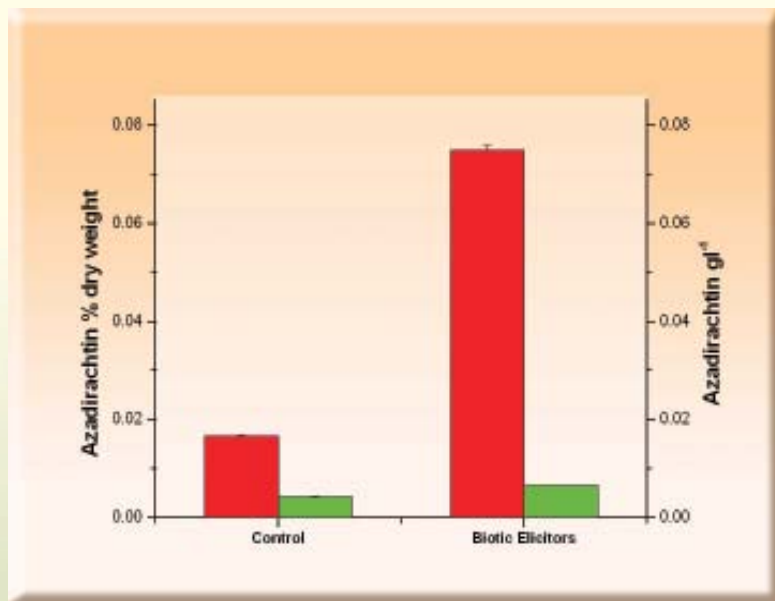


Fig. 7 : Effect of biotic elicitors on production of azadirachtin In hairy root cultures of *A. indica*

Hairy roots : ■ Medium : ■

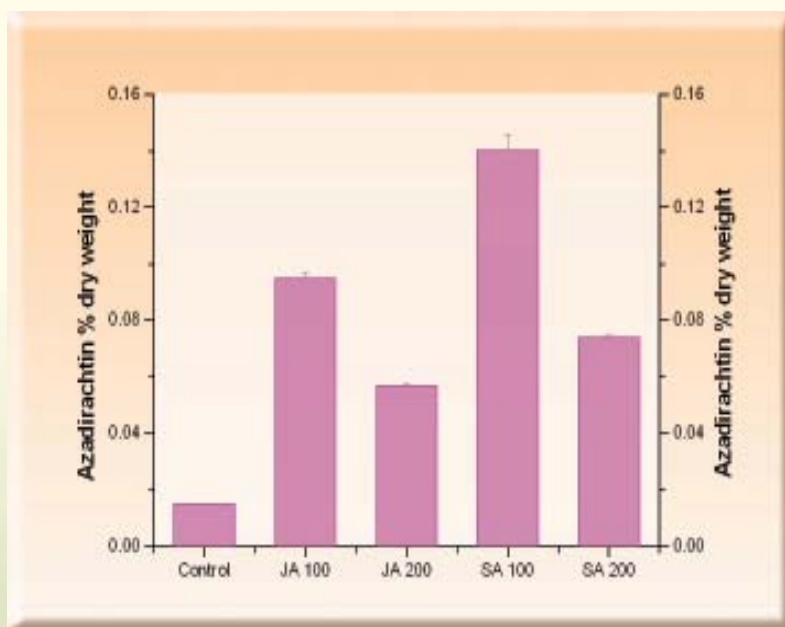


Fig. 8: Effect of signal compounds on production of azadirachtin by hairy root cultures of *A. indica*

Azadirachtin : ■

content in the culture medium was slightly increased in presence of biotic elicitor compared to control cultures.

Addition of signal compounds like jasmonic acid and salicylic acid at 100 and 200 mM increased the azadirachtin content in the roots as well as in the medium when compared to the control cultures. Out of the two concentrations of jasmonic acid and salicylic acid tested, 100 mM concentration was found to be better than 200 mM. The addition of jasmonic acid at 100 mM has shown a ~6 fold improvement in production of azadirachtin (0.095% DW) over the control cultures (0.016% DW). When cultures were supplemented with 200 mM of jasmonic acid, the production of azadirachtin (0.057% DW) was lesser than that produced at 100 mM concentration. When the hairy root cultures were treated with 100 mM of salicylic acid, there was a ~9 fold increase in azadirachtin production (0.14% DW) over the control cultures (Fig. 8). The results suggested that the accumulation of azadirachtin was favoured by low concentration of signal compounds in the culture medium. Similarly, hairy root cultures secreted maximum concentrations of azadirachtin

into the culture medium when treated with minimum concentrations of signal compounds (Fig. 9).

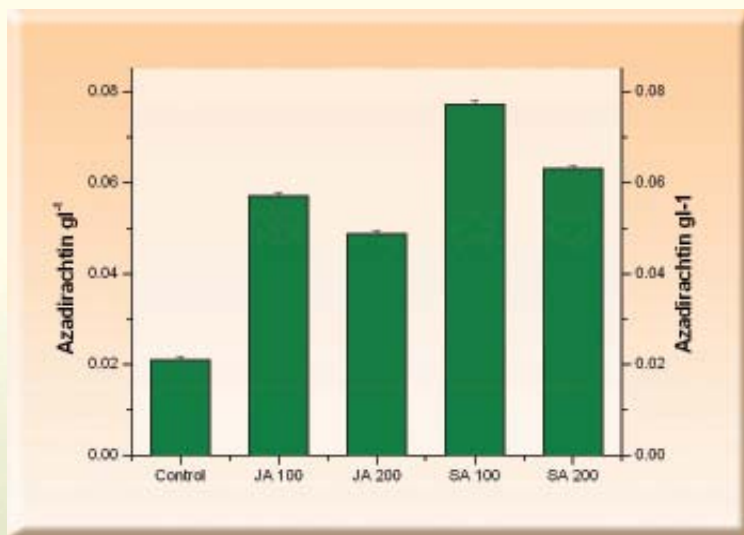


Fig. 9 : Effect of signal compounds on production of azadirachtin secreted into the medium by hairy root cultures of *A. indica*

Azadirachtin :

Discussion

Hairy roots induced by *A. rhizogenes* have received a lot of attention from plant biotechnologists for the production of secondary metabolites. The hairy roots can be indefinitely propagated on a synthetic medium without phytohormones (Tepfer and Tempe 1981; Doran 1997; Eapen and Mitra 2001). The main advantage of using hairy root cultures is due to their ability to grow in defined basal media without supplementation of phytohormones and due to their differentiated nature, they show genetic stability and tend to produce high levels of secondary metabolites characteristic of the species. In the present study, hairy root cultures were induced from 55-60% of cultures. Variations in virulence of bacteria and the vulnerability of the explants and genotype play an important role in determining the frequency of hairy root induction.

With the objective to achieve high biomass and azadirachtin production, the hairy roots were cultured on three different ionic strength media such as ON, MS and B5. It was found that the cultures grown in maximum ionic strength ON medium produced the maximum amounts of biomass and azadirachtin followed by MS and B5. The present results showed that ON medium containing higher ionic concentrations of inorganic salts compared to MS and B5, favoured growth and azadirachtin production. Altering macro and micronutrients of the cultured media are known to influence the production of bioactive molecules from cultured

tissues of several plants (Pan et al., 2004; Sivakumar et al, 2005). Prakash and Srivastava (2005) using *A. indica* cell suspension cultures found that optimizing media (NO_3) could enhance azadirachtin production. Allan et al, (2002) reported 0.007% DW azadirachtin in the hairy roots of *A. indica*. Accumulation of azadirachtin was studied in naturally grown plants of *A. indica* and found that normal roots contained 0.00032% DW of azadirachtin. Our experimental data showed that hairy roots developed from *A. indica* accumulated 0.016% DW azadirachtin, which is higher than that of naturally grown plant.

The low production of biopesticide azadirachtin in tissue cultures as compared to the seeds provides

alternative scope to adopt certain yield improvement strategies to enhance the productivity of azadirachtin. With this aim, we added biotic and signal compounds to the hairy root cultures and the results were quite promising. The addition of fungal cell wall fragments of *Claviceps purpurea* to the hairy root cultures significantly increased the azadirachtin content by 7-fold. Veersham *et al.*, (1995) reported that addition of biotic elicitors, cell extracts and culture filtrates of *Penicillium minioluteum*, *Botrytis cinerea*, *Verticillium dahliae* and *Gliocladium deliquescens* improved the production of taxol and related taxanes in *Taxus* species cell cultures. Enhanced production of sesquiterpenes by *S. tuberosum* cell cultures (Komaraih *et al.*, 2003) and saponin content by *P. ginseng* cell cultures (Jeong *et al.*, 2005) with biotic elicitors are known.

Methyl jasmonate has been shown to enhance the production of taxol and its analogues, rosmarinic acid, indole alkaloids, anthocyanins etc. in cell cultures of *Taxus sp.*, *Lithospermum erythrorhizon*, *Catharanthus roseus* and *Vaccinium pahale* (Yukimune *et al.*, 1996). In the present study, it was found that addition of jasmonic acid and salicylic acid into the culture medium enhanced the production of azadirachtin. Apparently salicylic acid was found to favour production of azadirachtin compared to jasmonic acid in the present study using *A. indica* hairy root cultures. Cultures grown in 100 mM concentration increased the azadirachtin production, whereas cultures grown with 200 mM concentration inhibited the azadirachtin production. The stress produced by these signal compounds increased the yield at low concentrations. High concentration resulted in loss of cell viability, demonstrating toxic effects. Thus, it can be concluded that the use of appropriate amount of signal compounds can increase the productivity of azadirachtin in hairy root cultures of *A. indica*.

References

1. Allan, E. J., Eeswara, J. P., Jarvis, A. P., Mordue (Luntz), A. J., Morgan, E. D and Stuchbury, T. (2002) Induction of hairy root cultures of *Azadirachta indica* A. Juss. And their production of azadirachtin and other important insect bioactive metabolites. *Plant Cell Rep.* 21, 374-379.
2. Ara, I., Siddiqui, B. S., Faizi, S., Siddiqui, S. (1989) Structurally novel diterpenoid constituents from the stem bark of *Azadirachta indica* (Meliaceae). *J. Chem. Soc., Perkin Trans. I*, 343-345.
3. Bouchez, D and Tourneur, J. (1991) Organization of the agropine region of the T-DNA of the Ri Plasmid from *Agrobacterium rhizogenes*. *Plasmid.* 25 (1), 27-39.
4. Chilton, M. D., Tepffer, D. A., Petit, A., David, C., Casse-Delbart, F and Tempe, J. (1982) *Agrobacterium rhizogenes* inserts T-DNA into the genome of the host plant root cells. *Nature (London).* 295, 432-434.
5. Dellaporta, J., Wood, J. B and Hicks, A. (1983) A plant DNA miniprep: version II. *Plant Mol. Biol. Rep.* 14, 19-21.
6. Doran, P.M., 1997. Hairy roots: culture and application. Harwood Academic Publishers. Amsterdam. The Netherlands. pp. 1-235.
7. Eapen, S and Mitra, R. (2001) Plant hairy root cultures: prospects and limitations. *Proc. Indian Natn Sci Acad. (PINS)* B67 Nos 3 & 4, 107-120.
8. Eilert, U., Wolters, B and Constable, F. (1986) Ultrastructure of acridone alkaloid idioblast in roots and cell cultures of *Ruta graveolens*. *Can. J. Bot.* 64, 1089-1096.

9. Fulzele, D. P., Heble, M. R and Rao, P. S. (1995) Production of terpenoids from *Artemisia annua* L. plantlet cultures in bioreactor. *J. Biotechnol.* 40, 139-143.
10. Gamborg, O. L., Miller, R. A and Ojima, K. (1968) Nutrient requirements of suspension cultures of soyabean root cells. *Exp. Cell. Res.* 50, 151-158.
11. Grundlach, H., Muller, M.J., Kutchan, T.M., Zenk, M.H., (1992). Jasmonic acid as a signal transducer in elicitor induced plant cell cultures. *Proc. Natl. Acad. Sci. USA.* 89, 2389-2393.
12. Hooykass, P. J. J., Klapcijk, P. M., Nuti, M. P., Schilperoot, R. A and Rorsh, A. (1977) Transfer of *A. tumefaciens* Ti plasmids to avirulent bacteria and *Rhizobium* explanta. *J. Gen. Microbiol.* 98, 477-484.
13. Jeong, G.T., Park, D.H., Ryu, H.W., Hwang, B., Woo, J.C., Doman, K.F., Kim, S.W., (2005). Production of antioxidant compounds by culture of *Panax ginseng* CA Meyer hairy roots: I Enhanced production of secondary metabolite in hairy root cultures by elicitation. *Appl. Biochem. Biotechnol.* 121-124, 1147-1157.
14. Komaraiah, P., Reddy, G.V., Reddy, P.S., Raghvendra, A.S., Ramakrishna, S.V., Reddanna, P., (2003). Enhanced production of antimicrobial sesquiterpenes and lipoxygenase metabolites in elicitor treated hairy root cultures of *Solanum tuberosum*. *Biotechnol. Lett* 25, 593-597.
15. Kuruvilla, T., Komaraiah, P and Ramakrishna, S. V. (1999) Enhanced secretion of azadirachtin by permeabilized margosa (*Azadirachta indica*) cells. *Indian J. Exp. Biol* 37, 89-91.
16. Murashige, T and Skoog, F. (1962) A revised medium for rapid growth and bioassays with tobacco tissue cultures. *Physiol Plant* 15. 473-497.
17. Namdeo A., Patil, S., Fulzele, D. P. (2002). Influence of fungal elicitors on production of Ajmalicine by cell cultures of *Catharanthus roseus*. *Biotechnology Progress* 18: 159-62.
18. Ohyama, K and Nitsch, J. P. (1972) Flowering haploid plants obtained from protoplasts of tobacco leaves. *Plant Cell Physiol.* 13, 229-236.
19. Pan, X.W., Xu, H.H., Liu, X., Gao, X., Lu, Y.T., (2004). Improvement of growth and camptothecin yield by altering nitrogen source supply in cell suspension cultures of *Camptotheca acuminata*. *Biotechnol. Lett* 26, 1745-1748.
20. Prakash, G and Srivastava A. K. (2005) Statistical media optimization for cell growth and azadirachtin production in *Azadirachta indica* (A. Juss) suspension cultures. *Process Biochemistry* 40, 3795-3800.
21. Sambrook, J., Fritsch, E. F and Maniatis, T. (1989) *Molecular cloning: a laboratory manual*, Cold Spring Laboratory Press, Cold Spring, Harbor, N.Y.
22. Savitha, B.C., Timmaraju, R., Bhagya laksami, N., Ravishankar, G.A., (2006). Different biotic and abiotic elicitors influence betalin production in hairy root cultures of *Beta vulgaris* in shake flask and bioreactor. *Process Biochem.* 41, 50-60.
23. Satdive, R.K., Fulzele, D.P and Eapen. S. (2001) *Biotechnology of Neem. Azadirachta indica*. L. In: *Role of Biotechnology in Medicinal and Aromatic Plants* (eds.) Khan, I. A and Khanum, A. Ukaz Publication, Hyderabad, pp. 168-181.
24. Sevon, N., Oksman-Caldentey, K.M., (2002). *Agrobacterium rhizogenes* mediated transformation : Root cultures as a source of alkaloids. *Planta Med.* 68, 859-868.

25. Slightom, J. L., Duran-Tardif, M., Jouanin, L and Tepfer, D. (1986) Nucleotide sequence analysis of TL-DNA of *Agrobacterium rhizogenes* type Plasmid. J. Biol. Chem. 261, 108-121.
26. Sivakumar, G., Yu, K.W., Hahn, E.J., Paek, K.Y., (2005). Optimisation of organic nutrients for ginseng hairy roots production in large scale bioreactors. Curr. Sci. 89, 641-649.
27. Tepfer, D and Tempe, J. (1981) Production d'agropine par des raciness transformees sous l'action d' *Agrobacterium rhizogenes* souche A44, C.R. Academy of science III (sciences de la vie) 292, 153-156.
28. Van der Esch, S. A., Gianacovo, G., Maccioni, O and Vitali, F. (1993) Preliminary results on the production of azadirachtin by plant tissue cultures of *Azadirachta indica*. G Bot Ital 127. 927-928.
29. Veeresham, C., Venkatesh, S and Shuler, M. L. (1995). Elicitation of *Taxus sp.* cell cultures for production of taxol. Biotechnol. Lett 17, 1343-1346.
30. Wysokinska, H., Chmiel., (1999). Hairy root cultures for Biotechnology. Acta Biotechnol. 17: 131-159.
31. Yukimune, Y., Tabata, H., Higuchi, Y and Hara, Y. (1996). Methyl jasmonate induced overproduction of paclitaxel and baccatin III in *Taxus* cell suspension cultures. Nature Biotechnol 14, 1129-1132.
32. Zid, S.A., Orihara, Y., (2005). Polyacetylenes accumulations in *Ambrosia maritime* hairy roots and cell cultures after elicitation with methyl jasmonate. Plant Cell Tiss. Org. Cult. 81, 65-75.

ABOUT THE AUTHORS



Dr Ramesh K Satdive joined BARC in 1997 after obtaining B.Sc. Degree in Agriculture from Mahatma Phule Krishi Vidyapeeth, Pune. He did his Ph.D. (Botany) from Mumbai University in 2004. His specialization is in the field of medicinal plant tissue culture. At present he is working on several important medicinal plants like *Azadirachta indica*, *Andrographis paniculata* and *Nothapodytes*

foetidai. He has initiated cell suspension and multiple shoot cultures for the above plants and is growing them in different types of bioreactors for production of anticancer bioactive compounds. To his credit he has around nine research publications in national and international journals and three in symposia.



Dr Devanand P. Fulzele joined the BARC in 1986 after postgraduation in Microbiology from Nagpur University. He has been working in the area of medicinal plant cell cultures and

bioreactor for large-scale cultivation and production of bioactive compounds. Dr. Fulzele obtained his Ph. D. degree in 1996 from Mumbai University for his work on regulatory aspects of secondary metabolites in medicinal plant tissue cultures. He was in Eberhard Karls University, Tübingen, Germany from July 1991 to October 1992 under Indo-German bilateral programme. His primary contributions are the design and development of bioreactors for cell and organ cultures for product synthesis. His work also includes design and development of different types of bioreactors at commercial levels. He has published many research papers in national and international journals. Dr. Fulzele has designed and developed first largest bioreactor in India and successfully commissioned at Indore for production of bioactive compounds. Dr. D. P. Fulzele is the recipient of the BARC Technical Excellence Award for the year 1998.



Dr Susan Eapen joined BARC in 1972 through 15th batch of Training School in "Biology and Radiation Biology" and is known for her contributions in "Plant

Biotechnology". Her major research areas are (1) Development of transgenic plants for insect and disease resistance (2) Developing plants for phytoremediation of toxic metals, radionuclides and xenobiotic pollutants (3) Production of bioactive molecules from in-vitro cultures of plants. She has around 100 publications in International and national journals and is a member of Maharashtra Academy of Sciences and The National Academy of Sciences, India. Currently she is heading the Plant Biotechnology and Secondary Products Section of NABTD, BARC.

PHOSPHATASE MEDIATED BIOREMEDIATION OF CADMIUM

Chitra Seetharam, A. S. Rao and S. K. Apte
Molecular Biology Division
Bhabha Atomic Research Centre
and

S. Suvarna, A. C. Udas and M. Sudersanan
Analytical Chemistry Division
Bhabha Atomic Research Centre

This paper won the Best Poster Award at the 16th Annual Conference of the Indian Nuclear Society (INSAC-2005), organized at Mumbai, during November 16-18, 2005.

Cadmium, a highly toxic metal, is carcinogenic, mutagenic and causes several diseases and metabolic disorders in humans exposed to it mainly through the food chain⁽¹⁻³⁾. There are a large number of anthropogenic sources, which release this metal into the environment. These include effluents from cadmium pigments, nickel- cadmium batteries, plastics, other electronic and metallurgical industries as well as motor vehicles and fertilizers.

Physico-chemical methods of heavy metal removal such as chemical precipitation, electroflotation, ion exchange, reverse osmosis and adsorption on activated charcoal etc. are generally not cost effective and unsuitable in places where the heavy metal concentrations are low but still above the permissible limits⁽⁴⁾.

Methods employing a biological agent- a natural or a genetically modified one, show great promise in achieving the above goal. Metal removal may be a simple adsorption of it on to the surface of the organism

i.e., biosorption, (e.g., yeast⁽⁵⁾, cadmium resistant strain of *Bacillus thuringiensis*⁽⁶⁾, *Sphingomonas paucimobilis*⁽⁷⁾ etc.). Another mode of metal removal is bioprecipitation through the precipitant ligands (inorganic phosphate, sulfide) generated by the organism. The metal may be precipitated as highly insoluble metal phosphate or sulfide⁽⁸⁻¹⁰⁾.

In this paper, we have presented the utility of a very simple biological system i.e., an *E. coli* expressing multiple copies of PhoN (acid phosphatase from *S. enterica subsp. typhi*) and having high specific activity for bioprecipitating cadmium from aqueous solution (Fig.1) Precipitation kinetics and pH dependence were also studied. An attempt was also made to draw a correlation between enzyme activity at different pH and the corresponding rate of metal precipitation.

E. coli DH5 α cells carrying phoN (a gene coding for acid phosphatase from a local isolate of *Salmonella*

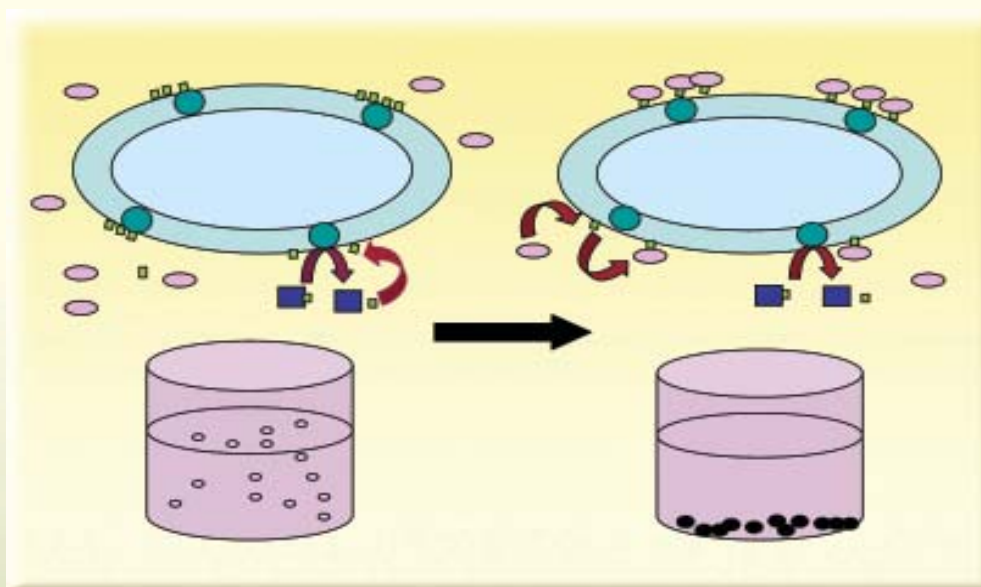


Fig. 1 : The precipitation of cadmium on the cell surface and settling of metal laden cells is represented here. PhoN protein (●) present in the periplasm of the cells cleaves a phosphomonoester (■) to release inorganic phosphate (■) which in turn precipitates cadmium (○) on the cell surface. The cadmium, which precipitates on the cell surface, results in the cells becoming heavy and settling down, making their removal easy.

enterica subsp typhi) on pUC18 vector (A. S. Rao unpublished work) were used for all the studies. The bacterium was grown aerated in LB medium with ampicillin (100 μ g/ml) to the late logarithmic growth stage, harvested and washed the cell pellet twice with saline and stored at 4°C for further use.

The cell bound PhoN was assayed by estimation of nanomoles of p-nitrophenol (pNP) released from p-nitrophenyl phosphate (pNPP) per mg of protein per minute by the hydrolytic action of the enzyme (11) which was found to be 800 \pm 100 U and this was higher than that of a similar *E. coli* clone i.e., 100-150 U (12). Further, the PhoN activity was unaffected at cadmium concentrations of 1-10 mM.

Cadmium precipitation studies were carried out using cells at an O.D_{600nm} of 0.3.

β -glycerophosphate (5mM) was incorporated as a substrate. Cadmium concentration used was 1mM (112ppm). The reaction was carried out in acetate buffer (2mM, pH ~7.0) as well as under unbuffered (distilled water, pH ~7) conditions at 30 °C and shaken at 50 rpm. Timed samples were withdrawn, centrifuged and cadmium was estimated in the supernatant in triplicates by alkaline Arsenazo-III and by AAS in later experiments.

The precipitation reactions were also set up in different buffers (100mM) of different pH. The buffers used were Acetate (pH 4 & 5); MES (pH 6); MOPS (pH 7) and Tris-Cl (pH 8 & 9). Appropriate controls were set up to rule out biosorption as the mode of removal of cadmium. The enzyme activity was also assayed at each pH tested for precipitation.

Time in hours	% Cadmium removed from solution
1	51.5
2	67.25
3	83.25

Table 1: 0.3 OD_{600nm} cells were used to precipitate cadmium from a solution containing 5mM β -glycerophosphate, 2mM Acetate buffer and 1mM Cd. Loss of cadmium from the supernatant with time is reported as percent removal from solution. The results are an average of four experiments.

Precipitation studies carried out using these cells showed that an average of ~83% of cadmium was removed from solution in 3 hours (Table 1). Further, studies were also carried out to estimate the cadmium in the pellet to ascertain whether the metal is, in fact, present in the pellet and recoverable. These results showed that the cadmium removed from the supernatant was seen associated with the cell pellet (data not shown).

Further studies to analyze the variation in the rate of precipitation as a function of pH revealed that no cadmium precipitation occurred at pH below 5.0. This shows that though \leq the enzyme activity is maximum at pH 5 as shown in Fig. 2, precipitation of the metal did not take place. This is probably due to the higher solubility of the metal phosphate,

via increased protonation of the phosphate in solution at lower pH as postulated earlier (13). These results indicate that the pH at which maximum enzyme activity was seen did not correspond with pH at which maximum precipitation of cadmium was obtained. However, above pH 7, the rate of precipitation seemed to vary in accordance with the variation in enzyme activity.

These results were confirmed using different buffers at the same pH. The rate of cadmium precipitation in 100 mM MOPS or MES at pH 6.5 was the same i.e. ~80% in 3 hours. 100 mM MES (pH 6.0) did not bring about any precipitation in 3 hours. However, upon prolonged incubation for 6 hours, precipitation was seen but to a lesser extent (only 35%, Fig. 2) compared to that at pH 6.5 and 7. The use of two different buffers having same pH, has also ruled out the possibility that the buffer components may be interfering in the precipitation reaction. Studies are in progress to confirm these observations.

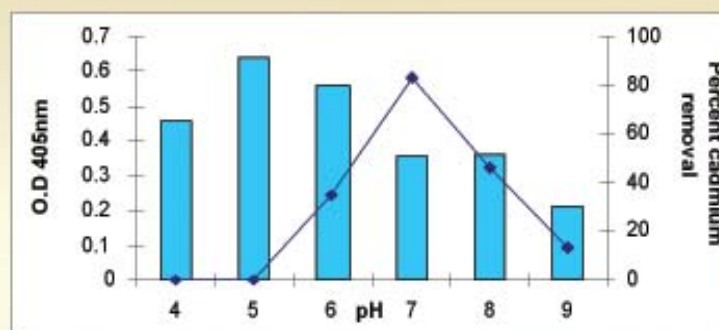


Fig. 2 : Data shows enzyme activity (bars) and cadmium precipitation (line) as a function of pH. The enzyme activity is reported directly as OD at 405nm recorded after the enzyme reaction is stopped with 0.2N NaOH once the reaction has proceeded for half an hour with pNPP as substrate. Values reported for the precipitation reaction are ones recorded 6 hours after the reaction was started, since at 3 hours no precipitation was seen at pH 6.

The rate of removal of cadmium mentioned here using a very simple biological system, i.e., *E. coli* cells with multiple copies of a single biocatalyst, PhoN, seemed to be very high compared to other bioremediation systems and is likely to have good potential for use in Cd containing industrial effluents having near neutral pH. It was also noted that the precipitation occurred to the same extent in distilled water also where no buffering was provided. Unlike cadmium, these cells with PhoN precipitated uranium from aqueous solutions having pH 4.5-9.0 (14).

Further work would involve testing different conditions like metal (Cd) concentration and cell density for cadmium precipitation, testing other heavy metals such as Cu, Pb etc. for precipitation and mixtures of metals found in waste sites.

References

1. Deknudt, G. and Deminatti, M. (1978) *Toxicology* 10 (1): 67-75.
2. Elinder C. G. and Kjellstrom, T. (1985) *Br. J. Ind. Med.* 42 (10): 651-65.
3. Cadmium ATSDR Toxicological Profiles April 1993, Prepared by Life Systems Inc for U.S Dept. of Health & Human Services.
4. Macaskie, L. E. (1990) *J. Chem. Tech. Biotechnol.* 49: 357-379.
5. Bashar Hadi, Margaritis, A., Berruti, F. and Bergougnou, M.(2003) *Intl. J. Reactor Eng.* 1: A47.
6. El-Helowl, E. R., Sabryl, S. A. and Amerl, R. M. (2000) *Biometals* 13(4): 273-280.
7. Tangaromusk, J., Pokethitiyook, P., Kruatrachue, M. and Upatham, E. S. (2002) *Bioresource Tech*; 85:103-105.
8. Sang-Weong, B, Clark, S. and Keasling, J. D. (2000) *Appl. Environ. Microbiol.* 66(9): 3939-3944.
9. Macaskie, L. E. and Dean, C. R (1984) *J. Gen. Microbiol.*130: 53-62.
10. Montgomery, D. M., Dean, C. R., Wiffen, P. and Macaskie, L. E. (1995) *Microbiology*, 141: 2433-2441.
11. Bolton, P. G. and Dean, C. R. (1972) *Biochem. J.* 127: 87-96.
12. Basnakova, G., Stephens, E. R., Thaller, M. C., Rossolini, G. M. and Macaskie, L. E. (1998) *Appl. Microbiol. Biotechnol.*50: 266-272.
13. Macaskie, L. E., Lloyd, J. R., Thomas, R. A. P. and Tolley, M. R.(1996) *Nuclear energy.* 35 (4): 257-271.
14. Lokhande, M., Achutan, P. V., Jambunathan, U., Ramanujam, A., Rao, A. S. and Mahajan, S. K. In Proc. of Nuclear and Radiochemistry (NUCAR)-2001 Symp. organized at University of Pune, Pune by Board of Res. in Nuclear Sciences, Dept. of Atomic Energy (BRNS-DAE) from Feb.7-10, 2001. pp224-5.

ABOUT THE AUTHORS



Ms. Chitra Seetharam, received her M.Sc. degree in Biotechnology from Mysore University in 2003. She joined Molecular Biology Division,

BARC through the 47th Batch of Training School. Her research interests involve microbe mediated bioremediation of environmental pollutants (organic and inorganic).



Dr Shree Kumar Apte joined BARC through the 16th batch of BARC Training School and is currently the Associate Director, Biomedical Group at Molecular Biology Division, BARC. His research interests relate to

underlying response of life forms to ionizing radiation and other environmental stresses and their biotechnological applications. He is an elected fellow of the Indian National Science Academy of Agricultural Sciences and Maharashtra Academy of Sciences.



Mr A. S. Rao obtained his M. Sc (Ag) in Microbiology in 1971 from G. B. Pant University of Agriculture and Technology, Pantnagar, U.P. He subsequently joined Bhabha Atomic Research Centre through the 17th batch of BARC Training

School in Biology and Radiobiology discipline in 1973. He initially worked on the development of biopesticides, especially those effective on economically important crop pests and mosquitoes. Currently, he is working in the Molecular Biology Division at BARC, on the development and use of genetically modified microbes for bioremediation of metals and organics relevant to nuclear industry.



Ms Suvarna Sounderajan was awarded B. Sc. Degree in chemistry from Mumbai University in 1994. She joined Electro chemical method section Analytical Chemistry Division in 1998 and is currently working at UTAF, Physico Chemical Method

section. She is involved in developing analytical procedures by voltammetric techniques as well as Spectro chemical techniques for the characterization of trace elements in various matrices eg. high purity materials, agricultural, biological, clinical, environmental and nuclear materials.



Dr M. Sudersanan, after graduating from the 11th batch of the Training School joined the Analytical Chemistry Division in 1968. He was awarded PhD from Mumbai University in the year 1975. His areas of expertise are Spectrochemical Techniques, Electrochemical

Techniques, Separation Sciences and Thermal Methods. He has over 200 publications in various international and national journals and symposia proceedings. He was keenly interested in academics therefore was closely associated with the Training School activities and also with the Mumbai University. He is an active member of many professional bodies like ISAS, ITAS etc.



Dr (Ms) A.C. Udas obtained PhD degree in Chemistry from Mumbai University in 1983. She joined Analytical Chemistry Division in 1983, and is currently working at UTAF, Physico Chemical Methods Section. She is actively involved in developing

methodologies and employing various Spectro chemical techniques for the characterization of trace elements in various matrices eg. high purity material, agricultural, biological, clinical and environmental samples. She is an EC member of ISAS and ICEST.

PPRA: AN IMPORTANT PROTEIN OF RADIATION RESISTANCE IN *DEINOCOCCUS* STIMULATES CATALASE ACTIVITY IN *ESCHERICHIA COLI*

Swathi Kota and Hari S. Misra
Molecular Biology Division
Bhabha Atomic Research Centre

This paper was awarded the Best Poster Prize at the “DAE-BRNS Life Sciences Symposium on Molecular Biology of Stress Response and its Applications”, held at BARC, Mumbai, during December 19-21, 2005.

Abstract

Deinococcus radiodurans is characterized by its exceptional capacity to tolerate the effects of various DNA damaging agents due to presence of the extraordinary DNA repair mechanism. DNA double strand break repair in *Deinococcus radiodurans* follows biphasic kinetics. The phase I, a RecA independent phase appears to be a DNA protective and preparatory phase for RecA dependent phase II repair. PprA, an important protein of radiation tolerance in *Deinococcus*, was shown to stimulate both NAD and ATP dependent *E. coli* DNA ligase activity. Here we found another interesting role of PprA in stimulation of *E. coli* catalase activity. Transgenic *E. coli* cells expressing PprA from *Deinococcus radiodurans* showed an improved tolerance to hydrogen peroxide while the effect of ionizing and non-ionizing radiation was similar to wild type. These cells showed nearly 3-fold higher catalase activity, which was mainly contributed by catalase E (KatE) and the levels of super-oxide dismutase were unchanged. The addition of purified PprA protein to cell free extract of non-recombinant *E. coli* cells has increased the catalase activity. But the PprA-antibody complex has no effect on the levels of catalase activity in-vitro. Furthermore, the addition of PprA antibodies to the cell free extract of PprA expressing *E. coli* cells has inhibited the catalase activity. The results suggest that free form of PprA per se stimulates the catalase activity in *E. coli*.

Introduction

Different reactive oxygen species (ROS) such as superoxide, singlet oxygen, hydroxyl and per-hydroxyl radicals are produced as the byproducts of metabolic processes in the cells and due to the lethal doses of ionising radiation (Halliwell and Gutteridge 1999).

Antioxidant enzymes such as catalases and super-oxide dismutases and antioxidant metabolites protect biomolecules from ROS mediated damage *in vivo*.

Deinococcus radiodurans, a bacterium, shows extreme resistance to the lethal and mutagenic effects of ionizing and non-ionizing radiation (Anderson et al

1956) as well as other physical and chemical DNA damaging agents (Smith et al 1992, Battista 2000). Different mechanisms including oxidative stress tolerance have been suggested, which help the organism to protect from the deleterious effects of these agents. Oxidative stress tolerance of *Deinococcus radiodurans* is supported by the presence of highly active antioxidant enzymes (Markillie et al 1999) and the existence of antioxidant metabolites in the system (Khairnar et al 2003; Misra et al 2004; Tian et al 2004). The factor which makes the antioxidant enzymes of *Deinococcus* much better than other bacteria has not been known. However, it has been shown previously that certain proteins upon interaction increase their specific activity and reaction kinetics. PprA was shown to stimulate both NAD-dependent and ATP-dependent *E. coli* DNA ligase activities *in vitro* (Narumi et al. 2004) and mutation in this gene makes the organism sensitive to gamma radiation (Kitayama et al 1983). Here we have demonstrated that over expression of PprA in a heterologous system like *E. coli* has increased the tolerance to hydrogen peroxide and the catalase E (KatE) activity was stimulated. PprA role in catalase activity stimulation was observed *in-solution*, which was very specific to the presence of PprA in free form. The results suggested the possible role of PprA in oxidative stress tolerance by stimulating catalase activity of *E. coli*.

Experimental

The *pprA* gene was PCR cloned from genomic DNA of *Deinococcus radiodurans* and expressed in *E. coli*. The effect of PprA expression on radiation and oxidative stress response of transgenic *E. coli* cells was monitored as total cell survival in comparison

with control. Recombinant PprA protein was purified using Ni-NTA agarose affinity chromatography. For seeing the effect of PprA on catalase activity *in vitro*, the enzyme activity was assayed both in presence and absence of purified PprA with and without PprA antibodies.

Results and Discussion

Higher tolerance of PprA expressing E. coli cells to oxidative stress

Transgenic bacteria expressing PprA showed insignificant change in non-ionizing radiation response and a marginal improvement for ionizing radiation response of wild type cells. However, these cells exhibited an enhanced tolerance to hydrogen

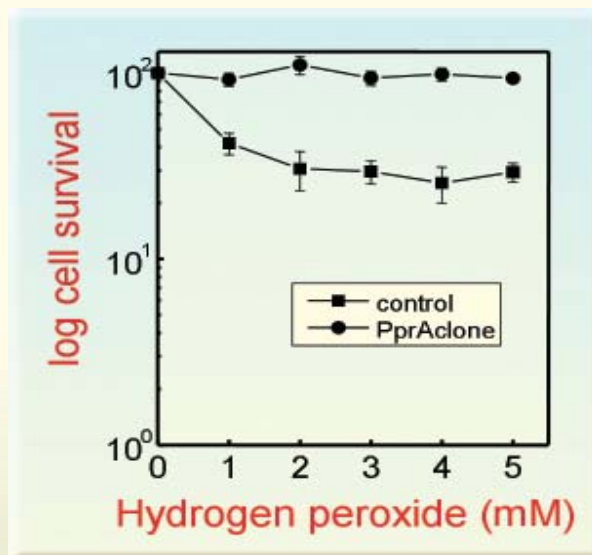


Fig.1 : Response of transgenic *E. coli* expressing PprA to hydrogen peroxide. Recombinant *E. coli* harbouring pET28a+ (control) and pETpprA (PprA clone) were exposed to different concentrations (1-5 mM) of hydrogen peroxide and cell survival was monitored on rich medium. Initial density of the cells taken for experiment were 6.02×10^8 cells / ml and 7.12×10^7 cells / ml for pET28a and pETpprA clones, respectively.

peroxide (nearly 2.5 to 3.5 fold higher cell survival) as compared to control (Fig. 1). This indicated the possible role of PprA in oxidative stress tolerance, which contributes though, to a little fraction to gamma radiation response of *E. coli*.

PprA expression differentially stimulates the antioxidant enzymes in E. coli

E. coli genome encodes for two types of catalases namely KatE and KatG. Differential role of these enzymes in radiation, mutagens and hydrogen peroxide response of *E. coli* have been demonstrated earlier (Loewen et al 1985; Mulder et al 1999; Sak et al. 1989). The increase in cellular oxidative stress tolerance has been believed due to the increase in antioxidant enzymes activity and recently to the presence of antioxidant metabolites in the cell (Khairnar et al 2003). So, the levels of catalase and super-oxide dismutase activities were investigated. Transgenic *E. coli* cells expressing PprA showed stimulation of soluble catalase activity by 2.8 fold (Fig. 2), while the activity of SOD remained nearly unchanged (data not shown). *In-gel* activity staining for catalases showed the stimulation of KatE activity while the levels of KatG activity in transgenic cells and control cells were similar (Fig. 3). This supports the hypothesis, which says that improved oxidative stress tolerance in presence of recombinant PprA was perhaps due to stimulation of KatE. Previously, the improved oxidative stress and gamma radiation tolerance was reported in transgenic *E. coli* cells expressing Ppr1, another radiation inducible protein from *Deinococcus radiodurans* (Gao et al, 2003). They demonstrated the correlation between the stimulation of KatG activity and enhanced protection from ionizing radiation while the levels of KatE activity remained unchanged.

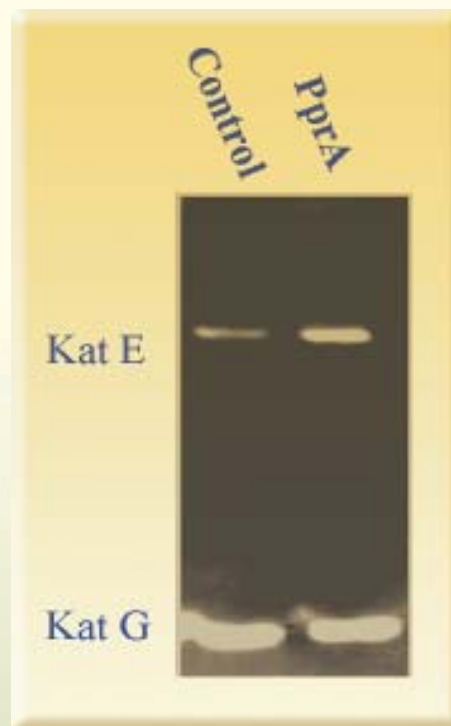


Fig. 2 : Transgenic *E. coli* cells expressing PprA showed activation of catalase activity. The cell free extracts of transgenic *E. coli* cells harbouring pET28a+ (control) and pETpprA (PprA), were separated on 7% native polyacrylamide gel and catalase activity was stained using standard protocol.

PprA stimulates catalase activity in solution

To understand the mechanism of catalase activity stimulation on over expression of PprA, its effect was monitored *in-vitro*. The purified recombinant PprA (36kDa) was added to the cell free extract from *E. coli* cells harbouring pET28a+ and total catalase activity was monitored. These samples showed 1.7 fold stimulation of soluble catalase activity. This effect of PprA was not observed when the protein was complexed with PprA antibodies. Results showed no stimulation of catalase activity in presence of PprA-antibody complex. On the other hand PprA antibodies

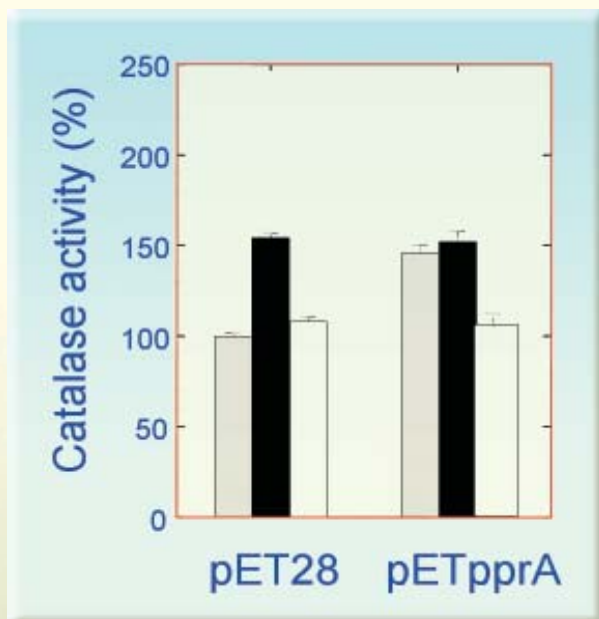


Fig. 3 : PprA-antibodies negate the PprA stimulation of *E. coli* catalase activity. Cell free extract of *E. coli* cells harbouring pET28a and pETpprA was incubated for 20min with 1.6 pmoles of purified PprA (Black) and 1.6 pmoles PprA – anti-PprA IgG complex (Empty) and catalase assay was carried out. The level of catalase activity in cell free extract without any treatment was treated as respective control (Grey). Catalase activity equivalent to 3.7 units per mg total protein represents 100 %.

showed reduction in the levels of catalase activity of *E. coli* cells over expressing recombinant PprA. These results strongly supported our hypothesis that PprA stimulates *E. coli* catalase activity by interacting with protein.

Acknowledgement

The authors are thankful to Dr S. K. Apte, for the critic in data analysis and Dr. Issay Narumi, JAERI, Japan for a generous gift of PprA antibodies.

References

1. Anderson A, Nordan H, Cain R, Parrish G, Duggan D (1956) *Food Technol* 10: 575-578.
2. Battista JR (2000) *Curr Biol* 10:R204 - R205.
3. Gao G, Tian B, Liu L, Sheng D, Shen B, Hua Y (2003) *DNA Repair* 2:1419-1427.
4. Halliwell B Gutteridge MC *Free radicals in Biology and Medicine*, Oxford University Press, Oxford, 1999, pp 105-35.
5. Khairnar NP, Misra HS, Apte SK (2003) *Biochem. Biophys Res. Comm.* 312:303-308.
6. Kitayama S, Asaka S, Totsuka K (1983) *J Bacteriol* 155:1200-1207.
7. Loewen PC, Switala J, Triggs-Raine BL (1985) *Arch Biochem Biophys* 243: 144-149.
8. Markillie LM, Varnum SM, Hradechy P, Wong KK (1999) *J Bacteriol* 181:666–669.
9. Misra HS, Khairnar NP, Atanu B, Priyadarshini I, Mohan H, Apte SK (2004) *FEBS Lett.* 578:26-30.
10. Mulder MA, Nair S, Abratt VR, Zappe H, Steyn LM (1999) *Microbiology* 145: 2011–2021
11. Narumi I, Satoh K, Cui S, Funayama T, Kitayama S, Watanabe H (2004) *Mol Microbiol* 54:278-285.
12. Sak BD, Eisenstark A, Touati D (1989) *Proc Natl Acad Sci USA* 86:3271–3275.
13. Smith MD, Masters CI, Moseley BEB. *Molecular Biology of radiation-resistant bacteria*, in RA Herbert and RJ Sharp (Eds), *Molecular biology and biotechnology of extremophiles*, Chapman & Hall, New York, NY, (1992) pp258-280.
14. Tian B, Wu Y, Sheng D, Zheng Z, Gao G, Hua Y (2004) *Luminescence*.

ABOUT THE AUTHORS



Ms Swathi Kota, M.Sc. Biochemistry from IARI, New Delhi, joined Molecular Biology Division, BARC after graduating from 46th batch of Biology-Radiobiology BARC Training School in 2002. Since then she has been actively involved in understanding the molecular mechanism underlying the extreme radioresistance of *Deinococcus radiodurans*. She has been a recipient of Homi Bhabha Meritorious Award for OCES-46th batch (Bioscience Group).



Dr Hari S Misra joined Bhabha Atomic Research Centre in 1990. Since then he has been working on molecular genetics of bacterial response to abiotic stress and development of insect resistant transgenic plants. Dr Misra is currently working on the elucidation of molecular mechanisms underlying the radiation response to biological system by employing the high throughput proteomics and genomics tools. His recent findings suggest the superior role of antioxidant metabolites in oxidative stress tolerance in bacteria. Dr. Misra is the recipient of INS Medal 2004 and an elected Fellow of Maharashtra Academy of Sciences, 2003.

SCREENING OF INDIAN CORN VARIETIES FOR AFLATOXIN RESISTANCE

Shruti S. Hajare, Sachin N. Hajare and Arun Sharma
Food Technology Division
Bhabha Atomic Research Centre

This poster paper was awarded the first prize in the subject area "Infestation Control and Food Protectants", at the 17th Indian Convention of Food Scientists and Technologists (ICFOST 2005) held at NIMHANS, Bangalore, during December 9-10, 2005.

Abstract

Corn (*Zea mays* L.), one of the major cereal crops, is also a suitable substrate for growth, development and activity of aflatoxigenic fungi causing major yield and economic losses. Among the different preharvest preventive measures applied for control, the use of inherent resistance mechanisms of the host plant represents a promising strategy. With this aim, twenty-one Indian corn varieties were examined. The results of a laboratory Kernel Screening Assay revealed 4 varieties with strong fungal resistance. All the varieties were further subjected to a detailed analysis for an antifungal protein, namely 14 kDa trypsin inhibitor (TI). A PCR based detection method revealed the presence of trypsin inhibitor (TI) gene in all the varieties. Its concentration in different varieties was determined by estimating the K_r which was found to be 7.0 $\mu\text{g/ml}$. Two of the resistant varieties showed high levels of TI, which was relatively low in susceptible varieties. Hence, this protein could be a promising selection marker for the initial screening. Studies on the pericarp wax content of the selected varieties exhibited no strong correlation between their wax content and resistance. Thus, among all the varieties screened, CML-142, P₁₉(Y)S₅-B-185-6-BBB, LM-6 and GY-39-1-328 were found to be the most promising varieties for use in commercial hybrids to develop fungal resistant varieties.

Introduction

Corn (*Zea mays* L.) is one of the major cereal crops of worldwide importance, traded as food, feed and an industrial grain crop in several countries including India. Unfortunately, it is also vulnerable to the growth of aflatoxigenic fungi, resulting into subsequent aflatoxin production, which causes major yield and economic losses (Oyebanji and Efiuwewwere 1999). Aflatoxins cause mortality and reduce productivity in farm animals and also are detrimental to humans, as high concentrations have been associated

with liver cancer. *Aspergillus flavus* may parasitically colonize silks and invade maturing corn kernels in the field producing aflatoxins (Payne and others 1988). Thus, aflatoxigenic fungi may infect the crop prior to harvest and remain throughout the harvest, storage and finally appear in corn products. Hence, preharvest prevention of aflatoxin contamination is probably the best and widely explored strategy.

In corn, among the various preharvest control mechanisms studied, host-plant resistance is supposed

to be the best and widely explored control strategy. It focuses on inhibition of fungal colonization and/or toxin production by *A. flavus* on the host plant, by the development of aflatoxin resistant inbreds (Brown and others 2003). It would also eliminate the need to detoxify large quantities of aflatoxin-contaminated seeds. The utilization of such resistant varieties has been the hope for developing resistant genotypes. The inherent resistance of corn kernels to *A. flavus* and aflatoxin contamination has been found to be associated with either the pericarp factors (morphological and chemical) and/or sub-pericarp factors (mainly antifungal proteins). These factors are under genetic control and hence, utilization of their protection in developing resistant genotypes has been of interest. Sources of resistance include inbred lines like Mp313, Mp420 (Chen and others 2002) and population like GT-MAS:gk (Widstrom and others 1987) and some drought tolerant genotypes (Tubajika and Damann 2001). However, a majority of these sources lack agronomic performance, which precludes their direct use in commercial hybrids (Betran and Isakeit 2004). This necessitates additional screening of corn germplasm for aflatoxin resistance, which can fulfill the agronomic needs.

The objective of the present study was to conduct a survey of corn varieties of Indian origin for aflatoxin resistance. Further, an attempt was made to correlate kernel resistance to different selection markers like an antifungal 14-kDa Trypsin inhibitor (TI) protein and kernel wax. A novel approach of enzyme kinetics was followed in TI protein studies.

Materials and Methods

Corn varieties

The kernels of 20 corn varieties were provided by All

India Co-ordinated Maize Improvement Project, Kolhapur, Maharashtra, India. One additional variety was purchased from a local market of Mumbai and labelled as 'Local'. All these varieties were cleaned, packed and stored at 4°C until further use, in order to retard insect infestation.

Mold strain

Aflatoxigenic strain of *Aspergillus parasiticus* NRRL 3145, potential producer of all the four major aflatoxins i.e. B₁, B₂, G₁ and G₂ was used in the present study.

Kernel screening assay

The kernel screening assay (KSA) was performed according to Tubajika and Damann (2001). Dry kernels of each variety were surface disinfected with sodium hypochlorite (0.5%) and rinsed with sterile D/W. Ten healthy, dried kernels of each variety were inoculated by dipping them into spore suspension (10⁵ spores/mL) of *A. parasiticus* (Sharma and Padwal-Desai 1985). The inoculated kernels were individually placed in wells of culture plate (24-well Nunc multidish, Nunclon, Denmark). The plates were incubated at ambient temperature (26±2°C) for 15 days, at relative humidity of 95±2%. At the end of incubation period the total number of infected kernels were enumerated. On the basis of fungal colonization the varieties were rated from 1-5 (1 = 1-20%, 2 = 21-40%, 3 = 41-60%, 4 = 61-80% and 5 = 81-100% of the kernels infected by fungus bearing conidia). Each experiment was repeated thrice.

Extraction of aflatoxins

Aflatoxin extraction from infected kernels was carried out as described by Widstrom and others (1987).

The kernels (10 No.) of each variety were crushed to powder in a pestle and mortar. This powder was extracted with chloroform: water (10:1). The toxins from the extract were purified using a silica gel column comprised of top and bottom layers of sodium sulphate and middle layer of activated silica gel. The extract was added to the column and washed initially with hexane, followed by ether and finally with methanol: chloroform (3:97) for toxin elution. The purified toxin fraction thus obtained was dried, processed and analysed by HPLC for quantification of total aflatoxins.

High Performance Liquid Chromatography (HPLC) of aflatoxins

The aflatoxins were analysed using HPLC (JASCO Int. Ltd, Japan) with modification of Holcomb and others (1996). The 10 μ l of sample (appropriately diluted) was injected on a reverse phase C18 (Hypersil ODS) column with 10 μ m particle size. The mobile phase comprised of methanol-water-acetonitrile (6:3:1) and the flow rate was 0.8 ml min⁻¹. The elution of toxin molecules was monitored using fluorescence detector set at excitation wavelength of 360 nm and emission wavelength of 440 nm. The JASCO Borwin Software was used to calculate the toxin content of the sample. The total area of the separated peak (of toxins) based on retention time was calculated.

PCR amplification and sequencing of the TI gene of corn kernels

The DNA from the kernels was extracted by the method of Mukherjee (1999). The DNA from kernels was extracted in buffer comprising of Tris-HCl (100 mM, pH 8.0), EDTA (50 mM, pH 8.0), NaCl (500 mM) and b-

mercaptoethanol (10 mM) and SDS (20%). It was further purified using chloroform and phenol (1:1). The DNA was precipitated using isopropanol and the pellet was dissolved in TE buffer (pH 8.0).

A PCR amplification of TI gene was performed as described by Chen and others (1999) using chromosomal DNA of corn kernels and the primer pair 2041 (5' GAGCTTACTTGGAGGGCATCGTCCGC 3') and 2164 (5' CATATGAGCGCCGGACCTCCTGC 3'). The molecular weight of the amplified PCR product was determined using DNA molecular size markers (pBR 322 DNA/ Hinf I digest, Bangalore Genei Pvt. Ltd., India) by electrophoresis on an agarose gel (1.2%) as described by Sambrook and others (1989).

The amplified product was purified using ExoSAP – IT (USB Corp, Ohio, USA) according to manufacturer's instructions and submitted for sequencing to Bangalore Genei Pvt. Ltd., Mumbai. The sequencing was performed using both the primers, by ABI Prism DNA sequencer. The sequence was then compared using Clustal W software (<http://www.ebi.ac.uk/clustalW>).

Purification of 14-kDa trypsin inhibitor protein (TI protein) from corn kernels

The 14-kDa trypsin inhibitor from dry kernels (50 g) was extracted as described by Chen and others (1998). Powdered kernels were extracted with phosphate-citrate buffer (pH 2.8). The pH of the crude extract was adjusted to 7.5 with 6 N NaOH. The supernatant was dialysed against sodium phosphate buffer (10 mM, pH 7.5) using a 10 kDa cut-off. The dialyzed crude extract was further subjected to ammonium sulphate precipitation to 80% saturation.

The trypsin-Sepharose 4B affinity column was prepared

by coupling trypsin (type III from bovine pancreas) to activated CH-Sepharose 4B according to manufacturer's instructions. The ammonium sulphate precipitated protein fraction was re-suspended in 10 mL of column loading buffer comprising of CaCl_2 (0.02 M), tris-chloride (0.05 M, pH 8.2) and NaCl (1.0 M) and loaded on the trypsin-Sepharose 4B column (equilibrated with the same buffer). The 14-kDa TI protein was eluted using glycine buffer (1.0 M, pH 2.1). Fractions collected were checked for absorbance at 280 nm and assayed for activity. The active fractions were pooled, dialysed against sodium phosphate buffer (10 mM, pH 7.5) and freeze-dried.

Trypsin inhibitor assay

The trypsin inhibiting activity of the purified 14-kDa TI protein was assayed using trypsin and N_α -benzoyl-DL-arginine b-naphthylamide hydrochloride (BANA) as a substrate as described by Barrett (1972) for lysosomal enzymes. One millilitre of sodium phosphate buffer (0.1 M, pH 6.8) system containing 7.5 μg of trypsin (1 mg/mL stock in D/W) and appropriate aliquot (approximately 150 μL) of TI protein was pre-incubated at ambient temperature ($26 \pm 2^\circ\text{C}$) for 10 min. To the same, 1 mM of BANA (10 mM stock in DMSO) was added and further incubated at 50°C for 10 min. The reaction was terminated by the addition of 1 mL GBC and PCMB reagent, prepared by mixing Fast Garnet GBC (0.2 mg/mL in 4% Brij 35) in equal proportion with PCMB reagent (10 mM), prior to use. The pink colored naphthylamine-GBC complex was measured at 520 nm.

Gel electrophoresis

The purity of the 14-kDa TI protein extracted from corn kernels was ascertained by both sodium dodecyl

sulphate-polyacrylamide gel electrophoresis (SDS-PAGE) and Non-denaturing gel electrophoresis (Native-PAGE) as described by Sambrook and others (1989). The protein bands were visualised using silver nitrate staining procedure according to Blum and others (1987). A mixture (10 μg) of standard proteins namely, trypsin, lactalbumin and aprotinin was used as molecular weight markers. A standard soybean trypsin inhibitor was also used as additional marker.

Estimation of protein

At different steps of purification, protein in the sample was measured by Bradford method (Bradford 1976). The standard curve was prepared using bovine serum albumin (BSA) as a standard protein. From the standard curve, the concentration of protein sample was determined. For purified TI, the protein concentration was determined using the formula:

$$A_{280}^{0.1\%} = 2.0 \text{ (Swartz and others 1977).}$$

Determination of inhibition constant (K_i) of TI protein

Standard K_m analysis: Standard K_m of trypsin (7.5 μg) was determined using different concentrations of BANA (0.05 - 1.6 mM). The Michaelis constant (K_m) and maximum velocity (V_{max}) of the trypsin for BANA was determined by Lineweaver-Burk plot.

Determination of K_i : The K_m' (apparent K_m of trypsin in presence of TI protein) was determined by incubating trypsin (7.5 μg) with different concentrations of BANA (as mentioned above) in presence of TI extracted from three different corn varieties viz. LM-6 (0.64 μg), Shaktiman (0.92 μg) and Local (0.94 μg). The inhibition constant (K_i) for trypsin

inhibitor was calculated using following equation,

$$K_m' = K_m \left(1 + \frac{[I]}{K_i} \right)$$

Where,

- K_m : Michaelis constant of uninhibited trypsin.
It is the substrate concentration at which, the velocity of the reaction is half the maximum velocity (V_{max}),
- K_m' : Apparent K_m of trypsin in the presence of trypsin inhibitor,
- [I] : Trypsin inhibitor concentration used for K_m' analysis and
- K_i : inhibition constant of the trypsin inhibitor for trypsin.

Determination of TI protein concentration in corn varieties

The crude protein extract (i.e. ammonium sulphate pelleted fraction) of all the corn varieties was prepared as described in protein extraction. Using this extract, the K_m' was determined for all the varieties. Further using this K_m' and K_i , the TI protein content of all the corn varieties was determined.

Determination of kernel wax content

The kernel wax from the selected varieties was estimated as described by Russin and others (1997). Fifty healthy kernels of 8 varieties, namely CML-142, P₁₉(Y)S₅-B-185-1-6-BBB [P₁₉(Y)], LM-6, GY-39-1-328 [GY-39], CML 430, CML 186, Madhuri and Hyd 9745 were selected for the present study. Kernels of each variety were immersed in 100 mL of distilled chloroform for 60 s to remove wax. The chloroform was partially concentrated in a flash evaporator at 40°C and further evaporated to dryness

under the stream of nitrogen. The weight of wax obtained from each genotype was determined.

Results and Discussion

Kernel Screening Assay (KSA)

Fungal colonization ratings (1-5) for corn varieties are depicted in Fig. 1. As shown in the figure, varieties showed differential response to fungal invasion. Varieties namely CML-142, P₁₉(Y)S₅-B-185-6-BBB, LM-6 and GY-39-1-328 showed relatively lower fungal colonization ratings, as the kernels exhibited least fungal infection. While CML-430, CML-186, CML-176, Madhuri, Pob-24-FSRRS-C-1 and Hyd-9745 exhibited significantly higher fungal colonization ratings, as the fungal infection was remarkably high on the kernels of these varieties. Fungal colonization on kernels of some of the resistant and susceptible varieties is shown in Fig. 2.

Aflatoxin Accumulation in Kernels

The aflatoxin levels in corn varieties used for KSA are shown in Fig. 3. There were no detectable levels of toxins in CML-142, LM-6 and P₁₉(Y)S₅-B-185-6-BBB, while GY-39-1-328 showed low concentrations of toxins. The toxin levels were significantly higher in CML-430, CML-176, CML-186 and Pob 24-FSRRS-C-1. Hyd-9745 though exhibited higher fungal colonization, showed low toxin accumulation.

Thus, KSA studies revealed resistant nature of CML-142, P₁₉(Y)S₅-B-185-6-BBB, LM-6, and GY-39-1-328 with significant inhibition of aflatoxigenic *A. parasiticus* growth and subsequent aflatoxin synthesis. Hence, these varieties were categorized into a group of resistant varieties. Further use of these varieties in

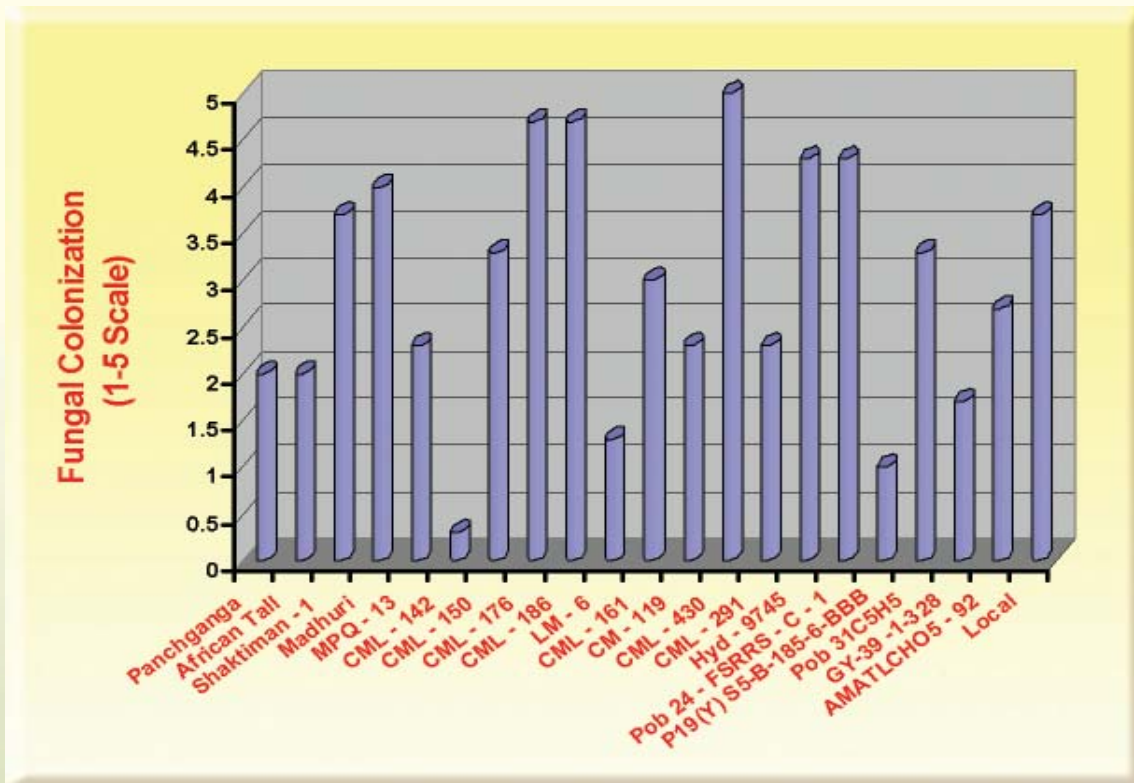


Fig. 1 : Kernel screening assay of corn varieties for *A. parasiticus* colonization. Fungal colonization was rated on a 1-5 scale (1=1-20% and 5=81-100% of the kernel surface covered by conidia). All data points are average of three independent experiments performed in triplicates.



Fig. 2 : Fungal colonization on corn varieties namely A), CML-142; B), LM-6; C), CML-186 and D), CML-430

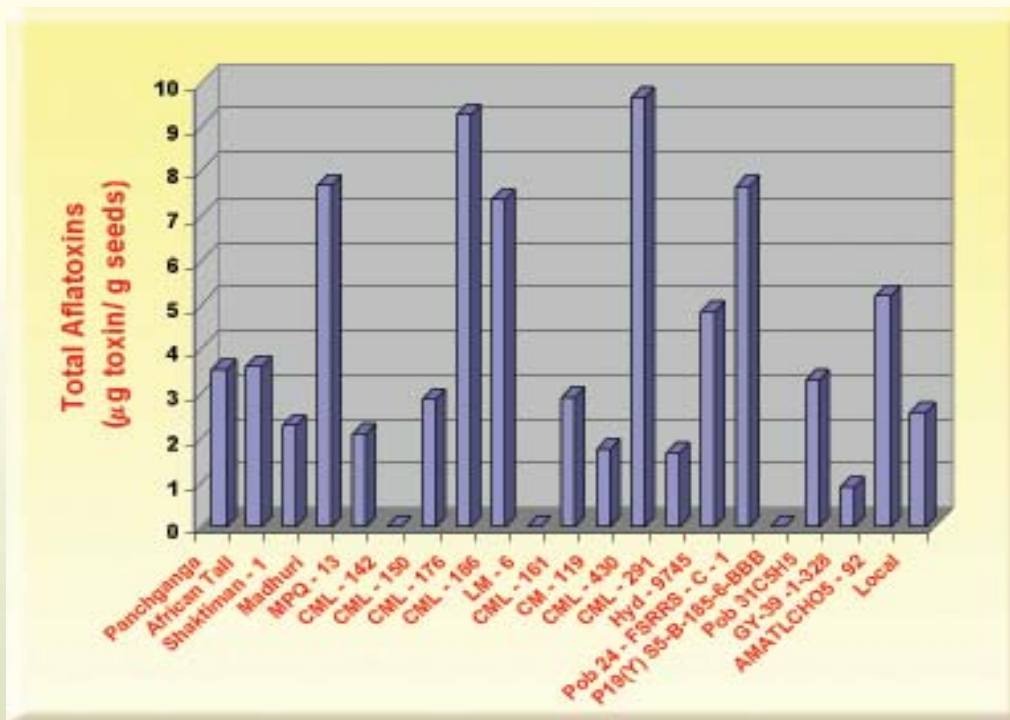


Fig. 3 : Aflatoxin concentration in kernels of corn varieties. The aflatoxins were extracted from the kernels used for KSA and the concentration of total toxins was determined using HPLC. All data points are average of three independent experiments performed in triplicates

breeding program could be beneficial to develop aflatoxin resistant cultivars. CML-430, CML-186, CML-176, Madhuri, Pob-24-FSRRS-C-1, and Hyd-9745 showed highest susceptibility to the *A. parasiticus* infection with higher levels of aflatoxins (except Hyd-9745). Thus, these varieties were grouped into aflatoxin susceptible varieties. The differential responses of corn varieties to fungal infectivity and toxin synthesis, thus, suggested that some fungal resistance mechanisms of kernels interfere in this process of infection and thereby lead to variation in fungal invasion.

Studies on 14-kDa Trypsin Inhibitor (TI) Gene

Studies by various researchers have shown that the constitutive levels of an antifungal, 14-kDa trypsin

inhibitor (TI) protein in kernels were associated with resistance to *A. flavus* infection and toxin production. This protein has both α -amylase and trypsin inhibitory activity. Purified TI protein initiated conidial rupture (Chen and others 1998) and inhibited both conidial germination and hyphal growth of *A. flavus* (Chen and others 1999a). In corn genotypes, TI protein concentration was found to vary, while in some varieties it was absent (Chen and others 1998; Tubajika and Damann 2001). Hence, Indian varieties were initially screened for its presence at gene level.

Studies with PCR amplification of TI gene from chromosomal DNA revealed the gene was present in all the varieties. Fig. 4 depicts the agarose gel electrophoresis of the PCR amplified product. A single

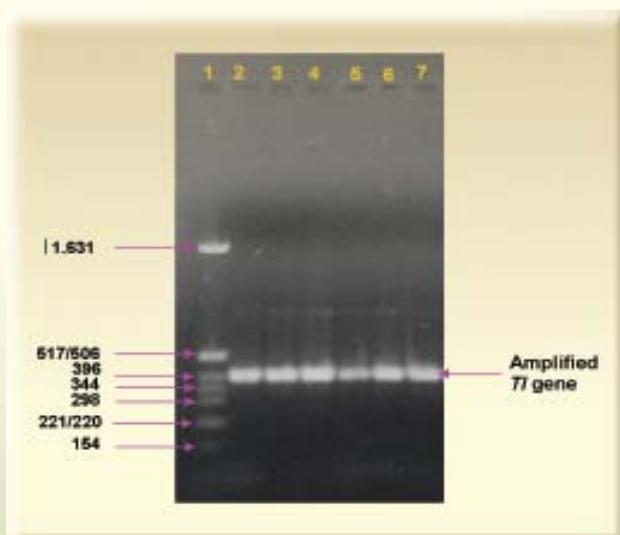


Fig. 4 : Agarose gel electrophoresis of pBR 322 DNA / *Hinf* I digest molecular size markers (Lane 1) and PCR amplified *TI* gene (marked by arrow in lanes 2-7) on agarose gel (1.2%).

band (marked by arrow in lanes 2-7) corresponding to 396 bp (Lane 1) indicated presence of *TI* gene in corn varieties. Further sequencing of this PCR amplified product (from 3 randomly selected varieties) showed 100% homology with the reported *TI* gene. The DNA sequencing studies also established its evolutionary conservation. As the studies confirmed presence of this gene in all the varieties including susceptible ones, it was felt necessary to estimate the level's of its expression in all the varieties.

Purification of TI Protein

A 14-kDa *TI* protein from corn kernels was purified to homogeneity from the crude extract by ammonium sulphate precipitation and trypsin-Sepharose 4B affinity chromatography.

Fig. 5 depicts the silver stained native (Fig. 5-A) and SDS-PAGE (Fig. 5-B) profiles of the purified *TI* protein. In both native as well as SDS-PAGE conditions, the purified *TI* protein appeared in two forms. The SDS-PAGE revealed that the major band, known as a virgins inhibitor, obtained was a single chain form of an intact 14-kDa *TI* protein (Fig. 5-B Lane 5). It was observed mainly during small-scale purification protocol. Whereas the two distinct bands, prominent in large-scale purification process were of 14 and 6-kDa in molecular weight (Fig. 5-B Lane 4). This two-chain form appeared due to the digestion of an intact *TI* protein by trypsin during elution step of purification and referred as the modified form. Similar

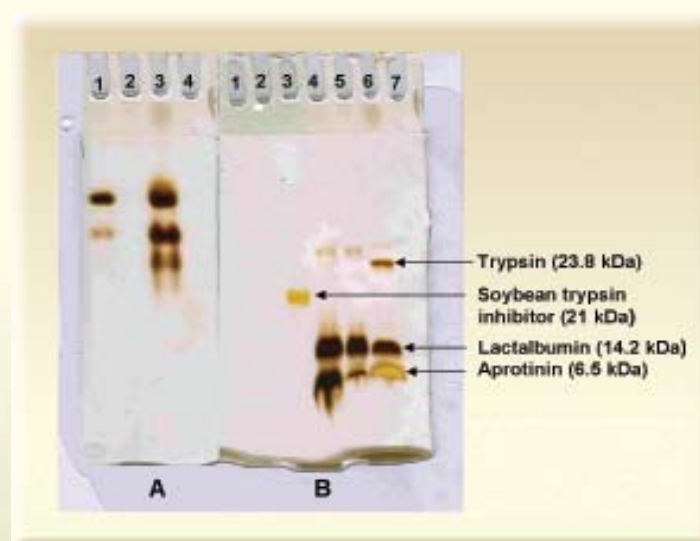


Fig. 5 : Polyacrylamide gel electrophoresis of trypsin affinity purified *TI* protein in A, non-denaturing (native) and B, denaturing (SDS) conditions.

A. Lane 1 and 3, purified *TI* protein.
B. Lane 3, standard protein of soybean trypsin inhibitor; Lane 4 and 5, purified *TI* protein and Lane 6, mixture of standard molecular weight markers including trypsin, lactalbumin and aprotinin.

observations were reported by Lei and Reeck (1986). Thus, both the forms were related to each other (Mahoney and others 1984). Further, the electrophoresis studies of TI protein in denaturing (in the presence of SDS) as well as in non-denaturing (native) conditions ascertained that these two forms were individual entities signifying their distinct nature.

Estimation of TI protein

Previous studies on various corn genotypes have reported the relative content of TI protein (Chen and others 1998; Tubajika and Damn 2001). Unlike that, in the present study the actual concentration of TI protein was determined following enzyme kinetics.

Fig. 6 shows the Lineweaver-Burk plot of TI protein obtained using BANA as a substrate. The K_m and V_{max} of trypsin was found as 0.4 mM and 0.01 nmoles/ml/min, respectively. In presence of TI protein, V_{max} of trypsin remained unchanged, while K_m showed concentration dependent increase in order LM-6 < Shaktiman < Local. This modified K_m was termed as apparent K_m (K_m'). The K_i calculated for all the three varieties using K_m , K_m' and $[I]$ (i.e. TI protein concentration) remained unchanged i.e. 7.0 $\mu\text{g/ml}$ (0.5 μM). Using this K_i , TI protein concentration in all corn varieties was determined.

Table 1 shows the total TI protein concentration in kernels of all the varieties. The high levels of TI protein in kernels of CML-142 and GY-39-1-328 suggested that this protein might play a significant role in their fungal resistance.

Whereas in LM-6 and P₁₉(Y)₅-B-185-6-BBB other resistant mechanisms may be prevalent as both these varieties showed low levels of TI protein. In susceptible varieties, the TI protein levels were markedly low. A marked difference in TI protein concentration was observed in other moderately susceptible varieties and the concentration of this protein was in accordance with their fungal resistance except CML-291 and CML-161. These varieties exhibited very low concentrations of TI protein, thus revealing role of other mechanisms in their partial resistance to fungal growth. Therefore, these results suggested probable involvement of TI protein in kernel's resistance.

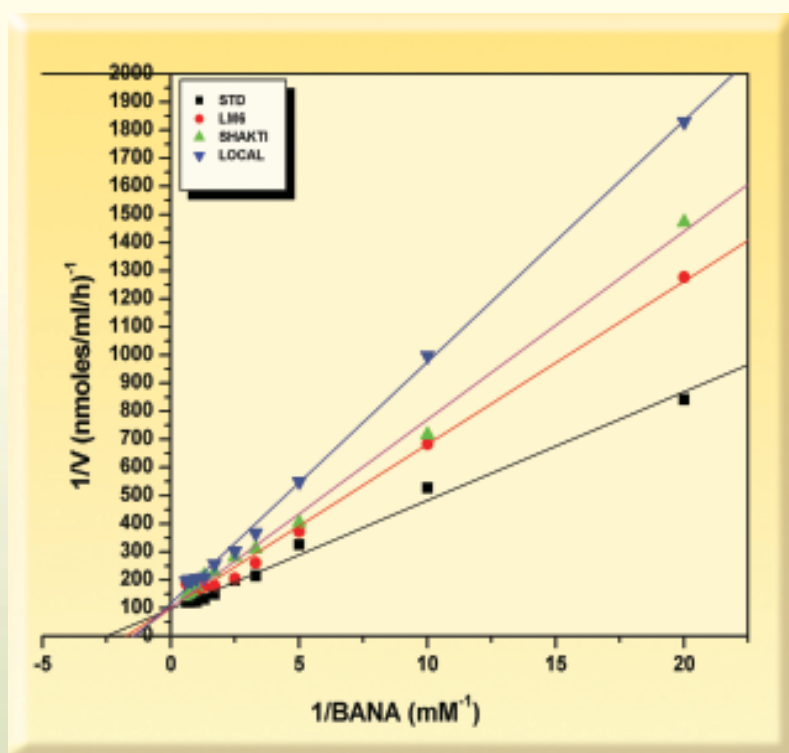


Fig. 6 : Lineweaver-Burk plot for 14-kDa TI protein obtained by a trypsin inhibitor assay using BANA as a substrate.

Table 1: Trypsin inhibitor concentration in Indian corn varieties

Variety	Trypsin inhibitor concentration* (µg of TI/g of seeds)	Response to <i>A. parasiticus</i> infection
LM-6	242.2	Resistant
P ₁₉ (Y)S ₅ -B-185-6-BBB	258	
GY-39-1-328	420	
CML-142	421.2	
CML-176	90	Susceptible
Pob-24-FSRRS-C-1	90	
Hyd-9745	132	
Madhuri	134	
CML-186	158	
CML-430	188	
CML-291	26.6	
CML-161	36	Moderately susceptible
African tall	130	
CML-150	130	
MPQ-13	131	
Pob31C ₁ H ₂ Bulk(ALM) HH-XB	132	
Local	180.8	
AMATLCHO5-82-1-1-36- 1-3-1-2-BBB	203	
Shaktiman-1	211.6	
CM-119	302	
Panchaganga	356	

*average of two sets of experiments

Table 2. Kernel wax content of corn varieties

Status of <i>A. parasiticus</i> infection	Corn variety	Kernel wax* (mg/50 kernels) ^b
Resistant	CML-142	2.5
	P ₁₉ (Y)S ₅ -B-185-6-BBB	2.0
	LM-6	3.0
	GY-39-1-328	1.5
Susceptible	CML 430	0.5
	CML 186	1.5
	Hyd 9745	1.5
	Madhuri	2.0

*Mean of two independent sets of experiments

^bAmount of kernel wax extracted from 50 kernels

Determination of Kernel Wax Content

The pericarp is the outermost portion of corn kernels and contains the layers of cutin and wax, which afford considerable protection against invasion by fungal pathogens (Russin and others 1997; Tubajika and Damann 2001). Earlier reports have revealed the presence of more pericarp wax in resistant varieties like GT-MAS:GK, Chunco, Arizona and Huffman (Russin and others 1997; Tubajika and Damann 2001). These observations were confirmed by the fungal inhibitory activity of pericarp wax assessed by in vitro antifungal bioassays (Russin and others 1997).

Table 2 illustrates the kernel wax content of 4 resistant and 4 susceptible corn varieties. Among the resistant varieties, higher wax content of LM-6 suggested its role in resistance to fungal invasion. While among susceptible varieties, CML-430 showed least wax content making it more prone to fungal invasion. However, the wax content of rest of the resistant varieties did not differ significantly as compared to susceptible ones. Thus, there was a weak correlation between wax content and kernels' susceptibility towards fungal infectivity.

Conclusion

Screening of 21 Indian corn varieties has revealed four varieties namely, CML-142, P₁₉(Y)S₅-B-185-6-BBB, LM-6 and GY-39-1-328 with significant inherent resistance to aflatoxigenic fungal infection. Use of these resistant

varieties holds a great promise, in raising commercial hybrids with resistance to toxigenic fungi.

An attempt made to correlate kernel's resistance to different factors like an antifungal 14-kDa TI protein and kernel wax revealed interesting results. Studies on trypsin inhibitor (TI) gene confirmed its evolutionary conserved nature. Further its expression in different varieties showed variation, which could govern the degree of resistance to fungal invasion. The high levels of TI protein in kernels of resistant varieties like CML-142 and GY-39-1-328 suggested that this protein might play a significant role in their fungal resistance. However, in remaining two resistant varieties, P₁₉(Y)S₅-B-185-6-BBB and LM-6, this was not true. Hence, it could be a promising selection marker for initial screening and further studies are essential to confirm the fungal-resistant nature of the corn varieties. Studies on another selection marker, kernel wax could not able to prove strong relation between its amount and resistance to fungal attack. However, the quality of wax in terms of its composition may govern the property of resistance.

References

1. Barrett AJ. 1972. Lysosomal Enzymes, Appendix Assay Methods. In: Dingle, JT, editor. Lysosomes a Laboratory Handbook. North holland: American Elsevier. p. 110-135.
2. Betran FJ, Isakeit T. 2004. Aflatoxin accumulation in maize hybrids of different maturities. *Agronomy J* 96: 565-570.
3. Blum H, Beier H, Gross HJ. 1987. Improved silver staining of plant proteins RNA and DNA in Polyacrylamide gels. *Electrophoresis* 8: 93-99.
4. Bradford MM. 1976. A rapid and sensitive method for the quantitation of microgram quantities of protein utilizing the principle of protein-dye binding. *Anal Biochem* 72: 248-254.
5. Brown RL, Chen ZY, Menkir A, Cleveland TE. 2003. Using biotechnology to enhance host resistance to aflatoxin contamination of corn (Minireview). *African Journal Biotechnol* 2(12): 557-562.
6. Chen ZY, Brown RL, Damann KE, Cleveland TE. 2002. Identification of unique or elevated levels of kernel proteins in aflatoxin-resistant maize genotypes through proteome analysis. *Phytopathology* 92(10): 1084-1094.
7. Chen ZY, Brown RL, Lax AR, Cleveland TE, Russin JS. 1998. Resistance to *Aspergillus flavus* in corn kernels is associated with a 14-kDa protein. *Phytopathology* 88: 276-281.
8. Chen ZY, Brown RL, Lax AR, Cleveland TE, Russin JS. 1999a. Inhibition of plant pathogenic fungi by a corn trypsin inhibitor overexpressed in *Escherichia coli*. *Appl Environ Microbiol* 65(3): 1320-1324
9. Chen ZY, Brown RL, Russin JS, Lax AR, Cleveland TE. 1999. A corn trypsin inhibitor with antifungal activity inhibits *Aspergillus flavus* α -amylase. *Phytopathology* 89: 902-907.
10. Holcomb M, Thompson HC, Cooper WM. 1996. SFE extraction of aflatoxins (B₁, B₂, G₁ and G₂) from corn and analysis by HPLC. *J Supercritical Fluids* 9: 118-121.
11. Lei MG, Reeck GR. 1986. Combined use of trypsin-agarose affinity chromatography and reverse phase high-performance liquid chromatography for the purification of single-chain protease inhibitor from corn seeds. *J Chromatography* 363: 315-321.

12. Mahoney WC, Hermodson MA, Jones B, Powers DD, Corfman RS, Reeck GR. 1984. Amino acid sequence and secondary structural analysis of the corn inhibitor of trypsin and activated Hageman factor. *J Biol Chem* 259: 8412-8416.
13. Mukherjee PK. 1999. Rapid extraction of plant genomic DNA suitable for restriction analysis and PCR amplification. *Asian Pacific J Mol Bio Biotech* 7(1): 95-96.
14. Oyebanji AO, Efiuwewwere BJO. 1999. Growth of spoilage mold and aflatoxin B₁ production in naturally contaminated or artificially inoculated maize as influenced by moisture content under ambient tropical condition. *International Biodeterioration and Biodegradation* 44: 209-217.
15. Payne GA, Hagler WM Jr, Adkins CR. 1988. Aflatoxin accumulation in inoculated ears of field-grown maize. *Plant Dis* 72: 422-428.
16. Russin JS, Guo BZ, Tubajika KM, Brown RL, Cleveland TE, Widstrom NW. 1997. Comparison of kernel wax from corn genotypes resistant or susceptible to *Aspergillus flavus*. *Phytopathology* 87: 529-533.
17. Sambrook J, Fritsch EF, Maniatis T. Eds. 1989. *Molecular cloning: A laboratory manual* (2nd Ed.). USA: Cold Spring Harbor Laboratory Press. R.4 p.
18. Sharma A, Padawal-Desai SR. 1985. On the relationship between pellet size and aflatoxin yield in *Aspergillus parasiticus*. *Biotechnol Bioeng* 27: 1577-1580.
19. Swartz MJ, Mitchell HL, Cox DJ, Reeck G. 1977. Isolation and characterization of trypsin inhibitor from opaque-2 corn seeds. *J Biol Chem* 252(22): 8105-07.
20. Tubajika KM, Damann KE. 2001. Sources of resistance to aflatoxin production. *J Agric Food Chem* 49: 21652-21656.
21. Widstrom WP, McMillian WW, Wilson DM. 1987. Segregation of resistance to aflatoxin contamination among seeds on an ear of hybrid maize. *Crop Sci* 27:961-963.

ABOUT THE AUTHORS



Ms. Shruti S. Hajare did her M. Sc. (Life Sciences) from University of Mumbai, and joined BARC in 1998 as a Ph. D. student under DAE fellowship. She is working on the

project entitled "Mycotoxin biogenesis and control in foods and feeds" She submitted her thesis to Mumbai University in April 2006.



Mr. Sachin N. Hajare did his M. Sc. (Zoology) from Pune University, and joined Food Technology Division, BARC, in 1998 after completing one-year Orientation Course (OCES- 41st Batch) in Radiobiology

discipline. He is working in the Food Science and Safety section of FTD and is currently working on control of mycotoxin producing fungi in foods and feeds.



Dr. Arun Sharma joined Training School of Bhabha Atomic Research Centre, Mumbai, in 1975, after finishing Masters degree in Microbiology from National Dairy Research Institute,

Karnal. He obtained his Ph. D. degree in Biochemistry from University of Bombay in 1984. He was a Post-Doctoral Associate at the Department of Plant Pathology, University of California, Riverside, USA, during 1990-1991, where he worked with Prof. Noel T. Keen on the avirulence gene D of *Pseudomonas syringae* pv. tomato. After returning to India, Dr. Sharma initiated work on *Xanthomonas campestris* pv. glycines, the etiological

agent of bacterial pustule disease of soybean. Since then he has been actively involved in studying the molecular biology of *Xanthomonas* with special reference to the mechanism of host-pathogen interaction. His other interests include biogenesis and control of aflatoxin in food and feed. Simultaneously, he has also been engaged in research related to radiation processing of food. He has more than 150 publications in national and international journals, including chapters in books and encyclopedias. He has participated as a delegate and expert in the co-ordinated research programs of the International Atomic Energy Agency. He has been the secretary of the Environmental Mutagen Society of India and Vice-President of Indian Society for Environmental Science & Technology. Dr. Sharma is currently Head, Food Technology Division, Bhabha Atomic Research Centre, Mumbai, India.

DEVELOPMENTAL STUDIES OF THE 20 MEV HIGH INTENSITY LINAC

P. Singh , S.V.L.S. Rao, Rajni Pande, T. Basak, Shweta Roy, M. Aslam,
P. Jain, P.K. Nema and S. Kailas
Nuclear Physics Division, Bhabha Atomic Research Centre
S. Krishnagopal
Raja Ramanna Centre for Advanced Technology, Indore
and
V.C. Sahni
Physics Group, Bhabha Atomic Research Centre

This paper was awarded the Best Paper (Poster) Award at the DAE-BRNS 50th Symposium on Nuclear Physics, held at BARC, Mumbai, during December 12-16, 2005.

In India, long-term economic exploitation of nuclear power is considerably dependent on an efficient utilization of the thorium through the reactor-based Th-U²³³ fuel cycle. Accelerator-Driven System (ADS) [1] has the potential to provide an additional route to an efficient use of the available uranium and thorium resources, besides offering a way towards nuclear waste incineration. Consequently, it has evoked considerable interest

in the nuclear community the world over as well as in India. Our effort, naturally is directed towards devising an ADS relevant to the ²³³U-Th cycle.

Accelerator Driven System (ADS) mainly consists of a sub-critical reactor coupled to a high power proton accelerator through high Z spallation target as outlined in Fig. 1. In the practical realization of ADS, the most challenging task is the development of a high energy

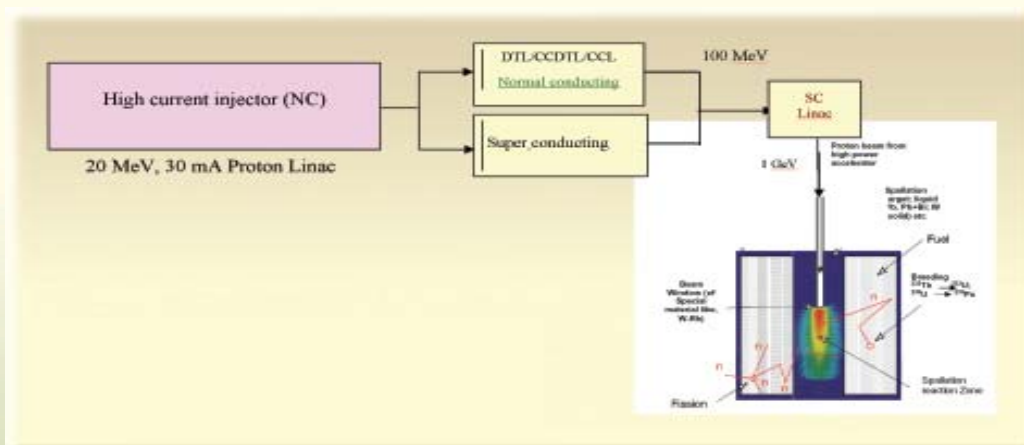


Fig. 1: Schematic of Accelerator Driven System.

(~ 1 GeV) and high current (~ 30 mA) proton accelerator to produce the intense spallation neutron source needed to drive the sub-critical reactor to the desired power. Also, it is necessary that the accelerator is reliable, rugged and stable in order to provide uninterrupted beam power to the spallation target, over long periods of time. It should also have a high efficiency (30-40%) for conversion of electric power to beam power. The loss of beam power in the accelerator must be less than 1 W/m so that hands-on-maintenance of the accelerator sub-assemblies can be safely done. For ADS, operation of accelerator should be in nearly CW mode to avoid undesirable thermal shocks to the fuel elements.

It is planned that the development of the 1 GeV accelerator for ADS will be pursued in three phases, namely, 20 MeV, 100 MeV and 1 GeV [2]. The most

challenging part of this CW proton accelerator is development of the low-energy injector, typically up to 20 MeV, because the space charge effects are maximal here. Therefore, BARC has initiated a programme for the development of a Low Energy (20 MeV) High Intensity Proton Accelerator (LEHIPA) as front-end injector of the 1 GeV accelerator for the ADS programme.

The major components of LEHIPA are a 50 keV ECR ion source [3], a 3 MeV Radio-Frequency Quadrupole (RFQ) [4] and a 20 MeV Drift Tube Linac (DTL) [5]. The Low Energy Beam Transport (LEBT) and Medium Energy Beam Transport (MEBT) lines match the beam from the ion source to RFQ and from RFQ to DTL respectively. The main criterion for the design of the linac is to have minimum beam loss. The layout of the 20 MeV accelerator is shown in Fig. 2.

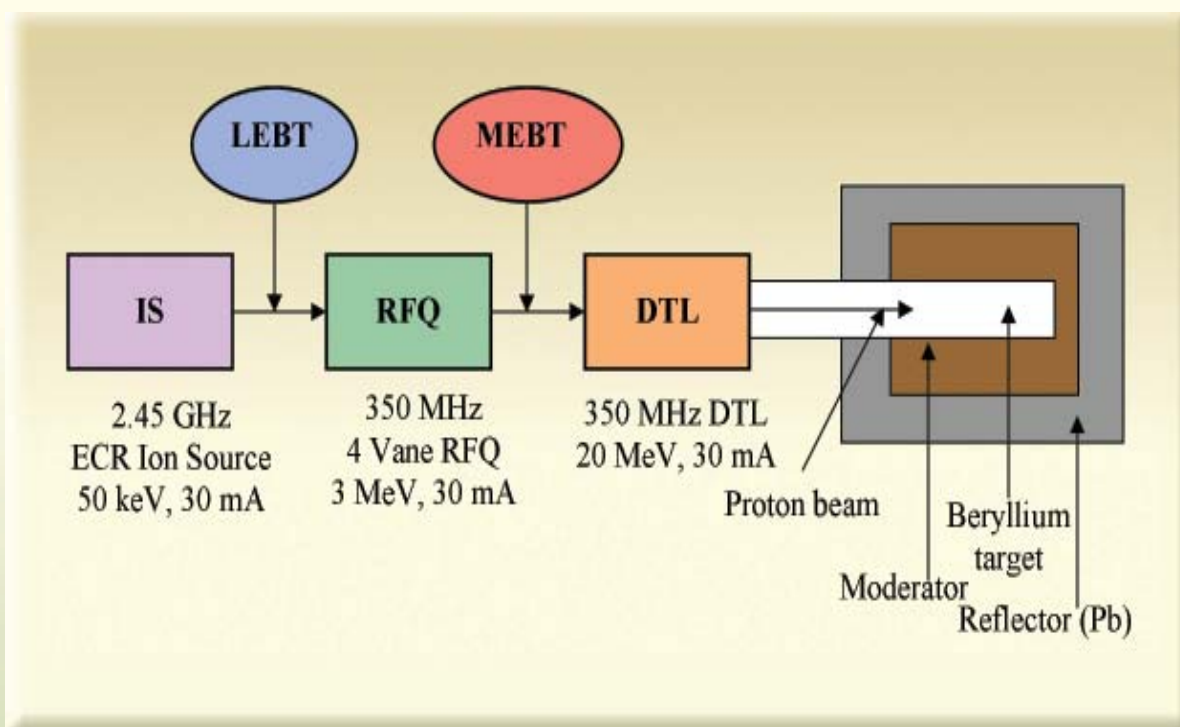


Fig. 2: Layout of LEHIPA.

The beam from LEHIPA will be used to generate neutrons via ${}^9\text{Be}(p,n){}^9\text{B}$ reaction. A neutron yield of 4.0×10^{15} n/sec [$S(E_p) = 4.476 \times 10^{11} \times E_p^{1.886} \times I$ n/s] [6] is expected to be produced for a 20 MeV proton beam of 30 mA current (Fig.3). This intense neutron facility may be used for various applications like production of radioisotopes, material science research and medical applications.

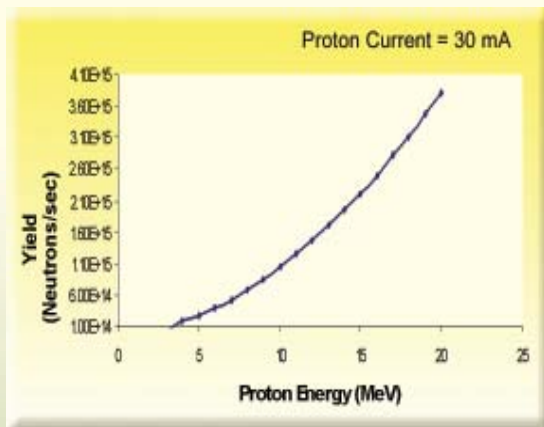


Fig. 3 : Neutron yield vs proton energy for beryllium target

The design of various components of LEHIPA is discussed below.

Ion Source

A 50 keV, 60 mA ECR ion source for LEHIPA is being developed by APPD, BARC [3]. In order to optimize the beam emittance, a five-electrode extraction geometry has been used.

Low Energy Beam Transport line (LEBT)

The dc proton beam from the ECR ion source is matched to the RFQ using LEBT. The main criterion for the design of the LEBT was to minimize the emittance growth with minimum beam loss. Two solenoids were used to focus

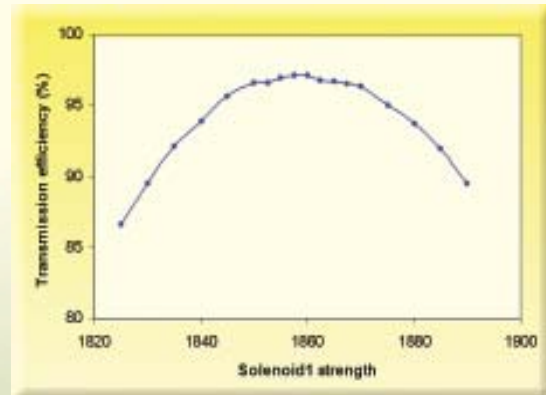


Fig. 4a: Transmission efficiency vs change in strength of solenoid 1.

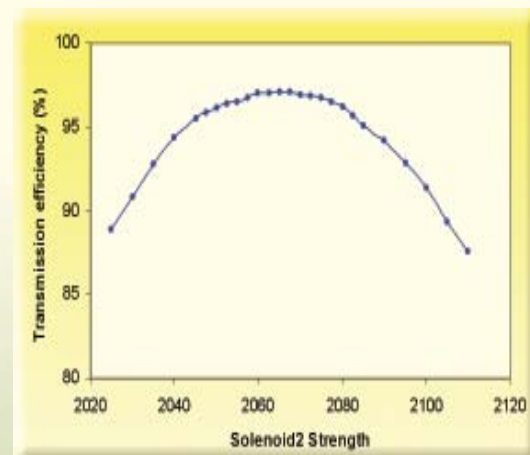


Fig.4b: Transmission efficiency vs change in strength of solenoid 2

and match the beam into the RFQ. Effects on the transmission through the RFQ if either solenoid strength changes from the designed value have also been studied and are shown in Figs. 4a and 4b. It can be seen that if magnetic field strength of either solenoid changes by ± 20 Gauss then the transmission at the end of the RFQ drops below 95%. At low energies space charge forces are very dominant and mainly responsible for increase in beam size and emittance. In order to reduce these effects, space charge compensation technique, in which electrons produced by ionization of a residual

gas neutralize the space charge of the beam, is used in the LEBT. Simulation studies show that there is no emittance growth in the LEBT when the beam is more than 95% space charge compensated [7]. Also the maximum beam radius reduces from 6.5 cm to 3.4 cm with compensation.

Radio-Frequency Quadrupole (RFQ)

The RFQ is a low-velocity, high-current linear accelerator with high capture efficiency. It focuses, bunches and accelerates the beam simultaneously. The physics design of the 350 MHz, 3 MeV, four vane RFQ has been done [8]. The input and output parameters of RFQ are listed in Table 1.

Table 1: Parameters of the RFQ.

Parameter	Value
Input energy	50 keV
Output energy	3 MeV
Beam current	30 mA
Frequency	350 MHz
Norm. RMS emittance	0.02π cm-mrad
Vane voltage	81.5 kV
Average bore radius	3.66-4.37 mm
Transmission Efficiency	97 %
Length	3.62 m
Total RF Power	430 kW
Peak electric field	32.96 MV/m

The geometry of the vanes of the RFQ for a resonant frequency of 350 MHz was optimized using the 2D electromagnetic code SUPERFISH [9]. The RFQ operates in the TE₂₁₀ mode, which cannot be excited in a closed cavity. In order to excite the RFQ in a TE₂₁₀ like mode, the vane ends are provided with undercuts to satisfy the

required boundary conditions. The vane undercuts have been optimized using 3D electromagnetic code MAFIA [10] to design the beginning and end cell of the RFQ [11]. The MAFIA model of the beginning cell is shown in Fig. 5.

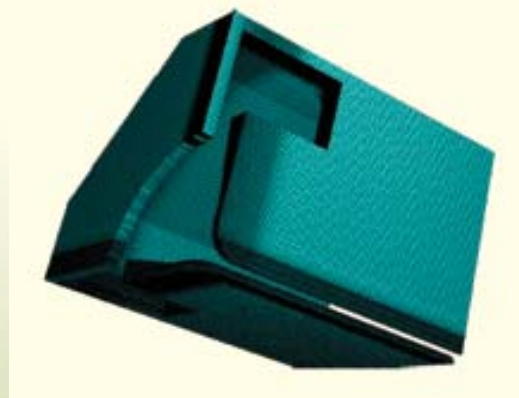


Fig. 5 : MAFIA model of the RFQ beginning cell with vane undercut

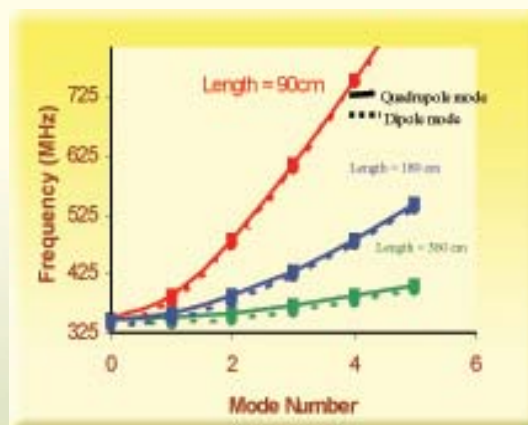


Fig.6: Variation of higher order dipolar and quadrupolar frequencies with RFQ length

The RFQ structure is normally operated at the cutoff frequency of the quadrupole mode, where for a 3.62 m long RFQ, the mode separation between the operating mode and the nearest higher order longitudinal mode is relatively small as shown in Fig. 6. As a result a single 3.62 m long RFQ will be

very difficult to tune and will be unstable. So in order to obtain transverse and longitudinal stability, the RFQ will be made in 4 segments of length about 90 cm each and the segments will then be joined together using resonant coupling technique. The resulting structure will be less sensitive to perturbations due to fabrication errors and the fabrication tolerances thus become easier [12]. The coupling cell has been designed in MAFIA and is shown in Fig. 7.

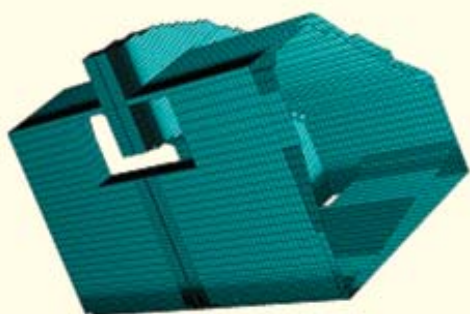


Fig. 7: MAFIA model of the coupling cell

Computer simulations using MAFIA were also done to study the frequency variation that can be tuned with the tuners. The effect of tuners on the electromagnetic field distribution was also studied. Fig. 8 shows a MAFIA model of one quadrant of RFQ cavity with tuner. A total of 32 tuners, each of diameter 4.5 cm will be used. The tuning range of each tuner is 26.5 kHz/mm per meter length of the RFQ.

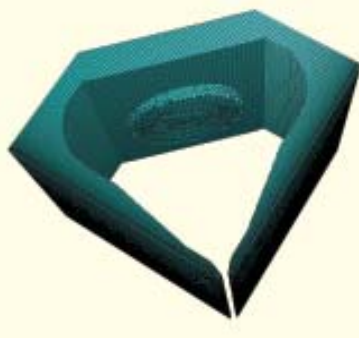


Fig. 8 : RFQ cavity with tuner

The vacuum required in the RFQ is 10^{-7} Torr. To achieve this, 24 vacuum ports have been designed in MAFIA as shown in Fig. 9. Each of these ports consists of six slots. The detuning due to each vacuum port is 112.5 kHz per meter length of the RFQ.



Fig. 9: RFQ cavity with vacuum port

The effect of various errors on the beam dynamics in the RFQ has been studied. The acceptance criterion for the error studies was 95% transmission through the RFQ. Detailed simulations of errors in the various parameters have been done, based on which the following tolerances have been specified: (i) alignment of the RFQ: $50 \mu\text{m}$ and 5 mrad; (ii) Energy deviation of the incoming proton beam: 0.5 keV; (iii) Stability of ion source power-supply: $< 1\%$; (iv) Tolerance on energy spread of beam from ion-source: 1%.

The integrated thermal/structural analysis of an RFQ is crucial to its design and operation. The total power dissipated in the RFQ structure is estimated to be 342 kW. This power dissipation can cause large temperature gradient in the RFQ structure along with distortion in the vane, which leads to detuning of the structure. The cooling scheme is designed to minimize temperature rise in the RFQ and control the detuning to less than 80 kHz. The inlet coolant water

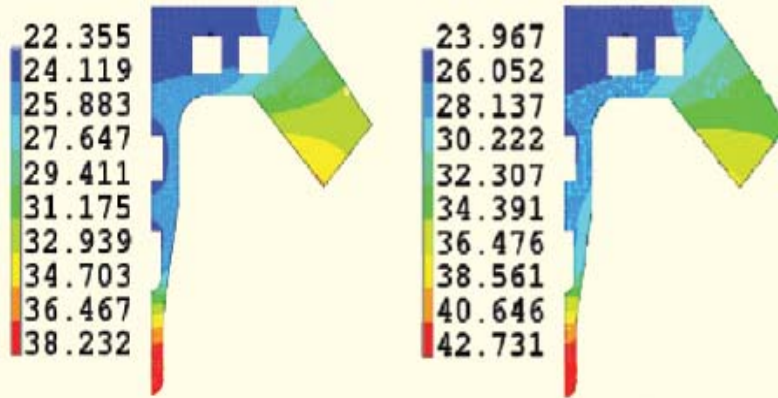


Fig. 10: Temperature distribution in the vane at the inlet and outlet

temperatures are chosen to be 16°C (vane tip) and 20°C (outer) [4]. The temperature distribution in the vane at the inlet and outlet are shown in Fig. 10.

The vane tip deflection at the inlet and outlet are 0.03 mm and 2.4 mm, which corresponds to the detuning of +30 kHz and +65 kHz respectively. The tolerance on the inlet coolant water temperature is estimated to be $\pm 0.1^\circ\text{C}$. The cooling system (LCW) for LEHIPA is being setup by RRDPA, BARC.

Medium Energy Beam Transport line (MEBT)

The MEBT has been used to match the beam from RFQ to DTL. It consists of 4 quadrupoles and two RF gaps for matching the beam in transverse and longitudinal planes. The total length of the MEBT is 1.04 m.

Drift Tube Linac (DTL)

The DTL can focus and accelerate a high intensity proton beam very effectively at low energies—typically from 3 to 50 MeV, where the space charge forces are

considerable. In LEHIPA, an Alvarez-type DTL is used to accelerate the beam from 3-20 MeV because of its higher effective shunt impedance as compared to Coupled Cavity Drift Tube Linac (CCDTL) (Fig. 11). Beyond 20 MeV, the bore radius has been increased from 1.1 cm to 1.4 cm which results in decrease of effective shunt impedance as seen in the figure below.

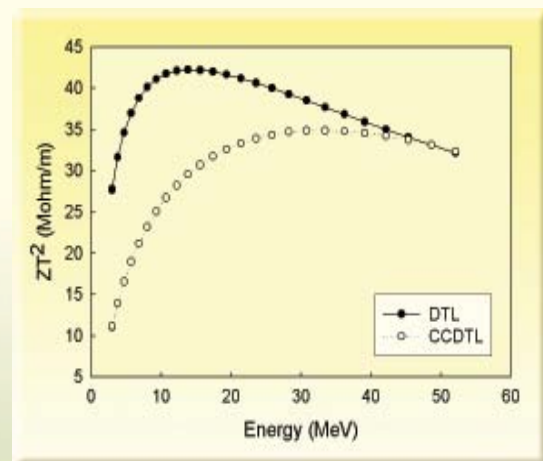


Fig.11: Comparison of effective shunt impedance vs energy for DTL and CCDTL

For minimum emittance growth, it is necessary to match the transverse phase advance per unit length in the RFQ and DTL. This requires quadrupole gradients of 80 T/m in the DTL if FODO (FD) lattice is used, making the design of electromagnetic quadrupoles (EMQs) difficult at low-energy end. However, if FOFODODO (FFDD) lattice is considered, the required quadrupole gradient is 46 T/m; making the design of

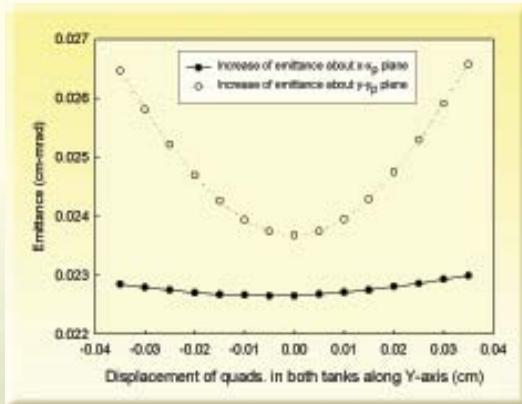


Fig. 12a: Variation of beam emittance with Quadrupole displacement

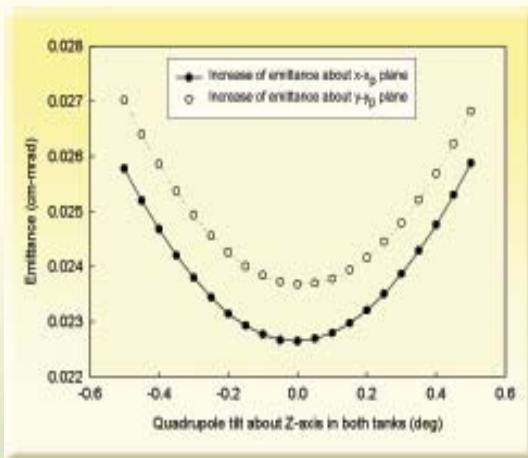


Fig. 12b: Variation of beam emittance with Quadrupole tilt

quadrupoles easier [13]. Also if the DTL is designed in 2 tanks, the quadrupole displacement and the quadrupole tilt in the tanks have to be restricted to within 100 mm in transverse planes and 0.6° about longitudinal plane as shown in Figs. 12a and 12b respectively. Alignment of quadrupoles to such precision over long lengths is very difficult. It is, therefore, planned to make the DTL in four short tanks having FFDD lattice. The RF power required in each tank is less than 500 kW, making the design of RF coupler also easier. However, the rms beam

size in a DTL having FFDD lattice is more than the rms beam size in a DTL having FD lattice. The aperture is consequently increased from 1.6 cm to 2.2 cm so that the aperture is more than 8 times the rms beam size in the DTL. The axial electric field in all the tanks will be kept constant at a value of 2.49 MV/m. The parameters of the DTL are listed in Table 2.

Table 2: Parameters of the Drift Tube Linac

Parameter	Value
Input energy	3 MeV
Output energy	20 MeV
Beam current	30 mA
Frequency	350 MHz
Diameter of cavity	54 cm
Diameter of drift tube	12 cm
Bore radius	1.1 cm
Axial electric field	2.49 MV/m
Total length	11.44 m
Beam transmission	100%
Focussing lattice	FFDD
Effective length of quad.	4.31 cm
Quadrupole gradient	46 T/m
Total power (Including 30% margin)	1.814 MW

Beam Dump

A target for beam dump of 600 kW proton beam from LEHIPA has been designed covering thermal and structural requirements. Thermal and mechanical stresses were examined both analytically and numerically in order to develop a procedure where the target dimensions could be optimized to allow the maximum amount of power to be placed on a

target for a given set of conditions. Optimizing a target generally involves the balancing of stresses on the hot and cold faces so that the target will not fail for the given set of conditions. A conical shape and nickel bulk was chosen for preliminary analyses of this target (Fig. 13) and design of the water-cooling system has been finalized.

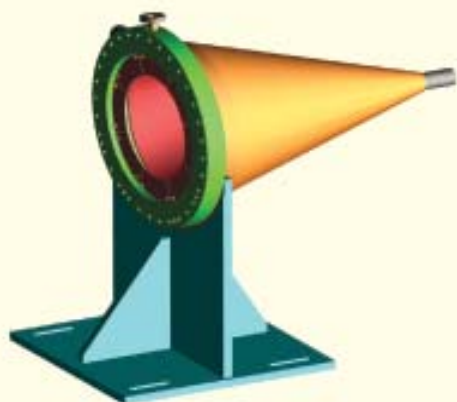


Fig. 13: Conical target for beam dump

400 keV RFQ

The 20 MeV linac involves handling of large RF powers at 350 MHz and fabrication of complex structures like RFQ. Presently, in BARC no experience exists in building long and complex structures such as CW RFQs, handling high RF power. It was therefore thought prudent to develop a small RFQ, which will also be useful to our department's programme. So it has been decided to develop a 400 keV, 1 mA deuteron RFQ at the same frequency of 350 MHz. In this context it was noted that there is an existing 400 kV DC accelerator for deuterons at the PURNIMA facility in BARC, which is used as a neutron generator. It produces a neutron yield of $\sim 10^9$ n/s, where the deuteron current is limited to around 100-200 μ A because of poor transmission through the

accelerating tube. In order to increase the flux by an order of magnitude it was felt that it would be useful to modify the ion source to get a beam current of 1 mA and replace the DC accelerator with an RFQ. As the beam transmission through the RFQ is more than 90%, this will increase the neutron yield to $\sim 10^{10}$ n/s (Fig. 14), which will enable experiments to be conducted with greater accuracy.

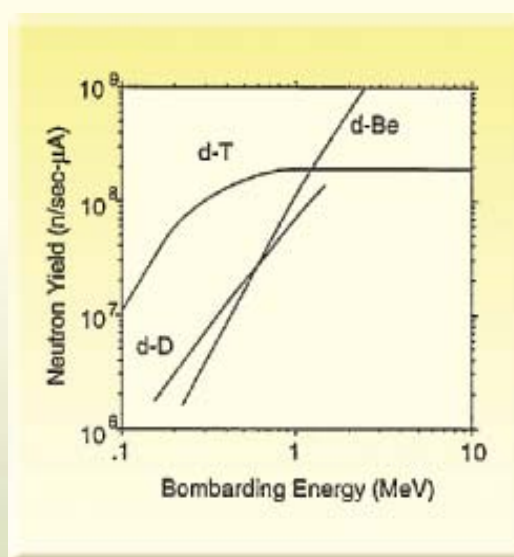


Fig. 14: Neutron yield vs deuteron energy

In addition to this, it will also generate useful experience, at an intermediate level of energy and RF power, in operating such systems. This experience will be of great value towards the ultimate objective of building and operating a 20 MeV, 30 mA proton linac.

It was therefore decided to build a deuteron accelerator consisting of a 50 keV ion source, and a 400 keV RFQ. The DC beam from the ion-source will be matched to the RFQ using a LEBT system, which has been designed with two solenoids. It is also

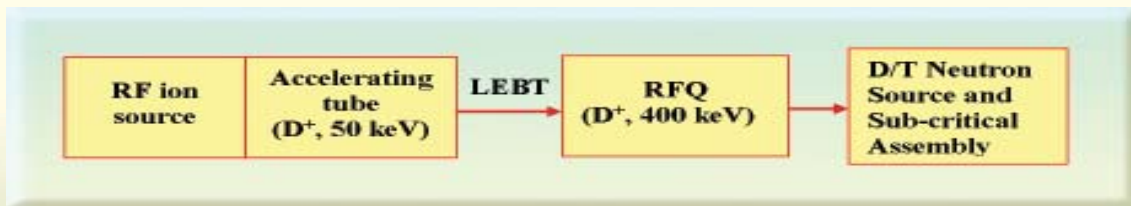


Fig. 15: Layout of the 400 keV deuteron accelerator based neutron source coupled to a sub-critical assembly

envisioned that in preparation for developing ADS type systems to gain some experience of coupling an external neutron source to a sub-critical reactor assembly [14], we should integrate the 14 MeV D/T neutron source to a light water, natural Uranium, sub-critical assembly. A schematic diagram of this total system is shown in Fig. 15.

The physics design of the 400 keV RFQ for deuteron beam has been completed [15]. The total length of this linac including its LEBT section is about 2.25 m. The transmission at the end of the linac is 95%. The detailed 3D design of this RFQ has been done, which includes the design of beginning and end cell, tuners and vacuum ports. The effect of tuners on the electromagnetic field distribution was studied [16]. The tuning range of 16 tuners (each of diameter 4.5 cm) is found to be [-2.1 MHz, 4.29 MHz] for a penetration of [-15 mm, 10 mm]. To achieve a vacuum of 10^{-7} Torr in the RFQ, 8 vacuum ports have been designed in MAFA, which cause a detuning of 900 kHz. This can be compensated by inserting the vacuum port assembly in the volume of the

RFQ by 3 mm.

Thermal analysis of this RFQ has also been done [17]. A total number of 24 longitudinal coolant channels were designed in the RFQ to remove ~ 68 kW of dissipated heat. It is found that frequency shift is almost zero at -0.2 mm tip deflection and increases with tip deflection on either side. It was also observed that the resonant frequency shifts by -70 kHz for every 1°C rise in the vane inlet cooling water temperature.

RF design of inductive couplers (40 kW each) has been done [18] and its complete assembly is shown in Fig. 16. The coupling coefficient can be varied from

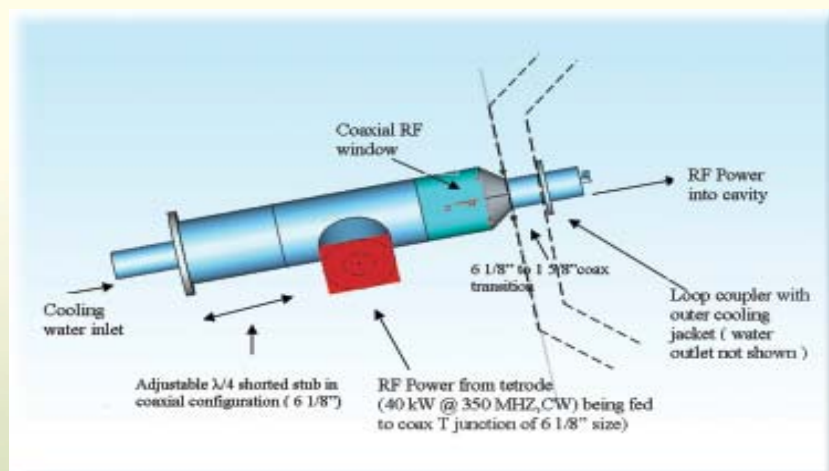


Fig.16: Schematic of 40 kW RF loop coupler assembly

0 to 1.5 by rotating the coupler inside the cavity. Resonant frequency shift of the quadrupolar mode of RFQ cavity with four loop couplers has been kept within 2 MHz. The maximum power loss density estimated on the coupler using MAFFIA code is about 56 W/cm². Cooling arrangement and its final mechanical design are being worked out.

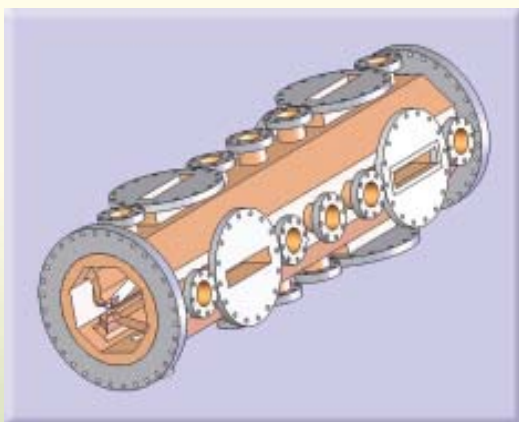


Fig. 17a: CAD model of 400 keV RFQ



Fig. 17b: Aluminium model of RFQ

To validate the simulations, a 50 cm aluminium model of the RFQ without modulations has been fabricated by MDPDS, BARC. The complete CAD and aluminium models of 400 keV RFQ is shown in Figs. 17 (a & b). The

resonant frequencies of different modes have been measured with VNA and were found to be in reasonable agreement with the simulations. Inductive couplers of different sizes have been used for RF measurements to study the variation of coupling coefficient. The results are being compared with the EM simulations using MAFFIA.

Future studies

A preliminary design of the 1 GeV, 30 mA CW proton linac for ADS has also been done [19]. This linac consists of a 3 MeV RFQ, DTL upto 50 MeV, CCDTL up 100 MeV and 5 cell superconducting elliptical cavities upto 1 GeV. The focussing lattice is FD in DTL and CCDTL and doublet in superconducting cavities. The DTL will be built in 5 tanks. The total length of the DTL is 28 m and the RF power required is about 4 MW. The CCDTL consists of 2 gap cavities. Its total length is 75 m and the RF power requirement is about 5 MW. The superconducting cavities consist of three sections $b=0.47$ (99.8-198.8 MeV), 0.62 (198.8-498.8 MeV) and 0.80 (498.8 MeV-1 GeV). The focussing doublets are placed after every 2 cavities in the first section, which will have 33 cryostats, after every 3 cavities in the second section having 40 cryostats and after every 4 cavities in the third section having 38 cryostats. Detailed design studies are in progress.

Summary & Conclusions

The physics design of LEHIPA, 20 MeV, 30 mA proton linac has been completed. Various sub-systems of accelerator have been designed and their procurement has been initiated. Development of fabrication techniques of RFQ and DTL structures has also been taken up inhouse (with CDM) as well as with industries. The LEHIPA facility will be housed in the basement of

Common Facility Building (CFB) at BARC. Construction of the building has commenced and installation of utilities like electrical power, cooling water plant and assembly of accelerator systems in CFB will begin in 2008.

In order to get hands on experience at relatively high RF power, a 400 keV RFQ for accelerating deuterons has been designed and is being fabricated. Major sub-systems of this device will be assembled and tested in VDG tandem hall. This RFQ will be used for generating 14 MeV neutrons by D-T reaction and will be used for studying neutron multiplication in a sub-critical assembly.

Acknowledgements

We thank Dr A. Kakodkar, Dr S. Banerjee and Dr S.S. Kapoor for their keen interest in this project. Several divisions of BARC (NPD, VPID, APPD, ED, RRDPD, CnID, RSSD, TSD, CDM, A&CED, RSD, LNPS, etc.) and RRCAT have contributed in this project and it is our pleasure to thank them all.

References

1. F. Carminati, R. Klapisch, J.P. Revol, J.A. Rubio and C. Rubbia CERN/AT/93-47 (ET); C. Rubbia et al; CERN/AT/95-44 (ET); CERN/LHC/96-01 (EET); CERN/AT/95-53 (ET); CERN/LHC/97-01 (EET).
2. S.S. Kapoor, "Roadmap for development of Accelerator Driven Sub-Critical Reactor Systems", BARC/2001/R/004.
3. P. Roychowdhury, P. Jain, V. Yadav, K.P. Dixit and R.C. Sethi, "Design and development of a high current Microwave ion source", Proc. InPAC-2003, Feb. 3-6, 2003, CAT, Indore, p 179.
4. T. Basak, B. Biswas, S. Kailas, S. Krishnagopal, Arvind Kumar, Rajni Pande, P.K. Nema, S.V.L.S. Rao, Shweta Roy, V.C. Sahni and P. Singh, "Physics Design of a Low Energy High Intensity Proton Accelerator", BARC/2004/I/007.
5. P. Singh, "Physics studies of the 20 MeV High Intensity Proton Accelerator", InPAC-2005, March 1-5, 2005, VECC, Kolkata, page 29.
6. H.J. Brede, G. Dietze, K. Kudo, U.J. Schrewe, F. Tancu and C. Wen et. al., "Neutron yields from thick Be targets Bombarded with deuterons or protons", Nucl. Instr. Meth. A274, 332 (1989).
7. Rajni Pande, S.V.L.S. Rao, T. Basak, P. Singh, P.K. Nema, S. Kailas, V.C. Sahni, A. Kumar, B. Biswas and S. Krishnagopal, "Effect of Space Charge Compensation on LEBT Design", Proc. DAE Symp. Nucl. Phys.(India), 46B, 466 (2003).
8. S.V.L.S. Rao, Rajni Pande, Shweta Roy, T. Basak, P. Singh, S. Krishnagopal, P. K. Nema, S. Kailas and V.C. Sahni, "Physics Design of the 3 MeV RFQ", InPAC-2005, VECC, March 1-5, 2005, page 60.
9. J.H. Billen and L.M. Young, POISSON SUPERFISH, LA-UR-96-1834. L.A.N.L.
10. MAFIA- Simulation Tool for Electromagnetic Analysis and Design, CST, Germany.
11. Rajni Pande, Shweta Roy, S.V.L.S. Rao, T. Basak, P. Singh, P.K. Nema, S. Kailas and V.C. Sahni, "3-D design of the RFQ cavity", DAE-BRNS Nucl. Phys. Symp., 47B(2004) 474.
12. L. M. Young, "Segmented Resonantly Coupled Radio-Frequency Quadrupole", PAC 1993.
13. T. Basak, Rajni Pande, Shweta Roy, S.V.L.S. Rao and P. Singh, "Comparison of FD and FFDD lattices for DTL", InPAC-2005, VECC, March 1-5, 2005, page 174.
14. R.P. Anand, T.K. Basu, B.K. Godwal, V.K. Handu, S. Kailas, P.K. Nema, M.M. Pande, B.V. Rama Rao, M.K.V. Rao, V.C. Sahni and P. Singh, "Design of a RFQ based 14 MeV Neutron Generator for studying neutron multiplication

- in a Sub-Critical Assembly”, Proc. DAE Symp. Nucl. Phys. (India), 46B, 574 (2003).
15. Shweta Roy, T. Basak, Rajni Pande, S.V.L.S. Rao, M. Aslam, P. Jain, P. Singh, P.K. Nema, S. Kailas and V.C. Sahni, “Physics design of a 400 keV RFQ for deuteron beam”, BARC/2005/I/005.
 16. Shweta Roy, Rajni Pande, T. Basak, S.V.L.S. Rao and P. Singh, “Design of tuner for the 400 keV deuteron RFQ”, InPAC-2005, VECC, March 1-5, 2005, page 58.
 17. M. Aslam, T. Basak, P. Jain, P. Singh and P.K. Nema, “Engineering design and analysis of 400 keV RFQ for deuteron beam”, DAE-BRNS Nucl. Phys. Symp., 47B(2004) 572.
 18. P. Singh, S.V.L.S. Rao, Rajni Pande, T. Basak, Shweta Roy, M. Aslam, P. Jain, S.C.L. Srivastava, Rajesh Kumar, P.K. Nema, S. Kailas, V.C. Sahni, “Accelerator Development in India for ADS Programme”, Proceedings of Workshop on physics of accelerator driven sub-critical systems for energy and transmutation, University of Rajasthan, Jaipur, Jan 23-25, 2006 –to be published in Pramana.
 19. Rajni Pande, Shweta Roy, T. Basak, S.V.L.S. Rao and P. Singh, “Beam Dynamics for the 1 GeV, 30 mA Linac for ADS”, submitted to InPAC-2006.

ABOUT THE AUTHORS



Dr. Pitamber Singh, a graduate of the 19th batch of BARC Training School, joined Nuclear Physics Division, BARC in 1976. He received his Ph.D. degree in Physics from Mumbai University in 1983. In addition to designing

and building the first 2 MV Tandem Accelerator, he has made an outstanding contribution in setting up the 6 MV Folded Tandem Ion Accelerator (FOTIA) facility at BARC. He was conferred DAE’s Technical Excellence Award for the year 2000 for his excellent contributions towards indigenous development of accelerator technology in the country. He is a life member of “The National Academy of Sciences, India”. Dr Singh is working on the development of High Intensity Proton Accelerators for the ADS programme of DAE. Presently, he is Head, FOTIA Section of the Nuclear Physics Division, BARC.



Mr S.V.L.S. Rao did his Masters in Physics from University of Hyderabad in 2000 and joined Nuclear Physics Division in 2001 after one year of Orientation programme at BARC. Shri Rao is presently involved in development of High Current Accelerators.



Ms. Rajni Pande is from the second batch of RRCAT Training School and is working in Nuclear Physics Division since 2002 as Scientific Officer. She did her M.Sc. in Physics from Lucknow University. Ms. Rajni Pande is involved in Physics Studies of the 20 MeV High Intensity Proton Accelerator being developed for ADS Programme.



Ms. T. Basak is working in Nuclear Physics Division, BARC as a Ph.D. student since 2002. She did her Masters in Physics from University of Mumbai. Ms. Basak is involved in Physics Studies of the 20 MeV High Intensity Proton Accelerator being developed for ADS Programme.



Ms. Shweta Roy is working in Nuclear Physics Division, BARC as a Scientific Officer since 2003. She is from the 46th batch of BARC Training School. She did her Masters in Physics from IIT, Delhi. Ms. Shweta Roy is involved in Physics Studies of the 20 MeV High Intensity Proton Accelerator being developed for ADS Programme.



Mr Mohammed Aslam obtained Bachelor degree in Mechanical Engineering from Madan Mohan Malviya Engineering College Gorakhpur. He joined 46th Batch of BARC training school. After completion of training, he joined Nuclear Physics Division of BARC and working on the 'high intensity low energy proton linac'.



Mr P.K. Nema is a mechanical engineer who joined BARC in 1972 as trainee officer. He had worked in the design and construction team of Dhruva reactor in BARC, Pelletron accelerator at TIFR and Indus-1 Synchrotron radiation source in RRCAT, Indore. His areas of special skill include mechanical design and manufacturing of precision components in particle accelerators and their metrology including alignments. He is presently coordinator of ADS programme in BARC.



Dr. S. Kailas, a graduate of the 14th batch of BARC training School, is Associate Director, Physics Group(N), BARC. His field of specialization is accelerator based nuclear physics research and applications. He is a Fellow of the Indian Academy of Sciences, Bangalore.



Mr Piyush Jain is Bachelor of Mechanical Engineering from Rajiv Gandhi Prodigiki Vishwavidyalaya (Bhopal). He joined 47th batch of BARC training school. After completion of training, he joined Nuclear Physics Division of BARC. Presently he is working in the high intensity low energy proton linac project.



Dr. V.C. Sahni holds dual positions, viz Director, Physics Group, BARC, Mumbai & Director, RRCAT, Indore. His current research interests include accelerators, synchrotron radiation sources and their utilization, condensed matter physics, building & using various kinds of advanced equipment for physics research & applications, including electron accelerators & lasers etc. Dr. Sahni is associated with many programs in different R&D institutions in the country. He is Fellow of National Academy of Sciences, India.

SELECTION FOR ABIOTIC (SALINITY AND DROUGHT) STRESS TOLERANCE AND MOLECULAR CHARACTERIZATION OF TOLERANT LINES IN SUGARCANE

V.Y. Patade, P. Suprasanna and V.A. Bapat
Nuclear Agriculture & Biotechnology Division
Bhabha Atomic Research Centre
and
U.G. Kulkarni
Department of Agricultural Biotechnology
Marathwada Agricultural University, Parbhani 431402

This paper was adjudged for the Best Poster Award in the National Conference on "Biotechnological Aspects Towards Cultivation, Utilization and Disease Management of Plants", held at Lal Bahadur Shastri Mahavidyalaya, Dharmabad, Nanded during 24-25 December 2005.

Abstract

Salinity and drought are the major environmental stresses, which greatly affect the plant productivity. Breeding for salinity is difficult and hence the intervention of mutagenesis and tissue culture can greatly facilitate the selection and isolation of useful tolerant lines. In the present study, *in vitro* mutagenesis was employed in the selection of salt and drought tolerant lines in popular sugarcane (*Saccharum officinarum* L.) cv. CoC-671. Embryogenic callus cultures were subjected to gamma irradiation at different doses (0, 10, 20, 30, 40 and 50 Gy). The 20 Gy irradiated cultures exhibited almost 50 % survival response. The embryogenic callus cultures were exposed to inhibitory levels of NaCl (42.8, 85.6, 128.3, 171.1, 213.9, 256.7, 299.5 and 342.2 mM) and polyethylene glycol (PEG 8000, 0.625, 1.25, 2.5, 3.75 and 5.00 mM). Irradiated and non-irradiated cultures showed decrease in callus growth with increasing selection pressure of salt. Salt stressed callus cultures accumulated proline compared to non-stressed calli. Na⁺ and K⁺ contents, quantified with an Atomic Absorption Spectrophotometer revealed clear-cut differences in salt stressed and non-stressed tissues. Leached out Na⁺ and K⁺ was much more than that of retained in tissue in both adapted and unadapted callus cultures. A total of 513 plants were regenerated from NaCl-tolerant calli grown up to 171.1 mM NaCl.

Molecular characterization using RAPD analysis revealed genetic polymorphism between the selected salt and drought tolerant lines from the control plants. RAPD of the putatively tolerant regenerants resolved 72 scorable markers from 9 out of 60 primers screened. Plantlets selected on 0.625 mM PEG (DRT 0.625) had accumulated maximum genetic changes to the control plant (0.69). The genetic similarity between the control and salt & drought tolerant lines ranged between 0.63 and 0.80. An interesting observation was recorded in case of RAPD profile obtained from primer OPH-07. An intense non-parental band was obtained among the selected drought tolerant lines. But the intensity of band exhibited decreasing trend with increasing selection pressure of PEG. The tolerant lines are being evaluated at field level for their genetic stability. The proper evaluation of these spontaneous and induced variants tolerant to salinity and drought may prove highly fruitful venture for its economic cultivation under the stress conditions.

Introduction

Sugarcane (*Saccharum officinarum* L.) is an important agro-industrial sugar crop, contributing about 70% of the world sugar production. Globally, it occupies about 20 Mha of land, a little about 2% of total cropped area, producing 1350 million MT of cane (FAO, 2004). Sugarcane is cultivated as a commercial crop in nearly 60 countries spread over the world. However, being a typical glycophyte, it exhibits stunted growth or no growth under salinity, with its yield falling to 50% or even more of its true potential (Subbarao and Shaw, 1985). Besides this, salinity in root zone of sugarcane decreases sucrose yield through its effect on both biomass and juice quality (Lingle and Weigand, 1996). A large acreage of land is affected with abiotic stress i.e., world's 20% cultivated land and nearly half of all irrigated land is affected by salinity (Rhoades and Loveday, 1990) and 93 Mha of cultivable land is rain fed.

A variation observed among the plants regenerated from cells and tissues termed somaclonal variation (Larkin and Scowcroft, 1981) has been considered a source of new plant genotype for crop improvement (Brettell et al 1886, Hedi and Bridgen, 1996). Somaclonal variation in combination with *in vitro* mutagenesis can be beneficial for the isolation of salinity and drought tolerant lines in a short duration employing *in vitro* selection (Samad et al 2001). *In vitro* selection has been used for selection of salt tolerance (Bressan et al 1985; Rosas et al 2003) and drought and frost tolerance (Adkins et al 1995; Remotti, 1998; Xing and Rajashekhar, 2001). However, the several variants are often unstable or non-heritable being epigenetic changes rather than genetic changes. Such epigenetic alterations may result false positive signals, if one seeks mutational change in a particular phenotype (Nelson, 1977; Schaeffer, 1981).

Evaluation and characterization of the spontaneous and induced variants against salinity and drought may prove highly fruitful venture for its successful cultivation in stress conditions. Therefore, analysis of the induced and spontaneous genetic variation in the regenerated plants is necessary for exploiting these variants for crop improvement. Various molecular techniques viz. RFLP, AFLP, RAPD, microsatellites and ISSR etc. are being used to characterize the induced genetic variation. Among these molecular techniques, Random Amplified Polymorphic DNA (RAPD) analysis (Williams et al 1990) is a simple, quick, easy to perform, require small amount of DNA for analysis and major advantage is that no prior sequence information required. These benefits justify the frequent application of the technique in genetic variability studies (Mondal and Chand, 2002; Bennici et al 2003 and Feuser et al 2003). Keeping these considerations in view, the present investigation was aimed at the *in vitro* selection for salinity and drought tolerance and characterization of the putative salt and drought tolerant regenerants of sugarcane cv. CoC-671, induced by gamma ray mutagenesis *in vitro*.

Materials and Methods

Plant Material

Embryogenic callus cultures of popular sugarcane cv. CoC-671 (Krishna) were established from young leaf explants and maintained through regular subcultures.

Multiplication of embryogenic calli

The callus was induced and multiplied on to MS medium supplemented with 100mg/l malt extract, 100mg/l L-glutamine, 1g/l casein hydrolysate, 5% coconut water, 1mg/l 2,4-D and 3% sucrose gelled

with 0.2% gel rite. The pH of medium was adjusted to 5.8 before autoclaving. The cultures were incubated in darkness at 25 ± 2 °C and subcultured at every three-week interval.

Radio sensitivity studies

Embryogenic calluses were subjected to gamma radiation using ^{60}Co , as a source in Gamma Cell 220 at dose rate of 9.6 Gy/min. The irradiation doses were 0, 10, 20, 30, 40 and 50 Gy.

Regeneration of plants

Plantlets were regenerated after 2-3 weeks of transfer of callus on regeneration medium, i.e., MS medium of the same composition as above but without 2,4-D. The rooted plantlets were hardened in the green house.

In vitro selection for salinity tolerance

Gamma irradiated and non-irradiated calluses (200 mg) were cultured on multiplication medium supplemented with different levels of salt-NaCl (0.0, 42.8, 85.6, 128.3, 171.1, 213.9, 256.7, 299.5 and 342.2 mM).

Estimation of proline accumulation

Free proline content of both adopted and non-adapted callus was determined as per the procedure of Bates (1973). 500mg non-adapted and adapted callus (exposed to different levels of salt) was used for the study.

Na⁺ and K⁺ analysis

Na⁺ and K⁺ content of both NaCl adapted and unadapted calluses were assayed by the procedure earlier reported (Basu et al. 2002). Na⁺ and K⁺ contents of both leachates and tissue extracts were quantified with an Atomic Absorption Spectrophotometer (GBC 904 AA, GBC

Scientific Equipment PTY LTD, Australia) and expressed as $\mu\text{mol g}^{-1}$ fresh weight.

RAPD analysis

DNA isolation

Genomic DNA was isolated from selected tolerant lines using a short protocol earlier standardized for sugarcane tissues in this laboratory (Desai et al 2005). 50 mg of the leaf tissue was used for the study. The isolated DNA (2 μl) was loaded on to 0.7 % agarose gel to detect the quality of DNA. The DNA sample was diluted with MilliQ water and the OD of different diluted samples was taken at 260 nm. The samples were then diluted so as to get the final concentration at 50 ng/ μl .

PCR optimization

The different components of PCR were optimized (Table 1) to get appropriate amplification product from the sugarcane genomic DNA. Various concentrations of genomic DNA (50, 100, 150 and 200 ng per 25 μl reaction mix), MgCl₂ (1.5, 2.5 and 3.5 mM) and *Taq* DNA polymerase (0.5 and 0.6 U) were used. For primer annealing, the different temperatures (35, 36, 37, 38, 39 and 40 °C) were tested.

Table 1: Primers selected for RAPD analysis

Sr.No	Primer	Sequence	G+C%
1.	OPH-03	5'-AGACGTCCAC-3'	60
2.	OPH-04	5'-GGAAGTCGCC-3'	70
3.	OPH-05	5'-AGTCGTCCCC-3'	70
4.	OPH-07	5'-CTGCATCGTG-3'	60
5.	OPH-09	5'-TGTAGCTGGG-3'	60
6.	OPH-12	5'-ACGCCCATGT-3'	60
7.	OPH-19	5'-CTGACCAGCC-3'	70
8.	OPA-03	5'-AGTCAGCCAC-3'	60
9.	OPA-02	5'-GAGGATCCCT-3'	60

Primer selection

Based on the previous investigations on RAPD analysis carried out with sugarcane embryogenic cultures and somaclones in this laboratory, the 60-decamer oligonucleotide primers from different sets (OPA, OPE, OPF and OPH) from Operon Technology Inc., USA were considered. Among the primers screened for sugarcane genome, the best-suited nine primers (Table 2) that showed distinct banding pattern were selected for the present RAPD study.

Table 2: Optimized PCR mastermix composition

Sr. No	Reagents	Vol. (µl)
1.	Assay buffer (10X)	2.50
2.	dNTPs (10 mM)	2.00
3.	Primer (30 ng/µl)	1.00
4.	MgCl ₂	1.00
5.	Taq DNA polymerase (3 U/µl)	0.20
6.	Sterile MilliQ water	13.30

PCR amplification

Amplification reactions were performed in a MJ Research, USA (PTC100) thermocycler. The reaction conditions were initial denaturation at 94°C for 5 minutes, 40 cycles each consisting of denaturation step of 1 min at 94°C, primer annealing at 37 °C for 1.5 min, primer extension at 72 °C for 2 min and final extension step at 72°C for 10 min.

The amplified products were subjected to agarose gel electrophoresis using 1.5% agarose and the gel was analyzed on a gel documentation system. The sizes of amplification products were determined by comparison

with λ DNA digested with *Hind* III and *Eco*RI marker.

Data analysis

RAPD bands were scored as present (1) or absent (0). The data was used for similarity-based analysis using the programme NTSYS-Pc (version 2.02) developed by Rohlf (1990). Jaccard's coefficient (F') was calculated using the programme SIMQUAL. Similarity coefficients were used to construct UPGMA (Unweighted Pair Group Method with Average) dendrogram.

Results

Radio-sensitivity studies of embryogenic callus cultures of sugarcane cv. CoC-671

Percent survival showed linear decreasing trend with increasing irradiation dose (Fig. 1). The highest survival was observed in the control cultures (85.7%) in terms of white proliferating clumps while the lowest survival was noted in 50 Gy irradiated cultures (Fig.2). The dose of 20 Gy was observed as the LD₅₀ dose for sugarcane embryogenic callus cultures. Regeneration

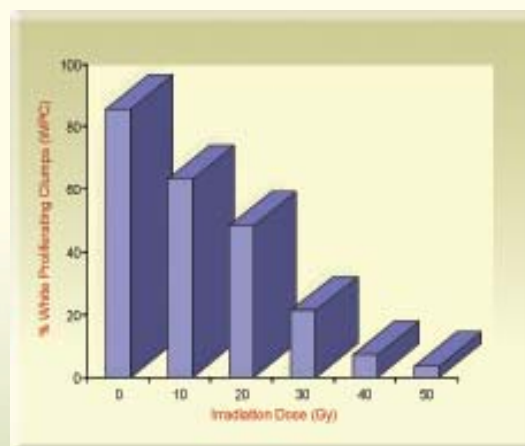


Fig. 1: Effect of gamma irradiation on survival of embryogenic calli of sugarcane cv. CoC-671

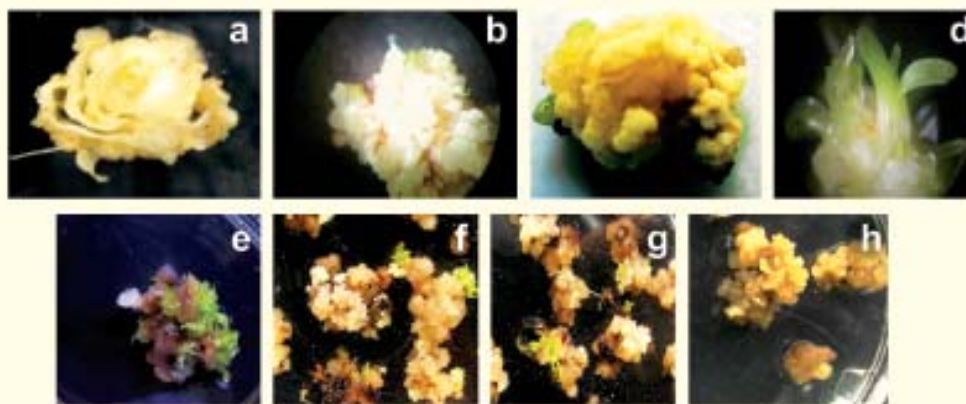


Fig.2 : Regeneration from irradiated calli of sugarcane cv. CoC-671
a- Induction of callus; b & c- stages in embryogenesis; d- Regeneration from control calli;
e, f, g & h- Initiation of regeneration from calli irradiated at 10, 20, 30 & 40 Gy respectively.

response of irradiated callus cultures was very less beyond 20 Gy gamma irradiation.

Studies on in vitro mutagenesis and selection for salinity tolerance

Irradiated callus cultures on salt selection media showed decrease in callus growth with increase in salt concentration (Fig. 3). In case of 10 Gy irradiated cultures, regeneration was observed only

in 85.6 mM NaCl selection medium. The cultures with 20 Gy irradiation showed regeneration in 42.8 mM and 85.6 mM NaCl selection medium. Survival was observed on selection medium with 213.9 mM NaCl concentration, in case of 30 Gy irradiated cultures. The 40 Gy irradiated cultures did not exhibit regeneration upon transfer to NaCl selection media. The 50 Gy irradiated cultures produced shoots in 128.3 salt selections.

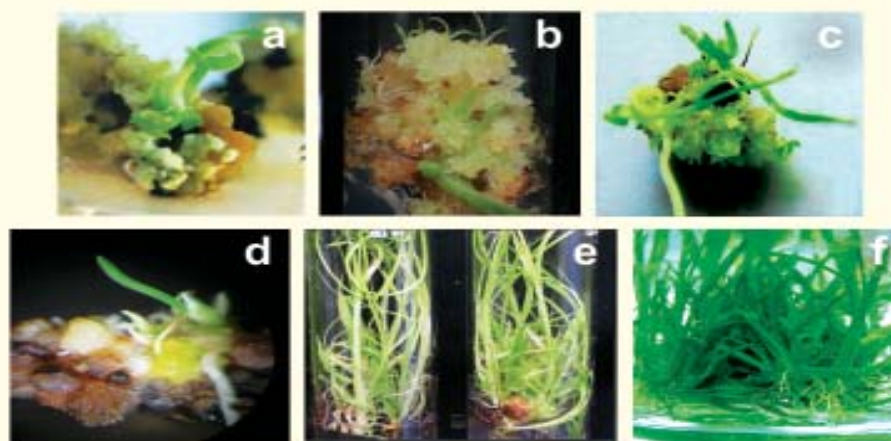


Fig. 3: Regenerants selected in vitro on different lethal doses of salt (NaCl) and PEG
a & b-Regeneration on PEG selection medium; c- shoots regenerated on 42.8mM NaCl;
d & e- regeneration on 171.1mM NaCl medium and f- rooting of the selected plantlets

Studies on proline accumulation in salt stressed callus cultures

The stressed calli (500 mg) were used to estimate proline accumulation. Salt stressed callus cultures exhibited higher levels of free proline content as compared to the control. The 85.6 mM NaCl stressed calli exhibited about 200% proline accumulation that of the control treatment. However, the stressed cultures with 128.3 mM and higher concentrations showed decrease in proline content with increasing salt concentrations.

Na⁺ and K⁺ analysis

a) *Sodium and Potassium content in unadapted NaCl stressed (6Hrs) callus cultures*

Leached out sodium was much more than that of retained in tissue (Fig. 4), but both leached and retained

if considered individually, exhibited linear accumulation with increasing concentration of NaCl in stress medium. The retained Na content was much higher than retained K except in control.

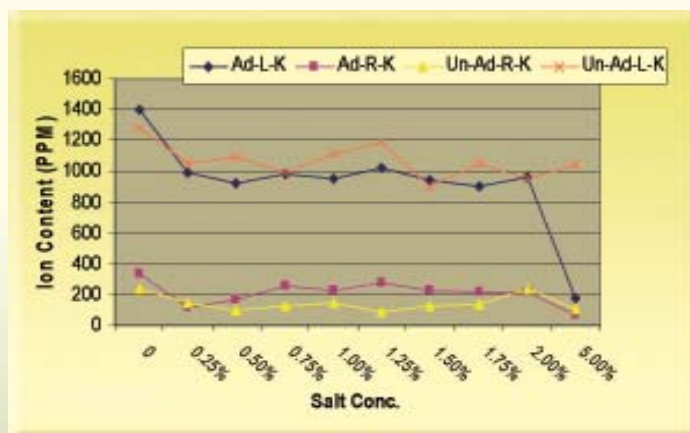


Fig.5 : Potassium ion content in adapted and unadapted NaCl stressed sugarcane calli

The leached out K (Fig. 5) was more than that of retained in tissue. The K retained exhibited little increase with increasing salt concentration. The content of K leached showed less variation with increasing salt concentration in stress medium.

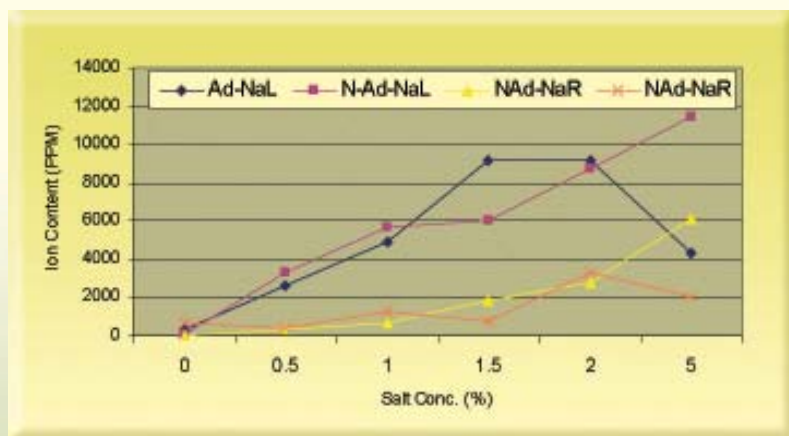


Fig.4 : Sodium ion content in adapted and unadapted NaCl stressed sugarcane calli

b) *Sodium and Potassium content in adapted and unadapted NaCl stressed (4Hrs) callus cultures*

The leached Na content in unadapted callus was found more than that of leached in adapted one. Retained sodium content in unadapted callus was more than that of retained in adapted callus up to 171.1 mM NaCl stress,

whereas for higher NaCl concentration sodium retained in adapted tissue was more than sodium retained in unadapted callus.

The sodium leached in both adapted and unadapted callus showed increasing trend with increasing NaCl concentration in stress medium.

The potassium leached in both adapted and unadapted callus did not exhibit any variation with increasing NaCl concentration. The same was true for in case of potassium retained in tissue. Potassium retained in adapted callus was observed to be higher than retained in unadapted callus. Inversely the potassium leached in adapted callus was lower than unadapted one.

Field Evaluation

The putatively tolerant sugarcane clones were hardened (Fig. 6) initially on sand and soil rite and then the hardened plantlets were transferred to polybags filled with potting mixture. About 90% survival was observed during initial hardening. The well hardened plants were then transplanted to field for studying the field performance of the clones (Fig. 7).

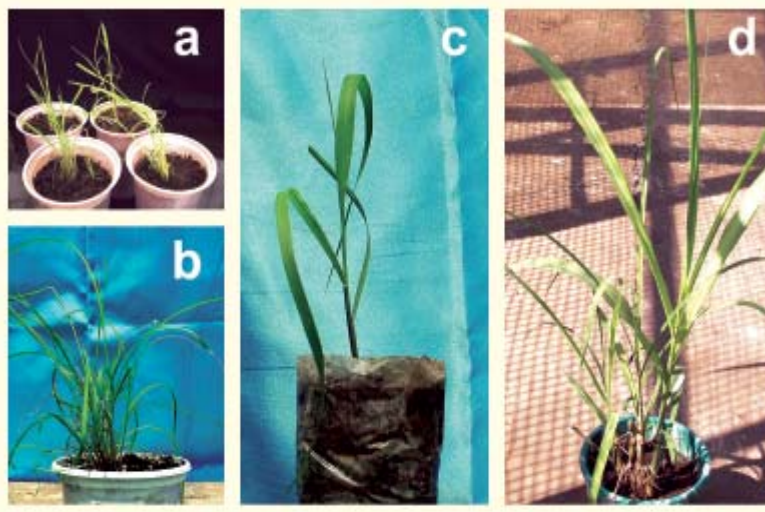


Fig. 6 : Hardening of *in vitro* selected salinity tolerant sugarcane clones a & b – Initial stages in hardening; c- Hardening in Poly bag containing potting mixture & d- Well hardened plant



Fig. 7 : Field evaluation of selected tolerant sugarcane clones

Optimization of PCR conditions for RAPD analysis

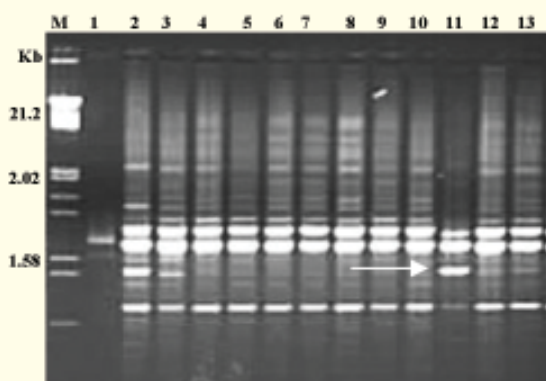
The optimization of PCR condition is of prime importance in RAPD analysis of genetic variability. Satisfactory results were not obtained following the PCR conditions in earlier reports (Saif et al 2001) for

sugarcane RAPD. The concentration of $MgCl_2$ affected the number and intensity of bands. The $MgCl_2$ (2.5 mM) produced scorable RAPD banding pattern whereas the concentrations below 2.5 mM produced faint bands or no bands due to increase in stringency with decrease in the concentration. Of the different concentrations of genomic DNA tried (50, 100, 150 and 200 ng per 25 μ l reaction mix), 150 ng was found optimum. The lower DNA quantity yielded less intense bands, whereas the higher concentrations added background effect. *Taq* DNA polymerase (0.6U) resulted good amplification of sugarcane genomic DNA as compared to 0.5 U. Of the different primer annealing temperatures (35,36,37,38,39 and 40 °C) opted, 37 °C was found to be optimum. Band number decreased above the annealing temperature of 37°C and no bands were observed above 39°C. The OPH-3 and OPH-20 were used for the PCR optimization. The same conditions (Table. 2) were found optimum for other primers as well as DNA samples

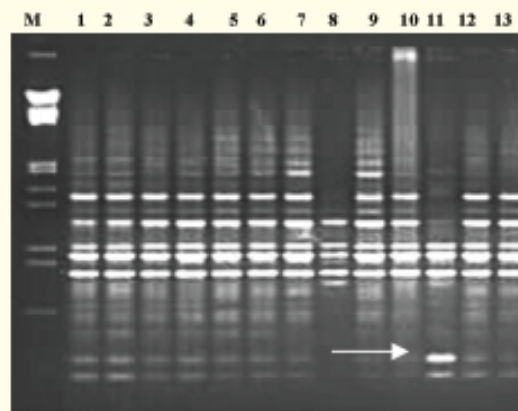
therefore followed as such in rest of the experiments.

RAPD analysis

The genetic variability among the *in vitro* mutagenized and selected plants was analyzed using RAPD molecular marker technique. Of the total 60 random decamer primers (OPH-A, OPH-C, OPH-D, OPH-E, OPH-F and OPH-H) screened, the nine decamer primers, those gave sufficient intense bands were selected for RAPD analysis. A total of 72 RAPD bands were obtained. On an average each primer produced 8 bands. The amplification products ranged from 0.1 Kb to 2 Kb. The primer OPH-05 (Fig. 8b) produced maximum 10 bands, out of which three were polymorphic. The primer OPH-09 produced five polymorphic bands from total of nine bands. An interesting observation was recorded in case of RAPD profile obtained from primer OPH-07 (Fig. 8a).



(a)



(b)

Fig. 8a: RAPD profile obtained with OPH-7

Fig. 8b: RAPD profile obtained with OPH-5

M- Marker (λ DNA/EcoRI & *Hind* III); 1- SLT 171.1 (10 Gy); 2- SLT 171.1 (20 Gy); 3- SLT 42.8; 4- SLT 85.6; 5-SLT 128.3; 6- control; 7-10 Gy; 8- 20Gy; 9- 50 Gy; 10-DRT 0.625; 11-DRT 1.25; 12-DRT 2.5; and 13-DRT 3.75

An arrow indicates an intense non-parental band obtained among the selected drought tolerant lines.

An intense non-parental band was obtained among the selected drought tolerant lines. But the intensity of band exhibited decreasing trend with increasing selection pressure of PEG. The RAPD profile revealed genetic polymorphism among the selected drought tolerant and salt tolerant lines from the control plant. The data on the presence or absence of bands from a particular primer for all the control, salt and drought tolerant & irradiated plants was used for similarity-based analysis and Jacquard's similarity coefficient was calculated. The genetic similarity between mother and regenerated

10 Gy irradiated callus on selection medium containing 171.1 mM NaCl (SLT 10 Gy) and regenerants from 20 Gy irradiated calli on selection medium containing 171.1 mM NaCl (SLT 20 Gy) into first group; regenerants on selection medium containing NaCl 42.8 (SLT 42.8), 128.3 (SLT 128.3), 85.6 mM (SLT 85.6) and PEG 3.75 mM (DRT 3.75) into second group; regenerants from 10 Gy (10 Gy), 50 Gy (50 Gy) irradiated calli, PEG 1.25 mM (DRT 1.25) and 2.50 mM (DRT 2.50) into third group; control, regenerants from 20 Gy irradiated callus (20 Gy) and plantlets selected on

selection medium containing PEG 0.625 mM (DRT 0.625) into fourth group. Interestingly, the dendrogram also separated SLT, DRT and irradiated regenerants horizontally into two groups suggesting that SLT regenerants completely delineated from others. SLT 171.1 (10 Gy) and SLT 171.1 (20 Gy) are placed together depicting the high similarity between them. The SLT regenerants are placed away from the control supporting the polymorphism revealed by RAPD profiles. This suggests that the irradiated and salt stressed regenerants are better for selection

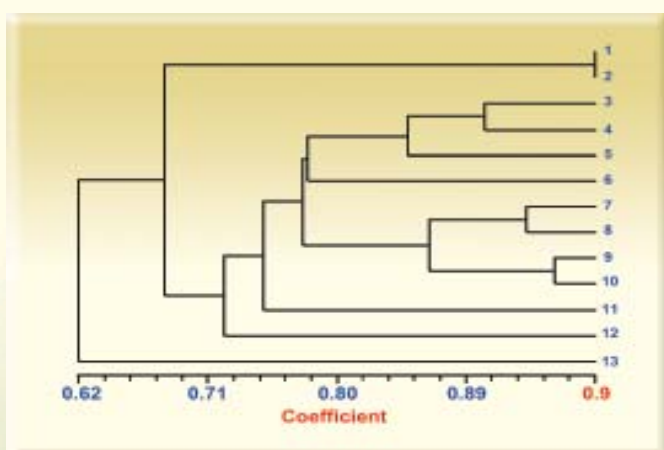


Fig. 9: Dendrogram showing genetic relationship between the parent (control) and regenerants selected on salt (NaCl) & PEG stress medium

1- SLT 171.1 (10 Gy); 2- SLT 171.1 (20 Gy); 3- SLT 42.8; 4- SLT 85.6; 5-SLT 128.3; 6- control; 7-10 Gy; 8- 20Gy; 9- 50 Gy; 10-DRT 0.625; 11-DRT 1.25; 12-DRT 2.5 and 13-DRT 3.75

plants was on an average 0.63. Plantlets selected on 0.625% PEG (DRT 0.625) had accumulated maximum genetic changes to the control plant (0.69). The genetic similarity between the control and salt & drought tolerant lines ranged between 0.63 and 0.80.

Based on the dendrogram (Fig. 9), the regenerants (Fig. 3) were divided into four groups based on secondary branching, which placed regenerants from

of mutants. The DRT regenerants are placed close to the control depicting that these did not accumulate much variation as compared SLT and SLT Gy. The coefficient of similarity of 0.8 to SLT 171.1 (10 Gy) and 0.63 to SLT 171.1 (20 Gy) suggest that regenerants have accumulated much variation compared to other regenerants. The value of 0.80 for SLT 171.1 (10 Gy) regenerants is much similar to control when compared

to others. The genetic distances of 0.63 to 0.8 suggest that there is a genetic variation among these regenerants at fine scale.

Discussion

Somaclonal variation occurs among the tissue culture regenerated plants. Cellular and molecular mechanisms behind the variations are mitotic irregularities leading to chromosomal instability, occurrence of gene amplification or deletion, gene inactivation or reactivation of silent genes, transposition and somatic crossing over, DNA methylation in case of epigenetic variation and point mutations (Larkin and Scowcroft 1981; Muler et al 1990). *In vitro* mutagenesis can be useful if results in additional effects with respects to mutation frequency and mutation spectrum in combination with quicker positive results and no effects on survival and fertility of the treated cultures. Crop breeding programme can be speeded up by combining the radiation technique with *in vitro* culture methods (Maluszynski et al 1995). *In vitro* mutagenesis has contributed to genetic improvement in several crop plants such as pineapple (Lepade et al, 1995), banana (Raop et al, 1995) and grape (Kuksova et al, 1997).

Detection of variants is of immense importance in order to utilize these in crop improvement. The variants may have genetic or epigenetic basis therefore early detection is of prime importance. It is rather difficult to detect the genetic variation from morphological features. Among the different molecular techniques, RAPD is widely used to study the variation at DNA level among the variants (Orapeza et al. 1995; Rout et al 1998; Soniya et al 2001; Geisteira et al 2002 and Bennici et al 2003).

At stringent annealing conditions, even slight base change at the primer-annealing site can result in

presence or absence of RAPD bands. It is therefore clear that *in vitro* mutagenesis and tissue culture conditions have induced varied amount of genetic changes among the selected the salt and drought tolerant plants from irradiated and non-irradiated callus cultures. The results from the present study are in conformity with the study by Saif et al (2001) on the detection of genetic variation using RAPD technique among the irradiated and salt stress (200mM NaCl) calli. Out of six primers used only two primers enabled the identification of polymorphism among variants of sugarcane. RAPD profile showed the polymorphism among irradiated 0-40 Gy and salt selected (0, 100, 150 and 200mM NaCl) variants. The present study on RAPD analysis of genetic variation among the *in vitro* selected drought and salinity tolerant from irradiated and non-irradiated callus cultures suggest that the variation can be detected at the stage of regeneration even before hardening in the green house. The technique has proved very sensitive for characterization of *in vitro* selected salinity and drought tolerant plants in sugarcane. In this study, dendrogram also separated SLT, DRT and irradiated regenerants horizontally into two groups suggesting that SLT regenerants completely delineated from others. SLT 171.1 (10 Gy) and SLT 171.1 (20 Gy) are placed together depicting the high similarity between them. The SLT regenerants are placed away from the control supporting the polymorphism revealed by RAPD profiles. This suggests that the irradiated and salt stressed regenerants are better for selection of mutants. The DRT regenerants are placed close to the control depicting that these did not accumulate much variation as compared SLT and SLT Gy. Lee et al (2002) could detect the radiation-induced variations in sweet potato using RAPD technique. However the

polymorphism could not be detected among regenerates from the non-irradiated calli.

The application of molecular markers technique will prove helpful to establish efficient system for selection in vitro the abiotic stress tolerant clones through in vitro mutagenesis. Mutagenesis through radiation in combination with tissue culture technique seems suitable for the improvement of vegetatively propagated crops (Maluszynski et al, 1995; Lee et al, 2002). The present study on RAPD analysis of genetic variation among the in vitro selected drought and salinity tolerant from irradiated and non-irradiated callus cultures suggest that the variation can be detected at the stage of regeneration even before hardening in the green house. The technique has proved very sensitive for characterization of in vitro selected salinity and drought tolerant plants in sugarcane. The proper evaluation of these spontaneous and induced variants against salinity and drought may prove highly fruitful venture for its economic cultivation under the stress conditions.

Conclusions

In vitro selection shortens the time considerably for selection of desirable trait under selection pressure and has been used for selection of abiotic stress. Somaclonal variation in combination with in vitro mutagenesis can be beneficial for isolation of salinity and drought tolerant lines in a short duration employing in vitro selection. Genetically stable somaclones, confirmed in field-testing can be used in a crop improvement program. The present study on RAPD analysis of genetic variation among the in vitro selected drought and salinity tolerant from irradiated and non-irradiated callus cultures suggest that the variation can be detected at the stage of regeneration even before hardening in the green house.

Acknowledgements

Authors would like to acknowledge cooperation and help from Dr. Nitin S. Desai, Dr. B. R. Majunatha, Mr J. Souframanien, NA&BTD and Dr. Sahayog N. Jamdar, FTD, BARC.

References

1. Adkins, S.W., Kunanuvatchaidach, R. and Godwin, I.D. (1995). Somaclonal variation in rice: Drought tolerance and other agronomic characters. *Australian Journal of Botany*, 43(2): 201-209.
2. Basu, S., Gangopadhyaya, G and Mukharjee, B.B. (2002). Salt tolerance in rice in vitro: Implication of accumulation of Na⁺, K⁺ and proline. *Plant Cell, Tissue and Organ Culture* 69: 55-64.
3. Bates, L.S. (1973) Rapid determination of free proline for water stress studies, *Plant and Soil*. 39: 205 – 207.
4. Bennici, A., Anzidei, M., Vendramin, G.G. (2003). Genetic stability and uniformity of *Foeniculum vulgare* Mill. regenerated plants through organogenesis and somatic embryogenesis. *Plant science* : 1-7.
5. Bressan, R.A., Singh, N.K., Handa, A.K., Kononowicz, A. and Hasegawa, P.M. (1985). Stable and unstable tolerance to NaCl in cultured tobacco cells. In: Freeling, M. (ed.) *Plant genetics: Proceedings of third annual ARCO Plant Cell Research Institute –UCLA symposium on Plant Biology: New Series*, A. R. Liss, New York: 755-769.
6. Brettell, R.I.S., Dennis, E.S., Scowcraft, W.R., Peacock, W.J. (1986). Molecular analysis of a

- somaclonal mutant of maize alcohol dehydrogenase. *Mol Gen Genet* 202:235-239.
7. Desai, N.S., Suprasanna, P., Bapat, V.A. (2005). Molecular Characterization Of Culture-Induced Genetic Variability Among Regenerated Plants Obtained Through Direct And Indirect Somatic Embryogenesis In Sugarcane. In : Proc. 26th PTCA (India) Conference & National Symp. Biotechnology. St. Aloysius College, Mangalore 208-219.
 8. F.A.O. (2004). <http://www.faostat.fao.org>
 9. Feuser, S., Meler, K., Daquinta, M., Guerra, M.P. and Nodari, R.O. (2003). Genotypic fidelity of micropropagated pineapple (*Ananus comosus*) plantlets assessed by isozyme and RAPD markers. *Plant Cell, Tissue and Organ Culture*, 72: 221-227.
 10. Geisteira, A.S., Otoni, W.C., Barros, E.G. and Moreira, M.A. (2002). RAPD-based detection of genomic instability in soybean plants derived from somatic embryogenesis. *Plant Breeding*, 121: 269-271.
 11. Hadi, M.Z., Bridgen, M.P. (1996). Somaclonal variation as a tool to develop pest resistant plants of *Torenia fournieri* Compacta Blue. *Plant Cell Tiss and Org Cult* 46:43-50.
 12. Kuksova, V.B., Piven, N.M., Gleba, Y.Y. (1997). Somaclonal variation and in vitro induced mutagenesis in grapevine. *Plant Cell Tiss and Org Cult* 49:179-186.
 13. Lapade, A.G., Velug, A.M.S., Santos, I.S. (1995). Genetic improvement of the queen variety pineapple through induced mutation and in vitro culture techniques. FAO/IAEA In: International Symposium, Vienna, 19-23 June 1995, IAEA-SM-340;145-146.
 14. Larkin, P.J. and Scowcroft, W.R. (1981). Somaclonal variation – a novel source of variability from cell cultures for plant improvement. *Theor Appl Genet*, 60: 197-214.
 15. Lee, Y.I., Lee, I.S., Lim, Y.P. (2002). Variations in sweetpotato regenerates from gamma ray irradiated embryogenic callus. *J. Plant Biotechnology*.4 (4): 163-170.
 16. Lingle, S.E. and Wiegand, C.L. (1996). Growth and yield responses of sugarcane to saline soil:II. Sucrose biochemistry in individual internodes. *Proc. Inter American Sugarcane Seminars* 93-102.
 17. Maluszynski, M., Ahloowalia, B.S., Sigurbjornsson, B. (1995). Application of in vitro mutation techniques for crop improvement. *Euphytica* 85:303-315.
 18. Mondal, T.K. and Chand, P.K. (2002). Detection of genetic variation among micro propagated tea {*Camellia sinensis* (L). O.Kuntze} by RAPD analysis. *In vitro Cell. Biol.-Plant*, 38: 296-299.
 19. Muler, E., Brown, P.T.H., Hartke, S. and Lorz, H. (1990). DNA variation in tissue-culture-derived rice plants. *Theor Appl Genet*, 80: 673-679.
 20. Murashige, T., Skoog, F. (1962). A revised medium for rapid growth and bioassays with tobacco tissue cultures. *Plant Physiol*, 15: 473-497.
 21. Nelson, O.E. (1977). The applicability of plant cell and tissue culture techniques to plant improvement. In Rubenstein I, Phillips R, Green CE (eds), *Molecular Genetic Modification of Eukaryotes*, Academic Press, New York 67-76.

22. Orapeza, M., Guevara, P., Garcia, E. and Ramirez, J.L. (1995). Identification of somaclonal variants of sugarcane (*Saccharum* spp.) resistant to Sugarcane Mosaic Virus via RAPD markers. *Plant Molecular Biology Reporter*, 13 (2): 182-191.
23. Rao, P. S., Ganapathi T.R., Bapat, V.A., Suprasanna, P. (1995). In vitro propagation and mutation induction in banana. IAEA-SM-340:191-192.
24. Remotti, P.C. (1998). Somaclonal variation and in vitro selection for crop improvement. In: Jain, S.M., Brar, D.S. and Ahloowalia BS (eds), Somaclonal variation and induced mutations in crop improvement. Kluwer Academic Publishers, Dordrecht 169-201.
25. Rhoades, J.D. and Loveday, J. (1990). Salinity in irrigated agriculture. In American Society of Civil Engineers, Irrigation of Agricultural Crops (Monograph 30) Steward BA and Nielsen DR (eds) American Society of Agronomists, 1089-1142.
26. Rohlf, F.J. (1990). NTSYS.Pc. Numerical taxonomy and multi variate analysis system, version 2.02. Applied bio statistics, New York.
27. Rosas, H.G., Garcia, S.S., Reyes, G.R., Ontiveros, J.L.R. and Villasenor, A.C.R. (2003). Preliminary results on in vitro selection for tolerance to chloride excess in avocado. *Revista Chapingo Serie Horticulture* 9(1): 39-43.
28. Rout, G.R., Das, P. and Raina, S.N. (1998). Determination of genetic stability of micropropagated plants of ginger using Random amplified Polymorphic DNA (RAPD) markers. *Bot Bull Acad Sin*, 39: 23-27.
29. Saif-Ur-Rashid, M., Asad, S., Zafar, Y. and Washeed, R.A. (2001). Use of radiation and invitro techniques for development of salt tolerant mutants in sugarcane and potato. IAEA-TECDOC, 1227: 51-60.
30. Samad, M.A., Begum, S., Majid, M.A. (2001). Somaclonal variation and irradiation in sugarcane calli for selection against red rot, water logged conditions and delayed or non-flowering characters. IAEA-TECDOC-1227: 45-50.
31. Schaeffer, G.W., (1981). Mutations and cell selections: Increased protein from regenerated rice tissue cultures. *Env Exp Bot*, 21: 333-345.
32. Soniya, E.V., Banerjee, N.S. and Das, M.R. (2001). Genetic analysis of somaclonal variation among callus derived plants of tomato. *Current Science*, 80 (9): 1213-1215.
33. Subbarao, M. and Shaw, M.A.E. (1985). A review of research on sugarcane soils of Jamaica. *Proceeding of Meeting West Indies Sugar Technol.* 2: 343- 355.
34. Williams, J.G.K., Kubelik, A.R., Livak, K.J., Raflaski, J.A. and Tingey, S.V. (1990). DNA polymorphism amplified by arbitrary primers are useful as genetic markers. *Nucleic Acids Res*, 18: 6531-6535.
35. Xing, W. and Rajashekar, C.B. (2001). Glycine betaine involvement in freezing tolerance and water stress in *Arabidopsis thaliana*. *Environ Expt Bot*, 46: 21-28.

ABOUT THE AUTHORS



Mr. Vikas Y. Patade has received his M.Sc. degree in Agril. Biotechnology from Marathwada Agricultural University, Parbhani. He was a state topper during his graduation and second topper during Post Graduation from MAU. Presently, he is working as a JRF in the BRNS research Project. His main thrust areas are in vitro mutagenesis & selection for abiotic stress tolerance, biochemical and molecular characterization of abiotic stress response and genetic transformation in sugarcane.



Dr. Umakant G. Kulkarni did his Ph. D in Genetics & Plant Breeding from University of Agricultural Sciences, Dharwad. He is responsible for the release of groundnut cultivars LGN-1 & LGN-2. He has served as the Head of Agricultural Botany and Biotechnology Department at Marathwada Agricultural University, Parbhani and Officer In-Charge, Tissue Culture Project. Presently he is the Associate Dean and Principal, College of Agriculture, Osmanabad, MAU, Parbhani.



Dr. Penna Suprasanna joined BARC in 1991 after obtaining his Ph.D. degree in Genetics from Osmania University, Hyderabad. He is working in the Plant Cell Culture Technology Section of NA&BTD and is engaged in plant biotechnological research on rice, banana and sugarcane. His contributions have been in the areas of cell and tissue culture, somatic embryogenesis, in vitro selection and transgenics. Dr. Suprasanna has to his credit, more than 90 research publications in journals and books published by national and international publishers. His interests are in using plant cell cultures for cellular and molecular genetic manipulation.



Dr. Vishwas A. Bapat is working in the area of plant tissue culture for the last 31 years. Currently he is heading the Plant Cell Culture Technology Section. The main thrust area of his work is on Micropropagation and Genetic Transformation of Plants. He has extensively contributed in the areas of clonal propagation, cell and protoplast culture, synthetic seeds, disease resistance and molecular farming. He has several publications in National and International journals to his credit. He is a Fellow of the National Academy of Sciences, India and the Maharashtra Academy of Sciences.

MEASUREMENT OF ATOMIC PARAMETERS OF SAMARIUM USING TWO-COLOR LASER-INDUCED FLUORESCENCE (LIF)

M L Shah, A K Pulhani, Vas Dev and B M Suri
Laser & Plasma Technology Division
Bhabha Atomic Research Centre

This poster paper was adjudged as one of the three Best posters at the National Symposium on "Recent Trends in Fluorescence Spectroscopy and its Applications; held at the Department of Physics, Kumaun University, Nainital during December 1-3, 2005

Laser Induced Photoionisation (LIP) and Laser Induced Fluorescence (LIF) techniques have yielded rich spectroscopic information for many elements^{1,2}. In LIP, atomic levels in energy region of interest are pumped by multi-step excitation and detected by further photoionisation. In LIF spectroscopy, the fluorescence is collected from the high lying energy levels populated by multi-step excitation. Recently we have identified several new energy levels using these techniques^{3,4}. From our work in atomic samarium, it is noted that many energy levels observed by one technique are not observed by other (and vice versa), which otherwise should be detectable from spectroscopic considerations³. In continuation of our work, we report here, the observation of new high-lying even-parity excited levels of samarium in the energy region 36051.52 cm⁻¹ to 36257.52 cm⁻¹ and their proposed total angular momentum (J) values. We also report second step excitation cross section of two transitions by using saturation method.

SA schematic diagram showing the experimental set-up and details employed in the present work can be found in A.K. Pulhani et al. 2005³. Photons from the first-step dye laser at wavelength λ_1 excite the samarium atoms to some intermediate level and photons from second-step dye laser at wavelength λ_2 excite them further to energy levels in the region of interest as shown in Fig. 1. The first-step dye laser

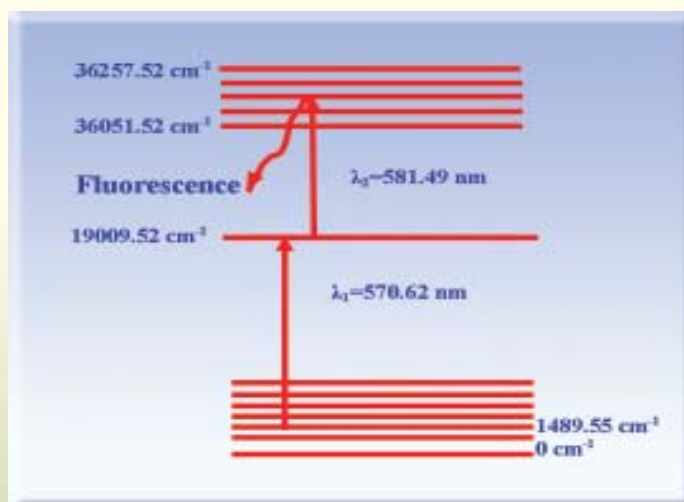


Fig. 1: Excitation scheme

wavelength was fixed by observing non-resonance fluorescence signal from the first-step excited level (19009.52 cm^{-1} to 292 cm^{-1}) and the wavelength (λ_2) of second-step dye laser was scanned in its tuning range. Fluorescence light emitted by samarium atoms was collected and focused by a lens assembly to the entrance slit of $\frac{1}{4}$ -meter monochromator, which was used in a tunable filter mode to cut off contributions from resonance fluorescence at excitation wavelengths and laser scattering from the windows. Output of monochromator was coupled to photomultiplier tube (PMT) at its exit slit for LIF signal, which was further processed by using boxcar averager. Two-color LIF spectrum was recorded as a function of tunable laser wavelength. Single-color fluorescence spectrum of the second-step tuning laser was recorded by blocking the first-step excitation laser and it was used to distinguish between single-color and

two-color resonances produced by the tuning laser. We have observed fifteen resonances by two-color LIF and assigned J values to these levels as listed in Table 1. We compared our observations with the results reported earlier in the same energy region by two-color three-photon ionization spectroscopy^{5,6}.

On comparison, we found four new resonances, which were not observed in earlier reported two-color three-photon ionization spectra^{5,6}. We have already established that fluorescence spectroscopy should be used to identify new levels in complement to two-color three-photon ionization spectroscopy³. Thus we propose four new energy levels in the energy region 36257.52 cm^{-1} to 36051.52 cm^{-1} .

Cross section Measurement: Measurement of photoexcitation cross-section from an excited state

Table 1: Observed two-color resonances and proposed new even parity states of Samarium when first-step excitation laser was fixed at 570.62 nm (1489.55 cm^{-1} (J=3) \rightarrow 19009.52 cm^{-1} (J=2)) transition and the second-step excitation laser was tuned from 577 nm to 587 nm.

Sr. No.	Our value (cm^{-1})	Relative intensity	Reported value (cm^{-1})	Reported J	Proposed New levels and J values
1	36257.52	Strong	36257.64	3	
2	36248.52	Medium	36248.15	2	
3	36224.52	Strong	36223.60	3	
4	36217.52	Medium	36217.11	3	
5	36201.52	Strong	36201.16	2	
6	36188.02	Strong	36188.80	2	
7	36171.52	Weak	New	-	New level, J=1-3
8	36168.52	Weak	New	-	New level, J=1-3
9	36162.52	Strong	36162.03	3	
10	36159.52	Medium	New	-	
11	36134.52	Strong	36133.72	3	
12	36105.52	Weak	New	-	New level, J=1-3
13	36086.52	Medium	36087.34	3	
14	36057.52	Medium	36057.51	2	
15	36051.52	Medium	New	-	New level, J=1-3

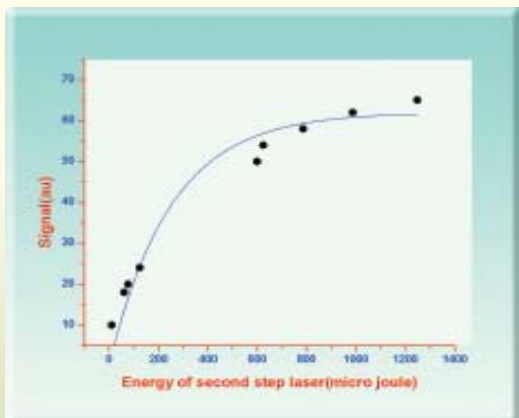


Fig. 2: Saturation curve for 19009.52 cm⁻¹ - 36224.52 cm⁻¹ transitions

of the neutral atom is of great interest from view point of both basic and applied research such as trace analysis and laser isotope separation etc. We have employed two-color LIF technique and saturation method for the measurement of second-step photoexcitation cross-sections of Sm⁷. The variation of two-color LIF signal was studied as a function of second-step laser pulse energy, keeping the first-step laser at saturation. Observation of saturation is quite apparent as shown in Fig.2, which is representative saturation curve for second step transition 19009.52 cm⁻¹ -36224.52 cm⁻¹. These saturation curves provided the values of excitation cross-section. The transitions for which cross section values measured are 19009.52 cm⁻¹ – 36257.52 cm⁻¹ and 19009.52 cm⁻¹ – 36224.52 cm⁻¹. The values of cross section of these transitions are 9.4x10⁻¹⁵ cm² and 1.9x10⁻¹⁴ cm² respectively. These values are reported for the first time, as there is no data reported earlier in the literature for the second-step excitation cross-sections.

We have identified four new even-parity energy levels of Samarium and measured the values of second step excited cross section of transitions 19009.52 cm⁻¹ –

36257.52 cm⁻¹ and 19009.52 cm⁻¹ – 36224.52 cm⁻¹, which are reported for the first time.

Acknowledgement

Authors would like to thank Dr. L M Gantayet, Head, LPTD, for his encouragement during this work.

References

1. Observation of new high lying odd levels of U (I) in two color multi photon ionization spectrum, B M Suri, K Dasgupta, P N Bajaj, K G Manohar et. al. , J. Opt. Soc. Am. B, J. Opt. Soc. Am. B 4, 1835-1836, 1987.
2. Laser spectroscopy of U (I) using stepwise excitation and fluorescence detection, E Miron, R David, G Erej et. al., J. Opt. Soc. Am. B 69, 256-264, 1979.
3. High-lying even-parity excited levels of atomic samarium, A. K. Pulhani, M. L. Shah, Vas Dev and B. M. Suri, J. Opt. Soc. Am. B 22, 1117 – 1122, 2005.
4. Two-color photoionization spectroscopy of uranium in a U-Ne hollow cathode discharge tube, Vas Dev, M. L. Shah, A. K. Pulhani and B. M. Suri, Applied Physics B 80, 587 – 594, 2005
5. Investigations of new high-lying even-parity energy levels of the samarium atom below its first ionization limit, T. Jayasekharan, M.A. N. Rizvi and G.L. Bhale, J. Opt. Soc. Am.B, 17, 1607 - 1615 (2000).
6. Observation of new even-parity states of Sm I by resonance ionization mass spectrometry, T. Jayasekharan, M.A. N. Rizvi and G.L. Bhale, J. Opt. Soc. Am.B, 13, 641- 648 (1996).
7. Measurement of oscillator strengths in Uranium using laser techniques, A Petit, R Avil, D L'Hermite and A Pailloux, Physica Scripta, Vol. T 100, 114-119, 2002 and references there in.

ABOUT THE AUTHORS



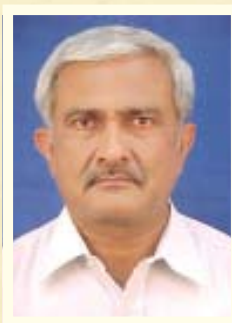
Mr Mukesh Lal Shah joined Laser and Plasma Tech. Division of BARC, in 2000, through 9th M. Tech. batch (Orientation Course for Engineering Postgraduates) of Training School. Prior to that, he obtained

M.Sc. in Physics from Kumoun Univ. Nainital and M Tech in Optoelectronics from G S Institute of Tech. and Science, Indore. He has been involved in laser spectroscopy of various materials of interest. His other interests include development of optical fiber based systems for laser spectroscopy applications.



Mr. Anil Kumar Pulhani obtained his Master's Degree in Chemistry from Punjabi University, Patiala. He joined BARC through 35th batch of training school. Since then he is working in the field

of laser spectroscopy of lanthanides and actinides. His current interests include trace level laser spectroscopy.



Dr. B. M. Suri joined the erstwhile Multi Disciplinary Research Section, BARC in 1975 after completing one year orientation course in Physics. Presently he is Head of Applied Spectroscopy

Section in Laser & Plasma Technology Division. He has been involved in setting up Laser spectroscopy laboratory and related research and development. He was awarded Ph. D. by Bombay University in 1985 for his work on optogalvanic effect in uranium discharges. He was a visiting scientist at the University of Mainz, Germany 1988-1990, where he was involved in pioneering development of Resonance ionization laser ion source for ultra-trace analysis applications. His current interests include laser spectroscopy and ultra-trace analysis. He has published about eighty papers in various national and international journals.



Dr. Vas Dev received his M.Sc (Hons School) degree in Physics from Panjab University, Chandigarh in 1982 and joined erstwhile Multi Disciplinary Research Section of BARC after graduating

from 26th batch of training School. His work on development of a frequency stabilized CO₂ laser and studies on dynamic instabilities led to completion of his Ph.D. degree from Bombay Univ. in 1991. He was a visiting Scientist to the University of Kaiserslautern, Germany during 1996-98. His recent research interest includes lasers and laser spectroscopy of lanthanides and actinides. He has published more than 40 research papers in various national and international journals.

FORMATION OF REDOX ACTIVE NANOSELENIUM ON REACTIONS OF OXIDIZING FREE RADICALS WITH SELENOUREA

Beena Mishra, K. Indira Priyadarsini and Hari Mohan
Radiation and Photochemistry Division
Bhabha Atomic Research Centre

and

P. A. Hassan
Chemistry Division
Bhabha Atomic Research Centre

This paper was adjudged as one of the Best Posters in the National Symposium on Radiation & Photochemistry (NSRP-2005) held at University of Karnatak, Dharwad, 17-19 January 2005

Abstract

Reaction of reactive oxygen and nitrogen species with selenourea were studied using different fast reaction techniques. In all these cases elemental selenium were produced as one of the reaction product. The size of the elemental selenium can be controlled to nanometer size by addition of bovine serum albumin or sodium dodecyl sulphate (SDS). The particle size, determined by dynamic light scattering studies (DLS), was dependent on the nature of the oxidant and on the amount of stabilizer. Nanoselenium separated from reactants by dialysis showed redox activity. The studies provide a new strategy of developing selenium compounds and modulating elemental selenium for therapeutic purpose.

Introduction

Selenium is an essential trace element for animals and humans, being a constituent of redox active enzymes like glutathione peroxidase, glycine reductase etc¹⁻³. Selenium compounds also exhibit antioxidant and radioprotecting activity and are free radical scavengers³⁻⁶. Selenium compounds employed for such studies are mostly in the oxidation states of +6,

+4 and -2; on the other hand there are only a few reports on elemental selenium with zero oxidation number (Se⁰). One of the reasons for these limited studies are due to the notion that colloidal selenium has very low bioavailability and biological activity. Recently it has been reported that particles of selenium stabilized to nanometer size exhibit high biochemical activity and have improved bioavailability⁷. There are both

Formation of elemental selenium on oxidation of selenourea

In all the experiments discussed above, treatment of selenourea solutions with any of the above oxidants turned the solutions into pink, which during the course of time changed to a gray precipitate. The possible mechanistic processes leading to the formation of selenium on oxidation of selenourea by the above oxidants is presented in scheme 1. The initially formed pink colored transparent solutions could be stabilized for days with the addition of proteins like BSA or surfactants like SDS, as these solutions are known to stabilize selenium particles by forming either protein conjugates or by the adsorption of surfactants on particle surface.

Characterization of the size of elemental selenium

The size of the elemental selenium particles were characterized by dynamic light scattering studies (DLS)⁹. Hydroxyl radical reaction of aqueous selenourea in the presence of oxygen produced Se nanoparticles that are stabilized by the addition of SDS. Fig. 1(a) and 1(b) show representative plots of the normalized intensity correlation function ($g^2(\tau)-1$) on irradiation of 50 mM and 200 mM selenourea solutions respectively. The shift of the correlation function to higher times with increase in selenourea concentration is an indication of increase in the relaxation time, which in turn reflects the increase in

the average size of Se nanoparticles.

The solid lines in Figs. 1(a) and 1(b) show the fit to the measured data using cumulants and the corresponding average hydrodynamic diameter increased with selenourea concentration, from 37 nm at 50 mM selenourea to a value of 52 nm at 200 mM selenourea. The size distribution is monomodal in nature with relatively small polydispersity (polydispersity index (P.I) < 0). The size distribution is practically unaffected with changes in absorbed dose of 65 Gy to 325 Gy or hydroxyl radical concentrations. In the absence of any stabilizer, oxidation by H_2O_2 produced highly polydisperse and larger particles of Se with average size of ~ 325 nm (Fig.1c) while the presence of stabilizers such as SDS or BSA decreased

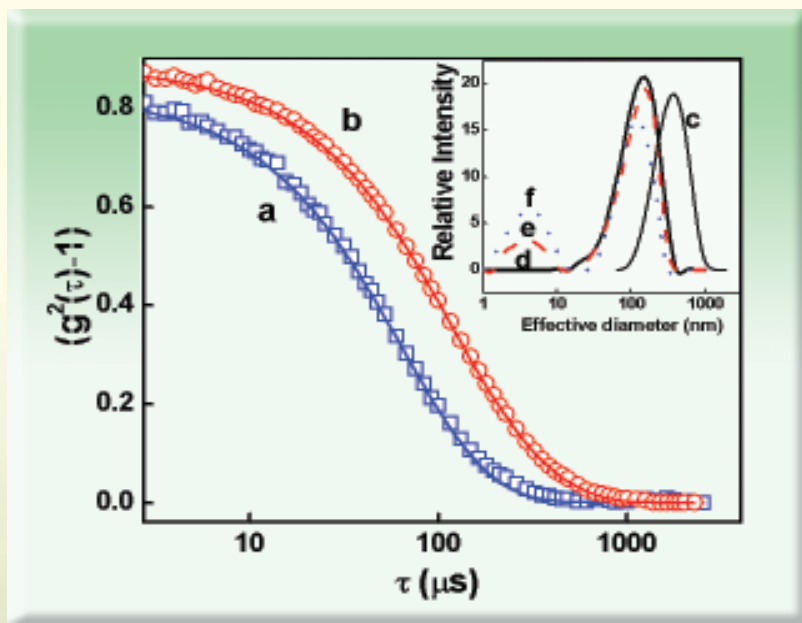


Fig. 1 : Variation of normalized intensity correlation function ($g^2(\tau)-1$) with time for Se nanoparticles prepared by OH radical reaction with different concentration of selenourea (a = [50 μ M], b = [200 μ M]). The solid lines are fitted to the data by the method of cumulants. The inset shows size distribution of Se nanoparticles at different concentration of BSA (c= [0 μ M], d = [10 μ M], e = [100 μ M], f = [200 μ M])

the particle size to ~ 100 nm.

The size distribution depends very much on the concentration of H_2O_2 , and stabilizers. In the presence of BSA, the size distribution is bimodal in nature with a major peak centered at around 100 nm and a minor distribution at around 10 nm. Fig.1c, 1d, 1e and 1f show the size distribution in the absence and in presence of 10, 100 and 200 mM BSA respectively. The intensity of the minor peak increased with increase in H_2O_2 or BSA concentrations while the peak positions remained approximately the same, indicating no significant change in the average size with BSA.

Similarly, singlet oxygen reactions with selenourea produced Se particles ranging in size from 20 to 170 nm in presence of SDS and the size varied with the initial singlet oxygen yield and the particles are highly polydisperse (Table 1).

The results listed in Table 1 suggest that oxidants with high rate constant produce smaller particles with low polydispersity. However this alone does not explain the size variation, probably other factors like reactivity, which is a product of rate constant and concentrations of the reactants and mode of initial electron transfer may also play an important role in determining the size and polydispersity of the particles. It is known that hydroxyl radicals react by electron transfer with selenourea; however the mechanism of reaction of other oxidants is not known. H_2O_2 is a mild oxidant and can cause both one and two electron reactions⁸. Singlet oxygen adds to double bonds by forming hydroperoxides, which eventually lead to formation of free radicals⁸. Hence it may not be possible to bring direct correlation between the size and the

initial rate constant.

Redox reactions of nanoselenium

The above solutions of nanoselenium were examined for their ability to participate in redox reactions with free radicals and molecular systems. For this, elemental selenium particles were generated by the reaction of H_2O_2 with selenourea, and the solutions were subjected to dialysis for 98 hours, so that the initial reactants do not interfere in these studies. The concentration of the selenium was determined by fluorimetric analysis using 1,2-diamino naphthalene. For the oxidation studies of nanoselenium, DCFA was employed. This compound is used as a marker for oxidative status in cells. For these studies, nano selenium solutions [~ 4 mg/ml] were mixed with DCFA solutions under neutral conditions and after about 3 hours, the solutions were excited at 502 nm and the fluorescence at 527 nm due to DCF was monitored. Under such conditions, DCFA undergoes slow hydrolysis and the hydrolyzed sample is oxidized by nanoselenium. A significant increase in the fluorescence in presence of nano selenium was observed indicating that it was able to oxidize dichlorodihydrofluorescein. Effect of particle size on oxidizing power of nanoselenium was also tested. For this, selenium particles of size 37 – 105 nm were mixed with DCFA solutions and the results showed that smaller the size of nanoselenium, larger is the fluorescence intensity at a given time. This result confirms that the oxidizing power of nanoselenium depends on the size of the nanoparticle.

We also studied the reaction of nanoselenium with $ABTS^{\bullet-}$ radicals, which in presence of compounds capable of donating electrons, is reduced to a colorless form. Reaction with $ABTS^{\bullet-}$ radicals was monitored by following the absorbance changes at 645 nm region in presence of nanoselenium as a function of time.

The results suggest that the decay of ABTS^{•+} radicals increased with decreasing particle size. This confirms that smaller size nanoparticle is able to reduce ABTS^{•+} more efficiently than the larger ones. In the above experiments, since the concentration of selenium is constant for a given reaction, the size dependency may either be due to change in number density of the particle or due to surface area. If the number density is responsible for this, one would expect a linear variation in these above activities with $1/r^3$ and if it is due to the surface area, linearity should be observed with $1/r$, where r is the radius of the particle. The above data show nearly linear variation with the inverse of particle radius, suggesting that the parameter correlating the redox reactivity is proportional to the total surface area of the particles. Thus, our results suggest that small size nanoselenium has greater potential to transfer electrons to radicals and other redox systems.

Conclusions

From the above results it can be concluded that selenourea reacts with a number of oxidants to produce elemental selenium. The selenium particles could be stabilized to nanometer size with the addition of BSA or SDS. The formation and characteristic size of the nano selenium depends mainly on the amount of selenourea undergoing oxidation and also on the type of oxidant and the amount of stabilizer. The stabilized selenium particles showed redox properties and participate in free radical and electron transfer reactions. Under cellular systems, due to the presence of large amount of proteins and other biomolecules, it is possible that much smaller size particles are produced under *in vivo* conditions.

References

1. Rosenfield, I.; Beath, O. A. *Selenium : geotoxicity, biochemistry, toxicity and nutrition*; Academic Press: New York, 1964.
2. Bock, A. In *Encyclopedia of Inorganic Chemistry*; Bruce-King R., Ed.; John Wiley: New York 1994, Vol.7, p 3700.
3. Muges, G.; du Mont, W.; Sies, H. *Chem. Rev.* **2001**, *101*, 2125.
4. Mishra, B.; Maity, D. K.; Priyadarsini, K. I.; Mohan, H.; Mittal, J. P. *J. Phys. Chem. A.*, **2004**, *108*, 1552.
5. Mishra B., Hassan P. A., Priyadarsini K. I., and Hari Mohan, *J. Phys. Chem. B*, **2005**, *109*, 12718.
6. Badiello, B.; Maggio, D. D.; Quintiliani, M.; and Sapora, O. *Int. J. Radiat. Biol.* **1971**, *20*, 61.
7. Zhang, J. S.; Gao, X. Y.; Zhang, L. D.; Bao, Y. P. *Biofactors* **2001**, *15*, 27.
8. Halliwell, B., and Gutteridge, J. M. C. *Free Radicals in Biology and Medicine*; Clarendon press: Oxford; 1989.
9. Pecora, R. In "Dynamic Light Scattering: Applications of Photon Correlation Spectroscopy" Plenum Press, New York, 1985.

ABOUT THE AUTHORS



Dr. K. Indira Priyadarsini joined Bhabha Atomic Research Centre in 1983. She is currently working on the elucidation of mechanisms of antioxidant action involving natural products and herbal

extracts with the potential application as radioprotectors, employing electron pulse radiolysis and invitro biochemical studies. Dr. Priyadarsini has co-authored more than 100 papers in peer reviewed international journals on radiation chemistry, photochemistry and radiation biology. She has been elected as the fellow of the National Academy of Sciences, India, and recipient of Homi Bhabha Science & Technology Award.



Ms. Beena Mishra received her M.Sc. degree in Chemistry with specialization in Inorganic Chemistry from Institute of Science, Mumbai, in 2001. She is a DAE fellow working in Radiation and Photochemistry Division,

BARC. She has submitted thesis for her Ph.D. degree in the subject entitled, "Free radical and transient studies of some biologically important organic and organometallic compound".



Dr. Hari Mohan joined Bhabha Atomic Research Centre in 1967. Since then he is actively involved in the study of fast reaction kinetics using accelerators and lasers. His research interests include free radical reactions of

halogenated and sulfur compounds and biomolecules of natural origin. He had co-authored more than 200 research papers in peer reviewed international journals. He superannuated in November, 2004 as Head, Radiation Chemistry Section of Radiation Chemistry & Chemical Dynamics Division of Bhabha Atomic Research Centre, Mumbai.



Dr. P. A. Hassan joined BARC in the year 1993, through 36th batch of Training School, and received Homi Bhabha Award. Since then, he has been working on the structure and dynamics of

association colloids such as micelles, their application in materials synthesis and rheology control of fluids. He has worked as a visiting researcher at the Laboratory of Complex Fluids, University of Louis Pasteur, Strasbourg, France. He pursued his post-doctoral research on soft condensed matter at the Department of Chemical Engineering, University of Delaware, USA. His research interests include structural transitions in micelles, liposomes, polymers, polyelectrolyte - surfactant interactions, nanomaterials and micro-rheology of complex fluids.

ONE-ELECTRON REDUCTION OF PYRROLOQUINOLINE QUINONE (PQQ), IN AQUEOUS SOLUTIONS: A PULSE RADIOLYSIS STUDY

Atanu Barik, K. Indira Priyadarsini and Hari Mohan
Radiation & Photochemistry Division
Bhabha Atomic Research Centre

and

H. S. Misra
Molecular Biology Division
Bhabha Atomic Research Centre

This paper was adjudged as one of the Best Posters in the National Symposium on Radiation & Photochemistry (NSRP-2005) held at University of Karnatak, Dharwad, 17-19 January, 2005.

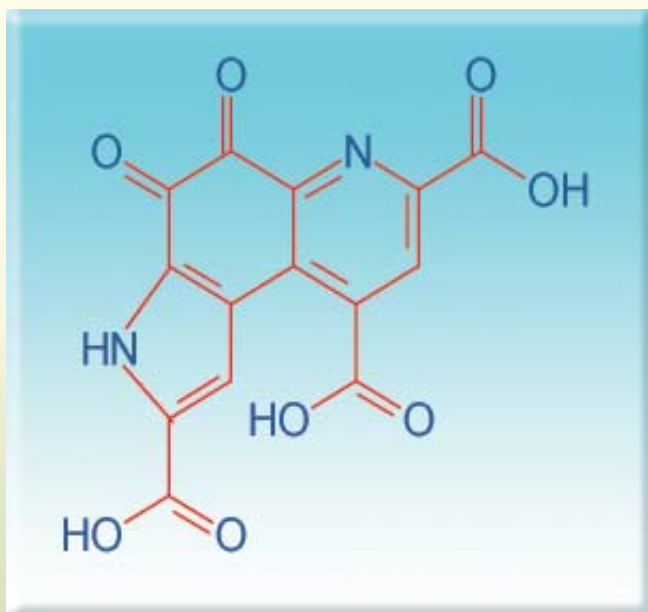
Abstract

One electron reduction of Pyrroloquinoline quinone (PQQ) was studied using pulse radiolysis technique. Reactions of hydrated electron, H atom, $\text{CO}_2^{\cdot-}$ radical and superoxide radicals produced very similar transient species. The radicals did not show decay in few milliseconds. The one-electron reduction potential of PQQ was determined at pH 7 using both methyl viologen and benzyl viologen couples and was found to be 0.36 ± 0.03 vs NHE.

Introduction

*P*yrroloquinoline quinone (PQQ) is a redox coenzyme [1], chemically it is known as 2, 7, 9-tricarboxyl-1H-pyrrolo [2, 3-f] quinoline-4, 5-dione. Though it is not synthesized in mammals, it occurs in several bacterial enzymes [2]. Trace level of PQQ has been found in human and rat tissues [2]. PQQ serves as a cofactor for a number of enzymes (quinoproteins) and particularly for some bacterial dehydrogenases [3]. Its unique redox cycling reaction

reflects striking biological properties [4]. The potential physiological role of PQQ in animals is not clear but it shows antioxidant activity by scavenging superoxide and hydroxyl radicals very efficiently and has the ability to inhibit lipid peroxidation [2,5]. On the other hand it acts as a pro-oxidant by producing hydrogen peroxide as an end product of PQQ redox cycling. In the redox process PQQ acts as an electron acceptor [2]. There are several reports describing the electrochemical properties of PQQ including potentiometric titration and cyclic voltammetry study [6]. The electrochemical



Scheme 1

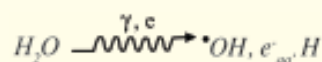
processes of PQQ may be reversible or irreversible depending on the nature of electrode used. Even the reversibility, in some cases depends on the pH of the solution. Pulse radiolysis is the best suited for studying such one-electron transfer processes accurately and has been proved to useful for estimation of one-electron reduction potential. In this paper we have discussed the one electron reduced product of PQQ by employing the pulse radiolysis technique.

Experimental

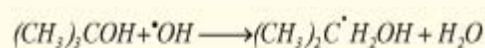
PQQ, methyl viologen, benzyl viologen were purchased from Sigma/Aldrich Chemicals, USA and used without any further purification. All other reagents used were of the highest purity available. Nanopure water from Milipore system was used for preparing the solutions and freshly prepared solutions were used for each experiment. 7 MeV linear electron accelerator of 50 ns pulse width was used for irradiation [7]. The absorbed dose was measured

using thiocyanate dosimeter [8]. Typical dose/pulse used for these studies varied from 10 to 12 Gy.

Radiolysis of water [5] produces e_{aq}^- , H^\bullet and $\bullet OH$ radicals in addition to the molecular products H_2 , H_2O_2 , H_3O^+ .



e_{aq}^- reaction can be studied by scavenging $\bullet OH$ radical by adding 0.3 M t-butanol under N_2 -saturated condition.



$CO_2^{\bullet -}$ radical is produced from 0.1 M $HCOONa$ under N_2O -saturated condition. $\bullet OH$ and H^\bullet react with formate ion to produce $CO_2^{\bullet -}$.



$O_2^{\bullet -}$ radical has been produced by reaction of oxygen with $CO_2^{\bullet -}$.



Results and Discussion

Ground state optical absorption spectrum of PQQ (3.63×10^{-5} M) in aqueous solutions exhibits absorption spectrum from 200 to 650 nm. PQQ has sharp and strong absorption at 248 nm, with a shoulder at 270 nm. It also shows a broad absorption at 330nm and 485 nm. The ground state pK_a values are 0.30, 1.60, 2.20, 3.30, 10.30. [9]

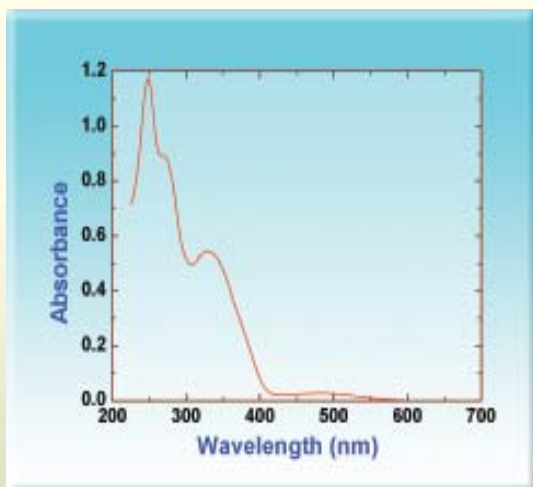


Fig. 1: Ground state optical absorption spectrum aqueous solutions of PQQ (3.63×10^{-5} M)

Reaction of reducing radical with PQQ

Pulse radiolysis of PQQ (3.63×10^{-5} M) was carried out with e_{aq}^- . The decay kinetics of e_{aq}^- at 700 nm was found to increase in presence of PQQ, and the bimolecular rate constant for the reaction of PQQ with e_{aq}^- was determined by following the decay of the transient absorption of e_{aq}^- at 700 nm and from the slope of the linear plot, the rate constant was estimated to be $1.81 \times 10^{10} \text{ M}^{-1}\text{s}^{-1}$. The transient obtained from the reaction of e_{aq}^- with PQQ shows absorption maxima at 330 nm and a broad band between 400 and 450 nm. Time resolved studies at 8 ms and 40ms after the pulse showed that the intensity of 450 nm band remained unchanged, whereas that of 400 nm band increases.

H atom reaction with PQQ at pH 1 under N_2 saturated condition shows almost similar type of transient absorption, where the 330 nm band was not observed. To get more details specific one electron reductant such as $\text{CO}_2^{\cdot-}$ was used to follow the transient behavior.

PQQ (5.08×10^{-5} M) reacts with $\text{CO}_2^{\cdot-}$ producing the transient having absorption band at 380 nm and small broad band with absorption maxima at 450 nm.

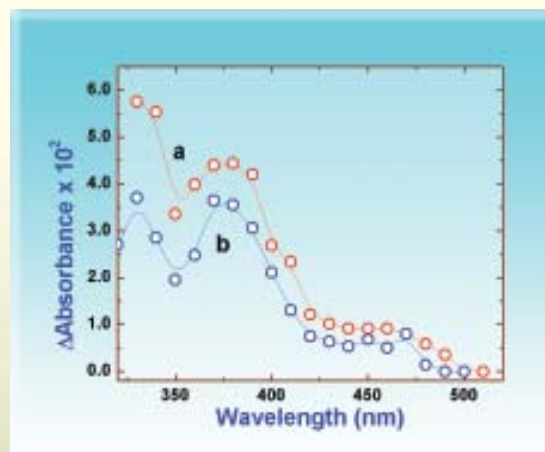


Fig. 2 : Transient absorption spectrum of PQQ in presence of 0.1 M HCOONa under N_2O (spectrum -a) and 1:1 N_2O and O_2 (v/v) saturated condition (spectrum -b).

PQQ reacts with $\text{O}_2^{\cdot-}$ forming a transient, which absorbs at 330 and 380 nm [5]. Superoxide radical can act as an oxidizing or reducing radical depending upon the condition. As the spectrum of the transient formed by the superoxide radical matches well with the spectra obtained from the e_{aq}^- or H atom. Thus superoxide reacts with PQQ (5.08×10^{-5} M) through reduction mechanism. The bimolecular rate constant of the reaction was measured from the formation kinetics at 380 nm and the typical value was $2.3 \times 10^8 \text{ M}^{-1}\text{s}^{-1}$.

One-electron reduction potential of PQQ at pH 7.0

Methyl viologen as a reference couple

The decay of radical cation of methyl viologen (600 nm) was affected on addition of low concentrations

of PQQ. These studies suggest the existence of following equilibrium reaction.



If this reversible electron transfer exists in equilibrium the observed first order rate constant (k_{obs}) under the condition of reversibility is given by following relationship.

$$k_{\text{obs}} = k_f[\text{PQQ}] + k_b[\text{MV}^{2+}]$$

where k_f and k_b are forward and backward rate constants. Rearranging this equation we get

$$\frac{k_{\text{obs}}}{[\text{MV}^{2+}]} = k_f \left(\frac{[\text{PQQ}]}{[\text{MV}^{2+}]} \right) + k_b$$

The (k_{obs}) was determined on monitoring the decay of $\text{MV}^{\bullet+}$ at 600 nm at different concentrations of MV^{2+} (10^{-4} to 10^{-5} M) and PQQ (10^{-5} to 10^{-6} M) in presence of 0.1 M formate. The plot of $k_{\text{obs}}/[\text{MV}^{2+}]$ as a function of

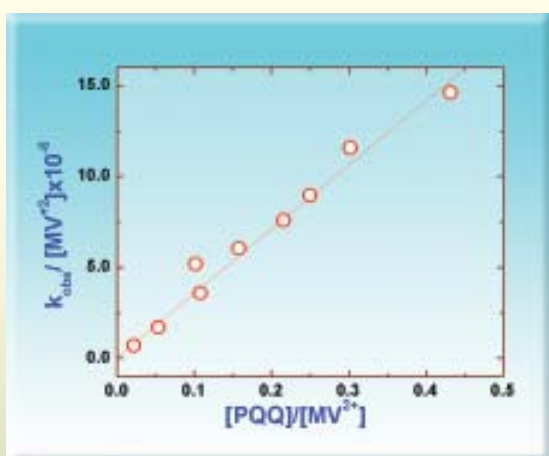


Fig. 3 : Plot of $k_{\text{obs}}/[\text{MV}^{2+}]$ vs $[\text{PQQ}]/[\text{MV}^{2+}]$ obtained on pulse radiolysis of N_2O -saturated aqueous solution of HCOONa (0.1 M) and different concentration of MV^{2+} and PQQ.

($[\text{PQQ}]/[\text{MV}^{2+}]$) (Fig. 3) gave a straight line with slope/intercept value of 79.76 corresponding to the equilibrium constant K (k_f/k_b).

The equilibrium constant and the potential of a system are related through the following Nernst's equation.

$$\Delta G = -n F \Delta E = -RT \ln K$$

where ΔG is the free energy change, ΔE is the difference in the electrode potential of the two couples involved, F is the Faraday constant and n is the number of electrons transferred in the reaction.

$$\Delta E = 0.059 \log (79.76) = 0.11$$

The standard reduction potential of $\text{MV}^{2+}/\text{MV}^{\bullet+}$ is -0.45 V vs NHE [10]. So the reduction potential of the couple $\text{PQQ}/\text{PQQ}^{\bullet-}$ is -0.34 V vs NHE at pH 7.

Benzyl viologen as a reference couple

The decay of radical cation of benzyl viologen (600 nm) was affected on addition of low concentrations of PQQ. These studies suggest the existence of following equilibrium reaction.



If this reversible electron transfer exists in equilibrium the observed first order rate constant (k_{obs}) under the condition of reversibility is given by following relationship.

$$k_{\text{obs}} = k_f[\text{BV}^{2+}] + k_b[\text{PQQ}]$$

where k_f and k_b are forward and backward rate constants. Rearranging this equation we get

$$\frac{k_{\text{obs}}}{[\text{PQQ}]} = k_f \left(\frac{[\text{BV}^{2+}]}{[\text{PQQ}]} \right) + k_d$$

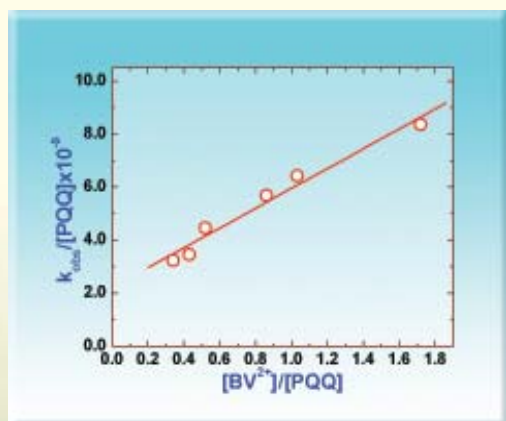


Fig. 4: Plot of $k_{\text{obs}}/[\text{PQQ}]$ vs $[\text{BV}^{2+}]/[\text{PQQ}]$ obtained on pulse radiolysis of N_2O -saturated aqueous solution of HCOONa (0.1 M) and different concentration of BV^{2+} and PQQ.

The (k_{obs}) was determined on monitoring the decay of BV^{2+} at 600 nm at different concentrations of BV^{2+} (10^{-5} M) and PQQ (10^{-5} M) in presence of 0.1 M formate. The plot of $k_{\text{obs}}/[\text{PQQ}]$ as a function of ($[\text{BV}^{2+}]/[\text{PQQ}]$) (Fig.4) gave a straight line with slope/intercept value of 1.684 corresponding to the equilibrium constant K (k_f/k_b).

$$\Delta E = 0.059 \log(1.984) = 0.013$$

The standard reduction potential of $\text{BV}^{2+}/\text{BV}^{+}$ is -0.374 V vs NHE [10]. So the reduction potential of the couple $\text{PQQ}/\text{PQQ}^{\bullet-}$ is -0.387 V vs NHE at pH 7. The average one electron reduction potential of $\text{PQQ}/\text{PQQ}^{\bullet-}$ was determined to be -0.36 ± 0.03 V vs NHE at pH 7.

Conclusions

PQQ undergoes one-electron reduction very easily. It reacts with reducing radicals like hydrated electron, H

atom, $\text{CO}_2^{\bullet-}$ radicals including superoxide radicals. The one-electron reduced species shows absorption spectrum at 300 to 500 nm region. The rate constants for these reactions are very high and show very effective reduction. The one-electron reduction potential of PQQ is -0.36 ± 0.03 V vs NHE and this value matches closely with that determined by cyclic voltammetry. As PQQ acts as coenzyme, this reduction potential will help to understand the mechanism for different enzyme activity.

Acknowledgements

The authors are thankful to Dr T. Mukherjee Director Chemistry Group and Dr S. K. Sarkar, Head, RPCD Division, BARC for their constant support and encouragement.

References

1. Kasahara, T. and Kato, T. Nature **422**, 832, 2003.
2. He, K.; Nukada, H.; Urakami, T. and Murphy, M.P. Biochem. Pharmacol. **65**, 67-74, 2003.
3. Magunusson, O.T.; Toyama, H.; Saeki, M.; Schwarzenbacher, R. and Klinman, J.P. J. Am. Chem. Soc. **126**, 5342-5343, 2004.
4. Bishop, A.; Paz, M.A.; Gallop, P.M. and Karnovsky, M.L. Free Radic. Biol. Med. **18**, 617-620, 1995.
5. Misra, H.S.; Khairnar, N.P.; Barik, A.; Priyadarsini, K.I.; Mohan, H. and Apte, S.K. FEBS Lett. **578**, 26-30, 2004.
6. Eckert, T.S.; Bruice, T.C.; Gainor, J.A. and Weinreb, S.M. Proc. Natl. Acad. Sci. USA **79**, 2533-2536, 1982.
7. Guha, S.N.; Moorthy, P.N.; Kishore, K.; Naik, D.B. and Rao, K.N. Proc. Indian Acad. Sci. (Chem. Sci.) **99**, 261-271, 1987.

8. Fielden, E.M.; Baxendale, J.H. and Busi, R.D. (Ed.). "The study of fast processes and transient species by electron pulse radiolysis", Reidel publishing Co. London, pp. 59, 1984.
9. Zhang, Z.; Tellekeratne, L.M.V.; Kirchoff, J.R. and Hudson, R.A. *Biochem. Biophys. Res. Commun.* 212, 41-47, 1995.
10. Wardman, P. *Free Rad. Res. Commun.* 14, 57-67, 1991.

ABOUT THE AUTHORS



Dr Atanu Barik obtained M. Sc. degree in Chemistry from Burdwan University (West Bengal) in 1999. After graduating from BARC Training School in 2000 (43rd Batch, Chemistry discipline), he joined Radiation & Photochemistry Division, BARC. Since then he is actively involved in free radical chemistry and excited state properties of important biomolecules employing photochemical and radiation chemical techniques. He has obtained Ph. D. degree in Chemistry from University of Mumbai in 2006.



Dr K. Indira Priyadarsini joined Bhabha Atomic Research Centre in 1983. She is currently working on the elucidation of mechanisms of antioxidant action involving natural products and herbal extracts with the potential application as radioprotectors, employing electron pulse radiolysis and invitro biochemical studies. Dr Priyadarsini has co-authored more than 100 papers in peer reviewed international journals on radiation chemistry, photochemistry and radiation biology. She has been elected as the fellow of the National Academy of Sciences, India, and recipient of Homi Bhabha Science & Technology Award.



Dr Hari S Misra joined Bhabha Atomic Research Centre in 1990. Since then he has been working on molecular genetics of bacterial response to abiotic stress and development of insect resistant transgenic plants. He is currently working on the elucidation of molecular mechanisms underlying the radiation response to biological system by employing the high throughput proteomics and genomics tools. His recent findings suggest the superior role of antioxidant metabolites in oxidative stress tolerance in bacteria. Dr. Misra is the recipient of INS Medal 2004 and an elected Fellow of Maharashtra Academy of Sciences, 2003.



Dr Hari Mohan joined Bhabha Atomic Research Centre in 1967. Since then he is actively involved in the study of fast reaction kinetics using accelerators and lasers. His research interests include free radical reactions of halogenated and sulfur compounds and biomolecules of natural origin. He had co-authored more than 200 research papers in peer reviewed international journals. He superannuated in November, 2004 as Head, Radiation Chemistry Section of Radiation Chemistry & Chemical Dynamics Division of Bhabha Atomic Research Centre, Mumbai.

PREPARATION OF ^{63}Ni ELECTRODEPOSITED SPECIAL CUSTOM-MADE SOURCES

Shyamala S. Gandhi, J.Udhayakumar and A. Dash
Radiopharmaceuticals Division
Bhabha Atomic Research Centre

This Paper received the Consolation Prize in the Poster Presentation Session at the NAARRI Annual Conference (NAC-2005) on "Radioisotopes and Radiation Technology: User's Perception and Experience", held at Multipurpose Hall, Training School Hostel, Anushaktinagar, Mumbai, during November 10-11, 2005.

Abstract

^{63}Ni is used as an ionization source in electron capture detector of Gas Chromatography. Different firms currently use such sources with a few tens of MBq activity, uniformly deposited on different size and shapes of metals. ECIL, Hyderabad, requested for ^{63}Ni beta ionization source of ~ 370 MBq (~ 10 mCi) on a delicate custom made holder, which was successfully carried out by us by electrodeposition method. This paper describes the fabrication of such ^{63}Ni custom-made source (exclusively coated on inner curved area of up to ~ 3.2 sq.cm. on Nickel alloy metal) in detail.

Introduction

^{63}Ni a pure beta emitter with half life of 100 years and $E_{\beta\text{max}}$ 0.067 MeV is used as low energy beta ionization source^[1]. β particles from ^{63}Ni source produce ionization resulting in a steady current in a stream of pure argon. When any other gas with a higher electron capture enters the chamber, the change in the current enables detection of the type and amount of the gas (Fig. 1)^[2]. A request was received from M/s Electronics Corporation of India Limited, Hyderabad for a ^{63}Ni source of ~ 370 MBq (10mCi) strength, in the form of a Nickel ring for use in Gas Chromatography equipment.

Electrodeposition is the most suitable technique for such preparations as thin films on prescribed dimensions, to achieve well-adhered deposit.

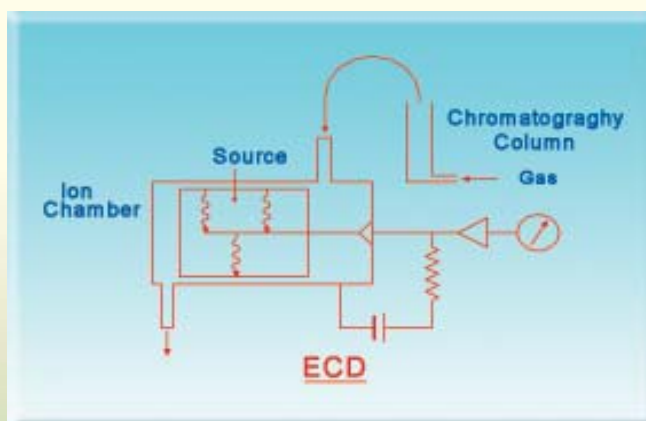


Fig. 1 : Ionization source set-up

Materials and Method

^{63}Ni was procured from M/s Amersham Biotech Pharmacia, UK. All other chemicals like Boric Acid, Nickel Chloride and Ethyl alcohol were of AR grade and procured from SD Fine Chemicals, Mumbai / BDH (India). The Nickel ring to be coated with ^{63}Ni was provided by ECIL, Hyderabad (Fig. 2).

A special cell was designed and used to mount Ni alloy ring holder. The Ni alloy holder was mounted suitably in between two thin rubber sheets and pressed tightly with butterfly screws ensuring no leakage of electrolyte (Fig.3).

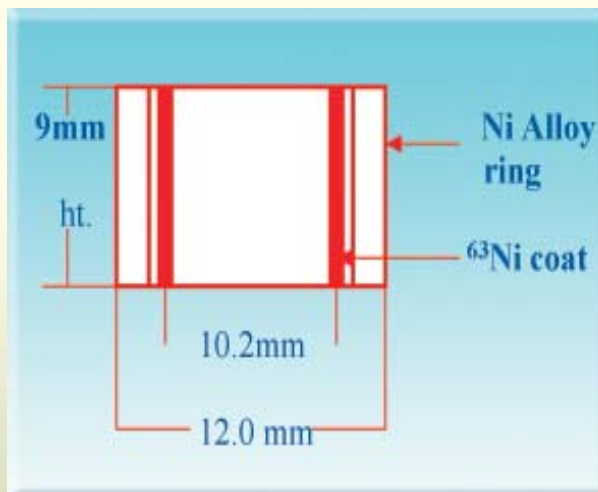


Fig. 2 : Nickel ring

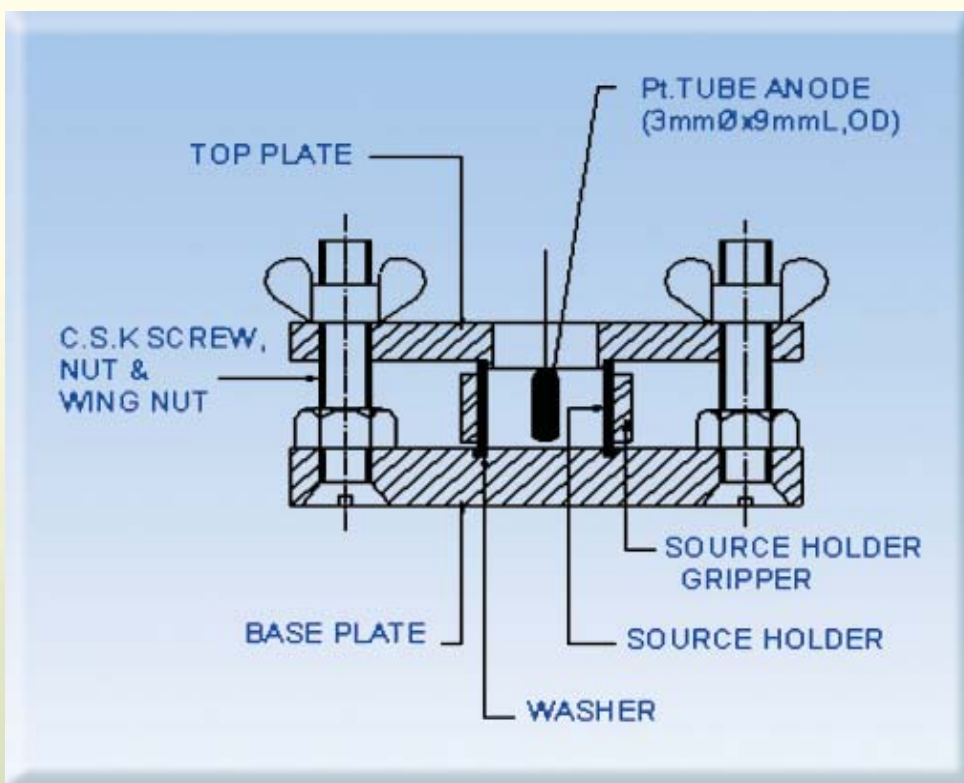
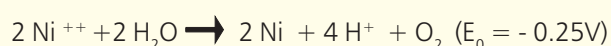


Fig. 3 : Electrodeposition cell assembly

Based on previous^[4] experience with preparing electro deposited ⁶³Ni sources, the following procedure was adapted. ~370 MBq (~10 mCi) of ⁶³Ni was to be deposited uniformly and accurately only in the inner curved portion of annular Ni Alloy ring holder of 12 mm diameter X 10 mm height with an inner diameter of 10.2 mm ID. The electrolyte (pH of 2–2.5) was composed of Boric acid (30 g/L), ~370 MBq (~10 mCi) ⁶³Ni as Nickel Chloride with a specific activity of 6.1 mCi/mg in a total volume of 0.8 ml. The electro-deposition was carried out for 4 hours maintaining electrolyte volume of 0.8ml, by addition of electrolyte (free from Ni carrier) occasionally to compensate for the loss of electrolyte volume. The source activity was assayed by drawing suitable electrolyte aliquots, before and after the electro-deposition. These samples were counted in the Liquid Scintillation Counter. At the end of electro-deposition, the source was washed with DDW, alcohol and dried. The electrodeposited ⁶³Ni source was heated to ~500°C to convert Ni to Nickel oxide and cooled. The source was then subjected to leach test for the adherence compliance quality in accordance with AERB standards.^[4]

The net electrolyte reaction is



Results

At the end of 4 hour electro-deposition, > 90% ⁶³Ni could be deposited. The leach test results indicated that < 0.01% of activity leached out, which was well within the permissible levels.

Conclusion

The electro deposition described is a very safe and reliable procedure to coat ⁶³Ni on any flexible dimensions of custom source holders. The specially developed electrodepositioning cell set-up is useful for plating on such small annular space area of the rings. Such sources are regularly supplied to various users on commercial basis through BRIT/DAE.

Acknowledgement

The authors acknowledge their sincere thanks to Dr V.Venugopal, Associate Director, RC & I Group and Dr (Ms.) Meera Venkatesh, Head, Radiopharmaceuticals Division for their encouragement and support. The authors also thank Mr B.G.Avhad, IAD, for extending fabrication support of electro- deposition cell set-up accessories in connection with the supply of ⁶³Ni electro-deposited custom source.

References

1. Radioisotopes Manual, Amersham, UK.
2. Industrial Gauging and Analytical Instrumentation Sources, Amersham International Plc.UK, 1986.
3. "Development of ⁶³Ni sources for Defence Related Applications" J.Udhayakumar et al. RPhD/BARC, (INSAC-2004), November 2004, BARC/Mumbai.
4. AERB Safety Standard no. AERB/SS/3 (Rev.1), Testing and Classification of Sealed Radioactive Sources, Oct.2001.

ABOUT THE AUTHORS



Ms Shyamala S. Gandhi obtained her B.Sc. degree in Physics from Mumbai University in 1993 and PG Diploma in Computer Science and Applications from SNTD University,

Mumbai in 1994 and joined BARC in 1997. She is involved in the regular fabrication of reference radiation sources, supplied to various users on commercial basis through BRIT. She has also participated in the development of custom made special sources such as polymer film sources using ^{60}Co and sources based on ^{147}Pm , ^{55}Fe and ^{63}Ni etc., for their use in various fields.



Dr Ashutosh Dash joined BARC in 1983 after successful completion of the 26th batch of training school. He obtained his PhD degree in Chemistry from Mumbai University in 1994. His

areas of expertise are fission products separation, large scale handling and vitrification of ^{137}Cs , separation of radioisotopes by ion exchange methods etc. He was on deputation to Korean Atomic Energy Research Institute (KAERI) as a Visiting scientist from November 2002 to April 2003. He was a member of IAEA sponsored CRP projects related to development of therapeutic radiation sources and development of generator technologies for therapeutic radionuclides. He is presently heading the T&RS Section of RPhD and looking after the program of production and supply of brachytherapy, industrial and reference sources. He has been involved in various capital plan projects of the Radiopharmaceuticals Division. He is a member of various departmental committees. He has more than 50 research publications including 10 publications in international journals. He is a life member of NAARRI, IANCAS and INS.



Mr J. Udhayakumar obtained his B.Sc. degree from Madras University in 1975 and joined BARC in 1976. He has worked on the development of ^{57}Co -mossbauer sources, ^{241}Am smoke detector source, ^{204}Tl sources etc.

He has also contributed to the development of ^{60}Co and ^{57}Co gamma film sources and ^{147}Pm source for beta dust monitors. He has been involved in the preparation of electrodeposited sources comprising of ^{57}Co , ^{60}Co , ^{125}I , ^{55}Fe , ^{109}Cd , ^{63}Ni etc. Presently he is responsible for the fabrication of reference sources supplied to various users on commercial basis through BRIT. He has one research paper in an international journal.

INFLUENCE OF IONIZING RADIATION ON PROTEIN DEGRADATION BY ENDOGENOUS PROTEASES IN POULTRY VISCERA

S.N. Jamdar, M.H. Kishore and P. Harikumar
Food Technology Division
Bhabha Atomic Research Centre

This poster paper won the Third Prize at the NAARRI Annual Conference (NAC 2005), held at Mumbai, during November 10-11, 2005.

Abstract

In poultry processing industry, viscera accounts for nearly 30% of the byproducts. It contains 10-13% proteins, 24-27% lipids and possesses 32-64% of the total proteolytic enzymes. A rapid method based on the degradation of tissue proteins by endogenous enzymes has been developed in our laboratory to retrieve 80-90% of the tissue proteins in the form of protein hydrolysates from poultry viscera (Bioresource Technol. 96 [1276-1284], 2005). The efficacy of this method is now evaluated in tissues hygienised by gamma radiation. Exposure to 5 to 10 kGy reduced the microbial load of poultry viscera by 4 to 6-log cycles while 20 kGy extended the shelf life to more than 60 days. Irradiation did not affect the activities of aminopeptidases, dipeptidyl peptidases and alkaline proteases while it inactivated aspartic protease only marginally. Consequently, the degradation of proteins by tissue autolysis was also unaffected by radiation processing. Thus, ionizing radiation could be used to extend the shelf life of poultry viscera, which in turn, could significantly reduce the cost of protein hydrolysate production.

Introduction

Poultry industry is flourishing globally with nearly 6.8×10^7 tonnes being processed every year (FAO statistics, 2005). It produces large quantities of organic by-products including the viscera, blood, feet, head and feathers (Ockeraman and Hansen, 2000); the utilization and disposal of which pose increasing challenges. The viscera, which constitutes nearly 30% of the total wastes, is rich in proteins and proteolytic enzymes (Jamdar et al 2005). It is estimated that in India, more than 1,44,000 tonnes of poultry viscera are produced annually in organized

sector alone. In the absence of suitable methods for the preservation and retrieval of nutrients, major portion of this by-product is being discarded resulting in environmental pollution (Fransen et al 1996) and loss of valuable nutrients (Rao et al 1996). We have developed a cost effective process based on tissue autolysis for the retrieval of intestinal proteins in the form of high quality protein hydrolyzates. One of the major constraints in this process is the high microbial load in viscera, which rapidly putrefy the tissue during handling and storage. The widely used methods such

as heat sterilization (Giri et al 2000, Nengas et al, 1999), acid stabilization (Cai et al 1995) and fermentation (Kherrati et al, 1998; Rao et al, 1996) are not suited to our scheme of protein retrieval, because of inactivation of tissue proteases (Jamadar et al 2004) and inadequate decontamination (Haapapuro et al, 1997). Thus, the need for a suitable method, which ensures decontamination of poultry viscera without the inactivation of proteases, has been felt.

In this context, application of gamma irradiation, which is recognized as an environment friendly cold sterilization process with least physical and chemical changes to food constituents, (Molins, 2001; Durante, 2002) holds promise. Tissue enzymes are relatively resistant to gamma radiation while microorganisms are highly susceptible. In the present paper, we report the status of protein degradation by endogenous proteases in radiation hygienized poultry viscera.

Methods

Poultry viscera, brought from local market were washed in tap water, blotted, weighed, sealed in polyethylene bags (15 cm x 20 cm) and exposed to different doses of gamma radiation (5kGy, 10 kGy and 20 kGy) in a package ⁶⁰Co γ -irradiator (dose rate 46 Gy/min) at ambient (26°C) temperature. The samples were stored at 4°C or 26°C.

Total aerobic bacteria, coliform bacteria and yeast and moulds were determined (BAM Online). The tissue samples were analyzed for protein, fat, moisture and ash according to AOAC method (1984). Lipid peroxidation was monitored in terms of thiobarbituric acid (TBA) values. (Alur et al 1995). The tissue autolysis was carried out at pH 2.8 and 60°C and the

levels of TCA (10%) soluble peptides at different time intervals were estimated by Miller's method. Total Volatile Basic Nitrogen (TVBN) was determined according to Farber and Ferro (1956).

Activities of aspartic protease, aminopeptidases were determined according to Jamdar and Harikumar (2005). Activity of alkaline proteases was determined as per method described by Thakore and Harikumar (1995).

Results and Discussion

Data presented in Table 1 shows the influence of gamma radiation on microbial population of chicken intestine during storage. A dose of 5 kGy extended the shelf life for 5 and 10 days at 26°C and 4°C respectively. The corresponding values for 10 kGy were 10 and 20 days. A dose of 5-10 kGy, which reduced the total viable count of bacteria, yeast and moulds by 4 to 5 log₁₀ units was sufficient to eliminate coliforms completely (<1 CFU/g tissue), while 20 kGy rendered the samples sterile. Similar degree of kill by ionizing radiation has been observed by Borrelly et al. (1998) who showed that ionizing radiation at 3kGy could reduce the count in raw sewage by 5 log₁₀ units. The efficacy of gamma radiation to eliminate both vegetative as well as spore forms of microorganisms from flesh foods have been demonstrated by many investigators (Molins, 2001; Farkas, 1998). Significantly, total count in irradiated samples (5 kGy and 10 kGy) even after storage for 10-20 days at 4°C (Table 1) remained 3-4 log cycle lower than that in unirradiated control (1.094 x 10⁷ CFU/g). No significant organoleptic degeneration was also discernible for these samples. This, along with the observation that low dose of ionizing radiation do not inactivate tissue proteases (Jamdar and Harikumar,

Table 1. Microbial Population of irradiated poultry viscera during storage¹

Sample	Storage (Days)	Log ₁₀ CFU/g				Statistical Significance		
		Total bacteria		Yeast and Mould		Total Coliform	Temp	Irr.
		4°C	26°C	4°C	26°C			
Unirradiated	0	7.0	7.0	7.0	7.0	6.9		
	0	3.6	3.6	2.7	2.7	ND		***
5 kGy	5	4.2	5.5	3.2	4.6	ND	A**/ B***	
	10	4.7	NA	3.9	NA	ND		
SEM		0.21	0.22	0.18	0.20			
10 kGy	0	1.7	1.7	1.2	1.2	ND		***
	5	2.0	2.6	1.8	2.0	ND	NS	
	10	2.6	5.4	2.6	4.3	ND	***	
	20	3.5	NA	3.4	NA	ND		
SEM		0.17	0.18	0.12	0.18			

¹ In samples exposed to 20 kGy the total bacteria, coliform, yeast and mould were <1 CFU/10g throughout the period of storage.

SEM for coliform count in unirradiated sample was 0.20

NA: Not analysed as the sample was organoleptically spoiled; NS: Not significant; ND: Not detected
Significance *** P < 0.001; ** P < 0.01; A**: significance for total bacterial count; B***: significance for total yeast and Mould count

2002), suggest that irradiation (5 kGy and 10 kGy) combined with storage at 4°C could be effectively employed for extending the shelf life of poultry viscera.

The biochemical changes induced by microbial proliferation as well as gamma radiation are monitored in terms of known parameters such as TVBN and TBA values (Table 2) (Alur et al. 1995). The levels of TVBN increased eight fold within 18h in unirradiated samples at ambient temperature while irradiated sample showed similar increase only after 62 days. The increase in TVBN value in unirradiated sample stored at 26°C

indicates microbial spoilage (Alur et al. 1995), while that in irradiated samples (20 kGy) could be attributed to production of non-protein nitrogen by autolytic degradation of proteins followed by decarboxylation and deamination. As expected, the TVBN values were lower in samples stored at 4°C, which could be ascribed to inhibition of bacterial proliferation and retarded activity of hydrolytic enzymes. One of the important parameters that has to be reckoned with in radiation hygienization of flesh foods, is lipid peroxidation. TBA values in unirradiated samples were 2.0 to 2.5 times lower than the

Table 2 Biochemical changes in poultry viscera during post irradiation (20 kGy) storage

Storage Days	TVBN (g/kg tissue)				TBA (mg/kg tissue)			
	Unirradiated		Irradiated		Unirradiated		Irradiated	
	4°C	26°C	4°C	26°C	4°C	26°C	4°C	26°C
0	0.3 ^z	0.3 ^z	0.5 ^x	0.5 ^x	3.5 ^x	3.5 ^x	6.7 ^x	6.7 ^x
1	0.5 ^x	2.6 ^z	0.5 ^x	0.7 ^x	3.6 ^x	4.9 ^x	7.0 ^y	8.2 ^y
2	0.6 ^y	NA	0.5 ^x	0.8 ^y	3.6 ^x	NA	9.0 ^y	9.4 ^y
5	0.6 ^y	NA	0.5 ^x	1.1 ^y	3.7 ^x	NA	10.1 ^y	12.1 ^z
10	NA	NA	0.6 ^x	1.4 ^z	NA	NA	13.2 ^z	13.3 ^z
20	NA	NA	0.8 ^y	1.7 ^z	NA	NA	15.3 ^z	17.1 ^z
62	NA	NA	1.3 ^z	2.5 ^z	NA	NA	9.1 ^x	9.2 ^x
SEM	0.02	0.08	0.03	0.12	0.06	0.09	0.65	0.61
Significance of effect	Temperature			A**/B***				NS
	Irradiation			NS			***	

NA: not analyzed, organoleptically spoiled (Unirradiated 1 day sample at 26°C was spoiled but analyzed to know the level in spoiled sample)
Significance: ***P < 0.01; **P < 0.02; *P < 0.05; ^{xz} means within column with different superscript differ significantly (P < 0.05)
A** significance on days 1 and 2; B*** Significance on days 5, 10, 20 and 62; NS: Not significant
Values are means of three independent experiments.

Table 3: Protease activity in irradiated poultry viscera (20 kGy)

Enzymes	Activity (µmoles/g/h)	
	Control	Irradiated
Aspartic protease	958.4	926.6
Alkaline proteases	1028.6	823.2
Cathepsin B	69.5	68.7
Aminopeptidases		
Arginine aminopeptidases	612.8	534.3
Glycine aminopeptidases	714.2	723.6
Valine aminopeptidases	246.7	302.7
Alanine aminopeptidases	2223.1	1908.7
Tryptophan aminopeptidases	795.7	738.7
Aspartic aminopeptidases	62.9	53.0
Serine aminopeptidases	199.7	168.2
Tyrosine aminopeptidases	1712.9	1688.8
Proline aminopeptidases	122.9	66.8
Histidine aminopeptidases	56.9	48.3
Phenylalanine aminopeptidases	2172.6	1995.8

corresponding irradiated samples throughout the storage period. The tissue showed significant increase in TBA levels immediately after irradiation as well as during storage (2.2 and 2.5 fold during 20 days at 4°C and 26°C). Increase in lipid peroxidation, though to a limited extent (1.3 fold) was also observed in unirradiated samples during storage which could be predominantly due to atmospheric oxygen, while an additional participation of radiation induced free radicals could explain the enhanced peroxidation in irradiated samples (Al-kahtani et al. 1996; Hampson et al. 1996). Our observation that TBA values diminished by 45% on prolonged storage (62 days), is in conformity with earlier reports of Auburg et al (1993), showing decreased levels of TBA

Table 4: Effect of irradiation on tissue autolysis

Time (h)	TCA soluble peptides (μ moles/g)	
	Control	Irradiated
0	16.50	18.55
0.25	46.10	48.50
0.5	50.35	54.15
1	64.50	66.75
2	70.75	73.50
3	77.75	78.75
4	85.75	88.00
6	90.00	92.87

during post irradiation storage. Data on the levels of aspartic protease, cathepsin B, alkaline proteases, and aminopeptidases are presented in Table 3. Exposure to a dose of 20 kGy resulted in 3%, 20%, 12%, 8% and 14.1% loss in activity of aspartic protease, alkaline protease, arg-aminopeptidase, phe-aminopeptidase and ala-aminopeptidase respectively. The levels of TCA soluble peptides released during autolytic degradation of irradiated (20 kGy) chicken intestine at pH 2.8 and 60°C are presented in Table 4. No significant difference was found in protein degradation after radiation treatment. The observation that irradiation did not cause any significant change in proteases activity as well as tissue autolysis is important while considering radiation hygienized poultry viscera for the preparation of protein hydrolysates or as a source of proteolytic enzymes for commercial applications. Moreover, the process, assures decontamination with little change in proximate composition, which is in agreement with the observations of Farag et al. (1999). Thus, irradiation could be used to hygienize poultry viscera before utilizing it for the preparation of value added products such as protein hydrolysates and proteolytic enzymes with minimum risk of spreading pathogenic organisms.

References

1. Al-Kahtani, H.A., Abu-Tarboush, H.M., Bajaber, A.S., Atia, H., Abou-Arab, A.A., El-Mojaddidi, M.A., 1996. Chemical changes after irradiation and post irradiation storage in tilapia and Spanish mackerel. *J. Food Sci.* 61, 729-733.
2. Alur, M.D., Doke, S.N., Warriar, S.B., Nair, P.M., 1995. Biochemical methods for determination of spoilage of foods of animal origin: A critical evaluation. *J. Food Sci. Technol.* 32, 181-188.
3. AOAC, 1984. *Official Methods of Analysis*, 14th edn. Assoc. Official Analytical Chemists, Washington, DC.
4. Auburg, S.P., 1993. Review: interaction of malondialdehyde with biological molecules- new trends about reactivity and significance. *Int. J. Food Sci. Technol.* 28, 323-335.
5. Borrely, S.I., Cruz, A.C., Del Mastro, N.O., Sampa, M.H., Somessari, E.S. 1998. Radiation processing of sewage and sludge. A review. *Progress in Nuclear Energy.* 33, 3-21.

6. Cai, T., Pancorbo, O.C., Merka, W.C., Sander, J.E., Barnhart, H.M., 1995. Stabilization of poultry processing by products and poultry carcasses through direct chemical acidification. *Biores. Technol.* 52, 69-77.
7. Durante, R.W., 2002. Food processors requirements met by radiation processing. *Rad. Phys. Chem.* 63, 289-294.
8. FAO statistics, 2005. FAO statistics of livestock production. apps.fao.org/faostat.
9. Farag, M., Dia El-Din, H., Mohamed, F.A., 1999. Effect of radiation processing as an integral part of the safe recycling animal waste. *Anim. Feed Sci. Tech.* 77, 267-280.
10. Farber, L., Ferro, M., 1956. Volatile reducing substances (VRS) and volatile nitrogen compounds in relation to spoilage of canned fish. *Food Technol.* 10, 303-304.
11. Farkas, J., 1998. Irradiation as a method for decontaminating food, A review. *Int. J. Food Microbiol.* 44, 189-204.
12. Fransen, N.G., Annemieke, M.G., Bert, A.P., Bijker, G.H., 1996. Pathogenic microorganisms in slaughterhouse sludge- A survey. *Int. J. Food Microbiol.* 33, 245-256.
13. Giri, S.S., Sahoo, S.K., Sahu, A.K., Mukhopadhyay, P.K., 2000. Nutrient digestibility and intestinal enzyme activity of *Clarias batrachus* (Linn.) juveniles fed on dried fish and chicken viscera incorporated diets. *Biores. Technol.* 71, 97-101.
14. Haapapuro, E.R., Barnard, N.D., Michele Simon, J.D., 1997. Review- Animal waste used as livestock feed: Dangers to human health. *Preventive Medicine*, 26, 599-602.
15. Hampson, J.W., Fox Jr, J.B., Lakritz, L., Thayer, D.W., 1996. Effect of low dose gamma radiation on lipids in five different meats. *Meat Sci.* 42, 271-276.
16. Jamdar, S.N., Harikumar, P., 2002. Sensitivity of catheptic enzymes in radurized chicken meat. *J. Food Sci. Technol.* 39, 72-73.
17. Jamdar, S.N., Harikumar, P., 2005. Autolytic degradation of chicken intestinal proteins. *Biores. Technol.* 96, 1276-1284.
18. Kherrati, B., Faid, M., Elyachioui, M., Wahmane, A., 1998. Process for recycling slaughterhouses wastes and by-products by fermentation. *Biores. Technol.* 63, 75-79.
19. Miller, G. L., 1959. Protein determination for large number of samples. *Anal. Chem.* 31, 964.
20. Molins, R.A., 2001. Potential social and economical benefits of food irradiation. In: Molins, R.A., (Ed.) *Food irradiation principles and applications*. Willey- Interscience, John Wiley and sons, inc., New York, pp.14-21.
21. Nengas, I., Alexis, M.N., Davies, S.J. 1999. High inclusion levels of poultry leals and related byproducts in diets for gilthead seabream *Sparus aurata* L. *Aquaculture*, 179, 13-23.
22. Ockerman, H.W., Hansen, C.L., 2000. Poultry By products. In: *Animal by product processing and utilization*, chapter 12. CRC press, New York, pp 439-455.
23. Rao, J. R., Mahendrakar, N.S., Chakrabarty, N.M., Raghavan, S.L., 1996. Utilisation of fermented fish and poultry offals in feed for common carp (*Cyprinus caprio*). *Seafood Export J.* 27, 17-23.
24. Thakore, D, Harikumar, P. 1995. Total proteolytic profiles in buffalo kidney cortex lysosomes. *Proc Indian Natn Sci Acad.* 61B, 371-376.

ABOUT THE AUTHORS



Dr Sahayog N. Jamdar Joined BARC in 1996 through BARC Training School (39th batch) and is working in the flesh food Biochemistry section, Food Technology Division. His major contribution is in understanding structure function relationships of proteases and preparation of value added products from poultry and fish processing wastes.



Dr P. Harikumar is presently the Head, Flesh Food Biochemistry Section, Food Technology Division. He joined BARC in 1967 after graduating from the university of Kerala, obtained M.Sc. and Ph.D. degrees from the University of Mumbai. He has carried out postdoctoral research at Roche Institute of Molecular Biology, Nutley, New Jersey, USA (1982-1984) and at University of Medicine and Dentistry, New Jersey, USA, (1998-1999) on "The Role of lysosomal proton ATPase and Ca²⁺ in the regulation of intracellular protein catabolism." His major contribution is in understanding the structure-function relationships of lysosomal proteases and their role in regulating the quality attributes of irradiated flesh foods and in the preparation of value added products from poultry and fish processing wastes.

MODIFICATION OF PROTEIN HYDROLYSATES BY CHICKEN INTESTINAL AMINOPEPTIDASES

M.V. Damle, S.N. Jamdar and P. Harikumar
Food Technology Division,
Bhabha Atomic Research Centre

This poster paper won the Third Prize in Biochemistry & Nutrition,
at ICFOST-2005, held at Bangalore, during December 9-10, 2005.

Abstract

Protein hydrolysates are economically important value added products in the food industry. Hydrolysis of food proteins is practiced for the improvement of nutritional characteristics, retarding deterioration, removal of toxic or inhibitory ingredients and modification of functional properties such as solubility, emulsification, foaming. Treatment with exopeptidases is often adopted to improve the consumer acceptability and functional properties of protein hydrolysates. Organoleptic acceptability of casein and soybean protein hydrolysates increased after hydrolysis with chicken intestinal aminopeptidases leading to marked reduction in the bitterness scores (4.3 to 2.5 and 3.8 to 2.5 respectively). Treatment with aminopeptidase did not affect the functional properties of the products. Highly purified as well as partially purified (isolated mucosa) enzyme systems could be successfully used for modification of protein hydrolysates. The commercial significance of chicken intestinal aminopeptidases for improving the acceptability of protein hydrolysates is discussed.

Introduction

Hydrolysis of food proteins is widely employed for value addition through improvement of nutritional characteristics, retarding deterioration, improvement of functional properties and removal of toxic or inhibitory ingredients (Clemente, 2000). Protein hydrolysates form important ingredient of medical diets for various ailments and are gaining acceptance as components of sports as well as weight control diets. One of the attributes that reduces the consumer acceptance of protein hydrolysates is the bitterness caused by the presence of low molecular

weight (>10 kDa) peptides containing pro, leu, tyr, phe, ala etc in specific combinations (Saha and Hayashi, 2001).

Methods such as solvent extraction (Lalasis and Sjoberg, 1978), adsorption onto matrices (Lin et al. 1997) and treatment with exopeptidases (Raksakulthai and Haard, 2003) have been employed for the debittering of protein hydrolysates. The processes based on the removal of bitter peptides render the hydrophobic amino acids unavailable in the final product leading to nutritional imbalance (Saha and Hayashi, 2001). Enzymatic debittering, though

considered technologically and nutritionally superior, possess limitations such as lack of economic viability and availability of broad specificity enzymes. In this context we have identified, chicken intestine, a poultry processing waste, as a rich and viable source of potential enzymes (Jamdar and Harikumar, 2005; Jamadar et al. 2003). In the present paper, we report an inexpensive immobilization system for debittering protein hydrolysates using chicken intestinal exopeptidases.

Materials and Methods

Materials

The naphthylamine derivatives of L-arginine, L-alanine, L-leucine, L-tyrosine, L-phenylalanine, L-tryptophan, PCMB, Brij-35, Fast Garnet GBC sulfate salt, cysteine, trypsin, Picryl sulfonic acid (TNBS), amino acid standard, o-phthaldehyde were purchased from Sigma chemicals St. louis.

Methods

All the experiments were carried out at 4 °C unless mentioned otherwise.

Separation of Mucosa : Chicken intestine was brought in ice from local abattoir soon after slaughter and freed of accompanying organs such as spleen and pancreas along with the overlying layer of fat and other connective tissue. The undigested food and faecal matter were flushed out with tap water. The intestines were cut longitudinally; mucosa was scraped out, packed in polythene bags and irradiated (20 kGy) in Gamma Cell (AECL, Canada).

Microbiological evaluation: 100 μ l of irradiated and unirradiated mucosa were inoculated in triplicate in 5 ml of sterile nutrient broth and incubated at 37°C for 24

hours. The suspension from these tubes (2nd day) was then spot inoculated onto sterile Plate count agar plates (2 spots per tube). The plates and the tubes were incubated at 37°C for 7 days and were observed daily for microbial growth.

Enzyme Assay: Aminopeptidase activity was determined by the method of Barrett (1972). The 1ml system with the appropriate aliquot of the enzyme and 0.1M sodium phosphate buffer pH 6.8 containing 1 mM cysteine and 1mM Amino acid β Nap was incubated at 50°C for 10 min. The reaction was terminated by adding 1 ml Fast Garnet GBC - PCMB reagent (0.2 mg/ml Fast Garnet GBC (in 4% Brij 35) and 10 mM PCMB reagent mixed equally just before terminating the assay). The absorbance of the pink colored naphthylamine-GBC complex was measured at 520 nm.

Preparation of Beads: The immobilized beads were prepared by entrapping the irradiated (20 kGy) mucosa (20 % v/v) in 3% Sodium Alginate (Loba Chemicals, India) and adding this solution dropwise into 0.3 M CaCl₂. The beads were left overnight in CaCl₂ for hardening and washed with distilled water the next day.

Preparation of casein hydrolysates: Trypsin (40 mg/L) was added to 10% suspension of food grade casein, prepared in distilled water, pH adjusted to 8.0 and incubated at 50 °C for 16 h. at the end of the incubation, the pH of the solution was adjusted to 4.0 with 1 N HCl, heated at 90 °C for 15 min and centrifuged at 10,000 g for 15 min. The supernatant was used as casein hydrolysate.

Soybean Protein hydrolysate: Soybean protein isolated from soybean flour (Qi et.al.1997) was suspended in distilled water (10% w/v), pH adjusted to 2.5 and incubated with pepsin (250 mg/liter) at 50°C for 16h. At the end of the incubation, the pH of the solution was adjusted to 4.0 with 1N NaOH, heated at 90°C

for 15 min and centrifuged at 10,000 g for 15 min and the supernatant was used as protein hydrolysate.

Debittering of protein hydrolysates: The scheme for debittering protein hydrolysates with immobilized chicken intestinal mucosa is presented in Fig.1. the calcium alginate beads entrapped with mucosa (30 g) were packed in a jacketed column (43 cm x 1.5 cm) maintained at 50°C. The bitter protein hydrolysate was passed through the column at a flow rate of about 45 ml/hr. the solution eluting from the column was collected. The debittering of the solution was assessed

by taste panel as well as RP- HPLC analysis.

Taste Panel analysis: The taste panelists (n=10) were selected on the basis of their responsiveness to caffeine. All the parameters such as appearance, odor and overall acceptability were scored on a 7-point hedonic scale. The bitterness was adjudged on a 5 point scale comparing it with caffeine concentrations 0% (not bitter -0), 0.025 % (Trace bitter-1), 0.5% (slightly bitter-2), 0.1% (bitter-3), 0.2% (very bitter-4) and 0.3% (extremely bitter-5).

Reverse Phase HPLC: the samples were analyzed by HPLC on a Symmetry C18 5mm (4.6 x 250 mm) column. 0.1% trifluoroacetic acid (TFA) in water (Solvent A), 0.1% TFA in 60% acetonitrile (Solvent B) were used as mobile phase. The separation was carried out at flow rate of 1 ml/minute and gradient elution of 0 to 5 min 100% solvent A, 5 to 45 minutes solvent A from 100 % to 0%, 45 to 50 minutes solvent A 0 %. Detection of peptides was carried out at 220 nm.

Amino Acid content: Total amino acid composition of freeze-dried samples was determined after invacuo hydrolysis in 6M HCl at 110°C for 24h. The o-phthaldehyde (OPA) amino acid derivatives were eluted on Symmetry C₁₈, 5µm (4.6 x 250 mm) column. The elution was carried out using gradient of 12.5 mM phosphate buffer pH 7.2 (Buffer A) and buffer A containing 50% acetonitrile (Buffer B). The separation was performed using a flow rate of 1 ml/min and a gradient as follows: 0 to 5 min 100% A, 5 to 15 minutes solvent A from 100 % to 80%, 15 to 70 minutes solvent A 40%, 70 to 80 minutes solvent A 0%. Detection of derivatized amino acid was monitored at 330 nm.

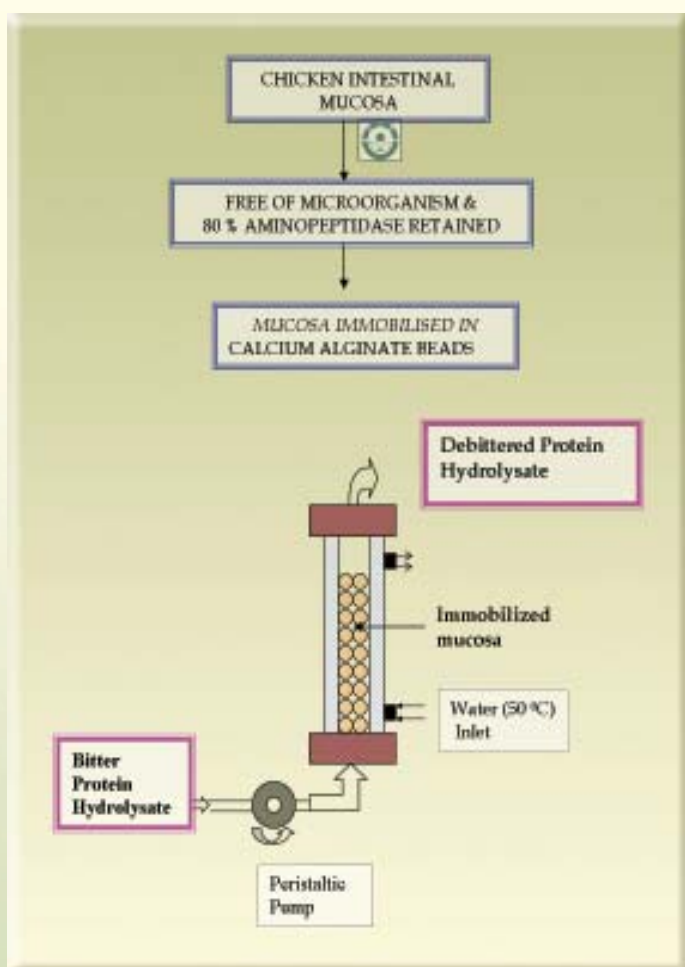


Fig. 1: Scheme for debittering of protein hydrolysates

Peptide chain length: The average peptide chain length of the samples was determined by the TNBS method (Adler-Nissen, 1979). The samples were appropriately diluted and dispersed in 1% SDS. To 50 μ l of the sample, 400 μ l of sodium phosphate buffer pH 8.2 and 400 μ l of 0.075% TNBS was added. After incubation in dark at 50 °C for 1 h, 800 μ l of 0.1 N HCl was added and the tubes were allowed to stand at room temperature for 30 min. the absorbance was measured at 340 nm. 100 mg of each sample was hydrolysed in vacuum at 100°C for 24 h and the total amino equivalents in the sample were quantified. The average peptide chain length was determined as per Nishiwaki et al, (2002) as the ratio of the number of free amino equivalents of the sample to the number of free amino equivalents of the acid hydrolysed counterpart.

Continuous debittering: Calcium alginate column containing immobilized mucosa was used for three days continuously debittering 3000ml of casein hydrolysate (5%). Three well spread out aliquots were drawn and were analyzed by Rp HPLC and taste panel. The column was also examined for leakage of aminopeptidase.

Statistical analysis: the statistical analysis has been carried out using Origin 6.1 pro software (Origin lab corporation, North Hampton USA). All the assays on the enzyme activity in beads have been carried out using sets of 5. All other assays have been performed in triplicate.

Results

Microbial status and aminopeptidase activities in irradiated mucosa: Irradiated (20 kGy) mucosa showed no microbial growth both under aerobic as well as anaerobic conditions indicating that the mucosa was sterilized by the treatment. Irradiation at 20kGy did not have any significant effect on aminopeptidases in the

mucosa (Fig. 2) which is apparent from less than 20% inhibition of hydrolytic activity on naphthylamide substrate of Arg, Ala, Leu, Phe, Tyr, and Trp their activities.

Aminopeptidase activity in beads: the aminopeptidase activity against b-Naphthylamide derivatives of arg. ala.

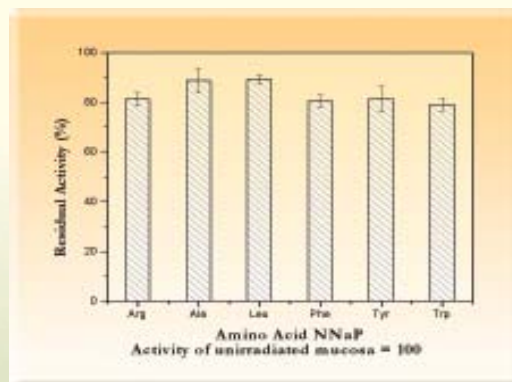


Fig. 2 : Aminopeptidase levels in irradiated mucosa

Table 1: Aminopeptidase activity in Ca-alginate beads.

Substrate (Amino acid β naphthylamide)	Activity (mMoles/bead/h)
Arg	331.45+9.85
Ala	323.75+18.00
Leu	311.41+5.90
Phe	275.72+6.64
Tyr	229.44+11.28
Trp	146.67+7.13

The activity reported is the average of three independent experiments \pm S.E.

leu, phe, tyr and trp in calcium alginate beads is presented in Table 1. The preference for the N terminal amino acid was in the order arg>ala>leu>phe>tyr>trp. Immobilization rendered the enzymes

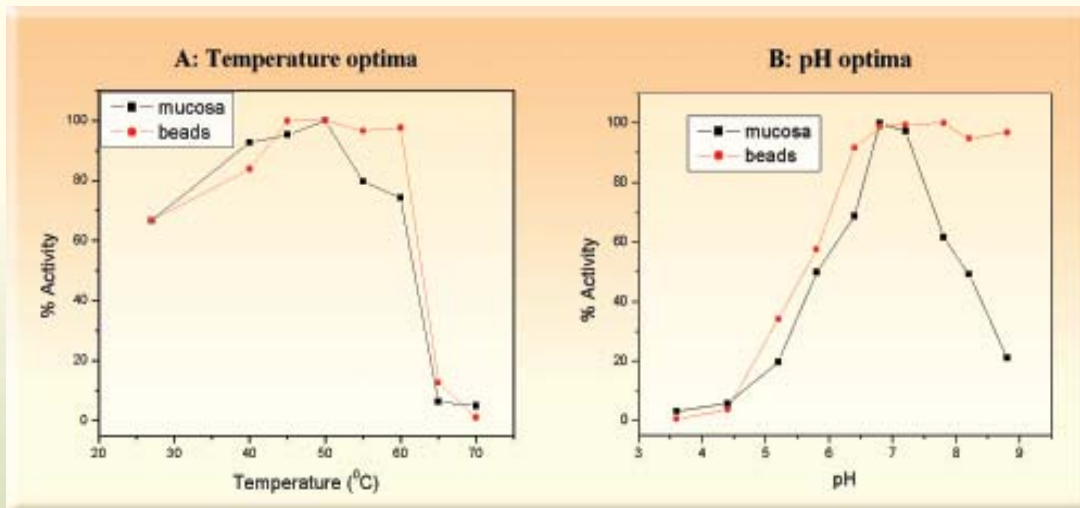


Fig. 3: Temperature and pH optima of aminopeptidases in mucosa and Ca alginate beads

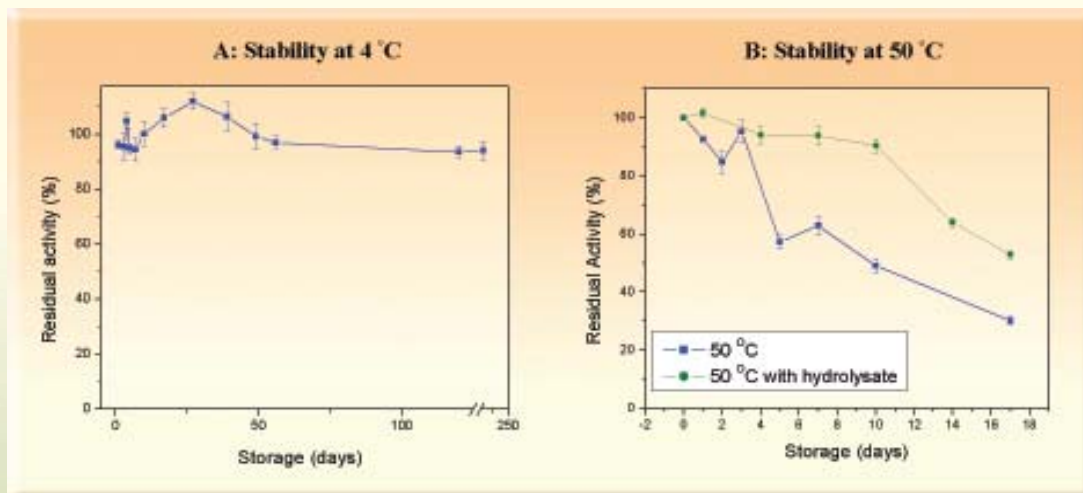


Fig. 4: Influence of temperature on the stability of aminopeptidase in beads

active over broader temperature and pH ranges (Figs. 3A and B) and stable (>90%) up to 200 days when stored at 4°C (Fig. 4A). At operational temperature (50°C), the beads retained activity for 4 days. In the presence of substrate (protein hydrolysate), the activity was retained for 10 days (Fig. 4B).

Modification of protein hydrolysates: The influence of

enzyme treatment on the sensory characteristics of casein and soybean protein hydrolysates is presented in Figs. 5A and 5B respectively. Both the products showed increased overall acceptability after enzyme treatment, Accompanied by decrease of bitterness of casein hydrolysate (4.30 to 2.40, Fig. 5A) as well as soybean hydrolysate (3.8 to 2.40, Fig. 5B).

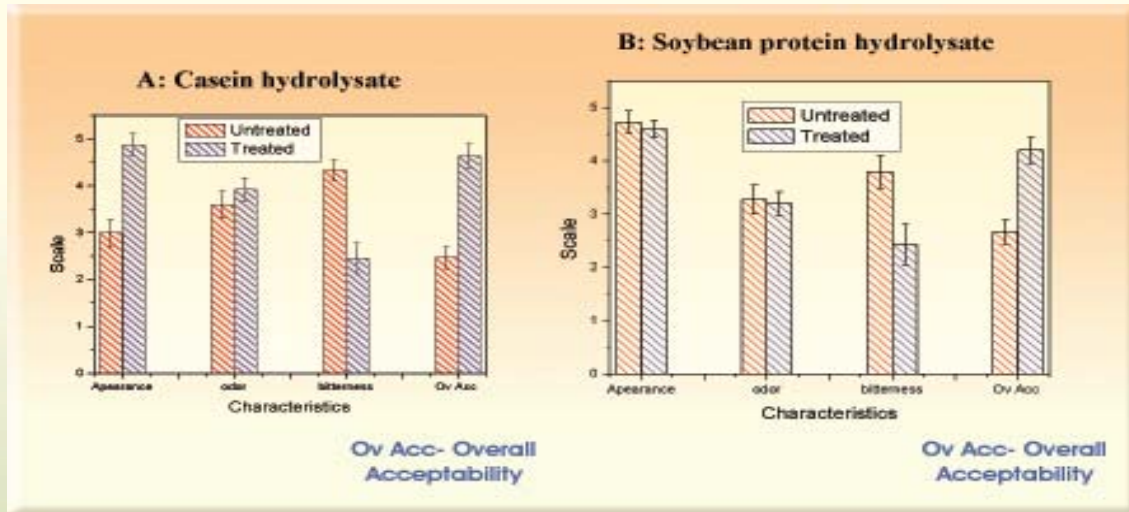


Fig. 5: Sensory analysis of casein hydrolysate and soybean protein hydrolysate

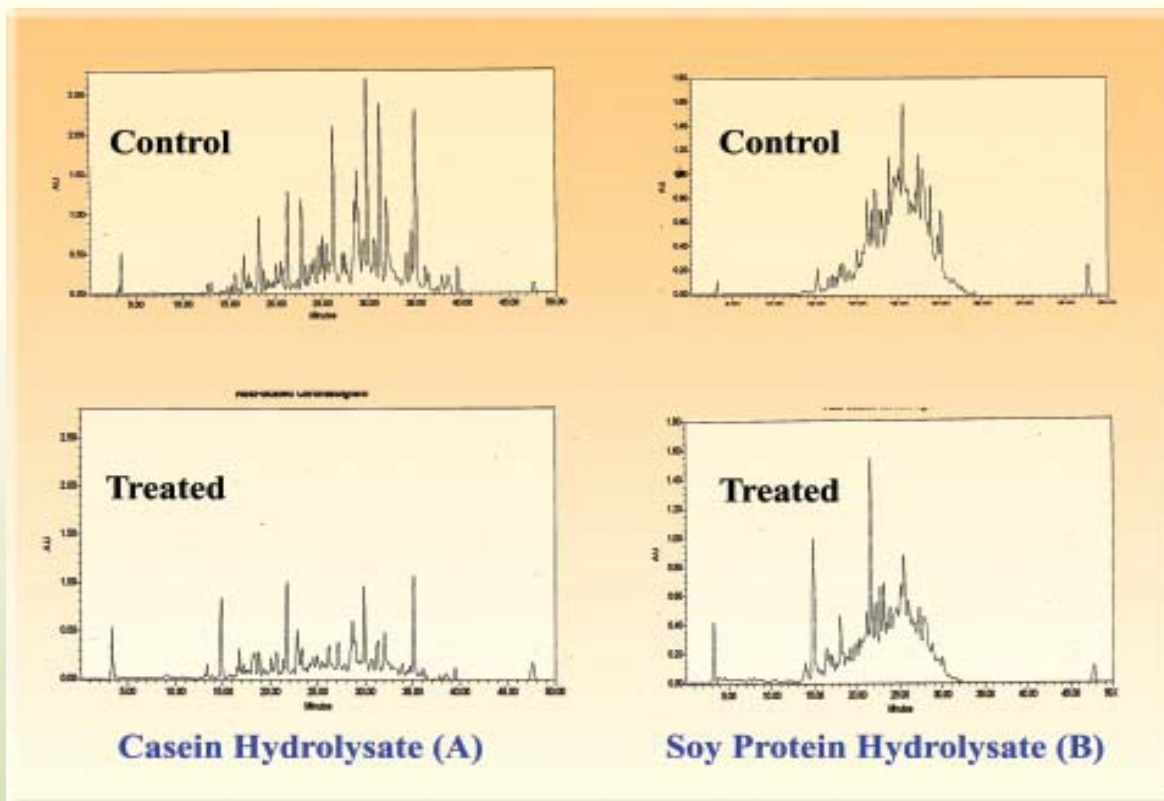


Fig. 6: RP HPLC profiles of protein hydrolysates after treatment

RP HPLC analysis: After enzyme treatment, peaks of casein hydrolysate (Fig. 6A) the at 27 min, 30 min, 32 min and 35 min were reduced with a concomitant increase in the peaks at 3 min, 15 min and between 17 – 25 min. For soybean hydrolysate (Fig. 6B) the region of fused peaks between 20- 35 min reduced with an increase in peaks in the region of 15 mins to 25 min.

Amino acid analysis: the amino acid content of the treated samples is presented in Table 2. Treatment with aminopeptidase did not affect the amino acid content of protein hydrolysates.

Table 2: Amino acid profile of protein hydrolysates after treatment.

Amino acid	Casein hydrolysate	Soybean protein hydrolysate
Asp	95.61	91.65
Glu	111.27	100.28
Ser	97.25	86.13
Gly	96.92	90.40
Thr	96.97	90.87
Arg	113.25	96.72
Tyr	97.29	92.69
Val	104.76	99.88
Met	96.10	97.42
Ile	105.05	98.35
Phe	100.24	92.19
Leu	97.07	99.19
Lys	97.74	93.99

(Values are expressed as % amino acid content of untreated sample and are an average of two independent experiments)

Peptide chain length: Hydrolysis by aminopeptidases resulted in a decrease in chain lengths of peptides in casein and soybean protein hydrolysates (Table 3). In

both the cases, the average peptide chain lengths were nearly half that of the untreated hydrolysates.

Table 3: Influence of treatment on peptide chain length of the protein hydrolysates.

	Average peptide chain length (Number of residues)	
	Casein hydrolysate	Soybean protein hydrolysate
Untreated	5.61	5.21
Treated	2.59	2.72

Values expressed are an average of two independent experiments.

Continuous operations: the effect of continuous operations on the debittering activity and retention of aminopeptidase was monitored. The RP HPLC profiles of the well spread out aliquots collected during the continuous operation of the column are presented in Figs. 7A-D [0h (Fig. 7A), 24h (Fig. 7B), 48h (Fig. 7C) and 72 h (Fig. 7D)]. the insert in Fig 7A (control) is the peak of potassium sorbate that had been added as a preservative and can be seen as a cut peak (26 min) in all the profiles. In all the aliquots collected a general shift in the peptide peaks from 25- 45 min to 3-22 min was observed. There was also a very scanty leakage of activity during the process. During the entire operation aminopeptidase activity (arginine naphthylamidase) of 169- μ moles/ h was detected in the hydrolysate (activity of 1 bead is 331 μ moles/h).

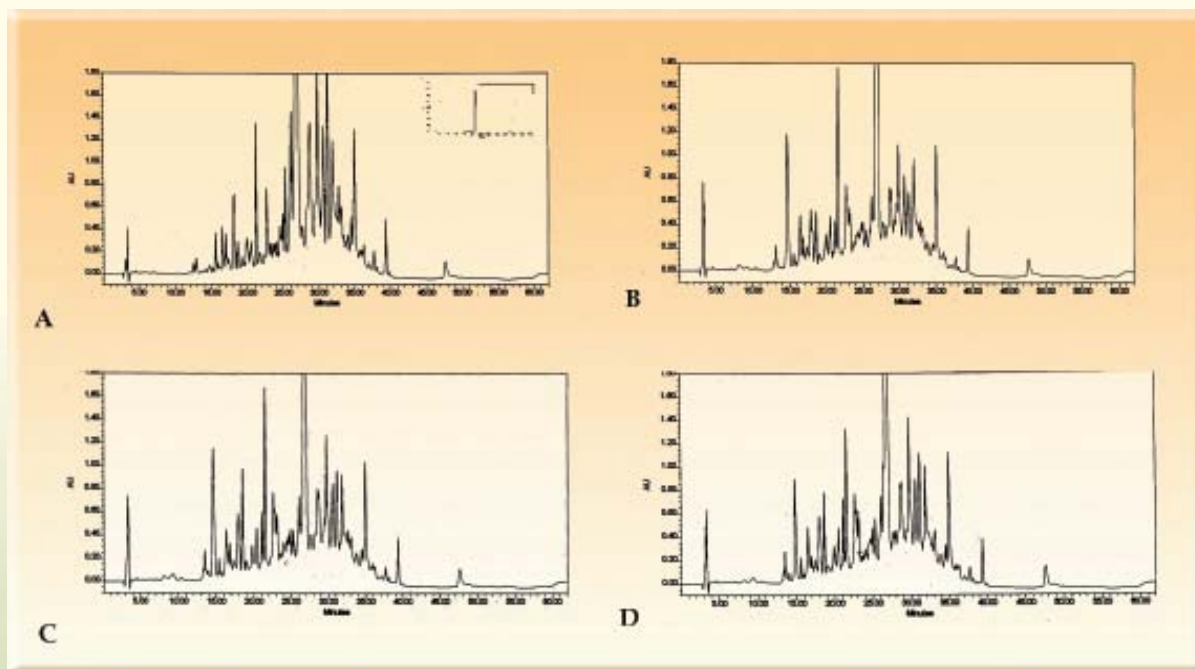


Fig. 7 : RP HPLC profiles of samples collected during the continuous operation of the column

Discussion

In the present paper a process for the debittering of protein hydrolysates using chicken intestinal mucosa is presented. The bitterness of protein hydrolysates is ascribed to peptides (<10kDa) rich in hydrophobic amino acids in certain specific sequences. The action of exopeptidases to bring about a reduction in bitterness of protein hydrolysates is well known (Raskulthai and Haard, 2003).

Intestinal mucosa which served as the source of aminopeptidases was rendered free of microflora by gamma irradiation (20kGy). Irradiation is a cold sterilization process and the eradication of the microorganism from the intestinal mucosa was accompanied by only a marginal loss (20%) of the aminopeptidase activities (Fig. 2) (Hwang and Hau, 1995).

Entrapment in Ca-alginate served as an easy method for the immobilization of chicken intestinal aminopeptidases. There also was no leakage of mucosal enzymes from the immobilized matrix. More importantly, aminopeptidase in the immobilized system exhibited broader temperature and pH optima as compared to the free mucosal aminopeptidases (Fig. 3A and B). Similar results on the broadening of temperature and pH optima have been reported earlier for other enzymes (Cohenford et al. 1986; Wilson et al. 1994; Varavinit et al. 2002). Immobilization also facilitated the stability of aminopeptidases (4A and B). The debittering capability of the immobilized system is apparent from the organoleptic studies (Figs. 5A and B). Debittering of protein hydrolysates was effected by a single pass of the hydrolysate through the immobilization system. Flow rate was maintained to allow a contact time of approximately 1h between the hydrolysates and the beads. Decrease in bitterness

could be ascribed to the degradation of hydrophobic bands as evidenced by the clear shift in RP HPLC profiles towards hydrophilic regions. Such a shift in the RP HPLC profiles has been shown (Nishiwaki et al. 2002; Minagawa et al. 1989) to be a characteristic feature of debittering. The taste panel studies also convincingly proved the reduction in the bitterness of the protein hydrolysates after the immobilized chicken mucosal peptidase acted on them. A reduction in the average peptide chain length for the hydrolysates after treatment was an indicator of the proteolytic action of the exopeptidases contributing to the debittering. Such a decrease in peptide chain length accompanying debittering has been reported by Minagawa et al (1989). The amino acid composition of both the hydrolysates was found unchanged on passing through the immobilized column. The adsorptive and extraction processes that bring about a debittering by the removal of constituent bitter peptides result in a nutritive loss as the bitter peptides contain many essential amino acids. The enzymatic debittering process devised by us could bring about debittering without affecting the nutritional composition. Continuous operation of the process was performed for over 3 days. The RP HPLC analysis of the samples well spread over the time period indicated that though there was a slight change in efficiency of the system, the peptide profile of the hydrolysates was concentrated more towards the hydrophilic region after treatment. Lack of measures to maintain the system under aseptic conditions and the potential of the hydrolysates to support microbial growth at enormous rates limited these studies. However, under batch set up it was observed that in the presence of the substrate the beads maintained the aminopeptidase activities for upto 10 days and we envisage that the column could at least be operated upto ten days.

Nonavailability of catalytically efficient peptidases in

economically viable quantities is the major limitation faced by industries attempting enzymatic debittering of protein hydrolysates. Since different types of amino acids are involved in imparting bitterness to protein hydrolysates, it is desirable to use a process, which uses a group of enzymes with varied specificities. In this respect, our process using chicken intestinal mucosa is endowed with multiple advantages such as the presence of multiple exopeptidases capable of acting on all the amino acid residues, high rates of catalytic efficiency and stability over a wide range of temperatures and pHs encountered in food industry operations.

References

1. Adler-Nissen J (1979) Determination of degree of hydrolysis of food protein hydrolysates by trinitrobenzenesulfonic acid. *J. Agric. Food Chem.* **27(6)**: 1256-1262.
2. Barrett AJ (1972) Lysosomal Enzymes, Appendix Assay Methods, In: *Lysosomes a Laboratory Handbook*, Dingle JT (Ed.) North Holland / American Elsevier, pp 110-135.
3. Clemente A (2000) Enzymatic protein hydrolysates in human nutrition. *Trends in Food Sci. and Technol.* **11**: 254-262.
4. Cohenford MA, Santoro PF, Urbanowski JC and Dain JA (1986) Effect of immobilization on physical and kinetic properties soluble and insoluble trypsin-albumin polymers. *Biotech. and Bioengg.* **28**: 736-740.
5. Hwang HI and Hau LB (1995). Effects of ionizing radiation on the enzyme activities and ultrastructural changes of poultry. *Radiat. Phys. Chem.* **46**: 713-716.

6. Jamadar VK, Jamdar SN, Dandekar SP and Harikumar P (2003) Purification and characterisation of aminopeptidase from chicken intestine. *J. Food Sci.* **68**: 438-443.
7. Jamdar SN and Harikumar P (2005) Autolytic degradation of chicken intestinal proteins. *Bioresource Technol.* **96**:1276-1284.
8. Lalasidas G and Sjoberg L (1978) Two new methods of debittering protein hydrolysates and a fraction of hydrolysates with exceptionally high content of essential amino acids. *J. Agric Food Chem.* **26**: 742-749.
9. Lin S-B, Nelles LP, Cordle CT and Thomas RL (1997) Physical factors related to C18 adsorption columns for debittering protein hydrolysates. *J. Food Sci.* **62**(5): 946-948.
10. Minagawa E, Kaminogawa S, Tsukasaki F and Yamauchi K. (1989) Debittering in bitter peptides of enzymatic hydrolyzates from milk casein by aminopeptidase T. *J. Food Sci.* **54**: 1225-1229.
11. Nishiwaki T, Yoshimizu S, Furuta M and Hayashi K (2002) Debittering of enzymatic hydrolysates using an aminopeptidase from the edible basidiomycetes *Grifola frondosa*. *J. Biosci. Bioeng.* **93**(1): 60-63.
12. Nishiwaki T, Yoshimizu S, Furuta M and Hayashi K (2002) Debittering of enzymatic hydrolysates using an aminopeptidase from the edible basidiomycetes *Grifola frondosa*. *J. Biosci. Bioeng.* **93**(1): 60-63.
13. Qi M, Hettiarachchy NS and Kalapathy U (1997) Solubility and emulsifying properties of soy protein isolates modified bt pancreatin. *J. Food Sci.* **62**(6): 1110-1115.
14. Raksakulthai R and Haard NF (2003) Exopeptidases and their action to reduce the bitterness in food: A review. *Cri. Rev. Food Sci. and Nutr.* **43**(4): 401-445.
15. Saha BC and Hayashi K (2001) Debittering of protein hydrolysates. *Biotechnology Advances* **19**: 355-370.
16. Varavinit S, Chaokasem N and Shobsnog S (2002) Immobilisation of thermostable α -amylase. *Science Asia.* **28**: 247-251.
17. Wilson SA, Peek K and David RM (1994) Immobilisation of proteinase from the extremely thermophilic organism Rt41A. *Biotech. and Bioengg.* **43**(4): 226- 231.

ABOUT THE AUTHORS



Mr. Madhujit Damle, M. Sc. (Microbiology) from University of Mumbai is a DAE fellow working in Flesh Food Biochemistry Section, Food Technology Division, BARC since

2001. He has submitted his Ph. D. thesis entitled " Studies of intracellular proteases and their action on tissue proteins" in April 2006.



Dr. P. Harikumar is presently the Head, Flesh Food Biochemistry Section, Food Technology Division. He joined BARC in 1967 after graduating from the University of Kerala, obtained M.Sc. and PhD

degrees from the University of Mumbai. He has carried out postdoctoral research at Roche Institute of Molecular Biology, Nutley, New Jersey, USA (1982-1984) and at University of Medicine and Dentistry, New Jersey, USA, (1998-1999) on "The Role of lysosomal proton ATPase and Ca^{2+} in the regulation of intracellular protein catabolism." His major contribution is in understanding the structure-function relationships of lysosomal proteases and their role in regulating the quality attributes of irradiated flesh foods and in the preparation of value added products from poultry and fish processing wastes.



Dr. Sahayog N. Jamdar Joined BARC in 1996 through BARC Training School (39th batch) and is working in the Flesh Food Biochemistry Section, Food Technology Division.

His major contribution is in understanding structure function relationships of proteases and preparation of value added products from poultry and fish processing wastes.

Edited & Published by : Dr. Vijai Kumar, Associate Director,

Knowledge Management Group & Head, Scientific Information Resource Division,

Bhabha Atomic Research Centre, Trombay, Mumbai 400 085, India.

Editorial Management : Ms. S.C. Deokathey,

Computer Graphics & Layout : P.A.S. Warriar, SIRD, BARC

BARC Newsletter is also available at URL: <http://www.barc.gov.in>

(for private circulation only)

